N.63 21105 NASA SP-34 PART 2

4449

SPACE FLIGHT HANDBOOKS

Volume 2

Lunar Flight Handbook

NATIONAL AERONAUTICS AND SPACE ADMINISTRATION



Printed Copy Price - Ots: \$6,00

SPACE FLIGHT HANDBOOKS Volume 2

Lunar Flight Handbook

PART 2 - LUNAR MISSION PHASES

444 p sefa

Prepared for the GEORGE C. MARSHALL SPACE FLIGHT CENTER

HuntsvIlle, Alabama Under Contract NAS 8-5031

(NASA-SP-34, Pl. 2) OTS: \$6.00



Office of Scientific and Technical Information NATIONAL AERONAUTICS AND SPACE ADMINISTRATION 1963
Washington, D. C.

FOREWORD

This handbook has been produced by the Space Systems Division of the Martin Company under contract NAS8-5031 with the George C. Marshall Space Flight Center of the National Aeronautics and Space Administration. The Lunar Flight Handbook is considered the second in a series of volumes by various contractors, sponsored by MSFC, treating the dynamics of space flight in a variety of aspects of interest to the mission designer and evaluator. The primary purpose of these books is to serve as a basic tool in preliminary mission planning. In condensed form they provide background data and material collected through several years of intensive studies in each space mission area, such as earth orbital flight, lunar flight, and interplanetary flight.

Volume II, the present volume, is concerned with lunar missions. The volume consists of three parts presented in three separate books. The parts are:

Part 1 - Background Material Part 2 - Lunar Mission Phases

Part 3 - Mission Planning

The Martin Company Program Manager for this project has been Jorgen Jensen; George Townsend has been Technical Director. Fred Martikan has had the direct responsibility for the coordination of this volume; he has shared the responsibility for the generation of material with Frank Santora.

Additional contributors were Robert Salinger, Donald Kraft, Thomas Garceau, Andrew Jazwinski and Lloyd Emery. The graphical work has been prepared by Dieter Kuhn and Elsie M. Smith. John Magnus has assisted in preparing the handbook for publication. William Pragluski, Don Novak, James Porter, Edward Markson, Sidney Roedel, Wade Foy and James Tyler have made helpful suggestions during the writing of this book.

The assistance given by the Future Projects Office at MSFC and by the MSFC contract management panel, directed by Conrad D. Swanson is gratefully acknowledged.

CONTENTS

	Volume II, Part 2 - Lunar Mission Phases
V	Earth Departure
VI	Earth-to-Moon Transfer VI-1
VII	Lunar Orbit
VIII	Descent to and Ascent from the Lunar Surface
IX	Moon-to-Earth Transfer
X	Earth Return X-1
	e preceding contents are Part 2 of Volume II. The remaining tw f Volume II contain the following:
	Volume II, Part 1 - Background Material
I	Introduction
II	Physical Data
III	The Earth-Moon System III-1
IV	Trajectories in the Earth-Moon System IV-1
	Volume II, Part 3 - Mission Planning
XI	Mission Planning XI-1
XII	Bibliography
	Appendix A Glossary
	Appendix B Symbols
	Index

CHAPTER V

EARTH DEPARTURE

Prepared by:

F. Santora
Martin Company (Baltimore)
Aerospace Mechanics Department
March 1963

Α.	Fixed Translunar Trajectory Technique	V - 2
В.	Variable Translunar Trajectory Technique	V-12
C.	Translunar Injection	V-14
D.	References	V-21
	Illustrations	V-23
	List of Illustrations	V-25

INTRODUCTION

Chapters II, III and IV presented material introductory to the problem of lunar flight such as analysis of the environment in which the space vehicle moves (including some numerical values of constants describing this environment), the geometry and dynamics of motion in earth-moon space and finally, a general classification of missions and trajectories and trajectory simulation in earth-moon space. The material in Chapters II, III and IV has been qualitative, or -if quantitative -- designed to provide background for a discussion of lunar trajectories. The present chapter is the first of six which present detailed trajectory data for the various phases of a lunar mission, giving detailed analyses and approaches to the problems, illustrating them with numerical examples, or giving parametric variations of trajectory variables whenever necessary. Chapter V discusses earth departure -that part of the total trajectory of any lunar mission between launch at a given time and site and injection into the desired translunar trajectory at the correct time and position. However, no discussion will be given of ascent trajectories from launch to booster burnout.

To accomplish its mission, a lunar spacecraft must be placed at a precise position at a precise time with a very accurate velocity. In order to attain these injection conditions, the spacecraft must first be launched from the earth's surface with the proper ascent trajectory. It is thus of utmost importance that this earth departure phase be as flexible as possible to ease the complexity of mission planning and to minimize the introduction of additional launch constraints. This consideration precludes discussion of direct ascent from launch to lunar trajectory injection (i.e., direct earth departure) by continuous rocket burning during this phase of the trajectory.

Generally the most practical, efficient, and likely technique of earth departure utilizes parking orbits about the earth prior to injection. Additionally, these parking orbits allow greater mission flexibility by providing:

- Time for final onboard and ground checkouts before injection is initiated.
- (2) Injection capability any time of the month, twice a day.
- (3) The same nominal ascent and injection trajectory profile for any mission.

The major disadvantages of this technique are the increased requirements for tracking, communication and computational facilities. Even so, these disadvantages will become less severe as more ground support equipment becomes operational and available for lunar mission support. Hence, parking orbits have been assumed for the earth departure phase throughout this chapter.

Flexibility from a flight mechanics point of view, as used here, is assessed in terms of launch frequency and launch tolerance. Launch

frequency is defined as the number of time periods for a possible launch during the month (lunar position in orbit) or during the day (earth rotation), while launch tolerance is the interval of time by which the launch can be expedited or delayed from the nominal launch time, still yielding the desired injection conditions.

There are two basic launch techniques that can be used to obtain launch frequency and launch tolerance. In the first technique, the earth parking orbit and translunar trajectory are fixed for a given injection time. Direct or indirect ascents are performed to attain the required parking orbit. The direct ascent solves the timing problem of arriving at the proper injection point at the correct time on the ground before launch. In the indirect ascent method, the spacecraft is launched at any time, and the timing problem is solved while in the parking orbit. The former method results in launch tolerances measured in terms of a few minutes and a launch frequency varying from one to four times a day. The indirect method is characterized by launch tolerances measured in hours, a frequency of one or two times a day, and a requirement of two additional rocket engine ignitions. Furthermore, waiting times in parking orbit prior to injection can easily be 24 hr for the indirect as compared to 2 hr for the direct ascent.

The second technique assumes a variation of the translunar trajectory with delay time resulting in a launch frequency of twice a day, with a corresponding launch tolerance of approximately 5 hr. Since no excess propellant is required to obtain this launch tolerance, there is no payload penalty. However, this is not the case for the first technique, where launch tolerances are governed by the amount of excess propellant available. This latter technique appears to be most favorable if an earth rendezvous is not required.

Additional propellant may also be required to salvage a mission in the event the vehicle cannot be injected at the preplanned time. Essentially, this propellant provides an injection frequency and injection time tolerance once the spacecraft is in its parking orbit. Excess propellant is also desirable for manned missions if an abort is required during the injection phase, when the spacecraft is being accelerated from earth-orbital to translunar injection speed.

The numerical data presented in this chapter represent launches from Cape Canaveral alone. Magnitudes of launch tolerances are obtained by assuming a hypothetical launch vehicle and are included solely for the purpose of giving insight into and comparison of the various aspects of the problem.

All data presented in this chapter is based on Keplerian orbits during ballistic flight, i.e., the earth is assumed spherically symmetric in concentric layers, and atmospheric drag and other nongravitational forces on the vehicle are neglected. (On occasion, effects of atmospheric drag and earth oblateness on the ascent trajectory will be mentioned.) In most cases, rocket thrust is simulated by an impulsive change in the veloc-

ity -- △ V; more details concerning the effects of finite burning times and a discussion of general orbital maneuvers are presented in Chapter VI of Ref. 1.

A. FIXED TRANSLUNAR TRAJECTORY TECHNIQUE

The timing and planning of a lunar mission reduces to the selection of a moon arrival date and time which depends on such mission considerations as solar illumination of the moon, the ability to establish prescribed orbits around the moon with circumlunar trajectories, and the ability to land at designated landing sites which are librating relative to earth. This selection of arrival time then fixes the translunar injection position ψ_0 , the injection time and the inclination of the translunar plane iVTL (Chapter IV, Section B). These fixed values, together with the injection radius and velocity, are then specific requirements for the lunar mission which must be met if the mission objectives are to be attained with the particular vehicle. This is illustrated by considering a one-minute delay in the arrival at the predetermined injection point. A late injection of this magnitude into a ballistic translunar trajectory can change the miss distance (pericynthion) at the moon by -26 km, the vacuum perigee altitude (for a circumlunar trajectory) by + 305 km, and the return inclination $i_{
m VTE}$ by 2 deg. Another,

and more severe example is an error in injection position. If the spacecraft is injected at the correct time but with an along-track position error of +11 km, the pericynthion of the ballistic circumlunar trajectory can change by + 135 km, the return vacuum perigee by -14, 250 km and the return trajectory inclination by 7.5 deg. Therefore, regardless of how the spacecraft leaves the earth's surface, it must satisfy the translunar injection requirements quite closely. Understandably, midcourse guidance can correct small errors at injection; but they must be small if the correction fuel requirements are not to become excessive and if the midcourse guidance scheme is to be easily mechanized. Major trajectory changes after injection require too much energy to be practical at this time and they should be avoided.

1. Launch Tolerance with Direct Ascent

a. Direct ascent without earth rendezvous

With the ballistic translunar trajectory fixed, the injection conditions of the spacecraft (radius and velocity vector) are also fixed. To achieve these injection conditions, a coast period and parking orbits are likely to be used during the ascent phase.

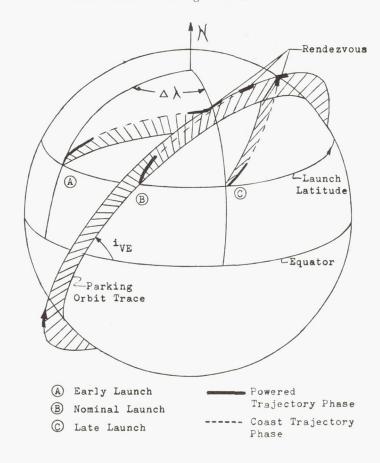
The inclination of the parking orbit to the equatorial plane is quite important. If this inclination is not the same as the inclination of the translunar trajectory to the equatorial plane, a lateral maneuver will be required at velocities between earth orbital and escape speed. This is expensive in fuel since a large velocity vector must be changed in direction or "turned." There-

fore, throughout the handbook, the parking orbit prior to injection is assumed to lie in the same plane as the initial translunar trajectory, and any lateral maneuvers, if required, will be performed during ascent into the parking orbit.

In order to satisfy the injection conditions, one can first visualize a "phantom" satellite in the parking orbit having the correct position for achieving the injection conditions at some predetermined time.

The problem now reverts to one that requires the spacecraft to ascend from the earth's surface and rendezvous with the phantom satellite. For mission planning, information is required as to the fuel penalty if the launch of the spacecraft is delayed on the ground.

In the direct ascent method, the spacecraft is boosted directly to the altitude of the parking orbit. The time of arrival at this altitude is planned such that the spacecraft and phantom satellite are coincident. The spacecraft is then injected into orbit, and it executes any turns that may be required to establish itself in the parking orbit plane during the orbit injection. In other words, a fictitious rendezvous is made with the phantom satellite. The direct ascent method is illustrated in the following sketch.



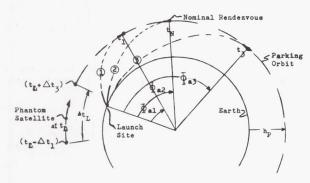
As can be seen, the spacecraft is accelerated from launch to some cutoff altitude. It then coasts to the parking orbit altitude, where ren-

dezvous is made with the phantom satellite. If a turn (i.e., orbit inclination change) is required, it is made during the second powered phase, as shown.

First, consider Case B in the sketch, where the launch site lies in the parking orbit plane and the phantom satellite is in the correct position, such that rendezvous occurs at the end of the ascent phase. For this case, no turn is required at the rendezvous point, and Case B will be considered as the nominal ascent trajectory in this discussion.

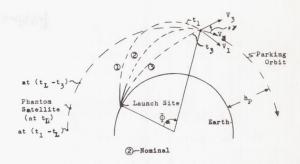
The next sketch shows three ascent trajectories (1, 2, 3) and the times of arrival at apogee (t_1 , t_N , t_3). Trajectory number two is the nominal ascent, and t_N is the nominal apogee arrival time, with the nominal launch time being t_L .

Now consider that for Case B, the phantom satellite was not at the correct position at launch (t_L), but instead was at (t_L - Δt_1) as shown



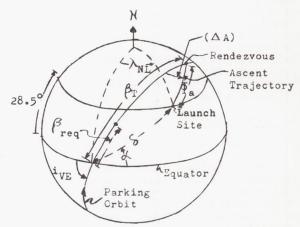
If Δt_1 is equal to the difference between the nominal apogee arrival time and t_1 ($t_N > t_1$), the spacecraft can still perform the rendezvous by flying the number 1 trajectory. This is called an early launch. The same reasoning applies if the phantom satellite occupies the position ($t_L + \Delta t_3$) at launch (late launch). If Δt_3 is equal to ($t_3 - t_N$) the spacecraft can rendezvous by flying the number 3 trajectory. In other words, by extending the ascent range Φ_a the spacecraft can be launched at any time in the interval $\Delta t_L = (t_3 - t_1)$, where Δt_L is the launch tolerance obtained by extending Φ_a from Φ_{a1} to Φ_{a3} .

Another method of obtaining launch tolerance consists of shaping the ascent trajectory. Consider the nominal ascent which arrives at the parking orbit altitude $h_{\mathbf{p}}$ with zero flight path angle (γ = 0). Now, for a given range angle $\Phi_{\mathbf{a}}$, allow the spacecraft to intersect the parking orbit with γ \neq 0, as shown in the following sketch:



Assume further that upon arrival at the parking orbit altitude $h_{\rm p}$ a rendezvous is performed, and the flight path angle is reduced to zero. Trajectory number 1 (early launch) arrives at $t_{\rm l}$, where $t_{\rm l} > t_{\rm N}$, and trajectory number 3 (late launch) arrives at $t_{\rm d} < t_{\rm N}$. By utilizing the same approach presented for the range extension method, it is similarly found that the launch tolerance from trajectory shaping is $\Delta t_{\rm L} = (t_{\rm l} - t_{\rm d})$.

Thus far, the discussion has been restricted to Case B where the launch site lies in the parking orbit plane. However, this is not true in general because as the phantom satellite progresses in its orbit, the launch site, on the rotating earth, rotates out of the parking orbit plane. The real situation, greatly exaggerated, is depicted in the sketch on page V-2 by the ascent trajectories A and C . Because of the earth's rotation, Case A occurs prior to the nominal launch time t_L and Case C after t_L , and it is evident that some turn is required if launch took place at those times. The following sketch gives the pertinent geometry for determining the required turn angle \triangle A which can be obtained from spherical trigonometry:



Ascent Turn Angle Geometry

$$\Delta A = \sin^{-1} \left[\pm \frac{\sin 28.5^{\circ} \cos i_{VE}}{\sin \phi_{a}} \right]$$

$$\frac{-\cos 28.5^{\circ} \sin i_{VE} \sin \lambda_{NL}}{\sin \phi_{a}}$$
(1)

where the launch site is assumed in the northern hemisphere for this formula to hold, and

- +28.5° = latitude of Cape Canaveral, the launch site

Equation (1) shows that the longitude of the launch site λ_{I} , the ascent range Φ_{a} , and the parking orbit inclination to the earth's equator i_{VE} , determine the magnitude of the required turn angle \triangle A. Furthermore, the minimum turn angle occurs when Φ_a = 90 deg. Assuming that the launch site is Cape Canaveral, which is at a latitude of +28.5 deg and $i_{\mbox{VE}}$ is limited to between 28.5 and 35 deg, typical values of Δ A are shown in Fig. 1 for the nominal case Φ_a = 90 deg. Since the phantom satellite moves along the parking orbit at approximately 4 deg/ min, and the launch site rotates with the earth at approximately 0.25 deg/min, the value of Δλ will always be small for a given nominal phantom satellite pass (see sketch on page V-2). Consequently, because of the short interval of time the phantom satellite is in a favorable rendezvous position in a given revolution, the required \triangle A is small. This particular point will become quite clear when the actual magnitudes of the launch tolerances are discussed

If $\triangle A$ and Φ_a are known, the required position of the phantom satellite β_{req} can be determined by use of spherical trigonometry (see the above sketch):

$$\beta_{\rm T} = \cos^{-1} \left[\left\{ \cos \phi_{\rm a} \cos \delta - \sin \phi_{\rm a} \sin \delta \cos \Delta A \right. \\ \left. \cdot \cos \left[\pm \left(\alpha - i_{\rm VE} \right] \right] \right\} \left\{ 1 - \sin \phi_{\rm a} \sin \Delta A \right. \\ \left. \cdot \sin \delta \sin \left[\pm \left(\alpha - i_{\rm VE} \right] \right] \right\}^{-1} \right]$$
 (2)

where

- (+) = launch site on the polar side of the orbital ground trace
- (-) = launch site on the equatorial side of the orbital ground trace

$$\alpha = \tan^{-1} \left[\frac{\tan 28.5^{\circ}}{\sin \lambda_{L}} \right]$$

$$\delta = \sin^{-1} \left[\frac{\sin 28.5^{\circ}}{\sin \alpha} \right]$$

then
$$\beta_{\text{req}} = \beta_{\text{T}}$$
 - ascent time $\left(\frac{\partial \beta_{\text{T}}}{\partial t}\right)$.

 \mathfrak{G}_{T} is the orbital central angle of the rendezvous point (measured northward from the ascending node of the parking orbit--see previous sketch).

But first, the required ascent range as a function of launch delay time must be determined. If a nominal launch (Φ_a = 90 deg) is possible at a given time (t_L), there are only two parameters which can be changed to effect a rendezvous at a later instant. These variables are the actual launch time t and the ascent range Φ_a . The motion of the phantom satellite as a function of these variables is given by:

$$dR_{req} = \frac{\partial R_T}{\partial t} dt + \left(\frac{\partial t}{\partial \Phi_a}\right) \left(\frac{\partial R_T}{\partial t}\right) d\Phi_a.$$
 (3)

Likewise, the motion of the intersection point of the parking orbit and ascent trajectory is given by

$$dR_{T} = \begin{pmatrix} \frac{\partial R_{T}}{\partial t} \end{pmatrix} \quad dt \\ \Phi_{a} = constant + \begin{pmatrix} \frac{\partial R_{T}}{\partial \Phi_{a}} \end{pmatrix} d\Phi_{a} \\ t = const$$
 (4)

In order to effect a rendezvous, the phantom satellite and the intersection point must be coincident. Therefore, by equating Eqs (3) and (4), the range extension as a function of launch time can be found as

$$\frac{d\Phi_{a}}{dt} = \frac{\frac{\partial R_{T}}{\partial t} - \left(\frac{\partial R_{T}}{\partial t}\right)}{\left(\frac{\partial R_{T}}{\partial \Phi_{a}}\right)} \Phi_{a} = constant - \frac{\partial R_{T}}{\partial \Phi_{a}} \frac{\partial R_{T}}{\partial t}$$

$$t = const$$
(5)

A typical magnitude of $d_\Phi^{}/dt$ for near-earth parking orbits is 55 deg/min. Thus if a nominal launch calls for $\Phi_a^{}=90$ deg, a launch can be made one minute before nominal by decreasing $\Phi_a^{}$ to 35 deg or one minute after nominal by increasing $\Phi_a^{}$ to 145 deg. In other words, for this practical range variation, launch tolerances obtained by range extension for the direct ascent technique are measured in minutes rather than hours. Note that Eqs (3), (4) and (5) apply to the range extension method only. Besides being used individually, the methods of range extension and trajectory shaping also can be used together to

obtain a launch tolerance as shown in the numerical example of Subsection A-1c below.

b. Direct ascent with earth rendezvous

It becomes immediately evident that if the phantom satellite were replaced by an orbiting vehicle, the launch tolerances given by the previous discussion are directly applicable. Therefore, if a mission entails a physical rendezvous with a fueling vehicle in earth orbit, for example, the methods for launching the spacecraft are not altered.

For the fixed translunar trajectory technique, the methods for launching and the launch tolerances for the fueling vehicle are identical to those of the spacecraft, since for an earth rendezvous mission with a subsequent translunar injection requirement, the fueling vehicle must first rendezvous with a phantom satellite and then the spacecraft must rendezvous with the fueling vehicle. Part of the mission planning must include the time required in parking orbit to perform the rendezvous maneuver, mate the vehicles and make final preparation for injection into the translunar trajectory.

c. Numerical example for direct ascent

The various concepts for direct ascents to the parking orbit and their relative merits can best be illustrated by a numerical example. Figure 2 presents launch tolerances obtained by range extension for a hypothetical launch vehicle with a burnout altitude of 185.2 km. The data shows that launch tolerance increases with increasing parking orbit altitude, and for the same range extension, it decreases with increasing initial ascent range. Both of these effects are evident from Eq (5), the first being due to the decrease of $\partial \, \mathbb{G}_T / \partial \, \mathbb{T}$ with increasing altitude, and the second due to increasing initial range.

Another aspect of the direct launch involves a set of orbit injection conditions (discussed in Section C) as well as launch tolerances for each orbital pass of the phantom satellite, since launch and rendezvous can take place on orbital revolutions prior to and after the nominal. This is also illustrated in the sketch showing direct ascent, whereby in Case A (early launch) the rendezvous with the phantom satellite may occur one revolution before the nominal, and in Case C (late launch) the rendezvous may occur one revolution after the nominal. Since the parking orbit period is approximately 90 min for the orbital altitudes considered, the launch site will have approximately a 22.5-deg longitude difference from the parking orbit plane for a pass before or after the nominal revolution. It becomes quite clear, for these cases, that much larger turns are required when the spacecraft intersects the parking orbit (Fig. 1). The additional ΔV of launching one revolution before nominal (due to turn) is approximately 1311 m/sec for the parking orbit inclination $i_{\rm VE}$ = 35 deg. This ΔV decreases with decreasing $i_{
m VE}$, but it still is 549 m/sec above nominal for $i_{\rm VE}$ = 29 deg. For launches

after nominal, the additional fuel requirement rises, but not nearly as sharply as for launches before nominal. A launch one revolution after nominal requires an additional Δ V = 762 m/sec for $i_{\mbox{\scriptsize VE}}$ = 35 deg and only 91.5 m/sec for $i_{\mbox{\scriptsize VE}}$ = 29 deg. For some cases, three or four launches per day are possible.

The velocity capability required $V_{\mbox{req}}$ for the nominal ascent (Case B) is given for the hypothetical booster in Table 1.

TABLE 1

Total Velocity Required for Nominal, No Turn, Rendezvous, $V_{\rm req}$ (m/sec)

 $h_{BO} = 185.2 \text{ km}$

Parking Orbit Altitude h _P	Asce	nt Range	Angle,	a (deg)
(km)	60	90	120	180
277.8 466.7 740.8	7848.3 7964.7 8136.9	7848.0 7958.0 8114.4	7847.4 7955.9 8107.1	7955.9

By extending the ascent range, the total velocity requirements are affected, the total velocity required being defined as

 ${
m V}_{
m req}$ = velocity at burnout + $\Delta {
m V}$ (injection and turns)

Table 1 shows that the required velocity decreases slightly with increasing ascent range. Thus, for the nominal case, launch tolerance is obtained with an attendant reduction in $V_{\rm req}$ and hence in fuel expenditure. Of course, $V_{\rm req}$ increases with parking orbit altitude, as can be seen from Table 1.

For the off-nominal case and the parking orbit inclinations of interest, practical turn angles from a standpoint of fuel requirements will vary from 0 to 4° .

Figure 3 shows that for a constant turn angle at $h_{\rm P}$ = 466.7 km the required velocity drops with decreasing range angle (see solid curves). However, the turn angle required will not remain constant as $\Phi_{\rm a}$ changes and the "dashed" curves in Fig. 3 show how the total velocity requirement varies. For range extensions from 60° to 90°, no additional velocity is required; but by extending the range beyond 90° and below 60°, the velocity required increases rapidly.

Launch tolerances as obtained from trajectory shaping have not been considered thus far. Essentially, the tolerances derived from the "shaping" method are limited only by the velocity capability of the booster and are dependent on the booster characteristics. Figure 4 presents the velocity requirement above nominal for obtaining launch tolerances by this method with the assumed booster and for $h_{\rm p}$ = 466.7 km. For a fixed $h_{\rm p}$

and a fixed launch time tolerance, the velocity requirement increases with decreasing ascent range angle.

It should be noted that the slopes of the ΔV versus Δt_L curves are quite steep and increase (not shown), with decreasing parking orbit altitude. In addition, more velocity is required to obtain a (+) launch tolerance (launch late) than a (-) tolerance. Practical tolerances ($\Delta V \simeq 300~\text{m/sec}$) again are measured in minutes.

A third method for generating tolerances is by combining the first two methods. This is possible by shaping the ascent trajectory for an early launch at the minimum ascent range angle and a late launch at the maximum range angle. Consider as an example a parking orbit (hp = 466.7 km, i_{VE} = 30.25°) and a booster (V req = 8186 m/sec, h_{BO} = 185.2 km). At this inclination (i_{VE} > 28.5°, the launch latitude) three launches daily are possible--two for Case B, since the parking orbit ground trace intersects the launch parallel at two points, and one for Case C, since the maximum turn angle required at Φ_{a} = 90° is approximately 2°, which is within the velocity capability of the booster, as illustrated in Fig. 3. Case B and Case C are illustrated in the sketch on page V-2.

Tables 2, 3 and 4 show the launch tolerances for this velocity capability using range extension only, trajectory shaping only, and a combination of the two methods for parking orbit altitudes of 277.8 km, 466.7 km, and 740.8 km. The nominal ascent range angle is 60° and, for the range extension method only, was varied to 180° for launch

tolerance. For the maximum turn case, the maximum ascent range angle is reduced to 125° because of the increased cost for turning (see Fig. 3). The nominal ascent range for trajectory shaping is 90° for the no-turn cases and approximately 65° for the turn cases.

Note that for the lower parking orbit altitudes

 $(h_D < 703.8 \text{ km})$ and for the no-turn case ($\triangle A = 0$), it is best to use the combination method. Above 703.8 km, the range extension method becomes the most efficient. Also note that if it is not practical to extend the ascent range from 60° to 180°, for example, limit Φ_{amax} to 120°, then the combination method is the most efficient. For the example, presented (V_{req} = 8186.6 m/sec and $i_{
m VE}$ = 30.25), a launch time tolerance of 3 min is available for the no-turn case at the parking orbit altitudes of interest. At $h_{\rm p}$ = 888.9 km, the entire velocity capability $V_{\mbox{req}}$ is required to establish a circular orbit, and therefore there is no excess velocity available for range extension or trajectory shaping. Consequently, there is zero launch tolerance at this altitude.

Tables 2, 3 and 4 also point out how the launch tolerances are reduced considerably for the maximum turn case because part of the excess velocity must be used to perform the turn.

One way of increasing the launch tolerances is to increase the velocity capability. For instance, by increasing the velocity capability of the previous example from 8186.6 to 8338.7 m/sec, the launch tolerance can be increased by one minute for a parking orbit altitude of 466.7 km.

TABLE 2 Launch Tolerance (min)

 $\rm h_{BO}$ = 185.2 km, $\rm h_P$ = 277.8 km, $\rm V_{req}$ = 8186.6 m/sec

	No Turn (Case B)			Maximum Turn (Case C)		
Method	-Tolerance	+Tolerance	Total Tolerance	-Tolerance	+Tolerance	Total Tolerance
Range extension	0	0.54	0.54	0	0.28	0.28
Trajectory shaping	. 1.76	0.85	2.61	0.68	0.42	1.10
Combination	1.76	1.24	3.00	0.67	0.56	1.23

 $\frac{\text{TABLE 3}}{\text{Launch Tolerance (min)}}$

 h_{BO} = 185.2 km, h_{P} = 466.7 km, V_{req} = 8186.6 m/sec

	No Turn (Case B)			Maximum Turn (Case C)		
Method	-Tolerance	+Tolerance	Total Tolerance	-Tolerance	+Tolerance	Total Tolerance
Range extension	0	1.68	1.68	0	0.86	0.86
Trajectory shaping	1.48	0.82	2.30	0.70	0.46	1.16
Combination	1.45	1.85	3.30	0.70	0.85	1.55

TABLE 4
Launch Tolerance (min)

 $h_{BO} = 185.2 \text{ km}, h_{P} = 740.8 \text{ km}, V_{req} = 8186.6 \text{ m/sec}$

	No Turn (Case B)			Maximum Turn (Case C)		
Method	-Tolerance	+Tolerance	Total Tolerance	-Tolerance	+Tolerance	Total Tolerance
Range extension	0	3.28	3.28	0	0	0
Trajectory shaping	0.81	0.66	1.47	0	0	0
Combination	0.62	2.37	2.99	0	0	0

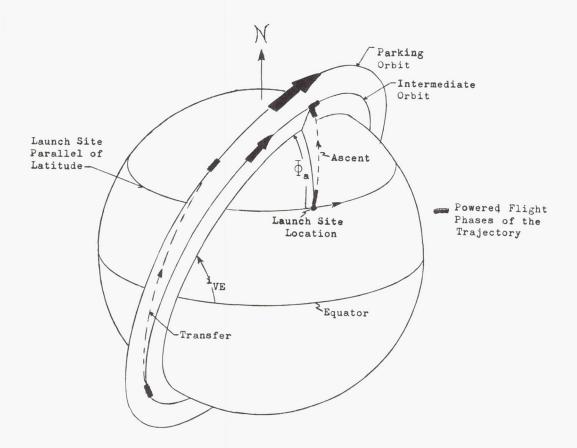
2. Launch Tolerance with Indirect Ascent

a. Indirect ascent without earth rendezvous

The indirect ascent method can be regarded as a generalization of the direct ascent method. The former method is illustrated in the following sketch.

In an indirect ascent, the spacecraft is launched at an arbitrary time into an ascent trajectory which intersects the parking orbit plane 90° downrange from burnout. This ascent range angle minimizes the turn angle as given by Eq (1). At the intersec-

tion of the ascent plane with the parking orbit plane, the spacecraft has reached the apogee of its ascent coast trajectory and is turned into and accelerated to the velocity of the predetermined intermediate or waiting orbit. The circular waiting orbit may be below or above the parking orbit, its most important characteristic being that it has a period different from the parking orbital period. This allows the spacecraft to wait in the intermediate orbit until the desired phase relationship with the phantom satellite is established. At this time the spacecraft transfers to the parking orbit by a Hohmann transfer and effects a rendezvous with the phantom satellite.



The indirect ascent method has the following characteristics: (1) Since the phantom satellite's position is ignored at launch, the launch tolerance is significantly larger than in the case of the direct ascent method. (2) Since there is generally a waiting period in the intermediate orbit and the transfer range angle is 180°, the time from launch to rendezvous can be many hours as compared to less than an hour for the direct ascent method. (3) Two additional powered phases are required. (4) The actual position of the rendezvous point cannot generally be controlled without excessive fuel penalties or longer wait times in the intermediate orbit. (5) The launch vehicle or booster must possess sufficient capability to deliver the spacecraft to higher altitudes than the nominal parking orbit because otherwise this method may become impractical due to the very long waiting times in the intermediate orbit.

In the numerical example which will be given later, it is assumed that the booster can deliver the spacecraft to any waiting orbit altitude between 185.2 and 740.8 km. The lower altitude limit is the result of unacceptably high drag decay rates for space vehicles with "normal" area-to-mass ratios, while the upper limit is the result of increasing radiation from the inner Van Allen belt, which may require heavier shielding of the space-craft, and to a lesser degree it is the result of increased energy requirements for the mission if the parking orbit is at a lower altitude.

In this range of waiting orbital altitudes, the time required to change the phase relationship be-

tween the spacecraft and the phantom satellite can be determined as soon as the parking orbit altitude is fixed. The following sketch shows the phantom satellite near the middle of the altitude band at $466.7~\mathrm{km}$. Assume that at a time t_0 , the

spacecraft and phantom satellite are in phase, $\Delta \beta'$ = 0, as shown. After one complete revolution of the phantom satellite t₁ the relative position

of the spacecraft to the phantom satellite has changed ($\Delta \beta' \neq 0$). In other words, the spacecraft has "gained" on the satellite for altitudes less than 466.7 km and has "lost" for altitudes greater than 466.7 km. The gain in central angle per revolution (i.e., angular displacement of spacecraft ahead of phantom satellite) is given by:

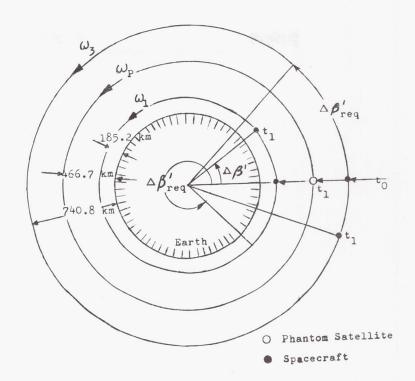
$$\Delta \beta' = t_1 (\omega_i - \omega_P)$$
 (6)

where $\boldsymbol{\omega}_{\mbox{\sc i}}$ is the angular velocity of the satellite in the waiting or intermediate orbit

or in terms of time the gain per revolution is

$$\Delta t = \Delta \beta / \omega_{i} \tag{7}$$

The maximum gain per revolution obtained from above is 5.7 min for a waiting orbit at 185.2 km, and the maximum loss is 5.7 min for one at 740.8 km if the parking orbit altitude is 466.7 km. Utilizing the same nomenclature but referring to t_1 as the position of the spacecraft at any time, and $\Delta\beta^{!}_{\ \ req}$ as the required phase relationship to



effect a Hohmann transfer to the parking orbit for rendezvous, the angle $\boldsymbol{\beta}$ to be gained or lost is:

$$\beta = \left| \triangle \beta_{\text{req}}^{\dagger} - \triangle \beta^{\dagger} \right|, \text{ gain for } \omega_{1}$$

$$\text{loss for } \omega_{3}$$
(8)

$$\beta = 360 - \left| \triangle \beta_{\text{req}}^{\dagger} - \triangle \beta^{\dagger} \right|$$
 , loss for ω_{1} (9)

with the number of spacecraft revolutions n required to achieve the proper phase relationship for rendezvous given by

$$n = \beta/\Delta\beta^{\dagger} \tag{10}$$

where $\Delta \beta^{\,\prime}$ is obtained from Eq (6) and n is not necessarily an integer.

Now assume that the nominal ascent trajectory corresponds to Case B (in the parking orbit plane, direct with Φ_a = 90°). After a few minutes of possible direct launches (direct launch tolerance) the phantom satellite is no longer in the proper phase relationship for rendezvous. The spacecraft must now ascend to a different altitude to correct for this phase differential, but in doing so, generates another differential because of the difference in ascent time from the nominal. Furthermore, the interception of the parking orbit plane occurs at a different location from the nominal, thereby introducing an additional phase differential. Finally, the transfer from the intermediate orbit requires a phase differential. Therefore, the total phase angle β to be made up in the intermediate orbit can be obtained from:

$$\beta = \Delta t_{L} \omega_{P} + (t_{a} - t_{aN}) \omega_{P} + (\beta_{T} - \beta_{TN}) + (180 - t_{tr} \omega_{P})$$

$$(11)$$

where

 Δt_{T} = launch tolerance

t = ascent time

ton = nominal ascent time

β_T = central angle from parking orbit node to interception of the parking orbit plane with the ascent trajectory

 $\beta_{\rm TN}$ = same as $\beta_{\rm T}$ except the ascent trajectory is nominal

ttr = transfer time from the intermediate orbit to the parking orbit.

Any booster burnout dispersions can be included in the second term on the right-hand side, waiting orbit dispersions into the third term; however transfer orbit and parking orbit injection dispersions will alter β .

Thus with knowledge of Δ β' for the intermediate orbit and of β for a particular launch tolerance, the number of revolutions required in the intermediate orbit can be found from Eq (10). But in order to obtain t_a , β_T and t_t for Eq (11), the intermediate orbit altitude relative to the parking orbit must be known. This altitude can be established through use of the previous sketch and Fig. 5. The constraints for ascent to a higher or lower intermediate orbit altitude are as follows--either set may be used; both reflect the phase conditions at injection into the intermediate orbit.

Set (1)

$$\Delta\beta_{\mbox{\scriptsize req}}^{\,\,\prime}$$
 - 180° $\bar{<}$ $\Delta\beta^{\,\,\prime}_{\mbox{\scriptsize req}}$ (lower alt)

$$\Delta \beta_{\text{req}}^{\prime}$$
 - 180° > $\Delta \beta_{\text{req}}^{\prime}$ (higher alt) (12)

Set (2)

$$\Delta \beta_{\text{req}}^{!} + 180^{\circ} > \Delta \beta^{!} > \Delta \beta_{\text{req}}^{!}$$
 (higher alt)

$$\Delta \beta_{\text{req}}^{\prime} + 180^{\circ} < \Delta \beta^{\prime} < \Delta \beta_{\text{req}}^{\prime} \text{ (lower alt)}$$
 (13)

For a parking orbit altitude h $_{\rm P}$ = 740.8 km, the waiting or intermediate orbit lies below it and there is no choice but to have an intermediate orbit lower than the parking orbit. In this case it is possible to have a phase difference β of 360°, which means that a maximum waiting time of 12.8 hr is possible at an altitude h $_{\rm i}$ = 185.2 km of the intermediate orbit. If the intermediate altitude is higher, for example, h $_{\rm i}$ = 466.7 km, the waiting time is doubled. The same waiting time applies if h $_{\rm P}$ = 185.2 km and the intermediate orbit is necessarily higher. Consider the case h $_{\rm P}$ = 466.7 km, h $_{\rm i}$ = 185.2 km where the maximum phase differential is 360°, the maximum waiting time is 25.6 hr. Of course, the maximum waiting time increases for 185.2 km < h $_{\rm i}$ < 466.7 km. If 185.2 km < h $_{\rm i}$ < 740.8 km, both constraints given by Eq (12) or Eq (13) can be utilized and the maximum waiting time is again reduced to 12.8 hr.

In the determination of parking and waiting orbit parameters, some neglected forces should be considered. Thus, at the lower orbital altitudes, i.e., near 200 km, atmospheric drag has a considerable effect on the trajectory of the spacecraft. The lifetime for a dense spacecraft, or low area-to-mass ratio, is of the order of days, while for a spacecraft with a high area-to-mass ratio it may be as low as a few hours. (For more details on lifetime, see Chapter V of Ref. 1.) Considering also orbit injection errors, a practical lower altitude limit for intermediate or parking orbits is 250 km.

Other corrections to Keplerian orbits are due to earth oblateness. For a circular orbit, the major secular effects are a correction to the orbital period and a correction to the location of the ascending node (regression of the nodes). During the earth departure phase, the motion of the phantom satellite in the parking orbit must be simulated from the translunar trajectory injection point back in time to the launch time \mathbf{t}_{L} . In other words, the phantom satellite position in orbit should reflect oblateness effects of the earth.

If the intermediate orbit altitude is different from that of the parking orbit, there will be a difference in regression rates between the two. Therefore, at the time of injection into the intermediate orbit, the plane of the intermediate orbit is established with the same inclination $i_{\rm VE}$ the parking orbit, but with an orbital plane that has a slightly different ascending node, or an offset. This offset gradually decreases due to nodal regression until, at the time of rendezvous, both the intermediate and parking orbit planes are coincident.

Oblateness effects can also be counteracted by applying small thrust impulses at the intersection

of the intermediate and parking orbit planes or by one pulse at rendezvous, or one at the intersection just prior to the rendezvous transfer maneuver. The additional ΔV requirement to counteract earth oblateness effects can be as high as 67 m/sec for a parking orbit altitude of 466.7 km and for a maximum of 24 hr in orbit.

b. Indirect ascent with earth rendezvous

Just as in Subsection A-1b, if the phantom satellite is replaced by a physical vehicle, the discussion given in the previous subsection, A-2-a, is directly applicable for indirect ascents of lunar spacecraft employing an earth rendezvous. The same launch tolerances and velocity requirements apply to the launch of the physical vehicle.

c. Numerical example for indirect ascent

Again, the various concepts for an indirect ascent will be illustrated by a numerical example. In order to allow a comparison with the direct ascent method, the parking orbit and hypothetical booster characteristics are assumed to be the same.

It has been established that the inclination of the parking orbit, the launch site latitude, and the launch delay time all have a bearing on the magnitude of the turn angle ΔA . It is assumed that the launch site is Cape Canaveral at a latitude of 28.5° N and that orbit inclinations, i $_{VE}$, are limited from 28.5 to 34.5° . Figure 5 presents the required ΔA for $\Phi_a=90^{\circ}$ from Cape Canaveral to various values of i_{VE} within the allowable band. The data are presented versus a time scale in increments of 1-hr launch delay time. The origin in time, t=0, is arbitrarily chosen in Fig. 5; it by no means represents the nominal launch time for the nominal, no-turn, direct ascent. This choice of time origin also applies to Figs. 6 through 12.

Again a hypothetical launch vehicle is assumed whose burnout altitude is 185.2 km. Typical velocity requirements for this booster are given in Table 5 below for parking orbit altitudes $\rm h_{\sc P}$ of 185.2, 466.7 and 740.8 km.

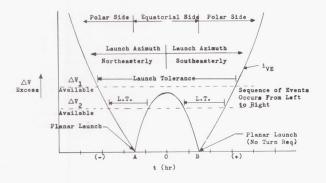
TABLE 5
Velocity Required for Indirect Ascents for Translunar Missions (m/sec)

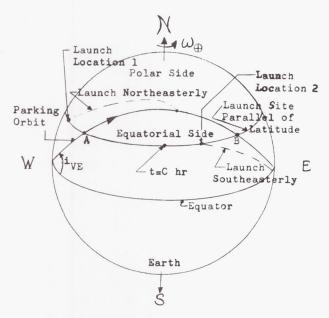
Parking Orbit Altitude h _P	185.2 km	466.	740.8 km	
Intermediate Or- bit Altitude h _i	740.8 km	185.2 km	740.8 km	185.2 km
V (burnout)	7816.9	7793.1	7816.9	7793.1
△V (injection)	297.8	0	297.8	0
△V (transfer)	311.2	162.8	164.6	311.2
ΣV (required to rendezvous)	8425.9	7955.9	8279.3	8104.3
ΔV (escape)	3226.0	3159.3	3159.3	3098.0
ΣV (required for mission)	11651.9	11115.2	11438.6	11202.3

However, the remainder of the discussion will assume that $h_{\mbox{\footnotesize{p}}}$ = 466.7 km, which is very close to a "rendezvous compatible orbit" of $^{\simeq}$ 485.2 km. A rendezvous compatible, or synchronous satellite orbit has an integral number of revolutions per sidereal day, and hence passes over the same areas each day. For circular orbits, the altitude alone determines rendezvous compatibility, but with earth oblatness effects taken into account, the altitude-inclination combination determines compatibility of orbits for rendezvous.

Figures 6 through 9 show the excess velocity requirements ΔV , i.e., the velocity required over a nominal, no-turn, direct ascent, for h_i = 185.2, 370.4, 555.6, 740.8 km, respectively. This velocity excess includes the excess increments for the launch, injection and turn, transfer and rendezvous phases. Note that in Figs. 6 through 9 the minimum excess velocity increases for $h_i > h_P$, since the spacecraft must lose altitude and hence potential energy to return to the parking orbit for rendezvous. The minimum excess is ΔV = 99.1 m/sec for h_i = 555.6 km and ΔV = 304.8 m/sec for h_i = 740.8 km.

The sketches below serve as an aid for interpreting Figs. 6 through 9.



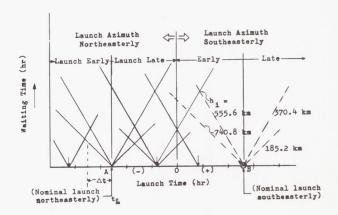


At t = 0, the launch site is halfway between the intersections of the parking orbit plane with the launch latitude on the equatorial side. Prior to this time, ascents are made northeasterly, A < 90° and southeasterly, A > 90°, afterward. The inertial launch azimuth A (great circle course on a nonrotating earth) is measured clockwise from geographic north through 360°. If the launch vehicle has an excess ΔV_1 available, it will have a continuous launch period (see sketch on page V-2). However, if only an excess ΔV_2 is available, the possible launch period LT will be discontinuous as shown in the first sketch.

Referring again to Figs. 5 to 9, it is possible to have a continuous launch tolerance for all parking orbit inclinations and the maximum ΔV excess required is on the order of 900 m/sec. The resulting launch tolerance can vary from 6 to 8 hr, depending on i_{VE} . For excess $\Delta V^{\prime}s$ less than about 900 m/sec, discontinuous and shorter launch tolerances will be experienced for the higher values of i_{VE} . However, continuous launch tolerances may still be realized for lower values of i_{VE} .

If the phantom satellite has the proper phase relation at the time the launch site is in the parking orbit plane, the nominal, no-turn, direct ascent to rendezvous is conducted. In this case no waiting time is required. If the launch vehicle and spacecraft are ready prior to the nominal time, and an ascent is performed, the proper phase relationship will not exist and the spacecraft must wait in an intermediate orbit. The spacecraft also must wait if a late launch is performed.

The waiting time in the intermediate orbit depends on the launch time. Figures 10 through 12 give the waiting time, in hours, for $\mathbf{h_i}$ = 185.2, 370.4, 555.6 and 740.8 km. Each figure represents a different $\mathbf{i_{VE}}$ in the possible band that can be established from Cape Canaveral launches. Data is shown emanating from a northeasterly nominal launch direction. Below is another auxiliary sketch illustrating the interpretation and use of the figures.



The sketch shows the regions of northeasterly and southeasterly launch azimuths. Since in general $\rm i_{\rm VE}$ >28.5°, the launch latitude, the launch

site will be in the parking orbit plane twice a day (points A and B in the previous sketches). If the launch took place at the nominal north-of-east launch time there would be zero waiting time. However, if the spacecraft is launched early, say at t_L - Δt , then, depending on h_i , the waiting time will vary accordingly as illustrated in the above sketch. Note the cyclic nature of the curves that originate at the "arrowheads." This is due to the phantom satellite achieving the proper phase re-lationship on succeeding revolutions. The interval of time between "phasings" is attained after one revolution plus an increment to account for the launch site rotation, i.e., the interval is slightly greater than the orbital period of the parking orbit. These "phasings" are denoted by arrows on the abscissas in Figs. 10 to 12 and the construction of the curves is accomplished by utilizing the same slopes for the straight lines as for the nominal launch. The phasing points do not necessarily occur on the southeasterly planar launch. However, if the nominal ascent is planned to occur at the southeast orbital plane intersection (point B and dashed curves in sketches), the phasing points are constructed in the same manner and with the same time intervals as they were for the northeasterly nominal launch. It becomes evident from the above discussion that the nominal ascent is not necessarily planned for either orbital plane intersection (points A and B). In fact, direct ascent (nominal launch) frequency may be higher for a given excess velocity if the phasing points are offset from the planar crossings.

Figures 10 to 12 essentially present minimum waiting times and the corresponding intermediate orbital altitudes as reflected by the constraints, Eqs 12 and 13.

B. VARIABLE TRANSLUNAR TRAJECTORY TECHNIQUE

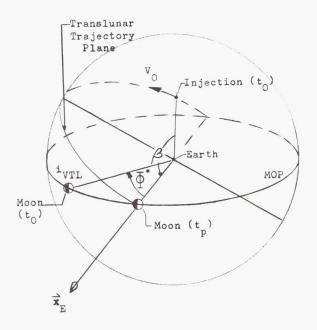
This technique is based on the fact that for any given translunar trajectory inclination $i_{\rm VTL}$ a specific trajectory can be found to satisfy constraints in flight time, pe icynthion altitude, and transearth inclination $i_{\rm VTE}$. For the class of circumlunar trajectories discussed in Chapter IV, this suggests that translunar trajectories with variable $i_{\rm VTL}$ be used to obtain a launch time tolerance (see Ref. 2, and also Chapter VI). This is opposed to the technique discussed in Section A, which assumes that the translunar trajectory inclination, $i_{\rm VTL}$, is fixed by the mission during the launch tolerance.

1. Launch Tolerance

a. Without earth rendezvous

Three assumptions will be made to simplify this discussion. (1) It can be shown for lunar trajectories that when the spacecraft is at pericynthion, t_p , the lunar position is nearly along the intersection \mathbf{x}_E of the MOP and the translunar trajectory plane established at injection, t_0 (see

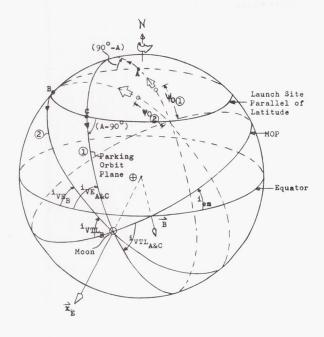
sketch below). This will be assumed exactly true



throughout this section. (2) Parking orbits around the earth are permissible; in fact, they are desirable because they allow the use of one efficient nominal ascent and orbit injection trajectory profile, provide final on-board and ground checkouts, and open the launch window considerably. (3) The moon's position at pericynthion (tp) is assumed fixed on x_E throughout the period of the launch time tolerance, and consequently the orientation of the earth's equatorial plane and MOP are assumed similarly fixed. The relatively slow motion of the moon around earth (about 1° of Φ^* in 2 hr) makes this assumption valid over a period of a few hours.

The next sketch illustrates how a launch time tolerance is obtained by varying $i_{\mbox{\scriptsize VTL}}.$ Theoretically, there is an infinite launch tolerance for this technique if there are no launch azimuth restrictions and if the launch vehicle possesses the additional energy requirements for retrograde launches (against the earth's rotation). Practically, however, this is not the case, since Cape Canaveral, for instance, has range safety constraints that restrict launch azimuths to $45^{\circ} \le A \le 110^{\circ}.$ In the illustrative example the launch azimuth is restricted to $70^{\circ} \le A \le 110^{\circ}.$

The following sketch shows the moon (x $_{\rm E}$) near its ascending node B at the time of pericynthion. The launch site is at 28.5° north latitude and is rotating with the earth, as indicated by the sequence of points, A, B, C on the sketch. At point A the launch site longitude is less than 180° west of the moon's longitude and A = 70°. This heading allows a parking orbit plane to be established (denoted by ① on the sketch) that passes through $x_{\rm E}$ and remains within the launch azimuth restriction. The resulting inclinations to the equator and



MOP are i_{VE_A} and i_{VTL_A} , respectively. The spacecraft remains in the parking orbit until it reaches the proper injection point ψ_0 and then is injected into a northerly direction relative

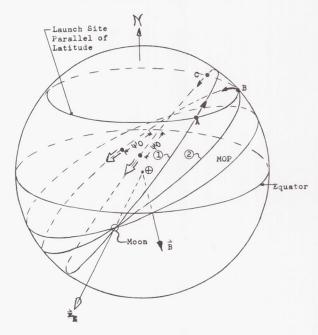
then is injected into a northerly direction relative to the MOP. North, relative to the MOP, is defined by the angular momentum vector of the lunar orbital motion.

If the spacecraft is launched due east (A = 90°), there is a launch point B that also allows the parking orbit (denoted by ② on the sketch) to pass through \mathbf{x}_{E^*} . Again the spacecraft remains in the parking orbit until position ψ_0 at which time a northerly injection takes place. This launch results in the minimum i_{VE} and i_{VTL} , as is evident from the sketch.

As the launch site rotates with the earth, point C is reached, requiring the maximum allowable launch azimuth (A = 110°) in order to pass through \vec{x}_E . Here, the parking orbit plane is the same as established when the launch was made at point A. Consequently $i_{VE}^{}$ and $i_{VTL}^{}$ are the same as for launch location A.

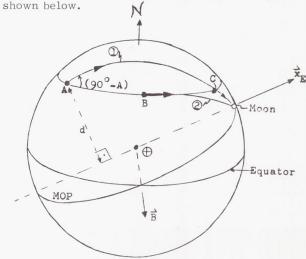
A launch is possible at any time that the launch site is between A and C. The translunar trajectories for this example are necessarily northerly and direct relative to the MOP, since a central angle $\beta > 150^\circ$ is required (see previous sketch) to intercept the moon if injection occurs close to perigee of the translunar trajectory.

When the launch site is east, but less than 180° east of the lunar longitude, another possible launch period exists. However, in this period translunar trajectories that depart from the earth southerly relative to the MOP are required as illustrated by the sketch below:



As before, in the time the launch site rotates from point A to B to C, the launch azimuths are 70°, 90° and 110° respectively, and within the azimuth restriction. The spacecraft waits in parking orbit (1) or (2) until the proper injection point ψ_0 is reached. At this time the spacecraft is injected in a southerly direction relative to the MOP. The shorter time required in the parking orbit for this case as compared to the inject north case can be noted by comparing the two sketches on this page. When the moon is near its descending node the opposite is true.

The two sketches above imply that ${\rm d}A/{\rm d}t$, the change in launch azimuth with launch time, is constant. This is true when the moon is at its descending or ascending node, but not when the moon is at some other orbital position, as



Here the moon is at its maximum northerly declination, and again the longitudes between A and B represent northeasterly launches and the longitudes from B to C represent southeasterly launches. Note that the perpendicular distances d between A and $\bar{\mathbf{x}}_E$ and C and $\bar{\mathbf{x}}_E$ are different. This causes a rapid variation in dA/dt when the site nears C, as can be visualized when the moon is considered as a pivot point. This is illustrated in Fig. 13, where the northeasterly and southeasterly launch tolerances are plotted separately for different lunar positions. Independently, the launch tolerance varies from 10 min to 4.74 hr. For the full range of launch azimuths the total available launch tolerance is 4.91 hr.

As pointed out previously, there are two launch periods available in one day. One period results in translunar trajectories that are northerly relative to the MOP, and the other period results in southerly translunar trajectories. Figure 13, although shown for northerly departures, also is applicable for southerly departures if the curve of northeasterly launches in Fig. 13 is used to represent southeasterly launches and vice versa.

Below is a table presenting typical delay times between injection during period I and injection during period II:

TABLE 6

Lunar Position	Max North	Max South	Desc/Asc Node
Injection (Period I)	Northerly	Northerly	Northerly
Launch time tolerance	4.91 hr	4.91 hr	4.91 hr
Delay time	38 sec	38 sec	7.19 hr
Injection (Period II)	Southerly	Southerly	Southerly
Launch time tolerance	4.91 hr	4.91 hr	4.91 hr

These data show a very short delay time between available launch periods for the moon at its maximum northerly or southerly declinations. For all practical purposes, a launch period of 9.82 hr is available at these times if both inject north and south trajectories are permitted.

The data presented in Fig. 13 and the above table are calculated for the year 1968, when the inclination of the MOP to the equatorial plane iem = 28.5°. Approximately nine years later, iem = 18.5°. The effect of this change on launch tolerance presented in Fig. 13 is to increase the minimum tolerance and decrease the maximum tolerance of the individual northeasterly or southeasterly launches. The total launch time tolerance will not be affected.

It is important to note that the technique outlined above does not require any turning of the velocity vector in flight at any time, although such maneuvers could be used to further increase the launch time tolerance. The only ΔV penalty of the launch vehicle is approximately 25 m/sec due to the varying component of the earth's rotational velocity in the flight direction for the range $70^{\circ} < A < 110^{\circ}$.

b. Launch tolerance with earth rendezvous

If a fueling vehicle is injected first into a parking orbit utilizing the variable trajectory technique, its launch tolerance can be obtained from the previous subsection. However, the spacecraft must now be launched to perform a rendezvous with the fueling vehicle. Since the parking orbit inclination of the fueling vehicle is fixed, the launch tolerance for the spacecraft is the same as for direct or indirect ascent of the fixed translunar trajectory technique.

The techniques for earth departure discussed in Sections A and B illustrate how the launch tolerance can be increased from minutes to many hours by the use of parking or parking and intermediate (waiting) orbits with only moderate fuel expenditure ($\triangle V$'s of the order of 300 m/sec). The increased launch tolerance is obtained at the expense of some increase in complexity and the number of rocket burning phases from launch to lunar injection. On the other hand, each burning phase can be used to correct for dispersions from previous phases, dispersions due to variable densities, earth oblateness, etc., and the additional time near earth can be used for tracking, checkout of equipment, and refueling by shuttle vehicles. Thus the small allowable delay time at the launch site for the one burning phase of a direct departure from earth has been traded for a large delay time at the launch site and small tolerances for each of several burning phases for an indirect departure from earth (i.e., one using parking or waiting orbits) which are simpler to achieve and give more control and reaction time during the earth departure phase of a lunar mission.

C. TRANSLUNAR INJECTION

Sections A and B have discussed launch techniques that result in the spacecraft arriving at the correct position at the correct time for injection into the translunar trajectory. Prior to injection, the spacecraft is in a parking orbit. But the question arises as to what can be done to salvage the mission if the spacecraft cannot be injected from this orbit at the proper time. This may be the result of a system malfunction that requires repair, a hold for injection because of the need of further verification of system status, or an off-design parking orbit.

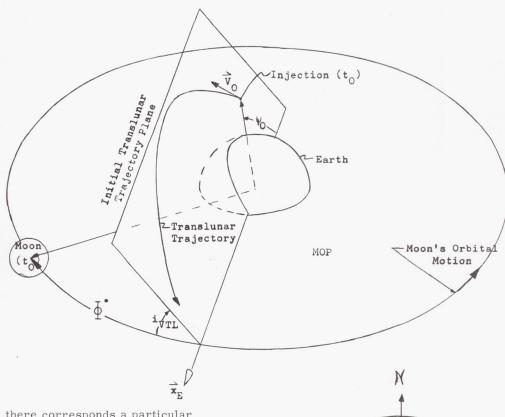
Furthermore, some missions require long waiting periods in a parking orbit prior to injection. Such a mission may be a lunar logistics mission wherein the freighter waits in a parking orbit while supplies are shuttled to it from the earth's surface. The following discussion is applicable to both the cases of a missed injection point and the logistics mission.

1. Injection Tolerance

A nominally ballistic translunar trajectory used for fulfilling a preplanned lunar mission is determined by the injection conditions: at a given time during the lunar month and during the launch tolerance at a given day there will be a resultant translunar trajectory plane inclined at an angle $\rm i_{VTL}$ to the MOP (see sketch below).

of the parking orbit, $i_{\mbox{VE}}$, is also constant, but its nodal regression rate cannot be ignored. The following sketch shows the physical situation and the nomenclature on the celestial sphere.

After the injection point has been missed, the moon continues in its orbit as indicated. The parking orbit regresses in a westerly direction for direct parking orbits and easterly for retrograde orbits; however, the launch restrictions



For this $i_{\rm VTL}$, there corresponds a particular injection velocity vector \vec{V}_0 , injection position ψ_0 , and moon lead angle Φ^* , to satisfy certain mission constraints such as miss distance at the moon, flight time to the moon, resultant orbital orientation about the moon, etc.

If the injection is not performed at time t₀, then the spacecraft will continue in its parking orbit until the next opportune time for injection arises. This time may occur after approximately one or several revolutions in the parking orbit provided the vehicle has a certain maneuvering capability. If the delay is such that the maneuvering capability becomes insufficient to cope with the off-design conditions, then a return to earth must be made, or the spacecraft continues in its parking orbit until its maneuvering capability allows an injection into the desired translunar trajectory. These cases will be discussed below.

Consider a delayed injection, where the spacecraft continues its flight in the parking orbit. Assume that the inclination of the MOP relative to the equatorial plane i em remains constant and that its nodal regression rate due to earth oblateness is negligible. The inclination

Regression due to earth oblateness

Equator

MOP

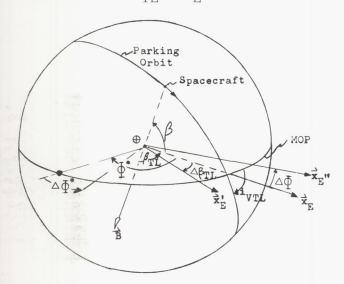
WE Moon at Pericynthion

(Moon at Injection)

at Cape Canaveral permit only easterly launches. The angle β_{TL} is measured from the ascending node of the MOP to the intersection of the parking orbit or translunar plane with the MOP $(\overrightarrow{x}_E$ axis) and is a function of i_{VE} and i_{em} . As can be seen the angle β_{TL} also varies with time as plotted under the title "Parking Orbit Regression Time Traces" in Figs. 14 to 16. The first two figures present

data for i $_{\rm em}$ = 26.5° and i $_{\rm em}$ = 28.5°, respectively. This represents the period from early 1966 when i $_{\rm em}$ = 26.5° through late 1968 when i $_{\rm em}$ = 28.5° to early 1972 when i $_{\rm em}$ is once again 26.5°. The parking orbit altitude assumed in these figures is that of a rendezvous compatible orbit (approximately 480 km) as explained previously in Subsection A-2b. The actual altitude varies slightly with i $_{\rm VE}$ and the figures reflect data for 28.57° \leq i $_{\rm VE} \leq$ 33.7°. Figure 16 shows the variation of $\beta_{\rm TL}$ for h $_{\rm P}$ = 185.2 km and i $_{\rm em}$ = 26.5° for comparison purposes.

Once the injection is missed, it will take approximately one revolution in the parking orbit (approximately 1.5 hr for a near-earth satellite) before another attempt is made. During this time the lunar position changes by $\Delta \, \varphi^*$ in its orbit (see sketch below), and the parking orbit shifts an amount $\Delta \beta_{TL}$ to $\tilde{x}^!_E$.



The inclination i_{VTL} also changes slightly (Fig. 17), and now the resulting lead angle after one revolution is equal to ($\Phi^* - \Delta \Phi^* - \Delta \beta_{TL}$). However, if the change in i_{VTL} is small the required lead angle remains essentially constant (see Chapter VI); therefore, if x_E is shifted by an amount $\Delta \Phi$ to x''_E prior to one revolution, another injection becomes possible.

where
$$\Delta \Phi \cong \Delta \Phi^* + \Delta \beta_{TI}$$
.

This technique can be extended for more than one revolution in the parking orbit and is only limited by the maneuvering capability $\triangle V$ to perform the shift.

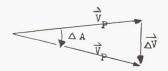
This shift, or parking orbit adjustment, can be accomplished by two methods. First, the orbital maneuver or adjustment takes place at $\beta=\pm~90^\circ$ so that the Δ V requirements are minimized. Second, the adjustment takes place at a point in the parking orbit that allows the nominal or design $i_{\rm VTL}$ and ϕ^* to be kept constant.

Only the former adjustment technique is discussed; the steps necessary to determine the amount of correction ΔV are listed below.

- (1) Determine the $i_{\mbox{VTL}}$, Φ^* required curve that satisfies the lunar mission from Chapters VI and XI.
- (2) Starting from the design or nominal injection time t_0 , determine β_{TL} as a function of time.
- (3) From (2), also determine actual $i_{\mbox{VTL}}$ as a function of time.
- (4) From (3) and (1), ascertain Φ^* required as a function of time.
- (5) From (2), knowing the moon's orbital position at any time, determine the actual lead angle Φ^* as a function of time.
- (6) From (5) and (4), find $\triangle \Phi$ by subtraction.
- (7) The orbital maneuver turn angle $\triangle A$ is given by

$$\Delta A = \sin^{-1} (\sin \Delta \Phi \sin i_{\text{VTL}})$$
.
(actual)

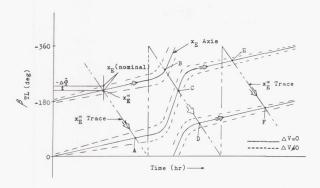
(8) Find the required ΔV through the following geometry, where $V_{\rm p}$ is the spacecraft speed in the parking orbit:



$$\Delta V = 2V_{P} \sin (\Delta A/2) \approx V_{P} \Delta A$$
 for small angles ΔA (15)

The above steps are then repeated in an iteration procedure, since $^{\rm i}{\rm VTL}$ (actual) slightly with $\Delta {\rm V}$. This variation, shown in Fig. 17 as a function of $\beta_{\rm TL}$, is very insensitive to modest values of $\Delta {\rm V}$. Also shown in Fig. 17 is the capability of shifting the parking orbit by $\Delta \Phi$, which is strongly dependent on the approximate time of pericynthion or $\beta_{\rm TL}$.

Below is a rough replica of a parking orbit regression time trace (see Figs. 14 to 16) to illustrate the above-described method for obtaining injection tolerances. The sketch shows one trace reflecting one value of $i_{\mbox{em}}$.

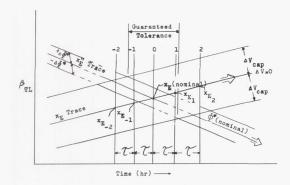


Assume that for a particular lunar mission the $\mathbf{x}_{\mathbf{E}}$ axis is located at the designated point in the sketch for a nominal or design injection. Assume further that the nominal translunar trajectory injection is south relative to the MOP and that there is a $\triangle V$ capability for adjusting the parking orbit. As was noted in the previous discussion, this △V capability can be used to shift the x $_{\rm E}$ axis by an amount equal to $\pm \Delta \Phi$. Therefore, the solid curves can be altered during any parking orbit revolution to another starting point on the dashed curves. It must be remembered that the nominal x_E axis on the solid curve also satisfies the required moon lead angle relationship **; and the relationship, given by x'!, moves at the same rate as the moon in its orbit and thereby establishes a second trace. The traces are coincident for the nominal injection but are separated until they are coincident again at points A, B, C, D, E and F. These

Before discussing these points it is helpful to examine in more detail what is occurring at the nominal injection point as shown by the following sketch.

coincident points represent other possible injec-

tion times.



The nominal point, x $_{E}$, is shown with its initial parking orbit at the injection point ψ_{0} . One revolution later, or after a time interval equal to the period τ of the parking orbit, the x $_{E}$ axis lies at

After two revolutions, the axis lies at etc. Considering the point \mathbf{x}_{E_1} , it is noticed that the x'' E trace is no longer coincident and a parking orbit adjustment must be made to shift \mathbf{x}_{E_1} to the $\mathbf{x''}_E$ trace. As can be seen, the amount of shift is within the $\triangle\,\mathrm{V}$ capability of the spacecraft even for the off-nominal x" $_{\rm E}$ traces. These off-nominal x" $_{\rm E}$ traces (± $\triangle\Phi^*$) are to be expected, since a change in i_{VTL} will necessitate a change in the lead angle, Φ^* , as pointed out previously. However, from Chapter VI, lead angle data indicates that $\Delta \Phi^*$ will generally be no greater than ±1° for an entire month and for the same mission. Therefore another chance for injection is possible at x_{E1}. If injection does not occur at $\mathbf{x}_{\mathbf{E}_1}$, another time interval τ must elapse before injection can take place at x E2. But at this point, one can see that $\mathbf{x}_{\mathbf{E}_2}$ cannot under all conditions be shifted to $\mathrm{x^{\prime\prime}}_{\mathrm{E}}$ because of insufficient maneuvering capability. Thus the injection tolerance in terms of injection frequency is 1 and in terms of time is a little longer than τ , or τ +. The maneuvering capability $\Delta V_{ ext{cap}}$ again becomes sufficient at point A in the previous sketch, where another injection frequency can be established. For purposes of illustration, let the above sketch also apply to point A, although the zero parking orbit revolution generally will not be coincident with the x_E and x''_E traces. Here, it is seen that an injection can be made at $x_{E_{-1}}$, $x_{E_{nominal}}$ and \mathbf{x}_{E_1} because both traces are starting from the far left before becoming coincident, whereas in the initial nominal case, both traces started at the coincident point. The injection frequency now is 3 and the guaranteed injection tolerance is $2\tau+$. The same reasoning applies to points

It was assumed that the nominal case resulted in an "inject south" case. At points A, C and E the resulting injection will be toward the north relative to the MOP and again toward the south at points B, D and F. If the nominal injection was toward the north, then the injections would be cycled correspondingly for the points.

B, C, D, E and F.

Figures 18 and 19 present actual data for two nominal cases occurring at $\beta_{\rm TL}$ = -220° and -65°. The first value represents conditions that result in a minimum injection frequency, and the second value gives a maximum frequency. A parking orbit altitude of 525.8 km is assumed together with $i_{\rm em}$ = 27.5° and $i_{\rm VE}$ = 30°.

Table 7 gives the guaranteed launch frequency and tolerance for the case where the injection is planned during the first parking orbit revolution after ascent from earth.

TABLE 7

	β_{TL}	=-220°	$\beta_{\rm TL}$ = -65°		
cap (m/sec)	Fre- quency	Tolerance (hr)	Fre- quency	Tolerance (hr)	
76.2	0	0	2	3.5	
152.4	0	0	4	6	
304.8	1	2.7	8	13	

Table 8 gives launch frequency and tolerance for an injection planned many orbital revolutions in advance, such as a logistics mission or injection under circumstances similar to point A on the sketch on page V-17, is mentioned above.

TABLE 8

A 7.7	β_{TI}	= -220°	β_{TL} = -65°		
(m/sec)	Fre- quency	Tolerance (hr)	Fre- quency	Tolerance (hr)	
76.2	0	0	5	7	
152.4	1	1.5	10	15.6	
304.8	4	5.8	20	31.5	

As can be seen $\Delta V_{\text{cap}} = 304.8 \text{ m/sec}$ will provide a launch frequency of at least 1 for the most unfavorable situation.

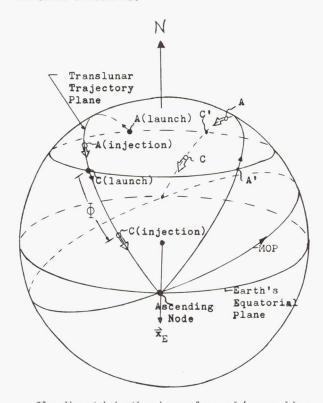
If an injection must be delayed until the next opportune time or a few succeeding opportune times (points A, B, C, D, E, F on the sketch on page V-17), necessary fuel and life support requirements must reflect this possible waiting time.

As a matter of interest, in Figs. 14 and 15, the minimum and maximum waiting times between possible translunar injections are noted. In Fig. 14, for example, the minimum waiting time between opportune injection times is 10 hr for $i_{\rm VE}$ = 28.57° and 12.4 hr for $i_{\rm VE}$ = 33.7°. The maximum waiting time is 253 hr for an $i_{\rm VE}$ = 28.57° and 250 hr for $i_{\rm VE}$ = 33.7°.

2. Propulsion System Requirements and Limitations During Injection

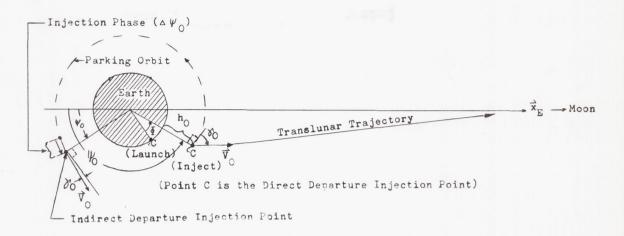
In the introductory paragraphs of the present chapter three advantages of earth departure by parking orbits were mentioned. The first, feasibility of final onboard and ground checkouts, should properly be discussed by the systems designer of a particular vehicle, so this point will not be elaborated in this Handbook. The increase in launch and injection capability has been discussed in detail in Sections A and B and Subsection C-1 of the present chapter. It remains to show why a parking orbit prior to injection leads to a single and most efficient injection trajectory profile. Additional use of the variable translunar trajectory technique (Section B), as opposed to the direct ascent, ensures a single and most efficient ascent trajectory.

The first sketch below illustrates on the celestial sphere the possible launch periods, points A to C, A' to C' on the launch parallel of latitude, for arrival at the moon when the moon is at its ascending node (see also Subsection C-1 for a more detailed discussion), while the second sketch illustrates the translunar trajectory injection parameters in the trajectory plane for the same conditions.



If a direct injection is performed (no parking orbit), the ascent range of from launch to injection is essentially constant or small for a given launch vehicle and it can only be launched during the period when the launch site is between points A, C, A', or C'. When Cape Canaveral is near position A, ψ_0 is typically 67°, with an ascent range angle Φ = 15°, and an injection flight path angle $\gamma_0 \simeq 30^{\circ}$. Similarly, when Cape Canaveral is near position C, ψ_0 = 143°, Φ = 15°, $\gamma_0 \approx 70$ °. If Cape Canaveral is located near point A' or point C', the required $\boldsymbol{\gamma}_0$ is negative and the spacecraft would lose altitude and atmospheric drag would cause a reentry. Another, completely impracticable, alternative would be to reverse the direction of vehicle motion. In fact, with a launch site in the northern hemisphere it becomes very difficult to perform direct departure lunar missions at all. For instance, with direct launches during the period when the moon is near its maximum northerly declination, zero launch frequency for many days of the lunar month can be expected.

In order to demonstrate the sensitivity of the flight path angle to energy expenditure, two representative plots of injection energy requirements to parabolic speed from a circular parking orbit are presented in Figs. 20 and 21. The characteristic



velocity of the maneuver is presented as a function of \mathbf{h}_0 (injection altitude) and γ_0 (injection flight path angle) for representative solid or liquid launch vehicles.

Figure 20 is for an initial thrust-to-weight ratio T/W_0 = 0.5 and Fig. 21 for T/W_0 = 1.5. A specific impulse $I_{\rm sp}$ = 420 sec is used, and the initial parking orbit altitude at which the maneuver is started is $h_{\rm p}$ = 183 km.

Note that the best flight path angle to minimize the energy requirements for this departure from the parking orbit is greater than 2° but less than 7° for values of $\rm T/W_{\rm 0}$ considered. The data presented in these figures are also indicative of the trends that can be expected for direct launches. An increase of Y_0 beyond 7° drastically increases the ΔV requirements. Therefore flight path angles of 30° or 70° would require very large quantities of fuel to counteract gravity losses during ascent, an inefficiency which is entirely unnecessary if parking orbits are employed prior to injection. It is obvious that if a given set of values $(V_0, h_0, \gamma_0, \Delta \psi_0)$ represent the most efficient injection, the ψ_0 required to fulfill a lunar mission with these injection conditions can be achieved by a parking orbit, as indicated in the previous sketch.

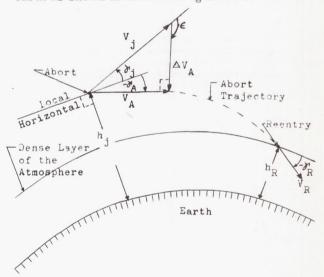
3. Abort During Injection

When the proper position of the spacecraft relative to the moon has been achieved in the parking orbit phase, the vehicle is accelerated to the translunar trajectory injection velocity. This maneuver is the injection phase, ($\Delta\psi_0$) and it establishes a ballistic trajectory with sufficient energy and the proper characteristics for the lunar mission. For a manned mission, it is highly desirable to provide for the safety of the crew in the event of a system malfunction, which

means guaranteeing the safe return of the space-craft to earth. Two methods can be used for a safe return during the injection phase. The first immediate return employs an abort maneuver that results in a re-entry of the spacecraft within a few minutes, while the second method, normal return, requires one revolution prior to re-entry.

a. Immediate return

The abort maneuver technique used for an immediate return calls for a maximum deflection of the spacecraft's velocity vector toward the earth as shown in the following sketch.



The spacecraft initially has a speed V_j and flight path angle Y_j at the time of abort. Thrust is then applied at a firing angle ε resulting in a characteristic velocity ΔV_A of the abort maneuver. The thrust orientation angle ε is such that the total deflection angle (Y $_j$ - γ_A) is a maximum for a given ΔV_A and is determined by:

$$\epsilon = \cos^{-1} \left(\frac{-\Delta V}{V_i} \right)$$
 (16)

Although the velocity of the spacecraft after the abort maneuver, V_A , is somewhat less than V_j , the flight path angle - γ_A is the prime criterion for establishing the abort trajectory. γ_A must be negative (V_A below the local horizontal) if re-entry is to be accomplished immediately.

However, at the re-entry point, the abort trajectory results in a re-entry velocity V_{R} and a re-entry flight path angle ${\bf Y}_{\rm R}$. If ${\bf Y}_{\rm R}$ is not sufficiently negative for V_R at the re-entry altitude h_R, then the spacecraft will skip back out of the atmosphere. Conversely, if γ_R is too steep, the spacecraft will undergo re-entry decelerations and heating rates beyond design limitations. Thus, there is an acceptable range of $V_{\rm R}$ and $v_{\rm R}$ at altitude h_R that permits a safe re-entry. By neglecting the atmosphere for the moment, the range of re-entry conditions (h $_{\rm R}$, V $_{\rm R}$, γ $_{\rm R}$) results in minimum and maximum vacuum perigee altitudes. This difference in altitudes is referred to as the "safe re-entry corridor" and is further discussed in Chapter X. Of course, this corridor depends on the configuration of the re-entering spacecraft.

In executing the abort maneuver, a minimum ΔV_A is needed if the abort trajectory is planned so as to acquire the upper limit or "skip boundary" of the re-entry corridor, since by doing this, $(\gamma_j - \gamma_A)$ is minimum. This upper limit is more commonly referred to as the "single pass overshoot boundary."

Such a boundary is shown in the lower left corner of Fig. 22 for a re-entering spacecraft with a lift-to-drag ratio of $\frac{L}{D}$ = -0.5, which is representative of a blunt-body space-craft configuration. The propellant requirement W_f for an L/D = 0 increases the mass ratio by about $\zeta = \frac{W_f}{W_0} \approx$ 0.03, which corresponds to an additional ΔV_A of approximately 150 m/sec over the value obtained from Fig. 22, as was pointed out in Ref. 3.

The boundary is presented as a function of the speed V and flight angle γ_j for various altitudes during the injection phase, and it assumes $h_P \! < \! 198.1$ km. It should be noted that the higher h_P , the more difficult it is to perform an immediate return. Figure 22 also allows the determination of the required ΔV_A for an immediate return abort during the injection phase for various values of T/W_0 and $I_{sp} = 420~{\rm sec.}$

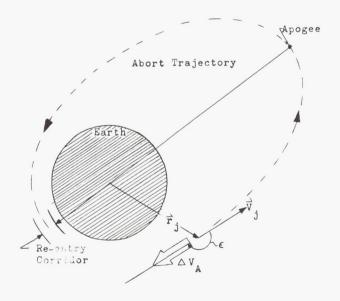
A source of ΔV_A losses arises from the implementation of the abort maneuver itself. Usually, the sequence of events consists of separating the spacecraft from the injection stage and orienting the spacecraft to the desired thrust attitude ε . This takes time, and it has been shown (Ref. 3) that a delay of only 30 sec requires an additional amount of propellant equivalent to

an additional amount of γ = $\frac{W_f}{W_0}$ = 0.07 to 0.10, which corresponds to ΔV_A = 350 to 500 m/sec. The reason for this is that the spacecraft velocity is near the parabolic speed, resulting in a centrifugal acceleration almost twice as large as the acceleration due to gravity and hence a rapid increase in γ_j ($\frac{d\gamma_j}{dt}$ = 0.05°/sec).

b. Normal return

From the previous subsection, it was found that an immediate return abort may require large amounts of propellant, especially if $T/W_0 < 4.0$ and $\rm h_P > 200~km$. This implies the use of high-thrust rocket engines, and possibly more than 40% of the spacecraft weight must be in the form of fuel and propellant system dead weight. If design consideration or operational concepts prohibit the immediate return method, then the abort must be conducted differently.

The normal return method is pictured in the sketch below.



If at a certain point in the injection phase (V_j, r_j) an abort becomes necessary, thrust is applied parallel to the velocity vector V_j but in the opposite direction (retrograde, $\epsilon=180^\circ$). This technique can be used since it minimizes the return time to earth and consequently provides a form of time control. After the abort burning phase, the spacecraft continues along its abort

trajectory until apogee. At this time, small midcourse corrections are made in order to ensure that the vacuum perigee of the abort trajectory lies in the re-entry corridor. There are two reasons for making the midcourse correction near or at apogee: (1) Perigee conditions can be changed most efficiently; (2) There is sufficient time for tracking and calculation of the actual abort trajectory prior to and after the midcourse correction.

Although the spacecraft may have a certain ΔV_A potential, it does not mean that the entire potential should be used for the abort maneuver. Generally only a portion of this capability will be used, as can be seen from Fig. 23. It presents the time to return to earth from abort to re-entry as a function of speed V_i at the time of abort for various $\triangle \boldsymbol{V}_{\boldsymbol{A}}^{} \boldsymbol{'} \boldsymbol{s}.$ Data are shown for an initial T/W_0 of approximately 1.1 and $I_{\rm Sp}$ = 420 sec. In this figure, for a typical injection trajectory profile as given in Table 9 below, it is noticed that if there is a limited control on $\Delta V_{\mbox{\scriptsize A}}$ application there is a corresponding limited control on the return time. This in turn allows some control of the geographical re-entry point. In the lower speed range, time of reentry can be controlled within $\tilde{2}$ hr for the ΔV_A 's quoted. This results in being able to vary the re-entry point by 30° in longitude. In the higher speed range, re-entry longitude control can vary from 150° to 360°. Thus, suitable and specific landing sites can be reached, thereby reducing the size of recovery forces and the number of required landing areas.

Also given in Fig. 23 are the apogee altitudes that result from an abort maneuver. These altitudes may be as high as 50,000 km, in which case two or more midcourse corrections are required to ensure safe re-entry. Depending on the inclination of the trajectory, there may be restrictions on apogee altitude because of the Van-Allen radiation belt.

In addition, the immediate return capability is shown to exist only in the very low-speed regime for the conditions presented.

TABLE 9
Typical Injection Trajectory Profile

Vj	h _j	Yj	
(m/sec)	(km)	(deg)	Notes
7,924.8	198.1	0	Parking orbit conditions
8,534.4	199.6	0.7	1
9,144	203.6	1.8	
9,753.6	210.3	3	Injection phase
10,363.2	220.1	5	V
10,972.8	233.2	7.6	Injection conditions

This concludes the discussion of abort during the injection phase. Abort and re-entry, prior to the parking orbit phase and while in the parking orbit, are considered earth-orbital type aborts. Re-entry and recovery data for earth satellites are presented in Chapters VIII and IX of Ref. 1, and abort data for the parking and intermediate orbit phases can be obtained from this reference.

D. REFERENCES

- "Orbital Flight Handbook," Martin Marietta Corporation, Space Systems Division, Baltimore, Md., ER 12684, 1963.
- Pragluski, W., "Launch Time Tolerance for Manned Lunar Missions," given at the "Proceedings of the Aerospace Support and Operations Meeting" of the Institute of the Aerospace Sciences in Orlando, Fla., 4 January 1961.
- 3. Slye, R., "Velocity Requirements for Abort from the Boost Trajectory of a Manned Lunar Mission," NASA TN D-1038, 1961.



ILLUSTRATIONS

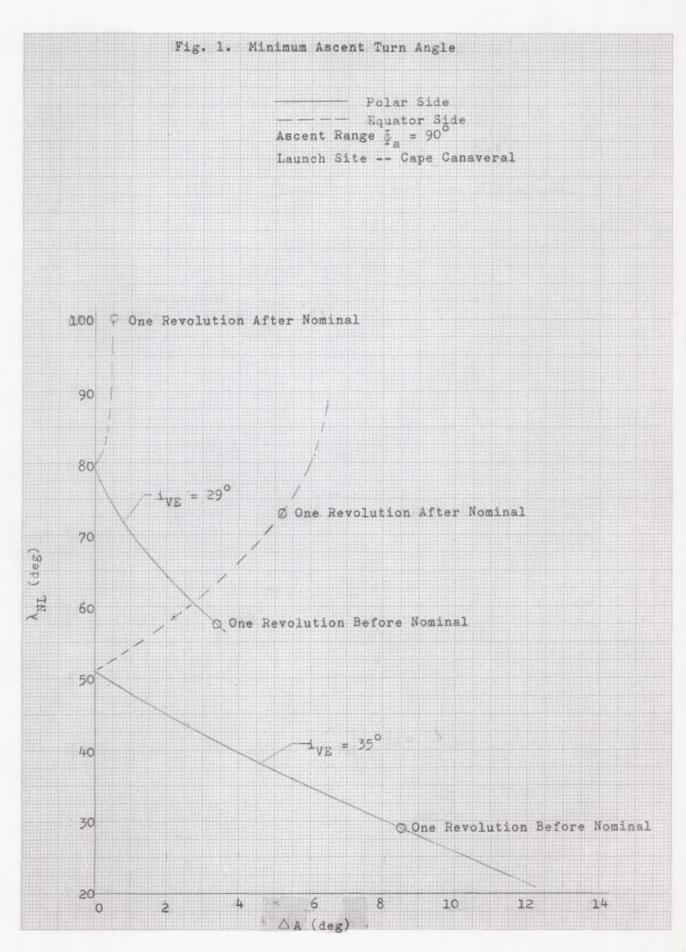


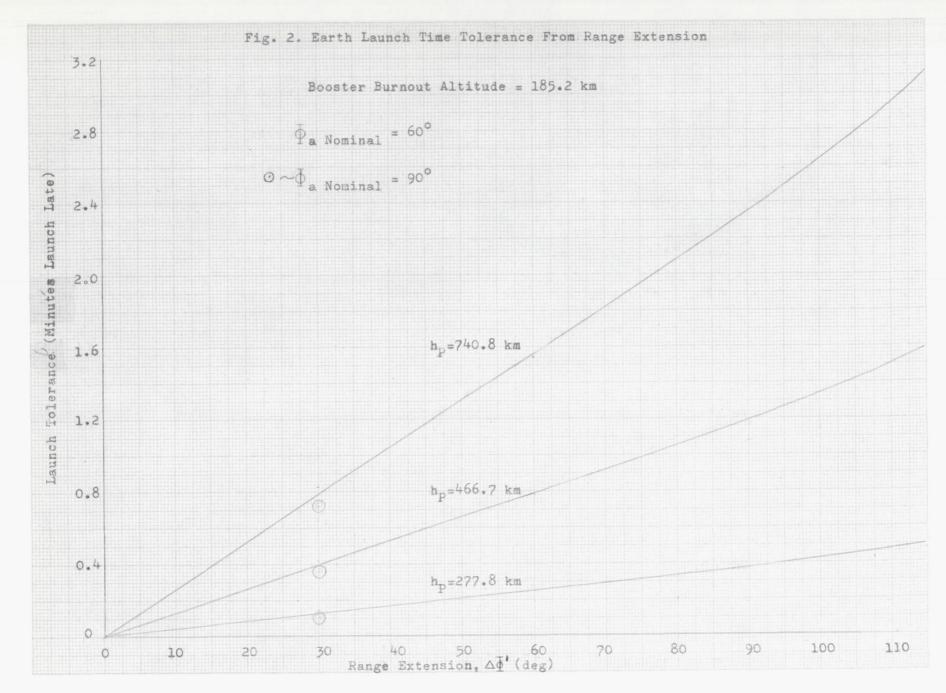
LIST OF ILLUSTRATIONS

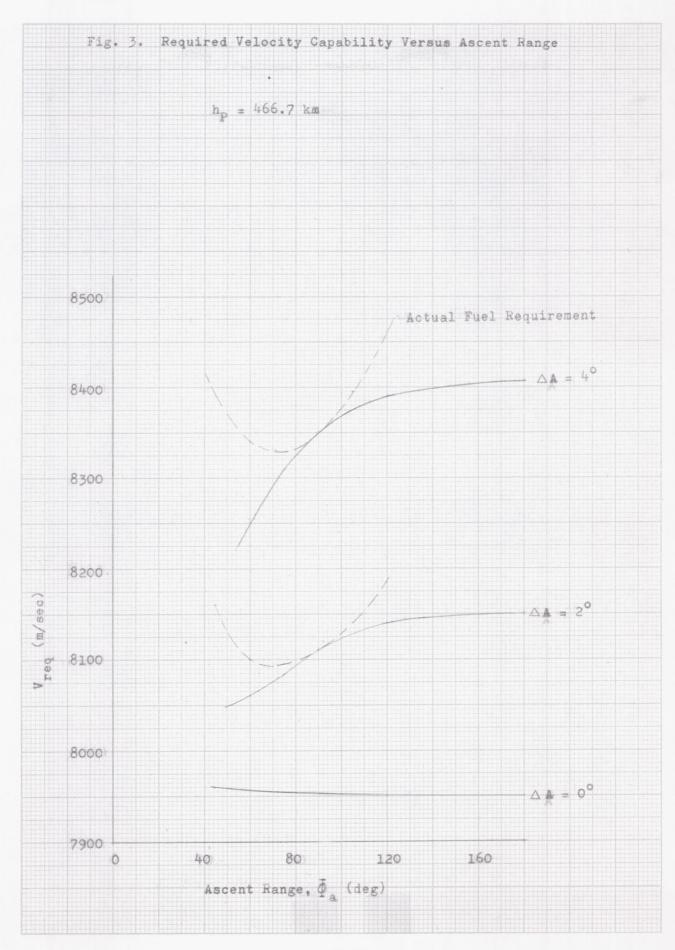
Figure	Title	Page
1	Minimum Ascent Turn Angle	V-27
2	Earth Launch Time Tolerance from Range Extension	V-28
3	Required Velocity Capability Versus Ascent Range	V-29
4	ΔV Versus Launch Time	V-30
5	Rendezvous Turn Angle Versus Launch Time	V-31
6	ΔV Required for Launch Tolerance	V-32
7	ΔV Required for Launch Tolerance	V-33
8	ΔV Required for Launch Tolerance	V-34
9	ΔV Required for Launch Tolerance	V-35
10	Waiting Time in Intermediate Orbit for Indirect Launches	V-36
11	Waiting Time in Intermediate Orbit for Indirect Launches	V-37
12	Waiting Time in Intermediate Orbit for Indirect Launches	V-38
13	Launch Tolerance	V-39
14	Parking Orbit Regression Time Trace	V-40
15	Parking Orbit Regression Time Trace	V-41
16	Parking Orbit Regression Time Trace	V-42
17	Moon Lead Angle and $i_{\mbox{\scriptsize VTL}}$ Change Curves	V-43
18	Injection Tolerance and Frequency for "Missed" Scheduled Injections (Case 1, $\beta_{\rm TL}$ = -220°)	V-44

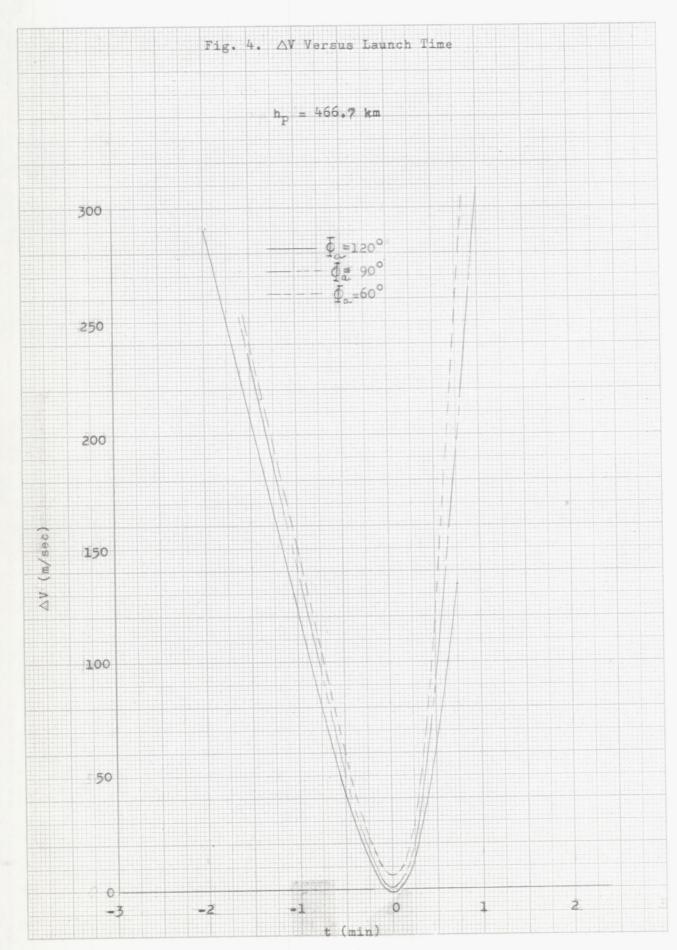
LIST OF ILLUSTRATIONS (continued)

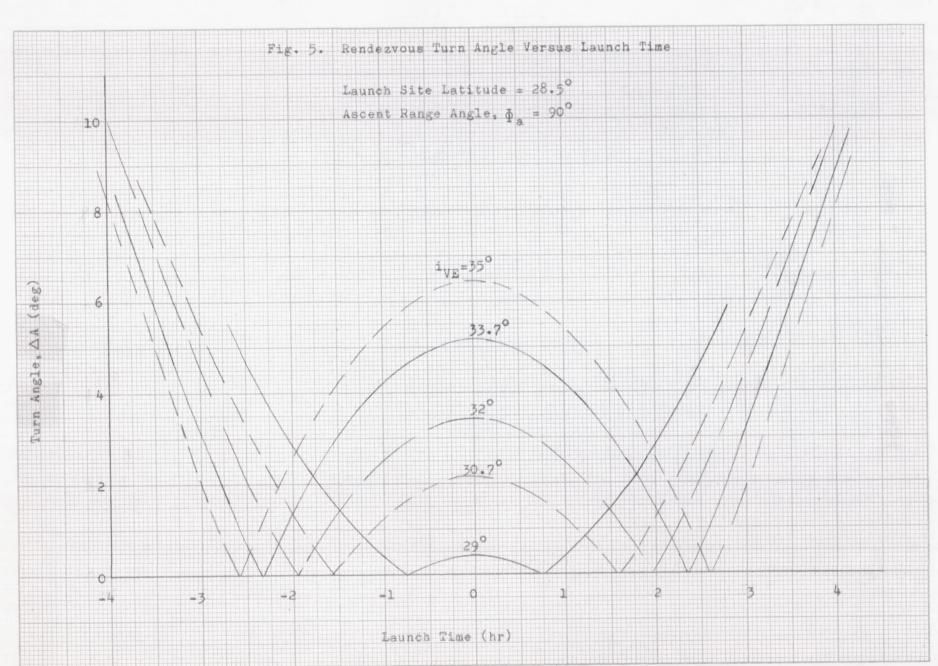
Figure	Title	Page
19	Injection Tolerance and Frequency for "Missed" Scheduled Injections (Case 2, $\beta_{\rm TL}$ = -65°)	V-44
20	Injection Energy Requirements to Parabolic Speed from a Circular Parking Orbit	V-45
21	Injection Energy Requirements to Parabolic Speed from a Circular Parking Orbit	V-46
22	Abort Velocity Impulse Required to Arrive at a Single-Pass Overshoot Boundary	V-47
23	Time to Return Versus Initial Abort Speed for a Typical Injection Phase	V - 48







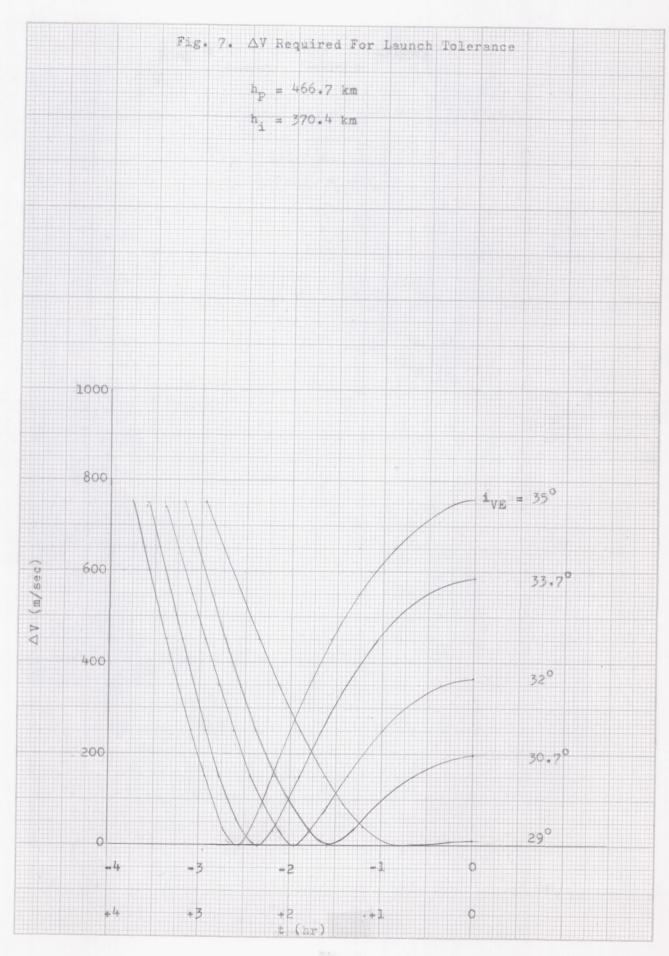


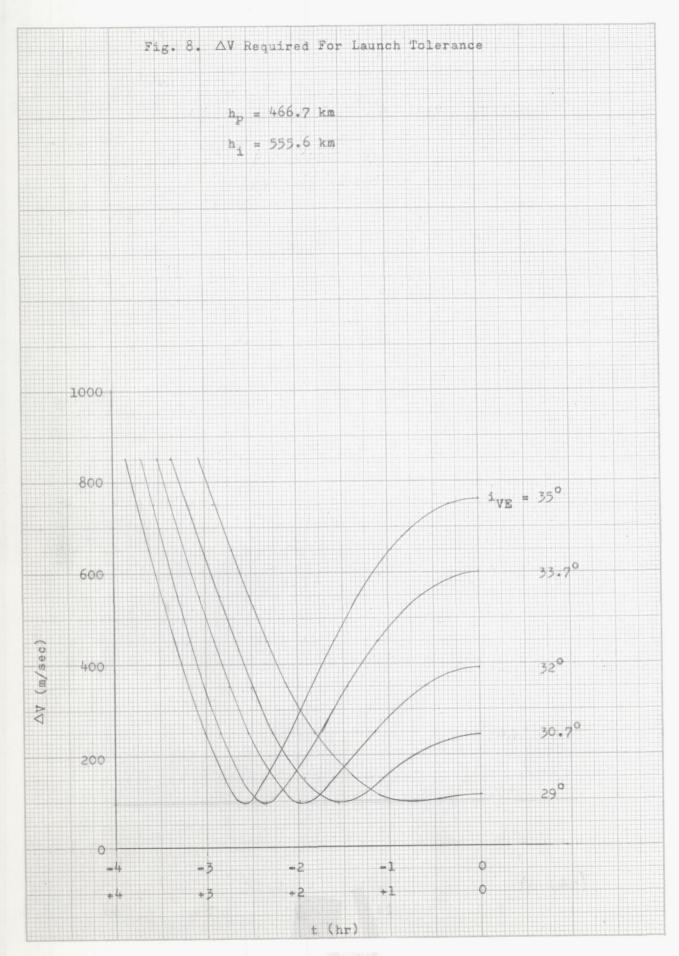


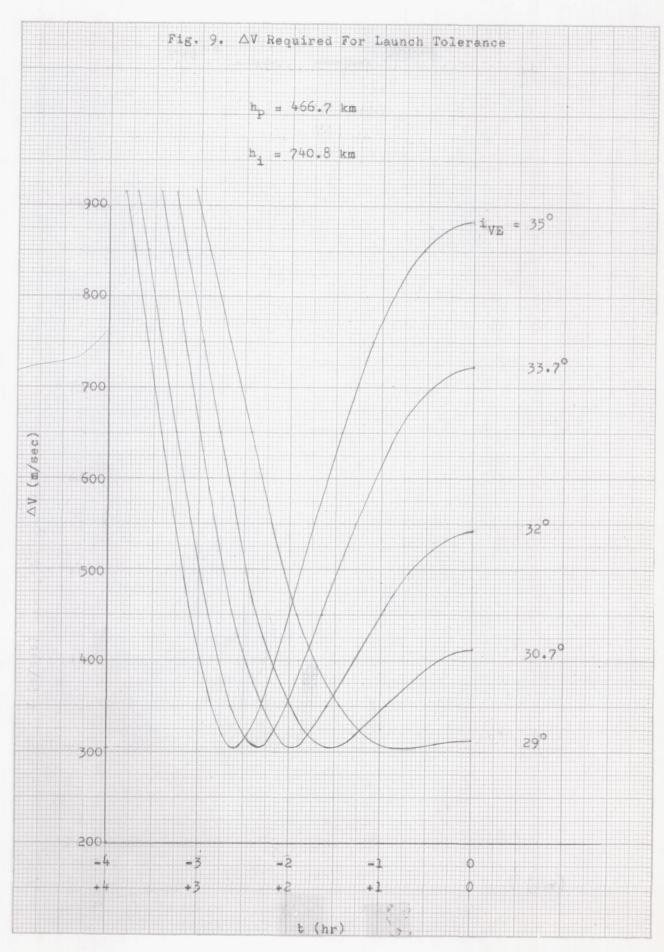
t (hr)

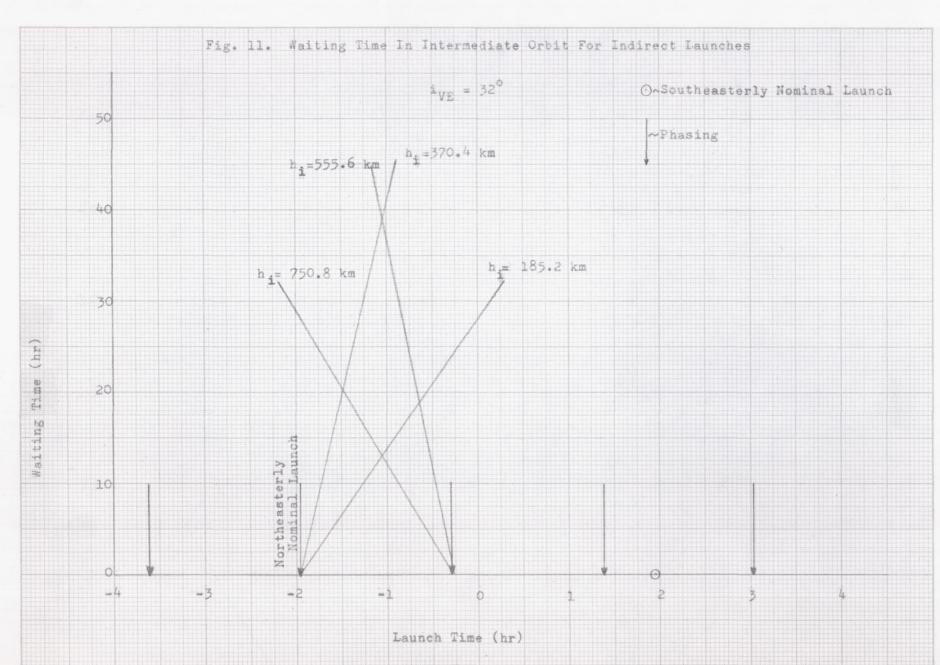
Fig. 6. AV Required For Launch Tolerance

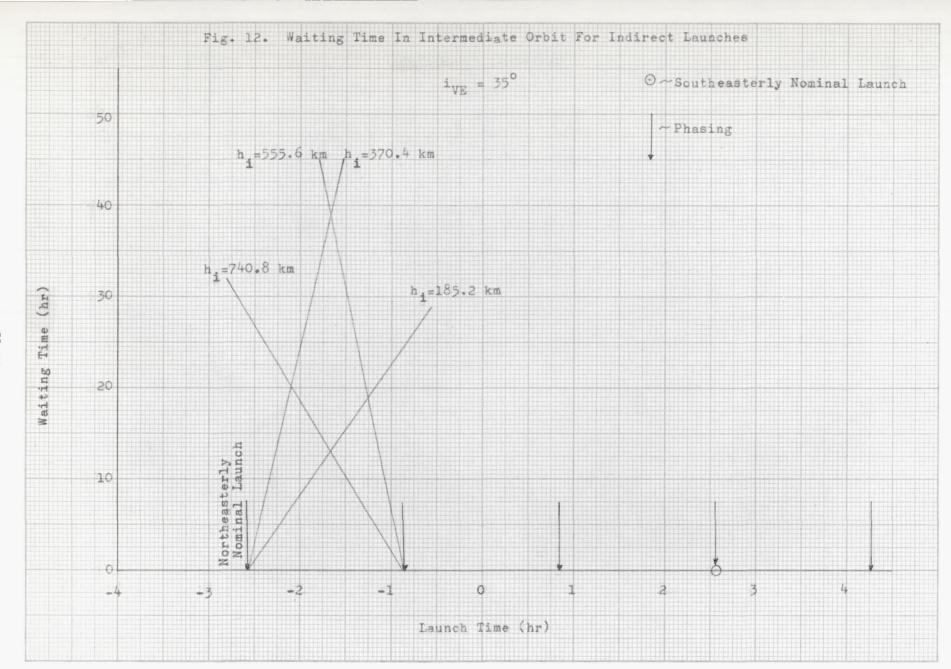
-3

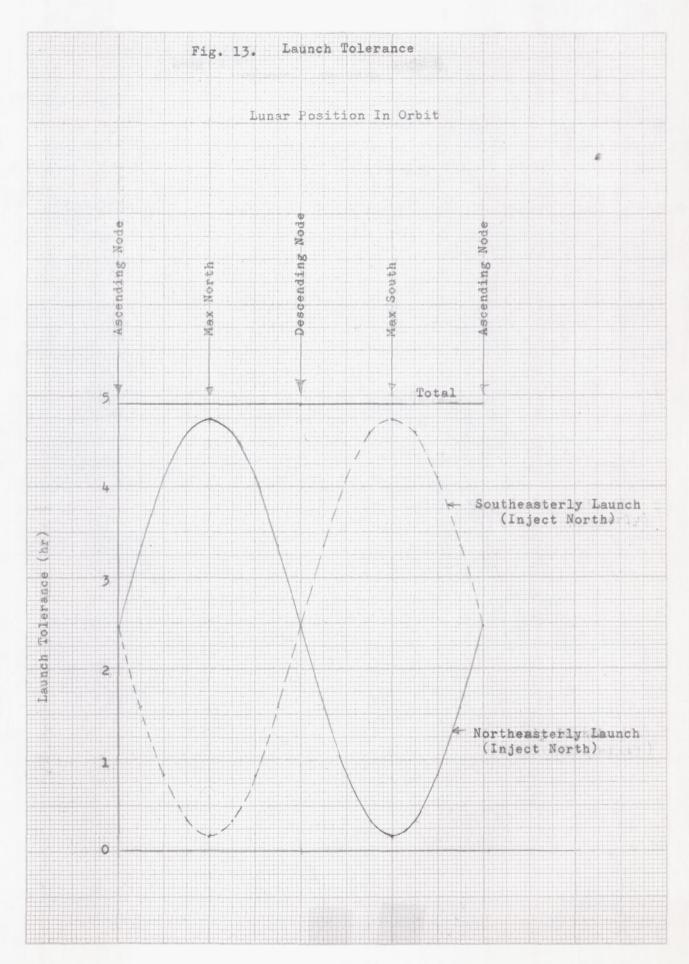


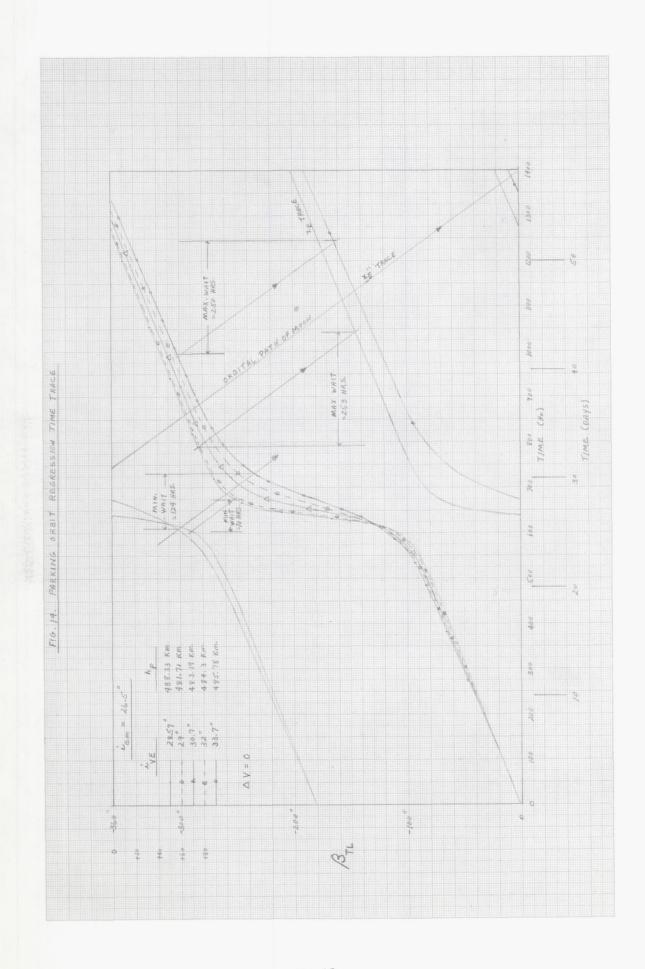


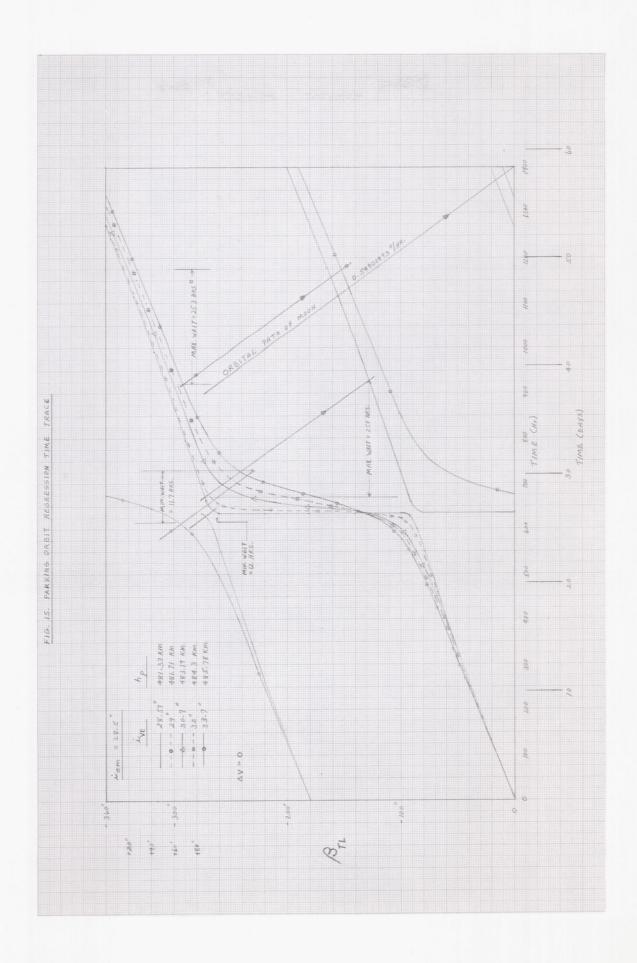


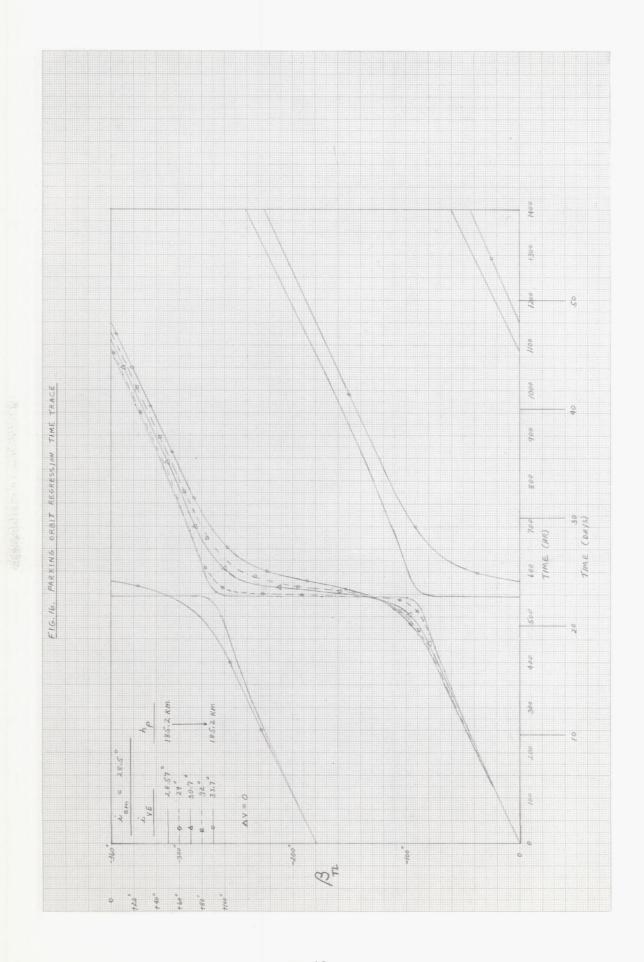












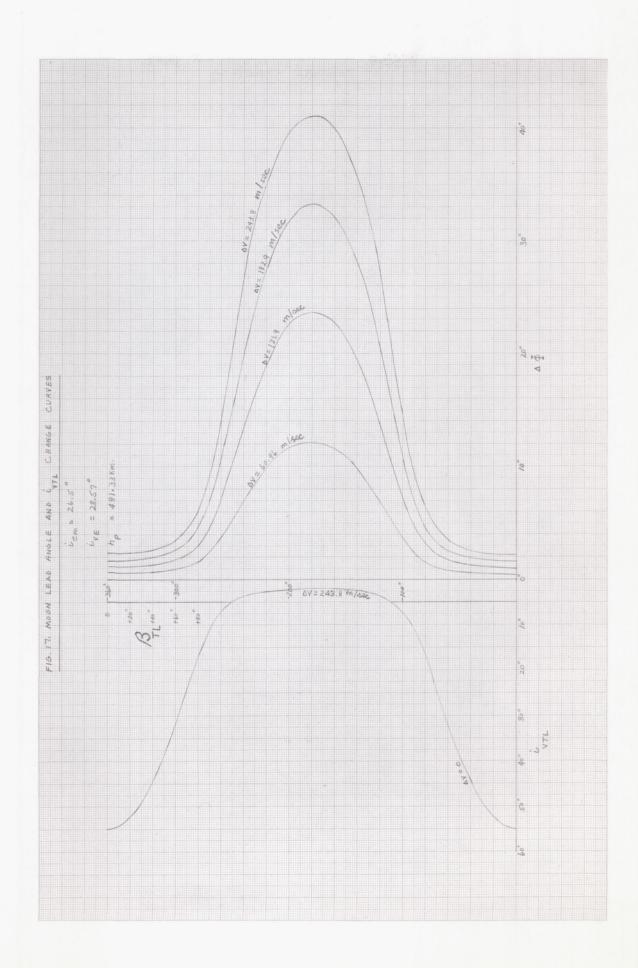


Fig. 18. Injection Tolerance And Frequency For 'Missed' Scheduled Injections (Case 1, β_{TL} = -220°)

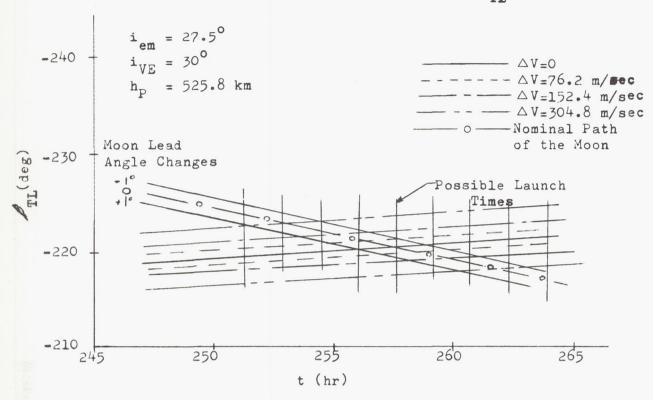
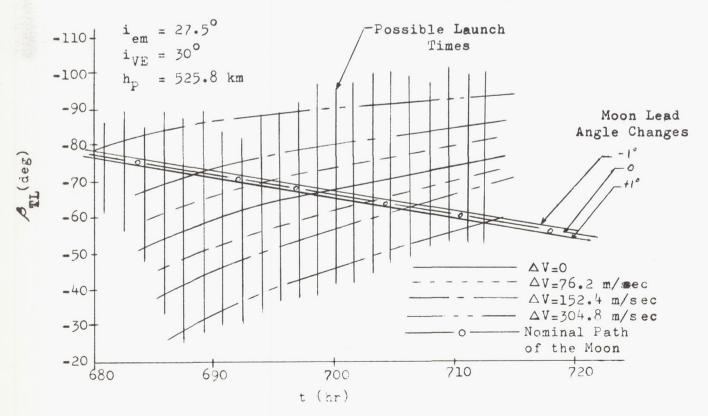
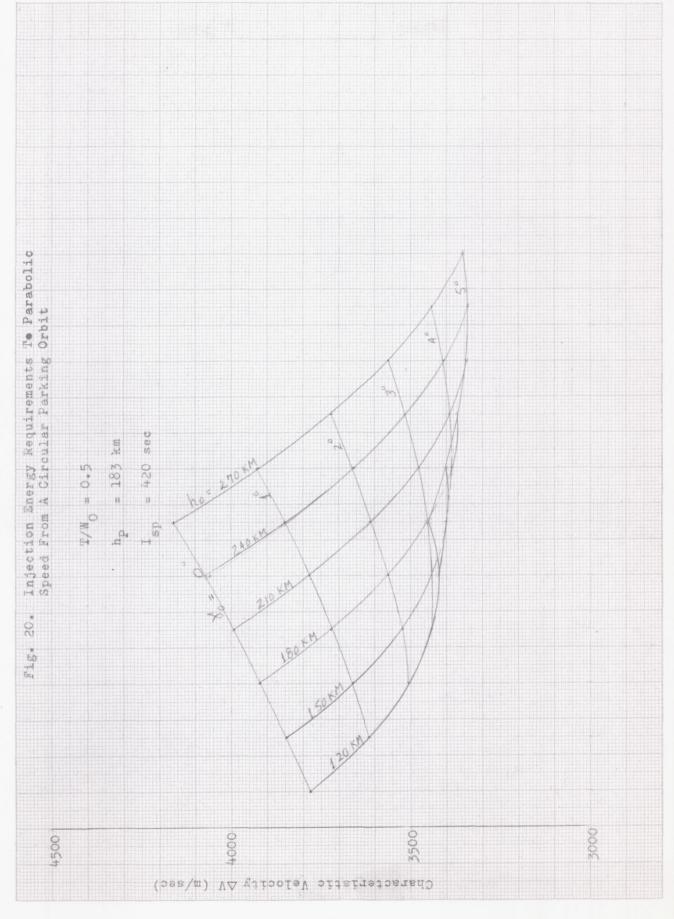
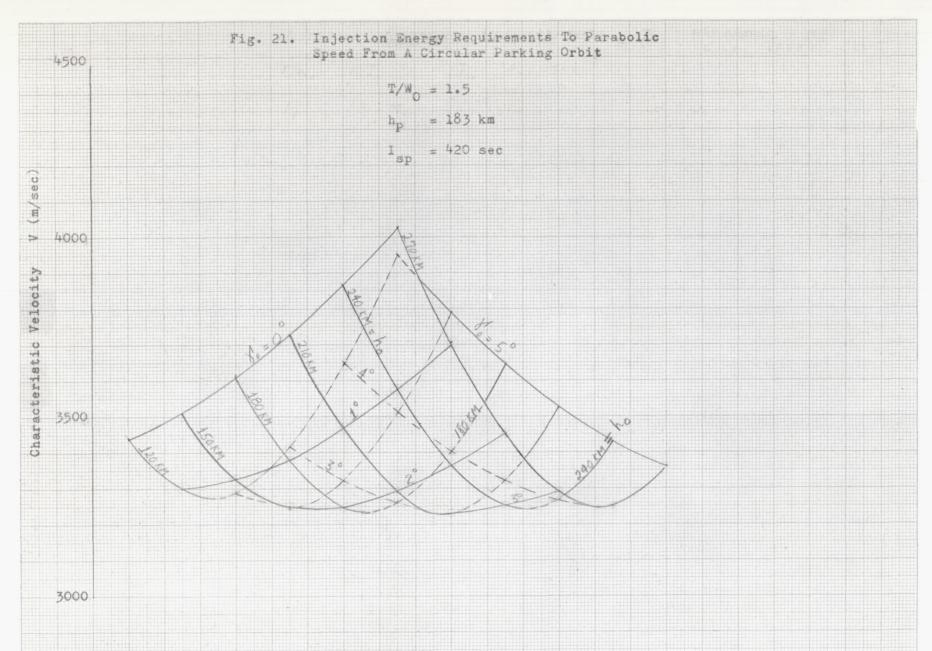
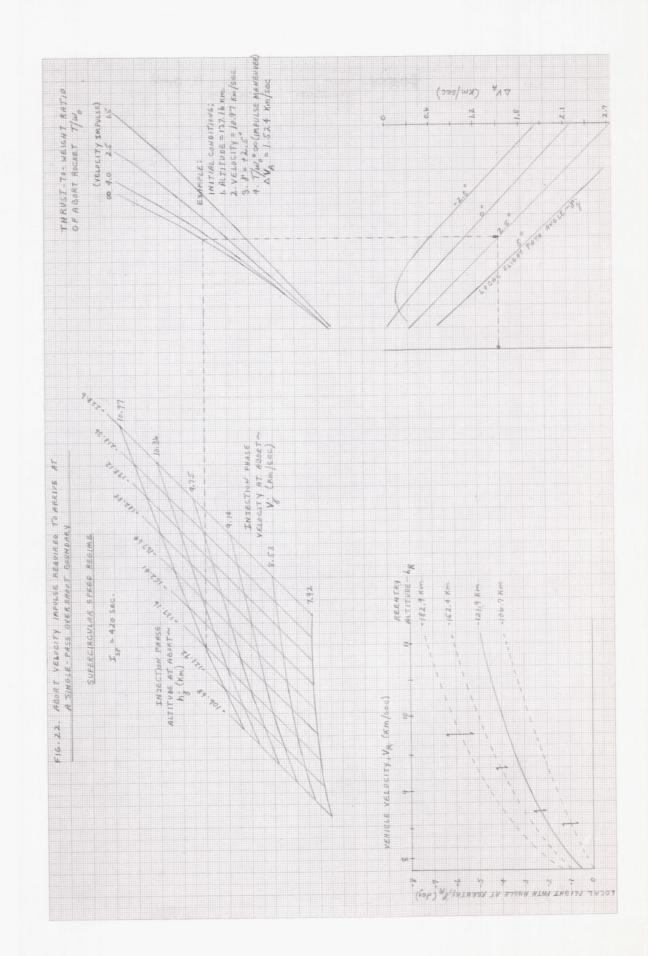


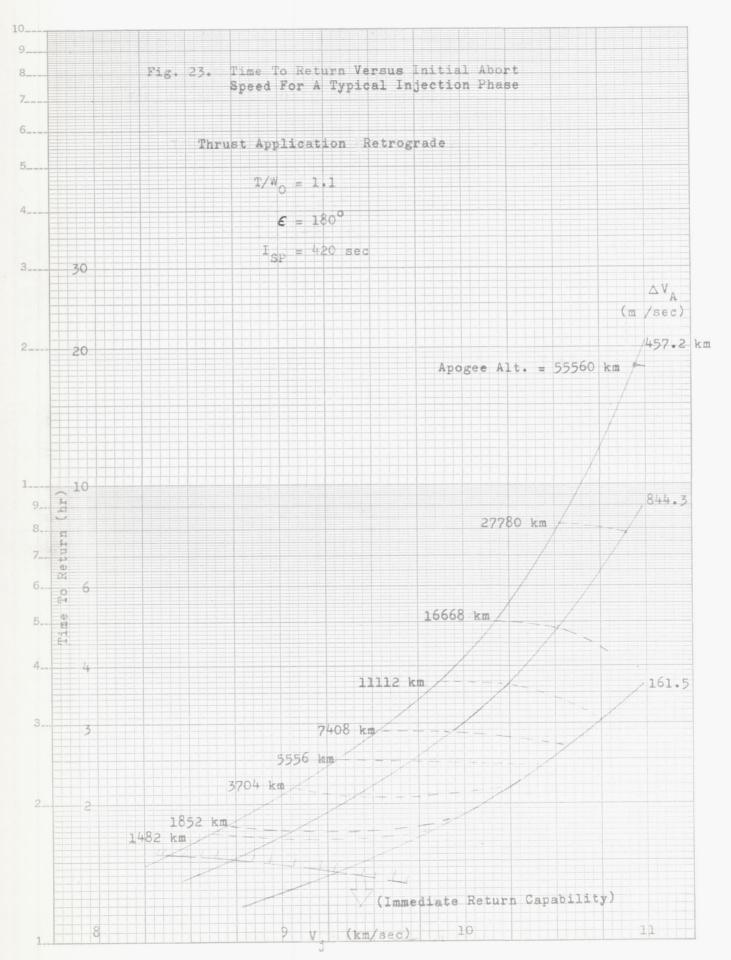
Fig. 19. Injection Tolerance And Frequency For 'Missed' Scheduled Injections (Case 2, TL = -65°)











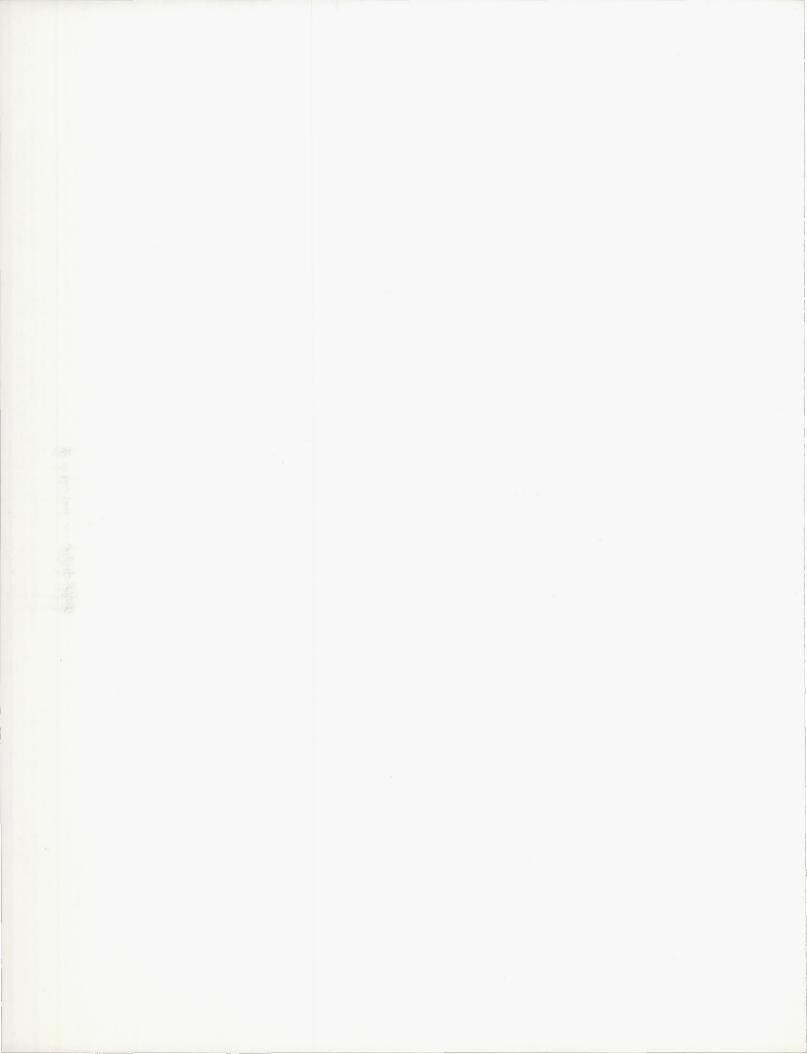
CHAPTER VI

EARTH-TO-MOON TRANSFER

Prepared by:

F. Santora, R. Salinger, F. Martikan, T. Garceau,
L. Emery, and D. Kuhn
Martin Company (Baltimore)
Aerospace Mechanics Department
March 1963

Α.	Injection Requirements for Lunar Trajectories	VI-1
В.	Navigational and Tracking Requirements	VI-7
С.	Midcourse Guidance and Energy Requirements V	T-15
D.	Translunar Abort	T-22
E.	References	T-27
	Illustrations	T-31
	Circumlunar Trajectory Catalogue	T-43



VI. EARTH TO MOON TRANSFER

Chapter V presented various techniques for leaving the launch site on the earth's surface and arriving at the proper injection conditions to establish a translunar trajectory satisfying certain mission constraints. These injection conditions consist of a specific time, velocity vector and radius vector. One purpose of Chapter VI is to graphically catalogue all possible injection conditions that reflect certain mission constraints in sufficient detail to serve as a primary source for design and mission planning work. Heavy emphasis is placed on circumlunar trajectories which return ballistically to earth; these were defined in Chapter IV and are described qualitatively and quantitatively in Section A, below. Although no data is presented in Chapter VI for the class of lunar trajectories that do not return ballistically to the immediate vicinity of the earth or approach trajectories, such data is included in Chapter IX. No injection data for lunar impact trajectories is included in the handbook except in discussion form in Chapters IV and VIII.

Chapter IV gives a description of the Voice technique which is used here to generate lunar trajectories by means of the patched two-body conics around the earth and moon. It is this technique that was used to generate the trajectory data found in this chapter and Chapters IX and XI. By referring trajectory data to the moon's orbital plane (MOP), which is a plane of symmetry, trends and tradeoffs between the various trajectory parameters are easily obtained and understood, and the number of graphs can be reduced. For the same reason, all data is general and thus applicable for any lunar position in orbit. If the lunar position in orbit at a certain date is needed. Chapter XI gives auxiliary graphs that allow interpretation of the general data of this chapter for specific dates. Comparisons with numerically integrated trajectories are also presented to prove the validity of the Voice data and to illustrate its

Sections B and C of this chapter present the better-known concepts of navigation and guidance used for lunar missions, mostly in qualitative form. Some numerical data is given to compare and illustrate the various concepts. Of special interest are the ground traces of several circumlunar trajectories shown in Figs. 4 and 5, and discussed in Subsection B-2 on tracking.

Finally, implications of performing an abort from a translunar trajectory are included in Section D, in which will be discussed and illustrated the timing of aborts for return to a particular earth base, nonplanar abort maneuvers and their consequences, and the possibility of establishing "abort way-stations" along the translunar trajectory.

A. INJECTION REQUIREMENTS FOR LUNAR TRAJECTORIES

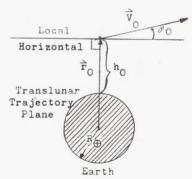
The data of this chapter concerns only circumlunar trajectories, as they are most likely to be used for manned lunar missions. A spacecraft in a circumlunar trajectory departs from the earth,

transfers ballistically to the vicinity of the moon, and achieves its closest approach, or pericynthion, as it passes behind the moon. The gravitational attraction of the moon turns the trajectory in the general direction of the earth, and the vehicle continues in a trajectory which brings it to the vicinity of the earth. The passage from the earth to the moon is referred to as the "translunar trajectory," while the return passage is termed the "transearth trajectory." This class of trajectory and possible related missions has been discussed and illustrated in Chapter IV.

1. The Circumlunar Trajectory Catalogue

The nomenclature of the Voice technique. which has been introduced in Sections B-8 and C of Chapter IV, is repeated here for convenience and discussed more fully because the graphical data of this chapter has been derived from this technique. The leading sketch, opposite, is a schematic showing the Voice Cartesian coordinate axes and some of the trajectory nomenclature and parameters. The x_E-axis is defined by the intersection of the translunar trajectory plane with the moon's orbital plane (MOP) and is directed toward the moon. The z_{E} -axis is defined by the angular momentum vector of the moon about the earth's center, while the y_E-axis completes the righthand coordinate system. The inclination of the translunar plane to the MOP is given by $i_{\mbox{\scriptsize VTL}}$ $0^{\circ} \leq i_{\mathrm{VTL}} \leq 180^{\circ},$ and is measured as shown in the leading sketch. The velocity and radius vectors at injection, or the initial conditions of the lunar trajectory, define the translunar plane.

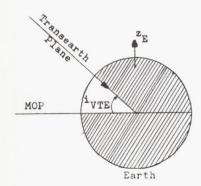
The injection conditions are specified as described below and illustrated on the following sketch:



 \vec{V}_0 is the injection velocity measured relative to the nonrotating $x_E y_E z_E$ system centered at the earth; γ_0 is the local flight path angle measured from the local horizontal to the velocity vector. The injection altitude, h_0 , is defined by h_0 = r_0 - R_{\oplus} , where \vec{r}_0 is the radius vector at injection and R_{\oplus} = 6371.02 km is the radius of an equivalent spherical model of the earth. The specification of the injection is completed by the angle ψ_0 , which orients the injection point with respect

to the Voice coordinate system and is measured from the negative x_E^{-axis} to \vec{r}_0 , as shown in the leading sketch, facing page VI-1.

A very important concept is that of the cardinal directions when the MOP is used as a reference plane for the trajectories in this handbook. By definition, the \mathbf{z}_{E}^{-} -axis is designated as the "North" direction and "East" is in the same direction as the moon's orbital motion about the earth. Thus, when $0 < i_{\overline{VTL}} < 90^{\circ}$, injection is in the northern hemisphere (relative to the MOP) and is direct, or in the direction of the lunar motion in orbit, or "East" (see Subsection A-8 of Chapter IV). When $90^\circ < i_{\mbox{VTL}} < 180^\circ$ the injection is again north of the MOP, but in this case the direction is a retrograde or, westward injection. The same reasoning applies for injections taking place in the southern hemisphere relative to the MOP. Since all data is presented with positive values of iVTL, the type of injection must be specified together with the value of iVTL; e.g., $i_{\rm VTL}$ = 60° (inject north), or $i_{\rm VTL}$ = 60° (inject south). In Chapters V and XI, Cape Canaveral is the launch site, and launch azimuths ${\rm A}_{\rm e}$ are arbitrarily restricted to $70^{\circ} < A_{e} < 110^{\circ}$. These values of A_e result in values of i_{VTL} equal to or greater than 0° but always less than 75°, as can be noted from Figs. 11 and 12 in Chapter XI. For this reason, data is given for $2^{\circ} \le i_{\rm VTL} \le 75^{\circ}$. The material is presented for the "inject north" case and must be reinterpreted for the "inject south" case, as will be discussed later in the chapter. A similar situation exists for the transearth trajectory, as was noted in Chapter IV. The transearth inclination to the MOP is denoted by iVTE and is measured positively, as shown. For convenience, the sketch is repeated here with an explanatory table relating return direction to



Transearth Trajectory Inclination

quadrant.

0° < i_{VTE} < 90° 90° < i_{VTE} < 180° -90° < i_{VTE} < 0° -180° < i_{VTE} < -90°

Return Direction

Direct from the north Retrograde from the north Direct from the south Retrograde from the south

The circumlunar trajectories have been graphically catalogued for specific mission constraints -namely, the pericynthion altitude $\ensuremath{^{\uparrow}\!h}_{\rm PL}$, the earthmoon distance $\,R_{\bigoplus}$, and vacuum perigee altitude of the transearth trajectory $\,h_{\rm PE}$. The circumlunar trajectory catalogue includes data for hpl. from 185.2 km to 5000 km where $h_{
m PL}$ = $r_{
m PL}$ -R $_{\ell}$ with $r_{\rm PI}$ the radius from the vehicle to the center of the moon at pericynthion and $R_{\mathcal{O}}$ = 1738.16 km is the radius of the spherical moon model. $R_{\oplus \emptyset}$ is varied from 56 ER (earth radii) to 64 ER, which represent the minimum lunar perigee radius and maximum lunar apogee radius, respectively, that can be encountered because of the eccentricity of the lunar orbit. The Voice data for these $\mathbf{R}_{\bigoplus \mathbf{Q}}$ was generated by keeping the angular momentum of the moon constant and assuming the moon to be in a circular orbit around the earth. All transearth trajectories have a vacuum perigee altitude of hpg = 46 km.

In addition to the injection conditions of i_{VTL} , V_0 , γ_0 , h_0 and ψ_0 , the flight time to pericynthion t_p and the total flight time from injection to perigee (T) also are recorded.

It is well to note at this time exactly what the catalogue contains and then to discuss each item separately in detail sufficient to provide a working knowledge of the material. The catalogue itself consists of Figs. C-1 to C-83 and contains the following trajectory constraints:

TABLE 1
Circumlunar Trajectory Catalogue

Case	R⊕((earth radii)	h _{PL} (km)	Figure Numbers	Pages		
1	56	185.2	C-1 to 8	IV-48 to 56		
2	56	1000	C-9 to 16	IV-57 to 64		
3	56	5000	C-17 to 24	IV-65 to 72		
4	60	185.2	C-25 to 32	IV-73 to 80		
5	60	1000	C-33 to 41	IV-81 to 89		
6	60	3000	C-42 to 50	IV-90 to 98		
7	60	5000	C-51 to 59	IV-99 to 107		
8	64	185.2	C-60 to 67	IV-108 to 115		
9	64	1000	C-68 to 75	IV-116 to 123		
10	64	5000	C-76 to 83	IV-124 to 131		

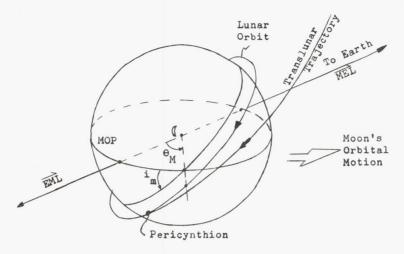
Trajectory data is given by the following variables as a function of $i_{\mbox{\scriptsize VTE}}$ for each of the above constraints:

(1)	V_0	(5) (6)	tp
(2)	Ψ_0	(6)	T
(3)	Φ^*	(7)	
(4)	ΔV	(8)	θ_{M}

The variables φ *, \triangle V, i_{m} and θ_{M} have not been mentioned previously in this chapter but will be discussed in sequence along with the others.

- (1) V_0 --the required injection velocity for the circumlunar mission. Figure C-1 shows \mathbf{V}_0 as a function of \mathbf{i}_{VTE} for $R_{\oplus 4}$ = 56 ER and $h_{\rm PL}$ = 185.2 km. The independent parameter is i_{VTL} , and its particular values are 2°, 30°, 60° and 75°. The first trend noticed is the fact that ${\rm V}_0$ increases as ${\rm i}_{\rm VTL}$ decreases. By referring to Figs. C-9 and C-17, it is observed that this trend remains the same and that the variation in \mathbf{V}_0 due to $\mathbf{i}_{\mathrm{VTL}}$ is 6 to 20 m/sec, depending on $h_{\rm PL}$ For $R_{\bigoplus \emptyset}$ of 60 and 64 ER (Figs. C-25, C-34, C-35, C-42, C-43, C-51, C-52, C-60, C-68 and C-76), this variation does not substantially change. Another trend indicates that V_0 is lower if the transearth trajectory is direct rather than retrograde. The difference between returning direct in the MOP and retrograde in the MOP is approximately 25 m/sec for all cases. It is also noticed that V_0 decreases as h_P increases but increases as $\mathbf{R}_{\bigoplus\emptyset}$ increases. The maximum V_0 encountered for the above cases is 10922.8 m/sec and occurs for $R_{\oplus 4}$ = 64 ER, i_{VTE} = 180°, h_{PL} = 185.2 km and $i_{VTI} = 2^{\circ}$.
- (2) ψ_0 --the injection position as given in Figs. C-2, C-10, C-18, C-26, C-35, C-44, C-53, C-61, C-69 and C-77. There is no appreciable change in the value of ψ_0 as $R_{\bigoplus \ell}$ is varied if h_{PL} is maintained constant. However, if h_{PL} is varied a significant change does occur.
 - (3) \$\psi^*\$--moon lead angle. This variable is discussed in Chapter IV, Section C, but for convenience is depicted in the sketch on page (ii) of this chapter. It is measured from the lunar position at injection to the x_E-axis, and its magnitude varies from 30° to 60°. This is a very important angle when obtaining numerically integrated trajectories.
 - (4) ΔV--required velocity impulse to enter a circular lunar orbit from the circumlunar trajectory. If the spacecraft were to enter a circular orbit about the moon at the time of pericynthion, a characteristic velocity impulse would be required to reduce the speed of the space vehicle to circular orbit velocity (see Chapter IV, Subsection A-4). Figures C-4, C-12, C-20, C-28, C-37, C-46, C-55, C-63, C-71 and C-79 present Δ V as a function of iVTE, and it is

- immediately noticed that \triangle V increases as i_{VTL} increases. By varying i_{VTL} from 2° to 75°, a \triangle V change of 30 to 60 m/sec may be realized, depending on h_{PL} . $R_{\Theta \ell}$ has little effect on this change but does influence the magnitude of the impulse by as much as 50 m/sec (\triangle V decreases as $R_{\Theta \ell}$ increases). Again, as is the case for V_0 , smaller values of \triangle V are required for direct return trajectories. The maximum \triangle V encountered for the cases in the above table is 1045 m/sec, which occurs for the following conditions: $R_{\Theta \ell}$ = 56 ER, i_{VTL} = 75°, i_{VTE} = 180°, i_{PL} = 185.2 km.
- (5) t_p--time from injection to pericynthion. As expected, t_p increases with i_{VTL}, since V₀ decreases with i_{VTL}; t_p also increases as h_{PL} and R_{⊕(} increase, and the longest times are realized with "direct" returns. This data is presented in Figs C-5, C-13, C-21, C-29, C-38, C-47, C-56, C-64, C-72 and C-80.
- (6) T--total flight time measured from injection to perigee. This particular variable is markedly influenced by ${\rm h}_{\rm PL}$. In fact, one may expect an increase of 35 to 65 hr (depending on ${\rm i}_{\rm VTE}$) by increasing ${\rm h}_{\rm PL}$ from 185.2 km to 5000 km. T is also increased by approximately 25 hr if ${\rm R}_{\rm \oplus 4}$ varies from 56 to 64 ER (with ${\rm h}_{\rm PL}$ held constant). The data giving T versus ${\rm i}_{\rm VTE}$ is found in Figs. C-6, C-14, C-22, C-30, C-39, C-48, C-57, C-65, C-73 and C-81.
- (7) i_{m} --inclination of the lunar orbit to the MOP, $0^{\circ} \le i_{m} \le 90^{\circ}$. If the spacecraft enters a lunar orbit at the pericynthion point (item 4), the resulting lunar orbit will be inclined to the MOP by an angle im. Because of the importance of this angle, a sketch showing i_{m} is repeated at this time from Chapter IV. Figures C-7, C-15, C-23, C-31, C-40, C-49, C-58, C-66, C-74 and C-82 present i_m, and a very interesting and significant result is that i m is limited to 25° for ${\rm h_{PL}}$ = 5000 km and to less than 15° for h_{PL} = 185.2 km. This clearly implies that high selenographic latitudes (25°) are inaccessible for landing or reconnaissance missions unless the velocity vector is turned at pericynthion. This maneuver requires relatively much fuel, and hence, circum-



lunar trajectories will result in fly-bys and lunar orbits that lie in a narrow band above and below the MOP. Furthermore, lunar librations will not improve this coverage to any great extent.

(8) θ_{M} --angle between the earth-moon line and the descending node of the lunar orbit, -180° $\leq \theta_{\rm M} \leq$ 180°. At the time of pericynthion ($t_{\rm p}$), the descending node of the trajectory plane is displaced θ_{M} degrees from the earth-moon line (EML). This angle is also shown in the above sketch, and it, together with im, completely describes the orientation of the trajectory plane at \boldsymbol{t}_{p} as well as the orientation of the circular lunar orbit that may be established at this point. Data relating θ_{M} with i_{VTE} for various $i_{\mbox{VTL}}$ are given in Figs. C-8, C-16, C-24, C-32, C-41, C-50, C-59, C 67, C-75 and C-83. Another important fact, not mentioned above, is that for a constant value of iVTL, an earth return is possible from any direction. This can be extremely useful in establishing operational concepts for lunar missions.

2. Generalization of the Catalogued Data

The catalogued data, extensive as it is, does not cover all parameters of the translunar trajectory. The material presented is applicable only for an injection flight path angle $\rm Y_0=5^\circ$ and an injection altitude $\rm h_0=250~km$. The following discussion presents methods whereby $\rm Y_0$ and $\rm h_0$ may be extended to other values.

First, consider that h_0 remains 250 km and it is desired to change γ_0 to a value $\gamma_0^{\rm I}$ other than 5°. It has been found that all data in the catalogue, except for ψ_0 , remains essentially the

same and any changes that do occur are altogether insignificant on the scale of the graphs. A new ψ_0 , denoted by ψ_0^{I} can be estimated to within ±0.2° for $\Delta\,\gamma_0$ as high as ±20° by means of the following empirical relation:

$$\psi_0^{\prime} = \psi_0 + 2 \triangle \gamma_0 \tag{1}$$
 where
$$\psi = \text{catalogue value}$$

$$\psi_0^{\prime} = \text{revised value of } \psi_0$$

$$\triangle \gamma_0 = \gamma_0^{\prime} - \gamma_0 = \gamma_0^{\prime} - 5^{\circ}$$

$$\gamma_0 = \text{catalogue value}$$

$$\gamma_0^{\prime} = \text{desired value of } \gamma_0$$

Values of ${}^{\gamma}_0^{}\!>\!25^\circ$ are improbable for earth departure by present boosters because of the higher fuel requirements, while values of ${\gamma}_0^{}<$ - 15° cause the spacecraft to re-enter the earth's atmosphere.

Next, consider that \mathbf{Y}_0 remains unchanged, i.e., $\mathbf{Y}_0^* = \mathbf{Y}_0$, and that it is desired to alter \mathbf{h}_0 by an amount Δ \mathbf{h}_0 . For Δ \mathbf{h}_0 less than ± 250 km, the data in the catalogue again does not change, with the exception of the injection velocity \mathbf{V}_0 . A new value of \mathbf{V}_0 , denoted by \mathbf{V}_0^* , can be determined for the desired \mathbf{h}_0 , which is denoted by \mathbf{h}_0^* through use of this equation derived from the conservation of energy in a restricted 2-body system:

$$V_0^{\dagger} = \left[V_0^2 - V_p^2 \left(\frac{\triangle h_0}{r_0} \right) \right]^{1/2}$$
 (2)

Observing that Eqs (1) and (2) are independent of each other, both γ_0 and h_0 may be varied together. An example of the use of these equations

is included in the second sample mission in Chapter XI.

If $h_0^{\, \bullet}$ is extended to 2000 km by means of Eq (2), small errors appear in the other parameters. These errors may be acceptable for feasibility trajectory calculations. The brief table below gives the maximum magnitude of these errors for the various parameters if the catalogued data is extended to $h_0^{\, \bullet}$ = 2000 km:

	Maximum Error
V_0	±1.5 m/sec
v_0 ψ_0	+1.3°
Φ *	±0,2°
$\triangle V$	-5 m/sec
tp	±0.3 hr
T	±0.6 hr
ⁱ m	-0.7°
$\theta_{\mathbf{M}}$	-3°

where:

parameter error = actual parameter valueestimated parameter value (from Eq (2)).

Therefore, the catalogued data in Figs. C-1 through C-83 can be applied to most circumlunar trajectories of interest. The catalogued trajectories are for the "inject north" case only as was mentioned previously. Since the reference plane is a plane of symmetry, the material can easily be reinterpreted for the "inject south" case by redefining the return inclination (i $_{\rm VTE}$) scale on the figures by:

$$i_{
m VTE}$$
 (inject south) = - $i_{
m VTE}$ (inject north) (3)

A simple example illustrates this readily. Suppose that for the "inject north" case, $i_{\rm VTL}$ = 60° and $i_{\rm VTE}$ = +40°, which is a return direct from the north. Therefore, for the "inject south" case, $i_{\rm VTL}$ remains the same, but $i_{\rm VTE}$ = -40°, which is a return direct from the south.

The lunar orbit orientation $\boldsymbol{\theta}_{\widetilde{M}}$ for the inject south case is interpreted in the following manner.

$$\boldsymbol{\theta}_{\mathrm{M}}$$
 (inject south) = $\boldsymbol{\theta}_{\mathrm{M}}$ (inject north) + 180°

3. Accuracy of Injection Conditions and Trajectory

Since the data presented in Figs. C-1 to C-83 was derived from an approximate force model of the earth-moon system, it is necessary to ascertain the accuracy of such data. To this end, the catalogued Voice trajectory data (patched conic force model) was spotchecked with numerically integrated trajectories which were generated by using the more accurate restricted 3-body force model with the moon in a circular orbit about the earth (angular momentum is constant). The

selected trajectories are considered extreme in the sense that they represent the maximum inaccuracy to be expected between the Voice and integrated trajectory results. For instance, high values of $i_{\mbox{\scriptsize VTL}}$ (>60°) and small values of $R_{\mbox{\scriptsize \oplus}\mbox{\scriptsize \emptyset}}$ (\simeq 56 ER) produce larger errors in V_0 , t_p and T.

Table 2 presents four circumlunar trajectories, giving the comparison of the previously discussed parameters. Trajectories 1 and 2 are presented to demonstrate the differences between the Voice and integrated results for the extreme conditions just mentioned. Below is a brief account of the likely errors that can be encountered in such extreme cases.

where the error is defined as the difference between the Voice and the restricted 3-body force model.

But more important than determining the acceptability of the Voice model is the substantiation of the trends indicated by Voice. Trajectory 1, for instance, shows the feasibility of leaving the earth with highly inclined trajectories and also returning with very high inclinations relative to the MOP. Trajectory 2 depicts in part the opposite case, i.e., injecting into a highly inclined translunar plane but returning with extremely low inclinations, in fact almost in the MOP. In trajectory 3, a complete reversal of trajectory 2 is shown. This trajectory has a very low inclined translunar plane (i_{VTL} = 2°) but returns to earth with a transearth inclination of approximately 75°. The last trajectory, number 4, has a remote pericynthion altitude ($h_{\rm PL}$ = 5000 km) and the moon is near apogee or at ${\rm R}_{\,\oplus\, \text{\scriptsize \it l}}\text{= }64$ ER. In addition, the entire circumlunar trajectory is essentially in one plane. Thus, some important trends indicated by Voice are easily verified by the numerically integrated trajectories given in Table 2, and it is possible to conclude that the inaccuracies inherent in utilizing a patched conic method are acceptable for initial feasibility trajectory studies.

As a final point, the resulting lunar orbit orientation about the moon (i_m,θ_M) is in remarkable agreement with that obtained by integrated trajectories. This fact is a major reason that the use of Voice data for mission planning, further discussed in Chapter XI, is practical. If desired, a more accurate value of θ_M can be obtained by applying an empirical correction, given by

 $\frac{\text{TABLE 2}}{\text{Comparison of Voice Trajectories with Numerically Integrated Restricted 3-Body Trajectories}} \\ \text{h}_0 = 250 \text{ km}, \ \gamma_0 = 5^\circ, \ \text{Inject North}$

Quantity	ity 1		2		3		4	
	Voice	Integrated	Voice	Integrated	Voice	Integrated	Voice	Integrated
R⊕((ER)	56.0	56.0	56.0	56.0	56.0	56.0	64.0	64.0
V ₀ (m/sec)	10896.661	10894.788	10889.214	10887.064	10903.696	10902.030	10890.007	10889.463
i _{VTL} (deg)	75.0	75.0	75.0	75.0	2.0	2.0	60.0	60.0
ψ_0 (deg)	18.7534873	18.456858	17.497310	17.090264	22.30213	22.209816	14 787743	14.562976
φ* (deg)	40.488397	41.201542	43.093934	44.149837	35.934781	36.316359	46.632338	47.461369
h _{PL} (km)	185.0305	185.4452	185.0630	185.2193	185.0750	185.4256	4998.8867	4999.7675
ΔV (m/sec)	3237.672	3296.0677	3131.953	3189.2988	3129.7472	3187.0975	2161.8967	2261.009
t _p (hr)	62.220	62.554	66.204	66.942	59.078	59.044	93.202	93.160
T (hr)	125.584	126.376	125.294	126.009	125.346	126.067	188.215	188.447
i _{VTE} (deg)	98.145	98.128	-178.9526	-178.9658	105.1679	105.1248	-115.5457	-115.5227
h _{PE} (km)	45.7893	44.2087	45.2795	43.3567	45.6254	43.7711	45.8436	54.7968
i _m (deg)	13.792493	14.308571	8.86063	9.0893964	8.8545358	9.09866	9.7478268	9.810085
θ _M (deg)	90.310615	91,203772	42.873267	44.390196	134.93123	132.6791	-1.9753935	-0.859943
θ* _M (deg)	91.162143	91.203772	43.7924	44.390196	133.2306	132.6791	-0.8012156	-0.859943

$$\Delta\theta_{\rm M} = \frac{+}{c} \left[0.22 + 0.000156 \, h_{\rm PL} \right],$$

$$C_0 \sin i_{\rm VTE} + 1 \tag{4}$$

where

+ holds for the "inject south" case

- holds for the "inject north" case

 \mathbf{C}_0 is obtained from Chapter XI, Section E; a constant derived from empirical data.

The corrected value of θ_{M} , θ_{M}^{*} , is given by

$$\theta_{M}^{*} = \theta_{M} + \Delta \theta_{M}$$

and is also noted in Table 2.

B. NAVIGATIONAL AND TRACKING REQUIREMENTS

Navigation is defined as the process of determining the position and velocity of a space vehicle; this process is usually accomplished by making observations such as star occultations by the moon, bearing lines to certain stars, angular diameters of the moon, earth and sun and from these observations computing the vehicle position and velocity vector. The problems of navigation in cislunar space, discussed in this section, are greater than those encountered in earth orbit since vehicle trajectories far from earth are significantly influenced by the lunar gravitational attraction, since trajectory sensitivities (the partial derivatives of trajectory parameters with respect to initial conditions) increase drastically, and because of uncertainties in the force model and in the astronautical constants. Thus, some means must be developed to determine the vehicle trajectory in flight, or the deviation of the actual trajectory from the nominal trajectory. The procedure used to determine the new trajectory is referred to as the navigation technique. The observations fundamental to a particular technique may be made from the spacecraft itself, from tracking stations on the earth, or from the lunar surface. A number of feasible navigation techniques for cislunar space can be devised if the methods for making the necessary navigational observations are available. The techniques discussed in this section include navigation by means of nominal or precomputed trajectories and trajectories computed in flight. A third technique, described as a "homing" technique (Ref. 1) utilizes line-of-sight orientation to ensure interception with the target. However, this technique has not yet been adequately proven for lunar missions, so it will not be discussed further.

The question remains of what to do when the deviation of the actual from the nominal trajectory has been determined, that is, how to return to the original trajectory or correct the actual trajectory in order to fulfill the mission. These midcourse guidance and energy requirements will be discussed in Section C.

1. Navigational Techniques

a. Observational considerations

Before discussing the details of various navigational techniques, it is necessary to decide what observations are to be made and how they are to be used in order to provide an improved estimate of position and velocity. Battin, in Ref. 2, has developed a procedure for statistically optimizing navigation for space flight. The detailed analysis will not be presented here, but a short account is given to emphasize the necessity of such a procedure.

In a typical self-contained space navigation system, observational data is gathered and processed to produce estimated velocity corrections by rocket burning (i.e., guidance corrections). Observational data may be gathered either by optical means or by radio. Fundamental to the navigation system is a procedure for processing observations which permits incorporation of each individual observation as it is made to provide an improved estimate of position and velocity. In order to optimize a navigation technique a number of alternate courses of action must be evaluated. The various alternatives, which form the basis of a decision process, concern the following:

- (1) Which navigational observation gives the most accurate position?
- (2) Does the best observation give a sufficient reduction in the predicted target error to warrant making the observation?
- (3) Is the uncertainty in the indicated guidance correction a small enough percentage of the correction itself to justify an engine restart and propellant expenditure?

The time interval from injection to arrival time at the aim point (near or on the moon) can be considered to be subdivided into a number of smaller intervals t₁, t₂, ... called "decision points." At each decision point one of three possible courses of action is followed: (1) a single observation is made; (2) a velocity correction is implemented; or (3) no action is taken. As a necessary step in the application of navigation schemes, certain rules must be adopted for the course of action to be taken at each "decision point." The number and frequency of observations must be controlled in some manner -- ideally by a decision rule which is realistically compatible with both the mission objectives and the capabilities of the observing device. If an observation is to be made, a decision is required regarding the type and the celestial objects to be used. Periodic guidance corrections must be applied and the number of impulses and times of occurrence must be decided.

Once the decision rules have been specified, it is necessary to test their effectiveness with some measure of performance. One typical objective is to minimize the miss distance at the moon. However, a reduction in miss distance

usually implies an increase in either the required number of observations or a greater expenditure of corrective propulsion--or both. This fact is demonstrated in Section C. In the face of conflicting objectives, present in any technique, compromises are clearly necessary, and a statistical simulation helps in arriving at an acceptable balance.

A common assumption is that secondary effects arising from the finite speed of light, the finite distance of stars, etc., are ignored in the observations. For the calculations, these effects at a particular reference point on the trajectory may be lumped together as a modification to the stored data which represents nominal reference values for the quantities to be observed at that point. Also, the question of simultaneous observations does not arise if the vehicle dynamics are governed by known laws and if deviations from a predetermined reference trajectory are kept sufficiently small to permit a linearization by expanding around the nominal trajectory point in a Taylor series and neglecting second and higherorder terms.

The essential problem is to select those observations which are, in some sense, most effective. For example, the requirement might be to make the selected observation at a certain time in order to get the maximum reduction in mean-squared positional or velocity uncertainty at that time. Of perhaps greater significance would be the requirement to select the observation which minimizes the uncertainty in any linear combination of position and velocity deviations. Specifically, one might select the observation which minimizes the uncertainty in the required velocity correction. As a further example, one might wish to select that observation which, if followed immediately by a velocity correction, would result in the smallest position error at the target or aim point.

The common methods for making navigational observations may be subdivided into three principal areas:

- Optical observation of the angles between several celestial bodies as seen from the vehicle.
- (2) Radio or optical tracking from the earth by determining the azimuth and elevation of the space vehicle.
- (3) Radio range (interferometer) and doppler measurements on the vehicle, the earth, or the moon.

Methods (2) and (3) will not be discussed since they are treated in Chapter XI of Ref. 1. However, a brief remark on the interferometer method of tracking and navigation will be made. For lunar flights it is possible to use the earth-moon separation as an interferometric baseline (Ref. 3). If a receiver could be established on the moon or at the libration points, it could easily be synchronized with a series of such stations on the rotating earth by means of line-of-sight communications. In this case the interferometer scheme illustrated in Chapter X of Ref. 1, where two transmitters are used at the ends of the baseline, operates in re-

verse. The phases of the transmitted waves are compared in the vehicle and the radio range from the vehicle to the stations can be determined. If each vehicle can carry sufficient computing equipment to transform and act on the received phase difference data, any number of vehicles can track themselves simultaneously from the same ground system. This system is similar to the hyperbolic LORAN navigation scheme now widely used by aircraft and ships.

The emphasis in this subsection will be on method (1)--angular observations of celestial bodies from the vehicle by optical methods. This technique will be most useful in early lunar flights since it has been proposed that navigation on manned lunar missions be handled by the crew and self-contained optical units be used for unmanned missions. Two types of measurements, one for small angles and one for large angles, will be described

Small angles, i.e., those less than a few degrees, may be measured within the field of view of an astronomical telescope. This type of measurement is particularly desirable for measuring the apparent diameter of the sun, earth or moon and the position of these bodies against their neighboring stellar background. The observations may be made directly, or the telescope may be used to photograph the sun, and/or moon and/or planets against the star background (Ref. 4). In the latter case the photographic plates could be read with an optical micrometer after developing. The photographic method has the advantage of "freezing" time, thus permitting a leisurely measurement of what was visible at a single instant. The technique requires local filtering to reduce the exposure of the image of the sun, moon or planet relative to the stellar background. It is presently used for determining the lunar ephemeris from the earth, yielding accuracies on the order of 0.01. These accuracies, of course, can not be expected from space vehicle observations. The photographic method requires a plate-reading micrometer; however, on a manned voyage it is very likely that an astronomical telescope and plate-handling equipment are on board for other than navigational purposes.

Large angles as well as small ones can be measured by a type of sextant which may be either hand-held or mounted in the vehicle. The sextant has several advantages over the telescope, notably:

- (1) Having separate light paths, a sextant requires no troublesome local filter; one light path or the other may be filtered as desired.
- (2) It measures large angles as well as small ones.
- (3) The optical requirements of a sextant's telescope are minimal, since the two objects whose separation is measured are brought into coincidence at a single point rather than being measured over an extended optical field.

Since a vehicle-borne sextant doesn't require manual support, it can be larger than a marine-

type sextant and can be equipped with a highmagnification telescope and a reading microscope for the vernier.

In a space vehicle, the optical system of such angular measuring instruments as sextants and star trackers have accuracies of the order of 0."1 to 1."0. However, the observational technique, reading errors, etc., permit practical accuracies of the order of only 10" for a single observation. This accuracy is quoted for a single observation of point sources such as stars; the tracking of extended images such as the earth and moon degrade, while the combination of a number of individual observations and their smoothing to determine a small vehicle trajectory arc enhance the practically achievable accuracy.

All optical observations are subject to planetary aberration due to the finite velocity of light and the relative motion of the observer and the celestial body. If a stationary telescope is pointed at a celestial body, it is pointing at the position where the celestial body was when the observed light left it rather than where it is when the light arrives at the space vehicle. These errors could be of the order of $10^{\rm m}$. The relative motion of the vehicle with respect to the observed object or stellar aberration causes celestial bodies to be displaced in the direction of the vehicle's velocity. This angular deviation, Δ , is given by the expression:

 $\Delta = \sin \phi \tan^{-1} \left(\frac{V_{\Delta}}{c} \right) \tag{5}$

where

φ = angle between the velocity vector and the line of sight to the observed object

 V_{Δ} = velocity of the space vehicle relative to the celestial body

c = velocity of light, 299,792.5 ± 0.1 km/ sec.

These errors are small and easy to correct because V_{Δ} /c is very small. For the worst case, ϕ = 90°, the deviation is about 20" for V_{Δ} = 29.8 km/sec.

Several types of navigational observations can be made from a space vehicle simultaneously in order to arrive at the best determination of position and velocity. For example: gyroscopic techniques can be used for angular measurements; accelerometers for measuring acceleration, primarily during rocket burning or near the moon and earth; radar techniques for velocity measurements; distance measurements from the apparent diameters of celestial bodies in the solar system; and time measurements from clocks and from the motion of celestial bodies in the solar system. These are all discussed extensively in Ref. 5.

b. Analysis of two navigational techniques

Two navigational techniques, referred to as technique 1 and technique 2, for determining spacecraft position by means of optical observa-

tions of celestial bodies will now be analyzed in detail. In technique 1 it is assumed that the nominal spacecraft position and velocity vectors are known so that perturbation methods may be employed in determining the actual position and velocity from the nominal. All measurements are assumed to be made at exact instants of time. Technique 2 on the other hand does not require a nominal trajectory, but the actual trajectory is determined directly from the observations. The same type of observation may be used in either navigational technique.

In technique 1, one type of observation to be considered is that of the angle A subtended at the space vehicle by the moon-earth line. By passing to the limit of infinite distance from either the earth or moon, corresponding angular measurements of the earth-star or moon-star line can be made. Referring to the sketch below, Δ and $\mathfrak q$ denote the nominal positions of the spacecraft and moon at the time of the measurement. Let $\overrightarrow{r}_{\bigoplus \Delta}$ be the vector from the earth \oplus to Δ and $\overrightarrow{r}_{\Delta}$ the vector from Δ to ℓ . With A denoting the angle at the space vehicle from the radius to the earth to the radius to the moon, we have

$$\cos A = -(\vec{r}_{\oplus \triangle} \cdot \vec{r}_{\triangle \emptyset})/r_{\oplus \triangle} r_{\triangle \emptyset}$$
 (6)

where $r_{\bigoplus \triangle}$ and $r_{\triangle \emptyset}$ denote magnitudes of the respective vectors $\overrightarrow{r_{\bigoplus \triangle}}$ and $\overrightarrow{r_{\triangle \emptyset}}$. Treating all changes as first order differentials, it can be shown that

$$\delta A = \left(\frac{\hat{n} - (\hat{n} \cdot \hat{n})\hat{n}}{r_{\oplus \Delta} \sin A} + \frac{\hat{n} \cdot - (\hat{n} \cdot \hat{n})}{r_{\Delta \ell} \sin A}\right) \delta \vec{r_{\oplus \Delta}}$$
(7)

where $\delta \vec{r}_{\ell} \Delta$ is the radius vector from the observed position to the nominal position of Δ with respect to earth, \hat{n} and \hat{m} are, respectively, the unit vectors from Δ toward θ and toward ℓ . Hence $\vec{r}_{\theta} \Delta = -r_{\theta} \Delta$ \hat{n} and $\vec{r}_{\Delta \ell} = r_{\Delta \ell}$ \hat{m} . The vector $\delta \vec{r}_{\theta} \Delta$ is small compared to $\vec{r}_{\theta} \Delta$. The two individual vector coefficients of $\delta \vec{r}_{\theta} \Delta$ in Eq (7) are vectors in the same plane in which the observation takes place and normal to the lines of sight to the earth and to the moon.

A second observation determines position by taking a stadiametric reading, or measuring the diameter of a celestial body. If D is the apparent diameter of the moon, the apparent angular diameter $2_{\rm V}$ is found from

$$\sin(\gamma) = D/2 r_{\wedge \alpha} \tag{8}$$

with the differential given by

$$\delta(2\gamma) = \frac{D \hat{m} \cdot \delta \vec{r}_{\oplus \Delta}}{(r_{\triangle I})^2 \cos(\gamma)}$$
 (9)

In technique 2, where the actual trajectory is computed without a nominal trajectory, this distance

measurement is usually used in conjunction with other measurements.

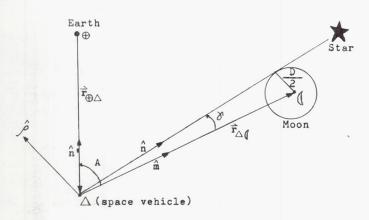
A third observation records the time of a stellar occultation by the moon. Let Δ and \emptyset be, respectively, the nominal positions of the space-craft and the moon at the time of observation, and let \hat{n} be a unit vector at the vehicle in the direction of the star occulted by the moon. With Y denoting the angle from the star radius to the moon radius as shown in the second sketch, we have, at the nominal instant of occultation,

$$\hat{\mathbf{n}} \cdot \hat{\mathbf{r}}_{\Delta \mathbf{I}} = \mathbf{r}_{\Delta \mathbf{I}} \cos \mathbf{Y} \tag{10}$$

Treating changes as first order differentials we obtain

$$\hat{\mathbf{n}} \cdot \delta \overrightarrow{\mathbf{r}}_{\Delta \mathbf{0}} = (\cos \gamma) \delta \mathbf{r}_{\Delta \mathbf{0}} - \mathbf{r}_{\Delta \mathbf{0}} \sin \gamma \delta \gamma$$

$$= (\cos \gamma) \hat{\mathbf{m}} \cdot \delta \overrightarrow{\mathbf{r}}_{\Delta \mathbf{0}} - \mathbf{r}_{\Delta \mathbf{0}} \sin \gamma \delta \gamma$$
(11)



The angular deviation δY is computed from a first order differential of 2 r $_{\Delta \sqrt{\!\!\!/}}$ sin Y = D:

$$\delta Y = -D \hat{m} \cdot \delta \vec{r}_{\Delta I} / 2 (r_{\Delta I})^2 \cos Y \qquad (12)$$

Furthermore, if $V_{\pmb{q}}$ and V_{Δ} are the respective inertial velocities of the moon and the spacecraft, and if δt is the difference between the observed and the nominal time of occultation, we have:

$$\delta \overrightarrow{r}_{\triangle \vec{Q}} = \overrightarrow{V}_{\vec{Q}} \quad \delta t - (\delta \overrightarrow{r}_{\bigoplus \triangle} + \overrightarrow{V}_{\triangle} \delta t)$$

$$= -\delta \overrightarrow{r}_{\bigoplus \triangle} - \overrightarrow{V}_{\vec{Q}} \triangle \delta t \qquad (13)$$

where $\widehat{\mathbb{V}}_{\P} \Delta$ is the velocity of the spacecraft relative to the moon. Then by combining Eqs (11), (12) and (13) we have finally:

$$\delta t = -\frac{\hat{\rho} \cdot \delta \vec{r}_{\oplus \Delta}}{\hat{\rho} \cdot \vec{V}_{\emptyset \Delta}}$$
 (14)

where $\hat{\rho}$ is a unit vector perpendicular to \hat{n} in the plane determined by the lines of sight to the moon and the star. The procedure could be reversed by considering star occultations by the earth.

Consider next the technique wherein the angle between the lines of sight to a star and the edge of the lunar disc is measured. From the sketch below.

$$\hat{\mathbf{n}} \cdot \hat{\mathbf{r}}_{\Delta \emptyset} = \mathbf{r}_{\Delta \emptyset} \cos (\mathbf{A}^* + \mathbf{Y}) \tag{15}$$

where A* is the angle to be measured. Taking total differentials and noting that $\delta \stackrel{r}{r}_{\oplus \Delta}$ = - & $\stackrel{r}{r}_{\Delta \emptyset}$, we obtain:

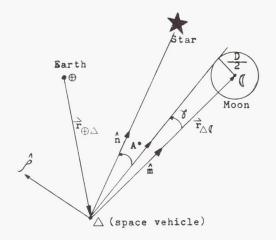
$$\frac{\rho \cdot \delta \overrightarrow{r_{\oplus \Delta}}}{r_{\Delta \mathbf{d}}} = \delta A^* + \delta Y$$

$$= \delta A^* + D \hat{\mathbf{m}} \cdot \delta \overrightarrow{r_{\oplus \Delta}} / 2 (r_{\Delta \mathbf{d}})^2 \cos Y$$

$$= \delta A^* + \tan Y \hat{\mathbf{m}} \cdot \delta \overrightarrow{r_{\oplus \Delta}} / r_{\Delta \mathbf{d}}$$
(16)

or finally:

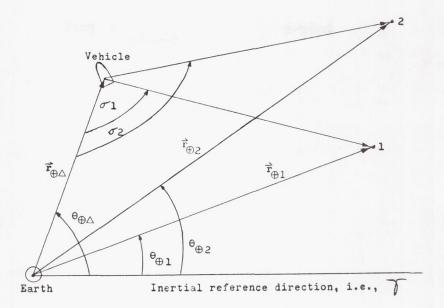
$$\delta A * = \frac{\rho \cdot \delta \overrightarrow{r}_{\bigoplus \Delta}}{r_{\Delta \emptyset} \cos \gamma} \tag{17}$$



For the measurement of the angle between a landmark on a planet or lunar surface and a star, let $\hat{\rho}$ be a unit vector perpendicular to the line of sight to the landmark and in the plane of measurement. Then if $\hat{\rho}$ is the vector position of the landmark relative to the center of the object, we have

$$\delta \mathbf{A} * = \frac{\hat{\rho} \cdot \delta \overrightarrow{\mathbf{r}}_{\bigoplus \Delta}}{\left| \overrightarrow{\mathbf{r}}_{\triangle \emptyset} + \overrightarrow{\rho} \right|}$$

Technique 2 does not use perturbations about a nominal trajectory, but angular measurements are converted directly to positional data. Optical instruments in the vehicle are used to establish bearing lines to point sources in the sky and the angles between the lines of sight are measured by a sextant. The conversion to positional information is illustrated in the following sketch, where the plane of the paper represents the plane of one set of two sextant readings. One bearing is assumed to be taken on the earth and the other sources, 1 and 2, are either stars, planets, or the moon. Define a nonrotating plane polar coordinate system $(r_{\bigoplus},\;\theta_{\bigoplus})$ with origin at the earth, in which the stars are assumed fixed. The unknown polar coordinates of the vehicle, $(r_{\bigoplus\Delta},$



 $\theta_{\bigoplus \Delta}$), can be expressed in terms of the measured angles σ_1 , σ_2 , $0^{\circ} \leq \sigma_1$, $\sigma_2 \leq 180^{\circ}$ and the known polar coordinates $(r_{\bigoplus 1}, \theta_{\bigoplus 1})$ and $(r_{\bigoplus 2}, \theta_{\bigoplus 2})$ of the sources 1 and 2, respectively, by use of trigonometry:

$$r_{\oplus \triangle} = \begin{bmatrix} r_{\oplus 1} & r_{\oplus 2} & \sin (\sigma_1 - \theta_{\oplus 1} - \sigma_2) \\ + & \theta_{\oplus 2} \end{bmatrix} \cdot \begin{bmatrix} (r_{\oplus 1})^2 & \sin^2 \sigma_2 + (r_{\oplus 2})^2 & \sin^2 \sigma_1 \\ - & 2 & r_{\oplus 2} & r_{\oplus 1} & \sin \sigma_1 & \sin \sigma_2 & \cos (\sigma_1 - \theta_{\oplus 1}) \\ - & \sigma_2 + & \theta_{\oplus 2} \end{bmatrix} \xrightarrow{-1/2}$$

$$r_{\oplus 1} & \sin \sigma_2 & \sin (\sigma_1 - \theta_{\oplus 1})$$

$$r_{\oplus 1} & \sin \sigma_2 & \sin (\sigma_1 - \theta_{\oplus 1})$$

$$r_{\oplus 2} & = \frac{-r_{\oplus 2} & \sin \sigma_1 & \sin (\sigma_2 - \theta_{\oplus 2})}{r_{\oplus 2} & \cos (\sigma_1 - \theta_{\oplus 2})}$$

$$\sin \theta_{\oplus 2} = \frac{-r_{\oplus 2} & \sin \sigma_1 & \sin (\sigma_2 - \theta_{\oplus 2})}{r_{\oplus 2} & \cos (\sigma_1 - \theta_{\oplus 2})}$$

$$(19)$$

$$\tan \theta_{\oplus \Delta} \approx \frac{-r_{\oplus 2} \sin \sigma_1 \sin (\sigma_2 - \theta_{\oplus 2})}{r_{\oplus 2} \sin \sigma_1 \cos (\sigma_2 - \theta_{\oplus 2})} - \sigma_1 \sin \sigma_2 \cos (\sigma_1 - \theta_{\oplus 1})$$
(19)

If source 1 is a distant star and source 2 represents the moon, these formulas simplify considerably, since $r_{\oplus 2}/r_{\oplus 1} \rightarrow 0$. Then

$$\mathbf{r}_{\oplus \Delta} = \mathbf{r}_{\oplus 2} \frac{\sin \left(\sigma_1 - \theta_{\oplus 1} - \sigma_2 + \theta_{\oplus 2}\right)}{\sin \sigma_2} \tag{20}$$

and

$$\theta_{\bigoplus \triangle} = \pi - \sigma_1 + \theta_{\bigoplus 1} \tag{21}$$

Differentials of Eqs (20) and (21) give an estimate of the errors induced in $r_{\bigoplus \Delta}$ and $\theta_{\bigoplus \Delta}$ by the measurement errors $\delta \sigma_1$ and $\delta \sigma_2$ and source position errors.

$$\delta r_{\oplus \triangle} = (\delta \sigma_1 + \delta \theta_{\oplus 2}) r_{\oplus 2} \frac{\cos (\sigma_1 - \theta_{\oplus 1} - \sigma_2 + \theta_{\oplus 2})}{\sin \sigma_2}$$

$$- \delta \sigma_2 r_{\oplus 2} \frac{\sin (\sigma_1 - \theta_{\oplus 1} + \theta_{\oplus 2})}{\sin^2 \sigma^2}$$

$$+ \delta r_{\oplus 2} \frac{\sin (\sigma_1 - \theta_{\oplus 1} - \sigma_2 + \theta_{\oplus 2})}{\sin \sigma_2}$$
(22)

$$\delta\theta_{\bigoplus \triangle} = -\delta\sigma_1 + \delta\theta_{\bigoplus 1} \tag{23}$$

The total effect of instrument and/or data errors in Eq (22) can be minimized by proper choice of sources 1 and 2. It is quite clear, for instance, that the cases σ_2 = 0, π , i.e., cases in which the moon, vehicle and earth are colinear, should be avoided. The simultaneous values σ_1 - $^\theta_{\bigoplus}1$ + $^\theta_{\bigoplus}2$ = 0, σ_2 = 90° reduce all errors but those for $\delta r_{\bigoplus}2$. Errors in the radial distance $r_{\bigoplus}\Delta$, $^\delta r_{\bigoplus}\Delta$, therefore determined primarily by the uncertainty in $r_{\bigoplus}2$, the distance of the moon from the earth.

If Eqs (22) and (23) are divided by dt, one obtains the time rates-of-change of $r_{\bigoplus \Delta}$ and $\theta_{\bigoplus \Delta}$:

$$\dot{\mathbf{r}}_{\oplus \Delta} = \dot{\boldsymbol{\sigma}}_{2} \frac{\sin \left(\sigma_{1} - \boldsymbol{\theta}_{\oplus 1} - \sigma_{2} + \boldsymbol{\theta}_{\oplus 2}\right)}{\sin \sigma_{2}} \\
+ \sigma_{2} \left[\left(\dot{\boldsymbol{\sigma}}_{1} + \dot{\boldsymbol{\theta}}_{\oplus 2}\right) \frac{\cos \left(\sigma_{1} - \boldsymbol{\theta}_{\oplus 1} - \sigma_{2} + \boldsymbol{\theta}_{\oplus 2}\right)}{\sin \sigma_{2}} \right] \\
- \dot{\boldsymbol{\sigma}}_{2} \frac{\sin \left(\sigma_{1} - \boldsymbol{\theta}_{\oplus 1} + \boldsymbol{\theta}_{\oplus 2}\right)}{\sin^{2} \sigma_{2}} \right] \tag{24}$$

$$\dot{\theta}_{\oplus \Delta} = -\dot{\sigma}_1 \tag{25}$$

The problem of obtaining these derivatives is discussed on p 21 of Ref. 3.

By combining the available observations and measurements, other approaches may be found through this technique. For instance, as an outgrowth of the above method, the position of a spacecraft in cislunar space may be determined by two stellar directions and a planetary source.

 Application of navigational technique 2 to lunar flight

The choice of stars and celestial bodies is of some importance if technique 2 is used for navigation in cislunar space. This aspect is discussed to some extent and illustrated by one example in the present subsection.

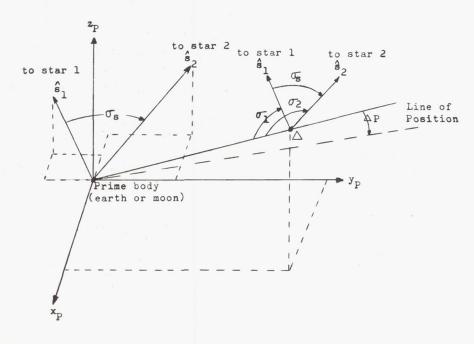
If the position of three bodies in space is known at a given time from calculated ephemerides, triangulation can be used to determine the position of the spacecraft at that time. In cislunar space one of the bodies will either be the earth or the moon, due to their proximity. The sun, any of the planets, and any of their moons suggest themselves for the other two celestial bodies. Unfortunately, these bodies cannot be used for lunar missions because of the inaccuracy developing from the large interplanetary distances as compared to the relatively small earth-moon distance. Therefore, the stars must be used.

It can be assumed with excellent accuracy that the stars are at an infinite distance from the earthmoon-spacecraft region. Hence the position of the stars is defined by their direction only and two stars and the earth or moon are not sufficient to determine the exact location of the spacecraft, but only a line of positions. The observation of the angle between one star and the prime body (earth or moon) from the spacecraft specifies its position as being on a cone with apex at the prime body (earth or moon), whose center line is directed toward the star, and

whose half-angle is given by the angle between the star and prime body. The additional observation of the angle between another star and the prime body specifies a second cone. The intersection between two cones with a common apex is specified by either one or two straight lines or no intersection occurs. However, since the spacecraft must be on the surface of both cones simultaneously, the last case is ruled out. If there is one line of intersection, which will be denoted "line of position, "then the spacecraft is known to be located somewhere on it. If there are two lines of intersection, then a proper choice of stars or a third angular measurement to get another star may settle on which line of position the vehicle is on. Approximate knowledge of the vehicle trajectory, of course, also determines the line of position. The location of the space vehicle on this line can be determined by stadiametric readings, a star occultation by a second prime body which may be another planet or the moon, by using another line of position determined from two stars and the second prime body, or by tracking from the earth or moon and subsequent data transmission to the spacecraft. The choice between these methods is dependent upon where the vehicle is relative to the earth or moon at the time.

In this navigation technique, it is important to know an optimum orientation of the two stars and the prime body chosen for observation in order to give the minimum error in the line of position due to errors in the two angular measurements. Another important question is whether the more prominent navigation stars can be used for position determination within an acceptable error, or if some of the less well-known stars have to be employed as well.

The geometry is illustrated in the following sketch. The origin of coordinates is at the center of the prime body, with Cartesian axes $x_p y_p z_p$ as shown. Vectors $\boldsymbol{\hat{s}}_1$ and $\boldsymbol{\hat{s}}_2$ are unit vectors in the direction of stars 1 and 2, $\boldsymbol{\sigma}_s$ is the angle between $\boldsymbol{\hat{s}}_1$ and $\boldsymbol{\hat{s}}_2$ which is known quite accurately



from the ephemeris, and the angles σ_1 and σ_2 are between the direction to the prime body and stars 1 and 2, respectively, $0^{\circ} \leq \sigma_1, \ \sigma_2 \leq 180^{\circ}$. The last two readings, made by the crew, establish the line of position.

The use of this navigation technique is illustrated below. The observational accuracy in the measurement of σ_1 and σ_2 is assumed at 6 ", and the worst possible combination of these two errors was used to define Δ P, the angular error in the line of position. Figure 1 shows the possible relationships between σ_1 and σ_2 which will result in ΔP = 0.006° or less for a star separation of σ_s = 60° in the case of the worst possible combination of errors in σ_1 and σ_2 . The line of position error (maximum) will be 0.006° on the boundary for the σ_1 and σ_2 combinations shown and will decrease as the σ_1 and σ_2 combinations move from the boundaries into the shaded area.

A natural goal is to choose stars which will keep the effect of reading errors to a minimum, but still make use of the more prominent navigation stars which have proved themselves to be easily identifiable over several centuries of naval navigation. With this in mind, the data presented in Fig. 2 is used in making the choice. The shaded areas shown represent the σ_1 and σ_2 combinations which will result in $\Delta P \leq 0.004^\circ$ for any σ_8 between 60° and 90°. For illustration, it can be seen that the range encompassed by σ_1 between 30° and 50° and σ_2 between 70° and 80° lies within the shaded area.

This data can be illustrated with an example using a circumlunar trajectory launched from Cape Canaveral on 14 June 1968 at 14:14 hr GMT. A view of the earth, as seen from the spacecraft three hours after injection into the translunar trajectory (a good time for first midcourse guidance corrections), is shown in Fig. 3 with the actual stellar background. The right side of the earth is illuminated by the sun, with Alaska and California appearing on the extreme right. The principal stellar constellations visible behind the earth are indicated on the figure. Using the earth's center as the celestial body, the σ_1 range (30° to 50°) and σ_2 range (70° to 80°) are shown traced on the celestial sphere. The required angular displacement between the two stars is 60° to 90° (shown on the bottom of the figure). Thus, star 1 must lie in the band labeled σ_1 range and star 2 in the band labeled σ_2 range. The distance between star 1 and star 2 must be 60° to 90°. Inspection of Fig. 3 shows many such separations between the prominent navigation stars. The spacecraft 3 hr after injection is typically 50,000 km from the earth, and an angular error of $\Delta P = 0.006^{\circ}$ corresponds to a position error of 5 km in the line of position.

Figures similar to Fig. 3 can be prepared for various times throughout the lunar mission. In the case of the illustrated circumlunar trajectory, figures for a later time will differ from Fig. 3 by a decreasing size of the earth and the earth's displacement due to its motion toward the upper left. When the vehicle approaches the moon, the moon with its star background can be used for navigation.

The main advantages of this navigational technique are:

- Observations can be planned well ahead of the mission on the ground.
- (2) In many cases the same pair of stars can be used for observations over long periods of time.
- (3) Observational errors can be minimized by proper choice of stars for navigation.
- (4) The time for navigational observations can be minimized.

The last point is important, as two observations must be made from the spacecraft for determining the line of position, and in the very early stages of lunar flight, the trajectory curves strongly (see Fig. 1 in Chapter IV), and the direction of the line of position changes relatively rapidly. This suggests that this navigational technique will yield better results farther from the prime body than in its immediate vicinity, and that it is not suitable for space vehicles in near-earth or near-moon orbits.

d. Concluding remarks

The problems of navigation are not completely solved even when position and velocity data are obtained and decision rules are applied. There still remains the problem of reducing this data to useful applications in corrections. For the case of smoothing and data reduction, reference can be made to Chapter XI of Ref. 1, while the differential correction technique is treated in Chapter VI of the same reference.

All navigational techniques mentioned have stringent data-processing requirements. Equations must be solved rapidly and accurately in order to support each technique.

The data processing could in principle be performed by analog computers, digital computers, or digital differential analyzers. Considerations of weight, volume, accuracy, and programming flexibility, however, preclude the use of the analog computer alone. For this reason, a navigational system must rely on digital data processors. The best compromise would appear to be a general-purpose digital computer capable of incremental computation for certain portions of the navigational problem. The mission duration anticipated for lunar flights requires a reliability sufficient for at least intermittent operation over long periods of time with a minimum of maintenance. Thus, the volume, weight, and secondary power available for the computer will necessarily be limited.

2. Tracking and Communications for Lunar Missions

The above discussion of navigation techniques illustrated the possibility of a vehicle in cislunar space performing the required navigational tasks independently of earth-based sensors. However, it remains extremely unlikely that ground monitoring, control, or coordination of a lunar mission for navigational or communication purposes will be dispensed with. This being the case, tracking of the spacecraft becomes a requirement for both manned and unmanned lunar missions. This subsection provides a qualitative description of tracking requirements for a typical lunar mission.

Since these requirements vary widely with the operational concept, a set of practical ground rules is needed. The following rules, illustrative of a typical lunar mission, have been established for the qualitative discussion of tracking:

- (1) Launch is planned from Cape Canaveral, in anticipation that the majority of lunar missions will originate there.
- (2) The launch azimuth $A_{\rm e}$ is restricted to between 70° and 110°, which is considered practical for the existing tracking facilities, range safety and launch tolerance requirements (see Chapter V).
- (3) Parking orbits are permissible.
- (4) The launch frequency must be twice a day.
- (5) The return or re-entry (if applicable) is adequately tracked.

Detailed quantitative tracking data for a given set of ground rules is usually obtained as a by-product of the trajectory calculation.

The first three ground rules are effectively illustrated by Figs. 4 and 5, which show typical ground traces of circumlunar missions launched from Cape Canaveral for a southerly and northerly lunar declination. With regard to the fourth ground rule, a launch frequency of twice a day can only be realized if injection into the translunar trajectory is allowed to take place in either a southerly direction along the Atlantic Missile Range (AMR) area or in a northerly direction along the Pacific Missile Range (PMR) area. Figures 4 and 5 show how the ground trace corresponding to a particular lunar trajectory with a specified launch azimuth is replaced by a ground swath corresponding to the band of possible launch azimuths. These ground swaths cover a large part of AMR and PMR. Since launch tracking facilities must be provided in these areas, it can be assumed that re-entry (for circumlunar missions) also occurs there. In fact, for the ground swaths in Figs. 4 and 5, re-entry occurs along PMR and the landings in the western part of the U.S.

Lunar missions are similar to earth orbital missions in many respects, and therefore, present Project Mercury techniques developed for tracking and communications can readily be used.

As mentioned previously, a logical assumption is that the overall coordination of the lunar mission will still be exercised by a ground control center. This control center will receive selected information concerning mission progress from the remote WTCN (Worldwide Tracking and Communications Network) stations during all phases of the mission and it uses this information to coordinate decisions and to advise and assist the vehicle if manned. Computational support for this control center is assumed to be provided by a computations and communications switching center (CCSC) such as exists at the Goddard Space Flight Center in Greenbelt, Maryland.

The CCSC computer determines trajectory parameters and steering corrections for normal or aborted missions and predicts the earth or lunar landing areas if applicable. WTCN stations exist at AMR and PMR in the Mercury Network, and as part of the DSIF (Deep Space Instrumentation Facilities). In addition, facilities are currently being planned for a primary landing site in southern Texas. An up-to-date list of the WTCN tracking facilities, their locations and a brief description is given in Chapter XI of Ref. 1.

In order to obtain an idea of tracking and communication requirements, a lunar mission is divided into several phases, as depicted in Figs. 4 and 5, and the requirements of each flight phase are briefly discussed.

During the launch phase and under direction of the ground control center, the CCSC computer predicts the boost phase trajectory, computes the look angles for the downrange radars, and transmits this data to the corresponding WTCN stations for use in vehicle acquisition. The vehicle boost phase is for the most part along the Project Mercury orbital mission range. These facilities are presently adequate to provide continuous tracking as well as voice and telemetry communications with the vehicle during the powered flight periods. Telemetry information is continuously collected at the ground stations with sufficient redundancy to minimize loss of data and obtain a smoothed trajectory from the many individual and overdetermining tracking observations. The ground control center also affirms the necessity for aborting the mission and in the case of an abort alerts the recovery forces for a manned mission. Injection into the parking orbit always takes place over an instrumented portion of the AMR, as the ascent range of "boosters" is small compared with the length of the AMR.

After parking orbit injection, the spacecraft waits for the proper moment to be injected into the translunar trajectory. For a northerly injection along PMR, this injection area varies from the vicinity of Australia to Hawaii. The actual injection point varies with the time of month and the launch time. To provide continuous tracking and monitoring during injection, it is very likely that additional tracking ships will be required to supplement the fixed site coverage along the PMR. The exact number will depend on launch azimuth variation, on injection requirements during the lunar month, on the operational concept and on the mobility of the tracking ships. If southerly injection along AMR is specified,

the same Project Mercury tracking range can be utilized. However, additional recovery forces may be required for manned missions in the event of an abort. It is also possible that additional tracking ships may be needed in this area, especially if the variable launch azimuth technique is used (see Chapter V).

Once the vehicle is injected into the translunar trajectory, its ground trace has the same general characteristics as indicated in Figs. 4 and 5. A very interesting feature of translunar and transearth trajectories is that for most of the mission, the ground trace will lie in a narrow band of almost constant latitude. This band will shift in latitude according to the time of month. In the above-mentioned figures, the maximum shift is from +35° latitude (northerly declination) to -35° latitude (southerly declination) under the present ground rules. This permits an easy plotting of the ground trace on maps using the Mercator projection. Another important and interesting characteristic of translunar and transearth trajectories is the "doubling back" or reversal of their ground traces. This characteristic is clearly shown in Figs. 4 and 5 and occurs within a few hours after injection and before re-entry. The reversal of the ground trace is due to the decrease of the angular velocity of the space vehicle with respect to the earth as it recedes from the earth (see Fig. 1 of Chapter IV), while the rotational rate of the earth about its axis remains constant. This becomes an advantage because the spacecraft will be overhead for a few hours when its angular velocity and the rotational rate of the earth are nearly the same, enabling continuous tracking at that time, which results in the determination of precise trajectory parameters.

During the translunar and transearth trajectory phases, the spacecraft is under continuous coverage by DSIF stations. They acquire and retain coverage from shortly after injection into a lunar trajectory until it returns to the vicinity of the earth (for a circumlunar trajectory) except for times when the vehicle is in the shadow of the moon. DSIF station coverage consists of two-way voice communications, telemetry and tracking, resulting in a steady updating of data and practically uninterrupted monitoring of mission progress. The ground control center, in turn, can refine the vehicle trajectory information and so inform a manned vehicle. Along the translunar and transearth trajectories, the CCSC computers systematically calculate and extrapolate the trajectory, and derive midcourse corrections. For a manned mission, these corrections are transmitted to the vehicle over a voice link for comparison with onboard navigational data. The onboard observations may provide the primary means of navigation, with ground-derived data providing redundancy, or vice-versa.

Since circumlunar and other lunar missions may involve passing behind the moon, and since the altitude and the predicted pericynthion point may be more accurately determined onboard than on the ground, data can be telemetered to earth just prior to occultation of the vehicle by the moon to permit ground computation of the trajectory so that the DSIF stations can reacquire

the spacecraft when line of sight is re-established. Likewise, during lunar orbits, vehicle sensors gather lunar data continuously, store the data while behind the moon, and transmit when visible to DSIF stations. On the transearth trajectory, DSIF stations again continuously cover the vehicle, receive any backlog of telemetry data, and provide the CCSC computers with trajectory data and voice reports in case of an unmanned mission for comparison. Final course corrections will be made after tracking data from earth tracking facilities refine the computer predictions, and ground-derived data and corrections are transmitted to the vehicle.

For the case of a manned lunar landing, continuous telemetry information from the lunar investigations and, very likely, television pictures will be transmitted to earth. Positional data collected during the lunar stay will allow the CCSC computer to provide information via DSIF voice link for comparison with the onboard navigation system. Earth computation may be either a primary or a supplementary source of data during the lunar takeoff and transearth trajectory injections.

Since there is an obvious operational advantage in having all manned lunar missions re-entering over the same ground facilities, it is desirable that the re-entry phase of the transearth flight occur either in a northerly direction along PMR or in a southerly direction along AMR. In this case, AMR and PMR tracking stations, the southern USA tracking stations, and backup and alternate landing sites along the AMR and the PMR can be used. There should also be provisions for emergency takeoffs or aborts from the lunar surface with safe returns to earth, which could be made at any time. As in the case of lunar injection, ships may be required along the PMR to provide continuous tracking during re-entry. The ship locations for any given day are again determined by variations of the ground swath over the lunar month and the mobility of the tracking ships.

C. MIDCOURSE GUIDANCE AND ENERGY REQUIREMENTS

Sections A of this chapter and of Chapter IX give the required injection conditions near earth for lunar missions. A translunar trajectory injection is specified by particular values of time, V_0 , γ_0 , h_0 , ψ_0 and i_{VTL} as defined in Section A above. But these nominal conditions cannot be achieved exactly because of injection guidance, navigation errors, and off-nominal booster performance. Therefore the actual translunar trajectory, as determined by the various navigation techniques, in all probability deviates from the desired or nominal trajectory, and thus may not satisfy the specific mission requirements. Hence, it becomes necessary that once or even several times during the flight to the moon, corrections be made to re-establish a trajectory that satisfies mission objectives. These corrections, more commonly called "midcourse guidance corrections," take the form of thrust impulses that adjust the actual or "errant" trajectory. Navigational observations and techniques as well as tracking and command from earth then serve as inputs which,

together with trajectory calculations, determine the magnitude and direction of the midcourse guidance correction.

In a general sense, there are two guidance concepts which can be used to correct the translunar trajectory:

- (1) Correct the errant trajectory to the aim point, which may be the nominal pericynthion point at the nominal pericynthion time, or correct the errant trajectory to some other pericynthion point and time in the case of approach and circumlunar trajectories. For lunar impact trajectories, the aim point is at a specified distance in front of the moon, such as entry into the lunar volume of influence. This may be regarded as an explicit guidance scheme.
- (2) Correct the errant trajectory back to the nominal trajectory (in position, velocity and time) some time prior to reaching the moon. This may be regarded as an implicit scheme.

The relative merits of these concepts are discussed below, together with some numerical data which was generated using a restricted three-body force model with the moon in a circular orbit at a radius of 60.32 earth radii except where noted otherwise.

1. Methods for Determining Midcourse Corrections

The problem of midcourse guidance is to compute the exact space vehicle velocity in an n-body force model (which for most cases of ballistic flight is sufficiently close to the actual trajectory as discussed in Section B, Chapter IV) for specified guidance objectives. Several approaches can be used, of which the following four are discussed below:

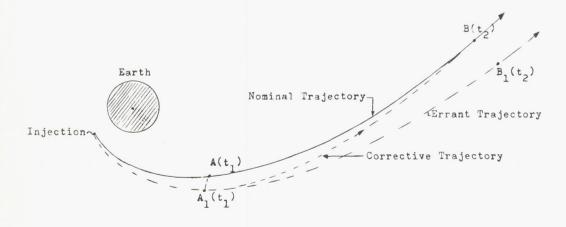
- (1) A linear differential correction scheme utilizing a nominal trajectory and precomputed trajectory sensitivities which are assumed to be constant.
- (2) A linear differential correction scheme utilizing trajectory sensitivities computed after launch (either on-board or on the ground).

- (3) A corrective trajectory technique which designs a new trajectory that satisfies mission specifications by means of the same method used to design the nominal trajectory.
- (4) A virtual mass technique utilizing two-body equations.

The first two methods involve the use of trajectory sensitivities. They are obtained by linearizing the nonlinear equations of motion by expanding in a Taylor series about a point of the trajectory and neglecting all but the zeroth and first order term. The coefficients of the first order term, which are the partial derivatives of trajectory parameters with respect to some such independent parameters as initial conditions, astronautical constants or time, are called trajectory sensitivities.

The first and best-known method used for determining the magnitude and direction of the midcourse correction is a linear differential correction scheme. In this scheme, a nominal translunar trajectory is assumed to satisfy all mission requirements, which in the case of a circumlunar trajectory consist of translunar inclination \mathbf{i}_{VTL} , pericynthion altitude \mathbf{h}_{PL} , inclination and orientation (\mathbf{i}_{m} , θ_{M}) of the orbit about the moon, and the transearth inclination \mathbf{i}_{VTE} . Due to injection errors, however, the actual trajectory will be displaced from the nominal, as shown below.

It is also assumed that the errant trajectory has been adequately determined by navigation or tracking before the point \mathbf{A}_1 is reached. The point \mathbf{A}_1 corresponds to a time \mathbf{t}_1 , after injection, when the midcourse correction is applied. Point A is the corresponding point on the nominal trajectory at time \mathbf{t}_1 with B and \mathbf{B}_1 being the points on the nominal and errant trajectory, respectively, at a time \mathbf{t}_2 , when it is desired to again "match" or intersect the nominal trajectory by a corrective trajectory. Since the errant trajectory is known prior to \mathbf{t}_1 through tracking and celestial navigation, the generalized position and velocity coordinates of the errant trajectory \mathbf{q}_B $\dot{\mathbf{q}}_B$ can be predicted at time \mathbf{t}_2 . These coordinates are then



compared to those of the nominal trajectory at point B and the differences Δq_B , $\Delta \dot{q}_B$ are obtained.

A first approach to defining the magnitude and direction of the midcourse direction involves the determination of the change in position and velocity components of the nominal trajectory as a result of characteristic velocity perturbations $\Delta\dot{q}_A$ at point A by means of integrated trajectories using a three-body force model. These partial derivatives $\left(\frac{\partial q_B}{\partial \dot{q}_A}\right,\frac{\partial \dot{q}_B}{\partial \dot{q}_A}\right)$ are the trajectory sensitivites

and are used in the following fashion to define the midcourse correction $\Delta \dot{q}_{i,\Delta}$:

$$\Delta q_{jB} = \sum_{i=1}^{n} \frac{\partial q_{jB}}{\partial \dot{q}_{iA}} \quad \Delta \dot{q}_{iA} \quad j = 1, 2, ..., m$$

$$\Delta \dot{q}_{jB} = \sum_{i=1}^{n} \frac{\partial \dot{q}_{jB}}{\partial \dot{q}_{iA}} \quad \Delta \dot{q}_{iA} \quad j = 1, 2, ..., m$$
(26)

where j and i are integers denoting the coordinate directions. For the rotating rectangular coordinate system \mathbf{x}_{R} \mathbf{y}_{R} \mathbf{z}_{R} of the restricted 3-body problem discussed in Subsection B-2 of Chapter III, Eq (26) take the form:

$$\Delta_{x_{RB}} = \frac{\partial x_{RB}}{\partial \dot{x}_{RA}} \Delta \dot{x}_{RA} + \frac{\partial x_{RB}}{\partial \dot{y}_{RA}} \Delta \dot{y}_{RA}$$

$$+ \frac{\partial x_{RB}}{\partial \dot{z}_{RA}} \Delta \dot{z}_{RA}$$

$$\Delta_{y_{RB}} = \frac{\partial y_{RB}}{\partial \dot{x}_{RA}} \Delta \dot{x}_{RA} + \frac{\partial y_{RB}}{\partial \dot{y}_{RA}} \Delta \dot{y}_{RA}$$

$$+ \frac{\partial y_{RB}}{\partial \dot{z}_{RA}} \Delta \dot{z}_{RA}$$

$$+ \frac{\partial y_{RB}}{\partial \dot{z}_{RA}} \Delta \dot{z}_{RA}$$

$$\Delta_{z_{RB}} = \frac{\partial z_{RB}}{\partial \dot{x}_{RA}} \Delta \dot{x}_{RA} + \frac{\partial z_{RB}}{\partial \dot{y}_{RA}} \Delta \dot{y}_{RA}$$

$$\Delta_{z_{RB}} = \frac{\partial z_{RB}}{\partial \dot{z}_{RA}} \Delta \dot{x}_{RA}$$

$$\Delta_{z_{RB}} \Delta \dot{z}_{RA}$$

In these three equations: the sensitivities $\frac{\partial x_{RB}}{\partial \dot{x}_{RA}}$,

etc., are known from the ground-computed trajectories; the errors in position at the aim point, Δx_{RB} , etc., are known from the trajectory prediction; and the required midcourse correction at A $(\Delta \dot{x}_{RA}, \ \Delta \dot{y}_{RA}, \ \Delta \dot{z}_{RA})$ can be obtained. Application of the midcourse correction at A_1

results in a corrective trajectory which arrives at the aim point B with a velocity $\dot{q}_{jB}+\dot{\Delta}\dot{q}_{jB}$ with components $(\dot{x}_{RB}+\dot{\Delta}\dot{x}_{RB},\dot{y}_{RB}+\dot{\Delta}\dot{y}_{RB},\dot{z}_{RB}+\dot{\Delta}\dot{z}_{RB})$. This velocity is not necessarily equal to the nominal trajectory velocity $(\dot{q}_j)_{nominal}$ If it is desired to match the trajectory in velocity as well as position at B, the midcourse correction at B is given by $\left[\dot{q}_j \right]_{nominal} - \left(\dot{q}_{jB} + \dot{\Delta}\dot{q}_{jB} \right) .$

The above approach tacitly assumes that the position errors at injection (not shown on the preceding sketch) are so small that they do not influence trajectory sensitivities and that the trajectory sensitivities at A are very nearly the same as those at \mathbf{A}_1 and therefore can be computed on the ground before the mission. This assumption has been validated by numerical integration for expected small errors at injection. Numerical data embodying the linear differential correction scheme is presented in the next subsection.

The second approach does not make this assumption, and, therefore, sensitivities are computed while in flight for the midcourse correction point A₁ after the parameters of the errant trajectory have been determined by navigation and tracking. In both approaches trajectory sensitivities are obtained through the generation of integrated trajectories whose initial conditions are the slightly perturbed nominal conditions at t₁. This fact has led to the almost universal acceptance of the idea that a capability for numerically integrating the n-body equations, or at least the 3-body equations for lunar trajectories (Chapter IV), is required from a guidance computer in the space vehicle if the second approach is used.

A third method which may also be employed, consists of designing an entirely new corrective trajectory in the same manner as the nominal trajectory was designed to satisfy the mission constraints. This new corrective trajectory intersects the errant trajectory at point A_1 , and it can be computed between injection and time t_2 by use of a perturbative scheme or an iterative scheme using a combination of n-body trajectories and the Voice technique. The midcourse correction is found very easily by determining the magnitude of ΔV_p and its direction necessary to reorient the errant velocity vector at A_1 to the corrective trajectory velocity vector at the same point.

A midcourse guidance scheme for cislunar space has been developed which would alleviate the demands for computers in the space vehicle (Ref. 6). The scheme uses modified 2-body trajectories to simulate n-body velocities by introduction of a

virtual mass into the earth-moon system which changes the earth's mass and relocates the barycenter. The use of the simple and inaccurate 2-body equations paradoxically permits an operational flexibility which cannot be attained so easily by numerically integrated 3-body and n-body trajectories due to the extreme sensitivity of trajectories to initial conditions.

The virtual mass technique essentially depends upon computing 2-body trajectories relative to a force center defined by the combined earth and virtual mass. The location of this force center is selected so that the plane, defined by the force center and points A and B, coincides with the initial n-body trajectory plane at A (as defined by the radius and velocity vectors relative to the force center). This force center is on the earth-moon line and lies between the center of the earth and the earthmoon barycenter. It represents an origin which defines the location for a Keplerian central mass that properly accounts for the out-ofplane distortion (drift) of the true trajectory (Chapter IV, Subsection A-8). The magnitude of the mass, or the strength of the central force field, must be adjusted so that the position and velocity at t1, corresponding to measurement from the force, define a trajectory which in fact passes through the aim point B. This technique of "biasing" the gravitational constant to account for the in-plane and out-of-plane distortion of course means that the flight time will differ from the actual time and must itself also be biased.

Thus, by knowing the position and velocity components of point B at to in this biased reference frame, the velocity vector required at A, to intercept B can be found by 2-body equations. This velocity vector is then compared to the actual velocity vector at A, and the direction and magnitude of the midcourse ΔV_{p} can be readily obtained. Preliminary analyses indicate that this biasing is independent of iVTL. A compact catalogue of virtual masses (location and magnitude) and time biases as a function of the time of the month can be prepared in advance for use during the mission. The virtual mass approach is a welcome step toward simplicity in determining guidance corrections and can be used as the primary method or as a manual backup for lunar missions.

2. Guidance Concepts

a. Guidance concept 1

Guidance concept 1 consists of correcting the errant trajectory to the nominal pericynthion point at the nominal pericynthion time—or correcting the errant trajectory to some other pericynthion point and time.

This concept suggests the use of the pericynthion position at t₂ as an aim point, which appears desirable since full advantage is taken of the focusing effect of the moon (Chapter IV, Subsection A-8). However, consideration must be given to the direction of flight at the peri-

cynthion point as well. Discussion of this facet of the problem is simplified if reference is made to the geometry of the lunar approach trajectory and the resulting lunar orbit as shown by the sketch in Section A page 4 of this chapter. The sketch shows the moon, the direction to earth (MEL) when the spacecraft reaches pericynthion, and the resultant lunar orbit if the spacecraft were injected into orbit at pericynthion with a retarding velocity impulse $\triangle V$. The orientation of the resultant lunar orbit is specified by the inclination i_m to the moon's orbital plane and the angle θ_M between the earth-moon line and the descending node. The pericynthion point is specified by $\beta_{\rm M}$, which is the orbital central angle measured positively toward the north from the descending node of the lunar orbit.

The nominal translunar trajectory will have a specific i_{m} , θ_{M} , and β_{M} associated with it. A single midcourse correction to an errant trajectory (a t_1 = 3 hr after injection, for instance) cannot result in arrival at the moon with the same im, $^{ heta}_{ ext{M}}$, and $^{ heta}_{ ext{M}}$. Any single impulse technique can be expected to fix one of the quantities, but not all three. The guidance concept under consideration fixes the pericynthion point. The resultant $i_{\, \rm m}$ and $\theta_{\, \rm M}$ cannot be matched without the addition of another velocity impulse at pericynthion. Yet, the correct i_m and θ_M is necessary. If the mission is circumlunar, an error in any of the re quired characteristics will result in an error in both vacuum perigee altitude and transearth trajectory inclination $i_{\ensuremath{\mathrm{VTE}}}$ at vacuum perigee. The total mission flight time will also be affected. If it is a lunar orbit mission, the desired lunar orbit would not be attained. This has more serious implications than the immediate situation mentioned. If it were a lunar landing mission, the resultant orbit would not go over the desired landing site. For illustrative purposes a completely ballistic circumlunar trajectory with i_{VTL} = 63.3°, h_{PL} = 463 km and $h_{\mathrm{PE}} = 45.720 \text{ km}$ is used.

 σ_{x} = 0.46 m/sec σ_{y} = 0.34 m/sec σ_{z} = 2.4 m/sec

These errors are used for the remainder of the discussion and are combined in various ways to yield a total velocity error, at injection, with a 99% probability. In this example the total injection velocity errors in the rotating trajectory coordinate system $\mathbf{x}_R\,\mathbf{y}_R\,\mathbf{z}_R$ become

 $\Delta \dot{x}_{R} = 1.18 \text{ m/sec}$

 $\Delta \dot{y}_{R} = 0 \text{ m/sec}$

 $\Delta \dot{z}_R = 5.23 \text{ m/sec}$

which are the same as those used in the third sketch below.

Trajectory sensitivities are determined for t_1 = 3 hr and the first adjustment method is used to calculate that a midcourse correction $^{\Delta}V_p$ = 7.3 m/sec is required to correct to the nominal pericynfhion point and time. The second correction, to reorient the velocity vector along the nominal trajectory, was $^{\Delta}V_v$ = 13.7 m/sec at pericynthion, and the total required $^{\Delta}V_{TOT}$ = 21.0 m/sec.

A feature of this concept which is somewhat expensive in fuel is the reorientation of the velocity vector to the desired direction at the aim point. This disadvantage can be eliminated, or almost eliminated, by changing the aim point to a new pericynthion position.

A large amount of data has been assembled in the present chapter and Chapter IX showing the relationships between the lunar orbit orientation (θ_{M} and i_{m}) and pericynthion point position β_{M} . The data are presented as a function of $i_{\mbox{VTL}}^{\mbox{\scriptsize M}}$ for approach trajectories (Chapter IX) and as a function of $\mathbf{i}_{\ensuremath{\mathrm{VTE}}}$ and $\mathbf{i}_{\ensuremath{\mathrm{VTL}}}$ for circumlunar trajectories which return to a specific vacuum perigee (Section A). A curve of required $\boldsymbol{\theta}_{M}$ versus \boldsymbol{i}_{m} can be determined as demonstrated in the sample mission I of Chapter XI (also Section A of Chapter XI). This data then fixes the $i_{
m VTE}$ for circumlunar flights and consequently β_{M} (see Section D Chapter XI). The required $\boldsymbol{\theta}_{\boldsymbol{M}}$ and $\boldsymbol{i}_{\boldsymbol{m}}$ curve can be obtained directly if a constant i_{VTE} is desired. Trajectories that do not return to a specific and safe vacuum perigee (Chapter IX) have a pericynthion position that varies with translunar flight time for a given $\boldsymbol{i}_m^{}$ - $\boldsymbol{\theta}_M^{}$ relationship. Thus, the corrected trajectory can be aimed at a new pericynthion point that satisfies the i_m - θ_M conditions. It must be remembered that, in general, a velocity correction is still required at this point.

This technique was used to correct the errant trajectory above. Again, midcourse corrections at 3 hr after injection were made along the velocity vector $\vec{V}_{\oplus \Delta}$, normal to the velocity vector in the plane of $\vec{r}_{\oplus \Delta}$ and $\vec{V}_{\oplus \Delta}$ (relative to earth) and a correction normal to this trajectory plane. These corrections will be referred to as $^{\Delta}V_{\oplus \Delta}$, $^{\Delta}Y$, and $^{\Delta}i$, respectively.

It was found that $^{\Delta}\mathrm{V}_{\bigoplus\Delta}$ changed h_{PL} efficiently, but not i_{m} or $^{\theta}\mathrm{M}$. On the other hand, $^{\Delta}\mathrm{Y}$ changed i_{m} and $^{\theta}\mathrm{M}$, but did not change h_{PL} effectively. The $^{\Delta}\mathrm{i}$ correction changed all of the pericynthion conditions, but not always in the correct directions or proportions. Therefore, a combination of $^{\Delta}\mathrm{V}_{\bigoplus\Delta}$ and $^{\Delta}\mathrm{Y}$ corrections was used in the midcourse maneuver, plus another correction at the new pericynthion point. The total velocity impulse required $^{\Delta}\mathrm{V}_{\mathrm{TOT}}$ was approximately 10.7 m/sec, compared to the 21.0 m/sec correction of the first approach above. Percentage-wise the differences in the two techniques may be large at times but in magnitude the differences may be wholly acceptable.

However, some difficulty may be encountered in determining the required midcourse maneuver. It has been shown analytically (Ref. 7) that the lunar miss distance or pericynthion is a linear function of the injection errors for an infinitesimal lunar mass (massless moon assumption). However, if the finite lunar mass is considered (patched conic or restricted 3-body technique), then the miss distance is related quadratically to the injection errors. It follows that for the linear trajectory sensitivities generated for conditions near the moon, a certain amount of cross-coupling in the sensitivities can be expected. This can be handled either by taking second-order terms in the Taylor series expansion or by repeated (and hopefully convergent) iteration by improved guesses at sensitivities. This cross coupling has indeed been noted in the above numerical example. The injection errors are large enough that the required midcourse correction was not readily obtained, in fact, a minimum of three iterations were required to obtain a satisfactory midcourse correction at the 3-hr point.

The following table shows a comparison between the linear differential correction scheme (methods one and two in Subsection C-1) and the third method for determining midcourse corrections in Subsection C-1, wherein a corrective trajectory is designed by use of the Voice technique (Chapter IV, Section C) and n-body force model trajectory calculations in conjunction determining the midcourse corrections. The trajectory under consideration is a circumlunar trajectory with the desired mission requirements noted in Table 3. The errant trajectory fulfills all the requirements satisfactorily except for the return vacuum perigee altitude. A hypothetical case is taken for which it is assumed that the midcourse correction takes place at the injection point. When the linear differential correction method without iterations was used, the obtained return perigee altitude was completely unacceptable and the pericynthion altitude was less satisfactory. However, use of the Voice technique and n-body trajectory calculations for obtaining the necessary correction, the resultant return perigee altitude becomes acceptable and all other mission parameters remain essentially the same. One trajectory can of course not be used as the basis of a final conclusion. However, together with the results of Egorov for impact trajectories (Ref. 7), the third method seems superior to the first two for the case of circumlunar trajectories,

TABLE 3

Comparison of Various Midcourse Guidance Schemes for a Typical Circumlunar Trajectory

Trajectory Variable	Mission Requirements	Errant Trajectory (n-body)	Corrected Trajectory (linear diff. correct.)	Corrected Trajectory (iteration with Voice) (n-body)
V ₀ (injection velocity) (m/sec)		10,963.736	10,963.756	10,963.786
γ ₀ (injection flight angle) (°)	2.668174	2.668174	2.668174	2.668174
h ₀ (injection altitude) (km)	182.88	182.88	182.88	182.88
ψ ₀ (injection position) (°)		13.9936314	13.1875706	13.1986777
iVE (translunar inclination) (°)	29.24953	29.384214	29.383332	29.382176
iVTEQ (transearth inclination)(°)	35.206	35.098407	35.566	35.386665
t _p (time to pericynthion) (hr)		73.734375	73.734	73.64034
T (total mission time) (hr)		147.101562	150	147.07816
h _{PL} (pericynthion altitude) (km)	185.0148	185.2000	173.1620	186.8668
h _{PE} (return vacuum perigee altitude) (km)	36.8061	215.4936	-1402.080	37.5
Φ* (moon lead angle) (°)		37.4512316	38.038309	38.0294507

when the trajectory passes from a earth-dominated gravitational field to a moon-dominated gravitational field and back again. It should be noted that the return vacuum perigee, i.e., when the vehicle passes through all three gravitational regions, is hardest to obtain by a linear differential correction scheme.

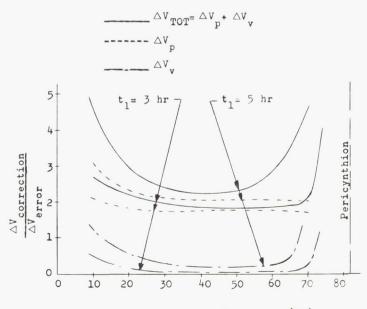
b. Guidance concept 2

Guidance concept 2 consists of correcting the errant trajectory back to the nominal trajjectory (in position, velocity and time) sometime prior to reaching the moon (Ref. 8).

Two approaches may also be used in imple-

menting this concept with the linear differential correction scheme. Either the midcourse correction can be made to return to the nominal trajectory as soon as possible (a truly explicit scheme) or to return to the nominal trajectory at some prearranged point and time. Ideally, either of these midcourse corrections is made in two parts. The first, at t1, is a velocity impulse which will return the spacecraft to the nominal trajectory at a specific point and time t2. The second correction is made at t2. to reorient the spacecraft's velocity vector along the nominal velocity vector. The velocity impulses required are referred to as $\Delta \, V_{\rm p}$, the first impulse to correct position, and $\triangle \hat{V_v}$, the second impulse to realign the spacecraft trajectory along the nominal trajectory.

The graphical data shown below is presented in a manner that allows a quick understanding of the orders of magnitude involved and of the efficiency of this concept.



Arrival Time At Aim Point, to (hr)

For this example, the nominal circumlunar trajectory has h_{PL} = 1852 km and an i_{VTL} = 9.1° at injection. The injection error is only in velocity. This error was applied in arbitrary directions, but only one set of typical data is presented. ΔV_p , ΔV_v and their sum ΔV_{TOT} per velocity error are shown as a function of arrival time t_2 on the nominal trajectory. The curves are shown for the midcourse correction being made at t_1 = 3 hr and at t_1 = 5 hr after injection.

For the effect of i_{VTL} at injection on the midcourse requirements, several trajectories have been investigated. All nominal trajectories are circumlunar, returning ballistically to a vacuum perigee of h_{PL} = 45.7 km, with h_{PL} = 463 km. The i_{VTL} of the trajectories is varied from 30° to 63.3°. The effect of i_{VTL} on midcourse requirements is shown below. The error conditions noted are for the most extreme cases encountered, and the coordinate system is that previously presented for the 1 σ errors. Only ΔV_{TOT} is shown, and the initial midcourse correction ΔV_{p} has been assumed at t_{1} = 3 hr.

This example typifies the differences between the first and second concepts. The first correction, ΔV_p , decreases as the aim point gets closer to pericynthion. The second correction, ΔV_v , increases as the moon is approached, a trend which becomes more severe with increasing values of $i_{\mbox{VTL}}$. In comparison, this concept requires a $\Delta V_{\mbox{TOT}}$ = 7.9 m/sec which is 25 to 60% less than required in the first concept.

The obvious points of the above figures are that:

- Delay in the midcourse correction results in increased propulsion requirements.
- (2) The required correction is greater when the inclination of the translunar trajectory plane (at injection) is increased.
- (3) For this concept, the best aim point on the nominal trajectory is approximately 75,000 km before reaching the moon.

Finally, most midcourse adjustment methods are readily adaptable to this guidance concept.

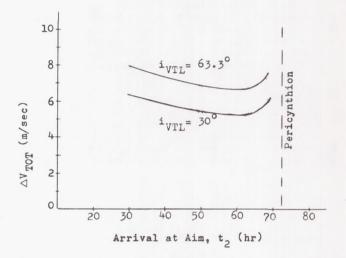
c. Midcourse guidance accuracy requirements

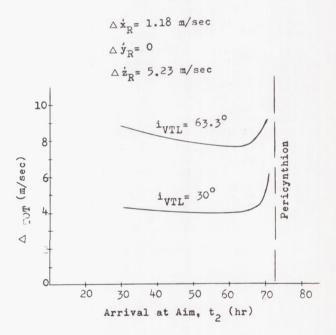
Several questions arise regarding midcourse guidance:

- (1) How accurate must be the navigational position and velocity determinations or the tracking of the vehicle from the earth and moon?
- (2) How accurately can the errant and corrective trajectories be predicted to the aim point?

(3) How accurately must the magnitude and orientation of the corrective velocity impulse be controlled in order to achieve the desired corrective trajectory?

$$\triangle \dot{\mathbf{x}}_{\mathrm{R}}$$
= .70 m/sec $\triangle \dot{\mathbf{y}}_{\mathrm{R}}$ = .51 m/sec $\triangle \dot{\mathbf{z}}_{\mathrm{D}}$ =6.20 m/sec





Again, since numerical values of position determination differ widely with the particular tracking and navigational equipment used, since the prediction depends on the force model and constants used in the trajectory simulation, and since the corrective velocity impulse depends on rocket engine characteristics, no quantitative results will be given.

A brief account of observational accuracies and some results of one navigational technique have been presented in Subsection B-1. Tracking by electronic means depends on the type of measurement made by the equipment, i.e., range, azimuth, elevation, photography against the star background, range measurements from several stations, etc., and on the accuracy of each individual tracking measurement. Usually, many measurements are taken, thus overdetermining the trajectory of the vehicle. The random errors can then be minimized by some smoothing technique which results in a trajectory which is better than one derived from the minimum number of tracking observations. Equipment bias errors, station location errors and atmospheric refraction errors (if the tracking is from earth) cannot be removed in this fashion but may be isolated by many observations with the tracking equipment in question. A more quantitative discussion of tracking equipment and smoothing techniques can be found in Chapter XI of Ref. 1.

The problems in trajectory simulation have been discussed in Section B of Chapter IV, and numerical comparisons between results obtained by use of several simple force models are scattered throughout the Handbook, most recently in Section A-2 of the present chapter.

The control of the corrective velocity impulses ΔV_p or ΔV_v depends on the thrust level of the rocket motor used for midcourse guidance, the burning time required to achieve the desired ΔV_p or ΔV_v , the accuracy of the accelerometers which control the thrust as well as the roundoff and truncation errors of the computer integrating the thrust acceleration to obtain ΔV_p or ΔV_v . These aspects have been discussed quantitatively in Chapters VI and XII of Ref. 1, and only a very brief description will be given here. The magnitude of the velocity impulse can be controlled by two different methods, with representative errors in each technique.

(1) Monitor propulsive inputs, a technique which attempts to control each of the propulsive parameters contributing to the velocity increment. The errors depend on the rocket engine control system and engine and fuel characteristics. Typical errors are:

Burning time $\Delta t_{\rm b}$ = 0.030 sec Mass flow rate $\Delta M_{\rm f}$ = 0.005 $M_{\rm f}$ Specific im-pulse $\Delta I_{\rm sp}$ = 0.004 $I_{\rm sp}$ Initial mass $\Delta M_{\rm 0}$ = 0

(2) Monitor the velocity increment directly, a technique requiring accelerometers and integrating computers. This system is more appropriate for the small midcourse corrections to be made; it has a typical error of $\Delta(\Delta V) = 10^{-4} \Delta V$ in the increment itself and $\Delta t_b = 0.030$ sec in shutdown time.

The individual midcourse velocity impulse can be controlled to within 0.01 to 0.1 m/sec by a conventional midcourse propulsion system. More accurate control is not necessary, but could be achieved by unconventional propulsion systems.

The directional control of ΔV_p and ΔV_v is not as critical since these velocity impulses are very small compared to the vehicle velocity vector V_Δ . Directional control of the thrust vector to within 1 to 5° from the nominal is considered sufficient in most cases, which can be achieved by a rudimentary attitude control system based on navigational observations.

If the navigational observations for position determination are in error, and the trajectory has not been determined or predicted accurately enough, or the midcourse velocity correction is in error, multiple midcourse corrections are required. These are not discussed here. However, additional data on nominal transearth midcourse guidance requirements will be given in Section B of Chapter IX.

D. TRANSLUNAR ABORT

In the translunar trajectory phase of a lunar mission, the vehicle is assumed to be in a ballistic two-body trajectory in the general direction of the moon. If a malfunction occurs on an unmanned mission which jeopardizes it or causes a mission failure, usually little action will be taken. However, if an emergency such as a solar flare or a meteoritic penetration occurs on a manned mission, it is abandoned and a turnaround or abort maneuver is performed to return the crew safely back to earth. This abort maneuver uses rocket burning to establish an abort trajectory with a prescribed vacuum perigee altitude and re-entry angle, within the safe re-entry corridor of the spacecraft. The essential parameters in such a maneuver are the propulsion requirements, the point along the translunar trajectory at which the abort is executed, and the eccentricity of the translunar trajectory. These parameters affect very strongly the time to return to earth and the possibility of landing at a preselected site.

In this section, requirements for abort maneuvers which result in the safe recovery of the vehicle will be presented. A simple method of obtaining acceptable return trajectories will be given in the first part. The problem of reaching preselected landing sites will then be discussed together with a consideration of aborts that occur both in and out of the plane of the initial trajectory. Finally, the requirements for establishing abort way-stations along the nominal trajectory will be discussed.

Only abort maneuvers initiated after injection and before the vehicle reaches a distance of approximately 200,000 km from earth will be considered. Beyond this distance, the effect of the moon begins to play a major role in determining the translunar trajectory, and the two-body trajectory assumption will no longer be accurate enough.

1. Abort to the Vicinity of Earth

In order to obtain a general idea of the requirements of the turnaround problem, several assumptions are made which simplify the calcu-

lations but allow the various parameters of interest to be found with sufficient accuracy. These assumptions are:

- (1) The model used for translunar and abort trajectories is a restricted two-body model, i.e., a vehicle of negligible mass moving in the central force field of a spherical earth. This allows the use of constant orbital elements for the description of these trajectories.
- (2) The abort maneuver consists of a single velocity impulse, ΔV_A .
- (3) The translunar and abort trajectories are confocal and have a perigee radius of 1 ER (earth radius).
- (4) Radiation belts are ignored.

The first concern is to determine ΔV_A requirements for abort together with the time to return to earth when performing abort maneuvers. Before this can be done, the velocity V_T and flight path angle γ_T must be known for any point along any translunar trajectory. In a system of units which measures the distance from the earth R in earth radii, and μ_{\oplus} = 1 is the gravitational constant of the earth, the resulting normalized velocity is expressible as:

$$V = \left[\frac{2}{R} - (1 - e_T)\right]^{-1/2}$$
 (28)

where e_T is the orbital eccentricity of the translunar trajectory.

The flight path angle γ , which is measured from the local horizontal to the velocity vector, may be found by use of the following equation:

$$\gamma = \cos^{-1} \left[\frac{(1 + e_T)/R}{2 - R(1 - e_T)} \right]^{1/2}$$
 (29)

Next, the limit of allowable eccentricities for the abort trajectories is required. For one constant and continuous band, an abort eccentricity \mathbf{e}_A = 1 is arbitrarily selected. Actually, this may be interpreted as a design limit and will be referred to as such. For a given distance from earth and a required perigee altitude, the minimum \mathbf{e}_A obtainable is realized when the semimajor axis \mathbf{a}_A is as small as possible. This requires that the radius at abort, \mathbf{R}_A , is the apogee, and, by assumption 3, above,

$$a_{A} = \frac{R_{A} + 1}{2}$$
 (30)

The resulting equation for the minimum allowable eccentricity is:

$$(e_A)_{\min} = \frac{(R_A - 1)}{(R_A + 1)}$$
 (31)

Figure 6 shows an envelope of allowable return eccentricities as a function of distance from the earth. There is actually no real upper limit above e_A = 1 provided that a proper negative abort flight path angle γ_Δ is achieved.

Knowing the orbital elements of the translunar trajectory and the required abort eccentricity, both the translunar trajectory conditions prior to abort (V_T , γ_T) and immediately after the maneuver (V_A , γ_A) are easily found.

The time to return to earth along any of the allowable orbits is computed with the classic two-body time equations of Ref. 1 and the results are shown in Fig. 7. This plot is true regardless of the eccentricity, \mathbf{e}_{T} , of the translunar trajectory and shows the return time as a function of the allowable \mathbf{e}_{A} for any \mathbf{R}_{A} .

The time to return may be altered for a given ΔV_A if the abort maneuver is such that the abort trajectory plane is different from the translunar plane. This is referred to as a "change in azimuth" and the consequences of such a maneuver are described here.

The change in azimuth $\Delta\,A$ is the angle between the original translunar trajectory plane defined by \overrightarrow{R}_T and \overrightarrow{V}_T or the $x_v\,y_v$ plane and the trajectory plane defined by $\overrightarrow{R}_\Delta$ and $\overrightarrow{V}_\Delta$.

Taking the dot product of the initial and final velocities, \overrightarrow{V}_T \overrightarrow{V}_A , the angle ϵ between \overrightarrow{V}_T and $\overrightarrow{V}_\Delta$ is obtained as

$$\epsilon = \cos^{-1} \left[\sin \gamma_{\rm T} \sin \gamma_{\rm A} + \cos \gamma_{\rm T} \cos \gamma_{\rm A} \cos \Delta A \right].$$

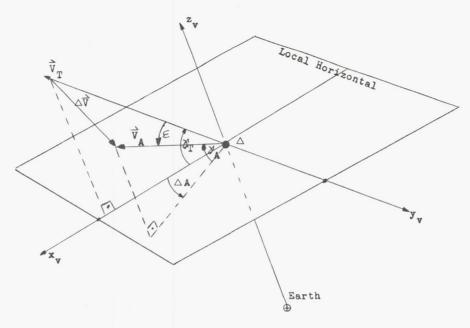
Thus, for a given \mathbf{Y}_T and \mathbf{Y}_A , ε increases with ΔA_{\bullet}

From the law of cosines,

$$(\Delta V_A)^2 = V_T^2 + V_A^2 - 2V_T V_A \cos \epsilon$$

it is seen that as ε increases, the required velocity impulse also increases for a given V_T and V_A . Therefore, for given initial conditions of V_T and V_A and a specific time to return, any change in heading will result in an increase in the required maneuvering impulse ΔV_A .

Figure 8 shows the ΔV_A needed to perform the abort maneuver at various distances from the earth without changes in heading. A (+ γ_A) in Figs. 7 and 8 indicates the region where, after the abort maneuver, the flight path angle is positive, and (- γ_A) is the region where the final flight path angle after abort is negative. For positive values of γ_A , the spacecraft must pass



through the apogee of the abort trajectory prior to returning to earth and perigee, while for the latter case, the spacecraft returns directly to the perigee of the abort trajectory. However, for obtaining a specific perigee latitude and longitude it may be more efficient, timewise, to maneuver out of the initial trajectory plane. This is demonstrated later in the section. The data given in Fig. 8 applies for $\mathbf{e_T}$ = 1.0. For $\mathbf{e_T}$ < 1.0 the $\triangle\,\mathbf{V_A}$ required to return to earth in a given time also decreases. In fact, the $\triangle\,\mathbf{V_A}$ is reduced by 10 to 15% if $\mathbf{e_T}$ is lowered from 1.0 to 0.98.

2. Abort to Preselected Landing Sites

Even during emergency situations, the problems of recovery might be reduced by the use of preselected landing sites. The results of performing in-plane abort maneuvers that return to a given perigee longitude will be presented in this section. They were obtained by using classical two-body results and by assuming that the abort maneuver is characterized by an impulsive change of velocity \triangle V $_{\rm A}$ at a distance R $_{\rm A}$ (in earth radii) from earth.

The nominal translunar trajectory prior to the abort maneuver used as an example is elliptical with injection at perigee $\rm h_0$ = 45.720 km, $\rm V_0$ = 11,055.1 m/sec, corresponding to an eccentricity $\rm e_T$ = 0.9668. This ellipse has an apogee radius approximately equal to the moon's average orbital radius of about 60 ER and an inclination $\rm i_{VE}$ = 36.5° to the equator.

Figure 9 presents the necessary information to estimate return perigee longitudes for various values of $\triangle\,V_A$ and R_A . The right-hand side of Fig. 9 shows the return time (time from the abort maneuver to return perigee which is also at $h_{\rm PE}$ = 45.720 km) as a function of R_A and $\triangle\!V_A$.

The left-hand side of the graph converts the return time into the longitude of abort trajectory perigee relative to the translunar trajectory (injection) perigee with the assumption that the latitude of the translunar trajectory perigee is equal to the latitude of the abort trajectory perigee. This assumption results in the removal of orbital inclination from the problem. However, the inclination and injection perigee latitude enter indirectly when the return perigee longitude is chosen. For example, assume that the injection latitude is 16.5° S and it is desired to land in Australia after an abort from a southeasterly launch from Cape Canaveral. This launch azimuth results in an approach to Australia from the northwest. Therefore, return perigee longitudes somewhat to the west of Australia are desirable.

Figures 10 and 11 have been obtained from Fig. 5 for three typical situations. Figure 10 shows $\triangle\,V_A$ and return time for abort maneuvers at various values of R_A with the requirement of landing in Australia. The injection perigee longitude and latitude are taken as 8.8° W and 16.5° S, which is representative for lunar launches from Cape Canaveral. The longitudes used for landings in Australia reflect an approach from the northwest. Figure 10 denotes the number of revolutions the earth has made (i.e., the number of sidereal days) before re-entry takes place, and the shaded band represents the width of the Australian continent.

Figure 11 presents the same information for landing in the United States and off the west coast. The injection perigee is assumed to be directly over Edwards Air Force Base which is representative of a lunar launch from Cape Canaveral on a trajectory inclination to the earth's equator of $i_{\rm VE}$ = 35° with a parking orbit prior to injection. The selection of return perigee longitude depends on the aerodynamic maneuvering capability of the lifting body re-entry vehicle, which is nearly tangent to the landing site latitude.

Therefore, four possible return perigee longitudes have been shown in Fig. 11. Perigee at 170° E longitude is representative of a return to Edwards Air Force Base with 7200 km of re-entry glide range. The other extreme would be a return perigee longitude at the east coast of the United States. This would represent the minimum reentry that could still remain within the boundaries of the United States. The much wider selection of return times compared to the Australian landings is apparent. This is due primarily to the fact that re-entry longitudinal maneuverability can be used to extend the choice of return perigee longitudes.

Subsection D-1 mentioned abort maneuvers that result in an abort trajectory out of the translunar trajectory plane. The discussion below demonstrates the feasibility of performing an abort maneuver with a change in azimuth $\triangle\,A$ resulting in reduced return flight times to reach a specific landing site.

In order to obtain representative data, a typical translunar trajectory was selected from which abort maneuvers were conducted in and out of the translunar plane at various distances from earth. The landing site is Edwards Air Force Base and the translunar trajectory is characterized by the following injection conditions:

Velocity	V_0	10,907 m/sec
Altitude	h ₀	231.953 km
Flight Path Angle	Υ ₀	3°
Longitude	λ_0	165° west
Latitude	φ ₀	26.35° north
Orbital Inclination	$i_{ m VE}$	35°
Orbital Eccentricity	e _T	0.9728

Results are presented in Fig. 12 which give the time-to-return from an abort as a function of \mathbf{R}_{Δ} and $\Delta\mathbf{A}$ for abort and translunar trajectories. The translunar (nominal) trajectory represents a no-maneuver condition and just gives the time to complete a circumlunar mission as a function of R on the translunar portion of the trajectory. The time-to-return from an abort maneuver depends on whether one particular landing site is desired, or a number of sites are available or simple earth return is sufficient. In the last case, it has been shown that the least $\triangle\, V_A$ is realized when the abort maneuver occurs in the nominal translunar trajectory plane. Figure 12 also gives the absolute minimum return time to earth for the values (\triangle V_A) max = 549 m/sec and (\triangle V_A)_{max} = 1829 m/sec illustrating that simple earth return requires less time than return to a specific site.

If return to a particular landing site such as Edwards Air Force Base is desired, then the arrival must be timed correctly because of the earth's rotation. The step functions on Fig. 9 represent the minimum time to return to Edwards Air Force Base for variable values of $\Delta\,\mathrm{V}_{A} \leq \left(\Delta\,\mathrm{V}_{A}\right)_{\,\mathrm{max}}$ and show the timing problem

for two values of (ΔV_A) $_{max}$ for abort trajectories with ΔA = 0°, ΔA = 10° and ΔA = 20°. The return times for out-of-plane abort to Edwards Air Force Base are in certain cases less than for in-plane aborts. The intersections of the out-of-plane step functions with the absolute minimum time curves in Fig. 12 denote these cases, and near these intersections the planar change ΔA should be decreased for increasing R_A to maintain minimum return times. As these intersections on the "return-to-Edwards" curves are approached, an increasingly larger Δ V_A is required and at the point of intersection the total available Δ V_A or (ΔV_A) max is used for abort.

The data in Fig. 12 indicates that definite benefits may be gained in performing abort maneuvers out of the translunar trajectory plane when landing at a specific site is required. Reductions in time-to-return of up to 5 hr over the in-plane returns can be realized for Edwards Air Force Base landings. If several landing sites are available the time to return could be reduced further. The restriction imposed by available tracking facilities has so far been ignored (see Subsection B-2). Since abort maneuvers out of the nominal trajectory plane change the abort trajectory inclination, the capability to track the vehicle during re-entry from existing facilities must be re-examined.

A point not illustrated in Fig. 12 is that the total time from the translunar abort decision to re-entry, \boldsymbol{t}_{R} , for landing at a particular site is the same for a large range of $\triangle V_A$ up to $(\triangle V_A)_{max}$, since for a successful abort the landing site which rotates with the earth must be near the abort trajectory plane. It does not matter whether the entire t_R is spent in an abort trajectory with a lower $\Delta\,\boldsymbol{V}_{A}$ or whether part of it is used in reaching a point on the translunar trajectory where ($\!\!\!(\triangle\,V_{\mbox{A}})\!\!\!\!/\mbox{ max}$ is used for the abort maneuver and the rest on the abort trajectory. This characteristic of translunar aborts to a given landing site suggests the selection of specific points or "abort way-stations" along the translunar trajectory for abort maneuvers, from which the vehicle can acquire the landing site with a fixed value of $\triangle V_A$. "Abort way-stations" allow the use of abort trajectories which can be precomputed on the ground prior to the lunar mission. However, they represent the least efficient abort maneuver from a standpoint of fuel requirements (i.e., the maximum value of $\triangle\,V_{\mbox{\scriptsize A}}$ is used for a given time to return). More material on way-stations is presented in the next subsection.

3. Abort Way-Stations

A method for obtaining abort way-stations, or points on the nominal translunar trajectory from which precomputed abort trajectories characterized with a fixed value of ΔV_{A} can be used, has been presented by Kelly and Adornato (Ref. 9). The method as described briefly in the present subsection is a modification of the one used in Ref. 9.

The following sketch illustrates the geometry of translunar abort with return to a specific landing site.

Assume a restricted two-body force model for the translunar and abort trajectories, and assume that they are in a common plane ($\triangle A = 0^{\circ}$). If we include the re-entry trajectory into the calculation, then an abort way-station as defined above must satisfy the following four constraints:

(1) Abort trajectories from the way-station must have acceptable flight path angles $\gamma_{\rm R}$ at re-entry:

$$\gamma_{\min} \leq \gamma_{R} \leq \gamma_{\max}$$
 (32)

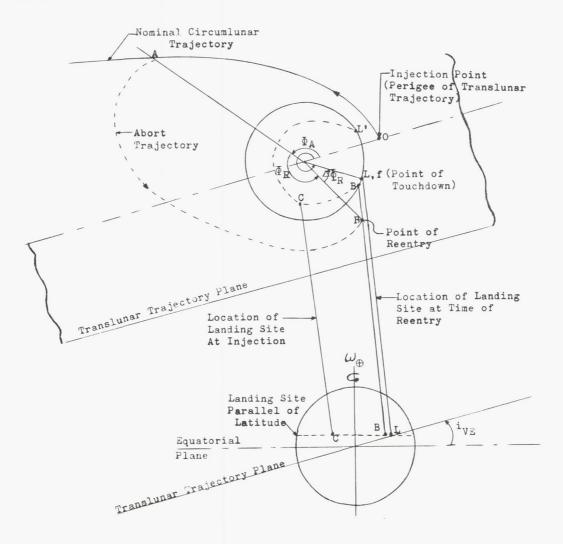
(2) Referring to the previous sketch, let 0 denote the vehicle and C the position of the landing site at translunar injection, let A denote the abort maneuver, B the location of the vehicle and landing site at re-entry and L, f the coinciding positions of the landing site and space vehicle, respectively, at vehicle touchdown. In addition, a double subscript notation is introduced for time, i.e.,

 $^{\triangle t}_{0\text{ -}A}$ is the time for the space vehicle to travel from translunar injection to abort and $^{\Delta}t_{B\text{-}L}$ the time for the landing site to rotate with the earth from B to L. With this notation, the first abort way-station imposes the following time constraint.

$$^{\Delta t}_{0-A} + ^{\Delta t}_{A-B} + ^{\Delta t}_{B-f} =$$
 $^{\Delta t}_{C-B} + ^{\Delta t}_{B-L}$ (33)

However, since the landing site rotates with the earth, it will be in the trajectory plane at the same location L once in each sidereal day (1 sidereal day = $86164.1 \, \mathrm{sec} = 23^{h} \, 56^{\, m} \, 4^{\, s}.1$) as long as the latitude of the landing site is less than the trajectory inclination. Thus, further abort way-stations are characterized by

$$^{\Delta}$$
 t_{0-A} + $^{\Delta}$ t_{A-B} + $^{\Delta}$ t_{B-f}
 $^{\Delta}$ t_{C-B} + $^{\Delta}$ t_{B-L} + (n-1) 86164.1 sec
(34)



where n = 1, 2, . . . is the number of the abort way-stations or sidereal days or complete rotations of the earth from injection. As long as the latitude of the landing site is less than the trajectory inclination, the site will intersect the translunar trajectory plane also at L' and a second set of abort way-stations can be computed for this site.

(3) Let Φ_A be the range angle from injection to abort (or true anomaly since injection occurs at perigee), Φ_R the range angle from abort to re-entry, and $\Delta\Phi_R$ the required longitudinal maneuverability of the vehicle from re-entry. The total range angle Φ_0 from injection to the point L of intersection of the landing site with the trajectory plane must satisfy

$$\Phi_0 = \Phi_A + \Phi_R + \Delta \Phi_R \tag{35}$$

(4) The range angle $\Delta\Phi_R$ is constrained by the longitudinal maneuvering capability of the vehicle, i.e.,

$$\left(\triangle \Phi_{\mathrm{R}} \right)_{\mathrm{min}} \leq \Delta \Phi_{\mathrm{R}} \leq \left(\triangle \Phi_{\mathrm{R}} \right)_{\mathrm{max}}$$
 (36)

For preliminary calculations the re-entry portion of the flight can be neglected in comparison with the translunar and abort trajectories. Then $\Delta t_{B-f} = \Delta t_{B-L} = 0$, $\Delta \Phi_R = 0$, and the restricted two-body force model results compiled in Chapter III of Ref. 1 can be used to determine abort way-stations for certain translunar abort trajectory characteristics and landing sites. If available, the re-entry trajectory parameters Δt_{B-f} and $\Delta \Phi_R$ can be obtained for certain space vehicle characteristics and added to the restricted two-body results to obtain more realistic abort way-stations.

A typical graph for determining abort way-stations has been given in Fig. 13. The dashed lines represent the required time from injection to when the landing site intersects the trajectory plane at L or $(\Delta t_{0-A}^{+} + \Delta t_{A-B}^{+} + \Delta t_{B-f}^{+})$ = constant for the first, second and third day. The curve of minimum time to re-enter corresponds to a change in flight path angle only by the abort maneuver, while the maximum time to re-enter corresponds to a change in velocity only with no change in flight path angle at abort. Both curves are for the same ΔV_A = 1529 m/sec. The intersections of the minimum time to re-enter curve with the dashed line represent abort way-stations and are denoted by dots on Fig. 13.

The abort way-stations on Fig. 13 correspond to the intersection of the ΔA = 0° step function with the curve labeled "absolute minimum time to return to earth (ΔV_A) " in Fig. 12. It is max

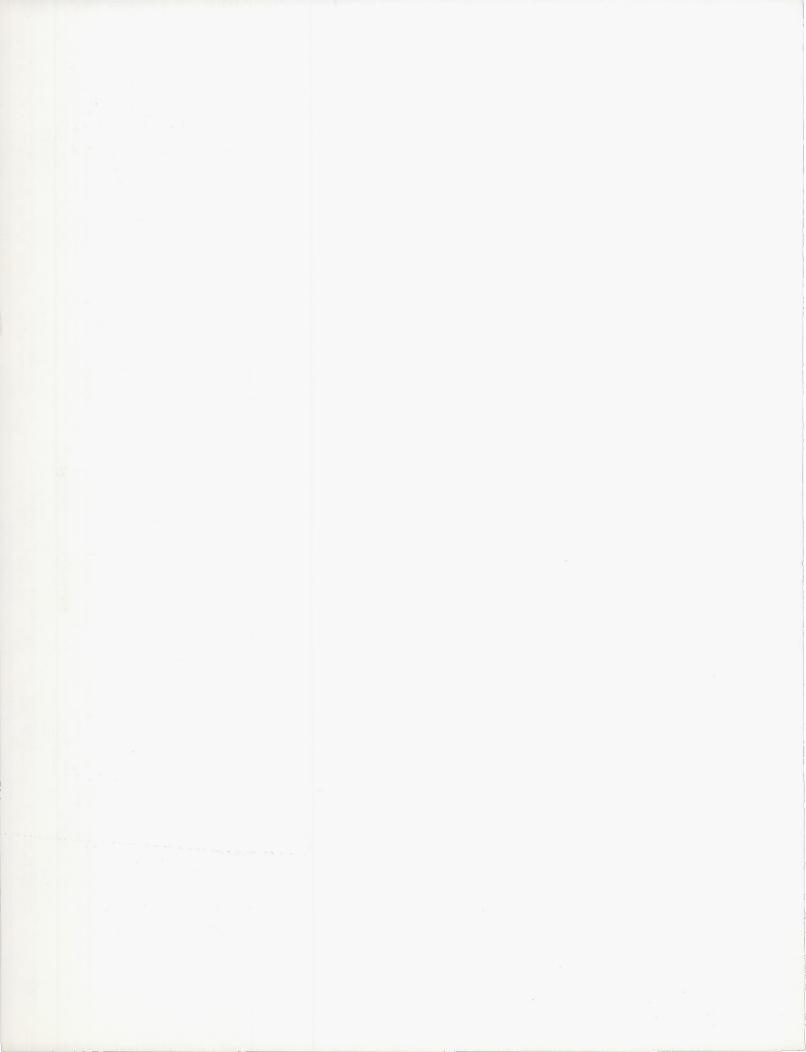
obvious that Fig. 12 presents much more information than Fig. 13--it gives abort way-stations for ΔA = 0°, ΔA = 10°, and ΔA = 20° which are the intersections of the step functions with the (ΔV_A) max

curves. In addition, lower values of ΔV_A can be obtained at a glance from Fig. 12. The near-horizontal part of the two-step function on Fig. 12 can be connected to yield a four-parameter set of curves where ΔV_A and ΔA are presented in the field of the graph together with the nominal trajectory (ΔV_A = 0), and R_A and time-to-return are the abscissa and ordinate, respectively. In this fashion, the maximum abort maneuver information can be presented on a single graph.

In practical design of abort trajectories (and way-stations), a set of graphs similar to Fig. 12 should be prepared for each prospective landing site and each location L and L' as soon as the nominal translunar portion of the trajectory has been determined. Results of re-entry trajectory calculations can be used to bias the curves obtained from the restricted two-body force model and thereby represent the actual situation more realistically.

E. REFERENCES

- "Orbital Flight Handbook," ER 12684, The Martin Company, Baltimore, March 1963.
- Battin, R. H., "A Statistical Optimizing Navigation Procedure for Space Flight," Instrumentation Laboratory, MIT, Cambridge, Massachusetts, May 1962.
- 3. Wheelon, A. D., "Midcourse and Terminal Guidance," Report No. 145, Space Technology Laboratories, Applied Physics Department, Los Angeles, California, June 1958.
- Porter, J. G., "Navigation Without Gravity," Journal of the British Interplanetary Society, Vol. 13, No. 2, March 1954, p 68.
- 5. "Navigational Techniques for Interplanetary Space Flight," Report No. 2752-15-F, University of Michigan, Willow Run Laboratories, Ann Arbor, Michigan, 1958.
- 6. Novak, D. H., "Two-Body Navigation and Guidance in Cislunar Space," ER 12447, Martin Company, Aerospace Systems Division, Baltimore, Maryland, May 1962.
- 7. Egorov, V. A., "Certain Problems of Moon Flight Dynamics," The Russian Literature of Satellites, Part I, International Physical Index, Inc., New York, 1958.
- 8. Pragluski, W. J., "Lunar Mission Midcourse Guidance Concept Trajectory Analysis, Lunar Landing Module," Technical Report No. 11, Martin Company, Baltimore, February 1962. (Unpublished)
- 9. Kelly, T. J. and Adornato, R. J., "Determination of Abort Way-Stations on a Nominal Circumlunar Trajectory," ARS Journal, Vol. 32, June 1962, pp 887 to 893.



ILLUSTRATIONS

Preceding Page Blank

LIST OF ILLUSTRATIONS

Figure	<u>Title</u>	Page
1	Star Choice Angles	VI-32
2	Star Choice Angles	VI-32
3	View from Spacecraft Towards Earth	VI-33
4	Typical Lunar Flight Ground Swath (southerly declination of the moon)	VI-34
5	Typical Lunar Flight Ground Swath (northerly declination of the moon)	VI-34
6	Minimum Eccentricity Allowable for Safe Earth Return	VI-35
7	Time to Return to Earth from any Point in a Translunar Trajectory	VI-36
8	Characteristic Velocity Impulse ΔV_A of the Abort Maneuver (no changes in azimuth)	VI-37
9	Time to Return for an Abort Maneuver from a Typical Translunar Trajectory	VI-38
10	Abort Velocity Impulse Required to Land in Australia for a Typical Translunar Trajectory	VI-39
11	Abort Velocity Impulse Required to Land in or Near the United States for a Typical Translunar Trajectory	VI-40
12	Complete Abort Data for a Typical Circumlunar Trajectory	VI-41
13	Abort Way-Stations for a Typical Circumlunar Trajectory	VI-42

FIG. 1. STAR CHOICE ANGLES

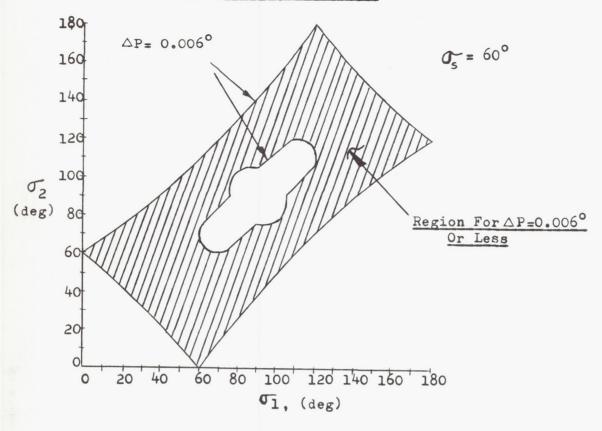


FIG. 2 STAR CHOICE ANGLES

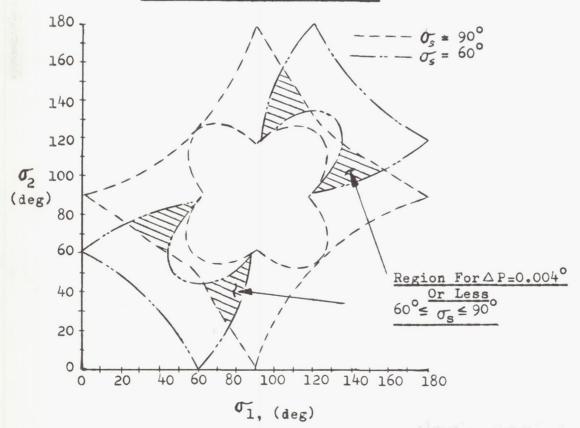
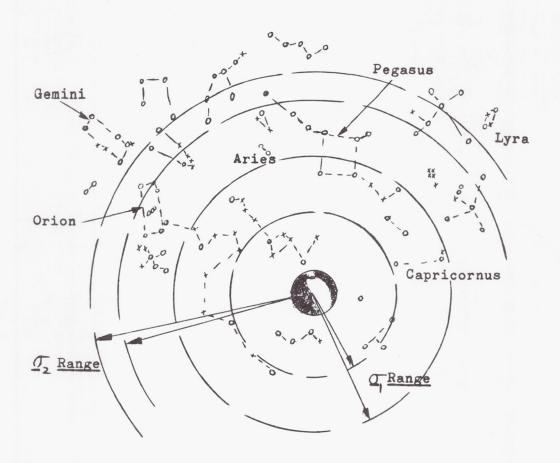


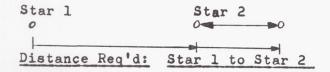
FIG. 3. VIEW FROM SPACECRAFT TOWARDS EARTH

Launch: 14 June, 1968, 14:14 Hr GMT View 3 Hours After Injection



Star Code:

- o 3rd. Magnitude or Brighter
- × 5th. Magnitude or Brighter



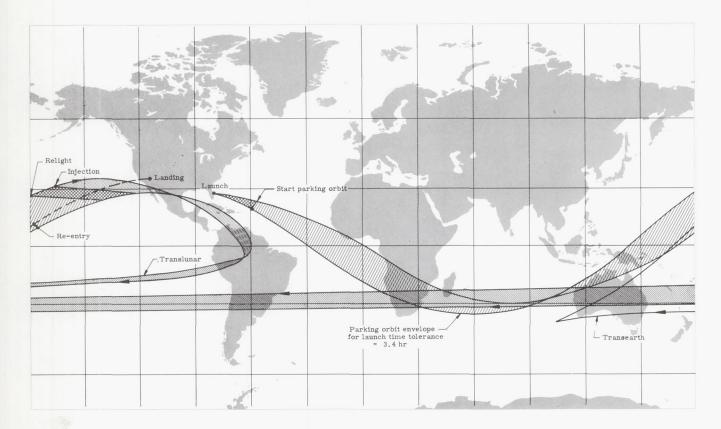


Fig. 4. Typical Lunar Flight Ground Swath (Southerly Declination of the Moon)

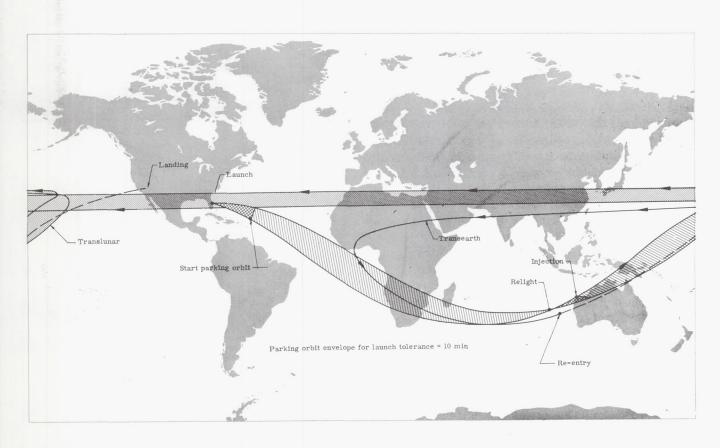
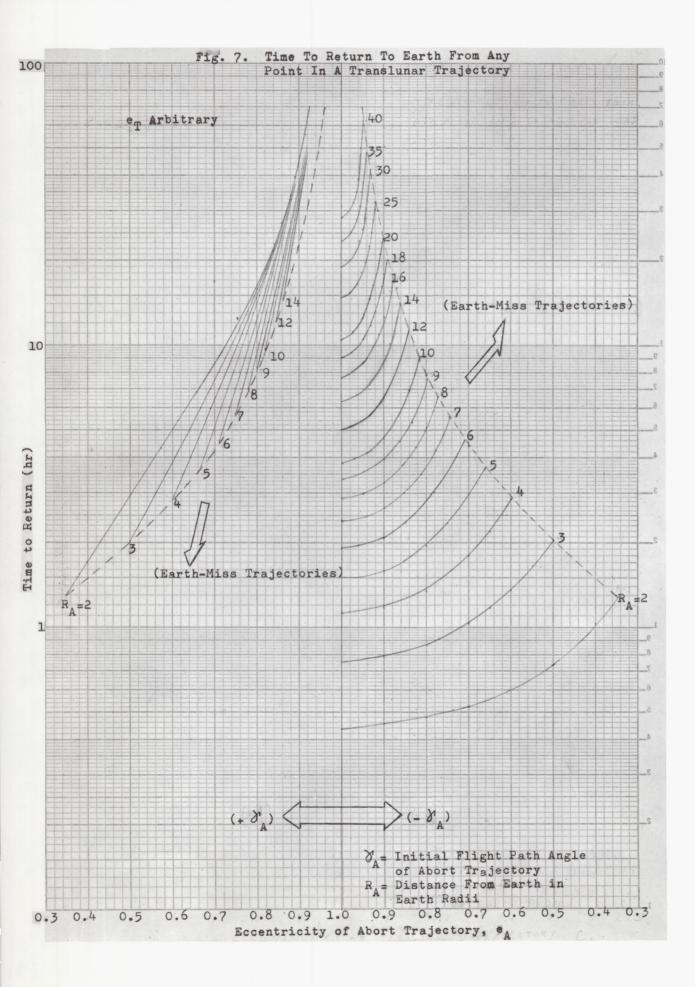
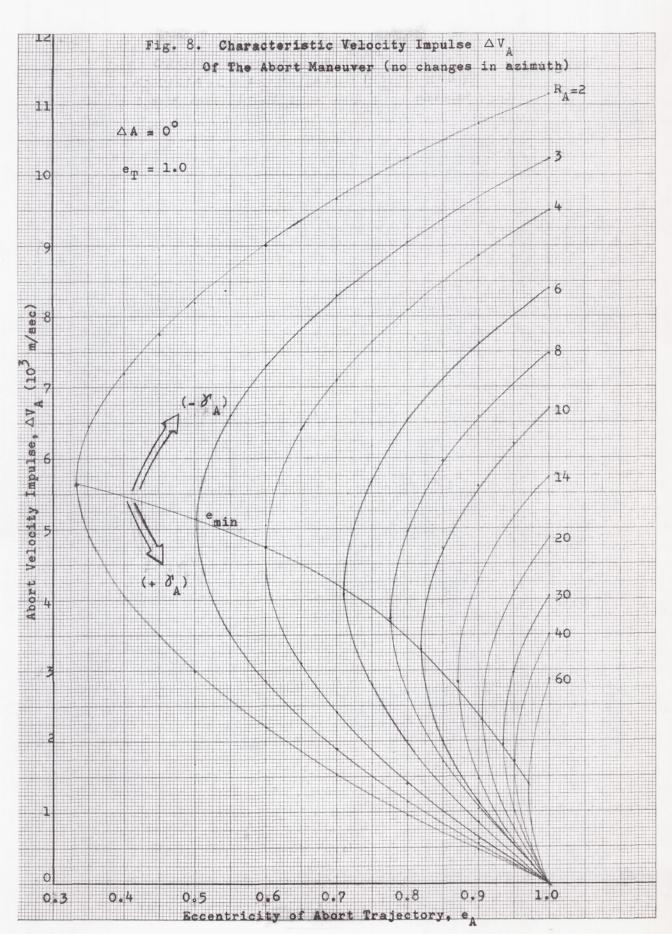
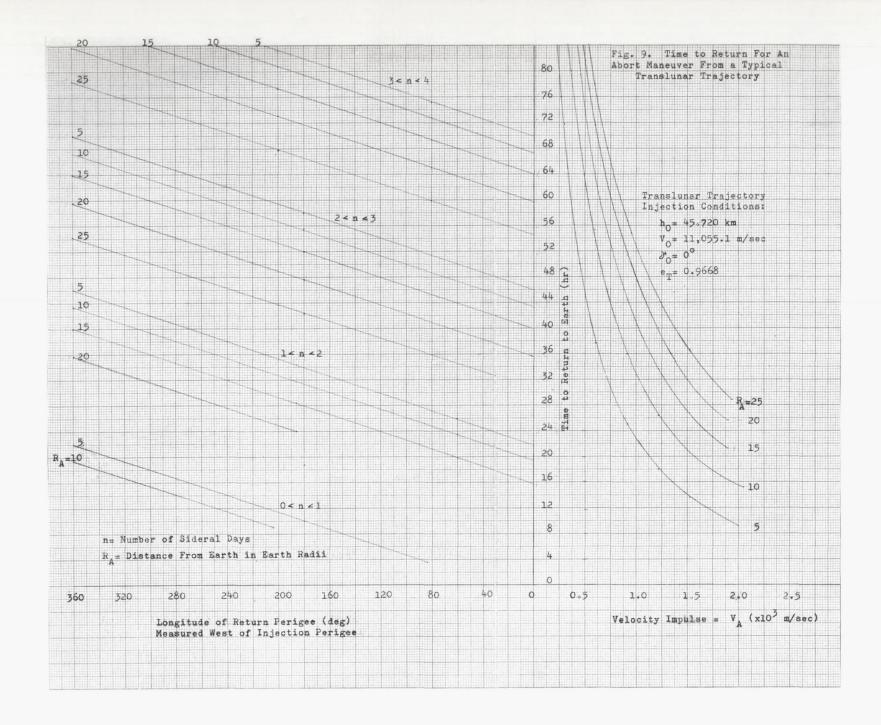


Fig. 5. Typical Lunar Flight Ground Swath (Northerly Declination of the Moon)

VI-35







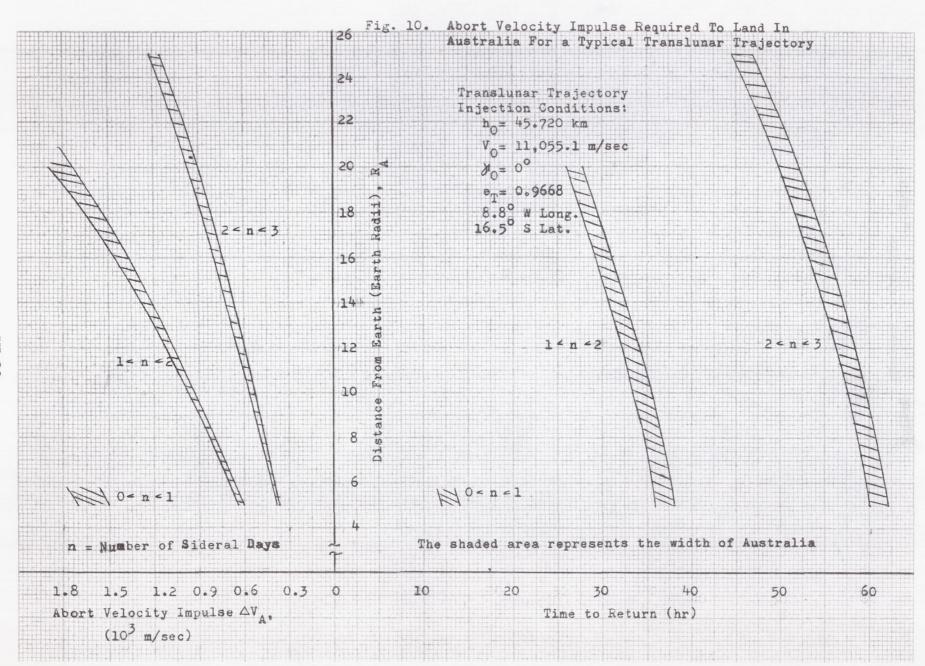
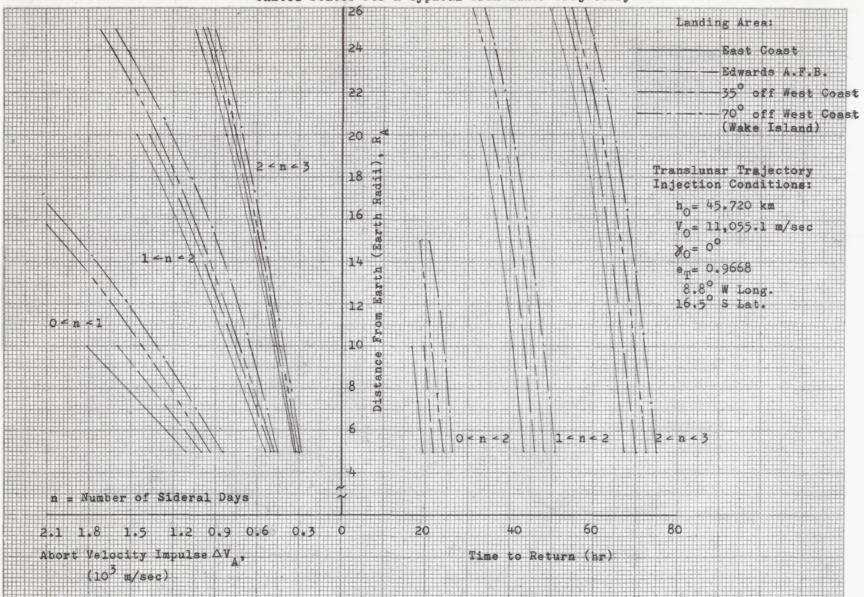
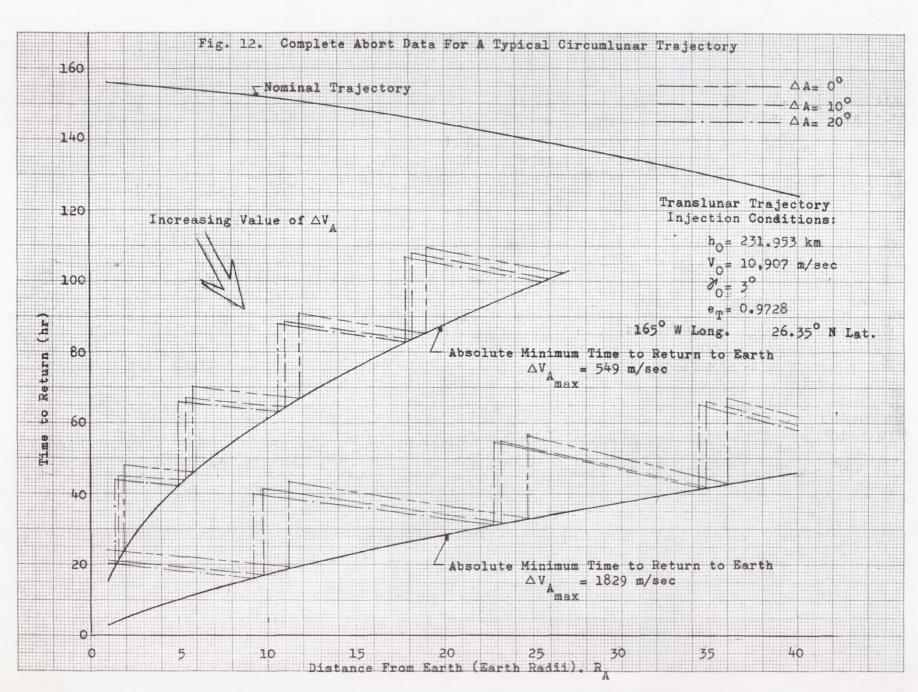
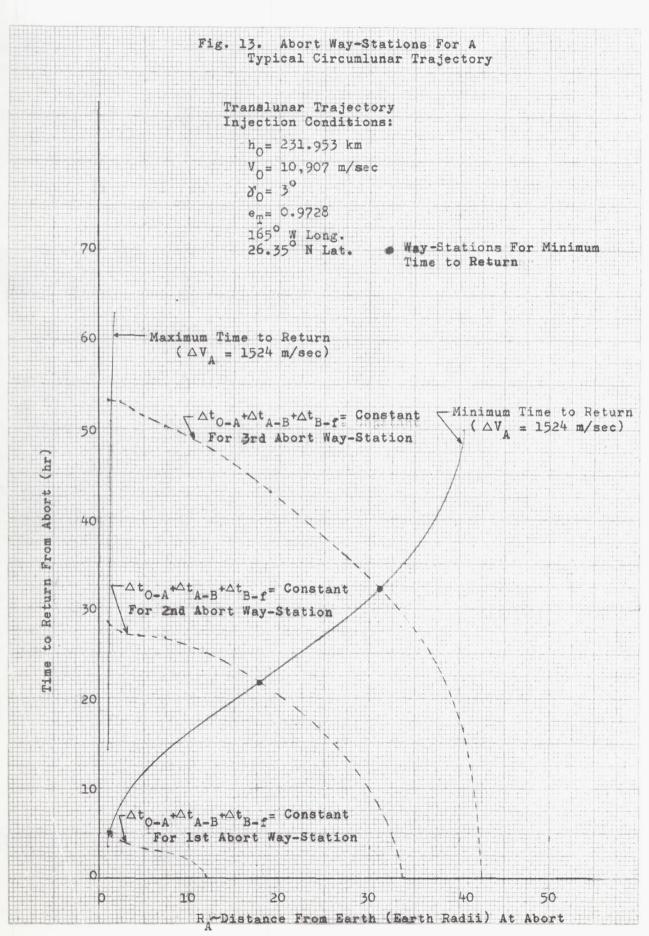


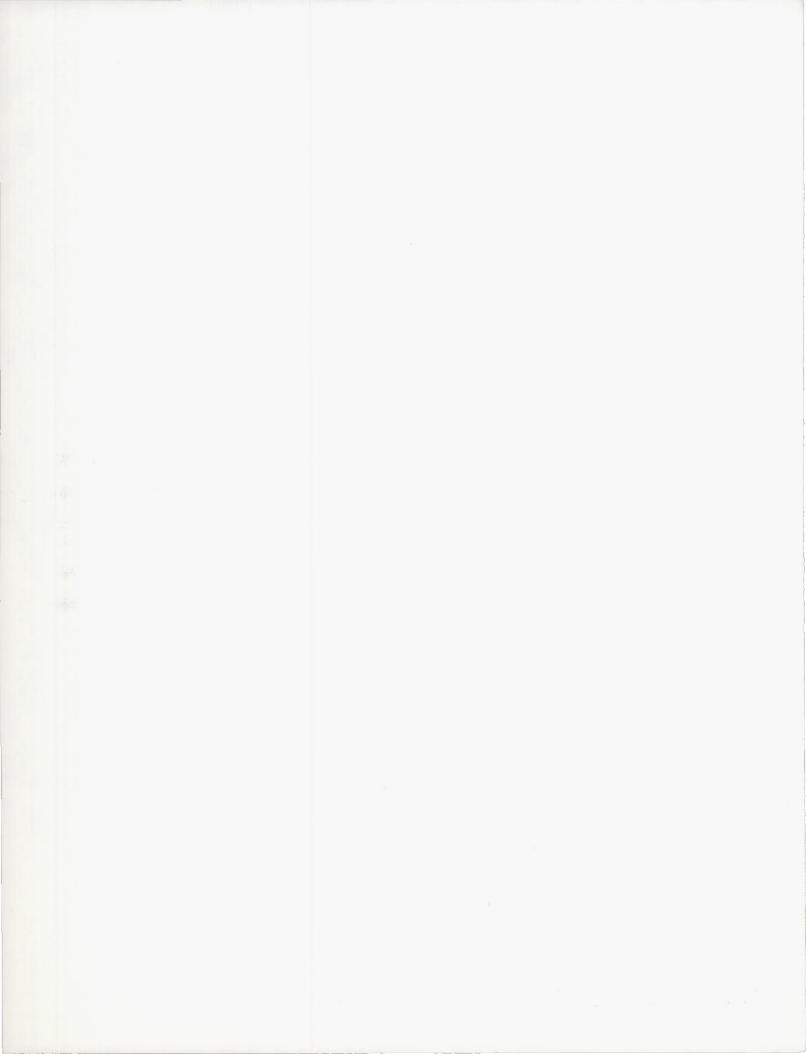
Fig. 11. Abort Velocity Impulse Required To Land In Or Near The United States For A Typical Translunar Trajectory







CIRCUMLUNAR TRAJECTORY CATALOGUE
Figures C-1 through C-83



CIRCUMLUNAR TRAJECTORY CATALOGUE

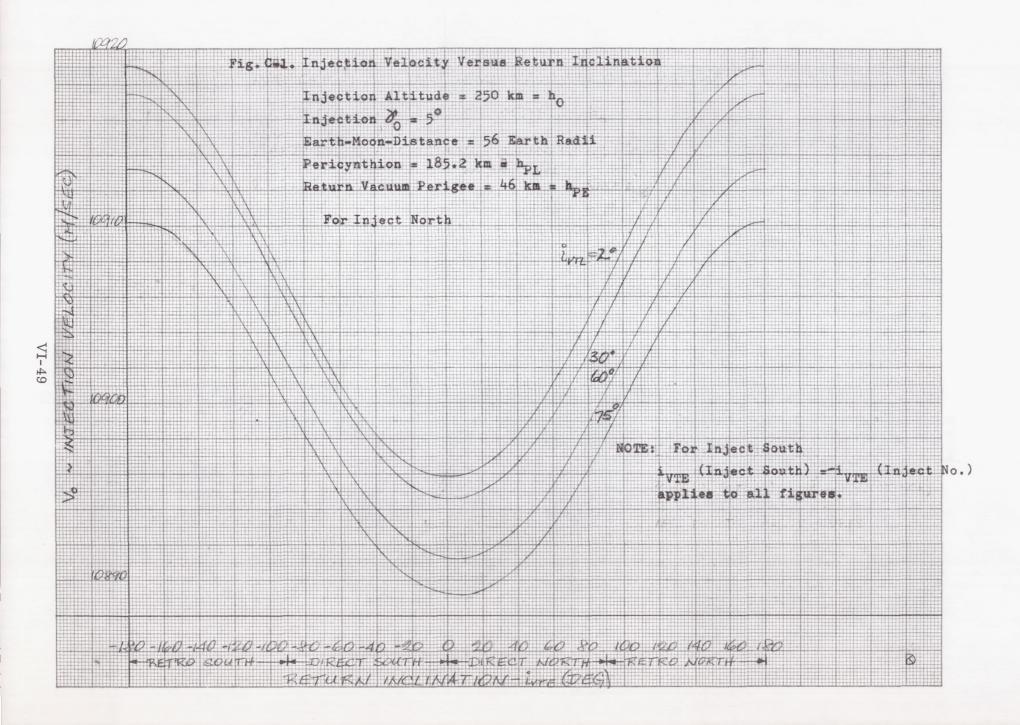
ation VI-49
Inclination VI-50
ation VI-51
Orbit Versus VI-52
clination VI-53
VI-54
Inclination VI-55
Inclination VI-56
ation VI-57
Inclination VI-58
ation VI-59
Orbit Versus VI-60
clination VI-61
VI-62
Inclination VI-63
Inclination VI-64
ation VI-65
Inclination VI-66
ation VI-67
Orbit Versus VI-68
clination VI-69
VI-70
Inclination VI-71

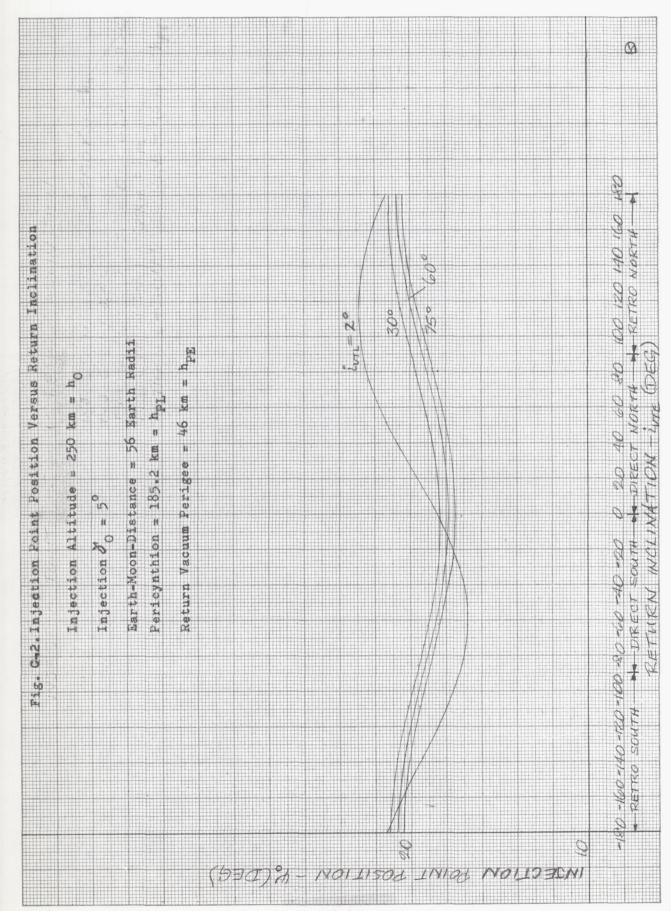
Preceding Page Blank

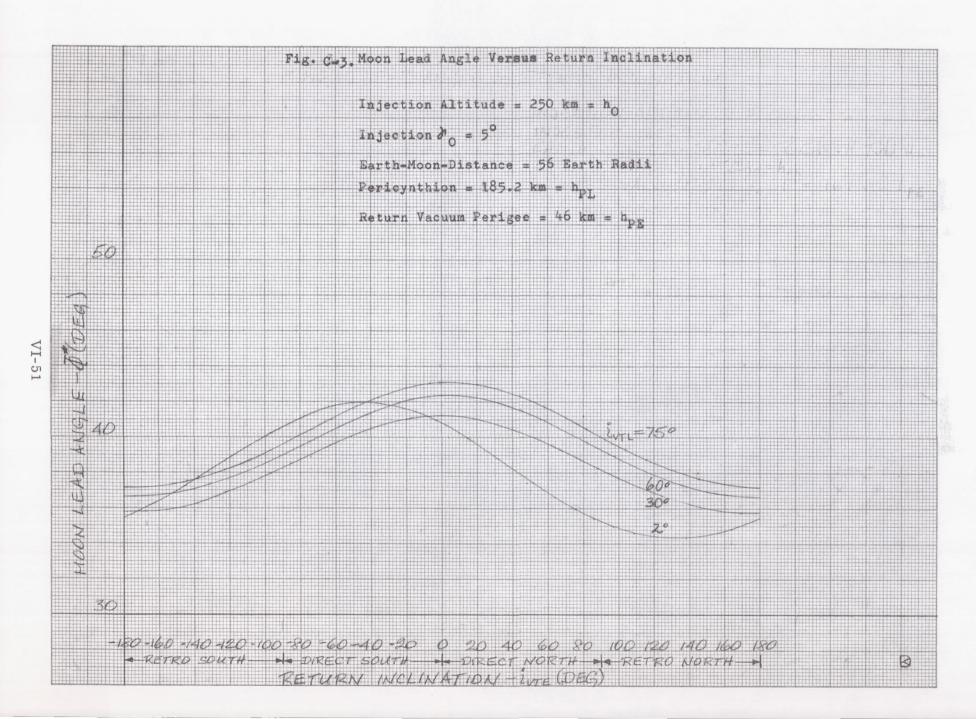
Figure	Title	Page
C-24	Lunar Orbit Orientation Versus Return Inclination	VI-72
C-25	Injection Velocity Versus Return Inclination	VI-73
C-26	Injection Point Position Versus Return Inclination	VI-74
C-27	Moon Lead Angle Versus Return Inclination	VI-75
C-28	ΔV Required to Enter Circular Lunar Orbit Versus Return Inclination	VI-76
C-29	Time of Pericynthion Versus Return Inclination	VI-77
C-30	Total Time Versus Return Inclination	VI-78
C-31	Lunar Orbit Inclination Versus Return Inclination	VI-79
C-32	Lunar Orbit Orientation Versus Return Inclination	VI-80
C-33	Injection Velocity Versus Return Inclination	VI-81
C-34	Injection Velocity Versus Return Inclination	VI-82
C-35	Injection Point Position Versus Return Inclination	VI-83
C-36	Moon Lead Angle Versus Return Inclination	VI-84
C-37	ΔV Required to Enter Circular Lunar Orbit Versus Return Inclination	VI-85
C-38	Time of Pericynthion Versus Return Inclination	VI-86
C-39	Total Time Versus Return Inclination	VI-87
C-40	Lunar Orbit Inclination Versus Return Inclination	V I- 88
C-41	Lunar Orbit Orientation Versus Return Inclination	V I- 89
C-42	Injection Velocity Versus Return Inclination	VI-90
C-43	Injection Velocity Versus Return Inclination	V I- 91
C-44	Injection Point Position Versus Return Inclination	VI-92
C-45	Moon Lead Angle Versus Return Inclination	VI-93
C-46	ΔV Required to Enter Circular Lunar Orbit Versus Return Inclination	VI-94
C-47	Time of Pericynthion Versus Return Inclination	V I- 95
C-48	Total Time Versus Return Inclination	VI-96

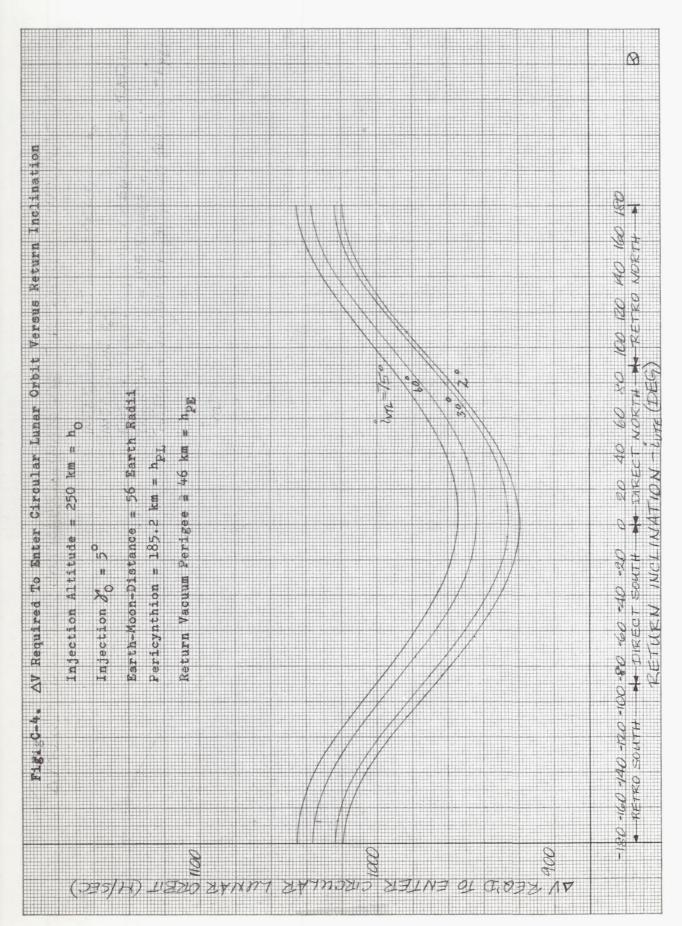
Figure	Title	Page
C-49	Lunar Orbit Inclination Versus Return Inclination	VI-97
C-50	Lunar Orbit Orientation Versus Return Inclination	VI-98
C-51	Injection Velocity Versus Return Inclination	VI-99
C-52	Injection Velocity Versus Return Inclination	VI-100
C-53	Injection Point Position Versus Return Inclination	VI-101
C-54	Moon Lead Angle Versus Return Inclination	VI-102
C-55	$\Delta\mathrm{V}$ Required to Enter Circular Lunar Orbit Versus Return Inclination	VI-103
C-56	Time of Pericynthion Versus Return Inclination	VI-104
C-57	Total Time Versus Return Inclination	VI-105
C-58	Lunar Orbit Inclination Versus Return Inclination	VI-106
C-59	Lunar Orbit Orientation Versus Return Inclination	VI-107
C-60	Injection Velocity Versus Return Inclination	VI-108
C-61	Injection Point Position Versus Return Inclination	VI-109
C-62	Moon Lead Angle Versus Return Inclination	VI-110
C-63	Δ V Required to Enter Circular Lunar Orbit Versus Return Inclination	VI-111
C-64	Time of Pericynthion Versus Return Inclination	VI-112
C-65	Total Time Versus Return Inclination	VI-113
C-66	Lunar Orbit Inclination Versus Return Inclination	VI-114
C-67	Lunar Orbit Orientation Versus Return Inclination	VI-115
C-68	Injection Velocity Versus Return Inclination	VI-116
C-69	Injection Point Position Versus Return Inclination	VI-117
C-70	Moon Lead Angle Versus Return Inclination	VI-118
C-71	$\Delta\mathrm{V}$ Required to Enter Circular Lunar Orbit Versus Return Inclination	VI-119
C-72	Time of Pericynthion Versus Return Inclination	VI-120
C-73	Total Time Versus Return Inclination	VI-121

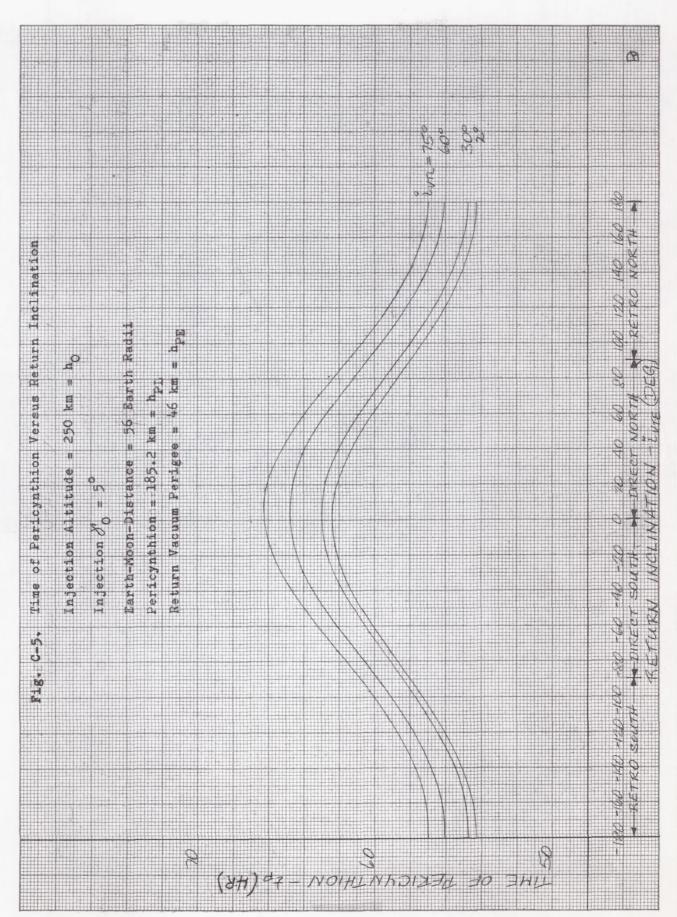
Figure	Title	Page
C-74	Lunar Orbit Inclination Versus Return Inclination	VI-122
C-75	Lunar Orbit Orientation Versus Return Inclination	VI-123
C-76	Injection Velocity Versus Return Inclination	VI-124
C-77	Injection Point Position Versus Return Inclination	VI-125
C-78	Moon Lead Angle Versus Return Inclination	VI-126
C-79	ΔV Required to Enter Circular Lunar Orbit Versus Return Inclination	VI-127
C-80	Time of Pericynthion Versus Return Inclination	VI-128
C-81	Time of Pericynthion Versus Return Inclination	VI-129
C-82	Lunar Orbit Inclination Versus Return Inclination	VI-130
C-83	Lunar Orbit Orientation Versus Return Inclination	VI-131

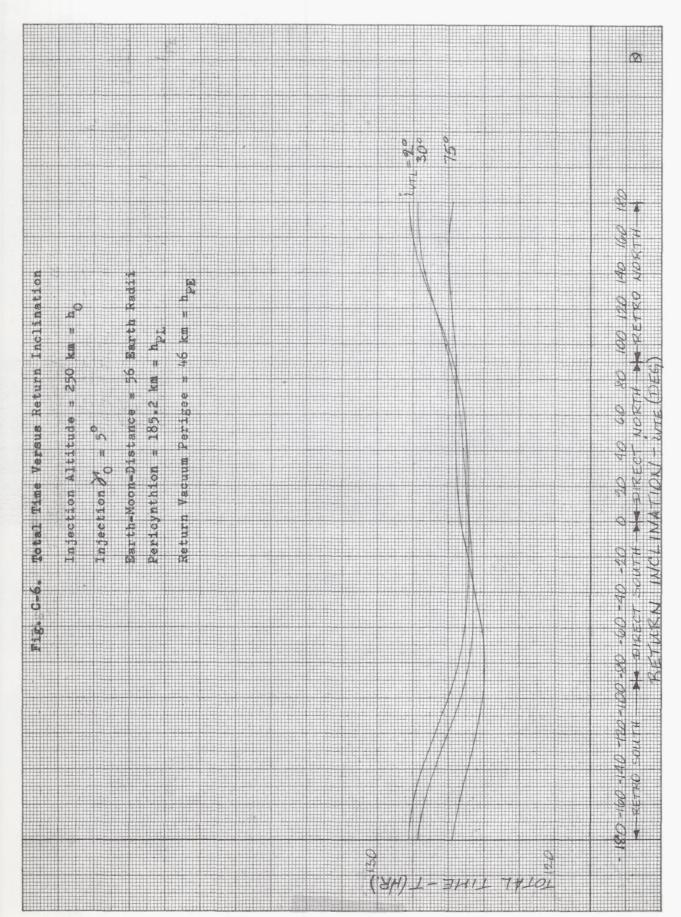


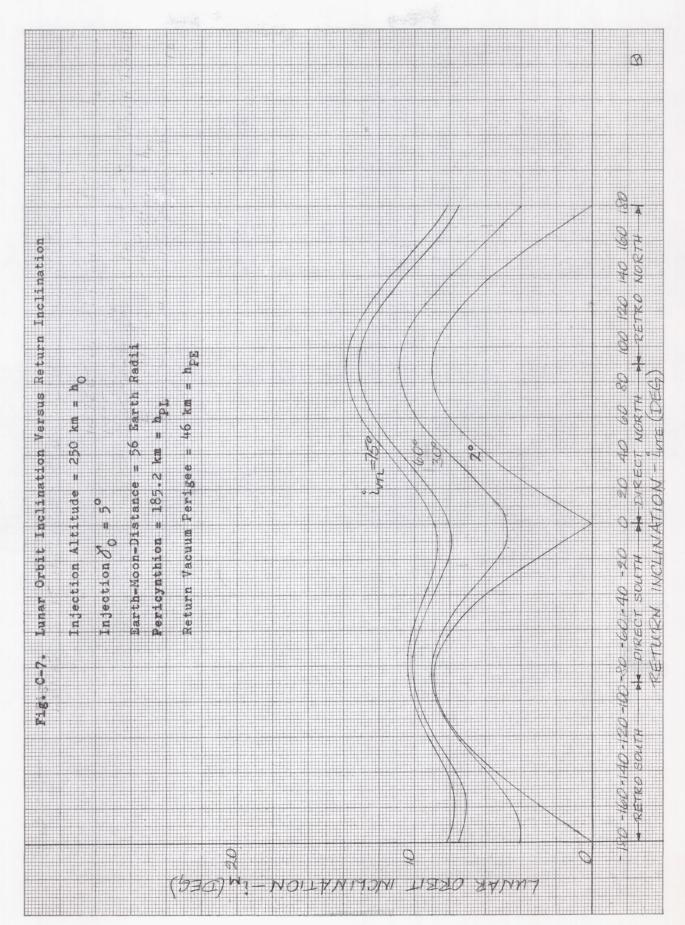


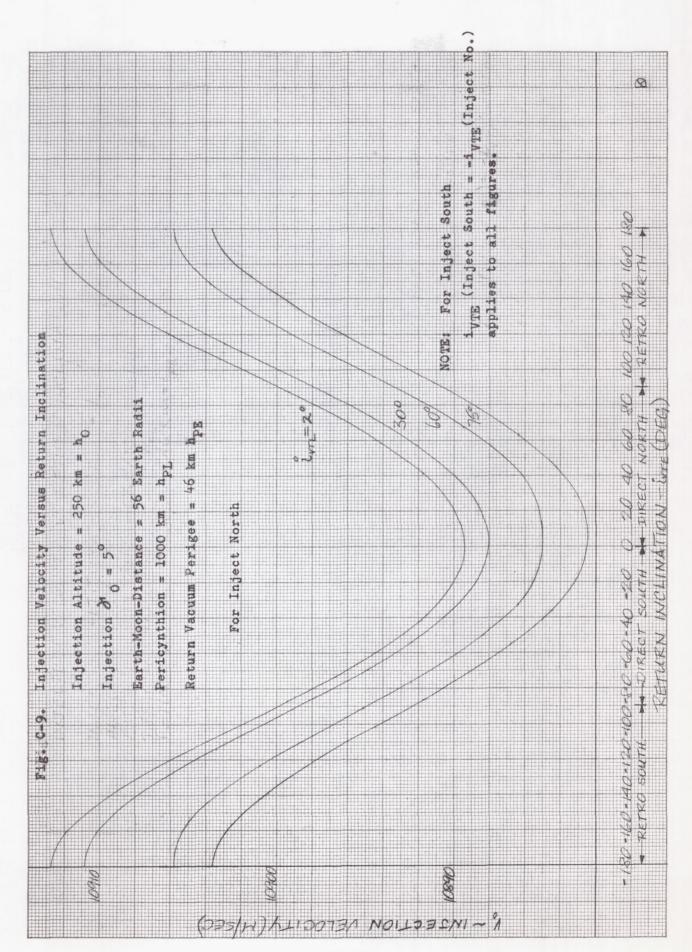


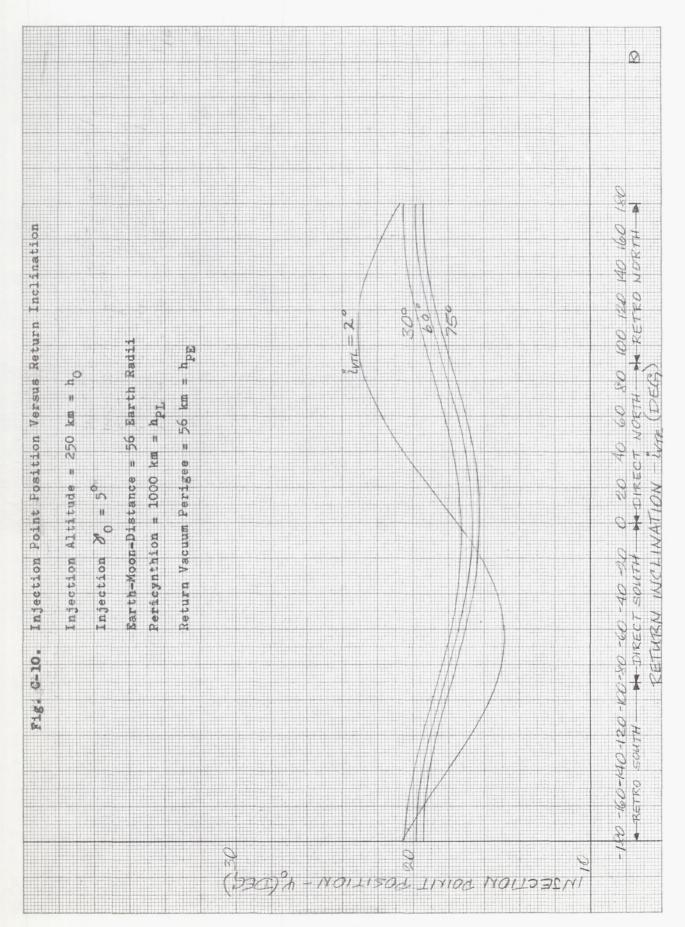




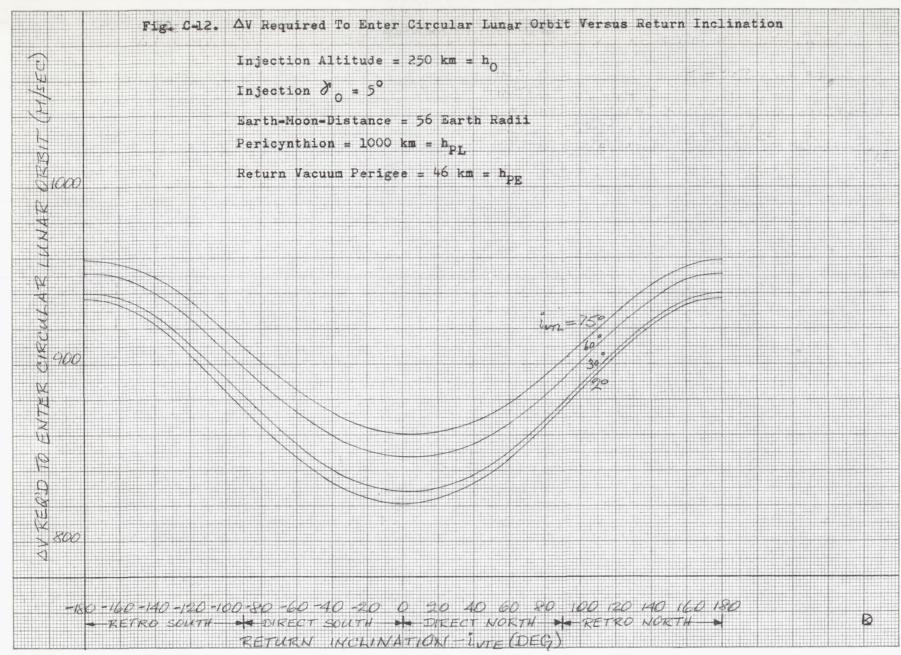


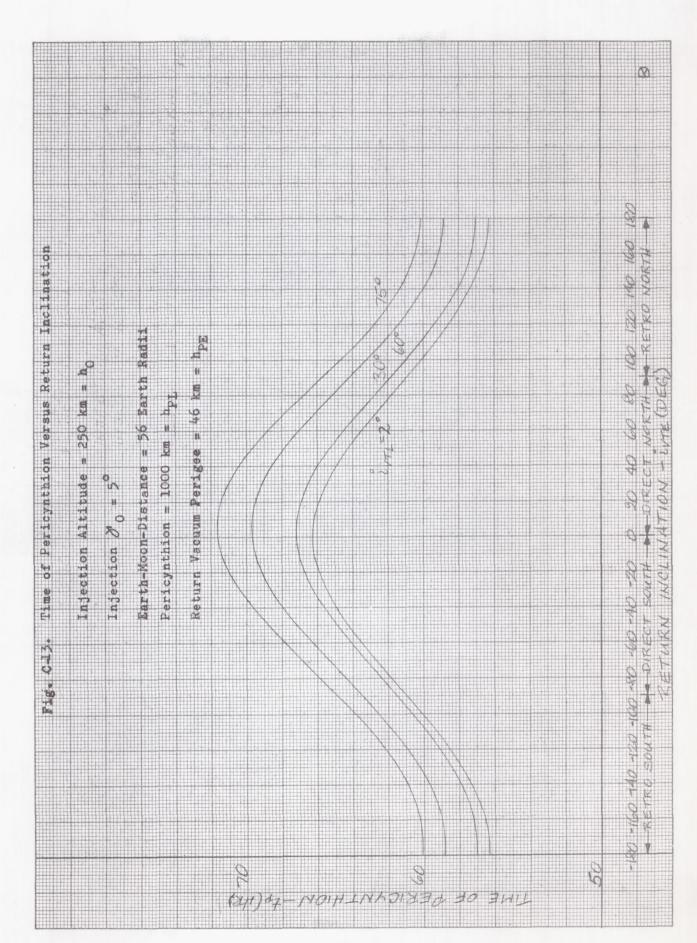


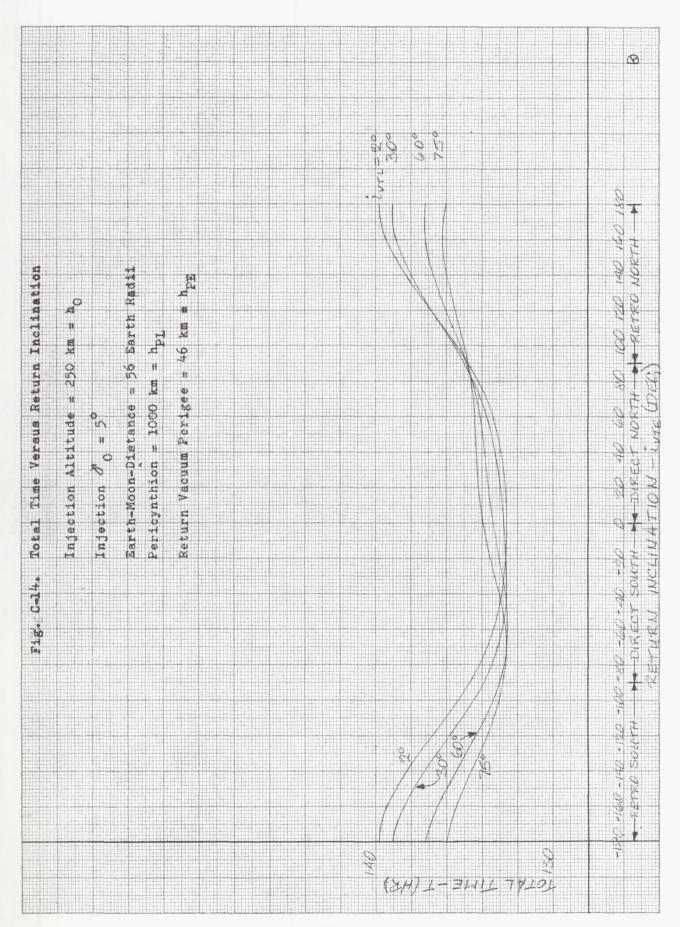


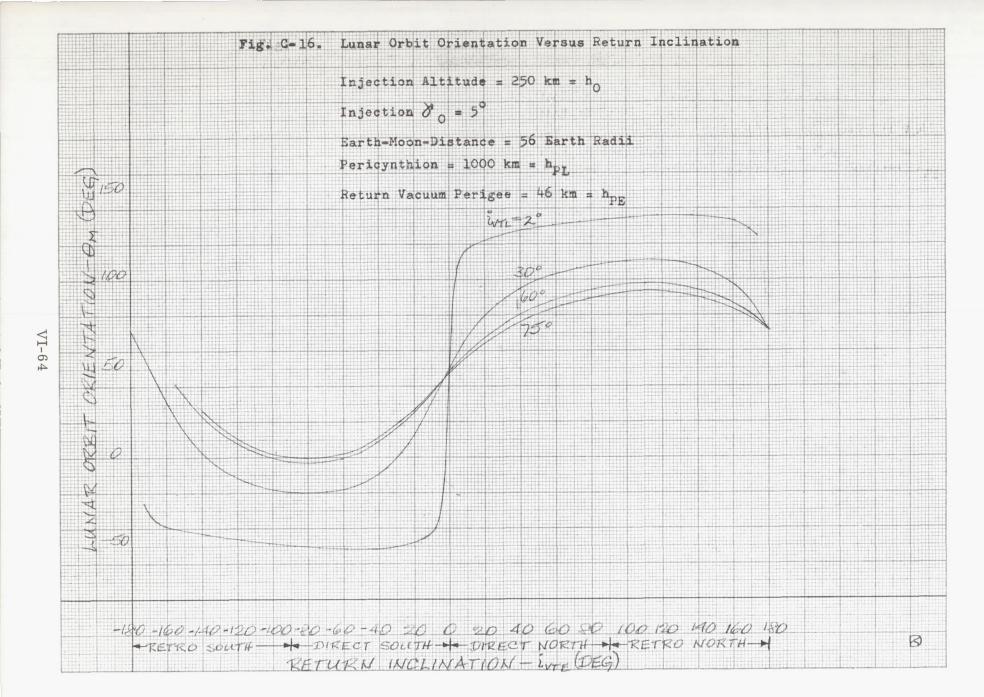


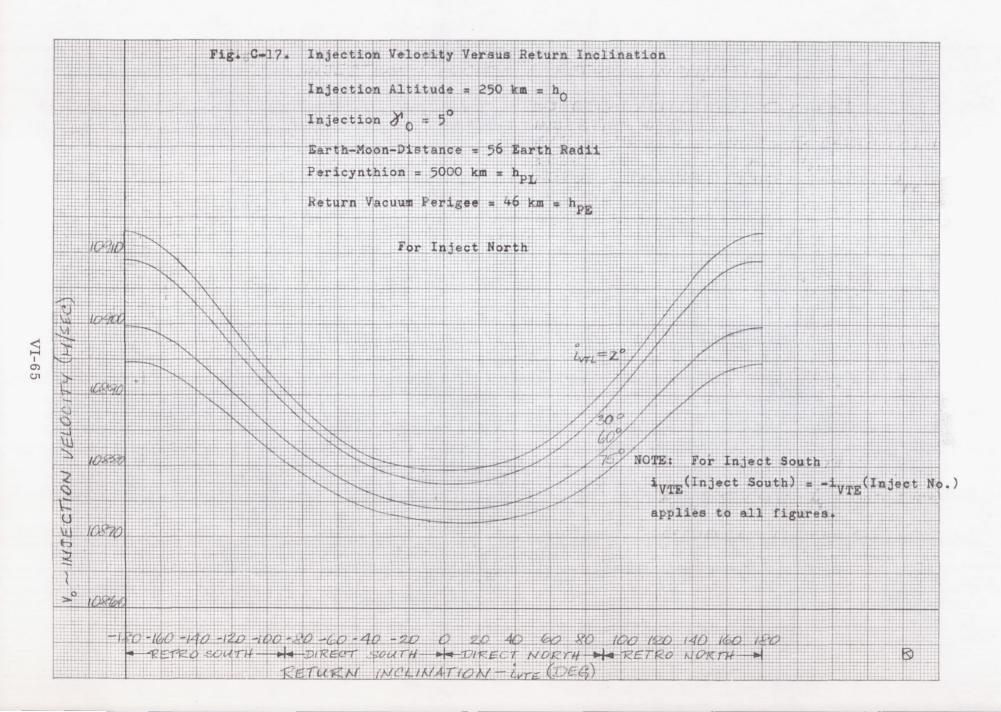


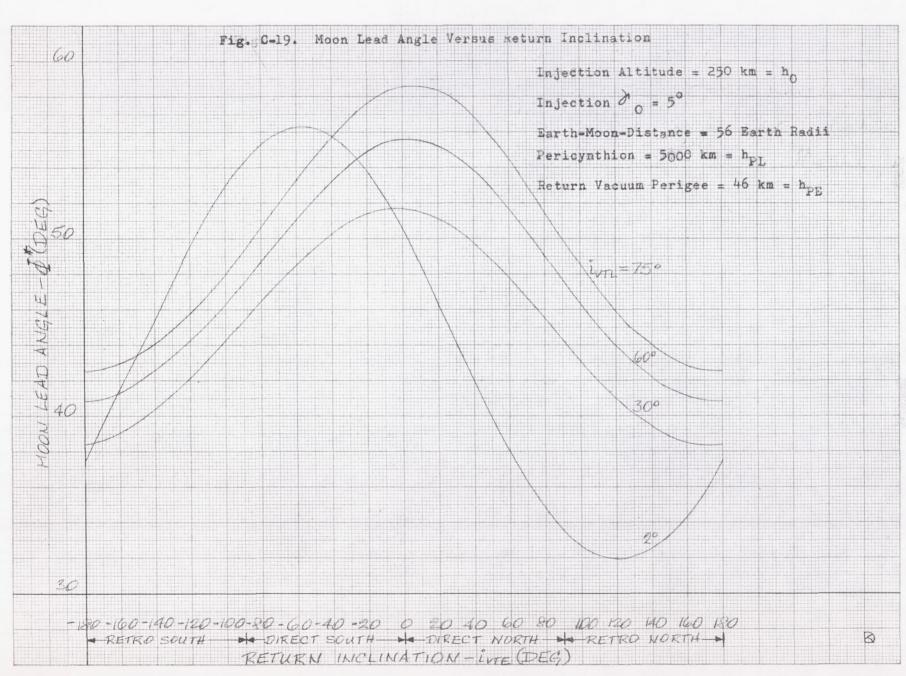




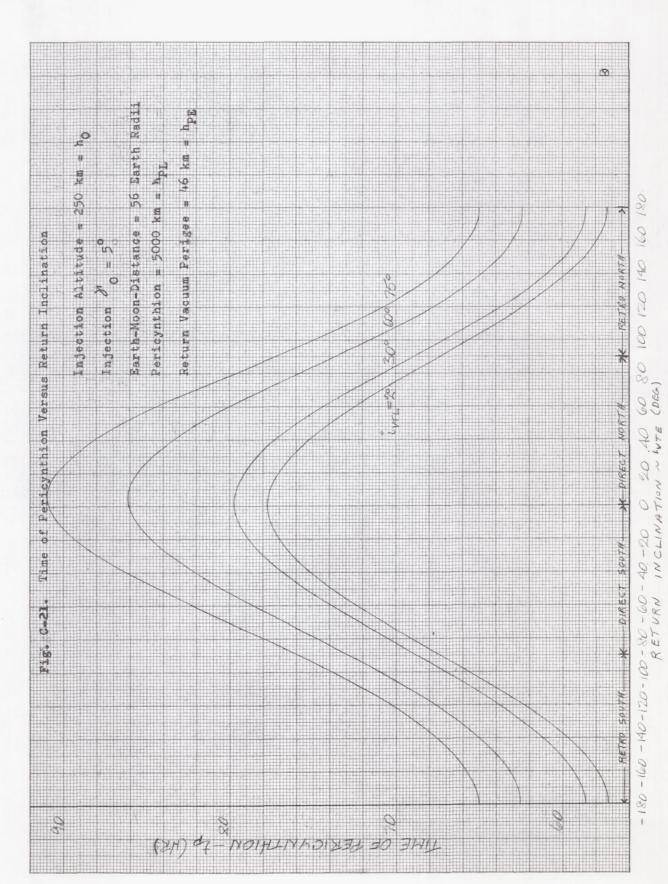


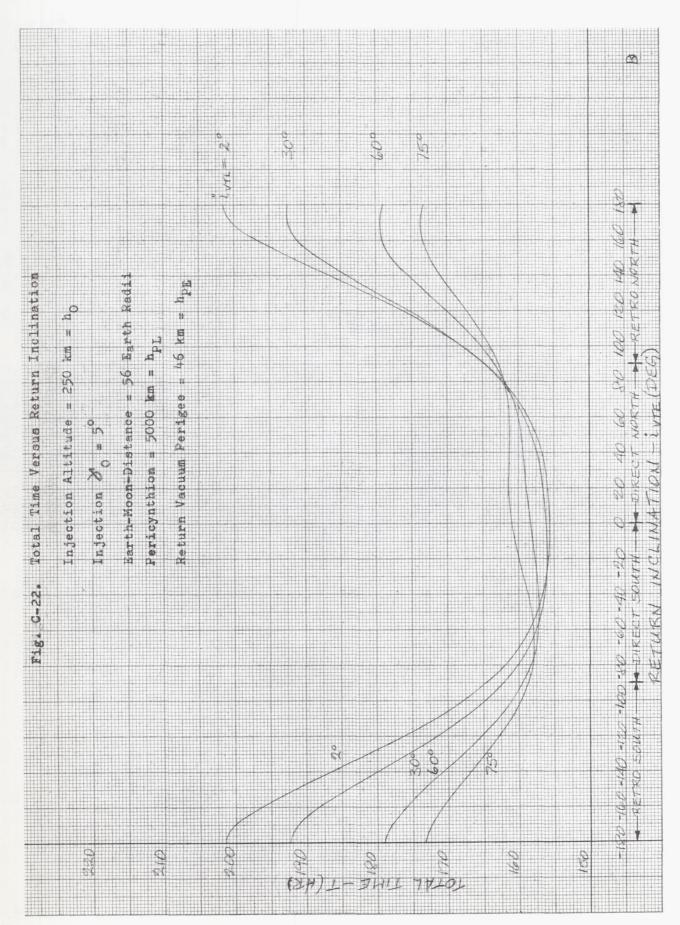


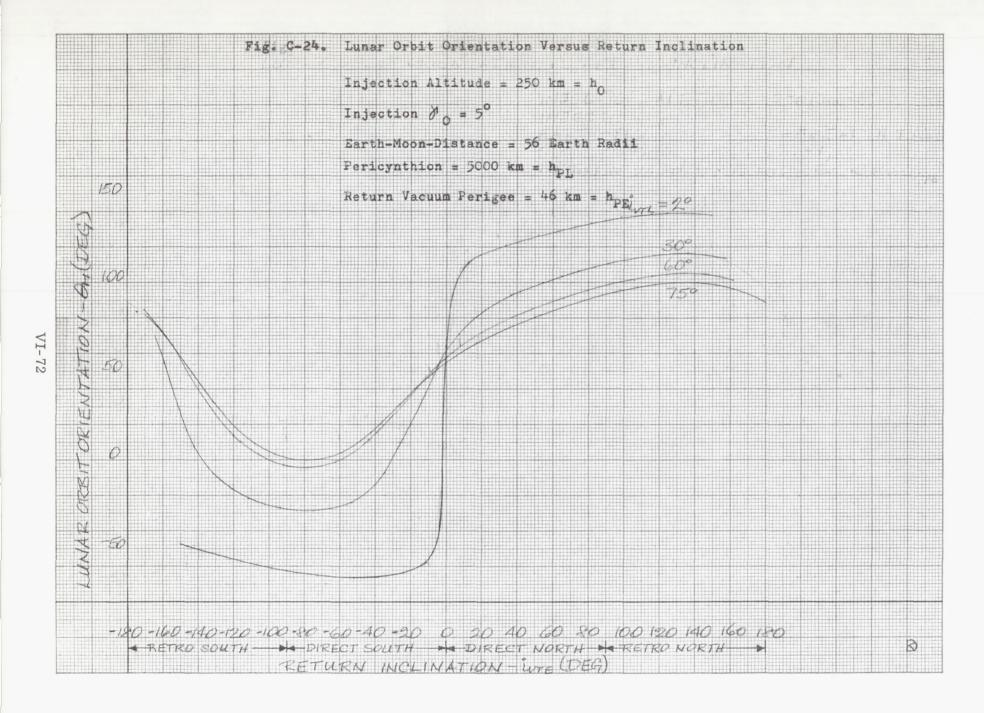


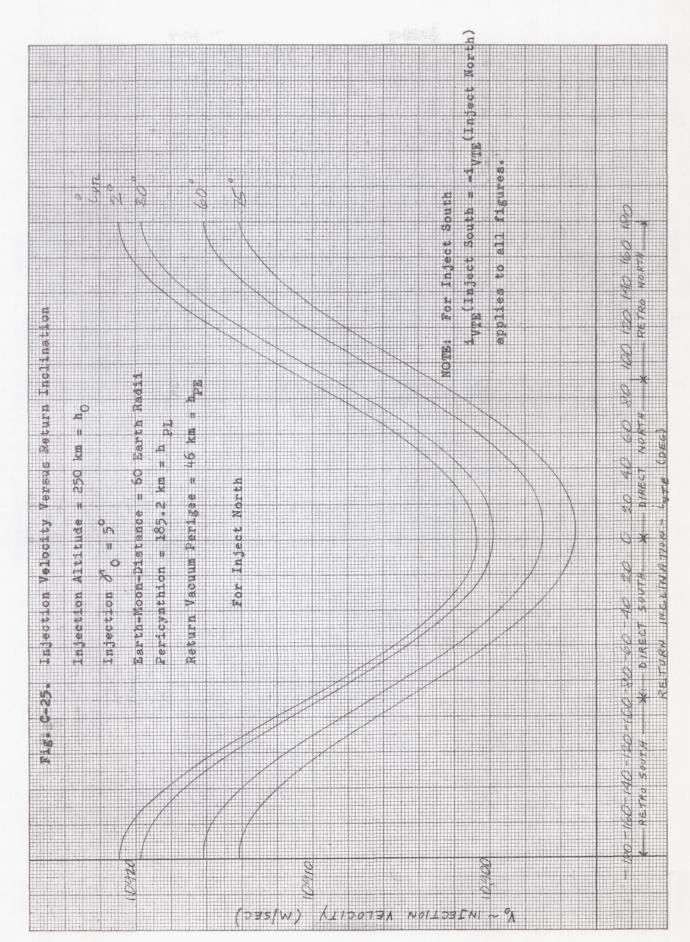


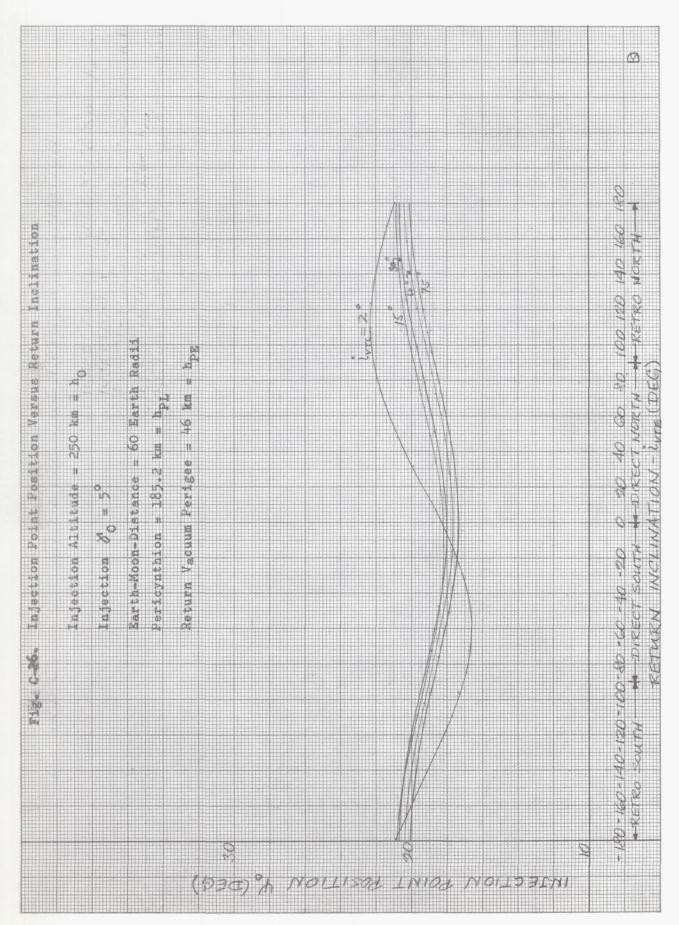
VI-68

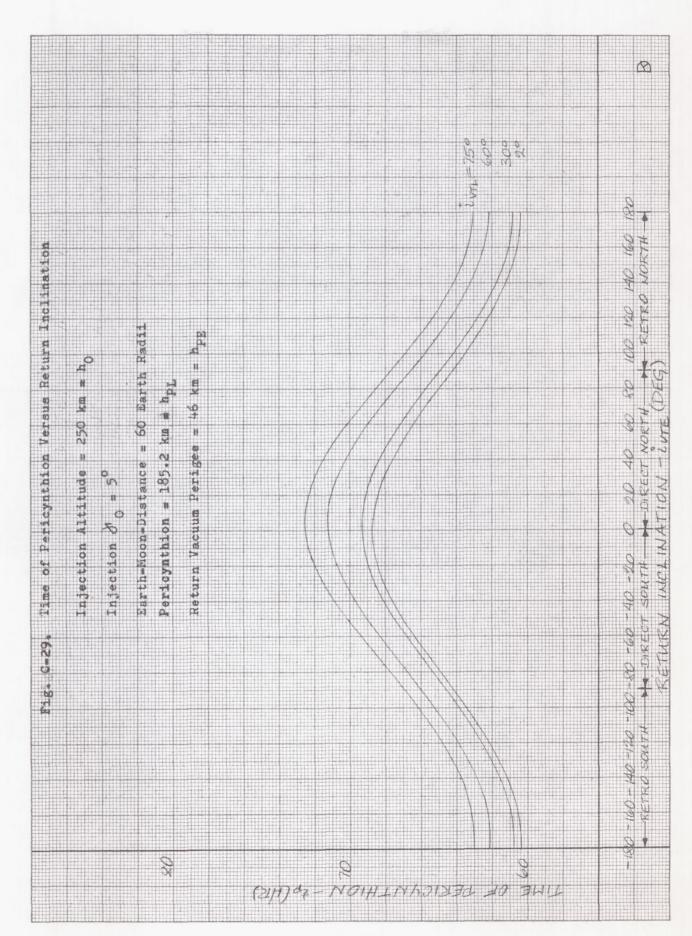


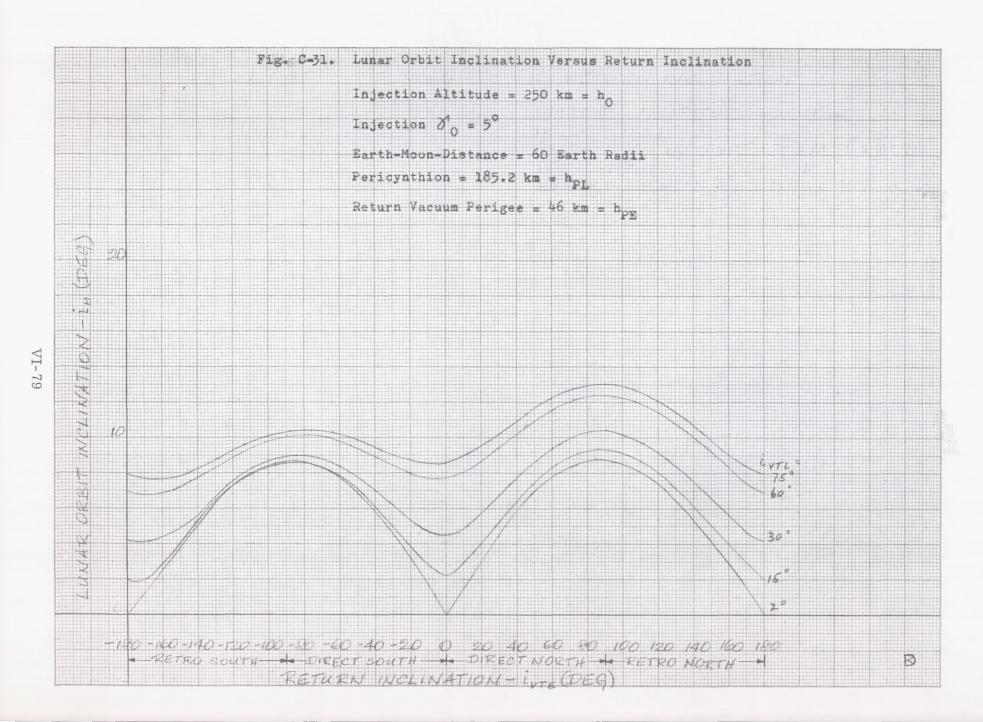


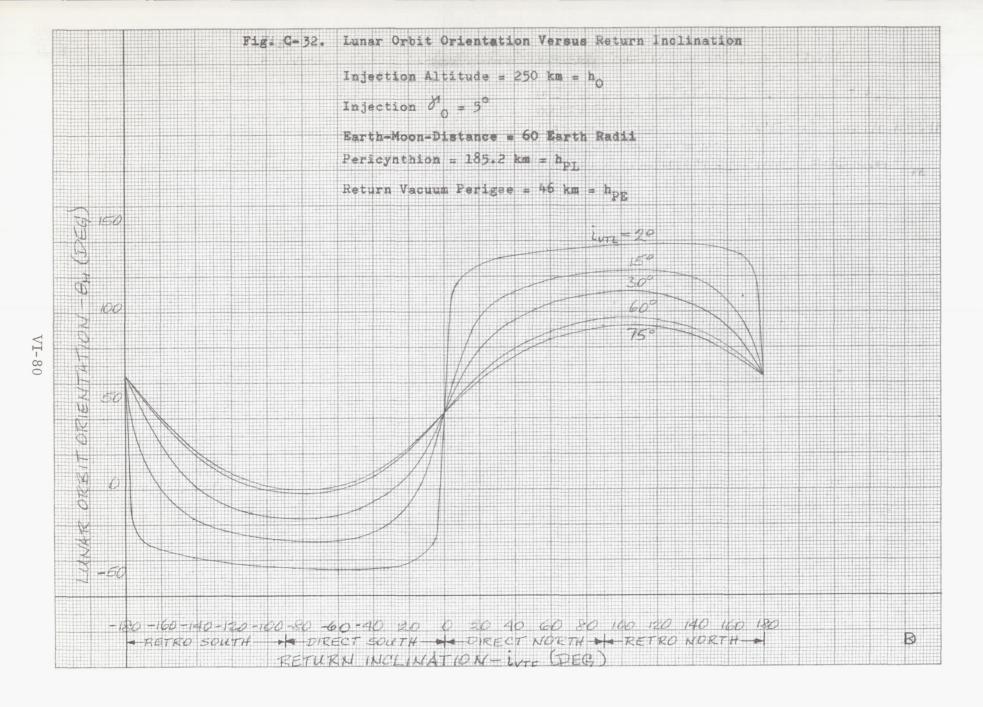


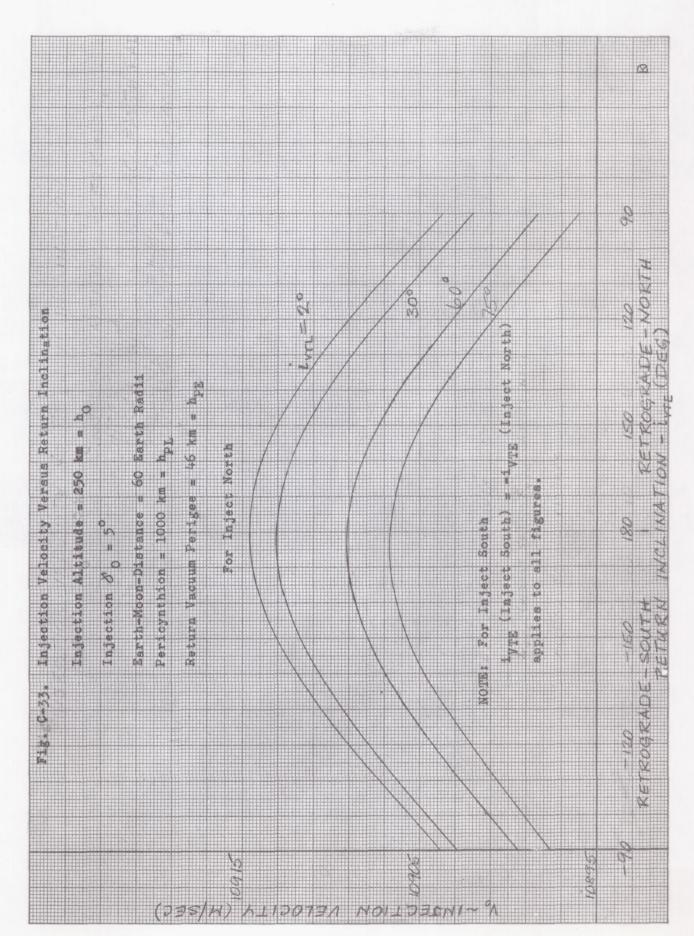


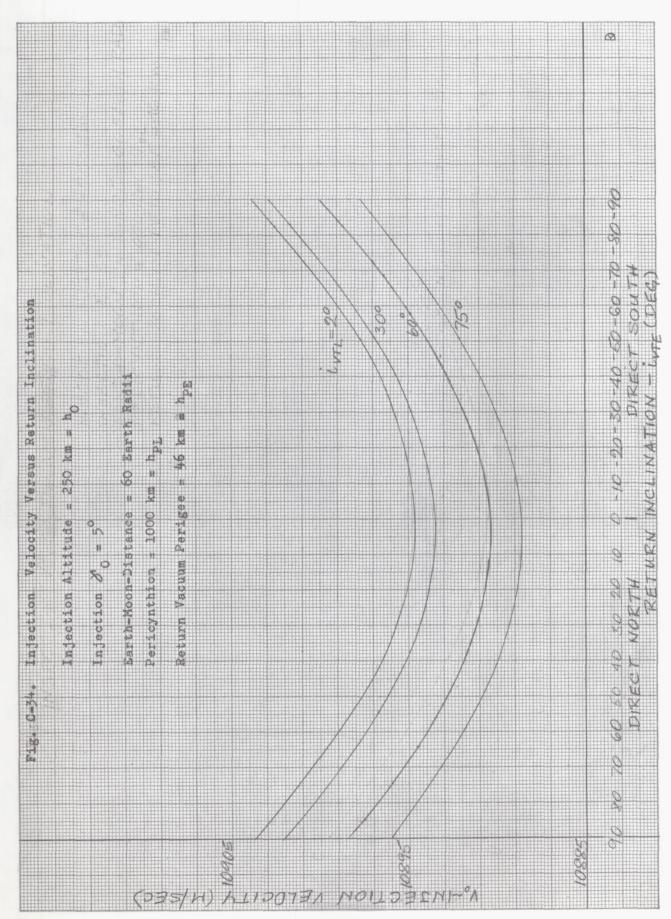


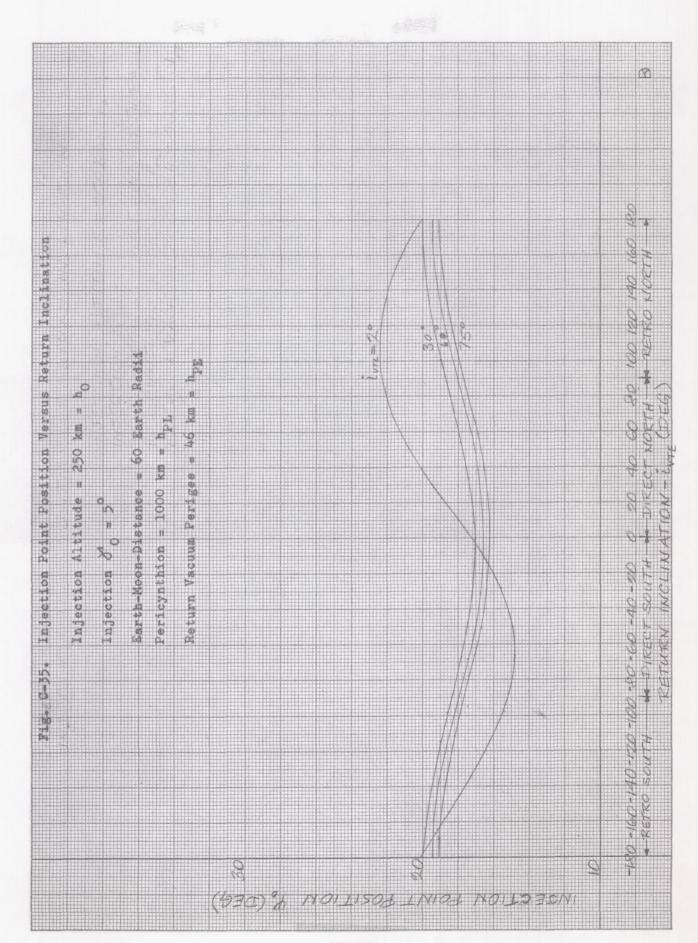


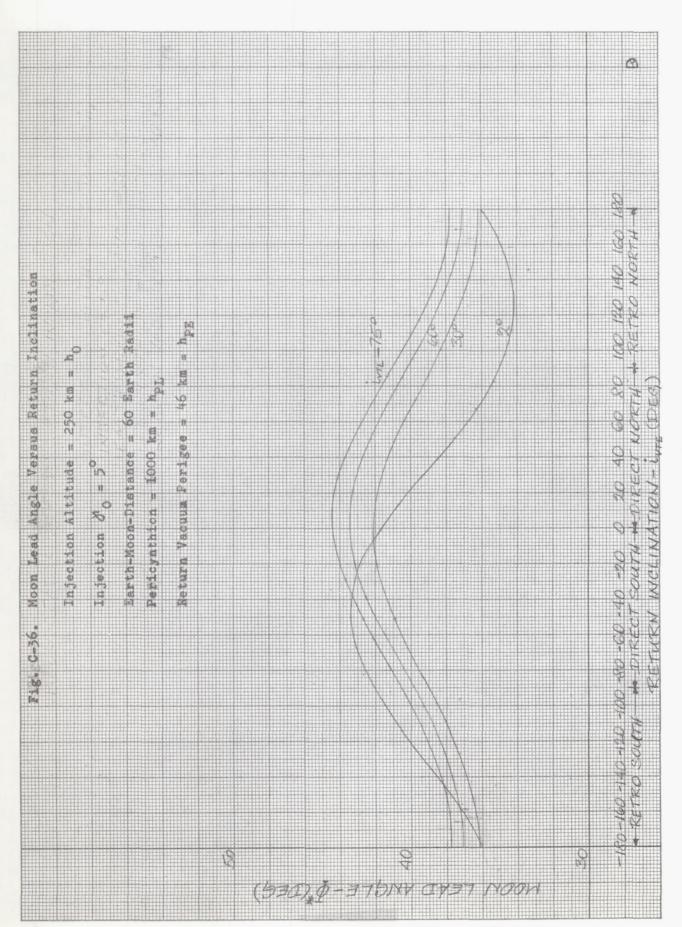




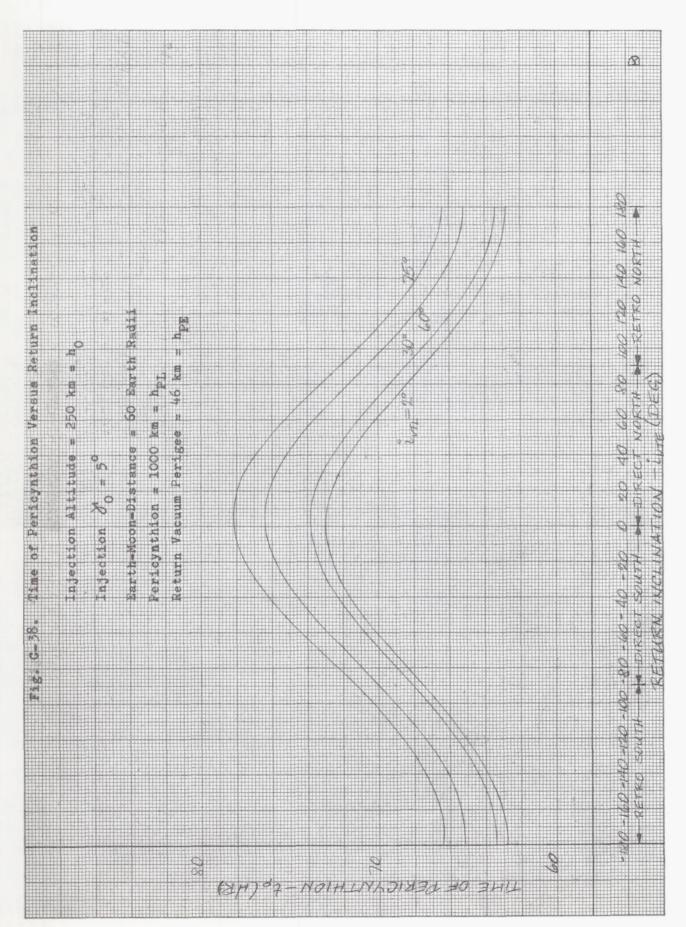


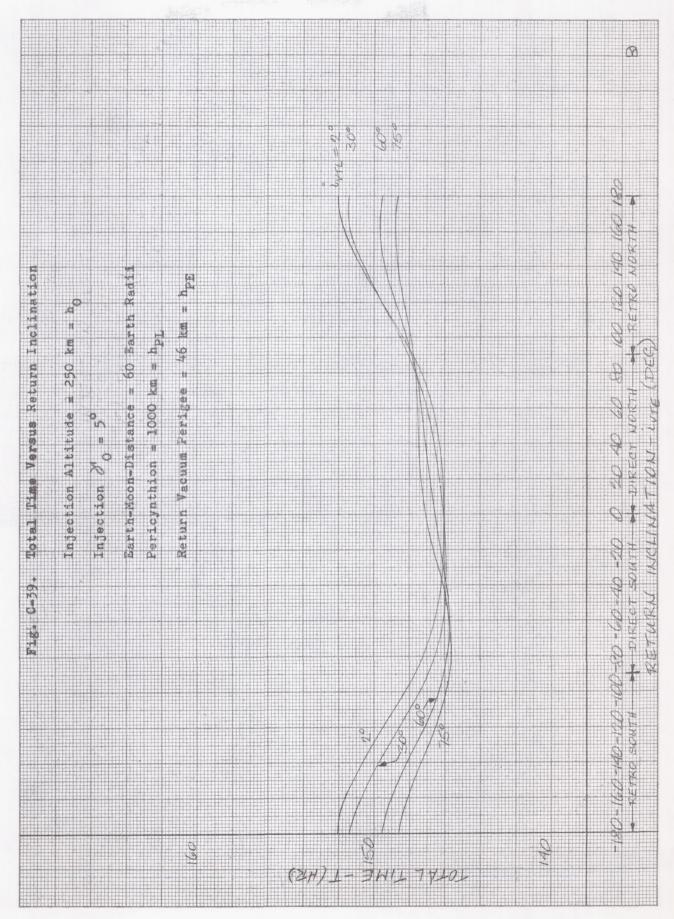




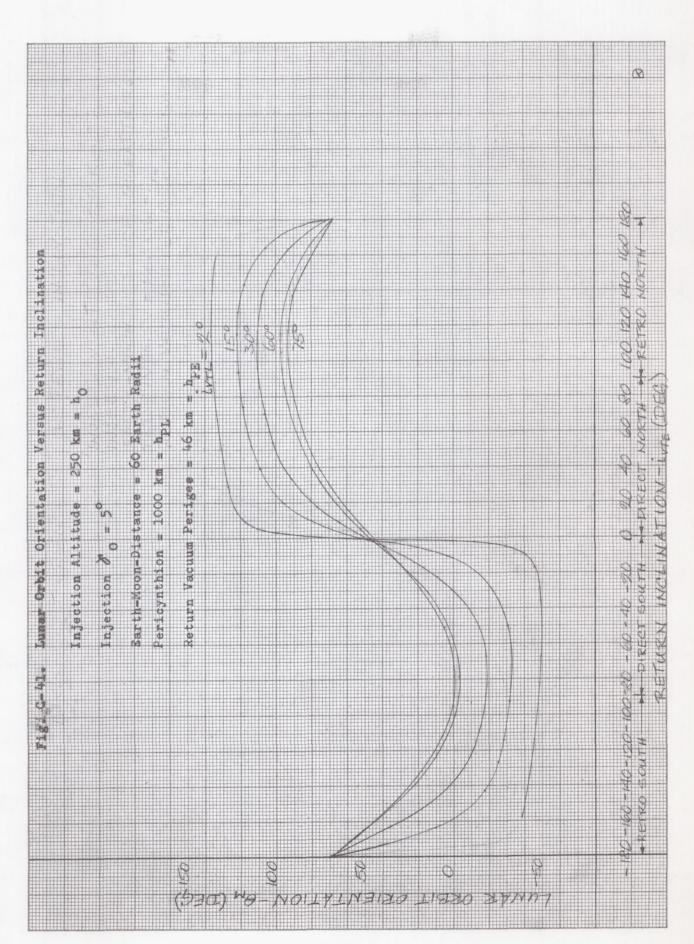


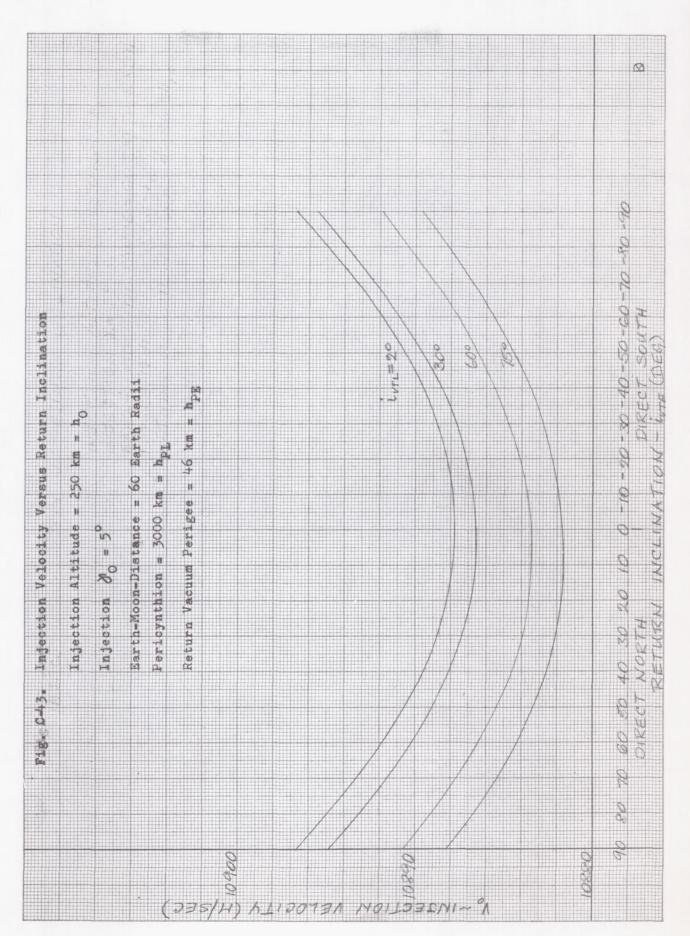
K E C C C C C C C C C C C C C C C C C C	
Injection Altitude = 250 km = h ₀ Injection O = 5° Barth-Moon-Distance = 60 Earth Radii Pericynthion = 1000 km = h _{PL} Return Vacuum Perices = 46 km = h _{PE}	

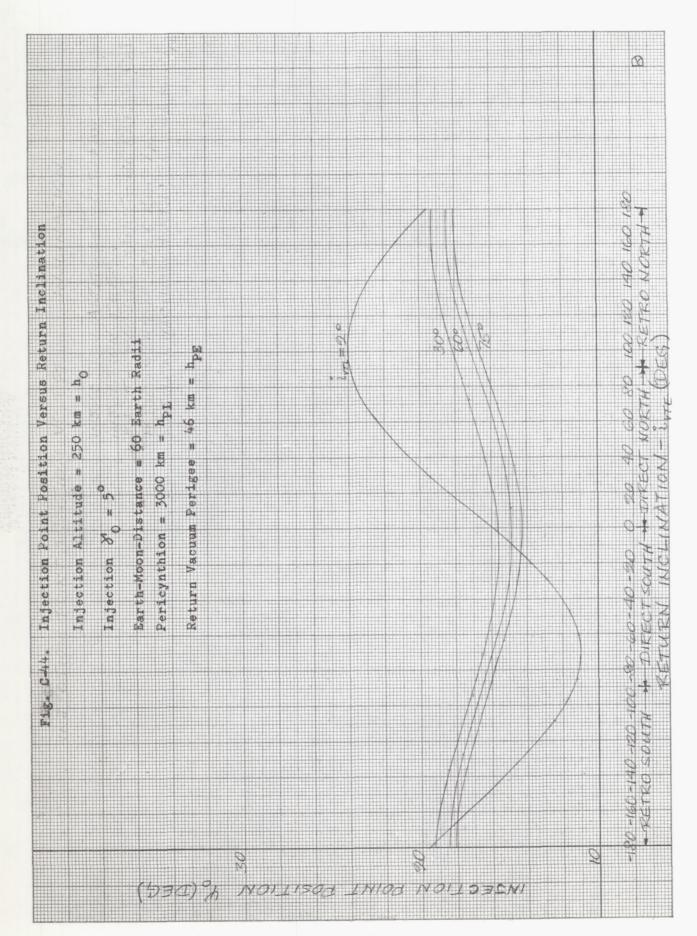




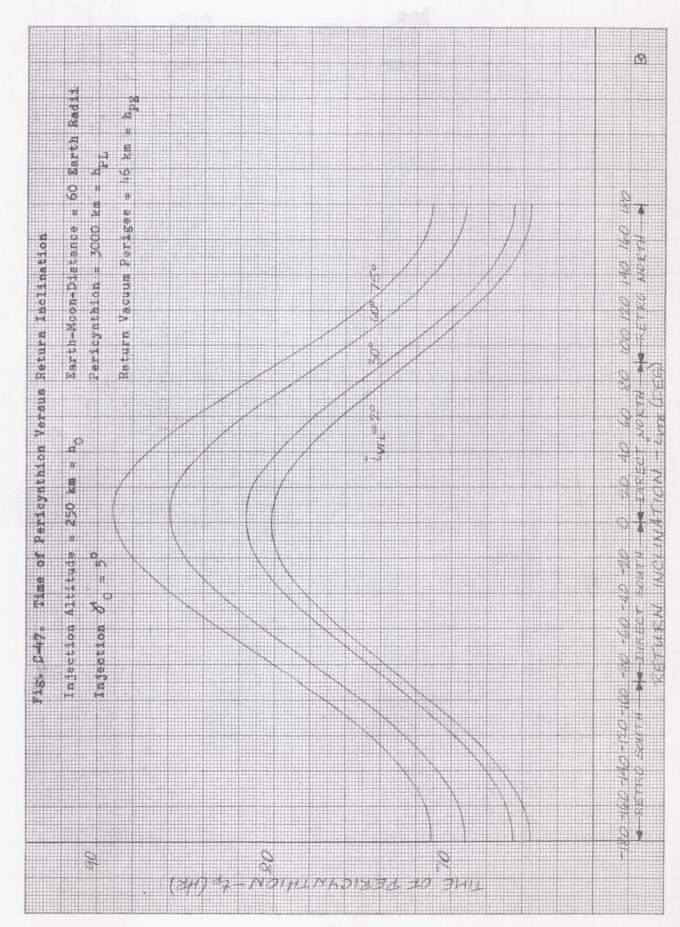
VI-88

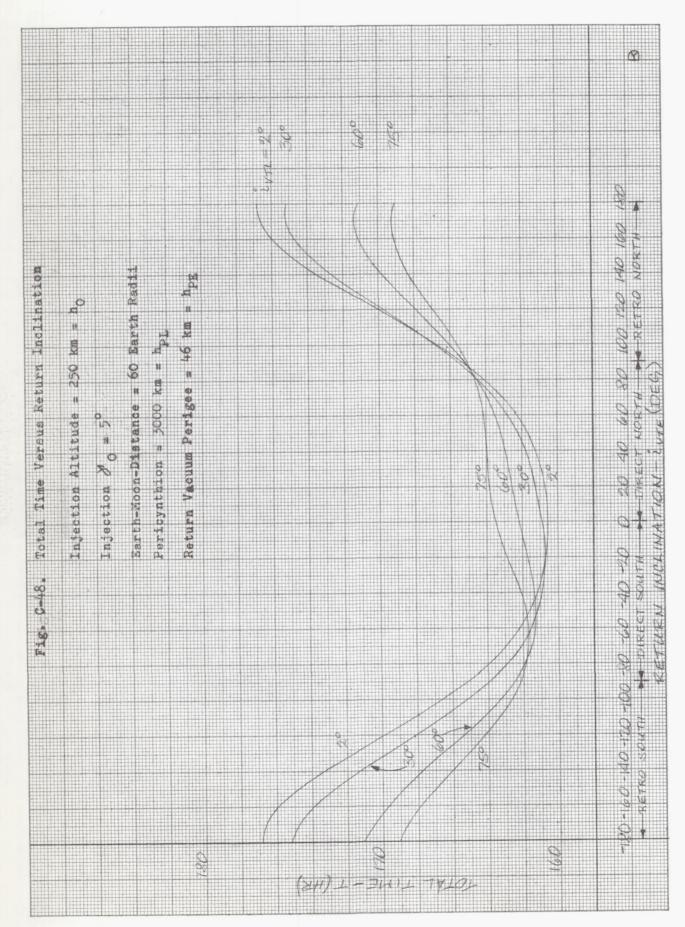


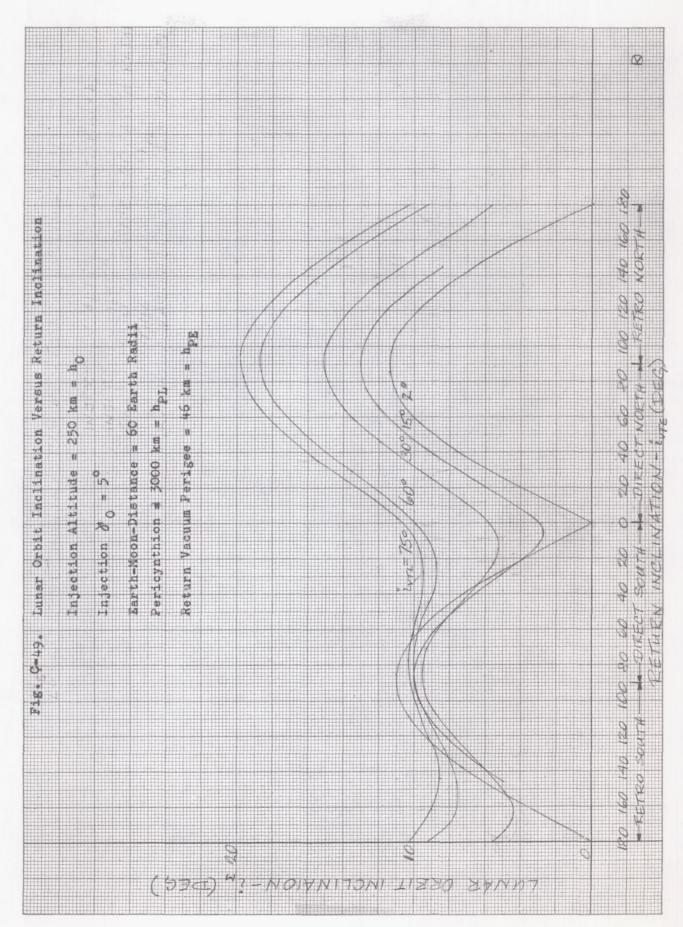


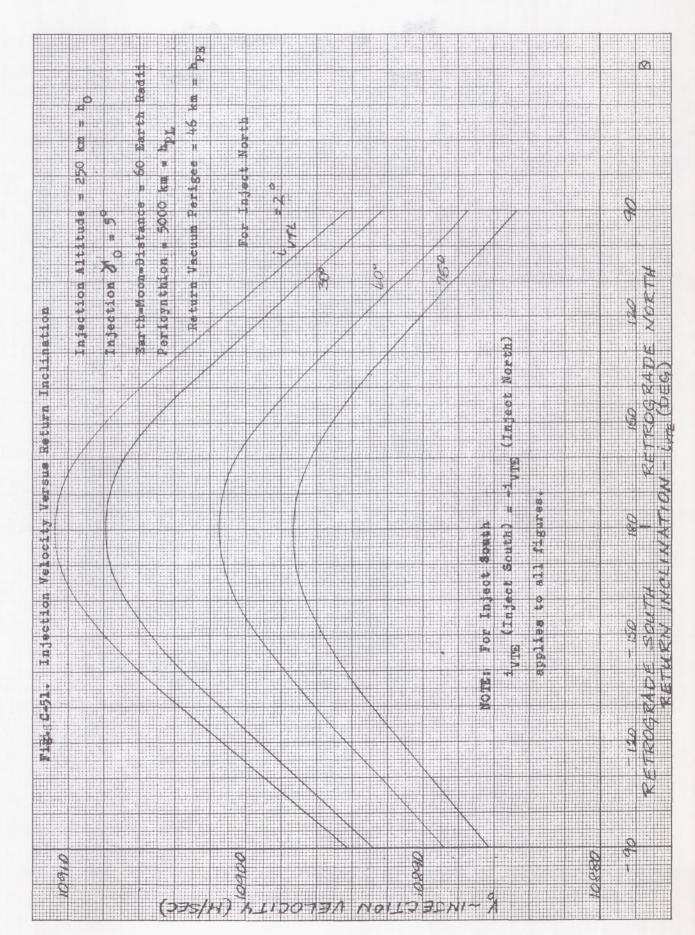


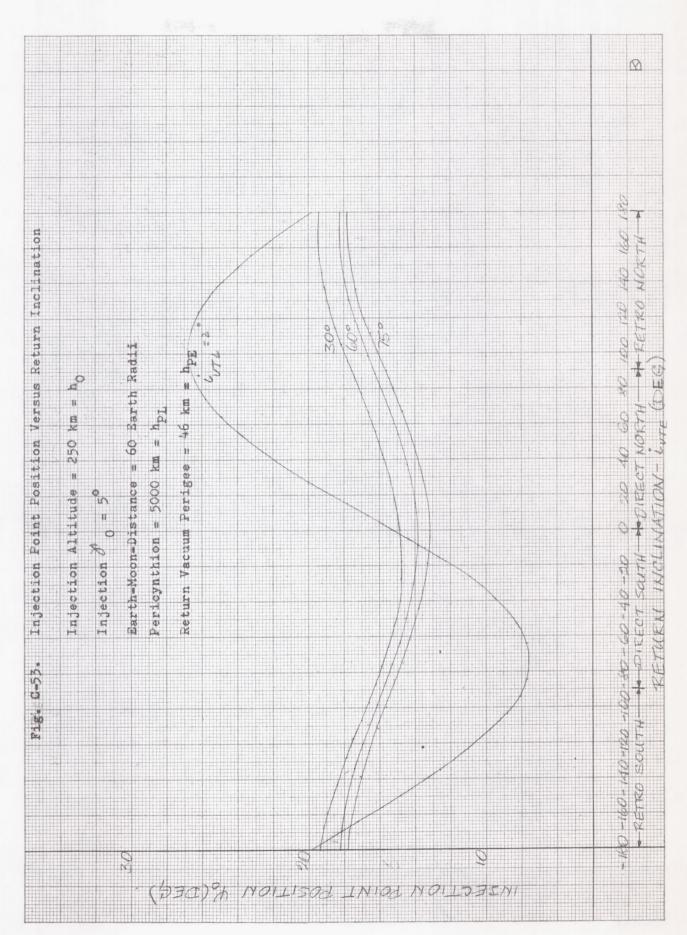
	.		2
Injection Altitude = 250 km = h_0 Injection $\partial^{i}_{0} = 5^{\circ}$ Earth-Moon-Distance = 60 Earth Radii	= hpl		0 20 40 60 80 100 120 140 160 180
Injection Altitude = 250 km Injection 8 0 = 5 Earth-Moon-Distance = 60 Ea	Pericynthion = 3000 km = hpl Return Vacuum Perigee = 46 km		-180 -160 -140 -120 -100 -80 -60 -40 -20 0
((D35/H) L	M KEDID LO ENLEK CIKCHTYK OBEI	



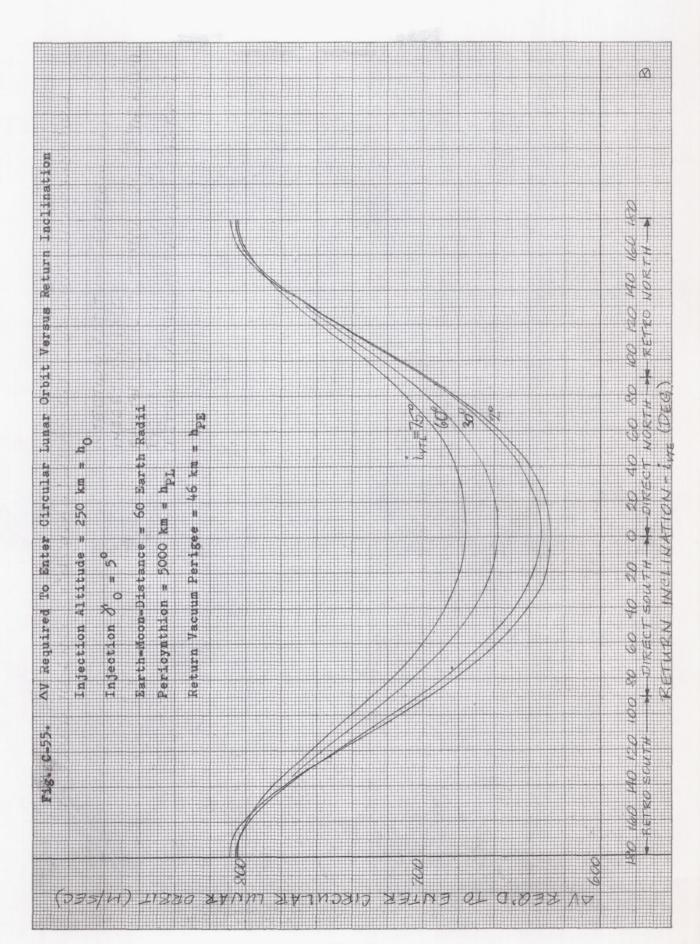


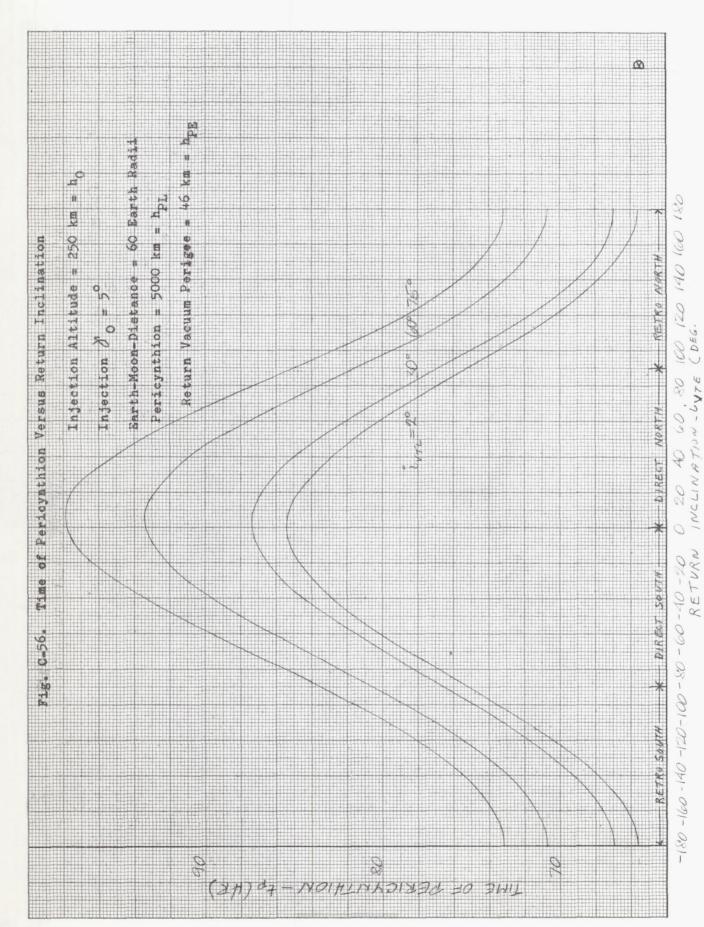




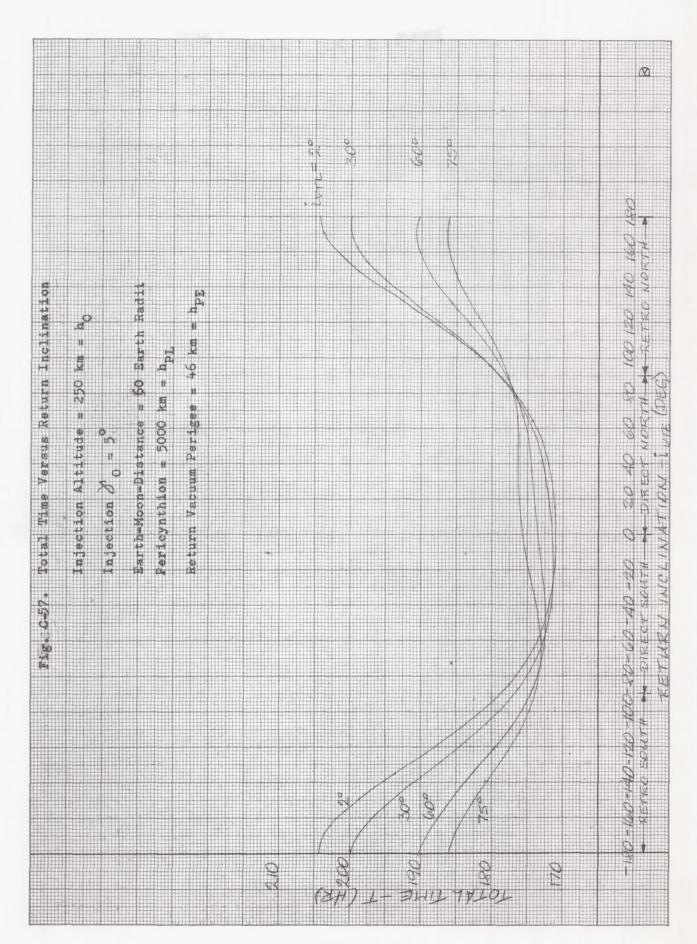


RETURN INCLINATION - in (DEG)



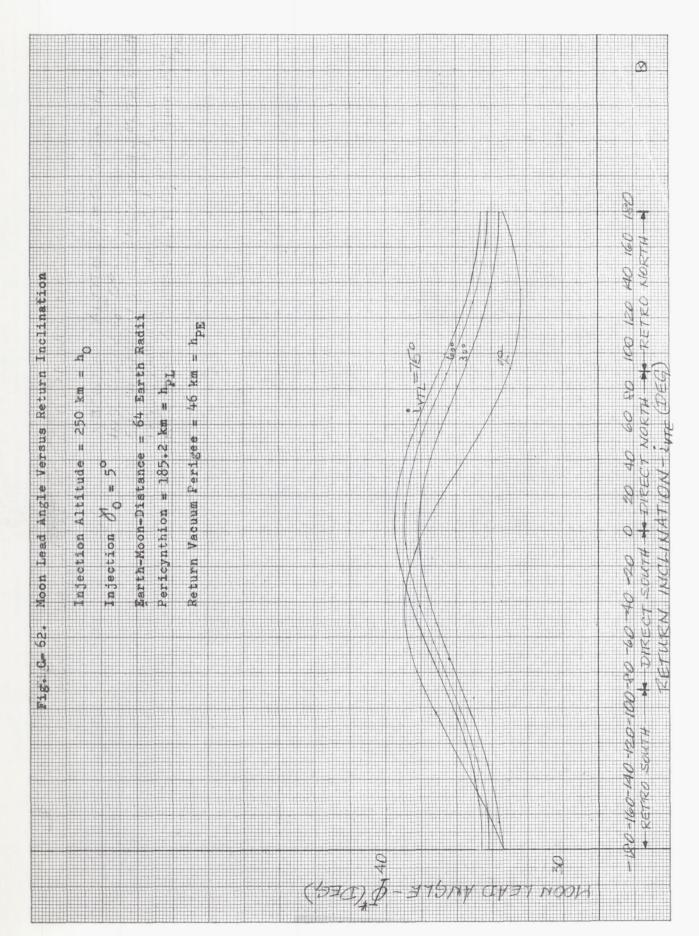


VI-104

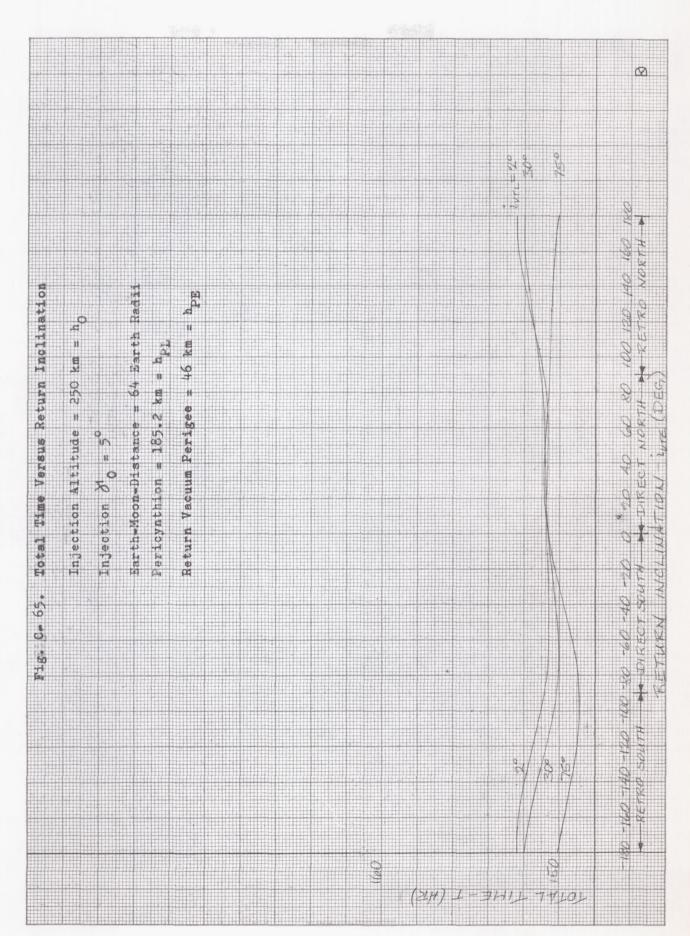


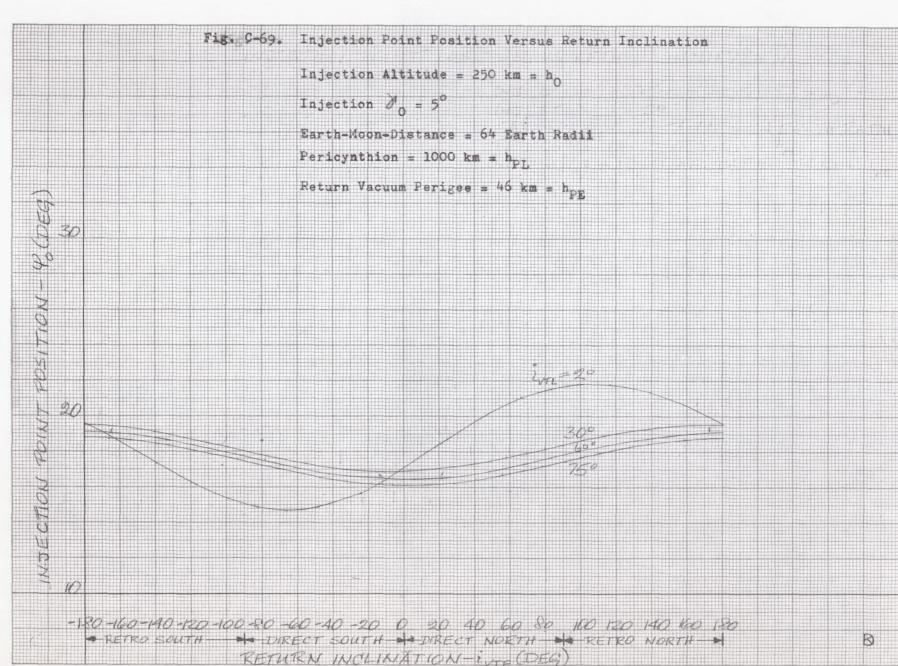
Injection Point Position Versus Return Inclination

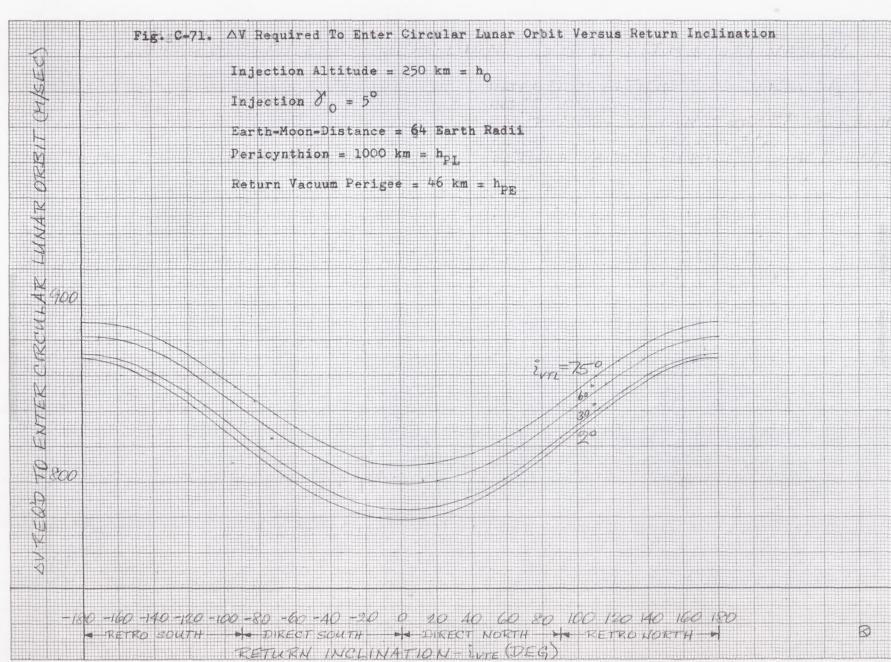


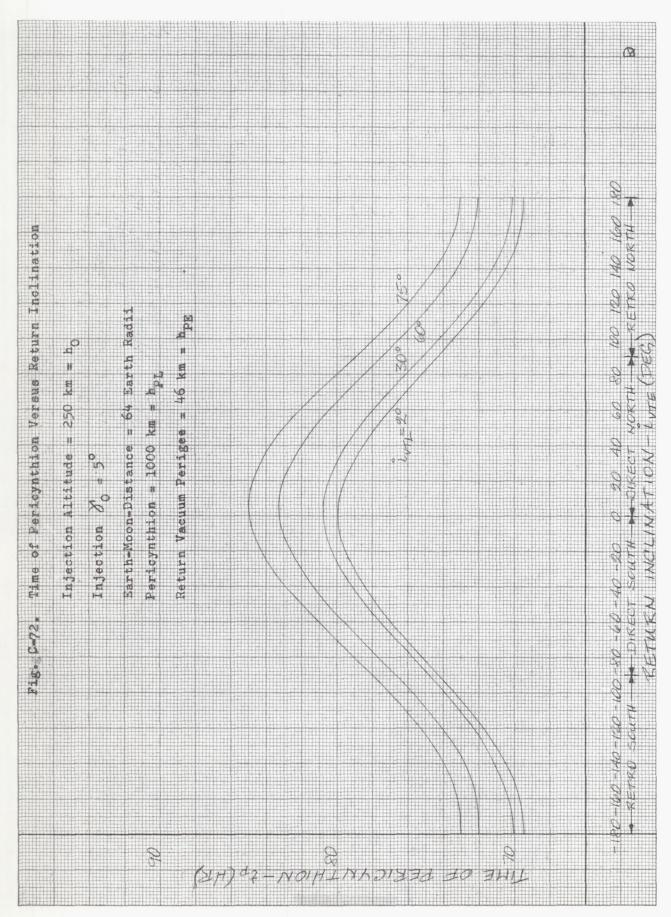


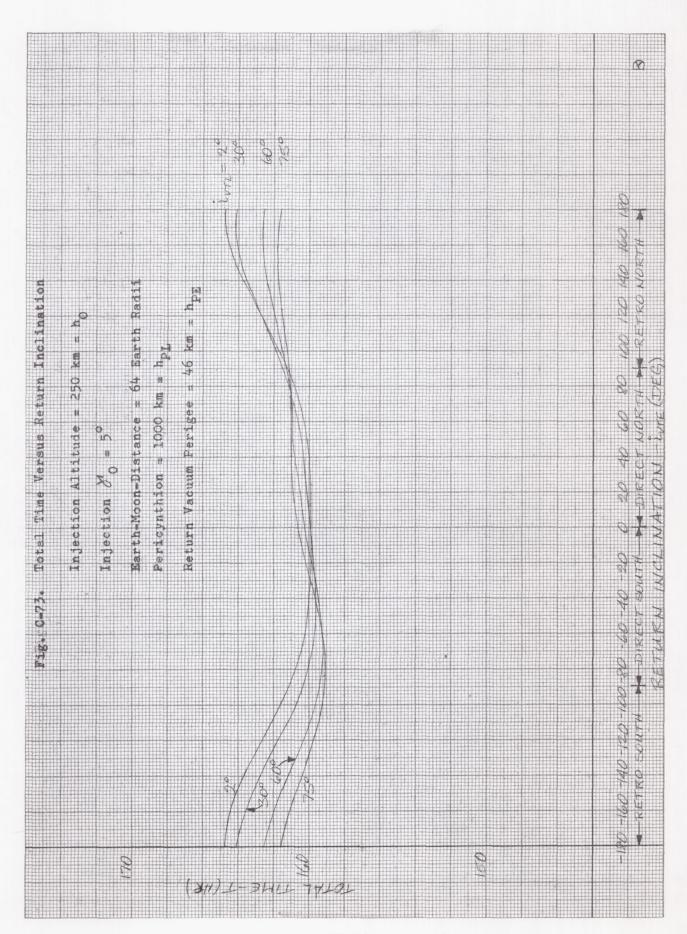
= 250 km = h _D . 2 km = h _D . 3ee = 46 km = h _D . 2m=76. 2					6
Injection Altitude = 25 Injection Altitude = 25 Earth-Moon-Distance = 6 Perioynthion = 185.2 km Return Vacuum Perigee = 6 Return Vacuum Perigee = 6		4 Earth Radii	46 km = hpg	247=75°	40 60 80 100 120 1
	Injection Al	W 2			-180-160-140-120-100-30-60-40-90 0



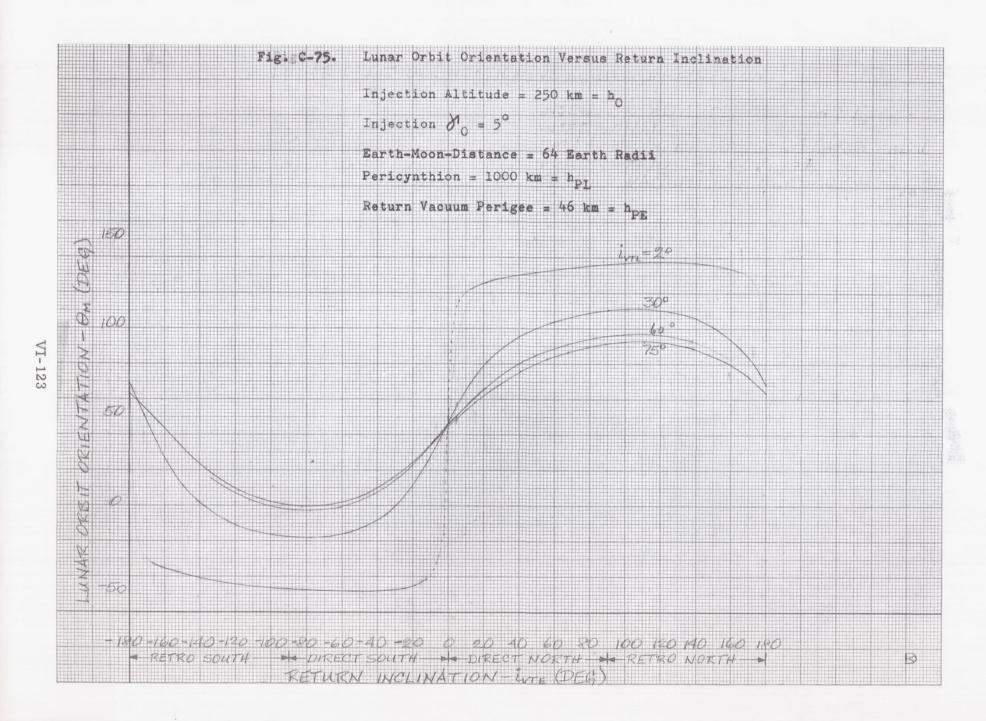


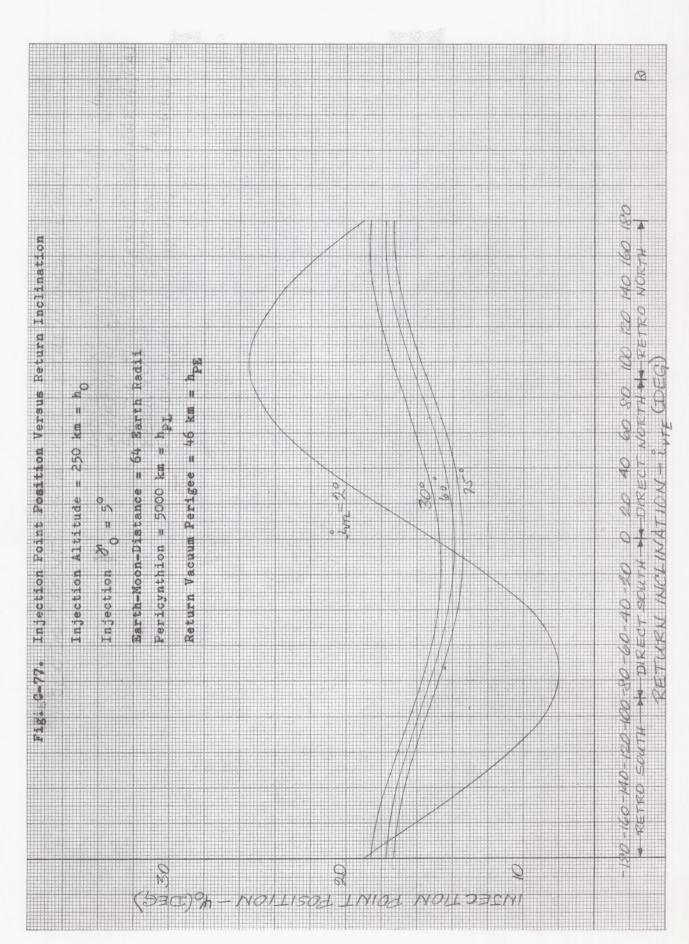


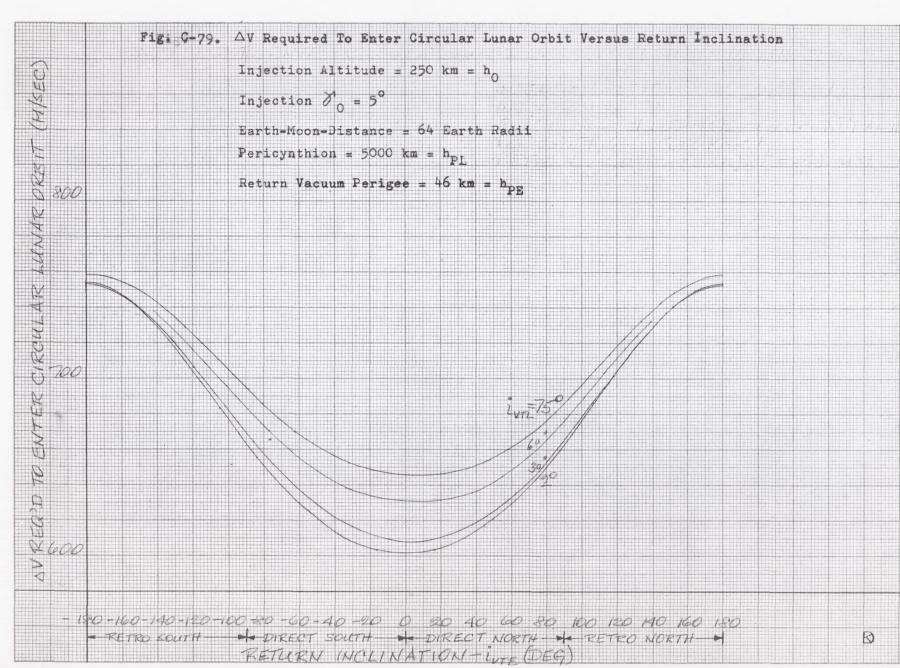




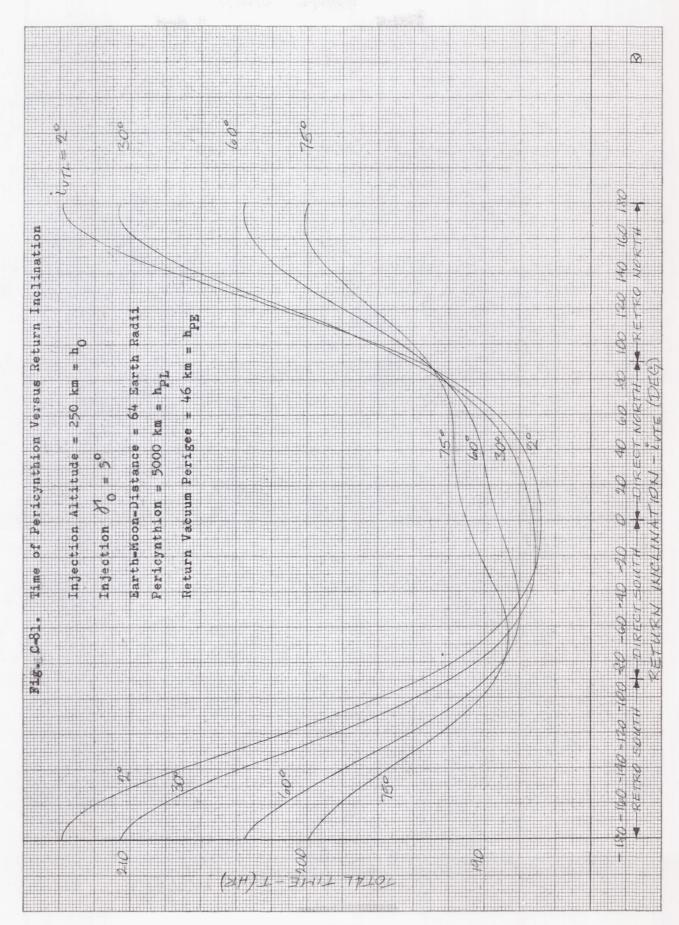
RETURNI INCLIMATION - ivre (DEG)



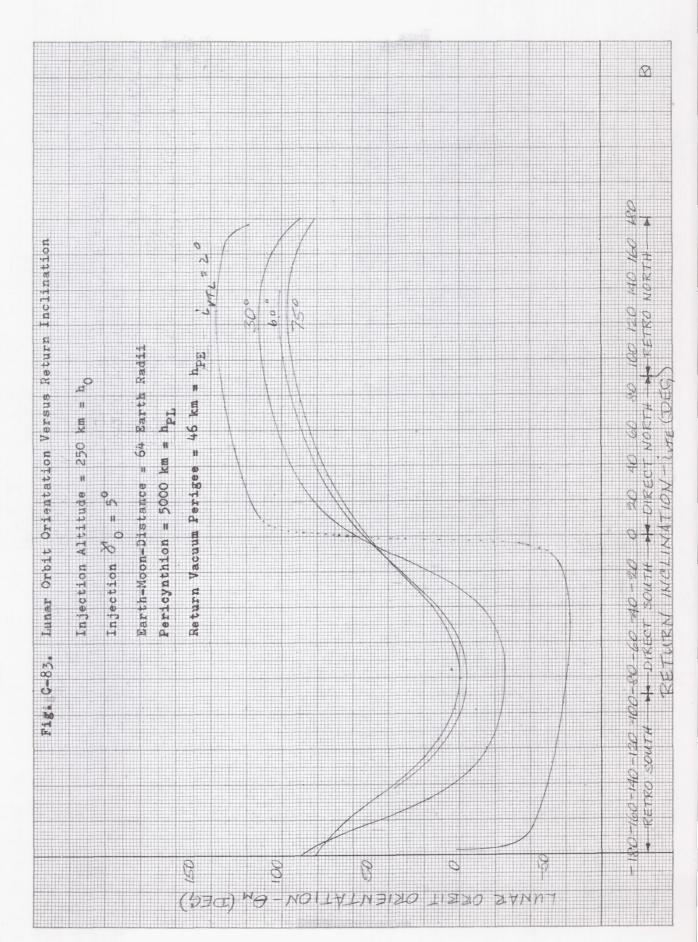


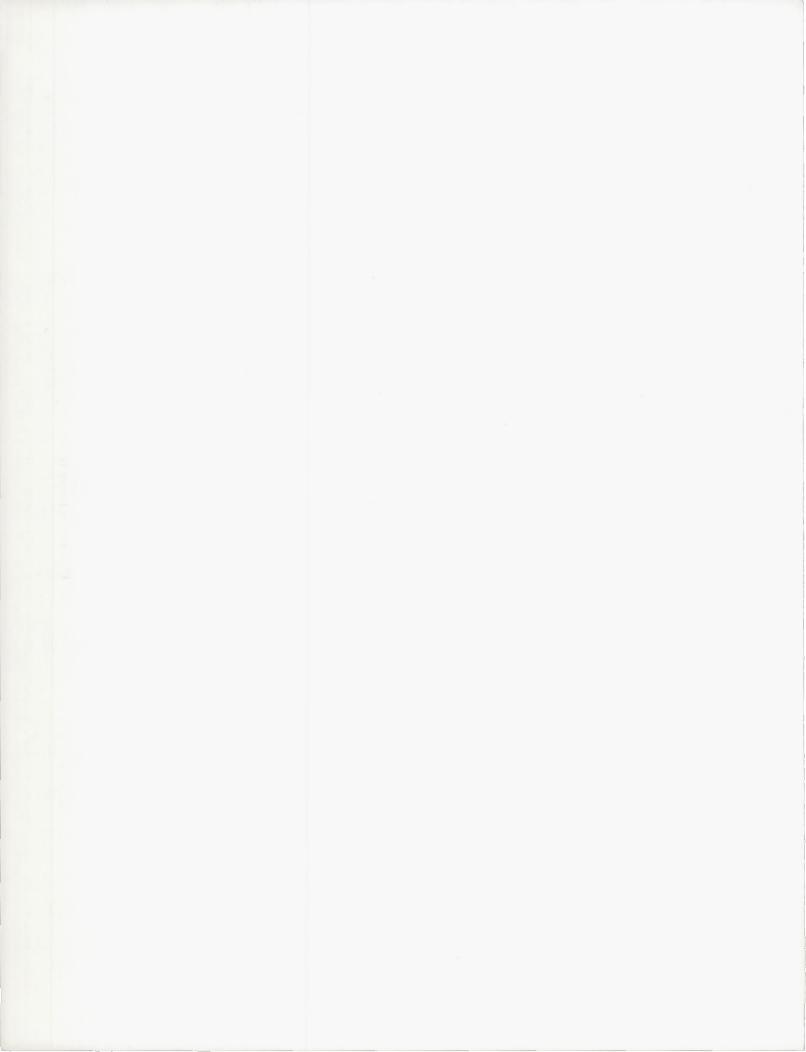


RETURN INCLINATION - Lyre (DEG)



RETURN INCLIMATION - EVE DEG





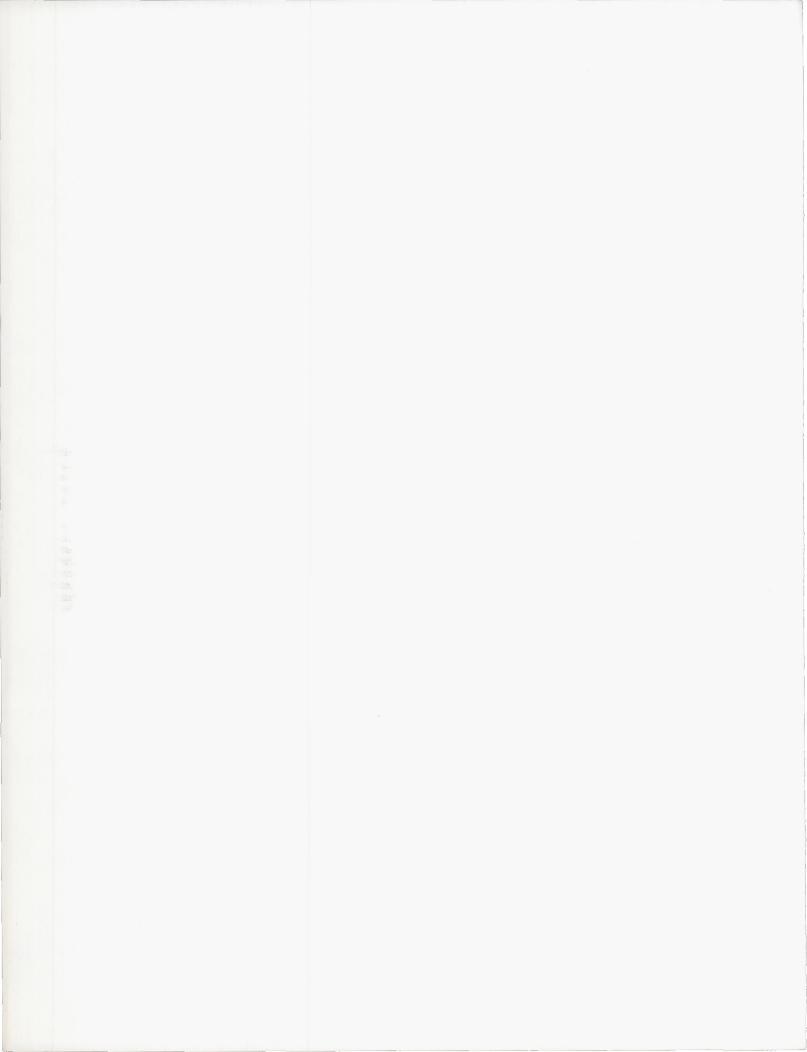
CHAPTER VII LUNAR ORBIT

Prepared by:

F. Martikan and R. Salinger

Aerospace Mechanics Department Martin Company (Balto.) March, 1963

Α.	Lunar Orbit Missions	VII-1
В.	Characteristics of Lunar Orbits	VII-1
С.	Entry and Departure Maneuvers Between Lunar Orbits and Transfer Trajectories	VII-9
D.	Lunar Orbit Determination Schemes	VII-11
E.	References	VII-12
	Illustrations	VII-15



A. LUNAR ORBIT MISSIONS

Lunar orbits are here defined as space vehicle trajectories which lie wholly within the Jacobi C2 region around the moon (Chapter III). They are very well suited for reconnaissance and surveillance missions where the objective is to obtain mapping and close-range scientific data. Orbits are useful in that a properly placed lunar satellite can stay in lunar orbit almost indefinitely, with its usefulness only limited by the life of the equipment. At the present time, it is planned that manned lunar missions will include a lunar orbit. In this case, the lunar orbit provides the safety feature of ballistic earth return prior to orbit entry, longer reaction time prior to landing at a preselected lunar site, smaller total fuel requirements, and smaller abort fuel requirements when compared to soft-landing lunar impacts (see Chapter VIII). In the lunar orbit phase, the space vehicle crew can determine repeatedly its position in orbit and the position of the landing site before the initiation of the deorbit maneuver. A logistics mission can employ a lunar "freighter" shuttling between an earth orbit and a lunar orbit, leaving material in lunar orbit for later use by the lunar expedition, to be called down at the time and place desired. When lunar exploration has advanced beyond the initial stage, rescue, communication, navigation, and possibly even travel between distant lunar bases may be accomplished by use of lunar orbits.

The lunar orbit phase is thus vital for almost all future missions, as soon as lunar exploration progresses beyond the stage of probes on approach or impact trajectories and beyond approach trajectories near minimum velocities. A brief description and classification of lunar orbit missions and missions using a lunar orbit phase has been given in Section A of Chapter IV. Lunar orbit parameters have also been discussed qualitatively and quantitatively in connection with the circumlunar trajectory catalogue (Section A of Chapter VI) and the transearth trajectory catalogue (Section A of Chapter IX). Both sample missions discussed in Chapter XI, Section G, one a landing and the other a reconnaissance mission, use a lunar orbit phase. In the mission discussion, the lunar orbital parameters, as they are limited by mission constraints, and methods for obtaining a first estimate of orbital parameters have been given.

In the present chapter, near-lunar satellite orbits are discussed in relative detail. In Section B, the characteristics of an orbit around the moon as affected by the triaxiality of the moon, the sun and the earth are discussed. These effects are compared, and it is shown that for a close lunar satellite, the sun's effects can be neglected. The equations of motion in a selenocentric coordinate system are derived from a potential function based on a triaxial moon. First-order secular changes in the orbital elements due to the moon's oblateness are presented in graphical form as a function of orbital inclination. Stability of a lunar orbit is briefly discussed. Finally, relationships for determining ground traces and longitude increments between successive ground traces are given.

This data is important for orbital parameter choice in lunar mapping, reconnaissance and surveillance missions.

Velocity requirements for entry into a lunar orbit in the form of summary plots are presented in Section C. The bulk of the material is based on the assumption that the effects of finite burning times are negligible. Results for two different types of trajectories (circumlunar and approach), based on a simplified earth-moon model, are presented and compared. It is seen that there are certain restrictions on the trajectory paramters that must be taken into account when planning a lunar mission.

In Section D, a qualitative discussion of lunar orbit determination schemes for both manned and unmanned vehicles in a lunar orbit is presented.

B. CHARACTERISTICS OF LUNAR ORBITS

In the design of lunar orbits the first and foremost concern is the determination of orbital parameters which best fulfill the mission objective. In most cases this requires eventually a rather accurate determination of space vehicle position with time, which involves either the use of general perturbation theories or a numerical integration on the digital computer if only short-time ephemerides of a lunar satellite are required. However, since very little graphical data on orbits around the moon has been published in the literature, and hardly any numerical evaluation of general perturbation theories as applied to lunar orbits has appeared, the discussion of this section will be directed toward a summary of important analytical results and the presentation of graphical material.

1. Keplerian Orbit Parameters

To obtain gross orbital characteristics, the moon may be considered a spherically symmetric body as a first approximation, with the influence of the earth and the sun neglected. Theoretically, this model is equivalent to one in which the lunar mass is concentrated at the center of the moon. The gravitational potential for this lunar model is

$$U_{\mathbf{q}} = \frac{\mu_{\mathbf{q}}}{r_{\mathbf{Q}}} \tag{1}$$

and the well-known restricted two-body Keplerian equations apply, as given in Chapter III, Section K (Ref. 1), for elliptic and circular orbits.

From a flight mechanics point of view, the period of revolution τ_0 for an elliptic orbit with semimajor axis a_0 as a function of a_0 ,

$$\tau_0 = 2\pi \sqrt{\frac{a_0^3}{\mu_{\mathbf{d}}}} \tag{2}$$

and the velocity of a satellite V_{C} in a circular orbit with radius r_0 as a function of r_0 ,

$$V_{\mathbf{C}} = \sqrt{\frac{\mu}{r_0}}$$
 (3)

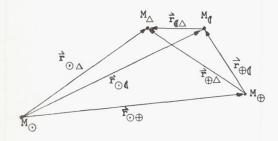
are of special interest. These parameters have been presented as a function of mean altitude $h_0 = a_0 - R_{\ell}$, where $R_{\ell} = 1738.16$ km is the radius of the equivalent spherical moon, and of circular orbit altitude $h_0 = r_0 - R_{\ell}$ in Figs. 1 and 2 for lunar orbits and close lunar orbits, respectively. For preliminary design calculations and for orbits of short duration, these numbers are a good approximation to the actual orbit.

However, these gross orbital characteristics are not good enough for a long-time satellite of the moon and for more accurate calculations. In this case, perturbing forces, which are small effects compared to the principal force of lunar attraction, have to be taken into account. The perturbing forces that will be discussed here are due to the gravity fields of the earth and of the sun and to the asphericity of the lunar gravity field.

2. Orbit Perturbations

a. Solar perturbation

Consider the gravitational attraction of the sun on a lunar satellite first. It can be shown that for a lunar satellite orbit, the effects of the sun can be neglected when compared to those of the earth. Let the masses of the lunar satellite, sun, moon, and earth be denoted by M_{Δ} , M_{\bigodot} , M_{\lozenge} , and M_{\bigoplus} , respectively. Assume an inertial frame of reference centered at the sun (which is a good assumption, since $\mathrm{M}_{\bigodot} >> \mathrm{M}_{\bigoplus}$, $\mathrm{M}_{\bigtriangleup}$) as shown in the sketch below:



The equation of motion of the lunar satellite is in vector form

$$\mathbf{M}_{\Delta} \left(\frac{\mathrm{d}^{2} \ \overrightarrow{\mathbf{r}}_{\odot \Delta}}{\mathrm{d}t^{2}} \right) = \overrightarrow{\mathbf{F}}_{\mathbf{M}_{\Delta}} \left(\mathbf{M}_{\odot} \right) + \overrightarrow{\mathbf{F}}_{\mathbf{M}_{\Delta}} \left(\mathbf{M}_{\bullet} \right) + \overrightarrow{\mathbf{F}}_{\mathbf{M}_{\Delta}} \left(\mathbf{M}_{\bullet} \right)$$

$$\tag{4}$$

or:

$$\mathbf{M}_{\Delta} \left(\frac{\mathrm{d}^{2} \overrightarrow{\mathbf{r}_{\odot}} \Delta}{\mathrm{d}t^{2}} \right) = \overrightarrow{\mathbf{F}} \left(\overrightarrow{\mathbf{r}_{\odot}} \Delta \right) + \overrightarrow{\mathbf{F}} \left(\overrightarrow{\mathbf{r}_{\odot}} \Delta \right) + \overrightarrow{\mathbf{F}} \left(\overrightarrow{\mathbf{r}_{\odot}} \Delta \right)$$
(5)

where
$$F_{M_{\Delta}} \equiv F_{M_{\Delta}} (M_{\odot}) \equiv F (r_{\odot \Delta}) = \frac{GM_{\odot} M_{\Delta}}{r_{\odot \Delta}} =$$

= $\frac{\mu \odot M_{\Delta}}{2}$ is the magnitude of the gravitational $r_{\odot \Delta}$

attraction of the sun on the lunar satellite, etc.

The motion of the moon is given by:

$$\mathbf{M}_{\mathbf{Q}} \left(\frac{d^{2} \overrightarrow{\mathbf{r}}_{\mathbf{O}\mathbf{Q}}}{dt^{2}} \right) = \overrightarrow{\mathbf{F}} \left(\overrightarrow{\mathbf{r}}_{\mathbf{O}\mathbf{Q}} \right) + \overrightarrow{\mathbf{F}} \left(\overrightarrow{\mathbf{r}}_{\mathbf{O}\mathbf{Q}} \right)$$
 (6)

where the force of the satellite on the moon is neglected (i.e., these equations are for a restricted 4-body problem). Using Eqs (4) and (5) and the relation $\vec{r}_{(\Delta)} = \vec{r}_{(\Delta)} - \vec{r}_{(\Delta)}$, it follows that:

$$M_{\Delta} \left(\frac{d^{2} \overrightarrow{r}_{\boldsymbol{\zeta} \Delta}}{dt^{2}} \right) = \overrightarrow{F} (\overrightarrow{r}_{\boldsymbol{\zeta} \Delta}) + \left[\overrightarrow{F} (\overrightarrow{r}_{\boldsymbol{\zeta} \Delta}) + \frac{M_{\Delta}}{M_{\boldsymbol{\zeta}}} \overrightarrow{F} (\overrightarrow{r}_{\boldsymbol{\zeta} \Delta}) \right] + \left[\overrightarrow{F} (\overrightarrow{r}_{\boldsymbol{\zeta} \Delta}) - \frac{M_{\Delta}}{M_{\boldsymbol{\zeta}}} \overrightarrow{F} (\overrightarrow{r}_{\boldsymbol{\zeta} \Delta}) \right]$$
or
$$(7)$$

$$\mathbf{M}_{\Delta} \left(\frac{\operatorname{d}^{2} \overrightarrow{r}_{\boldsymbol{\ell} \Delta}}{\operatorname{d} t^{2}} \right) = \overrightarrow{\mathbf{F}} \left(\overrightarrow{r}_{\boldsymbol{\ell} \Delta} \right) + \mu_{\bigodot} \mathbf{M}_{\Delta} \left[\overrightarrow{r}_{\bigodot \boldsymbol{\ell}} \right]^{3}$$

$$\frac{\overrightarrow{r}_{\bigcirc \Delta}}{\overrightarrow{r}_{\bigcirc \Delta}} \right] + \mu_{\bigoplus} M_{\Delta} \left[\frac{\overrightarrow{r}_{\bigoplus \emptyset}}{\overrightarrow{r}_{\bigoplus \emptyset}} - \frac{\overrightarrow{r}_{\bigoplus \Delta}}{\overrightarrow{r}_{\bigoplus \Delta}} \right] (8)$$

The magnitude of the second term on the RHS of Eq (8), which is due to the sun, can be approx-

imated by
$$\mu_{\odot}$$
 M_{Δ} $\left(\frac{r_{\emptyset \Delta}}{r_{\odot \emptyset}}\right)$ since $r_{\emptyset \Delta} << r_{\odot \emptyset}$;

the magnitude of the last term of Eq (8), which is due to the earth, can be approximated by $\mu_{\mathbf{A}}$ \mathbf{M}_{Δ}

$$\left(\frac{r_{\emptyset}}{r_{\bigoplus \emptyset}} \Delta\right) \text{ since } r_{\emptyset} \Delta << r_{\bigoplus \emptyset} \text{ . The ratio of }$$

these terms is given by:

$$\frac{\stackrel{M}{\bigcirc}}{\stackrel{M}{\bigoplus}} \left(\frac{\stackrel{r}{\bigoplus} \emptyset}{r_{\bigcirc} \emptyset} \right) \stackrel{3}{=} \frac{\stackrel{M}{\bigcirc}}{\stackrel{M}{\bigoplus}} \left(\frac{\stackrel{r}{\bigoplus} \emptyset}{r_{\bigcirc} \bigoplus} \right) \stackrel{3}{=} 0.00565,$$
(9)

which justifies the omission of the effects due to the sun when compared to those of the earth. Schechter (Ref. 2) uses Pontecoulant's lunar theory to obtain an idea of the sun's perturbative effect. Schechter considers a coplanar restricted four-body problem in the ecliptic plane; he expands the sun's gravitational field in a Taylor series around the instantaneous lunar position, and retains only the leading term of the series. The magnitude of the solar effect on a lunar satellite obtained there is roughly 0.3% as large as the effect exerted by the earth, or less than half of the approximate value obtained in Eq (9). Solar effects on lunar satellites can thus be considered higher-order effects and neglected.

b. Lunar asphericity perturbations

Before considering the actual magnitude of the earth's gravitational attraction, effects of lunar asphericity on lunar satellite orbits will be dis-

cussed; the earth perturbations will be compared later to those of lunar asphericity. Thus, we consider next the effects of the triaxially ellipsoidal shape of the moon on the satellite orbit. Assume that the moon and space vehicle are the only bodies in the dynamical system, and that the lunar potential is expanded in terms of spherical harmonics. By the use of MacCullagh's theorem (Ref. 3), the lunar potential U can also

be written in terms of the lunar moments of inertia. Several forms of U_{ℓ} which are widely used have been presented in Chapter II.

Another form of $U_{\boldsymbol{\ell}}$ which is given in terms of the selenographic coordinate system x_S , y_S , z_S is

$$U_{\ell} = \frac{\mu_{\ell}}{r_{S}} \left\{ 1 + \left(\frac{R}{r_{S}}\right)^{2} \left[\frac{3}{2} J_{2} \left(\frac{1}{3} - \left(\frac{z_{S}}{r_{S}}\right)^{2} \right) + 3 C_{2,2} \left(\frac{x_{S}^{2} - y_{S}^{2}}{r_{S}^{2}} \right) \right] \right\}$$

$$(10)$$

where R is the radius of the moon in the direction of the earth (denoted by a in Chapters II and IV) and J_2 , $C_{2,2}$ are the constant expansion coefficients, which can be defined in terms of the lunar moments of inertia as given in Chapter II. An advantage of Eq (10) is that it shows explicitly the two perturbative terms which are due to the asphericity of the moon. The J2 term represents the oblateness of the moon (i.e., the latitude dependence of the lunar radius), and the ${\rm C}_{2,2}$ term represents the ellipticity of the equator (longitude dependence of the lunar radius).

The selenographic coordinate system rotates with the moon, and before an explicit form for the gravitational force of the moon on the vehicle can be given, a transformation to the inertial (for this dynamical system) lunar equatorial coordinate system x, y, z, must be made.

This transformation is given by Eq (2) of Chapter III, and \mathbf{U}_{f} in the inertial coordinate system becomes:

$$U_{\ell} = \frac{\mu_{\ell}}{r_{\ell}} \left\{ 1 + \left(\frac{R}{r_{\ell}}\right)^{2} \left[\frac{3}{2} J_{2} \left(\frac{1}{3} - \left(\frac{z_{\ell}}{r_{\ell}}\right)^{2} \right) + \frac{3 - C_{2,2}}{r_{\ell}} \left[\left(x_{\ell}^{2} - y_{\ell}^{2}\right) \cos 2 \left(\Lambda_{s} + \omega_{\ell}^{2}\right) + 2 \sin^{2} \left(\Lambda_{s}^{2} + \omega_{\ell}^{2}\right) \right] \right\}_{(11)}$$

The equations of motion in the $\mathbf{x}_{\text{\tiny d}}$, $\mathbf{y}_{\text{\tiny d}}$, $\mathbf{z}_{\text{\tiny d}}$ coordinate system can be obtained by partial differentiation:

$$\ddot{x}_{\ell} = \frac{\partial U_{\ell}}{\partial x_{\ell}}; \quad \ddot{y}_{\ell} = \frac{\partial U_{\ell}}{\partial y_{\ell}}; \quad \ddot{z}_{\ell} = \frac{\partial U_{\ell}}{\partial z_{\ell}}$$

Carrying out the indicated operations, one ob-

rying out the indicated operations, one obsing
$$\frac{1}{x_{0}} = \frac{\mu_{0} \times_{0}}{r_{0}} \left\{ 1 + \frac{3 J_{2} R^{2}}{2 r_{0}^{2}} \left[1 - 5 \left(\frac{z_{0}}{r_{0}} \right)^{2} \right] - \frac{3 C_{2,2} R^{2}}{r_{0}^{4}} \left(x_{0}^{2} + 3 y_{0}^{2} + 2 z_{0}^{2} \right) \cos 2 \left(\Lambda_{S} + \omega_{0} \right) + 2 z_{0}^{2} \cos 2 \left(\Lambda_{S} + \omega_{0} \right) + 2 z_{0}^{2} \cos 2 \left(\Lambda_{S} + \omega_{0} \right) + 2 z_{0}^{2} \cos 2 \left(\Lambda_{S} + \omega_{0} \right) + 2 z_{0}^{2} \sin 2 \left(\Lambda_{S} + \omega_{0} \right) + 2 z_{0}^{2} \sin 2 \left(\Lambda_{S} + \omega_{0} \right) + 2 z_{0}^{2} \sin 2 \left(\Lambda_{S} + \omega_{0} \right) + 2 z_{0}^{2} \cos 2 \left(\Lambda_{S} + \omega_{0} \right) + 2 z_{0}^{2} \sin 2 \left(\Lambda_{S} + \omega_{0} \right) + 2 z_{0}^{2} \sin 2 \left(\Lambda_{S} + \omega_{0} \right) + 2 z_{0}^{2} \sin 2 \left(\Lambda_{S} + \omega_{0} \right) + 2 z_{0}^{2} \sin 2 \left(\Lambda_{S} + \omega_{0} \right) + 2 z_{0}^{2} \sin 2 \left(\Lambda_{S} + \omega_{0} \right) + 2 z_{0}^{2} \cos 2 \left(\Lambda_{S} + \omega_{0} \right) + 2 z_{0}^{2} \sin 2 \left(\Lambda_{S} + \omega_{0} \right) + 2 z_{0}^{2} \cos 2 \left(\Lambda_{S} + \omega_{0} \right) + 2 z_{0}^{2} \cos 2 \left(\Lambda_{S} + \omega_{0} \right) + 2 z_{0}^{2} \cos 2 \left(\Lambda_{S} + \omega_{0} \right) + 2 z_{0}^{2} \cos 2 \left(\Lambda_{S} + \omega_{0} \right) + 2 z_{0}^{2} \cos 2 \left(\Lambda_{S} + \omega_{0} \right) + 2 z_{0}^{2} \cos 2 \left(\Lambda_{S} + \omega_{0} \right) + 2 z_{0}^{2} \cos 2 \left(\Lambda_{S} + \omega_{0} \right) + 2 z_{0}^{2} \cos 2 \left(\Lambda_{S} + \omega_{0} \right) + 2 z_{0}^{2} \cos 2 \left(\Lambda_{S} + \omega_{0} \right) + 2 z_{0}^{2} \cos 2 \left(\Lambda_{S} + \omega_{0} \right) + 2 z_{0}^{2} \cos 2 \left(\Lambda_{S} + \omega_{0} \right) + 2 z_{0}^{2} \cos 2 \left(\Lambda_{S} + \omega_{0} \right) + 2 z_{0}^{2} \cos 2 \left(\Lambda_{S} + \omega_{0} \right) + 2 z_{0}^{2} \cos 2 \left(\Lambda_{S} + \omega_{0} \right) + 2 z_{0}^{2} \cos 2 \left(\Lambda_{S} + \omega_{0} \right) + 2 z_{0}^{2} \cos 2 \left(\Lambda_{S} + \omega_{0} \right) + 2 z_{0}^{2} \cos 2 \left(\Lambda_{S} + \omega_{0} \right) + 2 z_{0}^{2} \cos 2 \left(\Lambda_{S} + \omega_{0} \right) + 2 z_{0}^{2} \cos 2 \left(\Lambda_{S} + \omega_{0} \right) + 2 z_{0}^{2} \cos 2 \left(\Lambda_{S} + \omega_{0} \right) + 2 z_{0}^{2} \cos 2 \left(\Lambda_{S} + \omega_{0} \right) + 2 z_{0}^{2} \cos 2 \left(\Lambda_{S} + \omega_{0} \right) + 2 z_{0}^{2} \cos 2 \left(\Lambda_{S} + \omega_{0} \right) + 2 z_{0}^{2} \cos 2 \left(\Lambda_{S} + \omega_{0} \right) + 2 z_{0}^{2} \cos 2 \left(\Lambda_{S} + \omega_{0} \right) + 2 z_{0}^{2} \cos 2 \left(\Lambda_{S} + \omega_{0} \right) + 2 z_{0}^{2} \cos 2 \left(\Lambda_{S} + \omega_{0} \right) + 2 z_{0}^{2} \cos 2 \left(\Lambda_{S} + \omega_{0} \right) + 2 z_{0}^{2} \cos 2 \left(\Lambda_{S} + \omega_{0} \right) + 2 z_{0}^{2} \cos 2 \left(\Lambda_{S} + \omega_{0} \right) + 2 z_{0}^{2} \cos 2 \left(\Lambda_{S} + \omega_{0} \right) + 2 z_{0}^{2} \cos 2 \left(\Lambda_{S} + \omega_{0} \right) + 2 z_{0}^{2} \cos 2 \left(\Lambda_{S} + \omega_{0} \right)$$

These rather complicated equations of motion can be solved by numerical integration to yield the satellite position.

(15)

 $\sin 2 \left(\Lambda_{S} + \omega_{\ell} \right)$

Another approach to the problem is to express U_{\P} in terms of the orbital elements a, e, i, ω , ω^{I} , and f, which were defined in Subsection A-3c of Chapter III:

$$U_{\mathbf{Q}} = \frac{\mu_{\mathbf{Q}}}{r_{\mathbf{Q}}} \left\{ 1 + \left(\frac{R}{r_{\mathbf{Q}}}\right)^{2} \left[\frac{3}{2} J_{2} \left(\frac{1}{3} - \sin^{2} i \sin^{2} (f + \omega) \right) + 3 C_{2, 2} \left((\cos 2 (\Omega' - \omega_{\mathbf{Q}} t)) \left[\cos^{2} (f + \omega) - \sin^{2} (f + \omega) \cos^{2} i \right] \right] \right\}$$

$$- \sin^{2} (f + \omega) \sin^{2} (\Omega' - \omega_{\mathbf{Q}} t) \cos^{2} i \right\}$$

$$- \sin^{2} (f + \omega) \sin^{2} (\Omega' - \omega_{\mathbf{Q}} t) \cos^{2} i \right\}$$

where r_{q} can be expressed in terms of the elliptical elements of the satellite by:

$$r_{Q} = \frac{a (1 - e^{2})}{1 + e \cos f}$$
 (17)

and where f, the true anomaly, is related to ℓ the mean anomaly by the differential equation:

$$\frac{\mathrm{df}}{\mathrm{d}\ell} = \frac{\mathrm{a}^2}{\mathrm{r_0}^2} \sqrt{1 - \mathrm{e}^2} \tag{18}$$

It is now possible to form the perturbing function:

$$\Phi_{\mathbf{Q}} = \mathbf{U}_{\mathbf{Q}} - \frac{\mu_{\mathbf{Q}}}{\mathbf{r}_{\mathbf{Q}}} \tag{19}$$

and to use general perturbation methods to determine the time-variation of the orbital elements. The perturbing function Φ_{ℓ} can be divided into terms that arise due to $\boldsymbol{\mathrm{J}}_2$ and terms that arise due to $C_{2,\,2}$. The function Φ_{ℓ} can additionally be divided into secular terms, or terms that keep increasing with time, into longperiod terms, or terms that are periodic with an approximate period of the rotation of pericynthion, and into short-period terms, which are periodic with approximately the same period as the satellite period τ_0 . The desired term of $\Phi_{m{q}}$ can be substituted into the variation-ofparameter equations, one form of which is given by Eq (101) of Chapter III and other forms in Chapter III of Ref. 1, which form a set of six first-order ordinary differential equations completely equivalent to the equations of motion (13) through (15). These equations can then be solved for the secular, long-periodic and short-periodic variations in satellite orbital elements due to the lunar potential.

Consider the oblateness coefficient J₂. From Chapter II, it is seen that this expansion coefficient is the largest one in the lunar potential, and, hence, oblateness effects can be expected to be the most notable asphericity effects on the lunar satellite orbit. Of particular interest to the mission designer are the secular effects, since these increase with time and since it is often desired to obtain the average satellite behavior over a long period of time for lunar

orbital missions. Since the earth is also oblate, analytic work on near-earth satellites is also applicable for lunar satellites. In the following discussion of lunar oblateness effects, the secular effects will be discussed qualitatively, quantitatively, and finally, graphically. Periodic effects on the radius will be described only.

Due to the small oblateness of the moon $(J_2 < 1)$, the lunar satellite orbit is very nearly a circle or an ellipse. To first order in oblateness (using terms to J2 in the expansion of the gravitational potential), the orbital plane precesses around the lunar polar axis at a variable rate (nodal regression). In addition, the line of apsides defining the orientation of the satellite trajectory in the orbital plane rotates in this plane at a variable rate (apsidal rotation). The dependence of the mean motion, or the average rate of rotation of the satellite in the orbital plane, on the orbital inclination results in an oblateness correction to the period of the unperturbed (or restricted 2body) motion. Restricted 2-body motion is referred to as zero-order or unperturbed motion; if ${\bf J}_2$ is used, in addition, the motion is defined as second-order; the inclusion of $\mathrm{C}_{2,\,2}$ defines third-order motion; and all other, yet-to-bedefined spherical harmonic expansion coefficients of Un define fourth-order motion and are negligible.

The mean rate of nodal regression to firstorder has been found by many authors (Refs. 4 through 11 and others). In units of degrees per nodal period (time between successive ascending nodes), it is:

$$\frac{d\Omega}{dt} = -360 \cdot \frac{3}{2} J_2 \frac{R^2}{\bar{a}^2 (1 - e^2)^2} \cos i_0$$
 (20)

Since $\frac{d\Omega}{dt}$ = 0 (J₂ $\frac{d\beta}{dt}$), any one of the following expressions can be used to second-order in the denominator:

$${\rm a}^2\; {\rm (1\,-\,e^2)^2,\, a_0}^2\; {\rm (1\,-\,e^2)^2,\, \overline{a}^2}\; {\rm (1\,-\,e^2)^2,\,\, p^2,\,\, \overline{p}^2}$$

where a_0 is the Keplerian value of the semimajor axis, $p^2 = a^2 (1 - e^2)^2$ is the semilatus rectum of the orbit, r_0 is the average orbital radius $(r_0 \equiv p \text{ for Keplerian orbits})$, and a bar denotes an average value of the quantity about which it varies periodically for oblate moon orbits. The value of $\frac{d\Omega}{dt}$ is negative for a direct orbit $(i_0 < 90^\circ)$, i.e., it is a shift toward the west; while $\frac{d\Omega}{dt}$ is positive for a retrograde orbit $(i_0 > 90^\circ)$. For an equatorial orbit $(i_0 = 0^\circ, 180^\circ)$, the ascending node Ω is undefined, but $\frac{d\Omega}{dt}$ can be defined in the limit as $i_0 \to 0^\circ$ or $i_0 \to 180^\circ$. In Fig. 3, $\left(-\frac{d\Omega}{dt}\right)$ is plotted as a function of i_0 for three values of p.

It is seen from this figure that the nodal regression is largest for an equatorial orbit and zero for a polar orbit; it is larger for a circular orbit (e = 0) than for an elliptic orbit 0 < e < 1, and since it is a gravitational force, it decreases with the inverse square of the distance from the center of the moon.

The mean rate of apsidal rotation has been found by many authors (Refs. 4 through 11 and others); in units of degrees per nodal period, it is

$$\frac{d\omega}{dt} = 360 \frac{3J_2}{2} \frac{R^2}{\bar{a}^2 (1 - e^2)^2}$$

$$\cdot (2 - \frac{5}{2} \sin^2 i_0)$$
 (21)

For near-polar orbits, the perigee regresses, i.e., it moves against the direction of satellite motion, and $\frac{d\omega}{dt}$ is negative in value, while for near-equatorial orbits the perigee advances-i.e., it moves in the direction of satellite motion, and $\frac{d\omega}{dt}$ is positive in value. The inclination angles at which $2-\frac{5}{2}\sin^2i_0=0$, or $i_0\cong 63.45^\circ$ and $i_0\cong 116.55^\circ$ are known as critical inclination angles. Near the critical inclination, when $2-\frac{5}{2}\sin 2i_0=O(J_2)$, or approximately for inclinations between 62.45 and 64.45°, as well as between 115.55 and 117.55°, a second-order theory is insufficient to describe the apsidal motion, and Eq (21) does not hold. This case has been discussed by Struble (Ref. 12). Figure 4 presents the rate of apsidal rotation as a function of orbital inclination for three values of p. The perifocus location ω is undefined for circular orbits, but it is possible to define $\frac{d\omega}{dt}$ in the limit as $e\to 0$. The same general comments on the dependence of $\frac{d\omega}{dt}$ on e, p apply as in the case of $\frac{d\Omega}{dt}$.

The orbital period in unperturbed satellite motion is given by Eq (2) which has been plotted in Figs. 1 and 2.

In perturbed satellite motion, or when secondorder perturbing forces due to lunar oblateness act on the satellite, one can define three, in general distinct, periods of motion:

- (1) The anomalistic period, the time from one pericynthion to the next. In that time the elliptic angles (true, mean, and eccentric anomaly) increase by 360° , while the orbital central angle $\beta = \omega + f$ increases by more or less than 360° , depending on whether the apsidal rotation is against or in the direction of satellite motion.
- (2) The nodal period, also called draconic period, the time from one ascending node to the next. In that time the orbital central angle $\beta = \omega + f$

increases by 360° , since β is measured from the instantaneous position of the ascending node. The satellite does not, except at an orbit inclination of 90° , return to the same relative position in inertial space after one nodal period due to the regression of the nodes.

(3) The sidereal period, the time for the satellite to return to the same relative position in inertial space. In that time the satellite central angle as measured from a fixed reference, which is not to be confused with the central angle as measured from the ascending node, increases by 360°. In artificial satellite theory, the sidereal period is less important than the other two periods; it is rarely used, and it will not be discussed any further.

In many satellite calculations, especially in approximate ephemeris prediction, it is more convenient to use the nodal period τ_{β} than the anomalistic period, τ_{r} , since (especially for circular and near-circular orbits) the ascending node is a more easily identifiable point than pericynthion, except in the case of equatorial lunar orbits. Unfortunately, however, differing expressions have been obtained for it in the literature (compare the nodal periods derivable from mean motions given in Refs. 6, 7, 8, 10, 13, 14, 15, 16, 17, 18 among others).

An expression for the nodal period was derived from Struble's (Ref. 12) first-order theory by Martikan and Kalil (Ref. 13) for small eccentricities, $e=O\left(J_2\right)$, and shown to be compatible with expressions for the anomalistic period for large values of eccentricity by some numerical examples in Ref. 13:

$$\tau_{\beta} = \frac{2\pi}{\sqrt{\mu_{0}}} (\bar{a})^{\frac{3}{2}} \left\{ 1 - \frac{3}{8} J_{2} \frac{R^{2}}{\bar{a}^{2} (1 - e^{2})^{2}} \right\}$$

$$(7 \cos^{2} i_{0} - 1) , \qquad (22)$$

where \overline{a} is the mean semimajor axis of the perturbed orbit defined in terms of a reference Keplerian semimajor axis (which should not be used, since it is but a first estimate for a):

$$\overline{a} = a_0 \left\{ 1 - \frac{3}{4} J_2 \frac{R^2}{a_0^2 (1 - e^2)^2} \cdot (3 \cos^2 i_0 - 1) \sqrt{1 - e^2} \right\}$$
 (23)

The oblateness correction to the period as described by

$$\Delta \tau_{\beta} = \tau_{\beta} - \tau_{0} \tag{24}$$

has been presented in Fig. 5 as a function of inclination for three values of $\bar{p} = \bar{a} (1 - e^2)$.

Again the corrections are larger for a circular orbit (e = 0) than for an elliptic orbit 0 < e < 1, and it decreases with the inverse square of the distance from the center of the moon since it is a gravitational force.

Another important quantity of a lunar orbit is the variation of the orbital radius $r_{\mathbf{q}}$ with time. The radius in terms of orbital elements is given by Eq (17), and since the semimajor axis a and eccentricity e exhibit no first-order secular changes, $r_{\mathbf{q}}$ undergoes short-periodic changes since the term cos f in the expression for $r_{\mathbf{q}}$ undergoes short-periodic changes. If one uses Kork's form (Ref. 19) for the radius, which is equivalent to expressions derivable from Struble (Ref. 12), Kozai (Refs. 4, 20) and Izsak (Ref. 21) for eccentricities of order J_2 , then the expression for the instantaneous radius in one satellite revolution can be written.

$$\mathbf{r}_{\mathbf{Q}} = \tilde{\mathbf{a}} \left[1 - e \cos (\beta - \omega) + \frac{1}{4} J_2 \left(\frac{\mathbf{R}}{\tilde{\mathbf{a}}} \right)^2 \sin^2 i_0 \cos 2\beta \right],$$

$$e = O(J_2) \qquad (25)$$

The maximum variation in radius about the Keplerian orbit radius $r_{(0)} = \overline{a} \left[1 - e \cos (\beta - \omega) \right]$, if Eq (25) is compared with Eq (17), occurs for a polar close lunar satellite orbit ($i_0 = 90^{\circ}$, $\overline{a} \rightarrow R$). In this extreme case the radius variation due to lunar oblateness is given by

$$\Delta \mathbf{r}_{\mathbf{\ell}} = \mathbf{r}_{\mathbf{\ell}} - \mathbf{r}_{\mathbf{\ell}} \mathbf{0} \stackrel{\sim}{=} \pm \frac{1}{4} \mathbf{J}_{2} \bar{\mathbf{a}} = \pm 0.09 \text{ km}$$
 (26)

This radius variation decreases as the inclination decreases, $i_0 \stackrel{>}{>} 90^\circ\!,$ and it decreases with semimajor axis $\frac{R}{\bar{a}} < 1$, but altogether it is a very small variation. Similarly the short-periodic variations in e, i are rather small and result in position variations of about the same magnitude.

No explicit expressions exist for the effects of the terms of $\Phi_{\mathbf{C}}$ containing the equatorial ellipticity coefficient $C_{2,\,2}$ on lunar satellite orbit parameters. The numerical value of $C_{2,\,2}$ is one order of magnitude less than the value of J_2 , and one can expect the effects of equatorial ellipticity to be less than those of oblateness. Direct effects of $C_{2,\,2}$ on orbital elements can again be obtained by solving the variation-of-parameter equations using only the terms in $\Phi_{\mathbf{C}}$ which contain $C_{2,\,2}$ as a coefficient.

c. Earth perturbations

The next step in determining the motion of a lunar satellite is to compare the perturbing

effect of the earth with that of the lunar asphericity, where both effects vary with the altitude above the lunar surface. Lass and Solloway (Ref. 22) obtain an approximation for the earth's potential in the selenographic coordinate system. The acceleration of the lunar satellite due to gravitational attraction of the earth, which is the third term on the RHS of Eq (7), can be written as:

$$\frac{\vec{F}(\vec{r}_{\oplus\Delta}) - \frac{M_{\Delta}}{M_{\mathbf{Q}}} \quad \vec{F}(\vec{r}_{\oplus\mathbf{Q}})}{M_{\Delta}} =$$

$$\mu_{\oplus} \left\{ \frac{(x_{S} - \overline{r}_{\oplus\mathbf{Q}}) \hat{x}_{S} + y_{S} \hat{y}_{S} + z_{S} \hat{z}_{S}}{\left[(x_{S} - \overline{r}_{\oplus\mathbf{Q}})^{2} + y_{S}^{2} + z_{S}^{2}\right]^{3/2}} + \frac{\hat{x}_{S}}{\overline{r}_{\oplus\mathbf{Q}}} \right\}$$

$$(27)$$

Equation (27) becomes for $\bar{r}_S^2 << \bar{r}_{\oplus \emptyset}^2$, with $\bar{r}_{\oplus \emptyset}$ the fixed distance between the earth and the moon,

$$\frac{\hat{\mathbf{F}}(\hat{\mathbf{r}}_{\oplus\Delta}) - \frac{\mathbf{M}_{\Delta}}{\mathbf{M}_{\mathbf{Q}}} \hat{\mathbf{F}}(\hat{\mathbf{r}}_{\oplus\mathbf{Q}})}{\mathbf{M}_{\Delta}}$$

$$\frac{\mathbf{M}_{\Delta}}{\mathbf{M}_{\Delta}} = -\frac{\mu_{\oplus}}{\mathbf{M}_{\oplus}} (2 \mathbf{x}_{S} \hat{\mathbf{x}}_{S} - \mathbf{y}_{S} \hat{\mathbf{y}}_{S} - \mathbf{z}_{S} \hat{\mathbf{z}}_{S})$$

$$= -\frac{\mu_{\oplus}}{\mathbf{M}_{\Delta}} \left[2 \mathbf{x}_{S} \hat{\mathbf{x}}_{S} - \mathbf{y}_{S} \hat{\mathbf{y}}_{S} - \mathbf{z}_{S} \hat{\mathbf{z}}_{S} \right]$$

$$= -\frac{\mu_{\oplus}}{\mathbf{M}_{\Delta}} \left[2 \mathbf{x}_{S} \hat{\mathbf{x}}_{S} - \mathbf{y}_{S} \hat{\mathbf{y}}_{S} - \mathbf{z}_{S} \hat{\mathbf{z}}_{S} \right]$$

$$= -\frac{\mu_{\oplus}}{\mathbf{M}_{\Delta}} \left[2 \mathbf{x}_{S} \hat{\mathbf{x}}_{S} - \mathbf{y}_{S} \hat{\mathbf{y}}_{S} - \mathbf{z}_{S} \hat{\mathbf{z}}_{S} \right]$$

$$= -\frac{\mu_{\oplus}}{\mathbf{M}_{\Delta}} \left[2 \mathbf{x}_{S} \hat{\mathbf{x}}_{S} - \mathbf{y}_{S} \hat{\mathbf{y}}_{S} - \mathbf{z}_{S} \hat{\mathbf{z}}_{S} \right]$$

$$= -\frac{\mu_{\oplus}}{\mathbf{M}_{\Delta}} \left[2 \mathbf{x}_{S} \hat{\mathbf{x}}_{S} - \mathbf{y}_{S} \hat{\mathbf{y}}_{S} - \mathbf{z}_{S} \hat{\mathbf{z}}_{S} \right]$$

$$= -\frac{\mu_{\oplus}}{\mathbf{M}_{\Delta}} \left[2 \mathbf{x}_{S} \hat{\mathbf{x}}_{S} - \mathbf{y}_{S} \hat{\mathbf{y}}_{S} - \mathbf{z}_{S} \hat{\mathbf{z}}_{S} \right]$$

$$= -\frac{\mu_{\oplus}}{\mathbf{M}_{\Delta}} \left[2 \mathbf{x}_{S} \hat{\mathbf{x}}_{S} - \mathbf{y}_{S} \hat{\mathbf{y}}_{S} - \mathbf{z}_{S} \hat{\mathbf{z}}_{S} \right]$$

$$= -\frac{\mu_{\oplus}}{\mathbf{M}_{\Delta}} \left[2 \mathbf{x}_{S} \hat{\mathbf{x}}_{S} - \mathbf{y}_{S} \hat{\mathbf{y}}_{S} - \mathbf{z}_{S} \hat{\mathbf{z}}_{S} \right]$$

$$= -\frac{\mu_{\oplus}}{\mathbf{M}_{\Delta}} \left[2 \mathbf{x}_{S} \hat{\mathbf{x}}_{S} - \mathbf{y}_{S} \hat{\mathbf{y}}_{S} - \mathbf{z}_{S} \hat{\mathbf{z}}_{S} \hat{\mathbf{z}}_{S} \right]$$

$$= -\frac{\mu_{\oplus}}{\mathbf{M}_{\Delta}} \left[2 \mathbf{x}_{S} \hat{\mathbf{x}}_{S} - \mathbf{y}_{S} \hat{\mathbf{y}}_{S} - \mathbf{z}_{S} \hat{\mathbf{z}}_{S} \hat{\mathbf{z}}_{S} \hat{\mathbf{z}}_{S} \hat{\mathbf{z}}_{S} \right]$$

where grad is the gradient operator $\overline{\text{grad}} \approx \frac{\partial}{\partial x_S} \hat{x}_S + \frac{\partial}{\partial y_S} \hat{y}_S + \frac{\partial}{\partial z_S} \hat{z}_S$. The earth's potential for a lunar satellite can thus be approximated by

$$\mathbf{U}_{\bigoplus} \stackrel{\sim}{=} \frac{\mu_{\bigoplus}}{2 \, \overline{\mathbf{r}}_{\bigoplus}^{3}} \, \mathbf{r}_{\mathbf{S}}^{2} \left[1 - 3 \left(\frac{\mathbf{x}_{\mathbf{S}}}{\mathbf{r}_{\mathbf{S}}} \right)^{2} \right]$$
 (29)

The earth's potential U_{\bigoplus} can now be compared with the terms in the lunar potential U_{\P} , or more properly, the gradients of the potential, which are the gravitational forces, should be compared.

Numerical values for the ratio of the earth's potential as given by Eq (29), to the $\rm J_2$ and $\rm C_{2,\,2}$ terms of the lunar potential, as given by Eq (10), have been obtained. The approximations are only valid for close lunar satellites and crude enough so that no differentiation can be made if the satellite is between the earth and moon or on the opposite side of the moon. The results are presented in the following table where the ratios

$$\frac{J_{2}}{\text{earth}} = \frac{3\mu_{\P} R^{2} J_{2}}{r_{S}^{3}} / \frac{\mu_{\P} r_{S}^{2}}{2\overline{r}_{\P}^{3}} = 3\left(\frac{\mu_{\P}}{\mu_{\P}}\right)^{\frac{\overline{r}_{\P}}{R}} J_{2}$$
(30)

and

$$\frac{\mathbf{C}_{2,2}}{\text{earth}} = \frac{3\mu_{\mathbf{q}} \mathbf{R}^2 \mathbf{C}_{2,2}}{\mathbf{r}_{\mathbf{S}}^3} / \frac{\mu_{\mathbf{m}} \mathbf{r}_{\mathbf{S}}^2}{2\overline{\mathbf{r}_{\mathbf{m}}}^3} = 6\left(\frac{\mu_{\mathbf{q}}}{\mu_{\mathbf{m}}}\right) \left(\frac{\overline{\mathbf{r}_{\mathbf{m}}}}{\mathbf{R}}\right)^3 \mathbf{C}_{2,2}$$
(31)

are given as a function of lunar satellite altitude in lunar radii (LR):

h (LR)	J _{2/earth}	C _{2,2/earth}
0	84.7	15.0
1	10.6	1.87
2	3.14	0.55
3	1.32	0.23
4	0.68	0.12

The earth's perturbation equals the lunar $C_{2,\,2}$ term at an altitude of approximately 2700 km, and it equals the lunar J_2 term at an altitude of approximately 6100 km. For a close lunar satellite, the lunar asphericity terms predominate; these terms can be considered a first approximation to the motion of the lunar satellite.

d. Lunar atmospheric perturbations

The moon has an atmosphere which, at the surface, is estimated to be less than 10^{-12} times the density of the earth's atmosphere at sea level. Since the atmospheric drag forces are proportional to the density times velocity squared (for more data on aerodynamic forces see Subsection B-4b of Chapter IV), a hypothetical ratio of drag forces of a satellite of the earth orbiting at sea level and one of the moon at distance R_{\emptyset} can be found. This ratio is given by

$$\frac{D_{\text{d}} \text{ SL}}{D_{\text{\oplus}} \text{ SL}} \simeq \frac{\rho_{\text{d}} \text{ SL} V_{\text{d}}^{2} \text{ c}}{\rho_{\text{\oplus}} \text{ SL} V_{\text{\oplus}}^{2} \text{ c}} \simeq 10^{-12} \frac{(1.7)^{2}}{(7.9)^{2}} \simeq 5 \times 10^{-14}$$
(32)

where ρ_{\P} SL and ρ_{\P} SL are the sea-level atmospheric densities of the moon and earth, respectively, and V_{\P} c' V_{\P} c are the circular satellite velocities at zero altitude. This ratio might change by several orders of magnitude with lunar and earth orbital altitude, but by all accounts atmospheric drag is an utterly negligible force in lunar satellite orbits. Atmospheric drag acting on a circular lunar satellite orbit at an altitude of 10 km is less than the atmospheric drag of an earth satellite in a 1000-km circular orbit. Of course, data on the lunar atmosphere is still subject to conjecture.

e. Solar radiation pressure perturbations

The effect of solar radiation pressure has been discussed in Subsection B-4a of Chapter IV. The magnitude of the force is of the same order as in the case of earth satellites, since the moon and earth are about the same distance from the sun and, for close lunar satellites, shadow time must be considered, since for certain orbital parameters it may be as much as 40% of the total time in orbit.

3. Stability of Lunar Orbits

The final question in establishing orbital parameters for lunar satellites concerns stability of the orbit. The moon exerts a much smaller force on a lunar satellite than does the earth on an earth satellite at a comparable distance. Also, the perturbations on a near-lunar satellite due to the earth are much larger than the perturbations of the moon on near-earth satellites at a comparable distance. Only the effects of asphericity are more pronounced in the case of the earth than the moon, while solar perturbing effects are about the same for near-earth and near-moon satellites. Hence, stability of a lunar satellite is much more of a problem than the stability of an earth satellite. In particular, it is important to determine whether the combined gravitational attractions of the earth and sun (or other forces) can distort a lunar orbit sufficiently to cause the satellite to impact on the lunar surface.

The time period from the initially established orbit until impact has been given the name "lifetime" by some investigators. This term should not be confused with the term "lifetime" as it is applied to earth satellites, where it is the time period from the initially established orbit until atmospheric drag causes the satellite to re-enter the denser portions of the earth's atmosphere.

No investigations into stability have been performed for this chapter, but one note on the stability of lunar satellites has been reviewed. Schechter (Ref. 2) applies a modified version of Pontecoulant's lunar theory (see Ref. 23 for more details on this lunar theory) to the problem of motion of a lunar satellite. Schechter finds the maximum decrease of pericynthion radius Δr_{PL} as a function of r_{PL} = a (1 - e) is given approximately by

$$\frac{\Delta r_{PL}}{r_{PL}} \equiv \frac{(r_{PL})_{min} - r_{PL}}{r_{PL}} \sim -\frac{15}{8} \text{ em (1 + e)}$$
(33)

where m = $\frac{2\pi/\tau_0}{\omega_{\text{0}}}$ is the ratio of angular velocity

of the satellite in its orbit to the rotational rate of the moon. Schechter takes a conservative lunar orbit (from a perturbation standpoint) of e = 0.2, m = 1/15 (or a $^{\sim}$ 14,500 km), and the maximum decrease in pericynthion radius r_{PL} = a (1 - e) = 11,600 km is Δr_{PL} = $-\frac{15}{8}$ em r_{PL} (1 + e) = -350 km, or about 3%. The particular lunar satellite will have an infinite lifetime. However, these perturbations may in time increase the apocynthion radius sufficiently so that the mission requirements are not met.

4. Ground Traces and Longitude Increments

For reconnaissance, surveillance and mapping missions of the lunar surface from a near-moon orbit, the ground trace, or succession of subsatellite points on the lunar surface, and the longitude increments between successive ground traces are important. Both depend on the choice

of orbital parameters, and an orbit may be designed to cover certain regions of the moon and to provide a specific value for the longitude increment. The longitude increment that can be achieved for certain lunar orbits in turn is constrained by mission requirements, sensor limitations such as the field of view, the resolution, the image motion compensation required, and the maintainability of the system in the near-lunar environment.

In the following, only oblateness effects of the moon are considered, with lunar ellipticity and earth effects neglected. Also, since uniform picture quality and a simple image motion compensation system require circular or near-circular orbits for reconnaissance, surveillance and mapping missions, the case of a circular orbit around the moon will be treated separately.

During each revolution, the satellite ground track experiences a longitude increment of $\Delta \lambda_{\text{C}}$ degrees per nodal period to the west, where, under the preceding assumptions:

$$\Delta \lambda_{\mathbf{d}} = -\omega_{\mathbf{d}} (\tau_0 + \Delta \tau_{\beta}) - \frac{d\Omega}{dt} \frac{\text{degrees}}{\text{nodal period}}$$

$$= -\omega_{\mathbf{d}} 2\pi \left(\frac{r_S^3}{\mu_{\mathbf{d}}}\right) \left[1 - \frac{3}{8}J_2\left(\frac{R}{r_S}\right)^2 (7\cos^2 i_0 - 1)\right]$$

$$-360 \cdot \frac{3}{2}J_2\left(\frac{R}{r_S}\right)^2 \cos i_0 \frac{\deg}{\text{nodal period}}$$

$$(34)$$

where R \equiv a, the longest semiaxis of the moon, r_S is the radius of the circular lunar orbit, the minus signs indicate a shift to the west or negative selenographic longitude, $\lambda_{\rm c}$, and the nodal period is chosen because it gives the longitude increment at the same point in orbit. The first term on the right-hand side of Eq (34) above is due to the moon's rotation in one nodal period, while the second term is the average regression rate of the ascending node (or any other point on the ground track in this first approximation) due to lunar oblateness, as given by Eq (20), applied to a circular orbit. Since τ_0 is at least 6500 sec (see Fig. 2) and $\Delta\tau_{\beta}$ is at most 3 sec (see Fig. 5), the oblateness effect on the period is less than 1/2000 of the central force effect, and in view of the other approximations it can be neglected. Hence,

$$\Delta \lambda_{\ell} \stackrel{\sim}{-} - \omega_{\ell} 2\pi \left(\frac{r_{S}^{3}}{\mu}\right) - 540 J_{2} \left(\frac{R}{r_{S}}\right)^{2} \cos i_{0} \frac{\deg}{rev}$$
(35)

In order to obtain a qualitative idea of the magnitude of these effects for a 100-km circular equatorial orbit around the moon, one can obtain from Figs. 2 and 3 and from Eq (35), with $\omega_{\rm g} \simeq 1.52504 \times 10^{-4} {\rm deg/sec}$:

$$\Delta \lambda_{\text{Q}} \stackrel{\sim}{-} -1.079 - 0.102 \text{ deg/rev} = -1.181 \text{ deg/rev}$$
 (36)

In this extreme case the second term in Eq (35) (due to nodal regression, -0.102 deg/rev) is about one-tenth of the first term (due to the lunar rotation during one period, -1.079 deg/rev). Lunar oblateness effects on $\Delta\lambda_{\pmb{\ell}}$ are very significant, and cannot be ignored. They are as significant as in the case of a satellite orbit around the earth, primarily due to the much slower rotational rate $\omega_{\pmb{\ell}}$ of the moon about its axis. This smaller $\omega_{\pmb{\ell}}$ counteracts the effects of a smaller oblateness coefficient J_2 for the moon, as well as the weaker central force, as given by the gravitational constant $\mu_{\pmb{\ell}}$ of the moon as compared with $\mu_{\pmb{\Phi}}$.

Consider next a 1000-km circular equatorial orbit around the moon, for which

$$\Delta \lambda_{\text{q}} \stackrel{\sim}{-} -2.059 - 0.047 \text{ deg/rev} = 2.106 \text{ deg/rev}.$$
(37)

For this higher orbit, lunar oblateness accounts for only about one fortieth of the total $\Delta\lambda_{\P}$, showing that the weaker central force, as given by the gravitational constant μ_{\P} of the moon, increases the period and decreases the oblateness effects, or $\frac{d\Omega}{dt}$, considerably with altitude. Of course, there is a dependence of $\frac{d\Omega}{dt}$ on inclination-i.e., it decreases with increasing inclination and is zero for a polar orbit--while the period, and hence the first term of $\Delta\lambda_{\P}$, remains the same in this approximation.

For elliptic orbits, the term $\left(\frac{r_S}{\mu_{\mathfrak{C}}}\right)$ in Eqs 34 and 35 should be replaced by $\left(\frac{\overline{a}^3}{\mu_{\mathfrak{C}}}\right)$ and the term $\left(\frac{R}{r_S}\right)^2$ by $\left(\frac{R}{p}\right)^2$ in the same equations, where \overline{a} and $p = \overline{a}$ $(1 - e^2)$ have been defined in Subsection B-2b.

However, besides the longitudinal increment between revolutions, the location of the subsatellite point at any time during one revolution is of interest. To this end, consider a circular orbit around the moon and secular lunar oblateness effects with the exception of the oblateness effect on the period. The orbit ground trace, or the selenographic latitudes and longitudes of the subsatellite points as a function of time, can be computed in several steps. The satellite ground trace in a selenocentric nonrotating lunar equatorial coordinate system $\mathbf{x}_S \ \mathbf{y}_S \ \mathbf{z}_S$ can be found by spherical trigonometry. The declination δ_S of the subsatellite point is

$$\delta_{\rm S} = \sin^{-1} (\sin i_0 \sin \beta), -90^{\circ} \le \delta_{\rm S} \le 90^{\circ}$$
(38)

where

 $\beta = \beta_0 + \frac{\mathrm{d}\beta}{\mathrm{d}t} \, \mathrm{d}t$, $0^\circ \le \beta \le 360^\circ$ is the orbital central angle measured from the ascend-

 β_0 = 0 is the orbital central angle at the time of ascending nodal crossing of

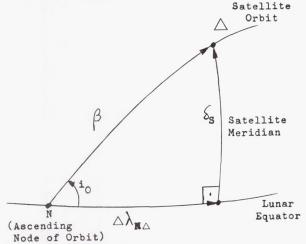
 $\frac{d\beta}{dt} = \frac{360}{\tau_0} \left(\frac{deg}{sec} \right)$ is the constant angular velocity of the satellite in its circular orbit,

dt, $0 \le dt \le \tau_0$ is an increment of time, measured from the ascending node to Δ .

The longitude of the subsatellite point relative to the ascending node, $\Delta\lambda_{N\Delta}$ is

$$\Delta \lambda_{\rm N\Delta} = \pm \cos^{-1} \left(\frac{\cos \beta}{\cos \delta_{\rm S}} \right)$$
, $0^{\circ} \le \left| \Delta \lambda_{\rm N\Delta} \right| \le 360^{\circ}$ (39)

where the positive sign applies for direct orbits $(i_0 < 90^{\circ})$, the negative sign applies for retrograde orbits (i_0 > 90°), and $\Delta\lambda_{\rm N\Delta}$ = 0 for polar orbits (i = 90°). The geometry of the satellite ground trace is illustrated in the following sketch:



By use of the vector relation,

$$\sin \Delta \lambda_{N\Delta} = \frac{\tan \delta_S}{\tan i_0}$$

and by use of Eq (38), Eq (39) can be written

$$\Delta \lambda_{N\Delta} = \pm \tan^{-1} (\cos i_0 \tan \beta)$$
 (40)

where + is for direct, - for retrograde and $\Delta\lambda_{\rm N\Delta}$ = 0 for polar orbits. In applying Eqs (38) and (40), great care must be taken to use the correct quadrants of the angles β and $\Delta\lambda_{N\Lambda}$.

On a rotating moon, the declination of the subsatellite point δ_{ς} becomes the selenographic latitude $\phi_{\mathcal{C}}$ directly, while an increment $\omega_{\mathcal{C}}$ dt must be added to $\Delta\lambda_{{\rm N}\Delta}$ in order to obtain the selenographic longitude $\Delta \lambda_{\text{$\mathbb{Q}$}\Delta}$ relative to the ascending node. The major effect of the lunar oblateness (the regression of the nodes) contributes the term

$$+\frac{\mathrm{d}\Omega}{\mathrm{d}t}\,\mathrm{d}t = -540\,\mathrm{J}_2\left(\frac{\mathrm{R}}{\mathrm{r}_\mathrm{S}}\right)^2\,\mathrm{cos}\,\mathrm{i}_0\,\mathrm{d}t$$
 (41)

to the longitude of the subsatellite point.

To summarize, the ground trace equations for circular orbits on a rotating moon, including the nodal regression, become

$$\phi_{\mathbf{Q}} = \sin^{-1} \left(\sin i_0 \sin \beta \right)$$

$$\lambda_{\mathbf{Q}} = \lambda_{\text{AN}} \pm \tan^{-1} \left(\cos i_0 \tan \beta \right) + \omega_{\mathbf{Q}} \quad \text{dt}$$

$$-540 \text{ J}_2 \left(\frac{\text{R}}{\text{r}_{\text{S}}} \right)^2 \cos i_0 \quad \text{dt}$$
(42)

where the positive sign applies for $i_0 < 90^{\circ}$, the negative sign for $i_0 > 90^{\circ}$, and $tan^{-1}(\cos i_0 \tan \beta) = 0$ for $i_0 = 90^{\circ}$,

$$\beta = \beta_0 + \frac{\mathrm{d}\beta}{\mathrm{d}t} \, \mathrm{d}t$$

(1) β is replaced by

 $\lambda_{\mbox{\scriptsize A}\,\mbox{\scriptsize N}}$ is the selenographic longitude of the ascending node.

Equations (42) can be used for elliptic lunar orbits if

> $\omega + f = \omega_0 + \frac{d\omega}{dt} dt + f_0 + \frac{df}{dt} dt,$ (43)where $\frac{d\omega}{dt}$ is the apsidal advance given

by Eq (21) and the subscript zero denotes conditions at the time of the ascending nodal crossing of the satellite.

- (2) $\frac{df}{dt}$ is not constant, but the true anomaly f must be expressed as a function of time through Kepler's equation.
- (3) The angle ω_{\P} dt is a function of f, as well as the angle $\frac{d\Omega}{dt}$ dt.

 (4) The factor $\left(\frac{R}{r_S}\right)^2$ in $\frac{d\Omega}{dt}$ must be replaced by $\left(\frac{R}{p}\right)^2$, where p = \overline{a} (1 e^2).

ENTRY AND DEPARTURE MANEUVERS BETWEEN LUNAR ORBITS AND TRANSFER TRAJECTORIES

The material in Section B described the effects of various forces on lunar orbits once they are

established. In this section, the ΔV requirements to establish lunar orbits from translunar trajectories and to inject into transearth trajectories from lunar orbits will be discussed. These maneuvers may be divided into three categories:

- (1) Velocity requirements assuming finite burning times and variable thrust-to-weight ratios of the rocket engine.
- (2) Velocity requirements for circumlunar trajectories assuming an impulsive maneuver.
- (3) Velocity requirements for one-way trajectories (injection into lunar orbit from a translunar trajectory or injection from a lunar orbit into a transearth trajectory) assuming an impulsive maneuver.

Figure 6 presents the ΔV requirements for entry into a circular lunar orbit at an altitude of 185.2 km from a typical approach trajectory when finite burning times and variable thrust-to-weight ratios are employed. These results were obtained by assuming that the entire maneuver was conducted in the trajectory plane, and that during rocket burning the thrust vector was parallel to the velocity vector at all times. The effect of offnominal conditions as the entry maneuver was initiated is not included.

Under these assumptions, the required change in velocity can be obtained from the rocket equation:

$$\Delta V = g_{\bigoplus 0} I_{sp} \ln \left(\frac{M_0}{M_e} \right) + \int_0^{t_b} g_{\ell} \sin \gamma \, dt.$$
 (44)

where M_0 is the initial mass and M_e the final mass of the space vehicle, t_b is the burning time, γ the flight path angle, $\mathrm{g}_{\bigoplus 0}$ the earth sea-level value and g_{\lozenge} the local value of the acceleration due to gravity. The first term on the right is an expression of the conservation of linear momentum and depends on the propellant consumed. This term takes into account the thrust-to-weight ratio, $\frac{\mathrm{T}}{\mathrm{W}_0}$, since the specific impulse I sp is defined as:

$$I_{sp} = \frac{T}{\dot{W}_{f}} \tag{45}$$

where \dot{W}_f is the propellant weight flow rate of the rocket engine. The second term takes into account the gravitational effects during rocket burning (change in flight path angle and change in altitude). The increase in vehicle velocity due to the local lunar gravity (the second term in Eq (44)) must be counterbalanced by an increase in total impulse of the vehicle's rocket engines. From Fig. 6 it can be seen that as T/W_0 increases, the velocity requirement reaches a lower limit. It

velocity requirement reaches a lower limit. It has been found that for practical lunar vehicles, the $\rm T/W_0\text{-}ratios$ are large enough so that the

differences between finite burning time and a velocity impulse maneuver (infinite thrust-to-weight ratio and infinitesimal burning time) are very small.

A general idea of the impulsive velocity maneuver requirements can be gained from Fig. 7 which presents a summary plot of these ΔV requirements for circumlunar trajectories. The manuever is performed at the pericynthion point of a circumlunar trajectory, and the lunar vehicle enters a circular orbit at the pericynthion altitude. The ΔV required to enter the circular orbit is the difference between the velocity of the vehicle on the trajectory at pericynthion and the circular lunar satellite velocity at the pericynthion altitude. The plot shows ΔV as a function of $h_{\displaystyle PL}$ for a maximum, average, and minimum earth-moon distance $\mathbf{R}_{\bigoplus \emptyset}$. Requirements for $\Delta \mathbf{V}$ depend on the translunar trajectory inclination, and a value of i_{VTL} = 75° with respect to the MOP was selected as this represents a limit for lunar missions launched from Cape Canaveral. For a translunar trajectory close to the MOP, e.g., 2°, the values of ΔV of Fig. 7 are reduced by an average of 33 m/sec. A transearth inclination of i_{VTE} = 60° with a direct north earth return was chosen to ensure that the return would always be direct. Since the maximum inclination of the MOP to the earth's equatorial plane is approximately 28.5°, this con-

For a retrograde return, there is an increase in the required ΔV . Data in Fig. 7 is based on circumlunar trajectories which were obtained by use of the Voice technique (see Chapter IV). To obtain a more realistic model of the earth-moon system, computer runs were made utilizing a restricted three-body trajectory program, and the results for a circularizing velocity impulse were compared with those obtained from the Voice program. The following table presents a comparison of the two programs for various trajectory parameters.

dition is satisfied.

ΔV Requirements for Lunar Orbit Entry (m/sec)

	Voice	Restricted 3-body	(△V) _{restricted 3-body} - △V(Voice)
$R_{\oplus 4} = 56 \text{ ER}$ $h_{\text{PL}} = 185.2 \text{ km}$ $i_{\text{VTL}} = 75^{\circ}$ $i_{\text{VTE}} = 34.6^{\circ}$	1034.024	1052.876	18.852
$R_{\oplus 4} = 56 \text{ ER}$ $h_{PL} = 185.2 \text{ km}$ $i_{VTL} = 75^{\circ}$ $i_{VTE} = 98.1^{\circ}$	986.842	1004.642	17.800
$R_{\oplus \ell} = 56 \text{ ER}$ $h_{\text{PL}} = 185.2 \text{ km}$ $i_{\text{VTL}} = 75^{\circ}$ $i_{\text{VTE}} = -178.9^{\circ}$	954.619	972.098	17.479
$R_{\oplus \P}$ = 56 ER $h_{\rm PL}$ = 185.2 km $i_{\rm VTL}$ = 2° $i_{\rm VTE}$ = 105.2°	953.947	971.427	17.480
$R_{\oplus \P} = 64 \text{ ER}$ $h_{PL} = 5000 \text{ km}$ $i_{VTL} = 60^{\circ}$ $i_{VTE} = -115.5^{\circ}$	658.946	689,156	30.210

As the table indicates, the velocity impulses for the restricted three-body force model are higher because in the restricted three-body force model, the vehicle is always under the gravitational influence of the moon, while in the Voice model, the vehicle is attracted by the moon only when it is within the lunar volume of influence. Thus, the vehicle velocity relative to the moon at pericynthion will be higher for the former case. A better approximation for Δ V can be obtained if the Jacobi integral calculation (Eq (76), Chapter III) is incorporated in the Voice program. The values of ΔV obtained by this method are higher than those from the integrated program but closer in magnitude than those obtained from the Voice program alone. Also, this method requires only a single additional computation whereas several trajectories must be calculated by numerical integration if the restricted three-body force model is

One result of considering finite burning time effects rather than impulsive values of ΔV is that h_{PL} of the translunar trajectory will normally be 2 to 4 km higher than the lunar orbital altitude, h_0 . For $\frac{T}{W_0} > 0.2$, the gravity losses for this maneuver are negligibly small.

For the case of one-way trajectories, i.e., translunar-to-lunar orbit or lunar orbit-to-transearth (Chapter IX), the values of the required ΔV vary over a larger range, since one set of constraints (either at the earth or at the moon) is removed. Figures 8 and 9 present the requirements for injection into a circular lunar orbit at an altitude of 185.2 km from a translunar trajectory using an impulsive maneuver. These figures differ from Fig. 7 in that lunar orbits with particular inclinations imand descending nodes $\theta_{\rm MTL}$ are shown, while in the latter figure, these mission constraints were not indicated. As will be discussed in Chapter IX, this data can be used equally well for injection from a lunar orbit into a transearth trajectory by a slight change of notation.

Figure 8 is for i_m = 2°. This low inclination of the orbit results in almost equatorial lunar orbits with a maximum i_0 = 8.7° due to the lunar librations in latitude which amount to 6.7°. In addition, the translunar trajectory inclination $i_{\rm VTL}$ is limited to a range of 30°, and $\theta_{\rm MTL}$ varies from 60° to 180°. However, these values shown in Fig. 8 can be extended due to symmetry about the MOP as discussed further in Section A of Chapter IX. The minimum ΔV for orbit entry is ΔV = 770 in./sec, for a transfer time about twice the usual transfer time of 60 hr.

In Fig. 9, i_m = 15°, and a wider range in all trajectory parameters is available. The maximum i_0 is 21.7° and i_{VTL} as well as θ_{MTL} is only restricted by the desired flight time and the available ΔV .

Additional plots for higher values of \boldsymbol{i}_{m} can also be obtained with corresponding increases in

the ranges of the lunar orbit and trajectory parameters.

The lunar orbit parameters referred to above (i $_{m}$ and θ_{MTL}) are not defined directly with re-

spect to selenographic coordinates, but rather with respect to coordinates referred to the MOP and the earth-moon line. Thus, to tie these orbits to ground traces on the lunar surface for a specific lunar mission date, a coordinate transformation must be made to obtain the selenographic latitude and longitude.

Figures 8 and 9 do not take into account the variation in the earth-moon distance or the variation in velocity requirements for lunar orbits higher than 185.2 km. A correction of $\Delta V = \pm 30$ m/sec must be made for distances other than the average earth-moon distance (60 ER). The higher the lunar orbit, the less ΔV is required to enter it. For $h_0 = 5500$ km the saving may be as high as 275 m/sec.

D. LUNAR ORBIT DETERMINATION SCHEMES

After a lunar vehicle (either manned or unmanned) has been placed in a lunar orbit, some means must be provided to determine the accuracy of the actual orbit achieved. This determination is important both for a reconnaissance mission and a lunar landing mission, since in both cases the location of certain lunar landmarks relative to the orbit plane is of the utmost importance. If the actual orbit differs much from the planned one, some corrections must be initiated in order to fulfill the mission objectives.

Lunar orbit determination schemes are similar for the manned and unmanned missions in that they both employ a combination of earthbased tracking facilities, instruments located in the vehicle, and possibly beacons on the lunar surface. However, for manned lunar missions, the primary responsibility for orbit determination will lie with the men in the space vehicle.

For a manned lunar mission, the essential instruments that will be required are the following:

- (1) Horizon scanner (utilizing Doppler radar).
- (2) Radar altimeter.
- (3) Sextant.
- (4) Clock.

A local vertical can be established with the horizon scanner, and thus measurements of the vehicle's orientation with respect to it can be made. By the use of the radar altimeter, an altitude-time history of the orbit is obtained. When the vehicle is over the lighted side of the moon, the horizon scanner and the sextant can be used in conjunction for angular readings between a star and a landmark on the moon. A similar measurement can be made between a star and the

local vertical when the vehicle is over the unlighted side of the moon. The period of the lunar orbit can be calculated by measuring the occultation of a star by the moon with the aid of the clock.

Since the orbital elements are not constants but will be continuously changing due to the triaxiality of the moon and the gravitational attractions of the earth and the sun, these readings by themselves will be useless. Therefore, some scheme for combining the individual instrument readings for determining the present and for predicting the future orbit of the space vehicle must be devised. One such method which will be described here is based upon a scheme used for midcourse guidance corrections.

At an arbitrary epoch (e.g., time of injection into lunar orbit), the position and rotational orientation of the earth and moon relative to the stars will be determined precisely. The position and velocity of the vehicle relative to the selenocentric nonrotating coordinate system $(x_{\boldsymbol{q}}\,,\,y_{\boldsymbol{q}}\,,\,z_{\boldsymbol{q}}\,,\,x_{\boldsymbol{q}}\,,\,x_{\boldsymbol{q}}\,,\,x_{\boldsymbol{q}}\,,\,x_{\boldsymbol{q}}\,,\,x_{\boldsymbol{q}}\,,\,x_{\boldsymbol{q}}\,,\,x_{\boldsymbol{q}}\,,\,x_{\boldsymbol{q}}\,,\,x_{\boldsymbol{q}}\,,\,x_{\boldsymbol{q}}\,,\,x_{\boldsymbol{q}}\,,\,x_{\boldsymbol{q}}\,,\,x_{\boldsymbol{q}}\,,\,x_{\boldsymbol{q}}\,,\,x_{\boldsymbol{q}}\,,\,x_{\boldsymbol{q}}\,,\,x_{\boldsymbol{q}}\,,\,x_{\boldsymbol{q}}\,,\,x_{\boldsymbol{q}}\,,\,x_{\boldsymbol{q}}\,,\,x_{\boldsymbol{q}}\,,\,x_{\boldsymbol{q}}\,,\,x_{\boldsymbol{q}}\,,\,x_{\boldsymbol{q}}\,,\,x_{\boldsymbol{q}}\,,\,x_{\boldsymbol{q}}\,,\,x_{\boldsymbol{q}}\,,\,x_{\boldsymbol{q}}\,,\,x_{\boldsymbol{q}}\,,\,x_{\boldsymbol{q}}\,,\,x_{\boldsymbol{q}}\,,\,x_{\boldsymbol{q}}\,,\,x_{\boldsymbol{q}}\,,\,x_{\boldsymbol{q}}\,,\,x_{\boldsymbol{q}}\,,\,x_{\boldsymbol{q}}\,,\,x_{\boldsymbol{q}}\,,\,x_{\boldsymbol{q}}\,,\,x_{\boldsymbol{q}}\,,\,x_{\boldsymbol{q}}\,,\,x_{\boldsymbol{q}}\,,\,x_{\boldsymbol{q}}\,,\,x_{\boldsymbol{q}}\,,\,x_{\boldsymbol{q}}\,,\,x_{\boldsymbol{q}}\,,\,x_{\boldsymbol{q}}\,,\,x_{\boldsymbol{q}}\,,\,x_{\boldsymbol{q}}\,,\,x_{\boldsymbol{q}}\,,\,x_{\boldsymbol{q}}\,,\,x_{\boldsymbol{q}}\,,\,x_{\boldsymbol{q}}\,,\,x_{\boldsymbol{q}}\,,\,x_{\boldsymbol{q}}\,,\,x_{\boldsymbol{q}}\,,\,x_{\boldsymbol{q}}\,,\,x_{\boldsymbol{q}}\,,\,x_{\boldsymbol{q}}\,,\,x_{\boldsymbol{q}}\,,\,x_{\boldsymbol{q}}\,,\,x_{\boldsymbol{q}}\,,\,x_{\boldsymbol{q}}\,,\,x_{\boldsymbol{q}}\,,\,x_{\boldsymbol{q}}\,,\,x_{\boldsymbol{q}}\,,\,x_{\boldsymbol{q}}\,,\,x_{\boldsymbol{q}}\,,\,x_{\boldsymbol{q}}\,,\,x_{\boldsymbol{q}}\,,\,x_{\boldsymbol{q}}\,,\,x_{\boldsymbol{q}}\,,\,x_{\boldsymbol{q}}\,,\,x_{\boldsymbol{q}}\,,\,x_{\boldsymbol{q}}\,,\,x_{\boldsymbol{q}}\,,\,x_{\boldsymbol{q}}\,,\,x_{\boldsymbol{q}}\,,\,x_{\boldsymbol{q}}\,,\,x_{\boldsymbol{q}}\,,\,x_{\boldsymbol{q}}\,,\,x_{\boldsymbol{q}}\,,\,x_{\boldsymbol{q}}\,,\,x_{\boldsymbol{q}}\,,\,x_{\boldsymbol{q}}\,,\,x_{\boldsymbol{q}}\,,\,x_{\boldsymbol{q}}\,,\,x_{\boldsymbol{q}}\,,\,x_{\boldsymbol{q}}\,,\,x_{\boldsymbol{q}}\,,\,x_{\boldsymbol{q}}\,,\,x_{\boldsymbol{q}}\,,\,x_{\boldsymbol{q}}\,,\,x_{\boldsymbol{q}}\,,\,x_{\boldsymbol{q}}\,,\,x_{\boldsymbol{q}}\,,\,x_{\boldsymbol{q}}\,,\,x_{\boldsymbol{q}}\,,\,x_{\boldsymbol{q}}\,,\,x_{\boldsymbol{q}}\,,\,x_{\boldsymbol{q}}\,,\,x_{\boldsymbol{q}}\,,\,x_{\boldsymbol{q}}\,,\,x_{\boldsymbol{q}}\,,\,x_{\boldsymbol{q}}\,,\,x_{\boldsymbol{q}}\,,\,x_{\boldsymbol{q}}\,,\,x_{\boldsymbol{q}}\,,\,x_{\boldsymbol{q}}\,,\,x_{\boldsymbol{q}}\,,\,x_{\boldsymbol{q}}\,,\,x_{\boldsymbol{q}}\,,\,x_{\boldsymbol{q}}\,,\,x_{\boldsymbol{q}}\,,\,x_{\boldsymbol{q}}\,,\,x_{\boldsymbol{q}}\,,\,x_{\boldsymbol{q}}\,,\,x_{\boldsymbol{q}}\,,\,x_{\boldsymbol{q}}\,,\,x_{\boldsymbol{q}}\,,\,x_{\boldsymbol{q}}\,,\,x_{\boldsymbol{q}}\,,\,x_{\boldsymbol{q}}\,,\,x_{\boldsymbol{q}}\,,\,x_{\boldsymbol{q}}\,,\,x_{\boldsymbol{q}}\,,\,x_{\boldsymbol{q}}\,,\,x_{\boldsymbol{q}}\,,\,x_{\boldsymbol{q}}\,,\,x_{\boldsymbol{q}}\,,\,x_{\boldsymbol{q}}\,,\,x_{\boldsymbol{q}}\,,\,x_{\boldsymbol{q}}\,,\,x_{\boldsymbol{q}}\,,\,x_{\boldsymbol{q}}\,,\,x_{\boldsymbol{q}}\,,\,x_{\boldsymbol{q}}\,,\,x_{\boldsymbol{q}}\,,\,x_{\boldsymbol{q}}\,,\,x_{\boldsymbol{q}}\,,\,x_{\boldsymbol{q}}\,,\,x_{\boldsymbol{q}}\,,\,x_{\boldsymbol{q}}\,,\,x_{\boldsymbol{q}}\,,\,x_{\boldsymbol{q}}\,,\,x_{\boldsymbol{q}}\,,\,x_{\boldsymbol{q}}\,,\,x_{\boldsymbol{q}}\,,\,x_{\boldsymbol{q}}\,,\,x_{\boldsymbol{q}}\,,\,x_{\boldsymbol{q}}\,,\,x_{\boldsymbol{q}}\,,\,x_{\boldsymbol{q}}\,,\,x_{\boldsymbol{q}}\,,\,x_{\boldsymbol{q}}\,,\,x_{\boldsymbol{q}}\,,\,x_{\boldsymbol{q}}\,,\,x_{\boldsymbol{q}}\,,\,x_$

$$\Delta \sigma = \sigma_{\rm c}(t) - \sigma_{\rm R}(t) \tag{46}$$

There will be a set of these equations for each of the times that the readings are taken.

This process is then repeated for each set of assumed initial conditions except for a change in each one of them, e.g., $\mathbf{x}_{\mathbf{q}} + \Delta \mathbf{x}_{\mathbf{q}}$, $\mathbf{y}_{\mathbf{q}}$, $\mathbf{z}_{\mathbf{q}}$; $\dot{\mathbf{x}}_{\mathbf{q}}$, $\dot{\mathbf{y}}_{\mathbf{q}}$, $\dot{\mathbf{z}}_{\mathbf{q}}$, etc. The differences in the actual and calculated readings are then expressible in terms of changes in coordinates by:

$$\Delta \sigma_{i} = \frac{\partial \sigma_{i}}{\partial x_{\mathbf{q}}} \Delta x_{\mathbf{q}} + \frac{\partial \sigma_{i}}{\partial y_{\mathbf{q}}} \Delta y_{\mathbf{q}} + \frac{\partial \sigma_{i}}{\partial z_{\mathbf{q}}} \Delta z_{\mathbf{q}} + \frac{\partial \sigma_{i}}{\partial \dot{z}_{\mathbf{q}}} \Delta \dot{z}_{\mathbf{q}} + \frac{\partial \sigma_{i}}{\partial \dot{z}_{\mathbf{q}}} \Delta \dot{z}_{\mathbf{q}} + \frac{\partial \sigma_{i}}{\partial \dot{z}_{\mathbf{q}}} \Delta \dot{z}_{\mathbf{q}}$$

$$(47)$$

where i denotes the i-th instrument reading. Utilizing a least squares technique which minimizes the differences Σ ($\Delta \sigma_i$)², Eq (47) is

solved for $\Delta x_{\boldsymbol{q}}$, $\Delta y_{\boldsymbol{q}}$, $\Delta z_{\boldsymbol{q}}^{i}$; $\Delta \dot{x}_{\boldsymbol{q}}$, $\Delta \dot{y}_{\boldsymbol{q}}$, and $\Delta \dot{z}_{\boldsymbol{q}}$. Thus, a set of initial conditions which when used with the equations of motion yield the best results consistent with the actual readings is obtained

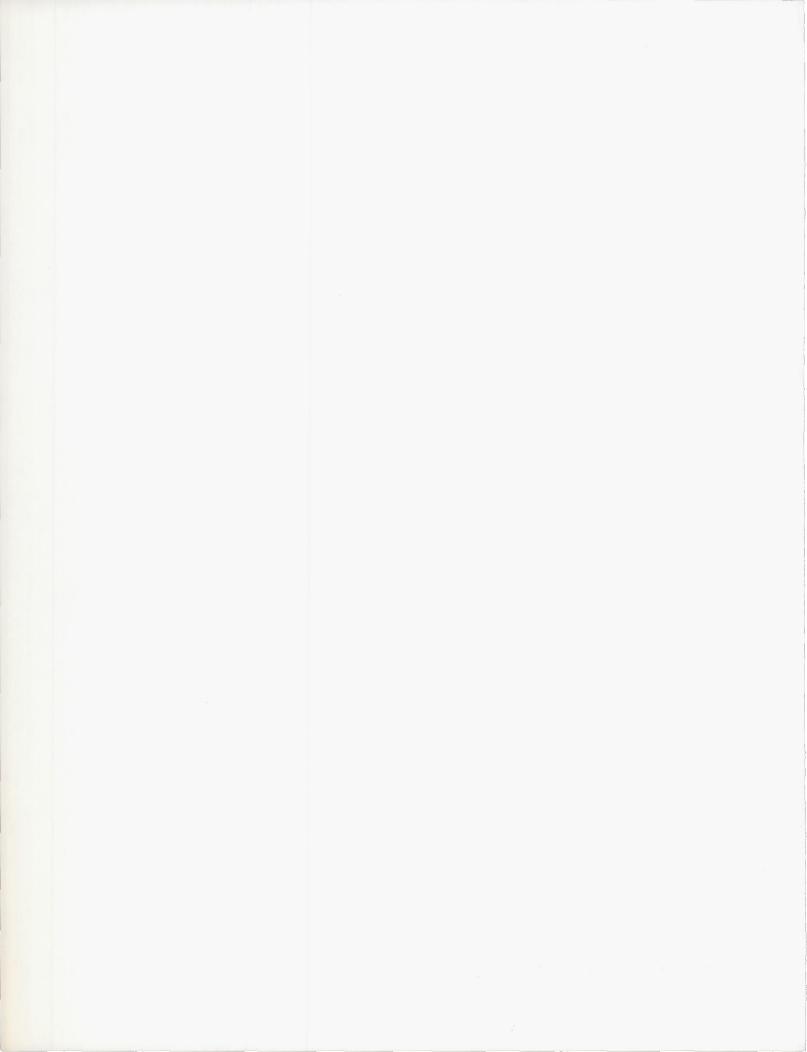
with the equations of motion yield the best results consistent with the actual readings is obtained. These results might be improved by several refinements--using a more detailed set of equations of motion, including statistical and instrument errors in the calculations, and using a more refined smoothing technique which weighs each of the readings differently.

For an unmanned lunar mission, orbit determination will be primarily based on data obtained by DSIF (Chapter VI). This system will be able to obtain the orbital altitude by knowing the precise location and dimensions of the moon. The orbital period will be calculated by adding the time the vehicle spends behind the moon to the time it is observed by the tracking facilities. Automatic equipment which might be included in an unmanned vehicle are a star tracker and a radar altimeter. These will give additional values of the orbital period and altitude.

E. REFERENCES

- "Orbital Flight Handbook," ER 12684, Martin Company, Space Systems Division (Baltimore), 1963.
- Schechter, H. B., "Multibody Influence on the Least Altitude of a Lunar Satellite," ARS Journal, Vol. 32, December 1962, p 1921.
- 3. Jeffreys, H., "The Earth, Its Origin, History, and Physical Constitution," University Press (Cambridge, England), 1952.
- Kozai, Y., "The Motion of a Close Earth Satellite," The Astronomical Journal, Vol. 64, No. 9, November 1959, p 367.
- Brouwer, D., "Solution of the Problem of Artificial Satellite Theory Without Drag," The Astronomical Journal, Vol. 64, No. 9, November 1959, p 378.
- 6. King-Hele, D. G., "The Effect of the Earth's Oblateness on the Orbit of a Near Satellite," Proceedings of the Royal Society, Vol. 247A, No. 4, August 1958, p 49.
- Vinti, J. P., "New Method of Solution for Unretarded Satellite Orbits," Journal of Research, N. B. S., Vol. 62B, No. 2, October-December, p 105.
- Blitzer, L., "Effect of Earth's Oblateness on the Period of a Satellite," Jet Propulsion, Vol. 27, No. 4, April 1957, pp 405-406.
- 9. Jaramillo, T. J., "The Combined Non-Linear Effects of Earth Oblateness and Atmospheric Drag on a Near-Earth Satellite," Wright Air Development Center WADC TR 59-513, AD No. 233184, October 1959.
- 10. Groves, G. V., "Motion of a Satellite in the Earth's Gravitational Field," Proceedings of the Royal Society, Vol. 254A, No. 1276, January 19, 1960, pp 48-69.
- 11. Anthony, M. L., and Fosdick, G. E., "Satellite Motions About an Oblate Planet," IAS Paper No. 60-57, IAS, National Summer Meeting, June, 1960, also published in Journal of Aerospace Sciences, Vol. 28, No. 10, October 1961, p 789.
- 12. Struble, R. A., "The Geometry of the Orbits of Artificial Satellites," Archive for Rational Mechanics and Analysis, Vol. 7, No. 2, 1961, pp 87-104.

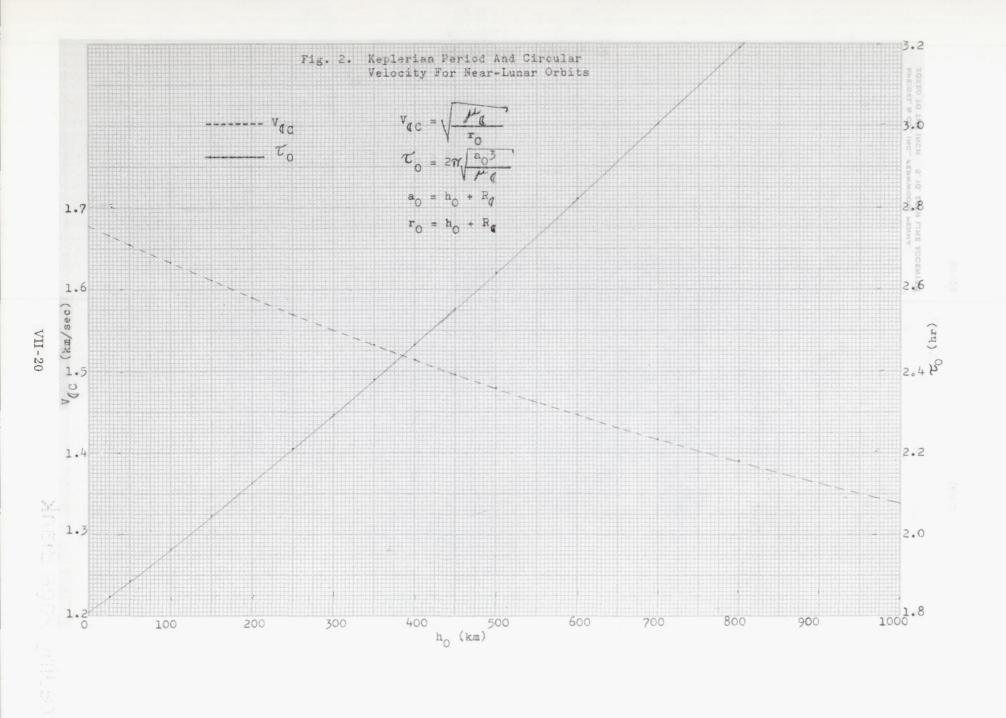
- 13. Martikan, F. and Kalil, F., "A Derivation of Nodal Period of an Earth Satellite and Comparisons of Several First-Order Secular Oblateness Results," unpublished note, also ER 12202, Martin Company (Baltimore), February 28, 1962.
- 14. Sterne, T. E., "The Gravitational Orbit of a Satellite of an Oblate Planet," The Astronomical Journal, Vol. 63, No. 1255, January 1958, p 28.
- 15. Sterne, T. E., "Development of Some General Theories of the Orbits of Artificial Earth Satellites," The Astronomical Journal, Vol. 63, No. 1264, November 1958, p 424.
- 16. Vinti, J. P., "Theory of an Accurate Intermediary Orbit for Satellite Astronomy," Journal of Research, N.B.S., Vol. 65B, No. 3, July-September 1961, p 169.
- 17. King-Hele, D. G., Walker, D. M. C., "Methods for Predicting the Orbits of Near-Earth Satellites," Journal of the British Interplanetary Society, Vol. 17, No. 1, January-February 1959, pp 2-14.
- 18. Blitzer, L., Weisfeld, M., Wheelon, A. D., "Perturbations of a Satellite's Orbit Due to the Earth's Oblateness," Journal Applied Physics, Vol. 27, No. 10, October 1956, pp 1141-1149.
- 19. Kork, J., "First Order Satellite Motion in Near-Circular Orbits About an Oblate Earth: Comparison of Several Results and Optimization for Minimum Altitude Variation," ER 12202, Martin Company (Baltimore), January 1962.
- 20. Kozai, Y., "Note on the Motion of a Close Earth Satellite with Small Eccentricity," The Astronomical Journal, Vol. 66, No. 3, April 1961, p 132.
- Izsak, I. G., "On Satellite Orbits with Very Small Eccentricities," The Astronomical Journal, Vol. 66, No. 3, April 1961, p 129.
- Lass, H. and Solloway, C. B., "Motion of a Satellite of the Moon," ARS Journal, Vol. 31, February 1961, p 220.
- Brown, E. W., "An Introductory Treatise on the Lunar Theory," Dover Publications (New York), 1960.

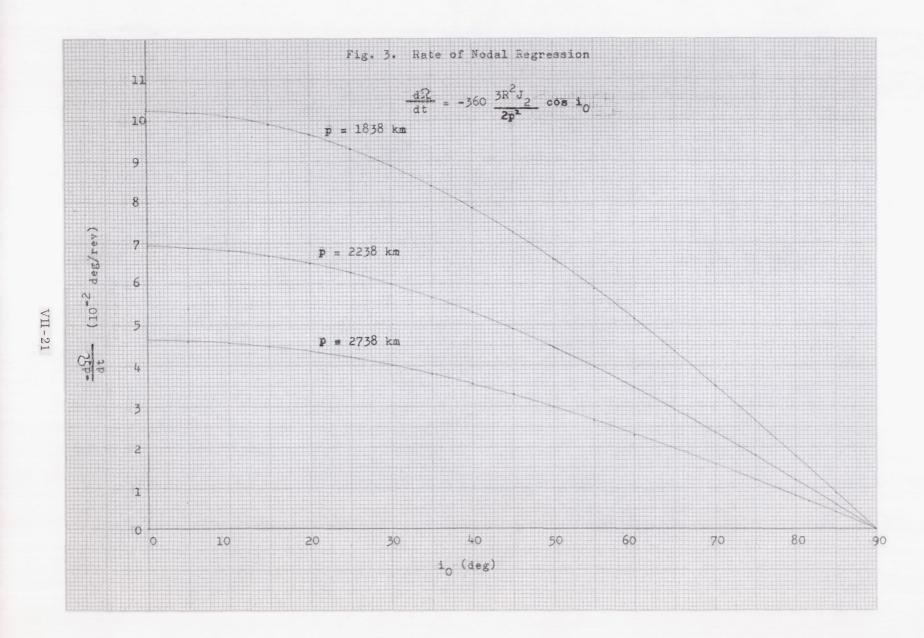


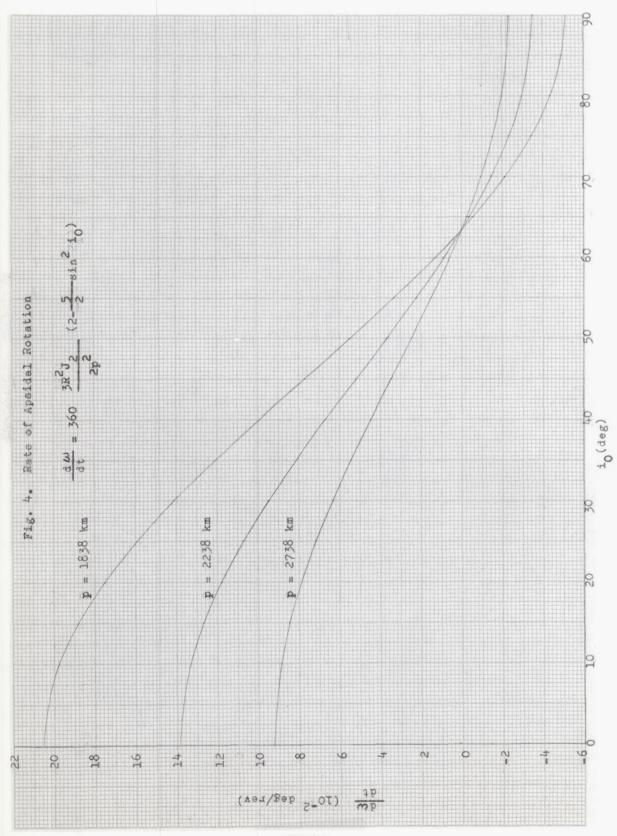
ILLUSTRATIONS

LIST OF ILLUSTRATIONS

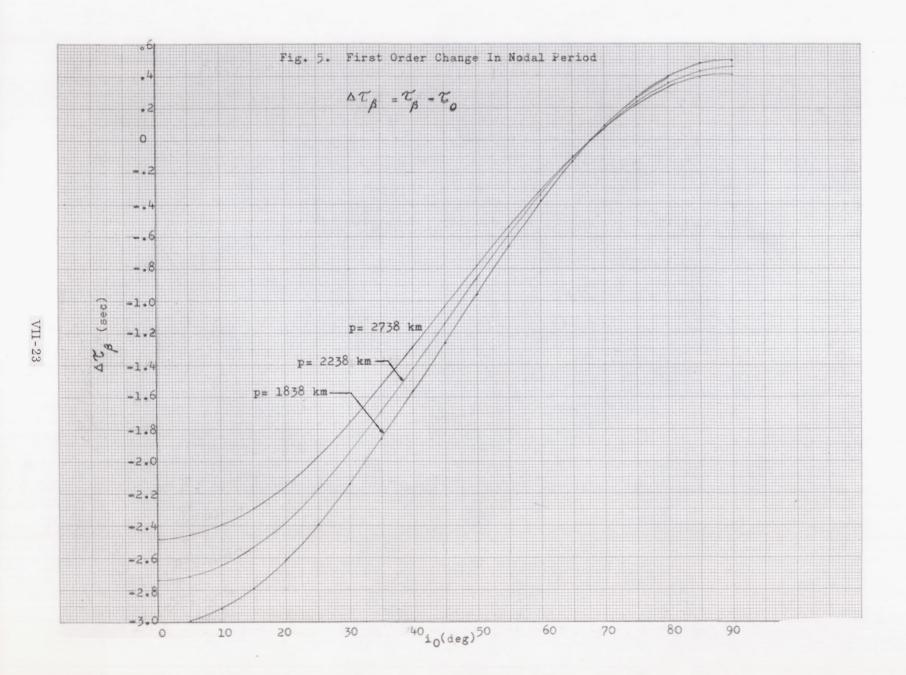
Figure		Page
1	Keplerian Period and Circular Velocity for Lunar Orbits	VII-19
2	Keplerian Period and Circular Velocity for Near-Lunar Orbits	VII-20
3	Rate of Nodal Regression	VII-21
4	Rate of Apsidal Rotation	VII-22
5	First order Change in Nodal Period	VII-23
6	Entry into Lunar Orbit	VII-24
7	ΔV Required for Injection into Circular Orbit for Circumlunar Trajectories	VII-25
8	Lunar Mission Parametersi _m = 2°	VII-26
9	Lunar Mission Parameters i _m = 15°	VII-27

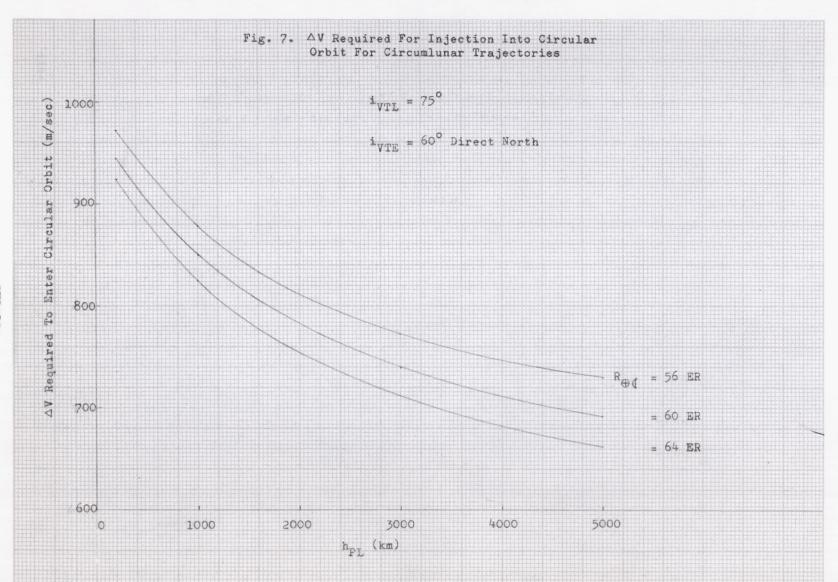






VII-22





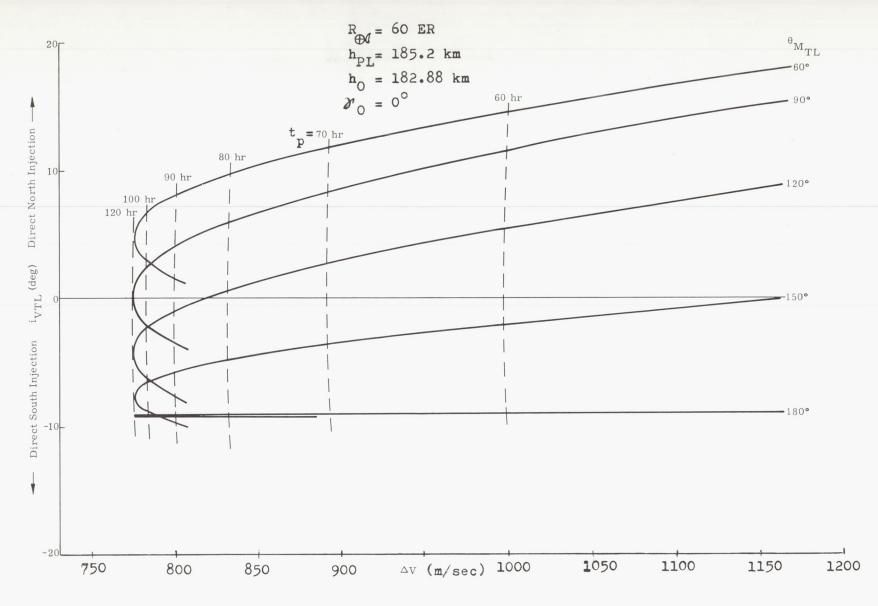


Fig. 8. Lunar Mission Parameters--i_m = 2°
(Approach Trajectories)

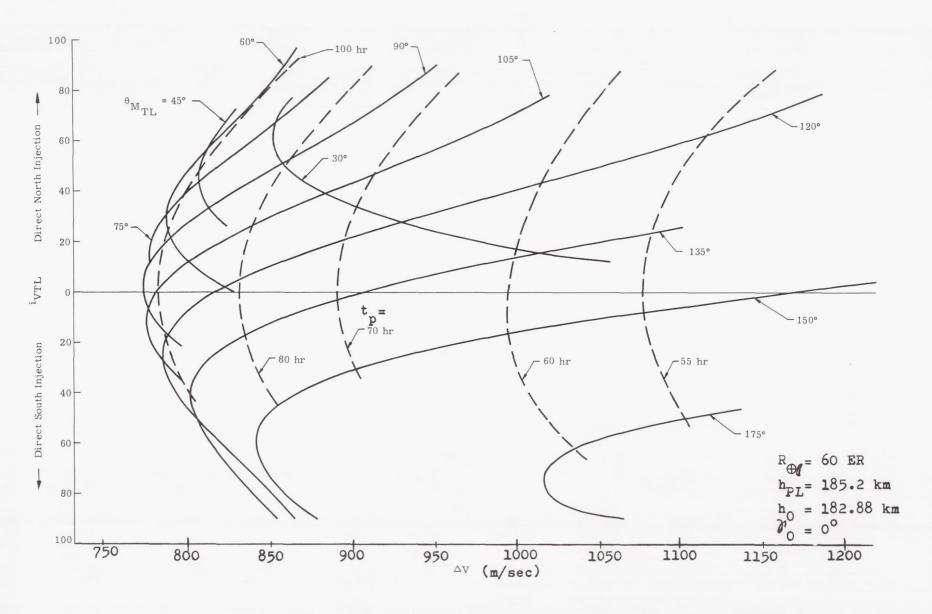
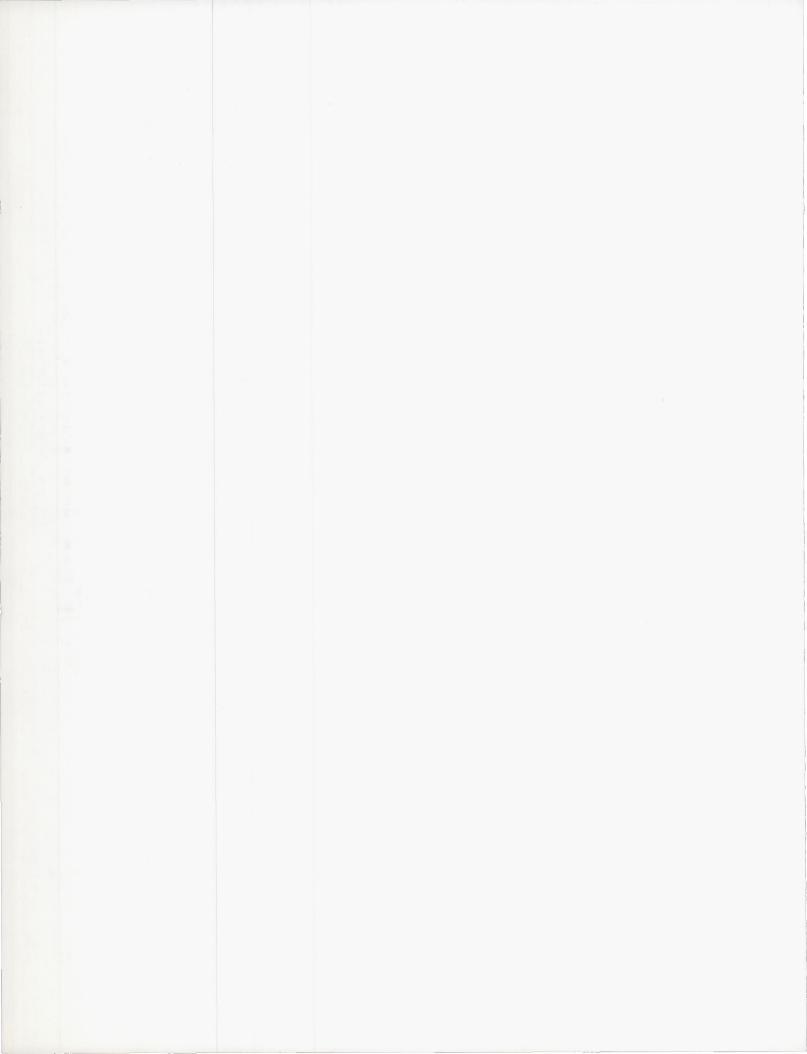


Fig. 9. Lunar Mission Parameters--i = 15°
(Approach Trajectories)



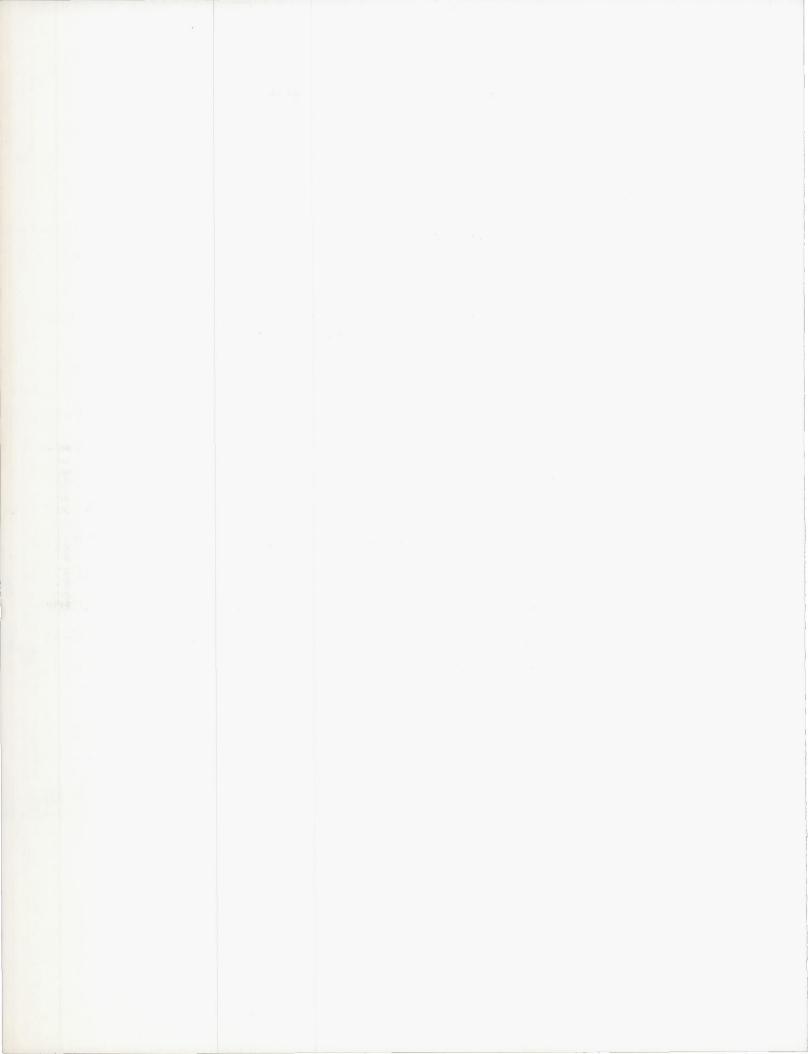
CHAPTER VIII

DESCENT TO AND ASCENT FROM THE LUNAR SURFACE

Prepared by:

J. D. Kraft, F. Santora, A. Jazwinski, F. Martikan, and R. Salinger Martin Company (Baltimore) Aerospace Mechanics Department March 1963

	Pag	е
Α.	Introduction VIII-	1
В.	Descent to Lunar Surface VIII-	1
C.	Ascent from Lunar Surface VIII-1	8
D.	Hovering and Translation Requirements VIII-2	1
E.	Lunar Landing Abort VIII-2	5
F.	References VIII-3	2
	Illustrations VIII-3	3
	List of Illustrations VIII-3	5



VIII. DESCENT TO AND ASCENT FROM THE LUNAR SURFACE

A. INTRODUCTION

The landing of a space vehicle on the surface of the moon in general involves retro-rocket deceleration to significantly reduce a relative vehicle approach speed which is on the order of 3 km/sec. The degree of reduction required and the techniques for achieving this velocity reduction are different for high-speed hard landings than for soft-landing instrument carriers and manned vehicles. Two main classes of ascent and descent trajectories may be distinguished:

- (1) Direct ascent from the lunar surface into a transearth trajectory or direct descent from a translunar trajectory to the lunar surface.
- (2) Ascent to a lunar satellite orbit prior to entering a transearth trajectory, which will be referred to as indirect ascent, and descent from a lunar satellite orbit after entering the lunar orbit from a translunar trajectory, which will be referred to as indirect descent

Although the direct case is straightforward and requires little explanation, various approaches are possible for achieving indirect ascent or descent, and these approaches are worthy of note. In the direct case, of course, the entire space vehicle, which is called landing module (LM), together with any related modules, descends from the translumar trajectory by use of one or more rocket deceleration phases to the lunar surface. On the other hand, in the indirect case, the space vehicle, on nearing the moon, is injected into a lunar satellite orbit. After this orbit is adequately determined, the indirect descent may proceed in either of two ways:

- (1) The vehicle separates into two modules, one containing the propulsion system and return spacecraft for the return trip to earth and the other comprising a shuttle. The shuttle vehicle is a minimal vehicle which is capable of being landed on the lunar surface; it can be used as a base for explorations, and it can be launched for a rendezvous with the return space vehicle, which has in the meantime remained in lunar orbit.
- (2) The entire orbiting space vehicle, including propulsion systems and fuel supply for the return to earth descends to the preselected point on the lunar surface. The portion of the vehicle which descends to the surface of the moon is known as the landing module (LM).

Both indirect approaches offer the advantages of greater flexibility in landing site selection and a longer period for final orbit determination. The shuttle approach offers the further advantage of smaller fuel requirements, since parts of the LM may be abandoned in lunar orbit, but it

requires more complex space vehicle systems due to the rendezvous requirement after ascent.

All data presented in this chapter is based on the assumption of a moon which is the only celestial body affecting the trajectory, which is symmetric in spherical layers and without an atmosphere. Thus all ballistic trajectories are Keplerian orbits. These assumptions are justified, since the short time spent during ascent and descent keeps the secular perturbations, which are neglected by making these assumptions, quite small.

Specific areas considered in each class of lunar ascent and descent trajectory include propulsion system requirements, types of trajectories, abort capabilities, guidance laws and control system requirements. The lunar ascent and descent phase of an impact probe or lunar landing mission can be further classified into such subphases as descent braking, hovering and translation prior to landing, launch from the lunar surface, and rendezvous (if required) with a lunar satellite vehicle. Each phase will be discussed separately. Material related to lunar ascent and descent is given as follows: Injection requirements for moon-toearth transfer are noted in Chapter IX, trajectory computation for the principal moon-to-earth or earth-to-moon transfers is considered in Chapters IV and VI, and some aspects of deorbit requirements are covered in Chapter VII. Keplerian orbit data is given in Chapter III of Ref. 1 in analytical and graphical form.

B. DESCENT TO LUNAR SURFACE

1. Direct Descent

Impact velocities with which an unretarded landing module (LM) strikes the moon vary from about 2.5 km/sec to 3.2 km/sec for typical earth-to-moon transfers. This terminal velocity (or unretarded impact velocity) is plotted as a function of transfer time in Fig. 1. Since the terminal velocity is equivalent to the velocity impulse required to stop the vehicle just before impact, it represents a lower bound on the velocity decrement required to decelerate and soft-land a vehicle with rocket burning. The actual deceleration or braking of the vehicle requires finite burning time and more fuel. Soft landings are characterized by impact velocities on the order of tens of meters per second. The degree by which the terminal velocity must be reduced by rocket braking depends on the nature of the mission.

a. Terminal velocity requirements

The greatest reduction in terminal velocity is required for manned vehicles. In this case impact should occur at less than about 5 m/sec (without shock absorption) so that the maximum impact deceleration be less than 15 $\rm g_{\bigoplus 0}$. For many instrument carriers, the soft landing requirement may be relaxed to several hundred $\rm g_{\bigoplus 0}$, resulting in a simplification of the landing guidance and control system. These missions may

employ mechanical or fluid shock absorbers or gas-filled balloons to reduce decelerations, but retro-rockets will still be required. Reference 2 estimates that a 200 newton payload, if slowed by retro-rocket to an impact speed of about 100 m/sec, could be landed by a collapsing balloon system with deceleration of 200 g $_{\bigoplus O}$. References (3) and (4)

consider stresses and penetrations with hard landings. Instrument packages may be mounted on top of high strength penetration spikes to avoid toppling and damage. Figure 2 shows the penetration of a rock surface material by a cylindrical body with a conical nose. The empirical Petry formula has been used to obtain the penetration depths plotted in Fig. 2:

$$P = K \frac{W}{D^2} f(V_i)$$
 (1)

where

P = maximum penetration depth

K = a constant varying with material and projectile shape

W = weight of projectile

D = diameter of projectile

f (V₂) = a function of impact velocity

The maximum resistive pressure associated with this penetration is plotted in Fig. 3. This pressure is independent of projectile weight. Both figures employ the compressive strength of the rock as a parameter, thus avoiding a specification of the type of lunar surface. Although opinions still differ as to the nature of the lunar surface, the primary surface material is rather thought to consist of porous rock than a thick dust layer (Ref. 5). At any rate, even for lunar probes, impact speeds should be reduced by retro-rockets to at least 100 m/sec for most payloads.

b. Braking technique

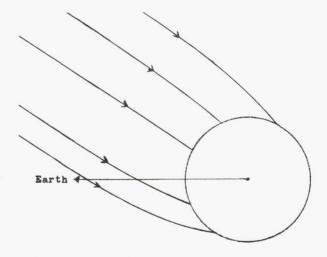
Direct descent braking is, then, a matter of reducing impact velocity from about 3 km/sec to less than 100 m/sec. The braking could be done most economically by applying maximum thrust over a minimum burning time in order to reach zero velocity just at the lunar surface. In the limiting case, the most efficient braking technique would apply, just before impact, an impulse equal in magnitude to the impact velocity. Of course, optimization based on the sole criterion of fuel economy results in a system requiring tolerance to high decelerations and stringent guidance and control system performance. Design of the lunar landing system must be based on a compromise between fuel economy on one hand and low decelerations and a simple guidance system on the other hand.

A braking technique for direct descent which achieves such a compromise might have the following qualitative characteristics: In the initial phase of the approach, which comprises the principal part of the landing trajectory, a high constant-thrust stage is employed to reduce

approach velocity significantly. During this phase only very crude guidance will be required. (The midcourse translunar guidance must achieve accuracies of the order of a few m/sec to assure impact, and errors of this order in the early braking phase can be tolerated.) A second phase, in which a variable thrust engine relying on accurate local velocity, altitude, and attitude sensors cancels the remaining velocity, must be initiated at a sufficiently high altitude to provide time to eliminate trajectory errors before touchdown. In manned missions this phase will probably terminate in a period of hovering and translation. Fuel economy of the vernier rocket is improved with increased throttleability, or range of thrust at which the engine can operate. The initial phase of constant-thrust burning could be accomplished in several periods of burning separated by a ballistic trajectory, although some means of attitude control is required at all times. The use of several periods of burning appears to relax certain guidance system requirements, but involves a more complicated propulsion system.

c. Direct descent trajectory analysis

All braking techniques considered for the descent phase must be evaluated in terms of fuel requirements, decelerations, complexity of the guidance scheme and similar parameters which can be obtained from the trajectory of the vehicle. The following sketch shows some typical ballistic lunar impact trajectories (i.e., those with no rocket braking in the vicinity of the moon) in the MOP which were obtained by use of the restricted three-body force model:



All strike the moon on the ascending arm; they leave earth direct, and the difference in injection velocity near earth between the outer trajectories on the sketch is approximately 25 m/sec.

In analyzing descent trajectories with rocket braking, or trajectories in general, analytic solutions are useful and desirable in that they show trends and provide a check on subsequent, more accurate, numerical solutions. On the other hand, these analytic trajectories may be unrealistic due to the restrictive assumptions that had to be made. The following assumptions underlie the simplest physical model which can

be used for analytical direct descent trajectories:

- (1) The descent is vertical to the surface of the moon.
- (2) The moon is homogeneous in spherical layers.
- (3) The lunar gravitational acceleration is constant during the braking phase.
- (4) Drag forces are neglected.
- (5) The mass flow rate and exhaust velocity of the braking rocket are constant.
- (6) The vehicle is a point mass and its attitude does not influence the trajectory; the attitude is only important in the correct aiming of the rocket engine.

The first assumption is justified for preliminary analysis since some typical direct descent trajectories approach the moon vertically, or nearly vertically, as can be seen from the preceding sketch. In addition, data generated from the vertical trajectory analysis is useful in describing off-vertical trajectories as long as thrust and vehicle velocity are colinear. The second assumption is quite reasonable, as can be seen from the lunar data in Section A of Chapter II, and it allows the treatment of all vertical trajectories as similar, regardless of the landing site location. Actually the first assumption implies the second. Concerning the third assumption, no serious inaccuracies result in the data if average values of gravitational acceleration are taken in each braking phase, especially when the altitude range during one braking phase is small compared to the lunar radius. Assumption (4) is certainly valid since the lunar atmospheric density at the

surface is probably less than 10⁻¹² of the sea level density of the earth's atmosphere. Assumptions (5) and (6) are the usual ones for a preliminary trajectory analysis. Furthermore, descent trajectories are usually so close to the primary body (in this case the moon) and of such a short duration that the gravitational attraction of other celestial bodies may be neglected.

With the foregoing assumptions, the equation of motion for vertical descent to the lunar surface with rocket burning becomes:

$$\mathbf{M} \frac{\mathrm{d}^2 \mathbf{h}}{\mathrm{d}t^2} = -\mathbf{V}_{\mathrm{ex}} \frac{\mathrm{d}\mathbf{M}}{\mathrm{d}t} - \mathbf{M}\bar{\mathbf{g}}_{\mathbf{\zeta}}$$
 (2)

where

M = mass of the vehicle, M = M₀ - Mt,
 M is a positive constant, M₀ the
 initial mass.

h = altitude of the vehicle above the lunar surface

t = time

V_{ex} = effective exhaust velocity of retrorocket (assumed constant) = average gravitational acceleration during braking

Successive integration of Eq (1) and evaluation of the boundary conditions,

$$t = 0: h = h_0, V = V_0$$

$$t = t_h: h = h_1, V = V_1$$

gives equations for the velocity and altitude after any given braking phase, which can be expressed in the form:

$$V_1 = V_0 + V_{\text{ex}} \left[\ln \left(1 - \zeta \right) + \frac{\overline{g}}{g_{\oplus 0}} \frac{\zeta}{\left(\frac{T}{W_0} \right)} \right]$$
 (3)

$$h_1 = h_0 + \frac{V_{ex}^2}{g_{\bigoplus 0}} \frac{1}{(W_0)}$$
 {(1 - ζ) ln (1 - ζ)

$$+ \zeta \left[1 - \frac{V_0}{V_{\text{ex}}} - \frac{\zeta \frac{\bar{g}_{\mathbf{c}}}{g_{\oplus 0}}}{2 \left(\frac{T}{W_0} \right)} \right]$$
 (4)

where

V₀ = vehicle speed (positive downward) at retro-rocket ignition

 \mathbf{h}_0 = altitude above the lunar surface at retro-rocket ignition

V_{ex} = effective exhaust velocity of the retro-rocket (assumed constant)

ζ = mass ratio of retro-rocket

$$\left(\zeta = \frac{W_f}{W_0} = \frac{\dot{M}}{M_0} t_1\right)$$

 $\frac{T}{W_0} \ \ \mbox{= initial thrust-to-weight ratio using} \\ \mbox{sea level weight at earth}$

Wo = earth sea level weight

 $g_{\bigoplus} 0 = acceleration of gravity at the surface of the earth$

g = average acceleration of lunar gravity over the altitude range during braking

Less accurately, the value of gravity at the lunar surface, \mathbf{g}_{\P} will be used instead of \mathbf{g}_{\P} in subsequent calculations and figures on vertical descent. For the case of one burning phase leading

to a soft landing with zero relative velocity to the

surface the end conditions are
$$t = t_b$$
: $h = h_1 = 0$, $V = V_1 = 0$

and, for this special case, Eqs (3) and (4) reduce respectively to:

$$\frac{V_0}{V_{\text{ex}}} = -\left[\ln\left(1-\zeta\right) + \frac{g_{\zeta}}{g_{\oplus 0}} - \frac{\zeta}{W_0}\right]$$
 (5)

$$\frac{h_0 g_{\bigoplus 0}}{V_{\text{ex}}^2} = -\frac{1}{\left(\frac{T}{W_0}\right)} \left[\zeta + \ln\left(1 - \zeta\right) + \frac{1}{2} \frac{g_{\emptyset 0}}{g_{\bigoplus 0}} - \frac{\zeta^2}{\left(\frac{T}{W_0}\right)} \right]$$
(6)

The nondimensional velocity parameter $\frac{V_0}{V_{ex}}$, and the nondimensional altitude parameter, $\frac{h_0 g_{\oplus 0}}{V_{ex}}$, are plotted in Figs. 4 and 5 as functions of mass ratio ζ and initial thrust-to-weight ratio $\frac{T}{W_0}$. If Eq (5) is solved for thrust-to-weight ratio, and the result substituted in Eq (6), the nondimensional altitude parameter is related to mass ratio and nondimensional velocity parameter.

$$\frac{g_{00}h_{0}}{V_{ex}^{2}} = \left[\frac{V_{0}}{V_{ex}} + \ln(1-\zeta)\right] \left[1 - \frac{1}{2} \frac{V_{0}}{V_{ex}} + \left(\frac{1}{\zeta} - \frac{1}{2}\right) \ln(1-\zeta)\right]$$
(7)

Since

eter as follows:

$$t_b = \frac{\zeta V_{ex}}{g_{\oplus 0} \frac{T}{W_0}}$$

Equation (5) can be used to relate burning time to mass ratio and velocity at retro-rocket ignition and define a nondimensional burning time param-

eter $\frac{g_{\bullet} o^{t}b}{V_{ex}}$ by the equation:

$$\frac{g_{(0)}^{t_b}}{V_{ex}} = -\left[\frac{V_0}{V_{ex}} + \ln(1-\zeta)\right]$$
 (8)

Equation (7) is plotted in Fig. 6, and Eq (8) is plotted in Fig. 7.

Error relationships for vertical descent may be evolved by taking differentials of Eq (3) and (4), where \overline{g}_{ζ} has been replaced by g_{ζ} 0. The results are as follows:

$$dV_{1} = dV_{0} + \left[\ln(1-\zeta) + \frac{g_{0}}{g_{0}} + \frac{\zeta}{\sqrt{\frac{T}{W_{0}}}}\right] dV_{ex}$$

$$+ V_{ex} \left[-\frac{1}{1-\zeta} + \frac{g_{0}}{g_{0}} + \frac{1}{\sqrt{\frac{T}{W_{0}}}}\right] d\zeta$$

$$-V_{ex} \frac{g_{\langle 0 \rangle}}{g_{\langle 0 \rangle}} \frac{\zeta}{\left(\frac{T}{W_0}\right)^2} d \left(\frac{T}{W_0}\right)$$

$$dh_1 = dh_0 + \left[\frac{2(h_1 - h_0)}{V_{ex}} + \frac{V_0}{V_{ex}} t_b\right] dV_{ex}$$

$$+ \frac{1}{\left(\frac{T}{W_0}\right)} (h_0 - h_1 + t_b^2 \frac{g_{\langle 0 \rangle}}{2}) d \left(\frac{T}{W_0}\right)$$

$$+ \frac{V_1 V_{ex}}{g_{\langle 0 \rangle} \left(\frac{T}{W_0}\right)} d\zeta - t_b dV_0$$

$$where t_b = \frac{V_{ex} \zeta}{g_{\langle 0 \rangle} \left(\frac{T}{W_0}\right)}$$

For the case of a single rocket braking period to a soft landing with zero velocity, nominal values are V_1 = 0 and h_1 = 0. Then

$$\begin{split} \mathrm{d}\, V_1 &= \mathrm{d}\, V_0 - \frac{V_0}{V_\mathrm{ex}} - \mathrm{d}\, V_\mathrm{ex} + V_\mathrm{ex} \left[-\frac{1}{1-\zeta} \right] \\ &+ \frac{g_{\,\, \downarrow \, 0}}{g_{\,\, \oplus \, 0}} - \frac{1}{\left(\frac{\mathrm{T}}{W_0}\right)} \right] - \mathrm{d}\zeta \\ &- V_\mathrm{ex} \, \frac{g_{\,\, \downarrow \, 0}}{g_{\,\, \oplus \, 0}} - \frac{\zeta}{\left(\frac{\mathrm{T}}{W_0}\right)^2} - \mathrm{d}\left(\frac{\mathrm{T}}{W_0}\right) \\ \mathrm{d}h_1 &= \mathrm{d}h_0 + \left(-\frac{2\,h_0}{V_\mathrm{ex}} + \frac{V_0}{V_\mathrm{ex}} \, t_\mathrm{b} \right) - \mathrm{d}\, V_\mathrm{ex} \\ &+ \frac{1}{\left(\frac{\mathrm{T}}{W_0}\right)} - \left(h_0 + t_\mathrm{b}^2 - \frac{g_{\,\, \downarrow \, 0}}{2}\right) \, \mathrm{d}\left(\frac{\mathrm{T}}{W_0}\right) \\ &- t_\mathrm{b} \, \mathrm{d}\, V_0, \quad \left[V_1 = 0, \, h_1 = 0 \right] - (12) \end{split}$$

De Fries (Ref. 6) derives results corresponding to Eq (11) for the case of n thrust on-off periods, i.e., n periods of constant thrust followed by periods of ballistic flight. The assumptions are the same as in the single-stage case. The value of the acceleration due to lunar gravity for the j-th powered phase is the constant value g at the time of rocket cutoff, while it is assumed variable during the ballistic flight phases. The error due to this assumption can be accounted for by including lunar gravity as an independent error source in the analysis. The results are reproduced here for convenience, and the notation is illustrated in the following sketch.

The error analysis is made by using a Taylor series expansion of the touchdown velocity (the velocity at the end of the n-th coasting period. which may be regarded as the initial velocity of a fictitious $(n+1)^{th}$ powered phase and is denoted by $V_{n+1,0}$) involving only first-order terms.

$$V_{n+1, 0} \left(h_{j0} + \Delta h_{j0}, \Delta V_{j} + \Delta (\Delta V_{j}), T_{j} \right)$$

$$+ \Delta T_{j}, g_{(j)} + \Delta g_{(j)}, V_{10} + \Delta V_{10}$$

$$= V_{n+1, 0} \left(h_{j0}, V_{j}, T_{j}, g_{(j)}, V_{10} \right)$$

$$+ \sum_{j=1}^{n} \frac{\partial V_{n+1, 0}}{\partial h_{j0}} \Delta h_{j0}$$

$$+ \sum_{j=1}^{n} \frac{\partial V_{n+1, 0}}{\partial (\Delta V_{j})} \Delta (\Delta V_{j})$$

$$+ \sum_{j=1}^{n} \frac{\partial V_{n+1, 0}}{\partial T_{j}} \Delta T_{j}$$

$$+ \sum_{j=1}^{n} \frac{\partial V_{n+1, 0}}{\partial g_{(j)}} \Delta g_{(j)}$$

$$+ \frac{\partial V_{n+1}}{\partial V_{10}} \Delta V_{10}$$

$$(13)$$

where the partial derivatives are given as follows:

$$\frac{\partial V_{n+1,0}}{\partial h_{j0}} = \frac{\partial V_{j+1,0}}{\partial h_{j0}} \frac{1}{V_{n+1,0}}$$
(1

+ continued

$$-\frac{\Delta V_{n}}{V_{n0}} \psi \qquad (j \neq n)$$

$$\frac{\partial V_{n+1,0}}{\partial \Delta V_{j}} \approx \frac{\partial V_{j+1,0}}{\partial \Delta V_{j}} \frac{1}{V_{n+1,0}} \quad (1$$

$$-\frac{\Delta V_n}{V_{n0}}$$
) ψ (j \ddagger n)

$$\frac{\partial V_{n+1,0}}{\partial T_{j}} = \frac{\partial V_{j+1,0}}{\partial T_{j}} \quad \frac{1}{V_{n+1,0}} \quad (1)$$

$$-\frac{\Delta V_n}{V_{n0}} \psi \qquad (j \neq n)$$

$$\frac{\partial V_{n+1,0}}{\partial g_{\emptyset j}} = \frac{\partial V_{j+1,0}}{\partial g_{\emptyset j}} \quad \frac{1}{V_{n+1,0}} \quad (1$$

$$-\frac{\Delta V_n}{V_{n0}} \psi \qquad (j \neq n)$$

$$\frac{\partial V_{n+1,0}}{\partial V_{10}} = \frac{\partial V_{20}}{\partial V_{10}} \frac{1}{V_{n+1,0}}$$

$$-\frac{\Delta V_{n}}{V_{n0}}$$
 ψ (j \div n) (14)

$$\frac{\partial V_{n+1,0}}{\partial h_{n0}} = \frac{g_{n}}{V_{n+1,0}}$$
 (j = n)

$$\frac{\partial V_{n+1,0}}{\partial \Delta V_{n}} = \frac{-V_{nf}}{V_{n+1,0}}$$
 (j=n)

$$\frac{\partial V_{n+1,0}}{\partial T_{n}} = \frac{1}{T_{n}} \frac{g_{n} M_{on} V_{ex}^{2}}{T_{n} V_{n+1}} \begin{bmatrix} \Delta V_{n} \\ V_{ex} \end{bmatrix}$$
$$-1 + e (j = n)$$

$$\frac{\partial V_{n+1,0}}{\partial g_{0n}} = -\frac{1}{2g_{0n}V_{n+1,0}} \left[(V_{n}) \right]$$

$$-\Delta V_{n}^{2} - V_{nf}^{2}$$
 (j = n)

$$\frac{\partial V_{20}}{\partial V_{10}} = \frac{V_{10} - \Delta V_1}{V_{20}} \qquad (j = n)$$

where

$$\psi = \begin{cases} V_{j+1, 0} & (n-j-1=0) \\ V_{j+1, 0} & (1-\frac{\Delta V_{j+m}}{V_{j+m}}) \\ m = 1, 2, \dots, (n-j-1) \end{cases}$$

denotes the product over m

M_{on} is the initial mass of the space vehicle at the n-th powered phase

The derivatives can be evaluated from Eqs (3) and (4), which are the solutions to the vertical descent equation of motion, with the subscript j denoting the j-th phase of rocket burning.

$$V_{jf} = V_{j,0} + g_{0j} \frac{M_{0j} V_{ex}}{T_{j}} \begin{pmatrix} 1 - e^{-\frac{\Delta V_{j}}{V_{ex}}} \end{pmatrix} - \Delta V_{j}$$

$$h_{jf} = h_{j0} - V_{j,0} \frac{M_{0j} V_{ex}}{T_{j}} \begin{pmatrix} 1 - e^{-\frac{\Delta V_{j}}{V_{ex}}} \end{pmatrix}$$

$$- \frac{g_{0j} M_{0j}^{2} V_{ex}}{T_{j}^{2}} \begin{pmatrix} 1 - e^{-\frac{\Delta V_{j}}{V_{ex}}} \end{pmatrix}^{2}$$

$$+ \frac{M_{0j} V_{ex}}{T_{j}} \begin{pmatrix} 1 - e^{-\frac{\Delta V_{j}}{V_{ex}}} \end{pmatrix}$$

$$- \frac{\Delta V_{j}}{V_{ex}} e^{-\frac{\Delta V_{j}}{V_{ex}}}$$

$$V_{j+1,0} = 2\mu_{0} \begin{pmatrix} \frac{1}{h_{j0}} - \frac{1}{h_{jf}} \end{pmatrix} + V_{jf}^{2} \qquad (15)$$

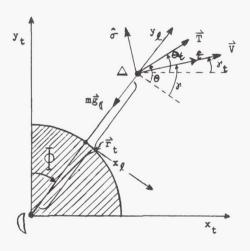
where M_{0j} is the initial mass of the vehicle at the j-th burning phase.

A complication is introduced when the assumption of vertical descent is dropped since the analytic solutions for descent trajectories comprised by Eqs (3) and (4), or (5) and (6), apply only for vertical descent. The accurate solution for nonvertical trajectories involves a numerical approach, since the equations of motion are not integrable in closed form. However, the vertical descent solutions are useful, rather than good, approximations for description of nonvertical trajectories when altitude and velocity in the vertical case are interpreted as range and range rate. Accuracy of the approximation is increased if the thrust and vehicle velocity vectors are colinear during the braking phases of descent, so that the trajectory is almost a straight line until the very final, low-velocity phase, when the trajectory curves over to the local vertical on the moon. The sketch on page VIII-2 shows that ballistic trajectories approach the moon almost on a straight line, since the maximum curvature of the hyperbolic selenocentric approach trajectory is near pericynthion, which is below the lunar surface for impact trajectories.

The next step in the calculation of descent trajectories would be the numerical solution of a general two-dimensional descent trajectory. The physical model implies that any phases of rocket burning take place in a trajectory plane which at the same time contains the center of the moon; its trace on the lunar surface is a great circle, and this model is compatible with the spherical moon assumption. The standard inverse-square variation of $g_{\mbox{\sc d}}$ with vehicle distance from the

center of the moon is assumed in two-dimensional trajectories, thus retaining only assumptions (2), (4), (5) and (6) of the ones listed on pages VIII-2 and -3 for the physical model underlying two-dimensional descent trajectory calculations.

Consider two coordinate systems in the trajectory plane. One is a selenocentric system which is regarded as inertial and has its origin at the center of the moon, the y_t axis directed toward the northernmost point of the trajectory plane and the x_t axis toward the ascending node in the lunar equatorial plane. The second coordinate system is a local one similar to the topocentric system, but with origin at the instantaneous subvehicle point and the y_ℓ -axis directed toward the vehicle. Both coordinate systems, the unit vectors $\hat{\sigma}, \ \hat{\tau}, \$ and the forces acting on the vehicle are illustrated in the following sketch (positive values for all quantities are shown):



In inertial coordinates, the vector equation of motion is

$$\widetilde{Mr_t} = \overrightarrow{T} + M\overrightarrow{g_d},$$
(16)

where

$$M = M_0 - \frac{T}{V_{ex}}$$
 $t_b = instantaneous vehicle mass$

M₀ = constant vehicle initial mass (prior to rocket burning)

T = rocket thrust

 V_{ex} = effective exhaust velocity

th = time of rocket burning

 \vec{r}_{+} = vehicle radius vector

The digital computer usually integrates the scalar equations of motion, which will be obtained next. The components of the forces tangential and normal to the flight path (which is along the unit

vector $\hat{\tau} \equiv \frac{\vec{V}}{\vec{V}}$), can be obtained from the preceding sketch.

$$F_{\tau} = T \cos (\theta - \gamma) - Mg_{\ell} \sin \gamma$$

$$F_{\sigma} = T \sin (\theta - \gamma) - Mg_{\ell} \cos \gamma$$
(17)

where

 θ = thrust attitude angle (the angle between local horizontal or \mathbf{x}_{ℓ} -axis and the thrust direction)

γ = flight path angle (the angle between the local horizontal or x_ℓ -axis and the velocity vector).

If these force components are further resolved into the \mathbf{x}_t and \mathbf{y}_t directions, one can write the scalar equations of motion

$$x_{t} = \cos Y_{t} \left[\frac{T}{M} \cos (\theta - Y) - g_{\ell} \sin Y \right] - \sin Y_{t} \left[\frac{T}{M} \sin (\theta - Y) - g_{\ell} \cos Y \right]$$
(18)

$$y_{t} = \sin Y_{t} \left[\frac{T}{M} \cos (\theta - Y) - g_{\ell} \sin Y \right] + \cos Y_{t} \left[\frac{T}{M} \sin (\theta - Y) - g_{\ell} \cos Y \right] (19)$$

where

 Y_t = inertial flight path angle (for angle between the x_t - axis and the velocity vector)

These differential equations are integrated to solve for \dot{x}_t and \dot{y}_t , which in turn are integrated to solve for x_t and y_t . The following auxiliary definitions are of interest, and they are usually computed for each trajectory printout interval.

$$V = \sqrt{\dot{x}_t^2 + \dot{y}_t^2}, \text{ the selenocentric (inertial)}$$

$$velocity \text{ of the vehicle}$$

$$r = \sqrt{x_t^2 + y_t^2}, \text{ the distance of the vehicle}$$

$$from the center of the moon$$

 $\mathbf{y}_{\ell} \equiv \mathbf{h} = \mathbf{r} - \mathbf{R}_{\ell}$, where \mathbf{R}_{ℓ} is the radius of the spherical moon

$$\Phi = \tan^{-1} \left(\frac{x_t}{y_t} \right)$$

$$y_t = \tan^{-1}\left(\frac{y_t}{x_t}\right)$$

$$\gamma = \sin^{-1} \left(\frac{y_t y_t + x_t x_t}{r V} \right)$$

In some cases it is convenient to write the component equations of motion tangential and normal to the instantaneous flight path. If we

define a unit vector $\hat{\tau} = \frac{V}{V}$ tangential to the flight path and define a unit vector $\hat{\sigma}$ normal to the flight path, the velocity is by definition $\vec{r_t} = \vec{V} = V\hat{\tau}$, and the acceleration is given by

Thus the tangential and normal scalar equations of motion become

$$\dot{V} = F_{\sigma}, V \dot{\gamma}_{\dagger} = -F_{\sigma},$$
 (20)

where F_{τ} and F_{σ} are given by Eqs (17).

Once the range of possible trajectory parameters for the direct descent trajectory has been narrowed down, and the landing area has been selected, some typical precision trajectories should be calculated. The vehicle can now move in three dimensions, and the most accurate values are used for the physical constants. This would result in lifting the assumption of a moon homogeneous in spherical layers, but using a moon homogeneous in ellipsoidal shells. The buildup and tailoff of rocket thrust in a given burning period can also be simulated, and any lateral maneuvering which can reduce the hovering and translational requirements on the LM can be introduced into the computer simulation.

equatorial coordinates $\mathbf{x}_{\mathbf{q}}$ y $\mathbf{z}_{\mathbf{q}}$ (assumed inertial for this case), including the triaxially ellipsoidal shape of the moon, are given in Chapter VII. Thrust accelerations add terms $\frac{\mathbf{T}_{\mathbf{x}}}{\mathbf{M}}$, $\frac{\mathbf{T}_{\mathbf{y}}}{\mathbf{M}}$, $\frac{\mathbf{T}_{\mathbf{y}}}{\mathbf{M}}$, and to the equation of motion in the $\mathbf{x}_{\mathbf{q}}$, $\mathbf{y}_{\mathbf{q}}$, and $\mathbf{z}_{\mathbf{q}}$ directions, respectively. The transformations of $\mathbf{T}_{\mathbf{x}}$, $\mathbf{T}_{\mathbf{y}}$, $\mathbf{T}_{\mathbf{z}}$ to components $\mathbf{T}_{\mathbf{u}}$, $\mathbf{T}_{\mathbf{v}}$, $\mathbf{T}_{\mathbf{w}}$, which are in a coordinate system $\mathbf{x}_{\mathbf{v}}$, $\mathbf{y}_{\mathbf{v}}$, $\mathbf{z}_{\mathbf{v}}$, are given in Chapter IV-B-4 e (the only change in the transformation equations is a formal change of the $\mathbf{\Phi}$ -symbol to the $\mathbf{\ell}$ -symbol). This coordinate system has its origin at the center of gravity of the vehicle, the $\mathbf{z}_{\mathbf{v}}$ -axis in the direction of the radius vector, the $\mathbf{x}_{\mathbf{v}}$ -axis in the general direction of

motion in the trajectory plane but perpendicular

The equations of motion in selenocentric lunar

to $\mathbf{z}_{_{\mathbf{V}}}$, and the $\mathbf{y}_{_{\mathbf{V}}}$ -axis perpendicular to the trajectory plane to complete the right-hand Cartesian coordinate system.

d. Trajectory optimization

The previous subsection described the physical models and the corresponding equations of motion -the tools of the trajectory analyst. In order to obtain a particular solution to the equations of motion, or a trajectory, further information is needed, for example: the initial conditions for descent (position, velocity, vehicle mass) must be obtained from translunar trajectories, the characteristics of the rocket engine and the fuel must be specified, and the important question, "How should the space vehicle be steered, or, what is the variation of thrust attitude angle θ with time during rocket burning?" must be answered. Since there are an infinite number of possible trajectories between the initial position and velocity for a direct descent and the final lunar landing site position and touchdown velocity, the number of trajectories analyzed must be reduced drastically. This leads naturally to a problem of trajectory optimization: what trajectory maximizes or minimizes some criterion of performance Q, where Q might be the fuel expended during descent, payload on the lunar surface, cost, etc.? Of course, the lunar descent phase must be integrated with the other trajectory phases of the particular lunar mission.

Optimization problems may be classified into two categories:

- (1) Pure trajectory problems, where all vehicle and rocket engine characteristics, such as initial weight, thrust, etc., are specified and the trajectory that optimizes some aspect of performance is sought.
- (2) Space vehicle design problems, where the mission is specified, and payload weight, landing site location, rocket engine and fuel characteristics or similar parameters are sought.

Various trajectory optimization schemes, primarily based on the calculus of variations, the method of steepest descent, Pontryagin's maximum principle or dynamic programming have appeared in the literature. A general approach will be outlined in Subsection B-2e and applied to the case of descent from lunar orbit. Although this approach could also be used in analysis of direct descent, the discussion of this optimization scheme will be deferred until later, and only results of two simpler approaches, one a space vehicle design problem and the other a trajectory problem, will be given here for nominally vertical trajectories.

Reference 7 treats a space vehicle design problem. In it are treated the optimum thrust-to-mass ratios $f_0 = \frac{T}{M_0}$ for the simple, vertical descent with one burning phase to a soft landing at zero touchdown velocity under the assumption of constant thrust and constant gravity (the trajectory of Eqs (5) and (6)). A further assump-

tion is that the total mass of the propulsion system \mathbf{M}_p (mass of tanks, thrust chamber, propellant reserves, plumbing, etc.), can be expressed by the linear form

$$M_p = A + B M_f + CT$$
 (21)

where

 $M_{\rm f}$ = total propellant mass

A = fixed propulsion system mass, i.e., the mass that does not vary with engine size

B, C are constants of proportionality, where

- B = ratio of the propulsion system mass that depends on ${\rm M_{ ilde{f}}}$ (or the propellant scalable system mass) to ${\rm M_{ ilde{D}}}$
- C = ratio of the propulsion system mass that depends on T (or the thrust scalable system mass) to $M_{\rm p}$

T = thrust.

The constants A, B and C are rocket engine design parameters. Figure 8 gives the optimum in terms of a nondimensional impact velocity $\frac{1}{2}$

parameter
$$\frac{V_i}{V_{ex}}$$
, where V_i is the ballistic lunar impact velocity given in Fig. 1 as a function of

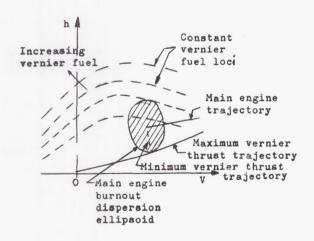
impact velocity given in Fig. 1 as a function of transit time, and in terms of the nondimensional propulsion system parameter $[(g_{00}^{C})/(1+B)]$.

The region of the parameter $g_{\ell \, 0} \, C \, / (1+B)$ for liquid propulsion systems is shaded in Fig. 8. The parameter C is smaller for solid rockets than for liquid systems because the solid rocket system mass is largely dependent upon the propellant mass and not too dependent upon thrust level. Therefore, payload acceleration tolerances would generally be exceeded if the optimum thrust for solid rockets were chosen. Figure 9, also from Ref. 7, shows the penalty in payload weight resulting from braking at other than optimum thrust level. For typical impact velocities, the payload is not too sensitive to changes in thrust-to-weight ratio.

Reference 8 outlines an optimization procedure for a trajectory problem based on a two-engine braking system. The basic braking technique to be optimized is chosen for simplicity and reliability as follows. A high constant-thrust, solid-propellant engine provides the major portion of the braking. After main retro-rocket burnout a variable-thrust, liquid-propellant engine reduces the remaining velocity before impact and corrects for dispersions in altitude and velocity at burnout of the solid engine. The nominal program of this vernier engine involves a descent at minimum thrust until sensors reveal a velocity-altitude combination which permits soft landing by maximum vernier thrust operation for the remainder

of flight. Based on this preliminarily defined braking technique, the optimization is then concerned with apportionment of velocity reduction between the two engines such that total braking system weight is minimized. The technique is indicated first in the case of vertical descent and then extended to off-vertical approaches. The numerical optimization procedure is illustrated in the following sketch and may be outlined as follows:

- From given main engine terminal conditions and engine characteristics, a dispersion ellipsoid in the h, V, Y space is established.
- (2) The computer then iterates to find the point of tangency of this ellipsoid and a surface of constant vernier fuel. This point represents the maximum vernier fuel required for the chosen nominal burnout point.
- (3) From the vernier fuel mass corresponding to the tangent surface, the total engine weight (vernier weight plus main engine weight) is computed.
- (4) Curves of main engine weight and vernier weight as functions of nominal main engine terminal velocity are generated by repeated computer runs. The optimum terminal velocity is then the one corresponding to the minimum sum of vernier and main engine weight.



e. Guidance laws for direct descent soft landings

From the trajectory analysis and optimization phase of the design, one or several trajectories will have been selected for the proposed direct descent to the lunar surface. But how will the vehicle stay on the desired trajectory? The

guidance, which is concerned with obtaining the input information required for the desired trajectory, such as altitude and velocity, and the guidance laws, which are used to control the vehicle so that it stays near the desired trajectory, for direct descent trajectories form the subject of the present subsection.

A multitude of guidance laws have been studied in connection with the lunar landing mission. However, only a few laws can be considered here in any detail. It is instructive to consider first a few simple guidance laws which can be used in connection with nominally vertical descent, the case for which analytic approximate solutions have been derived. These guidance laws for vertical descent will be considered in this section; a guidance law applicable to nonvertical trajectories will be analyzed in detail in Section B-2d (discussing indirect descent) since typical trajectories for ascent to or descent from a lunar satellite orbit deviate further from the vertical than do typical direct ascent and descent trajectories.

In the case of direct descent, guidance in the early phases of descent may be relatively simple. The system may consist of altimeter and horizon sensor, and a constant-thrust rocket engine.

Velocity need not be measured during initial braking, first because the velocity would have to be controlled by midcourse guidance to a few m/sec to avoid missing the moon completely and, secondly, because accurate velocity determination might be difficult at high altitude. In the final braking phase more refined guidance will be required to eliminate trajectory errors before touchdown. The altimeter must be supplemented by a Doppler system in the vehicle so that both altitude and velocity may be monitored. For this final phase a variable thrust engine will be required to implement the guidance commands.

Reference 9 considers several guidance laws for use in nominally vertical descent:

(1) Vertical channel

$$a_c = \frac{1}{2} \frac{\dot{h}^2 - \dot{h}_f^2}{h - h_f} + g_{\ell}$$
 (22)

or $a_c = a_{nom} + K(t) \left\{ \dot{h} - \left[2 (a_{nom} - g_{\ell}) (h - h_f) + \dot{h}_f^2 \right]^{1/2} \right\}$ (23)

where

a = command acceleration

h = instantaneous downward velocity

h_f = desired final downward velocity

h = instantaneous altitude

h_f = desired final altitude

a_{nom} = nominal acceleration

K(t) = programmed gain factor

(2) Horizontal channel

$$\omega_{\text{VC}} = -f(t) \frac{V_{\text{W}}}{V_{\text{U}}} = -k \frac{V_{\text{W}}}{r_{t}}$$
 (24)

$$\omega_{WC} = f(t) \frac{V_V}{V_U} = k \frac{V_V}{r_t}$$
 (25)

where

 $\omega_{\rm VC}$ = command pitch rate

 ω_{WC} = command yaw rate

 V_{u} = velocity component along roll (thrust)

V_v = velocity component along pitch axis

 $V_{_{\mathrm{W}}}$ = velocity component along yaw axis

k = gain constant

r_t = slant range along thrust axis to lunar surface

Next, these guidance laws will be discussed. By means of Eq (22), when a deviation from the nominal trajectory is sensed, the thrust is controlled to produce a new constant acceleration trajectory which terminates with the required final velocity and altitude. That is, this guidance law is explicit; it does not depend upon storage of the complete nominal trajectory. The law does not force the vehicle to fly the nominal trajectory but simply steers for the desired final values. It may be obtained by integration of the equation of motion during vertical descent, under the assumption that $\frac{T}{M}$ and g_{ℓ} are constant:

$$F \equiv M (f - g_{\ell}) = M\dot{h}$$
 (26)

where

f = $\frac{T}{M}$ is the constant acceleration due to thrust.

From the conservation of energy

$$\int F dh = change in kinetic energy$$

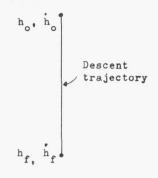
or

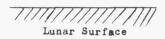
$$\int_{h_0}^{h_f} M (f - g_i) dh = \frac{1}{2} M (\dot{h}_0^2 - \dot{h}_f^2)$$
 (27)

which becomes

$$f - g_{\mathbf{q}} = \frac{1}{2} \frac{\dot{h}_0^2 - \dot{h}_f^2}{\dot{h}_0 - \dot{h}_f}$$
 (28)

after integration over the indicated interval.





The guidance law of Eq (23) is an example of an implicit guidance law; that is, the vehicle follows a nominal trajectory in the guidance phase. A deviation of the actual velocity h from the desired instantaneous velocity,

$$\sqrt{2 (a_{\text{nom}} - g_{\ell}) (h - h_f) + \dot{h}_f^2}$$
, (29)

generates a command correction to the nominal acceleration. This law forces the vehicle to follow the nominal trajectory.

In the absence of errors, both laws would produce identical trajectories. However, Cheng and Pfeffer (Ref. 9) find that the closer adherence to the nominal trajectory resulting from use of Eq (23) results in less variation in acceleration. When the LM attitude is nearly vertical, the altitude h and altitude rate h may be replaced by slant range $r_{\rm t}$ and velocity along the thrust axis $V_{\rm u}$, respectively, in Eqs (22) and (23), so that the raw data need not be transformed.

Equations (24) and (25) form a proportional rate guidance law for horizontal maneuvers. The angle between the velocity vector and the thrust vector is used to generate angular command rates $\boldsymbol{\omega}_{\text{VC}}$ and $\boldsymbol{\omega}_{\text{WC}}$. The thrust and velocity are not forced to be colinear throughout flight as in the case of a gravity turn trajectory (Subsection C-2b), but this situation is gradually achieved by touchdown time.

2. Indirect Descent (descent from lunar orbit)

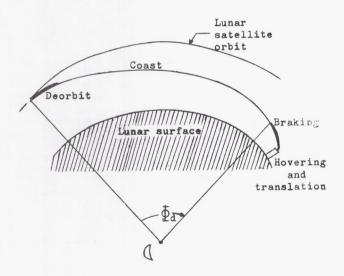
The direct descent method for achieving a hard or soft landing will probably only be used for instrument carriers, since any failure in the rocket braking system would result in a lunar impact speed of about 3 km/sec for the space vehicle. In contrast, the most commonly used descent technique for manned and even some unmanned vehicles will probably use an approach or circumlunar trajectory for the translunar portion of the flight. Of these two trajectories the latter would be preferable, since any failure in the rocket braking system would allow a ballistic return of the vehicle to the vicinity of the earth. Lunar descent from the approach and circumlunar trajectory is performed in two stages -- a braking from the translunar trajectory,

which is a hyperbolic trajectory around the moon, to circular or elliptic lunar orbits and subsequently a descent from this orbit to the lunar surface by the entire landing module (LM). This approach allows maximum flexibility in choice of landing site, since with a lateral maneuver during or subsequent to the braking into lunar orbit, any orbital inclination can be obtained. Furthermore, with additional fuel consumption, the indirect descent technique allows more time for observations and corrections before landing. However, the technique is more complex than direct descent from a translunar trajectory.

a. Descent technique

Descent from a lunar satellite orbit to a soft landing on the lunar surface will probably involve the following routine, although other techniques are possible:

(1) In the shuttle concept, after separation from the orbiting vehicle, the shuttle vehicle experiences a retrothrust during what will be termed the deorbit phase of descent. Of course, this technique is not restricted to the shuttle case but can be applied to an indirect descent of the entire vehicle. The deorbit maneuver requires a velocity impulse of $\Delta V \approx 100 \text{ m/sec.}$



- (2) Following deorbit the (LM) coasts in a ballistic elliptical trajectory to an altitude of perhaps 20 or 30 km.
- (3) A final braking phase reduces the LM velocity to less than 50 m/sec by the time the vehicle has descended to an altitude of a few hundred meters.
- (4) During the terminal braking phase, lateral velocity is reduced to zero and the thrust vector is pitched over into a vertical or hovering attitude.

(5) During the final phase of descent, the vehicle is capable of hovering and translation. This capability is discussed in Section D below.

Since descent from orbit, or indirect descent, necessarily involves curved, nonvertical trajectories, the analytic trajectory solutions possible for vertical direct descent (Section B-1c) are useful as approximations no longer. All indirect descent trajectories must be computed by numerical integration of the equations of motion. (Section B-1c includes various simple forms of the equations to be integrated.) Also, guidance law for indirect descent must be more general, and therefore more complicated, since these laws cannot rely on approximations which assume small angles between the thrust vector and the local vertical. On the other hand, many approaches which will be applied to analysis of indirect descent are obviously applicable in the cases of direct descent which deviate considerably from vertical.

b. Indirect descent trajectories

Various factors prevent a general analysis of descent trajectories. The number of parameters involved is very large (orbit altitude, descent range, individual propulsion system specifications, vehicle weight, to mention a few). Even after a descent technique such as the one discussed in the previous subsection has been chosen for a given mission, trajectories will differ somewhat, depending on the choice of guidance law or pitch program. Therefore, generality must be sacrificed, and trajectories will be presented for a particular hypothetical mission, a particular vehicle, and for limited ranges of trajectory variables.

The particular case investigated is descent from a circular orbit of 185.2-km altitude. Various trajectories were computed with a two-dimensional point-mass trajectory program and plotted in Figs. 10 through 14 for parameters given in the following table. Nominally constant pitch rates (θ_t = const) were used in generating these trajectories.

Sample Braking Trajectories

Figure No.	$\frac{\mathbf{T}}{\mathbf{W}_0}$	Descent Range, ⁴ d (deg)	Initial Altitude, h ₀ (km)	Terminal Altitude, h _f (km)	Specific Impulse Isp (sec)
10	0.45	90	18.29	0.304	309
11	0.45	180	18.29	0.304	309
12	0.45	Synchronous* 95	18.29	0.304	309
13	0.45	Synchronous 95	12.19	0.304	309
14	0.45	Synchronous 95	27.43	0.304	309

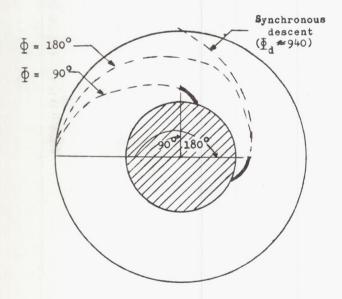
*Synchronous, or equal period, descent is discussed in Section D

The ordinates for these figures give altitude in km (left-hand ordinate) and the corresponding time from braking ignition (right-hand ordinate). Time increments are also indicated along each curve by data points. For a given altitude or time the four curves on each figure determine the vehicle velocity magnitude, V; the local flight path angle, Y; the range from braking rocket ignition, and the pitch angle with respect to inertial coordinates, $\theta_{\rm r}$, on the appropriate abscissa scales.

c. Braking requirements

Figures 15, 16 and 17 summarize a parametric computer analysis of propulsion system requirements for descent from orbit and, in particular, for the braking phase. All of these figures relate to descent from a 185.2-km circular orbit, for which the braking phase trajectories of Figs. 10 through 14 are typical.

Figure 15 shows a typical complete descent trajectory. Figure 16 shows the characteristic velocity, $\Delta V \equiv -V_{\rm ex} \ln{(1-\zeta)}$, required during the braking phase as a function of initial thrust-to-weight ratio for several descent range angles.



Whereas the $\Phi_{\rm d}$ = 90° and $\Phi_{\rm d}$ = 180° descents are initially tangent to the lunar satellite orbit, the synchronous descent (involving a coast phase of the same orbital period as the lunar satellite orbit) begins with a nontangential deorbit. This factor explains the greater economy of the $\Phi_{\rm d}$ = 90° and $\Phi_{\rm d}$ = 180° cases as shown in Fig. 16. Figure 17 shows the same functional relationship, velocity decrement required versus initial thrusto-weight ratio, for various initial braking altitudes for a synchronous descent. One curve for a higher value of specific impulse is also included

for comparison. Figure 18 is a plot of the same variables as Figs. 16 and 17, except that Fig. 18 includes the deorbit phase requirements in addition to those for the braking phase. The forms of these curves indicate the existence of an optimum thrust level for each set of nominal system and orbit parameters from the flight mechanics point of view.

d. Guidance law for indirect descent braking

Just as there is an optimum thrust magnitude, there is also an optimum direction, and the guidance and control system must keep the vehicle reasonably close to this optimum for descent. The control law (or guidance law) for descent from lunar orbit should be as flexible, efficient, as simple as possible, and should permit manin-the-loop operation for system reliability. A predictive guidance technique, which has been demonstrated in a simulation program (Ref. 10), appears to fulfill these requirements very well and will therefore be discussed in this subsection.

The guidance operational phase of the descent from orbit described in Subsection B-2a begins during the ballistic phase 30 sec before the braking thrust is initiated. During braking, the thrust vector must be controlled in such a manner that the range and range rate go to specific values simultaneously. The thrust magnitude should experience as small a variation as is practical to minimize the requirements for engine throttling. Fuel consumption must not be penalized by the thrust vector control.

These requirements are not compatible. For example, minimum fuel consumption dictates constant thrust (Ref. 11), but range control dictates variable thrust. Again, minimum fuel consumption with a range restraint dictates a complicated thrust vectoring system, whereas the guidance information must be displayed simply to reduce human reaction time. There are other conflicting requirements. The predictive law selected represents a reasonable compromise. Lawden (Ref. 12) has noted that an extremum of a payload function is obtainable for a point particle in a constant gravitational field with mass a function of time, if the thrust vector direction in the two-dimensional case is represented by the time-dependent bilinear function of the form

$$\tan \theta_t = \frac{a - bt}{c - dt}$$
 (30)

where $\theta_{\rm t}$ is the thrust vector angle in an inertial two-dimensional coordinate system. Fried (Ref. 13) has shown that d = 0 if range is unrestrained, and Perkins (Ref. 14) has indicated that the law (30) is applicable to a braking type of maneuver. It can also be shown that another form similar to Eq (24) is obtained when a three-dimensional trajectory is considered, and the thrust vector is resolved in two directions. The thrust in this discussion is assumed to act along the longitudinal or roll axis of the vehicle.

Consider any set of orthogonal Cartesian axes \mathbf{x}_t \mathbf{y}_t \mathbf{z}_t and a rotation about one of these axes to form a new Cartesian set $\mathbf{x}_t^{'}$ $\mathbf{y}_t^{'}$ $\mathbf{z}_t^{'}$. Define a

rotation about the $\mathbf{z}_{t}\text{-axis}$ as yaw angle $\psi_{t}\text{,}$ a rotation about the z_t -axis as pitch angle θ_t and a rotation about the x_{+} -axis as roll angle ϕ_{+} . Next consider a three-dimensional lunar landing trajectory.

A notable characteristic of solutions for a and b in Eq (30) is that the product (bt) is generally small for braking trajectories in selenocentric space and with initial decelerations greater than 5 m/sec². With this observation, it is possible in a first approximation to linearize the pitch angle θ_{+} and the yaw angle ψ_{+} :

$$\theta_{t} = \theta_{t0} + \dot{\theta}_{t}t$$

$$\psi_{t} = \psi_{t0} + \dot{\psi}_{t}t$$
(30a)

Therefore, in a first approximation, an Euler angle program having constant first derivatives represents an efficient thrust vector control. Furthermore, the requirement that range and range rate be driven to specified values simultaneously is satisfied in two of the three dimensions. The third (longitudinal range) is satisfied if the thrust magnitude and ignition point are allowed to vary within specific bounds to accommodate errors in ignition time and system performance. Finally, an Euler angle program of this form is quickly assimilated and understood by a human pilot.

Solution of the differential equations of motion for guidance purposes needs to be only approximate, provided that the solution is convergent. That is, as the vehicle approaches the target, it becomes more accurate. It is necessary that the initial inaccuracies do not jeopardize the later stages of the trajectory. In addition, the predictive system exhibits a closed-loop response, so that inaccuracies due to constant errors or computational roundoffs are driven to zero.

The differential equation of motion in vector

$$\frac{d^2 \stackrel{\rightharpoonup}{r}}{dt^2} = -\frac{\mu_{\ell}}{r^3} \stackrel{\rightharpoonup}{r} + \frac{\stackrel{\rightharpoonup}{T}}{M}$$
 (31)

In development of the prediction equations, the following approximations can be made:

- (1) Thrust and mass flow are constant.
- (2) The vehicle behaves like a point mass.
- (3) The change in $\frac{\mu_{0}}{r^{3}}$ is small when compared to $\frac{T}{M}$.

For these assumptions, Eq (25) becomes

$$\left(\frac{d^2}{dt^2} + \omega^2\right) \stackrel{\rightharpoonup}{r} = \frac{\stackrel{\rightharpoonup}{T}}{M_0 - \dot{M}t}$$
 (31a)

where
$$\omega = \sqrt{\frac{\mu_{\mathbf{q}}}{R_{\mathbf{q}}}} = \text{constant.}$$
 (31b)

This form of differential equation is amenable to solution by the method of variation of parameters. A complementary solution is:

$$\vec{r}_{c} = \vec{C}_{1} \sin \omega t + \vec{C}_{2} \cos \omega t$$
 (32)

where \vec{C}_1 and \vec{C}_2 are constant vectors

The particular solution has the form

$$\vec{r}_{p} = \vec{A}(t) \sin \omega t + \vec{B}(t) \cos \omega t$$
 (33)

The three dependent variables, \vec{r} , \vec{A} and \vec{B} must satisfy Eqs (31) and (33) and one additional, arbitrary condition which will be imposed. Differentiation of Eq (33) gives

$$\frac{d\vec{r}}{dt} = \vec{A}\omega \cos \omega t - \vec{B}\omega \sin \omega t + \vec{A}\sin \omega t + \vec{B}\cos \omega t$$

The third arbitrary condition may be specified as
$$\overset{\checkmark}{A}$$
 $\overset{\checkmark}{\sin \omega t}$ + B cos ωt $\overset{\triangle}{=}$ 0 (34)

so that

$$\frac{d\vec{r}}{dt} = \vec{A} \omega \cos \omega t - \vec{B} \omega \sin \omega t$$
 (35)

Differentiation of Eq (35) and substitution of Eq

$$\frac{d^{2}\vec{r}}{dt^{2}} = -\omega^{2}\vec{r} + \vec{A}\omega\cos\omega t - \vec{B}\omega\sin\omega t \qquad (36)$$

which, with Eq (31), reduces to

$$\overrightarrow{A} \omega \cos \omega t - \overrightarrow{B} \omega \sin \omega t = \overrightarrow{T}$$
(37)

Simultaneous solution of Eqs (34) and (37) gives

$$\frac{\vec{A}}{\vec{A}} = \frac{\vec{T}}{\omega M} \cos \omega t$$

$$\frac{\vec{B}}{\vec{B}} = \frac{\vec{T}}{\omega M} \sin \omega t$$
(38)

Then the solution becomes

$$\vec{r} = (\vec{r}_0 - \frac{1}{\omega} \int_0^{\tau} \frac{\vec{T}}{M} \sin \omega t \, dt) \cos \omega \tau$$

$$+\frac{1}{\omega}\left(\dot{\vec{r}}_{0}^{+}+\int_{0}^{\tau}\frac{\vec{T}}{M}\cos\omega t\,dt\right)\sin\omega\tau\tag{39}$$

$$\vec{r} = (\vec{r}_0 + \int_0^{\tau} \frac{\vec{T}}{M} \cos \omega t \, dt) \cos \omega \tau$$

-
$$(\omega \vec{r}_0 - \int_0^{\tau} \frac{\vec{T}}{M} \sin \omega t \, dt) \sin \omega \tau$$

where τ denotes the final time.

For the case of short burning times,

sin ωτ 2 ωτ

cos ωτ 2 1

and Eq (39) reduces to

$$\vec{r} \simeq \vec{r}_0 \cos \omega \tau - \int_0^{\tau} \frac{\vec{T}}{M} t dt + \left(\dot{\vec{r}}_0 + \int_0^{\tau} \frac{\vec{T}}{M} dt \right) \tau$$

$$\dot{\vec{r}} \simeq \dot{\vec{r}}_0 + \int_0^{\tau} \frac{\vec{T}}{M} dt - \left(\dot{\vec{r}}_0 - \int_0^{\tau} \frac{\vec{T}}{M} t dt \right) \omega^2 \tau$$
(40)

Equations (40) are the approximate prediction equations in this explicit guidance law. The components of the thrust vector \overrightarrow{T} in the \mathbf{x}_t \mathbf{y}_t \mathbf{z}_t coordinate system at any time t are:

$$T_{x}(t) = T(t)\cos(\theta_{t} + \dot{\theta}_{t}t)\cos(\psi_{t} + \dot{\psi}_{t}t)$$

$$T_{y}(t) = T(t)\cos(\theta_{t} + \dot{\theta}_{t}t)\sin(\psi_{t} + \dot{\psi}_{t}t) \qquad (40a)$$

$$T_{z}(t) = T(t)\sin(\theta_{t} + \dot{\theta}_{t}t)$$

If the thrust is assumed constant, and θ_t and ψ_t are assumed to be of the same order as ω , approximate analytic solutions for A and B may be derived. To the first order in ωt , the components of A and B in the x_t y_t z_t coordinate system are:

$$\begin{split} \mathbf{A}_{\mathbf{x}} &\approx \frac{1}{\omega} \left[\mathbf{J}_{1} \cos \theta_{t} \cos \psi_{t} - \mathbf{J}_{2} \left(\dot{\theta}_{t} \sin \theta_{t} \cos \psi_{t} \right. \right. \\ &\left. + \dot{\psi}_{t} \sin \psi_{t} \cos \theta_{t} \right) \right] \\ \mathbf{A}_{\mathbf{y}} &\approx \frac{1}{\omega} \left[\mathbf{J}_{1} \cos \theta_{t} \sin \psi_{t} - \mathbf{J}_{2} \left(\dot{\theta}_{t} \sin \theta_{t} \sin \psi_{t} \right. \right. \\ &\left. - \dot{\psi}_{t} \cos \psi_{t} \cos \theta_{t} \right) \right] \\ \mathbf{A}_{\mathbf{z}} &\approx \frac{1}{\omega} \left[\mathbf{J}_{1} \sin \theta_{t} + \mathbf{J}_{2} \dot{\theta}_{t} \cos \theta_{t} \right] \\ \mathbf{B}_{\mathbf{x}} &\approx \mathbf{J}_{2} \cos \theta_{t} \cos \psi_{t} - \mathbf{J}_{3} \left(\dot{\theta}_{t} \sin \theta_{t} \cos \psi_{t} \right. \\ &\left. + \dot{\psi}_{t} \sin \psi_{t} \cos \theta_{t} \right) \\ \mathbf{B}_{\mathbf{y}} &\approx \mathbf{J}_{2} \cos \theta_{t} \sin \psi_{t} - \mathbf{J}_{3} \left(\dot{\theta}_{t} \sin \theta_{t} \sin \psi_{t} \right. \\ &\left. - \dot{\psi}_{t} \cos \psi_{t} \cos \theta_{t} \right) \\ \mathbf{B}_{\mathbf{z}} &\approx \mathbf{J}_{2} \sin \theta_{t} + \mathbf{J}_{3} \dot{\theta}_{t} \cos \theta_{t} \end{split}$$

where

$$J_1 = -V_{ex} \ln (1 - \zeta)$$

$$J_2 = \frac{t}{\zeta} (J_1 - V_{ex} \zeta)$$

$$J_3 = \frac{t}{\zeta} (J_2 - \frac{V_{ex} \zeta}{2} t | \zeta)$$

$$V_{\text{ex}} = \frac{T}{\dot{M}}$$
 is the effective exhaust velocity $\dot{\zeta} = \frac{\dot{M}t}{\dot{M}}$ is the mass ratio

The commanded pitch, pitch rate, yaw and yaw rate for the bilinear guidance law, θ_{tc} , $\dot{\theta}_{tc}$, ψ_{tc} and $\dot{\psi}_{tc}$, can be determined explicitly:

$$\sin \theta_{tc} = \frac{\frac{\omega A_{z} \frac{J_{3}}{J_{2}} - B_{z}}{J_{1} \frac{J_{3}}{J_{2}} - J_{2}}}{\frac{J_{3} \frac{J_{3}}{J_{2}} - J_{2}}{J_{3} \cos \theta_{tc}}}$$

$$\sin \psi_{tc} = \frac{\frac{B_{z} - J_{2} \sin \theta_{tc}}{J_{3} \cos \theta_{tc}}}{\frac{\omega A_{y} \frac{J_{3}}{J_{2}} - B_{y}}{J_{1} \frac{J_{3}}{J_{2}} - J_{2}}}$$

$$\dot{\psi}_{tc} = \frac{\omega A_{y} + (\dot{\theta}_{tc} \frac{J_{2} \sin \theta_{tc}}{J_{2} \cos \theta_{tc}} \frac{-J_{1} \cos \theta_{tc}}{\cos \psi_{tc}}) \sin \psi_{tc}}{\frac{J_{2} \cos \theta_{tc} \cos \psi_{tc}}{J_{2} \cos \theta_{tc}}}$$

where ζ and t can be computed from the following empirical approximations, with the subscript k denoting the value at a given time t:

$$\zeta = 1 - \exp\left[\frac{1}{V_{\text{ex}}} \left(\dot{S} + 2g_{q} \frac{h - h_{k}}{V + V_{k}} \right) \right] ;$$

$$(V + V_{k}) > 0$$

$$t = \left| \frac{S^{2}}{\dot{S} \cdot \dot{S} \left[\frac{1}{\ln(1 - \zeta)} + \frac{1}{\zeta} \right] + \dot{r}_{k} \cdot \dot{S}} \right| \frac{1}{K_{k}}$$

$$(40e)$$

with

$$\vec{S} = \vec{r} - \vec{r}_k$$

The function \mathbf{K}_k depends on its value at the preceding step, \mathbf{K}_{k-1} , and can be computed from the following relation:

$$K_{k} = \left(\frac{\stackrel{\rightarrow}{S}_{plp} \cdot \stackrel{\rightarrow}{S}_{plp}}{\stackrel{\rightarrow}{S} \cdot \stackrel{\rightarrow}{S}}\right) K_{k-1}$$
(41)

where the predicted slant range vector is

$$\vec{S}_{plp} = \vec{r} - \vec{r}_{plp}$$

With a pilot in the loop, the equations for t and \bar{K}_k are not required. The pilot performs the same function as these equations by manipulating the throttle.

During the manual mode, the predictions are acted upon directly by the pilot. He does not use

the angles θ_{tc} and $\dot{\theta}_{tc}$, or ψ_{tc} and $\dot{\psi}_{tc}$, but he sees the effects which the instantaneous values of θ_t , $\dot{\theta}_t$, ψ_t , $\dot{\psi}_t$ will have on the terminal (or landing) conditions. Then, using the appropriate control, he adjusts his attitude until the prediction is favorable. Thus, in a sense, the pilot is solving for the correct attitudes and attitude rates by trial and error by use of the predictive displays.

In the terminal phase, as in the braking phase, provision may be made for both automatic and manual control. A guidance law for the terminal phase (Ref. 15) is

$$\frac{\vec{T}}{M} = g_{\ell} \frac{\vec{R}_{\ell}}{R_{\ell}} - \frac{(\vec{S} - \vec{S}_{t})}{\left(1 + \frac{h}{h_{0}}\right)^{2}} K_{1} - K_{2} \vec{S}$$
(42)

where

R = central body radius vector to landing site

S = slant range vector from target to vehicle

 K_1 , K_2 = thrust sensitivity coefficients

The capability of the guidance law has been tested in a lunar landing simulator which required a total of 294 operational amplifiers, utilizing four Reac C-400. Two Reac C-100 and an expanded EA 231R analog computers. Fuel consumption during the manual braking runs was generally within two percent of that required for an identical automatic run. Pilot displays are so simple for the predictive law that, in most cases, a "safe" flight was flown on the second or third attempt. The pilot's performance was best when augmenting the automatic system, and his inclusion, in general, improved the total system performance. In some cases, with marginal initial conditions, the pilot was able to recover control and save the vehicle in a situation in which use of the automatic system would have resulted in an impact.

e. Trajectory optimization

Up to this point optimum maneuvers have only been mentioned in passing. The purpose of this subsection is thus to include a more detailed discussion of trajectory optimization.

The trajectory optimization field, and for that matter the solution of variational problems in general, has acquired considerable impetus during the last few years. To the classical calculus-of-variations approach have been added methods based on steepest descent, the Pontryagin maximum principle, and dynamic programming. These latter are very closely related to the calculus of variations and are reducible to it, at least in the limit.

Most recently, steepest descent has dominated the scene. Considerable success has been realized in obtaining approximate optima by this method. The abandonment of the classical indirect approach (calculus of variations), which yields exact optima, in favor of this approximate method, was stimulated by the difficulty encountered in solving the

two-point boundary value problem (in general with one unknown boundary) which results from the classical approach.

A new systematic scheme for solving the two-point boundary value problem with one unknown boundary has recently been developed (Ref. 16). Its feasibility and advantages have been demonstrated (Ref. 17) on a simple trajectory optimization problem which possesses an analytical solution (Ref. 18). The method of solving the variational boundary value problem is here applied to solve for the steering program resulting in maximum payload in the braking phase of a lunar landing maneuver. The method will now be briefly outlined, and some representative results will be presented.

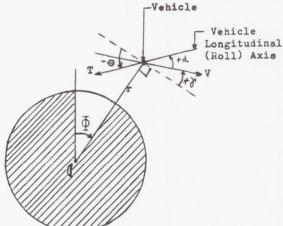
It is assumed that the moon is spherical and does not rotate. Trajectories in a plane are considered so that the equations of motion may be written (see sketch below)

$$\dot{V} = -\frac{T}{M}\cos(-\gamma - \theta) - \frac{\mu_{0}}{r^{2}}\sin\gamma$$

$$\dot{\gamma} = \frac{T}{MV}\sin(-\gamma - \theta) + \frac{V}{r}\cos\gamma - \frac{\mu_{0}\cos\gamma}{r^{2}V}$$

$$\dot{r} = V\sin\gamma$$

$$\dot{\Phi} = \frac{V\cos\gamma}{r}$$
(43)



Thrust is assumed constant so that the condition of maximum payload is equivalent to that of minimum rocket burning time.

The first necessary condition of the calculus of variations (Euler-Lagrange equations) results in a boundary value problem. The constraint equations (43) have to be solved together with the Euler-Lagrange equations, where conditions are imposed at both boundaries, and where the terminal boundary--terminal (minimum) time--is unknown.

Linear perturbations around some nominal (nonoptimal) solution of this boundary value problem are considered. This new set of linear, ordinary differential equations defines an adjoint set. Solutions of the adjoint equations are Green's functions, which relate perturbations in initial conditions to terminal conditions. Appropriate linear combinations of the Green's functions yield the

desired perturbations in the unknown (estimated) initial conditions, and the terminal time, which will result in desired changes in the terminal conditions which have to be met. The process is iterative in nature, since the equations (43) are nonlinear, and converges rapidly to the solution of the Eulerian boundary value problem.

This method was applied to the problem at hand. The pertinent constants are:

$$\mu_{\ell} = GM_{\ell} = 4905.927 \text{ km}^3/\text{sec}^2$$

$$R_{\ell} = 1738.236 \text{ km}$$

$$T/W_0 = 0.45$$

$$I_{\text{sp}} = 309 \text{ sec}$$

$$g_{\oplus 0} = 9.80665 \text{ m/sec}^2$$

$$M_0 = 9979 \text{ kg}.$$

The Eulerian boundary value problem was solved for the initial conditions:

$$V_0 = 1.74 \text{ km/sec}$$

 $Y_0 = 0^{\circ}$
 $h_0 = 18,288 \text{ m}$

which represent the conditions during synchronous ballistic descent, at pericynthion, or at the start of braking. Two sets of terminal conditions were solved for:

$$\gamma_{.1} = -90^{\circ}$$
 $h_{1} = 304.34 \text{ m}$

(2) $V_{1} = 0.001 \text{ km/sec}$
 $\gamma_{1} = -10^{\circ}$
 $\gamma_{1} = 304.34 \text{ m}$

(1) $V_1 = 0.001 \, \text{km/sec}$

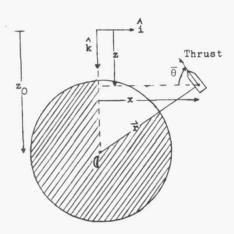
The solutions appear in Fig. 19. Terminal flight path angle constraints were not accurately met because the simplicity of the integration scheme limited the accuracy. (This was a pilot program.) The other terminal conditions were satisfactorily met. It should be pointed out that the accuracy with which terminal constraints are met is strictly a function of accuracy in the integration (Ref. 18).

A few comments are in order. It may be observed that all the maneuvering necessary to change the terminal flight path angle occurs optimally at the end of the trajectory. This is a rather apparent result since it is easiest to change the flight path angle when velocity is lowest. It is observed that fuel expenditure for this maneuvering is rather low, so that the same optimum trajectory may be flown almost to the end no matter what the desired terminal orientation. The nearlinearity of the θ -curve implies that a bilinear tangent steering program is an excellent approximation. (This is an exact optimum in a constant gravitational field; see previous subsection.)

It is pointed out that the trajectories shown in Fig. 19 yield maximum payload for the exact terminal conditions attained.

A second approach to the control optimization problem is presented in Ref. 19 and applied to the braking phase of lunar landing, i.e., that phase of descent from about 15 km to a few hundred meters above the lunar surface. Briefly, the method involves piecewise linear approximations to a nominal trajectory in a two-dimensional inertial coordinate system. The required control, as obtained from solving the matrix Riccati equation, is optimum in the sense that a performance index is minimized for a specified set of performance matrices.

The notation of Ref. 19, as defined in the following sketch, has been retained.



The equations which provide the mathematical model of the system to be controlled are the equations of motion in the two-dimensional inertial coordinate system, which become:

$$\dot{x} = -\mu_{\mathbf{d}} \frac{x}{r^{3}} - g_{\mathbf{\Theta}0} I_{\mathrm{sp}} \frac{\dot{M} \cos \overline{\theta}}{M_{0} - M_{\mathrm{f}}}$$

$$\dot{z} = \mu_{\mathbf{d}} \frac{z - z_{0}}{r^{3}} - g_{\mathbf{\Theta}0} I_{\mathrm{sp}} \frac{\dot{M} \sin \overline{\theta}}{M_{0} - M_{\mathrm{f}}}$$

$$(44)$$

where

I_{sp} = specific impulse of the propellant

g_{⊕0} = sea-level acceleration due to earth gravity

M = mass flow rate

 M_0 = initial mass of the vehicle

 M_f = mass of fuel expended

 $\bar{\theta}$ = 180- θ_t , pitch angle relative to the negative x-axis

Control of the vehicle is to involve a variation of $\bar{\theta}$ and \bar{M} . Linear approximations to these equations may be written in terms of perturbations about the nominal trajectory, $x_0 = x - x_{nom}$, $x_0 = x - x_{nom}$, etc., by means of Taylor series. For example,

$$\dot{x}_{0} = \frac{\partial \dot{x}_{0}}{\partial x} \dot{x}_{0} + \frac{\partial \dot{x}_{0}}{\partial z} \dot{z}_{0} + \frac{\partial \dot{x}_{0}}{\partial M_{f}} \dot{M}_{f0} + \frac{\partial \dot{x}_{0}}{\partial M} \dot{M}_{0} + \frac{\partial \dot{x}_{0}}{\partial \bar{\theta}} \dot{\theta}_{0}$$

$$+ \frac{\partial \dot{x}_{0}}{\partial \bar{\theta}} \dot{\theta}_{0} \qquad (45)$$

where all partial derivatives are evaluated for nominal values. The linearized equations can be written in matrix form as

$$\overset{\cdot}{\mathbf{X}} = \left[\mathbf{F}(t) \right] \overset{\rightharpoonup}{\mathbf{X}} + \left[\mathbf{G}(t) \right] \overset{\rightharpoonup}{\mathbf{u}}$$
 (46)

where X is the state vector which in this case has as components the variables which describe the behavior of the system, i.e.,

$$\vec{X} = \{ x_0, x_0, z_0, z_0, M_{f0} \}$$

and u is the control vector with the control variables as components, i.e.,

$$\vec{u} = \{ \dot{M}_0, \, \bar{\theta}_0 \}$$

The time-varying coefficient matrices [F(t)] and [G(t)] are approximated by constant values for a given increment of time:

$$\begin{bmatrix} \mathbf{f} \\ \mathbf{f}_{21}(t) & 0 & \mathbf{f}_{23}(t) & 0 & \mathbf{f}_{25}(t) \\ \mathbf{0} & 0 & 0 & 1 & 0 \\ \mathbf{f}_{41}(t) & 0 & \mathbf{f}_{43}(t) & 0 & \mathbf{f}_{45}(t) \\ \mathbf{0} & 0 & 0 & 0 & 0 \end{bmatrix}$$

$$\begin{bmatrix}
G \end{bmatrix} = \begin{bmatrix}
g_{21}(t) & g_{22}(t) \\
0 & 0 \\
g_{41}(t) & g_{42}(t) \\
1 & 0
\end{bmatrix}$$

$$f_{21}(t) = \frac{\partial x_0}{\partial x} \Big|_{nom} = \mu_{\{1, nom - 1, nom - 2, 0\}} \frac{2x_{nom}^2 - (z_{nom} - z_0)^2}{(x_{nom}^2 + (z_{nom} - z_0)^2)^{5/2}}$$

$$f_{23}(t) = \frac{\partial x_0}{\partial z}\Big|_{nom} = f_{41}(t) = \frac{\partial z_0}{\partial x}\Big|_{nom}$$

$$= 3\mu_{1} x_{\text{nom}} \frac{z_{\text{nom}} - z_{0}}{\left[x_{\text{nom}}^{2} + (z_{\text{nom}} - z_{0})^{2}\right]^{5/2}}$$

$$f_{25}(t) = \frac{\partial \ddot{x}_0}{\partial M_f}\Big|_{nom} = -g_{\oplus 0}I_{sp} \dot{M}_{nom} \frac{\cos \overline{\theta}_{nom}}{(M_0 - M_f_{nom})^2}$$

$$f_{43}(t) = \frac{\partial \ddot{z}_0}{\partial z} \bigg|_{\text{nom}} = \mu_0 \frac{2 \left(z_{\text{nom}} - z_0\right)^2 - x_{\text{nom}}^2}{\left[x_{\text{nom}}^2 + \left(z_{\text{nom}} - z_0\right)^2\right]^{5/2}}$$

$$\mathbf{f}_{45}(\mathsf{t}) = \left. \frac{\partial \ddot{\mathbf{z}}_0}{\partial \mathbf{M}_{\mathrm{f}}} \right|_{\mathrm{nom}} = -\mathbf{g}_{\oplus 0} \mathbf{I}_{\mathrm{sp}} \, \dot{\mathbf{M}}_{\mathrm{nom}} \, \frac{\sin \, \overline{\boldsymbol{\theta}}_{\mathrm{nom}}}{\left(\mathbf{M}_0 - \mathbf{M}_{\mathrm{f}_{\mathrm{nom}}}\right)^2}$$

$$g_{21}(t) = \frac{\partial \dot{x}_0}{\partial \dot{M}}\Big|_{\text{nom}} = -g_{\oplus 0} I_{\text{sp} \overline{M_0 - M_f}_{\text{nom}}}$$

$$g_{22}(t) = \frac{\partial \dot{x}_0}{\partial \overline{\theta}} \bigg|_{\text{nom}} = g_{00} I_{\text{sp}} \dot{M}_{\text{nom}} \frac{\sin \overline{\theta}_{\text{nom}}^{\bullet}}{M_0 - M_{f_{\text{nom}}}}$$

$$g_{41}(t) = \frac{\partial \ddot{z}_0}{\partial \dot{\mathbf{M}}} \bigg|_{\text{nom}} = -g_{\oplus 0} \mathbf{I}_{\text{sp}} \frac{\sin \overline{\theta}_{\text{nom}}}{\mathbf{M}_0 - \mathbf{M}_{\mathbf{f}_{\text{nom}}}}$$

$$\mathbf{g}_{42}(\mathsf{t}) = \left. \frac{\partial \ddot{z}_0}{\partial \theta} \right|_{\mathrm{nom}} = -\mathbf{g}_{\oplus 0} \mathbf{I}_{\mathrm{sp}} \, \dot{\mathbf{M}}_{\mathrm{nom}} \, \frac{\cos \, \overline{\theta}_{\mathrm{nom}}}{\, \overline{\mathbf{M}}_0 - \, \mathbf{M}_{\mathrm{f}_{\mathrm{nom}}}}$$

These equations comprise the linear model.

The optimum control uwill be that which minimizes the specified performance index, which is, in general, a function of the form

$$\mathcal{J}(\vec{\mathbf{u}}) = \lambda \left[\vec{\mathbf{X}}(\mathbf{t_f}), \mathbf{t_f} \right] + \int_{0}^{\mathbf{t_f}} L(\vec{\mathbf{X}}, \vec{\mathbf{u}}, \mathbf{t}) d\mathbf{t}.$$

For the lunar landing problem the performance index selected is

$$\mathcal{J}(\vec{\mathbf{u}}) = \frac{1}{2} \vec{\mathbf{X}}^{\mathrm{T}} (\mathbf{t}_{\mathbf{f}}) [\mathbf{S}] \vec{\mathbf{X}} (\mathbf{t}_{\mathbf{f}})$$

$$+ \frac{1}{2} \int_{0}^{t_{\mathbf{f}}} {\vec{\mathbf{X}}^{\mathrm{T}}} [\mathbf{Q}(\mathbf{t})] \vec{\mathbf{X}}$$

$$+ \vec{\mathbf{u}}^{\mathrm{T}} [\mathbf{R}(\mathbf{t})] \vec{\mathbf{u}} d\mathbf{t}$$

The matrices [S], [Q(t)] and [R(t)] may be selected to meet such requirements as accuracy and the amount of control available. The significance of these matrices will be indicated by the solution.

Minimization of a given performance index may be based upon Pontryagin's maximum principle, which states that a necessary condition for an optimum u is that there must exist

a continuous vector $\vec{\psi}$ such that the Hamiltonian function

$$H = L + \vec{\psi}^T \stackrel{:}{\vec{x}}$$

is minimized by \vec{u} . The conditions that $\vec{\psi}$ must satisfy are

$$\vec{\psi}_i = -\frac{\partial H}{\partial X_i}$$

and

$$\vec{\psi}_{i}(t_{f}) = -\frac{\partial \lambda}{\partial X_{i}}$$
 $t = t_{f}$

The Hamiltonian then becomes

$$\begin{split} \mathbf{H} &= \frac{1}{2} \, \overrightarrow{\mathbf{X}}^{\mathrm{T}} \, \left[\overrightarrow{\mathbf{Q}} \, \, \overrightarrow{\widetilde{\mathbf{X}}} + \frac{1}{2} \, \overrightarrow{\mathbf{u}}^{\mathrm{T}} \, \, \left[\overrightarrow{\mathbf{R}} \, \, \overrightarrow{\mathbf{u}} + \overrightarrow{\psi}^{\mathrm{T}} \, \, \right] \, \overrightarrow{\mathbf{X}} \\ &+ \, \overrightarrow{\psi}^{\mathrm{T}} \, \left[\overrightarrow{\mathbf{G}} \, \, \overrightarrow{\mathbf{u}} , \right] \end{split}$$

which is minimized with respect to u by setting

$$\frac{\partial H}{\partial u_i} = 0$$

which gives the optimum u,

$$\vec{u} = - \begin{bmatrix} R \end{bmatrix}^{-1} \begin{bmatrix} G \end{bmatrix}^T \vec{\psi}$$
.

The solution for $\overrightarrow{\psi}$ is assumed to have the form

$$\vec{\psi} = [P(t)] \vec{X}.$$

Then P(t) is found to satisfy the nonlinear matrix Riccati equation,

$$\begin{bmatrix} \dot{\mathbf{P}}(t) \end{bmatrix} - \begin{bmatrix} \mathbf{P}(t) \end{bmatrix} \begin{bmatrix} \mathbf{G} \end{bmatrix} \begin{bmatrix} \mathbf{R} \end{bmatrix}^{-1} \begin{bmatrix} \mathbf{G} \end{bmatrix}^{\mathrm{T}} \begin{bmatrix} \mathbf{P}(t) \end{bmatrix}$$

$$+ \begin{bmatrix} \mathbf{F} \end{bmatrix}^{\mathrm{T}} \begin{bmatrix} \mathbf{P}(t) \end{bmatrix} + \begin{bmatrix} \mathbf{P}(t) \end{bmatrix} \begin{bmatrix} \mathbf{F} \end{bmatrix} + \begin{bmatrix} \mathbf{Q} \end{bmatrix} = 0$$

An additional constraint is the final value of the ${\it Riccati}$ equation,

$$[P(t_f)] = [S].$$

The $\begin{bmatrix} S \end{bmatrix}$ matrix affects only the final values of control, whereas the $\begin{bmatrix} Q \end{bmatrix}$ matrix influences the error of the state vector \overrightarrow{X} . The $\begin{bmatrix} R \end{bmatrix}$ matrix penalizes the system for using too much control.

Detailed results from application of the optimum theory to the lunar landing problem are presented in Ref. (19). Final trajectory errors are on the order of one meter per 300 meters initial error in position and one m/sec per five m/sec initial error in velocity. Controls that would use small amounts of additional fuel for off-nominal trajectory conditions are obtained. For 3000-meter initial error in position, about 18.2 kg of additional fuel are required. For initial errors in velocity of 9 m/sec, 146 kg of additional fuel are required.

C. ASCENT FROM LUNAR SURFACE

1. Direct Ascent

The goal of the direct lunar ascent phase is accurate injection of the vehicle into a certain transearth trajectory. Since no intermediate or parking orbit is involved, the required injection conditions are the final values to be achieved by the direct ascent trajectory. Figures 20a and 20b give some indication of typical final value requirements for lunar ascent trajectories. The magnitude and direction of the final velocity vector required at an altitude of 93 km (50 naut mi) for injection into 70- and 80-hr return-time transearth trajectory are given as functions of lunar longitude for launch sites lying in or close to the MOP. The magnitude of the required velocity vector exhibits little variation with burnout point longitude. For example, variation for the 80-hr orbit injection is from 2497 to 2490 m/sec. Direct ascent from a lunar landing base is possible for bases over a wide range of the lunar surface if sufficient propellant is available.

Define an angle η measured from the moonearth direction on the far side of the moon, positive in the direction of the moon's angular rotation, $\widehat{\omega}_{\ell}$. From Fig. 20a it can be seen that, in the region of most probable landing sites in the MOP given by $-180^{\circ} < \eta < -100^{\circ}$, the required flight path angle is close to 90° , i.e., the ascent trajectory must be nearly vertical. For this reason, the vertical trajectory analysis of Subsection B-1c is again useful as a closed-form approximate solution. Under the assumptions of constant gravity g_{ℓ} , constant mass flow rate M, and constant exhaust velocity V_{ex} , Eqs (3) and (4) apply in the case of vertical ascent, except that the signs of all velocities (V_0 and V_1) should be reversed if vehicle speed is to be measured positive upward. These equations, evaluated for the initial conditions,

$$t = 0$$
: $h_0 = 0$, $V_0 = 0$

give the following burnout conditions:

$$\frac{V_{B0}}{V_{ex}} = -\left[\ln\left(1 - \zeta\right) + \frac{g_{00}}{g_{00}} \frac{\zeta}{T/W_{0}}\right] \quad (47)$$

$$\frac{h_{B0} g_{\oplus 0}}{V_{\text{ex}}^{2}} = \frac{1}{T/W_{0}} \left[(1 - \zeta) \ln (1 - \zeta) + \zeta - \frac{1}{2} \frac{g_{0}}{g_{\oplus 0}} \frac{\zeta^{2}}{T/W_{0}} \right]$$
(48)

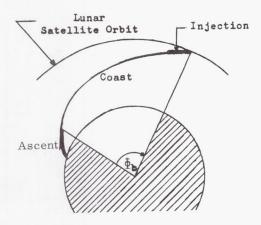
Equation (47) has the same form as Eq(5), so that Fig. (4) gives $\frac{V_{B0}}{V_{ex}}$ for vertical ascent as well as $\frac{V_0}{V_{ex}}$ for vertical descent.

2. Indirect Ascent

a. Ascent technique

The ascent technique which will be investigated as being most typical is analogous to the descent technique discussed in Subsection B-2a.

- The term "ascent phase" will be ascribed to the initial powered liftoff portion of ascent.
- (2) Following the initial powered phase, the space vehicle coasts in an elliptical orbit to a desired parking orbit altitude.
- (3) The vehicle is injected into the parking orbit.
- (4) For the shuttle concept, the shuttle vehicle (LM) executes a rendezvous with the orbiting module (MOM).



These phases are considered below.

b. Indirect ascent trajectories and requirements

Several sample trajectories for ascent to a 185.2-km circular orbit are shown in Figs. 21 through 25. These figures show range; velocity, V; flight path angle with respect to local horizontal, γ ; and pitch angle with respect to inertial coordinates, θ_t , on the abscissa scales corresponding to altitude or flight time on the ordinates. The pitch program for these runs was based on a nominally constant pitch rate, $\dot{\theta}$ = const. Propulsion system and trajectory parameters for these sample ascents are given in the following table. Ascent range, as indicated in the previous sketch, is the lunar central angle between initial liftoff and orbit injection burnout.

Sample Ascent Trajectories (initial phase only)

			Burnout Altitude	
Figure No.	$\frac{\mathbf{T}}{\mathbf{W}_0}$	Φ _b (deg)	h _{B0} (km)	I _{sp} ,
21	0.2	180	15.24	315
22	0.39741	60	36.58	315
23	0.39741	180	21.34	315
24	0.7	60	18.29	315
25	0.99138	180	15,24	315

Figure 26 shows a typical complete ascent trajectory.

The total velocity increment required for ascent and injection into a 185.2-km circular orbit is shown as a function of initial thrust-to-weight ratio for several range angles in Fig. 27. These curves are based on a parametric computer study utilizing approximately constant pitch rates. The improvement in fuel economy of this type of program over a gravity turn trajectory is indicated by a gravity turn data point on Fig. 27. For the particular conditions of the run

(
$$I_{sp}$$
 = 315 sec, Φ_b = 75°, $\frac{T}{W_0}$ = 0.4) the gravity

turn trajectory was less efficient by about 30 m/sec.

Although, as indicated by Fig. 27, the gravity turn is not a particularly efficient pitch program, it is one of the basic types of ascent trajectories and deserves some mention. Reference 20 presents an analysis of this type of trajectory. A gravity turn is one in which the thrust is always maintained parallel to the vehicle velocity vector. (The special case of vertical descent, i.e., both thrust and vehicle velocity in the vertical direction during flight, was solved analytically in Subsection B-1c.) This type of trajectory is particularly useful for planetary ascents since it keeps the aerodynamic moments low during ascent in the denser parts of planetary atmospheres. The equation of motion for a gravity turn is the same as Eq (2) for one-dimensional descent, except that vector notation must be used to allow for two-dimensional motion:

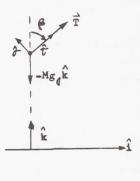
$$M \frac{d\vec{V}}{dt} = \vec{T} - M g_{\ell} \hat{k}$$
 (49)

where

V = vehicle velocity vector

T = thrust vector

k = unit vector normal to lunar surface



From the definition of the gravity turn,

$$\overrightarrow{T} = T \hat{\tau}$$

where the unit vector $\hat{\tau} = \frac{\vec{V}}{V}$

With resolution of the equation of motion along $\hat{\tau}$ and $\hat{\sigma}$, a unit vector normal to $\hat{\tau}$ in the plane of motion, Eq (49) becomes, in component form

$$\frac{dV}{dt} = g_{q} \left(\frac{T}{W} - \cos \beta \right)$$

$$V\beta = g_{q} \sin \beta$$
(50)

where β = thrust orientation angle with respect to vertical.

For constant $g_{\mathbf{0}}$, say $g_{\mathbf{0}0}$, and constant $\frac{T}{W}$ these equations can be integrated in closed form.

$$V = V_0 \frac{\left(\tan\frac{\beta}{2}\right)^{\left(\frac{T}{W}-1\right)} \left(1+\tan^2\frac{\beta}{2}\right)}{\left(\frac{T}{W}-1\right)} \left(\tan\frac{\beta_0}{2}\right) \left(1+\tan^2\frac{\beta_0}{2}\right)}$$
(51)

$$\frac{\dot{M}}{\dot{M}_0} t = \frac{V_0}{\dot{V}_{ex}} \qquad \left(\tan\frac{\beta}{2}\right)^{\left(\frac{T}{\dot{W}}-1\right)} \begin{bmatrix} \frac{1}{\frac{T}{\dot{W}}-1} + \frac{\tan^2\frac{\beta}{2}}{\frac{T}{\dot{W}}+1} \end{bmatrix} \\ \left(\tan\frac{\beta}{2}\right)^{\left(\frac{T}{\dot{W}}-1\right)} \begin{pmatrix} \frac{1}{\frac{T}{\dot{W}}-1} + \frac{\tan^2\frac{\beta}{2}}{\frac{T}{\dot{W}}+1} \end{bmatrix}$$

(52)

However, this analytic solution is not as useful as that obtained for vertical descent (Subsection B-1c.). Reference 15 outlines a numerical solution to Eq (50) for the following conditions:

- (1) Constant g and T
- (2) Constant mass flow rate M
- (3) The initial velocity is zero, and the trajectory is initially vertical.

The solution proceeds as follows:

$$u(\tau) = -\frac{T}{W_0} \ln (1 - \tau) + \int_0^{\tau} \psi(s) ds$$
 (53)

$$\tan\frac{\beta}{2} = \left(\frac{1+\psi}{1-\psi}\right)^{\frac{1}{2}} \tag{54}$$

where

$$\psi(\tau) = \tanh \left[\int_{\tau}^{1} \frac{ds}{\frac{T}{W_0} \ln(1-s) - \int_{0}^{s} \psi(s^{\dagger}) ds^{\dagger}} - k \right]$$

(Solved by iteration)

$$u = \frac{V \frac{T}{W_0}}{V_{ex}}$$

$$\tau = \frac{\dot{M}}{M_0} t$$

c. Lunar rendezvous

A mission employing the shuttle concept requires that the shuttle be able to rendezvous with an orbiting module (MOM) in lunar orbit. In many ways, this rendezvous is easier to perform than an earth orbit rendezvous. Lunar orbit speed is much lower than earth orbit speed, and the ratio of lunar orbit period to lunar rotation rate is very favorable with regard to launch frequency. The more difficult aspects of the lunar orbit rendezvous are associated with the unfamiliar topography, the lack of ground facilities for tracking the orbiting vehicle, and the planning of the ascent guidance commands.

The rendezvous maneuver can be conveniently considered as consisting of three phases, the ascent phase, closing phase and docking phase. During the ascent phase the target vehicle (MOM) is acquired electronically or optically by the intercepting shuttle vehicle. The second phase includes the closing trajectory from acquisition to the vicinity of the target vehicle, where the third phase, docking, takes place.

The ascent phase must be considered in the problem of orbital rendezvous because it is in this phase that the timing problem of hitting the target is solved. A shuttle vehicle on the lunar surface (rotating with a period of about 28 days) must be launched with the objective of intercepting the target vehicle, which is orbiting with a period of about two hours. The ascent phase can accomplish the interception objective by either of two basic approaches, direct rendezvous or indirect rendezvous. The indirect rendezvous is illustrated and fully discussed in Chapter V. The shuttle vehicle is launched into an intermediate parking orbit without considering the position of the target vehicle in its orbit at launch time. The intermediate parking orbit and target orbit are coplanar but have different altitudes and, therefore, different orbital periods. Because of the period difference, the relative angular position of the two vehicles changes with time. When the proper relative position is achieved, the shuttle vehicle is accelerated into a transfer orbit which terminates in the vicinity of the target vehicle, where final acquisition can be made. Thus, the timing problem is solved with the shuttle in orbit.

The direct rendezvous technique is also fully discussed in Chapter V. Here, the shuttle vehicle is not launched until the relative position of the launch site and the orbiting vehicle is that required for direct ascent and acquisition. The timing problem is solved on the ground before launch in the case of direct rendezvous.

At only two times in every 28 days can the shuttle be launched into an intercept trajectory which is optimum from the standpoint of propellant consumption. Therefore, the shuttle must have more than the optimum amount of propellant in order to widen the launch time tolerance. Important considerations in allocating this fuel surplus are the desired launch-time tolerance, target orbital altitude and inclination, and the time available for rendezvous.

Two means of increasing the launch-time tolerance are available. These means, range extension and trajectory shaping, are discussed in detail in Chapter V. With range extension, the ascent trajectory reaches its apogee at the target orbit altitude, as in the optimum ascent case, but the ascent range is varied as a function of time to provide launch time tolerance. Direct ascent rendezvous timing involves matching the interception point of the ascent trajectory and the target orbit with the target vehicle (MOM) itself. The amount of launch time tolerance to be gained by range extension can be determined by comparing the motion of the interception point and the target and making them coincide.

The second means of increasing the launch time tolerance is by trajectory shaping (see Chapter V). If a nominal ascent is taken to be one in which the shuttle arrives at the parking orbit altitude with zero flight path angle, then launch-time tolerance can be obtained by flying an ascent trajectory that would pass through the target point with a nonzero positive or negative flight path angle. Such a flight path, of course, would require correction to zero flight path angle at orbit altitude. Ascents resulting in a positive flight path angle at intercept permit "launch late" launch time tolerance. When the ascent trajectory includes an apocynthion, time is lost in transfer, and "launch early" time tolerance is provided. Figure 28 shows the lunar launch time tolerance available from trajectory shaping. Figure 29 shows the total excess velocity requirement for increasing launch time tolerance by range extension and trajectory shaping for sample out-of-plane launches.

Launch tolerances for missions that do not entail the shuttle concept are essentially unlimited. From Chapter IX it is seen that a return to earth can be made in any transearth trajectory plane and the return is completely independent of the launch time. This and the fact that there are no launch azimuth restrictions result in the ability of launch at any time.

The second phase, the closing phase, may be accomplished in various ways, including tail chase, inverse tail chase, and lateral rendezvous techniques. In the tail chase, the shuttle overtakes the MOM from behind. The shuttle must travel at a speed greater than the circular orbit speed of the target and so will gain altitude during closing. Therefore, the closing phase for the tail chase method must begin behind and below the targets. In the inverse tail chase, the target (MOM) overtakes the intercepting shuttle, which must be placed ahead of and above the target. The tail chase and inverse tail chase are shown in Fig. 30. Lateral rendezvous, shown in Fig. 31, involves placing the shuttle in an orbit at the same altitude as the target orbit. The two orbits cross after a certain time to permit rendezvous.

Each of the techniques has its advantages and disadvantages. The tail chase permits radar sensing from the shuttle vehicle without lunar surface background, but requires excess fuel to catch up to the target. The inverse tail chase is relatively economical, but the lunar surface may provide an undesirable radar background to the target during acquisition. Both direct and inverse tail chases

involve curved flight paths which make line-ofsight steering difficult. The lateral rendezvous approach does not entail any problems of surface background, and cross-coupling between velocity and altitude does complicate steering so much as in the other techniques. The lateral approach ranks between the two tail-chase techniques in economy.

After the closing phase, with the shuttle in the same orbit as the MOM with approximately 10 meters separation, the docking phase will complete the rendezvous. If the only reason for rendezvous is to permit refueling, docking may involve either structural mating of the two vehicles or simply use of a probe and drogue. On the other hand, if crew or supplies must be interchanged, then structural mating, seals and air locks are necessary. Precise attitude and translation control will be required on the "seeker" vehicle, and, at the minimum, the target vehicle (MOM) must be attitude-stabilized. Attitude control of the MOM may be necessary if there is a possibility of a large discrepancy in attitude between the two vehicles. In order that damaging impacts be precluded, closure rate should be reduced to zero when the vehicles are some distance apart. A docking mast could then be extended from one vehicle to engage a receptacle on the other vehicle and thus serve to pull the two vehicles together at a closely controlled rate.

Rendezvous has not been discussed in great detail, since there is essentially little difference in philosophy between lunar orbit rendezvous and earth orbit rendezvous, which has been considered extensively in the literature, e.g., Ref. 21 and Chapter VII of Ref. 1. There are only quantitative differences due to the weaker gravitational field and smaller radius of the moon. These differences will tend to make lunar orbit rendezvous easier than earth orbit rendezvous at the same altitude. Circular orbit speeds involved in lunar rendezvous closures are on the order of 2 km/sec as against 8.5 km/sec for low altitude earth orbit rendezvous. A typical lunar orbit rendezvous is shown in Fig. 32.

d. Guidance laws

While a wide variety of guidance laws are applicable to the problem of ascent from the lunar surface, only one will be singled out as an example. The law selected is that described in Subsection B-2d in connection with the descent braking trajectories. This law is equally applicable to the case of indirect ascent and, in fact, has been used to generate the thrust orientation program for the trajectories plotted in Figs. 21 through 26.

D. HOVERING AND TRANSLATION REQUIREMENTS

Most manned lunar landings will require the capability to hover above the landing site while final observations of the site are made. These observations will primarily concern the suitability of landing site terrain. Because the area immediately beneath the hovering vehicle (LM) might prove unfavorable (due to uneven rocks, large crevices or deep dust deposits, for example), the landing

module (LM) should be capable of translating, i.e., maneuvering laterally, during the final descent phase. This subsection considers propellant requirements and optimum conditions for hovering and translation.

Since hovering altitude and translation range are very small compared to the lunar radius R, and since propellant weight required in this phase is small compared to vehicle weight, very good analytic approximate solutions of the equations of motion may be obtained. The case of constant vehicle acceleration and the case of constant thrust with constant propellant flow rate will be investigated. For convenience the analyses consider vertical and horizontal motion separately. Therefore, the results can be used directly if hovering and translation are accomplished by separate orthogonal rocket engines. However, if the required thrust orientation is obtained by gimbaling a single engine or by pitching the entire vehicle, the thrust, position, and velocity as computed should be interpreted as components of the resultant vector quantity.

1. Constant Acceleration

Although motion under constant thrust with constant flow rate is generally a more realistic basis for propulsion analysis, the small mass ratios required for hovering and the extreme simplicity of analysis make the case of constant acceleration useful for preliminary investigations. Let the landing vehicle (LM) be required to translate with uniform acceleration and deceleration while hovering at constant altitude. The local x $_{\ell}$ y $_{\ell}$ coordinate system can then be assumed an inertial system, and the total horizontal translation denoted by x $_{\ell t}$ can be obtained from the familiar expression for rectilinear motion,

$$\mathbf{x}_{\ell t} = \begin{bmatrix} \frac{1}{2} & \frac{\mathbf{T}_{\mathbf{x}}}{\mathbf{M}} \left(\frac{\mathbf{t}_{\mathbf{b}}}{2} \right)^{2} \\ \end{bmatrix} 2 = \frac{\mathbf{T}_{\mathbf{x}}}{\mathbf{M}} & \frac{\mathbf{t}_{\mathbf{b}}^{2}}{4}$$
 (55)

where

 $\frac{T_x}{M}$ = constant horizontal thrust acceleration

t_b = total hovering time (i.e., horizontal rocket burning time)

The constant thrust required is

$$T_{x} = \frac{4x_{\ell t} W}{g_{\oplus 0} t_{b}^{2}}, \qquad (56)$$

where W = $g_{\oplus 0}$ M is the constant vehicle weight.

Since $T_x = I_{sp} \stackrel{\bullet}{W_{fx}}$ and $W_{fx} = \stackrel{\bullet}{W_{fx}} t_b$, Eq 56 becomes

$$W_{fx} = \frac{4x_{\ell t}W}{g_{\theta 0} I_{sp} t_{b}}.$$
 (57)

 W_{fx} is the total fuel weight lost due to burning of the horizontal translation engine and W_{fx} is the fuel

weight flow rate $\dot{W}_{fx} = \dot{M}_{fx} g_{\oplus 0}$.

The weight of the propellant required to hold the vehicle at constant altitude during translation, \mathbf{W}_{fy} , is seen from

$$T_{y} = I_{sp} \dot{W}_{fy} = Mg_{0}$$
 (58)

to be

$$W_{y} = \dot{W}_{fy} t_{b} = \frac{W g_{0} t_{b}}{g_{0} I_{sp}}$$
 (59)

The total propellant used for hovering and translation is

$$W_{f} = W_{fx} + W_{fy} = \frac{W}{g_{\bigoplus 0} I_{sp}}$$

$$\left[\frac{4 x_{\ell t}}{t_{b}} + g_{\emptyset 0} t_{b}\right]$$
(60)

For minimum total fuel, to translate a given distance $\mathbf{x}_{\text{ft}},$

$$\frac{dW_f}{dt_b} = \frac{W}{g_{\oplus 0}I_{sp}} \left[-\frac{4x_{\ell t}}{t^2} + g_{\ell 0} \right] = 0, \tag{61}$$

01

$$t_{b} = 2\sqrt{\frac{x_{\ell t}}{g_{0}}}$$

$$T_{x} = T_{y} = W\frac{g_{0}}{g_{0}}$$

$$\frac{W_{f}}{W} = \frac{4\sqrt{x_{\ell t} g_{0}}}{g_{0} I_{SD}}.$$
for minimum W_{f}
(62)

2. Constant Thrust

a. Translation

It is possible to derive simple analytic solutions to the equation of translatory motion under the assumptions of constant thrust and constant mass flow rate. This case is much more realistic than that of constant acceleration previously considered. The equation of motion is

$$M \frac{d^2 x_{\ell}}{dt^2} = T_x \tag{63}$$

where

M = instantaneous total vehicle mass

x_a = horizontal translation

 T_x = constant thrust component in the horizontal (x_{ℓ}) direction

The thrust program selected is the simplest possible. A constant thrust $T_{\rm x}$ is applied for approximately half the burning time, at which point the thrust is reversed to decelerate the LM to zero horizontal velocity when the desired translation distance has been traversed. Velocity at the beginning of the translation will be assumed zero. Thus, this constant thrust routine is analogous to the constant acceleration scheme previously outlined. The time of thrust reversal, t_1 , obviously will not be half the burning time, t_b , because the vehicle will be lighter during the deceleration phase than in the acceleration phase due to the weight of propellant expended during translation.

The equation of motion may be rewritten:

$$\ddot{x}_{\ell} = \frac{\frac{T_{x}}{M_{0}}}{1 - \frac{\dot{M}}{M_{0}} t}$$
(64)

where

 M_0 = initial total vehicle mass

M = total constant mass flow rate (including any flow from vertical hovering rockets during the translation)

The first integration of this equation gives the expression for the horizontal velocity of the LM at any time during the acceleration phase;

$$\dot{x}_{\ell} = -\frac{T_{x}}{\dot{M}} \ln \left(1 - \frac{\dot{M}}{\dot{M}_{0}} t\right) + \dot{x}_{\ell 0};$$

$$\dot{x}_{\ell 0} = 0$$
(65)

The second integration and evaluation of the constant of integration for the initial condition \mathbf{x}_{ℓ} = 0 at t = 0 gives the relation for horizontal position. In particular, at an arbitrary time \mathbf{t}_{1} , the horizontal position and velocity components are as follows:

$$\mathbf{x}_{\ell 1} = \frac{\mathbf{T}_{\mathbf{x}} \mathbf{M}_{0}}{\dot{\mathbf{M}}^{2}} \left[(1 - \zeta_{1}) \ln (1 - \zeta_{1}) + \zeta_{1} \right]$$

$$\dot{\mathbf{x}}_{\ell 1} = -\frac{\mathbf{T}_{\mathbf{x}}}{\dot{\mathbf{M}}} \ln (1 - \zeta_{1})$$
(66)

where $\zeta_1 = \frac{\dot{M}}{M_0} t_1$ is the mass ratio for rocket burning from t_0 to t_1 .

At this time the thrust is reversed, i.e., the vehicle obeys the equation of motion

$$\hat{\mathbf{x}}_{\ell} = -\frac{\frac{\mathbf{T}_{\mathbf{x}}}{\mathbf{M}_{0}}'}{1 - \frac{\mathbf{M}}{\mathbf{M}_{0}}'} \mathbf{t}$$
 (67)

where $M_0' = M_0 - \dot{M} t_1$ is the total vehicle mass at beginning of the deceleration phase.

Successive integration of this equation and evaluation of the constants of integration for the initial conditions of the deceleration phase, \mathbf{x}_{ℓ} = $\mathbf{x}_{\ell\,1}$ and $\dot{\mathbf{x}}_{\ell}$ = $\dot{\mathbf{x}}_{\ell\,1}$ at t = \mathbf{t}_{1} , determine the position from the start of the translation and the velocity at any time during this phase.

$$\dot{x}_{\ell} = \frac{T_{x}}{\dot{M}} \ln \left(1 - \frac{\dot{M}}{\dot{M}_{0}} t\right) - \frac{T_{x}}{\dot{M}} \ln \left(1 - \frac{\dot{M}}{\dot{M}_{0}} t_{1}\right) + \dot{x}_{\ell 1}$$

$$x_{\ell} = \frac{T_{x}}{\dot{M}} \left[-\frac{\dot{M}_{0}}{\dot{M}} \left(1 - \frac{\dot{M}}{\dot{M}_{0}} t\right) \left\{ \ln \left(1 - \frac{\dot{M}}{\dot{M}_{0}} t\right) + \left(t_{1} - t\right) \ln \left(\left(1 - \frac{\dot{M}}{\dot{M}_{0}} t_{1}\right) + \left(1 - \frac{\dot{M}}{\dot{M}_{0}} t_{1}\right) \right\}$$

$$+ \frac{\dot{M}_{0}}{\dot{M}} \left(1 - \frac{\dot{M}}{\dot{M}_{0}} t_{1}\right) \ln \left(1 - \frac{\dot{M}}{\dot{M}_{0}} t_{1}\right)$$

$$+ t_{1}$$

$$+ \frac{\dot{M}_{0}}{\dot{M}} \left(1 - \frac{\dot{M}}{\dot{M}_{0}} t_{1}\right) \left\{ \ln \left(1 - \frac{\dot{M}}{\dot{M}_{0}} t_{1}\right) - 1 \right\}$$

The rather formidable position equation simplifies considerably on evaluation at the end point $t = t_b$, $x_\ell = x_{\ell t}$, $x_\ell = 0$. The velocity equation gives, for $x_\ell = 0$ at $t = t_b$,

$$0 = \frac{T_{x}}{\dot{M}} \ln \left[\frac{1 - \frac{\dot{M}}{M_{0}} t_{b}}{\left(1 - \frac{\dot{M}}{M_{0}} t_{1}\right) \left(1 - \frac{\dot{M}}{M_{0}} t_{1}\right)} \right]$$
(69)

which provides a simple relation between total burning time and the thrust reversal time.

$$t_b = 2t_1 \left(1 - \frac{\dot{M}}{M_0} t_1\right) = 2 \frac{M_0'}{M_0} t_1$$
 (70)

Substitution of this relation in the position equation gives, in terms of mass ratio

$$\mathbf{x}_{\ell t} = \frac{\mathbf{T}_{\mathbf{x}} \, \mathbf{M}_{0}}{\dot{\mathbf{M}}^{2}} \left[- (1 - \zeta_{1}) (1 - 2 \zeta_{1}) \right]$$

$$\left\{ \ln (1 - 2 \zeta_1) - 1 \right\}$$

$$- \zeta_1 (1 - 2 \zeta_1) \ln (1 - 2 \zeta_1)$$

$$+ (1 - \zeta_1) \ln (1 - \zeta_1) + \zeta_1$$

$$+ (1 - 2 \zeta_1) \left\{ \ln (1 - 2 \zeta_1) - \ln (1 - \zeta_1) - 1 \right\}$$

$$(71)$$

which reduces to

$$\mathbf{x}_{\ell t} = \frac{\mathbf{T}_{\mathbf{x}}}{\dot{\mathbf{M}}} \quad \mathbf{t}_{1} \left[\ln (1 - \zeta_{1}) + 2 \zeta_{1} \right]$$
where
$$\mathbf{t}_{1} = \frac{1 - \sqrt{1 - 2 \frac{\dot{\mathbf{M}}}{\dot{\mathbf{M}}_{0}}} \, \mathbf{t}_{b}}{2 \frac{\dot{\mathbf{M}}}{\dot{\mathbf{M}}_{0}}}$$

Mass ratios for hovering and translation generally should be less than ζ = 0.01. For such small mass ratios the previous expression for translational distance can be approximated by:

$$x_{\ell t} \approx \frac{T_x}{M_0} \frac{t_b^2}{4} \left(1 + \frac{1}{4} \frac{\dot{M}}{M_0} t_b\right), 1 >> \left(\frac{\dot{M}}{M_0} t_b\right)^2$$
(72)

This solution obviously approaches that for constant acceleration (or constant mass with constant

thrust since acceleration = $\frac{T_x}{M}$) as M approaches

zero. Translational distance is plotted as a function of initial thrust-to-weight ratio and burning time in Fig. 33.

b. Vertical descent from hover

If the LM is to descend and reach zero altitude at the end of the translation time, t_b, the vertical component of motion is described by the following equation.

$$M \frac{d^2 y_{\ell}}{dt^2} = T_y - M g_{\ell 0}$$
 (73)

or

$$\frac{d^2 y_{\ell}}{dt^2} = \frac{\frac{T_y}{M_0}}{1 - \frac{\dot{M}}{M_0}} - g_{\ell 0}$$
 (74)

where

 y_{ℓ} = altitude above the lunar surface

T_v = vertical component of thrust

M = total mass flow rate (including any flow from horizontal rockets).

With the assumptions of constant thrust T_y , constant mass flow rate, M, and constant lunar gravity g_0 , this equation can be integrated as in Subsection

B-1c. However, in the case of final descent from hover, the initial conditions are $\mathring{y}_{\ell} = 0$ and $y_{\ell} = y_{\ell 0}$ at t = 0. For this case, integration of the above equation of motion gives:

$$\dot{y}_{\ell} = -\frac{T_{y}}{\dot{M}} \ln \left(1 - \frac{\dot{M}}{\dot{M}_{0}} t\right) - g_{\ell 0} t$$

$$y_{\ell} = \frac{T_{y} \dot{M}_{0}}{\dot{M}^{2}} \left[\left(1 - \frac{\dot{M}}{\dot{M}_{0}} t\right) \ln \left(1 - \frac{\dot{M}}{\dot{M}_{0}} t\right) + \frac{\dot{M}}{\dot{M}_{0}} t \right] - g_{\ell 0} t^{2} + y_{\ell 0}$$

$$(75)$$

For \dot{y}_{ℓ} = 0, y_{e} = 0 at t = t_{b} , these equations give

$$t_{b} = -\frac{T_{y}}{g_{0\dot{M}}} \ln (1 - \zeta)$$
 (76)

$$y_{\ell 0} = -\frac{T_y}{\dot{M}} t_b \left[\left(\frac{1}{\zeta} - 1 \right) \ln \left(1 - \zeta \right) + 1 \right] + \frac{g_{\ell 0} t_b^2}{2}$$
 (77)

where $\zeta = \frac{\dot{M} t_b}{M_0}$ is the total mass ratio. Sub-

stitution of the first equation for $\mathbf{T}_{\mathbf{y}}$ in the second equation provides the relation

$$y_{\ell 0} = g_{\ell 0} t_b^2 \left[\frac{1}{\zeta} - \frac{1}{2} + \frac{1}{\ln(1-\zeta)} \right]$$
 (78)

For small mass ratios, as will generally be the case for the final phase of descent, the following approximation is convenient.

$$y_{\ell 0} \approx \frac{g_{\ell 0}^{t_b}^2}{12} \zeta \left(1 + \frac{\zeta}{2}\right), 1 > \zeta^2$$
 (78a)

c. Hovering

Hovering precisely at a chosen altitude obviously requires variable vertical thrust,

$$T_y = M g_{0} = M_0 g_{0} \left(1 - \frac{\dot{M}}{M_0} t\right).$$

If a constant thrust $T_y = M_a g_{(0)}$ were applied, the solution of the equation of motion with initial conditions $y_\ell = y_{\ell (0)}$, $\dot{y}_\ell = 0$ at t = 0 does not permit the constraints \dot{y}_ℓ $(t_b) = 0$ or y_ℓ $(t_b) - y_\ell$ (0) = 0 except for the theoretical limit $t_b = \zeta = 0$. However, with choice of a slightly lower constant thrust level, the condition \dot{y}_ℓ $(t_b) = 0$ can be achieved. From Eq (75) for the given initial conditions,

$$\dot{y}_{\ell,t} = -\frac{T_y}{\dot{M}} \ln \left(1 - \frac{\dot{M}}{M_0} t_b\right) - g_{40}^{t} b$$

$$y_{\ell t} - y_{\ell 0} = \frac{T_{y} M_{0}}{\dot{M}^{2}} \left[\left(1 - \frac{\dot{M}}{M_{0}} t_{b} \right) \ln \left(1 - \frac{\dot{M}}{M_{0}} t_{b} \right) + \frac{\dot{M}}{M_{0}} t_{b} \right] - \frac{g_{\ell 0} t_{b}^{2}}{2}$$
(79)

where the subscript $^{\rm t}$ signifies a value at time $^{\rm t}_{\rm b}$. For small mass ratios the first equation gives

$$\dot{y}_{lt} \approx t_b \left[\frac{T_y}{M_0} \left(1 + \frac{1}{2} \zeta \right) - g_{(0)} \right], \ 1 > 5 \zeta^2$$
 (80)

so that the end constraint $\dot{y}_{\ell\,\,t}$ = 0 is possible if the constant thrust is selected such that

$$T_{y} \approx M_{0} g_{(0)} \left(1 - \frac{\zeta}{2}\right) \tag{81}$$

Substitution of this value in the second equation of (46) determines the change in altitude during the "hover,"

$$y_{\ell\,0} - y_{\ell\,t} \approx \frac{1}{12} g_{\ell\,0} t_b^2 \zeta, 1_{>>} \zeta^2$$
 (82)

d. Simultaneous translation and hovering or descent

If the vertical and horizontal components of thrust are provided by separate engines, the solutions of Subsections D-2a through D-2c apply directly for simultaneous translation and hovering or descent. For touchdown at the same instant as the required translation is completed, the simultaneous equations are, from Eqs (43) and (45) and $\dot{M} = \dot{M}_{\nu} + \dot{M}_{\nu}$

$$x_{\ell t} = \frac{x_{t}}{4} + \frac{y_{t}}{4} + \frac{y_$$

$$+\frac{1}{16} \zeta^2 V_{ex} t_b$$
 (83)

$$y_{l0} \simeq \frac{g_{l0}t_b^2}{12} \le (1 + \frac{\zeta}{2})$$
 (84)

where ${\rm V_{ex}}$ = exhaust velocity of each engine. For given mission requirements ${\rm x_{\ell\,t}}$ and ${\rm y_{\ell\,0}}$, the required values of ζ and ${\rm t_b}$ are determined by these equations. No optimization is possible since the problem is completely determined. In the case of simultaneous translation and hovering with constant thrust components, only the first of the two previous equations is a condition. Therefore, a value of ${\rm t_b}$ can be selected which optimizes the

mass ratio $\zeta = \frac{W_f}{W_0}$. Values of ζ and t_b selected in this way then determine the change in eltitude

in this way then determine the change in altitude which must be accepted,

$$y_{\ell 0} - y_{\ell t} \approx \frac{1}{12} g_{\ell 0} t_b^2 \zeta.$$
 (85)

Conditions for minimum ζ , $\zeta_{\rm m}$, are obtained by setting

$$\frac{\mathrm{d} \zeta}{\mathrm{d} t_{\mathrm{b}}} = 0 \tag{86}$$

in the equation resulting from differentiating Eq (83) with respect to ζ . The results are:

$$x_{lt} \approx x_{lt} (\zeta, t_b)$$
, are

$$t_{b} \simeq \frac{\zeta_{m} V_{ex}}{2 g} \left(1 + \frac{\zeta_{m}}{2}\right)$$

$$x_{\ell t} \simeq \frac{\zeta_{m} V_{ex} t_{b}}{4} \left(1 + \frac{1}{4} \zeta_{m}\right) - \frac{g_{0} t_{b}^{2}}{4} \left(1 - \frac{1}{4} \zeta_{m}\right)$$

$$y_{\ell 0} - y_{\ell t} \simeq \frac{1}{12} g_{0} t_{b}^{2} \zeta_{m}$$
(87)

where ζ_m is the minimum ζ .

It can be seen that these expressions approach those derived in the constant acceleration case in the limit as $\zeta \to 0$,

$$\zeta = \frac{2 g_{0}t_{b}}{V_{ex}}$$

$$x_{\ell t} = \frac{g_{\ell 0} t_b^2}{4}$$
.

These equations demonstrate the utility of Fig. 34 as an accurate approximation for the minimum fuel required to hover and translate simultaneously.

E. LUNAR LANDING ABORT

It is anticipated that the majority of landing missions in the near future will not employ direct (impact) trajectories to the landing site. In the case of manned landings, crew safety is jeopardized by use of direct trajectories, while for reconnaissance flights (manned or unmanned), the lunar areas that can be covered are severely limited. Since most impacting lunar probes have no abort requirements, this section is based on a flight wherein the spacecraft is maneuvered into a circular orbit about the moon from which the landing phase begins. This phase is initiated by a deorbit maneuver, after which the vehicle descends on a landing coast trajectory to a lunar altitude of approximately 18 km, at which point a braking maneuver is initiated. The braking maneuver decelerates the vehicle to hover condition at a low altitude of approximately 600 meters from which translation and final letdown are accomplished.

During the landing phase, it may become imperative to cut short the intended mission and to alter the course of the spacecraft. Typical reasons for such action could be propulsion failures, "unsafe" trajectories, guidance malfunctions, solar flare activity, etc.

In this section various techniques of abort during the landing phase will be discussed, with emphasis on the manned mission; these techniques are similar in most respects to those presented in Refs. 22 and 23. In Technique I the apocynthion altitude of the abort trajectory equals the initial circular orbit; in Technique II the apocynthion altitude of the abort trajectory exceeds the altitude of the initial

circular orbit; and in Technique III the abort trajectory is circular and has an altitude equal to the abort altitude. Each one of the abort techniques above can be performed with or without rendezvous. In addition, abort maneuvers occurring during the final braking and hovering phases will be discussed.

1. Abort with Return to Orbit (Technique I)

a. Abort Technique I without rendezvous

The pertinent orbital relations are illustrated in the following sketch:

Landing Coast Trajectory

Abort Trajectory

Abort Trajectory

Ava

Initial
Circular
Orbit

The vehicle is initially in a circular orbit of altitude h_0 , and the orbit departure angle Θ is measured from the pericynthion point of the landing coast trajectory to the deorbit point along the circular orbit with origin taken at the center of the moon. A spherical moon is assumed and altitudes are measured with respect to the lunar surface. The abort trajectory has an apocynthion altitude of h_0 , and a downrange aim angle (ϕ_A) is defined as the central angle between the abort point and the apocynthion of the abort trajectory. All rocket burning is simulated by a velocity impulse $\Delta V,$ where ΔV_A is the characteristic velocity impulse required to establish the abort trajectory. Upon arrival at the apocynthion of the abort trajectory, the vehicle is injected back into the circular orbit by a circularizing velocity impulse $\Delta V_{_{\rm C}}$. Hence, the total velocity impulse required to execute an abort and to inject into a circular orbit is $\Delta V_{\rm T}$ = $\Delta V_A + \Delta V_C$.

Figure 35 presents $\Delta V_{\rm T}$ versus downrange angle ($\Phi_{\rm A}$) for three abort altitudes, namely, $h_{\rm A}$ = 152.4 km, 91.4 km, and 18.3 km, with an initial circular orbit altitude of h_0 = 185.2 km. For this case, the orbit departure angle is Θ = 178° and the pericynthion altitude of the landing coast trajectory is $h_{\rm PL}$ = 18.3 km. Decreasing the orbit departure angle

For the case of a type A abort trajectory, the vehicle ascends to the apocynthion after the abort maneuver. If at this time the vehicle fails to inject into the circular orbit, it will descend toward pericynthion, and if this pericynthion is less than some minimum altitude, there will be an impact.

@ from 178° to 150° (not shown) increases the

 $\Delta\,V_{\mathrm{T}}$ requirements from 3 to 10 m/sec. This

figure shows that there is an optimum downrange angle to "aim" which minimizes the $\Delta\,V_{\mbox{\scriptsize T}}$ require-

ments. However, in some cases, where hpi is

negative, this aim point must be adjusted to avoid impact with the lunar surface. This physical

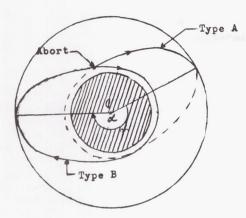
limitation is indicated on the figure and refers to two types of abort trajectories as shown in the

following sketch.

A type B abort trajectory descends through its pericynthion first before attaining the circular orbit altitude. The limitation with this type of trajectory is again that the pericynthion altitude be above the lunar surface.

In the present discussion, an abort trajectory was designated as safe if it attained a pericynthion altitude of no less than 11 km. This choice was based on the moon's topographical characteristics and was taken to avoid lunar mountains with an ample margin of safety.

The restriction of a pericynthion above the lunar surface may be eliminated if the reliability is deemed high enough to assure that an injection into the circular orbit will always take place. It may also be eliminated if design features account for such a contingency. However, for the present, this restriction is not waived. As can be seen from Fig. 35, this restriction on the pericynthion altitude of the types A and B abort trajectories essentially describes a safe abort window which is defined by the angle α as shown in the following sketch. Figure 36 presents α as a function of circular orbit altitudes h_0 for several values of $h_{\rm A}$. It



can be seen that α decreases rapidly with abort altitude. But even at low abort altitudes, the window is sufficiently wide ($\alpha \simeq 40^\circ$) to affirm the success of manual or emergency backup control modes. The safe abort window is independent of the other orbital elements of the landing coast trajectory and is a function of the abort altitude and initial circular altitude alone. Active abort procedures as described above may become necessary because of unacceptable coast trajectories, probability of stage explosions, ease of planning the return flight to earth, etc. This abort procedure requires two rocket engine ignitions.

Passive abort procedures require one ignition, and they utilize a landing coast trajectory that returns to or intersects the initial circular orbit altitude where the circularizing maneuver is performed. If the braking phase has begun, an active abort becomes mandatory.

b. Abort Technique I with rendezvous

For the problem of rendezvous (shuttle concept) the vehicle consists of two modules, the landing module (LM) and the lunar orbital module (MOM). At the deorbit point the LM leaves the MOM and establishes a landing coast trajectory while the MOM continues in the original circular orbit (see next sketch). In the event of an abort during descent, the objective of the LM is to establish an abort trajectory whose apocynthion is at the circular orbit. The slant range $(r_{\rm LM})$ is the distance

between the LM (actually the shuttle) and the MOM at the time of abort.

The case for which the abort trajectory allows the LM to arrive coincident with the MOM is defined as a "perfect rendezvous." This, however, may not always be desirable because of velocity impulse requirements and lunar impact restrictions. Thus, the LM can either lead or lag the MOM after reestablishing the original circular orbit

If the LM lags the MOM, a "catch-up" maneuver (gain) is required. For separation angles ξ greater than a certain amount, such maneuvers result in trajectories that impact the moon if performed in one revolution.

Should the LM lead the MOM (a more likely case), a "drop-back" maneuver (loss) is required. The limiting factor for the loss maneuver can arbitrarily be chosen to be the loss of line of sight between

the two vehicles. The limiting separation angles are given in Table 1 with the corresponding circular orbit altitude (h_0) .

TABLE 1

h ₀ (km)	+\$	-ξ	
92.6 185.2 370.4	14n° 26n° 47n°	37° 51° 69°	where n is the number of revo- lutions of the MOM and LM

Performing an indirect rendezvous of this nature requires three rocket engine ignitions. By restricting the number of revolutions of the gain or loss orbits to one, the elapsed time from the maneuver to the closing phase is approximately two hours.

The total velocity impulse required to abort and rendezvous with these maneuvers is shown in Figs. 37, 38, and 39 for initial orbital altitudes of 92.6, 185.2, and 370.4 km, respectively. Each figure presents several abort altitudes for an orbit departure angle of 178°. The pericynthion altitude of the landing coast trajectory is chosen in all cases to be 18.3 km. The figures show that for a 1.0-km increase in h_0 , the minimum $\Delta\,\mathrm{V}$ in-

creases ± 0.5 m/sec and occurs at downrange aim angles ($\Phi_{\rm A}>~160$ °) greater than those required for perfect rendezvous.

Table 2 presents a comparison of the minimum total $\Delta\,V$ requirements with and without rendezvous considerations. The quantities shown do not include a perfect rendezvous with data for an orbit departure angle $_{\odot}$ = 178° and a circular orbit altitude h_{0} = 185.2 km.

TABLE 2

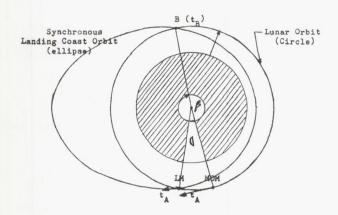
h _{PL}		Δ V indirect rendezvou i.e., with gain or loss maneuvers (m/sec)	
18.3	18.3	105	37
	91.4	100	40
	152.4	70	38

Conditions for a perfect rendezvous are also indicated in Figs. 37, 38 and 39, and it is seen that compared with the minimum $\Delta V^{\dagger}s$ listed above the ΔV requirements increase significantly by hundreds of meters per second. The required downrange aim angle for perfect rendezvous is less than 95°. Figure 40 presents the velocity requirements for direct rendezvous (i.e., without gain or loss maneuver) as a function of abort altitude and various initial orbital altitudes. Also shown in the figure are the requirements for an orbit departure angle Θ = 95° for h₀ = 185.2 km.

This particular departure angle bears significant interest because it provides a passive abort capability (i.e., the LM is allowed to coast to the lunar orbit altitude and an adjustment of the velocity to

circular orbit velocity (ΔV_c) is included) that allows rendezvous to take place in approximately two hours, as explained below.

Consider an initial circular orbit altitude \mathbf{h}_0 with the associated period τ_0 :



If the landing coast trajectory also has the period τ_0 , then the LM will lead the MOM at t_A , but the modules will be coincident at t_B , or when the orbital central angle β = 360° at which time the rendezvous maneuver is executed. The impulse requirement for this maneuver at the initial orbital altitude stated above (h_0 = 185.2 km) is 138.5 m/sec. For each initial orbit altitude, there is a departure angle that results in such a synchronous coast trajectory. Other departure angles may require several revolutions, or even days, before coincidence is attained.

The ΔV requirements versus downrange aim angle for an active abort (i.e., when the LM is put on the abort trajectory as soon as possible) from a synchronous orbit are given in Fig. 41. Data is presented for the case mentioned above (h $_0$ = 185.2 km), and the downrange aim angle required for a perfect rendezvous is indicated. The minimum velocity impulse is approximately 45 m/sec over the impulse required for the 178° orbit departure.

The downrange aim angle necessary for perfect rendezvous is shown in Figs. 42, 43, and 44 as a function of abort altitude for $h_0 = 92.6$, 185.2, and 370.4 km, respectively. Also included in these figures are the downrange angles that result in a plus and minus 1° separation angle between the LM and MOM when the LM arrives at apocynthion. These figures may be interpreted in several ways. First, assuming that the separation distance (= 35 km) is the reasonable limit of the guidance and propulsion capability of the LM for the closing phase, the curves represent an acceptable rendezvous window. This window decreases rapidly as the abort altitude decreases. Secondly, if the position-time history of the MOM is not exactly as planned (for example, if there exists a separation angle of -1°), but the LM abort guidance is accurate,

the increase in ΔV requirements may be found. This is accomplished by noting that a decrease in downrange angle (Figs. 42 through 44) is accompanied by an increase in abort velocity impulse (Figs. 37 through 41).

Figures 42 through 44 are presented for orbit departure angles of 178°. Included in Fig. 43, is the departure angle of 95° (synchronous orbit). A decrease of the departure angle results in a rotation of the $\Phi_{\rm A} {\rm versus} \; {\rm h}_{\rm A} \; {\rm curves}$ in Figs. 42 through 44, which lowers the rendezvous window at higher abort altitudes and slightly decreases the window size. A reduction of pericynthion altitude ${\rm h}_{\rm PL}$ of the coast trajectory (not shown) raises the rendezvous window and increases its size.

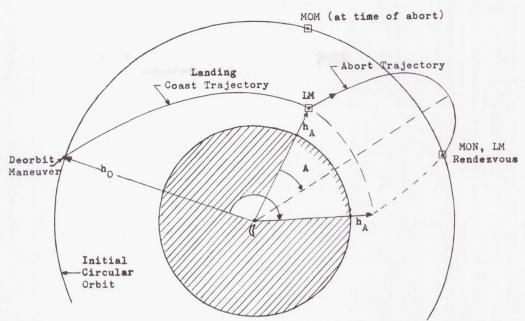
Superimposed on Figs. 42, 43 and 44 is the impact restriction for type A abort trajectories. As is noticed, if "safe" abort trajectories are specified, perfect rendezvous at all times is not possible and gain or loss maneuvers have to be performed. These maneuvers increase the rendezvous time by 2 hr. It was found that type B abort trajectories do not affect the rendezvous problem because the downrange angles at which they occur are far removed from those required for perfect rendezvous.

Another important aspect of rendezvous missions is the slant range between the LM and MOM during the landing phase. The maximum slant range occurs at the initiation of the braking phase (to hovering and landing) as shown in Fig. 45. This figure presents the slant range as a function of altitude during the landing coast trajectory for initial circular orbit altitudes of 92.6, 185.2 and 370.4 km. The maximum slant ranges for an orbit departure angle of 178° are 185, 410 and 820 km, respectively. After braking begins, the slant range decreases to values equivalent to the initial circular orbit altitudes, i.e., at some point during the braking or hovering phase MOM is directly overhead.

2. Abort with Return to Orbit and Perfect Lunar Rendezvous (Technique II)

The following sketch illustrates this technique. In this method the abort trajectory is such that its apocynthion altitude exceeds the circular orbit altitude. This allows the MOM to "catch up" while the LM is still in its abort trajectory above the circular orbit altitude, so that both arrive at the same time at the rendezvous point at altitude \mathbf{h}_0 . Figure 46 presents the total $\Delta \mathbf{V}$ required to abort and rendezvous from a descent use of a synchronous orbit as a function of time from the deorbit maneuver. The solid curve corresponds to Technique I and the dashed curves to the present method (Technique II) for three values of time from abort to rendezvous. An auxiliary scale in Fig. 13 indicates the abort altitude $\mathbf{h}_{\mathbf{A}}$.

Depending on the time requirements, the savings in ΔV (i.e., fuel savings) by use of Technique II instead of Technique I can be quite large. Table 3 presents the velocity requirements for the two techniques when a perfect rendezvous is considered. The circular orbit altitude h_{Ω} is



185.2 km, and the orbit departure angle is 95°.

TABLE 3

111111111111111111111111111111111111111								
Tech- nique I ΔV ΔV (m/sec)								
hA		Time from	Abort to Re	ndezvous				
(km)	(m/sec)	1000 sec	3000 sec	5000 sec				
20	1290	960	425	205				
30	940	765	390	220				
60	595	560	330	210				
100	360	390	260	190				
160	195	195	170	150				

It is seen from Table 3 that for low abort altitudes the velocity requirements using Technique II are significantly smaller. This is due to the fact that larger downrange angles are possible with this method. However, for high abort altitudes, the advantage is not as great and the differences reduce to zero as h_{Δ} approaches h_{Ω} .

In addition, the ΔV requirements for a typical braking phase are included in Fig. 46. It is seen that during the braking phase, the fuel savings of Technique II diminish. The maximum propulsion requirement ($\simeq 1750 \text{ m/sec}$) for abort occurs, as is expected, at the end of braking.

3. Circular Abort Trajectory (Technique III)

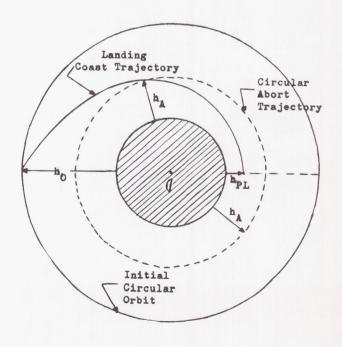
This type of abort is pictured in the sketch at the right. If an abort becomes necessary during the landing coast trajectory, another alternative to the two previously discussed techniques is to establish a circular orbit at the abort altitude and leave the LM in this orbit for an indefinite time.

This abort technique is attractive for non-rendezvous missions and for missions that require establishment of very low circular orbits about the moon. Table 4 gives the Δ V re-

quirements for orbit departure angles of 178° and 95° as well as the $\triangle V$ required for passive aborts. Passive aborts return to the initial circular altitude of 185.2 km and include the adjustment of the velocity to the circular orbit velocity. Impulse requirements may be either larger or smaller than the passive maneuver, depending on the orbit departure angle (Θ).

 $h_0 = 185.2 \text{ km}, h_{PL} = 18.3 \text{ km}$

hA		ΔV, Θ= 178° (m/sec)		95° ec)
(km)	Passive	Active	Passive	Active
152.4 121.92 91.44 60.96 30.48	36.6 36.6 36.6 36.6 36.6	61.9 72.1 74.1 67 50	138.5 138.5 138.5 138.5 138.5	138.4 133.7 125.4 108.8 85.2



4. Abort During the Hovering Phase

Final letdown to the lunar surface requires that the landing module possess a rate of descent appropriate to the type of landing, whether for soft or hard landings. For soft landings, which are considered in this section, the most crucial stage of the letdown maneuver occurs within 30 meters of the lunar surface. If an abort becomes necessary during this time, important considerations are the abort thrust-to-weight ratio, the reaction time and the design structural limit of the LM.

The objective of the abort during this phase is to establish a positive rate of climb before impact with the lunar surface, or to ensure that a touchdown on the surface will be within mission design limits.

The landing safety boundaries are illustrated for a typical abort thrust-to-weight ratio of $\frac{T}{W_0}$ = 0.422. It is assumed that the delay time to ignite the abort engines or increase engine

thrust to the desired emergency value is one second. During this reaction interval, the LM is assumed to descend ballistically $(\frac{T}{W_0} = 0)$ from an

initial altitude and an initial rate of descent. Figure 47 gives a safety boundary for the case that impacts without use of emergency thrust and for the conditions stated above. If the initial conditions of the LM are to the left of the boundary, the module can recover before impact and initiate an ascent back to orbit. To the right, impact cannot be avoided. Included in the figure is an arbitrary impact structural limit of 6 $\rm g_{\bigoplus,0}$ (with shock ab-

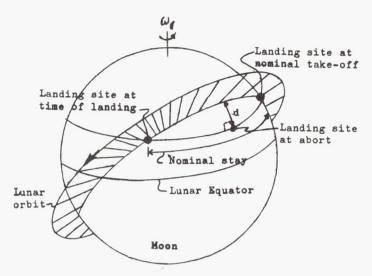
sorbers) based on free fall ($\frac{T}{W_0}$ = 0). Initial conditions to the right of this limit are structurally unsafe for free fall to the surface.

Also included in the figure is a typical descent as executed by an automatic landing system. As long as the descent is to the left of the boundaries, the letdown is continued in a normal fashion. However, if the altitude is greater than 11 meters and the descent reaches the safety limit, abort propulsion is initiated followed by an ascent to orbit. When the altitude is less than 11 meters, the main landing propulsion is terminated at the limit and the module drops in. It is further assumed that the horizontal component of velocity is within the stability margin of the LM while it is below 11 meters of altitude.

5. Lunar Surface Abort

After completion of a lunar landing, the module will remain on the surface for a selected interval of time. If during this stay time an abort becomes necessary, the module will initiate an ascent phase. For missions that do not entail lunar rendezvous, the launch is accomplished in a normal manner. That is, the module is rolled to the desired azimuth, and the ascent is carried on without changes from the nominal ascent trajectory. However, for the case where lunar rendezvous is a consideration, the launch azimuth is somewhat restricted.

The sketch below illustrates how plane changes become necessary when aborting with the requirement to rendezvous for a launch-compatible orbit.



This type of orbit passes over the landing site once the landing phase, and again after a nominal stay time, so that both ascent and descent occur essentially in the orbit plane. Since the moon is rotating, the landing site will not lie in the plane of the orbiting MOM at all times. Therefore, a launch at any time during the nominal stay time and after the stay time will result in the site being displaced from the orbital plane.

The maximum displacement is given in Fig. 48 for aborts made after one-half the nominal stay time, for aborts one day past the nominal stay time, and for various landing-site latitudes. This range is zero for sites on the lunar equator and increases with site latitude.

Aborts from the lunar surface should be successful. Although any vehicle will be designed for high reliability, the question still arises as to what can be done in the event of a primary guidance failure. The possibility of such an emergency requires some type of backup guidance system.

For illustrative purposes, a backup system utilizing strapped down gyros and three orthogonally mounted accelerometers is assumed. Such a system would require a man to complete the guidance loop. Module attitude is related to him from the gyros and velocity from the accelerometers.

The above manual ascent technique is considered the simplest. It consists of lifting off and rising vertically for an interval of time. The module is then pitched to a desired inertial thrust attitude $\boldsymbol{\theta}_t$, which is measured from the \boldsymbol{x}_t -axis

to the thrust axis, and this attitude is maintained constant in inertial space until engine cutoff. It is assumed that the nominal mission specifies the establishment of a lunar orbit at 185.2 km. Therefore, after thrust cutoff, the module coasts

TABLE 5

T/W ₀	t _t (sec)	θ _t (deg)	$\frac{\partial h_{AL}}{\partial t_t}$ (m/sec)	$\frac{\partial \Phi_0}{\partial t_t}$ (deg/sec)	$\frac{\partial h_{AL}}{\partial \theta_t}$ (m/deg)	$\frac{\frac{\partial \Phi_0}{\partial \theta_t}}{(\deg/\deg)}$	θh _{AL} ðt _b (m/sec)	θΦ0 θt b (deg/sec)	t _b
0.4	60	20.7	0	-0.3	19507	0.5	8336	1.5	340
0.4	100	17,5	-204.2	-0.32	20970	0	10741	2	350
0.4	100	13	-1143.	0.4	25146	2.5	8918	3.2	360
0.6	60	17	0	-0.2	22068	0.75	14246	2.35	220
0.6	100	11.8	-323.1	-0.4	23590	0	7699	2.55	230

to an apocynthion altitude of 185.2 km, at which time injection into a circular orbit is made. Two thrust-to-weight ratios have been investigated for a fuel specific impulse of $I_{sp} = 315$ sec, and the results are presented in Fig. 49. The ascent range angle Φ_0 , range angle measured from liftoff to orbit injection is shown as a function of tilt time with burning time as a parameter. Also noted in the figure are the acceptable limits of tilt time as determined from trajectory sensitivities. Sensitivities are determined by assuming errors of 1 second in tilt time $(t_{\scriptscriptstyle +})$ and burning time t_h plus 1° in θ_t (inertial thrust or pitch attitude), and with out-of-plane maneuvers not being considered. These errors are considered representative. The areas of decreasing, minimum, and rapidly increasing sensitivities for the thrust-to-weight ratios are shown in

Typical sensitivities are listed in Table 5, where \mathbf{h}_{AL} = apocynthion altitude.

Conditions in the area of decreasing sensitivity result in a maximum rectangular dispersion area from the nominal point of 66.6 km in altitude and 222 km in range on arrival at apocynthion for the above-mentioned errors. This maximum dispersion rectangle is shown by the curve marked "limit" in Fig. 49. Note also the limited amount of range control as shown in Fig. 49. For both values of T/W_0 , the range angle Φ_0 can be varied from 40 to 70 degrees. As the tilt time is prolonged, the ΔV requirements increase, as can be seen in Table 6. Compared to guided ascents (Section C), the ΔV requirements increase by 60 to 90 m/sec. Also included in Table 6 is the required pitch attitude θ_{\star} .

As can be seen from the above discussion, lunar ascent utilizing this backup technique is feasible. However, for missions involving a lunar rendezvous, launch time tolerances are drastically reduced because of the restricted range control.

This implies that additional stored pitch programs, preferably with constant rates, be used to increase range control. These pitch programs can be generated with clocked potentiometers, and the backup technique is again found to be quite feasible.

The initial pitch angle (θ_{t0}) , pitch rate (θ_{t}) , and burning time t_{b} required to extend (Φ_{0}) to 180° are shown in Fig. 50. The pitch rate (θ_{t}) is held constant throughout the burning phase, with data presented for $T/W_{0} = 0.4$, $T/W_{0} = 0.7$ and $I_{sp} = 315$ sec.

Much of the data on lunar abort presented in this section is illustrative of the various techniques and representative of some present plans for lunar landing abort, rather than being of a parametric nature. The number of parameters is too large to be presented over all values of each trajectory variable. Practical limits on the variables are often prescribed by the available hardware at the time of the mission, and they

TABLE 6

		-		
T/W ₀	t _t (sec)	t _b (sec)	ΔV (m/sec)	θ _t (deg)
0.4	20	340	194.8	20.4
0.4	60	340	1962.9	20.7
0.4	100	340	200.2	20.4
0.4	20	350	1877.6	16.5
0.4	60	350	1941.6	17.0
0.4	100	350	2004.1	17.5
0.4	100	360	2276.3	13.0
0.6	20	220	1872.7	16.9
0.6	60	220	1910.2	17.0
0.6	100	220	1923.6	16.3
0.6	20	230	1851.4	8.3
0.6	60	230	1881.8	11.3
0.6	100	230	1929.1	11.8

can be further restricted by the choice of abort technique as was illustrated in this section.

F. REFERENCES

- Orbital Flight Handbook, ER 12684, Martin Company, Space Systems Division (Baltimore), 1963.
- Schrader, C. D., "Lunar and Planetary Soft Landings by Means of Gas-Filled Balloons," Technical Paper 2480-62, ARS Lunar Missions Meeting, 17 to 19 July 1962.
- Lang, H. A., "Lunar Instrument Carrier--Landing Factors," Rand Corporation Report RM-1725, 4 June 1956.
- 4. Rinehart, J. S., "Stresses Associated with Lunar Landings," J. British Interplanetary Society, Vol. 17, 1960, pp 431 to 436.
- "Proceedings of the Lunar and Planetary Exploration Colloquium," Vol. III, No. 1, 15 May 1962, p 75.
- deFries, P. J., "Analysis of Error Progression in Terminal Guidance for Lunar Landing," NASA TN D-605, July 1961.
- 7. Wrobel, J. R., and Breshears, R. R.,
 "Lunar Landing Vehicle Propulsion Requirements," Paper No. 1121-60, ARS Semi-Annual
 Meeting, 9 to 12 May 1960.
- 8. Mason, M., and Brainin, S. M., "Descent Trajectory Optimization for Soft Lunar Landings," IAS Paper No. 62-11, presented at the IAS 30th Annual Meeting, New York, 22 to 24 January 1962.
- 9. Cheng, R. K., and Pfeffer, I., "A Terminal Guidance System for Soft Lunar Landing," Technical Paper 1912-61, ARS Guidance Control and Navigation Conference, 7 to 9 August 1961.
- Markson, E., Bryant, J., and Bergsten, F., "Simulation of Manned Lunar Landing," Paper No. 2482-62, ARS Lunar Missions Meeting, 17 to 19 July 1962.
- 11. Berman, L. J., "Optimum Soft Landing Trajectories, Part 1, Analysis," MIT, AFOSR 519, March 1961.

- 12. Lawden, D. F., "Dynamic Problems of Interplanetary Flight," Aeronautical Quarterly, Vol. 6, 1955, pp 165 to 180.
- 13. Fried, B. D., "Trajectory Optimization for Powered Flight in Two or Three Dimensions," Space Technology, J. Wiley and Sons, Inc., 1959.
- 14. Perkins, C. W., "Optimum Retro-Thrust Trajectories," M. S. Thesis, MIT, June 1960,
- 15. Markson, E. E., "Thrust Programming for Terminal Maneuvers in Space," Proceedings of IAS Meeting on Aerospace Support and Operations, Orlando, Florida, 4 to 6 December 1961.
- Jazwinski, A. H., "Integration of Two-Point Boundary Value Problems with One Unknown Boundary," A-PD-113, General Dynamics/ Astronautics, 17 May 1962.
- 17. Jurovics, S. A., and McIntyre, J. E., "The Adjoint Method and Its Applications to Trajectory Optimization," ARS Journal, 32 (9), September 1962, pp 1354 to 1358.
- 18. Jazwinski, A. H., "New Approach to Variational Problems in Trajectory Optimization," ER 12700, Martin Company Space Systems Division (Baltimore), November 1962.
- 19. Tyler, J., and Foy, W., "Application of Optimal Control Theory to a Lunar Landing Vehicle," RM-230, Martin Company (Baltimore), August 1962.
- 20. Culler, G. J., and Fried, B. D., "Universal Gravity Turn Trajectories," J. of Applied Physics, Vol. 28, No. 6, June 1957, pp 672 to 676.
- 21. Jensen, J., Townsend, G., Kork, J., and Kraft, D., "Design Guide to Orbital Flight," McGraw-Hill, 1962.
- 22. Bartos, G., and Greenberg, A., "Abort Problems of the Lunar Landing Mission," ARS Preprint 2490-62.
- 23. Kelly, T. J., "Abort Considerations for Manned Lunar Missions," ARS Preprint 2478-62.

ILLUSTRATIONS



LIST OF ILLUSTRATIONS

Figure	Title	Page
1	Lunar Impact Velocity Without Rocket Braking	VIII-39
2	Target Penetration for Sectional Density, W/D ² = 1	VIII-40
3	Maximum Resistive Pressure Between Payload and Rock Target	VIII-41
4	Vertical Descent	VIII-42
5	Vertical Descent	VIII-43
6	Vertical Descent	VIII-44
7	Vertical Descent	VIII-45
8	Variation of Optimum Thrust/Mass Ratio with Propulsion-System Mass Parameter	VIII-46
9	Effect of Off-Optimum Thrust Level on Payload Soft-Landed with Zero Touchdown Velocity	VIII-46
10	Braking Trajectory 1	VIII-47
11	Braking Trajectory 2	VIII-48
12	Braking Trajectory 3	VIII-49
13	Braking Trajectory 4	VIII-50
14	Braking Trajectory 5	VIII-51
15	Typical Lunar Landing Trajectory	VIII-52
16	Characteristic Velocity Requirement for Braking Phase	VIII-53
17	Characteristic Velocity Requirement for Braking Phase of Synchronous Orbit Descent	VIII-54
18	Characteristic Velocity Requirement for	VIII-55

LIST OF ILLUSTRATIONS (continued)

J	rigure	Title	Page
	19	Optimum Braking Phase of Lunar Landing	VIII-56
	20a	Requirements for Injection into an 80-Hour Return-Time Transearth Trajectory	VIII-57
	20b	Transearth Trajectory Injection Requirements	VIII-58
	21	Ascent Trajectory 1	VIII-59
	22	Ascent Trajectory 2	VIII-60
	23	Ascent Trajectory 3	VIII-61
	24	Ascent Trajectory 4	VIII-62
	25	Ascent Trajectory 5	VIII-63
	26	Typical Lunar Ascent Trajectory	VIII-64
	27	Characteristic Velocity $\triangle V$ Required for Ascent to an 185.2-km Circular Orbit	VIII-65
	28	Excess $\triangle V$ Required Versus Launch Time Tolerance for Lunar Rendezvous	VIII-66
	29	Excess $\triangle V$ Required for Out-of-Plane Ascent	VIII-67
	30	In-Plane Rendezvous Techniques	VIII-68
	31	Lateral Rendezvous	VIII-69
	32	Typical Lunar Orbit Rendezvous Profile	VIII-70
	33	Horizontal Translation	VIII-71
	34	Minimum Propellant for Translation While Hovering at Constant Altitude	VIII-72
	35	Total △V Required to Abort from a Lunar Landing Coast Trajectory	VIII-73
	36	Safe Abort Window (Non-Impact Trajectories)	VIII-74

LIST OF ILLUSTRATIONS (continued)

Figure	Title	Page
37	ΔV Required to Abort and Rendezvous at 92.6 km (50 N Mi) from a Landing Coast Trajectory	VIII-75
38	ΔV Required to Abort and Rendezvous at 185.2 km (100 N Mi) from a Landing Coast Trajectory	VIII-76
39	ΔV Required to Abort and Rendezvous at 370.4 km (200 N Mi) from a Landing Coast Trajectory	VIII-77
40	Total $\triangle V$ Required for Perfect Rendezvous Versus Abort Altitude	VIII-78
41	ΔV Required to Abort and Rendezvous at 185.2 km (100 N Mi) from a Landing Coast Trajectory	VIII-79
42	Down Range Angle Required for a Lunar Rendezvous from an Abort Along a Landing Coast Trajectory	VIII-80
43	Down Range Angle Required for a Lunar Rendezvous from an Abort Along a Lunar Landing Coast Trajectory	VIII-81
44	Down Range Angle Required for a Lunar Rendezvous from an Abort Along a Lunar Landing Coast Trajectory	VIII-82
45	Slant Range Versus Altitude of Landing Coast Trajectory	VIII-83
46	Velocity $\triangle V$ Required to Abort and Rendezvous from Synchronous Orbit Descent	VIII-84
47	Landing Safety Boundaries	VIII-85
48	Maximum Landing Site Out-of-Plane Range for Aborted Missions	VIII-86
49	Emergency Backup Guidance Capability	VIII-87
50	Pitch Rate and Initial Pitch Angle Required for Range Extension	VIII-88



3.2 3.1 3.0 3.0 3.0 2.9 2.8 2.7 2.6 2.5 40 50 60 70 80 90

Fig. 1. Lunar Impact Velocity Without Rocket Braking

Earth-to Moon Transit Time (hr)

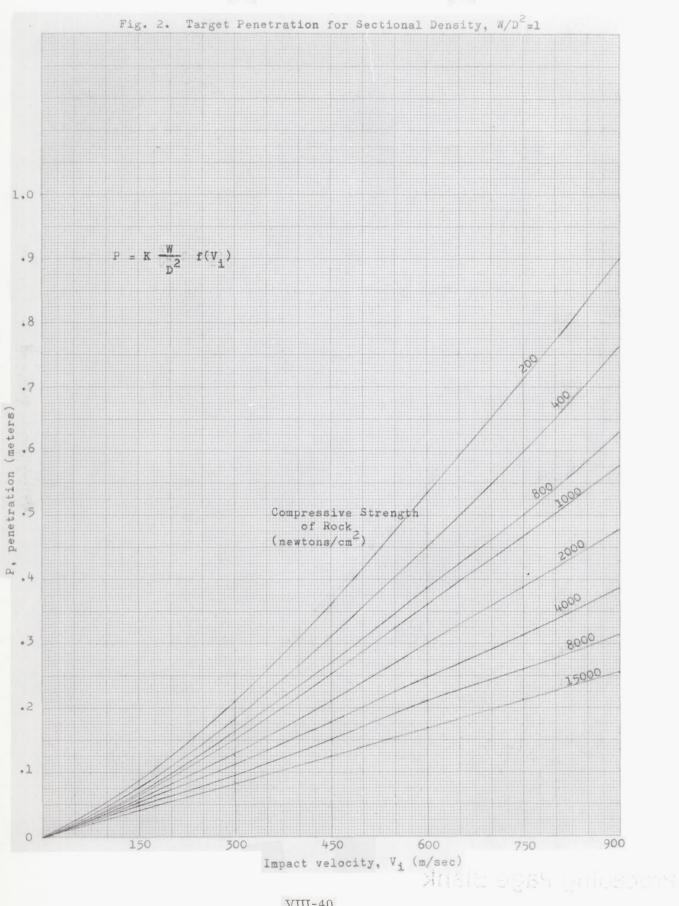
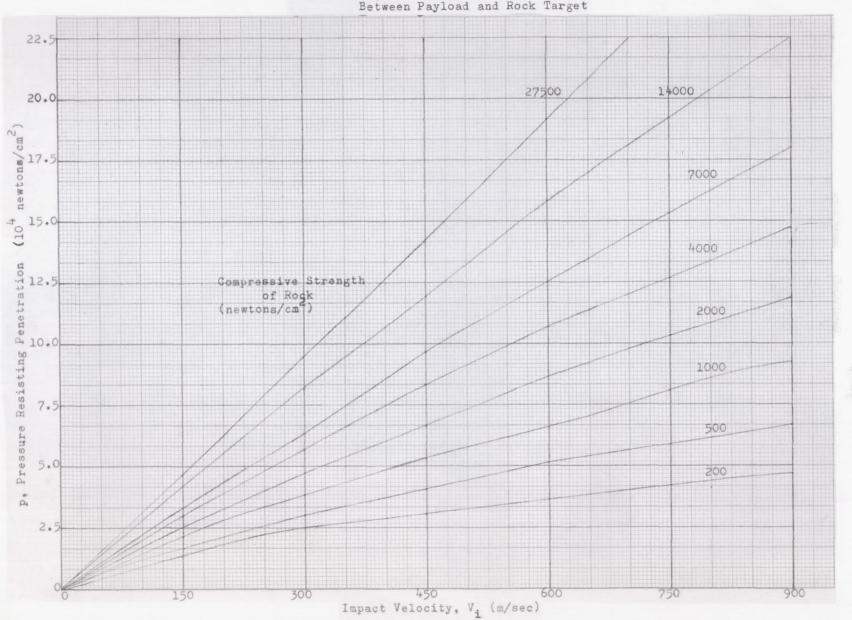
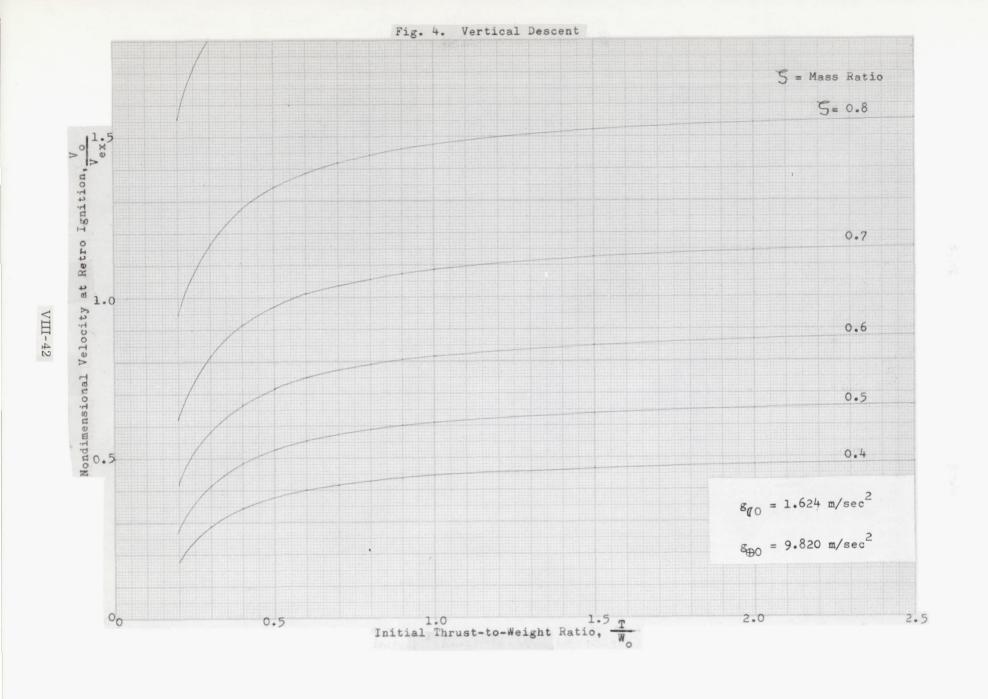
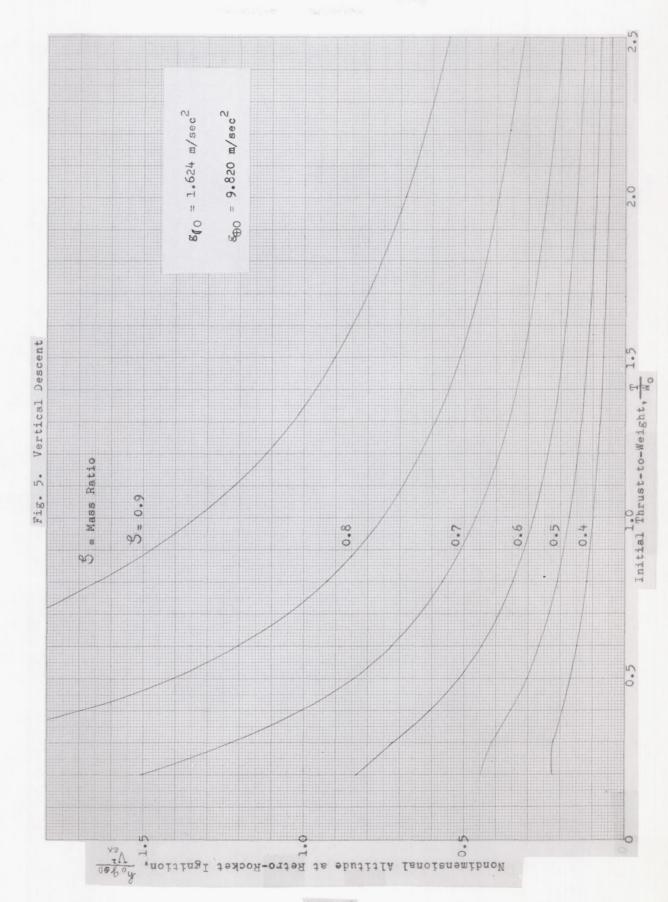


Fig. 3. Maximum Resistive Pressure
Between Payload and Rock Target







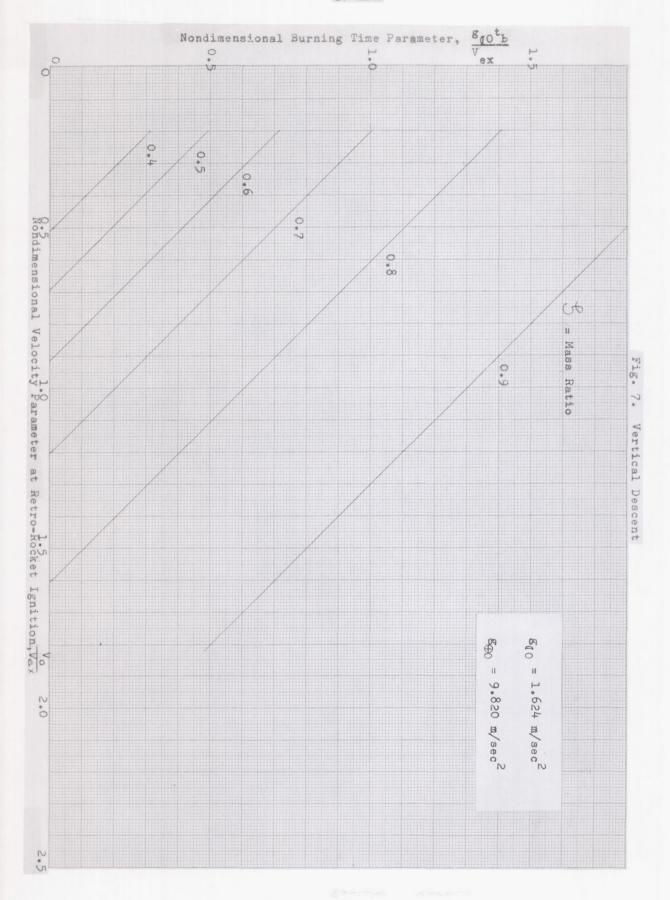
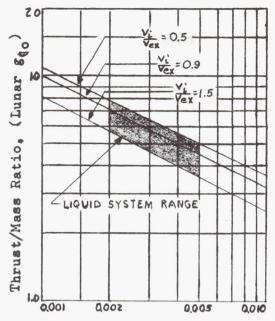


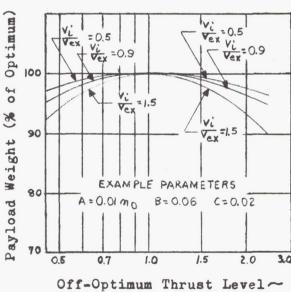
Fig. 8. Variation of optimum thrust/mass ratio with propulsion-system mass parameter



Propulsion System Mass Parameter ~

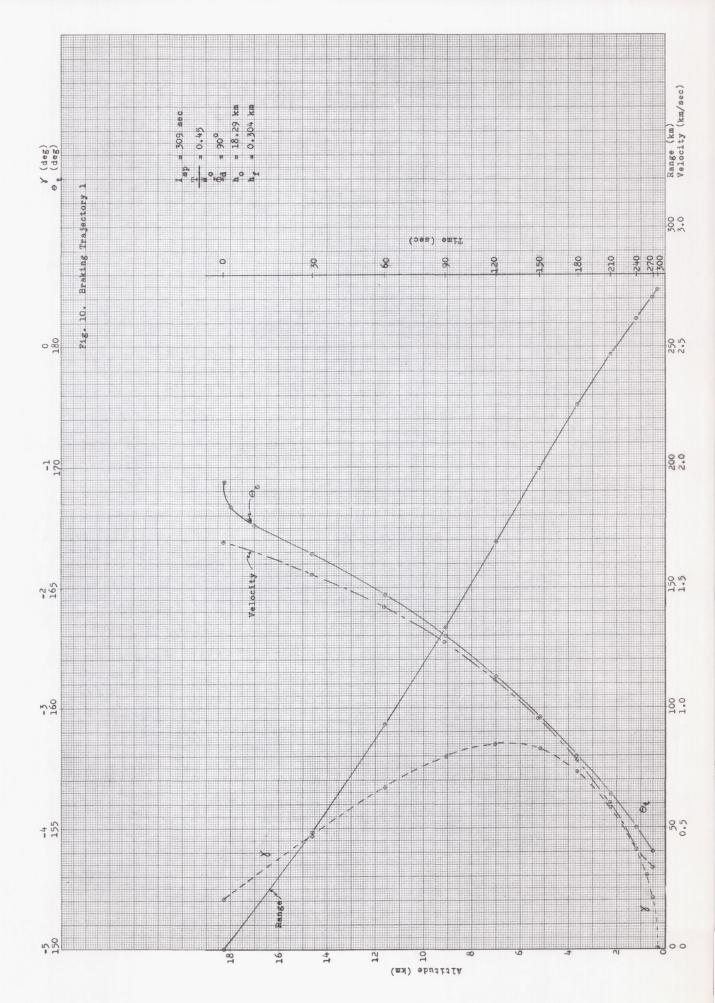
$$\frac{g_{00} v_{ex}}{(1 + B)}$$

Fig. 9. Effect of offoptimum thrust level
on payload soft-landed
with zero touchdown
velocity

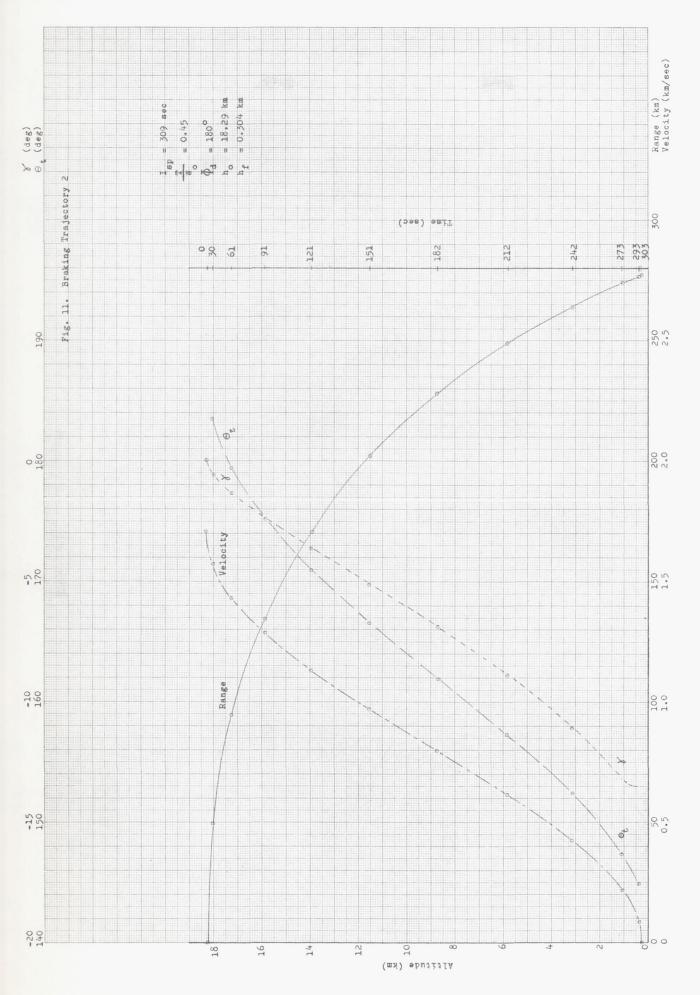


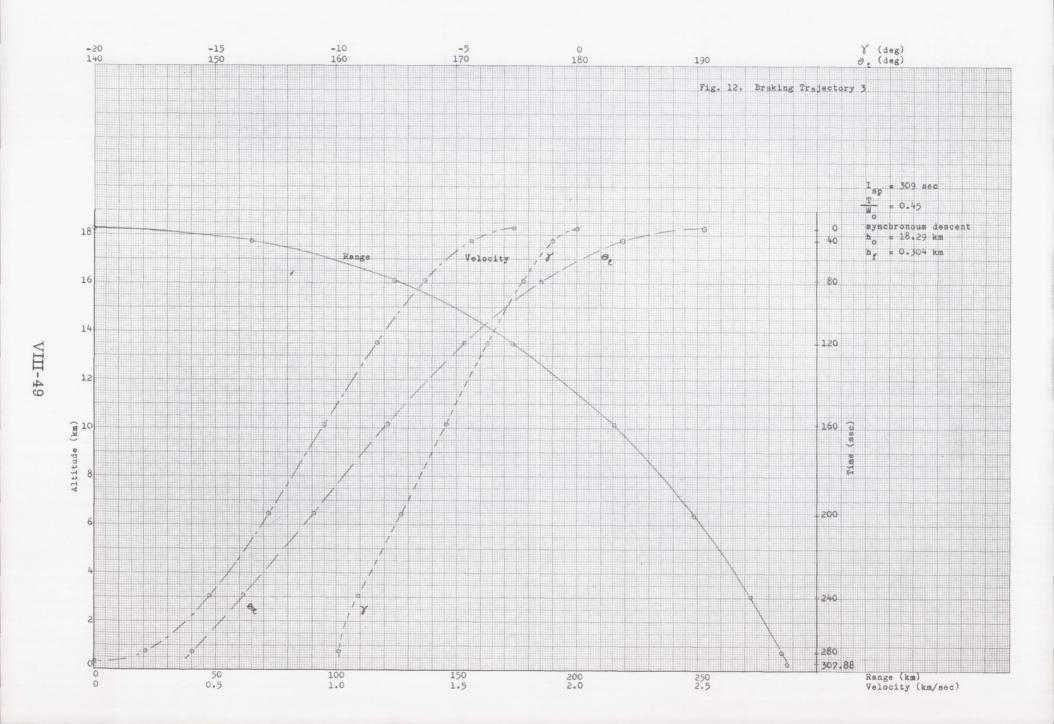
Off-Optimum Thrust Level $(T/W_0)/(T/W_0)$ opt.

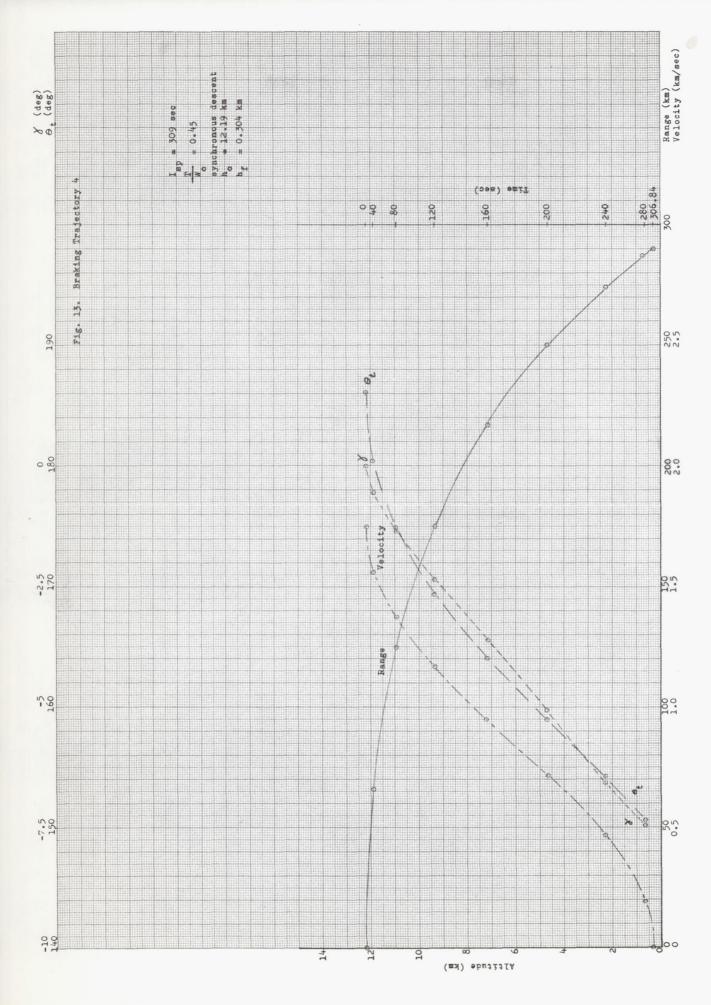
Data For Vertical Descent With a Single Burning Phase.



VIII-47



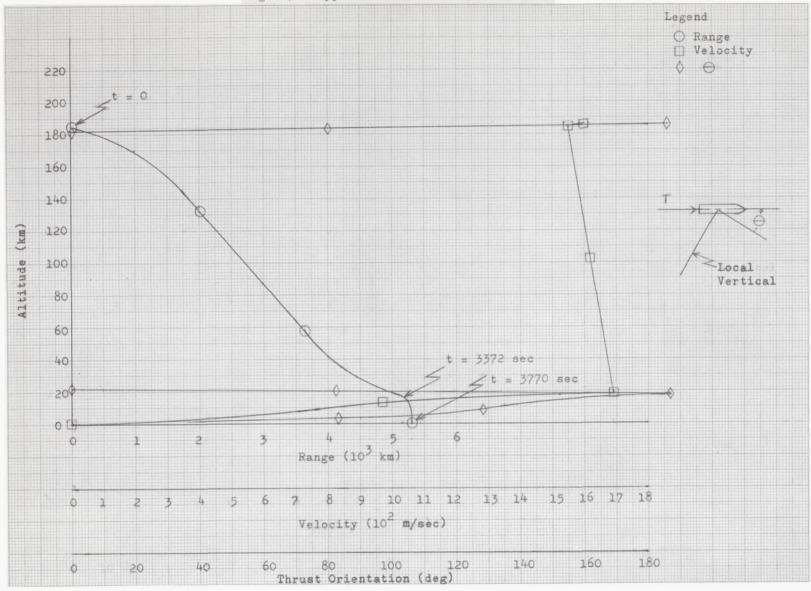


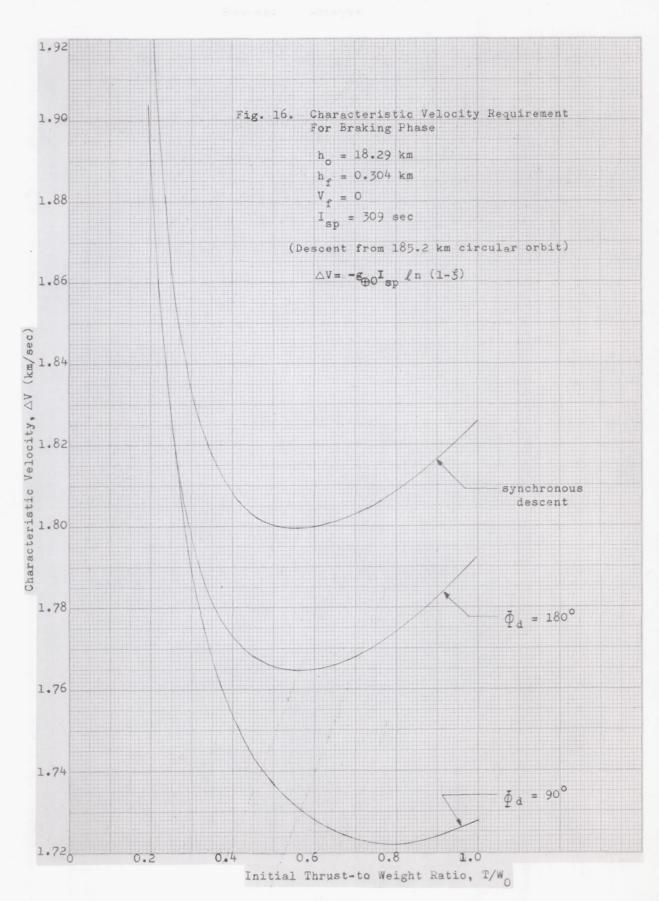


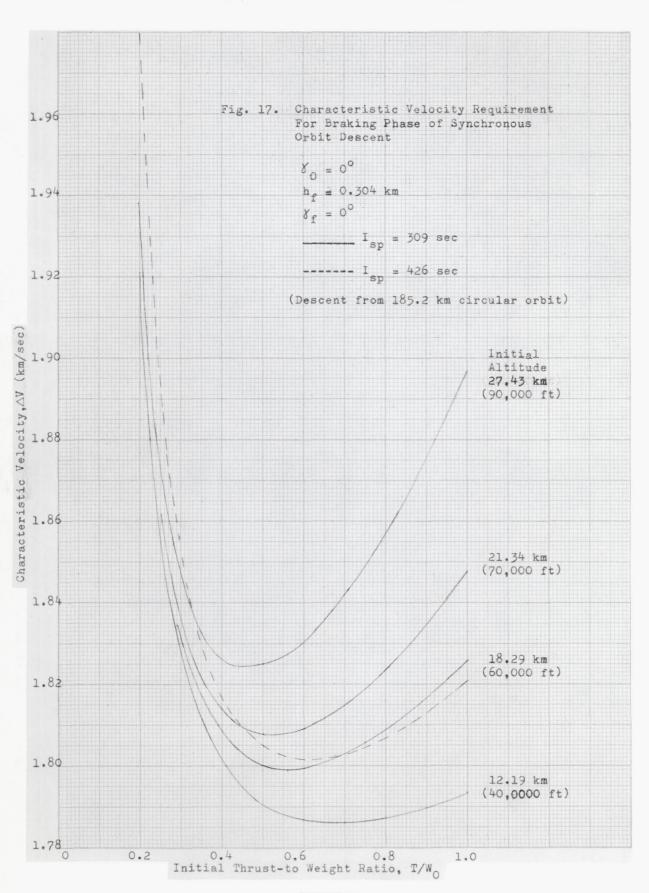
γ (deg) Θ (deg)

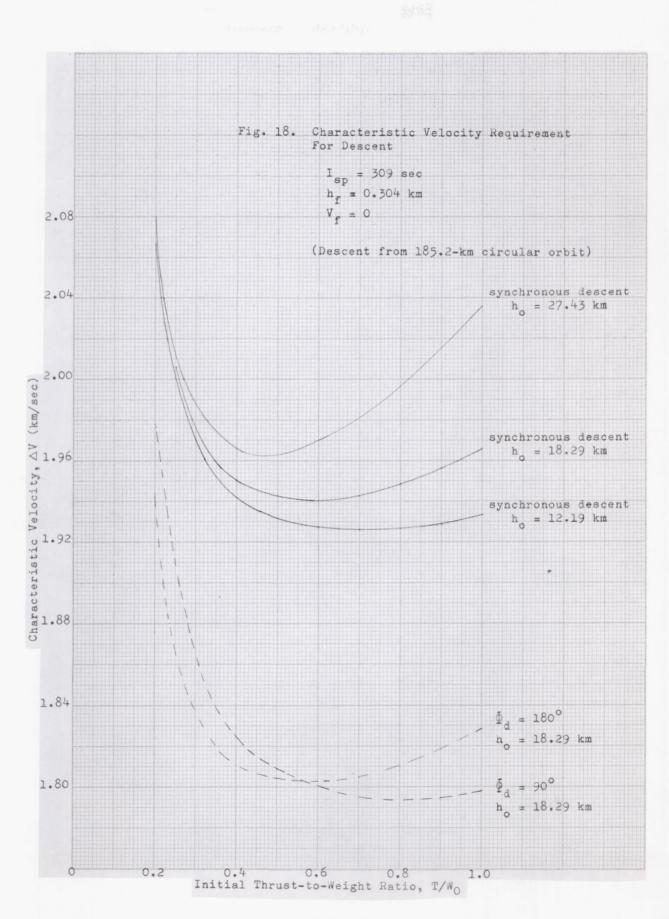
-20 -15 -10 -5

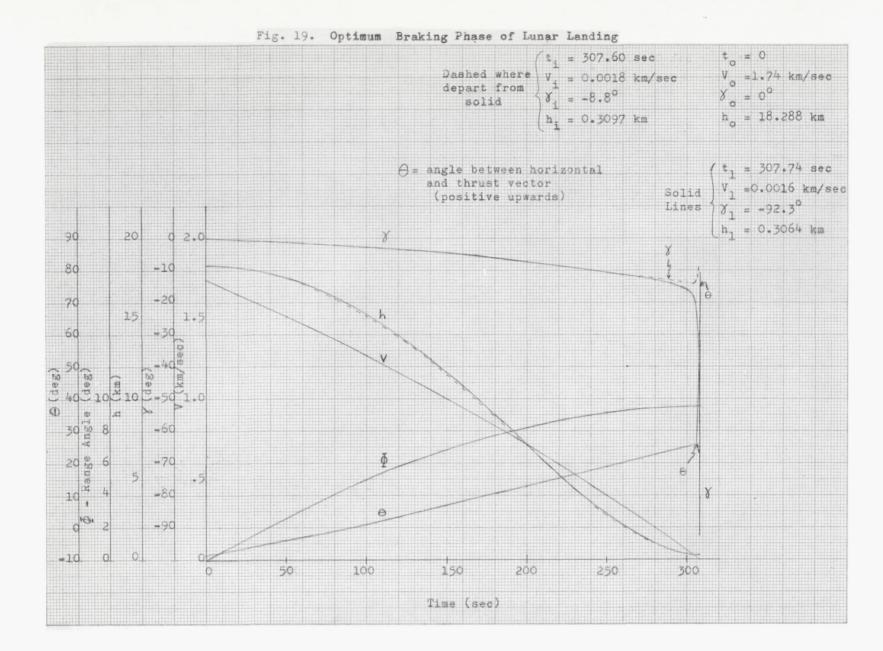
Fig. 15. Typical Lunar Landing Trajectory











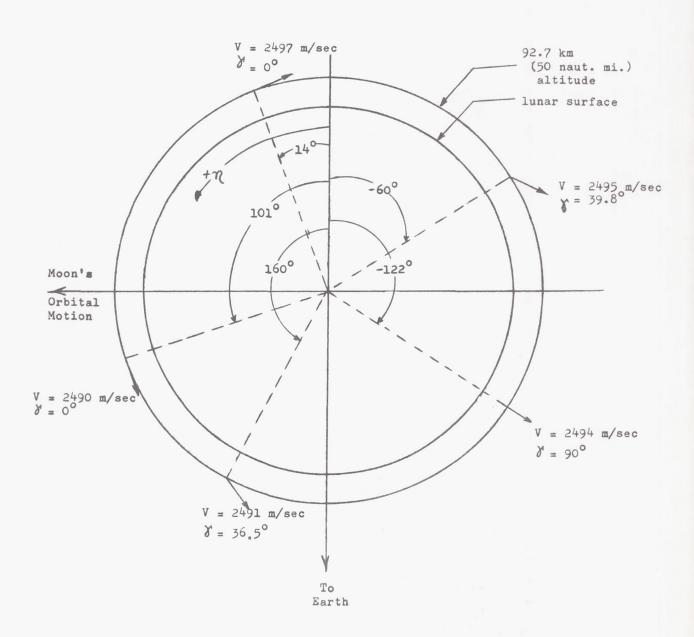
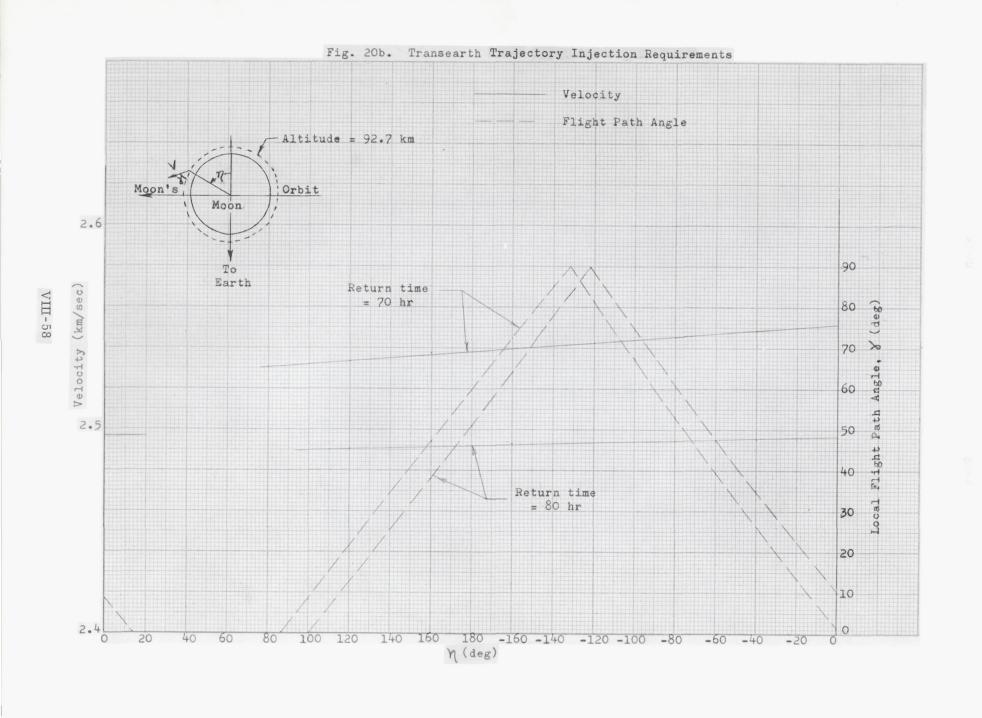
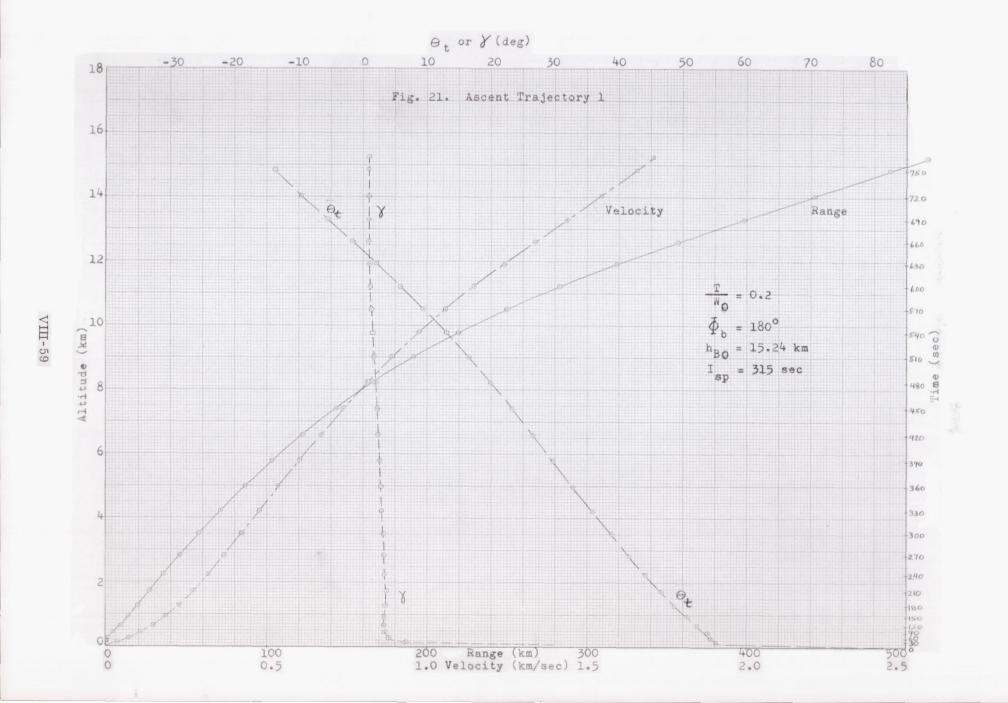
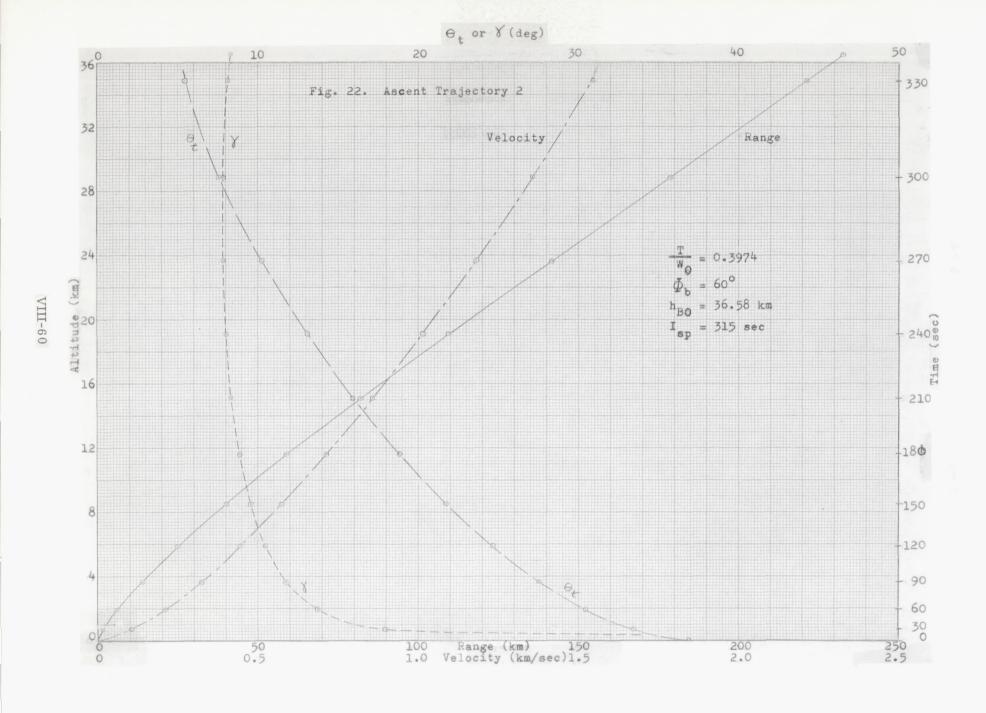
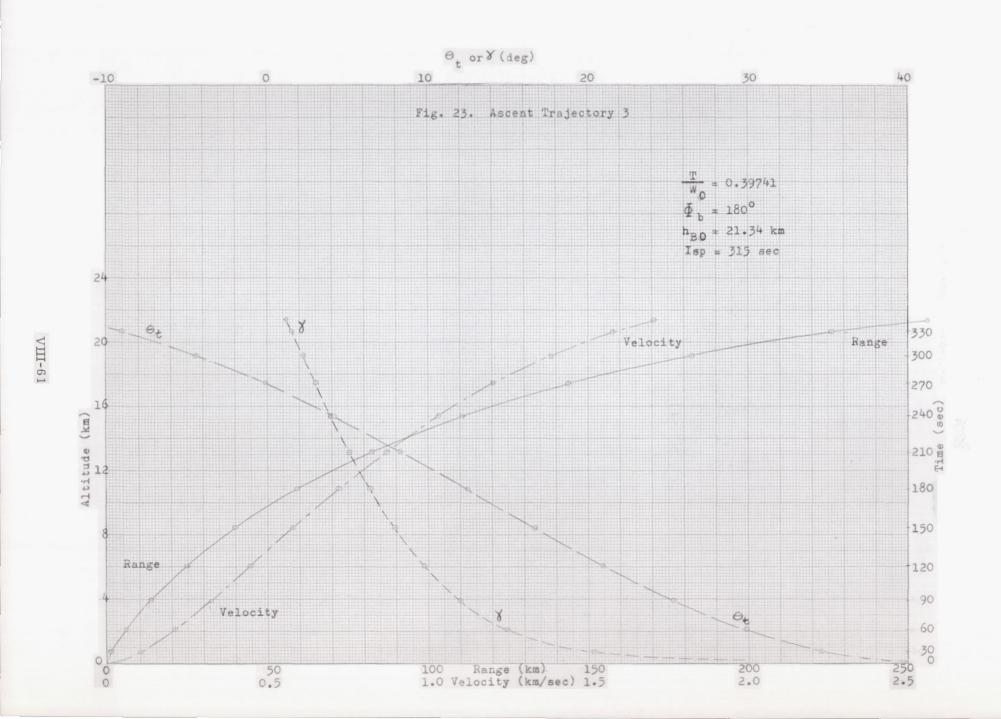


Fig. 20a. Requirements for Injection Into An 80-Hour Return-Time Trans-Earth Trajectory









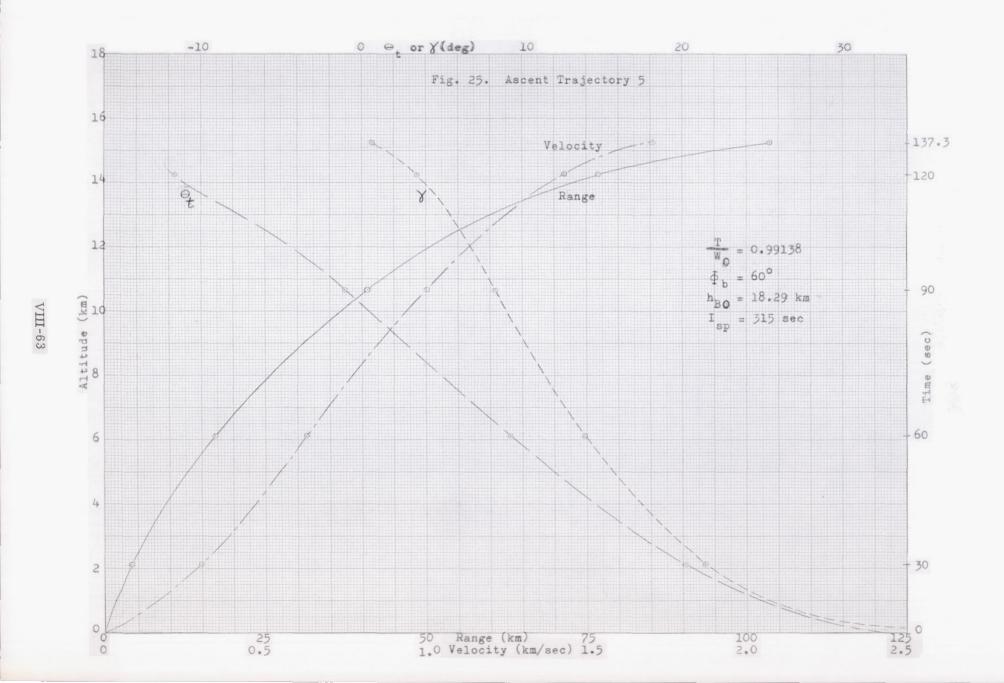


Fig. 26. Typical Lunar Ascent Trajectory

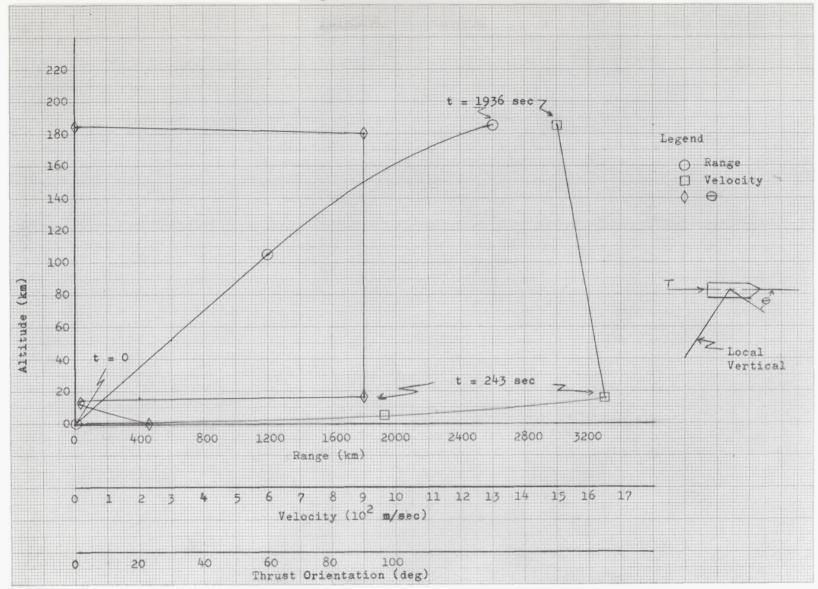


Fig. 27. Characteristic Velocity ΔV Required For Ascent to an 185.2-km Circular Orbit

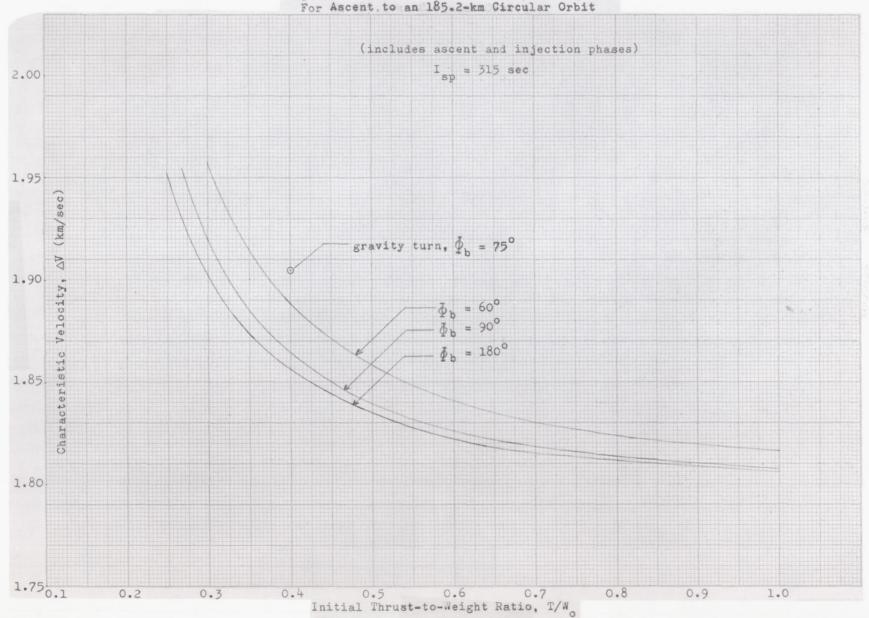
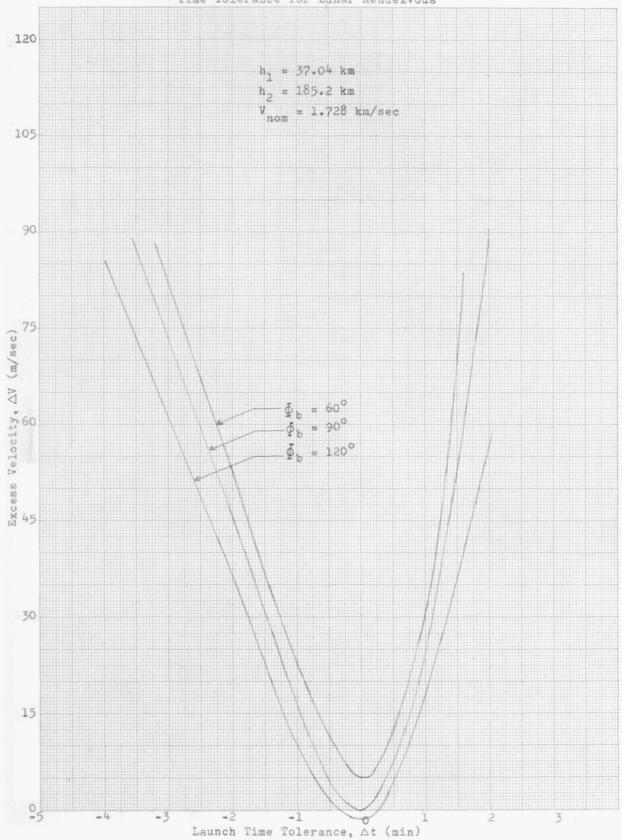


Fig. 28. Excess ΔV Required Versus Launch Time Tolerance for Lunar Rendezvous



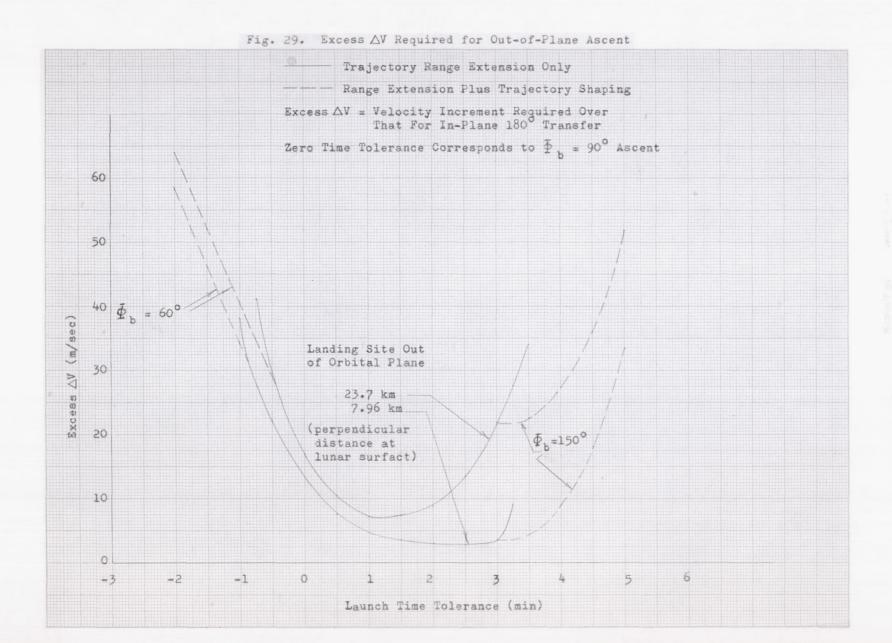
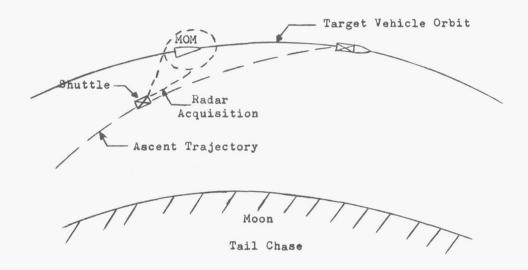


Fig. 30. In-Plane Rendezvous Techniques



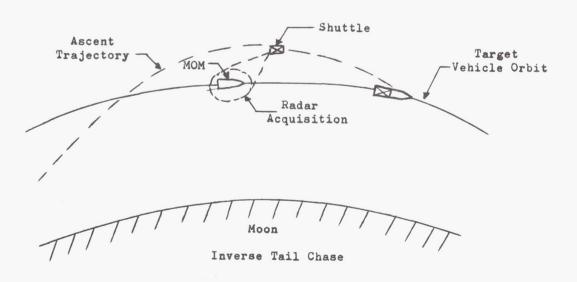


Fig. 31. Lateral Rendezvous

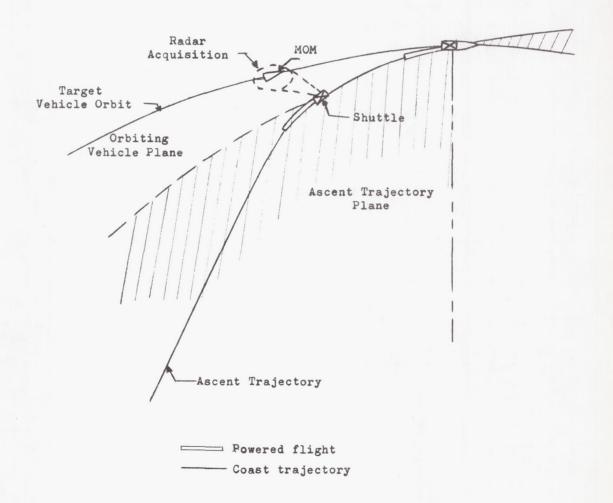
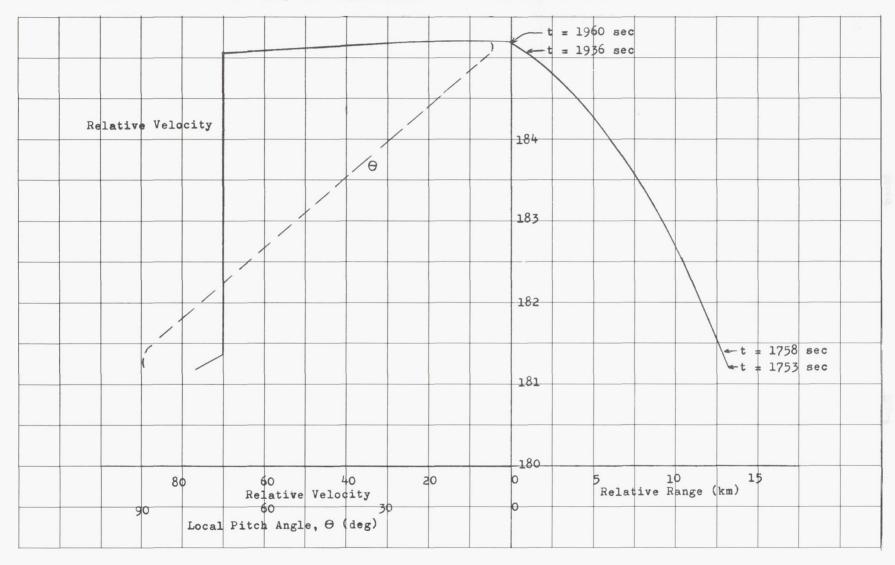
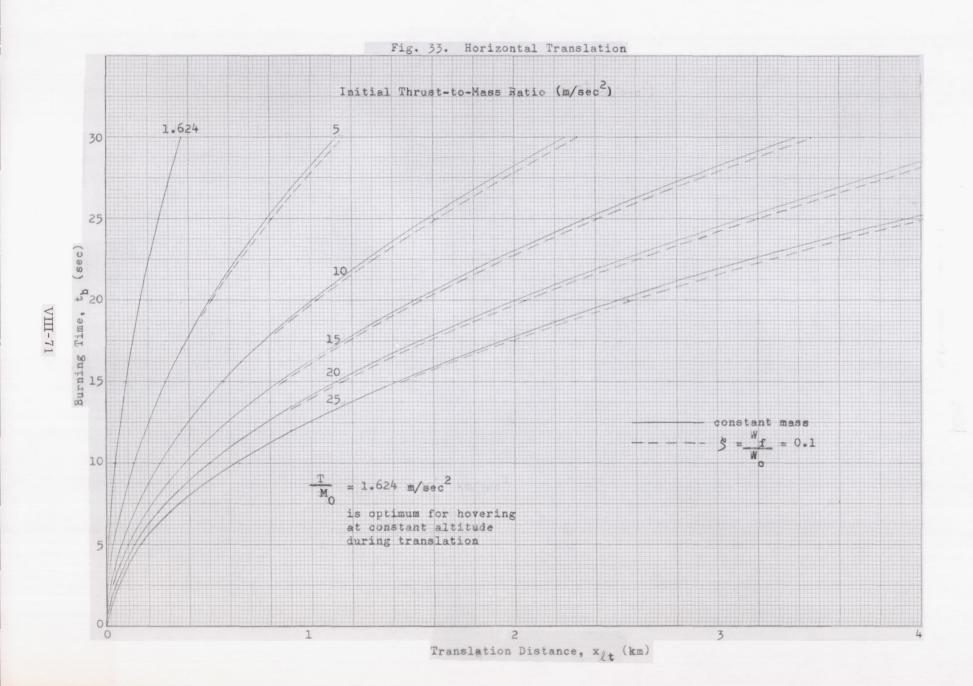
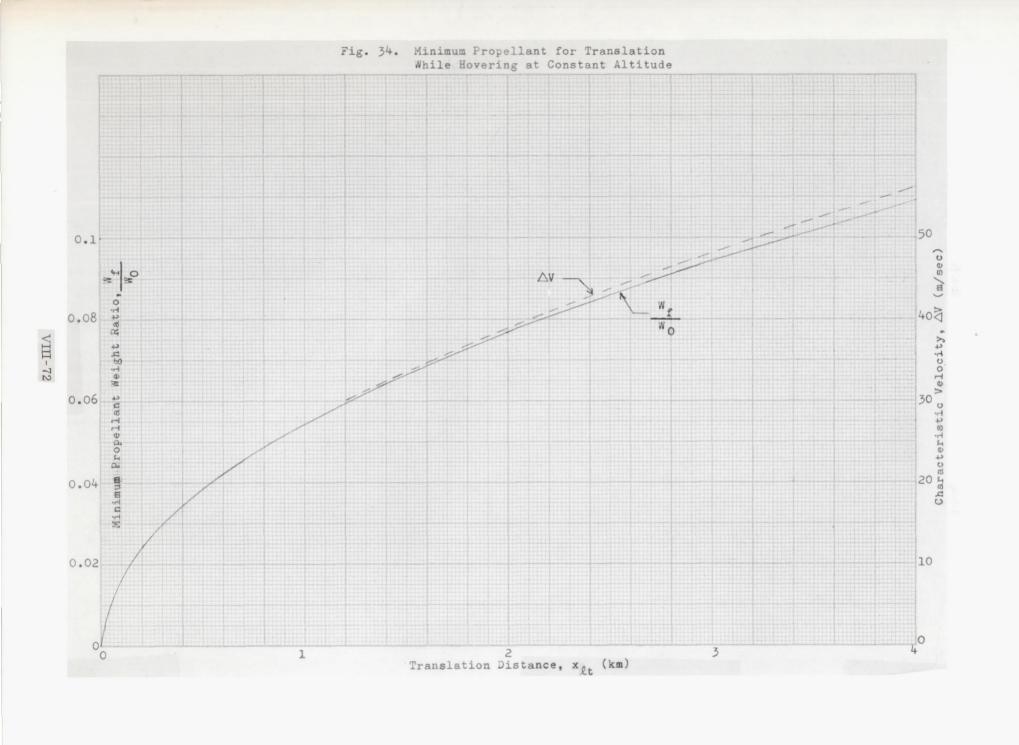
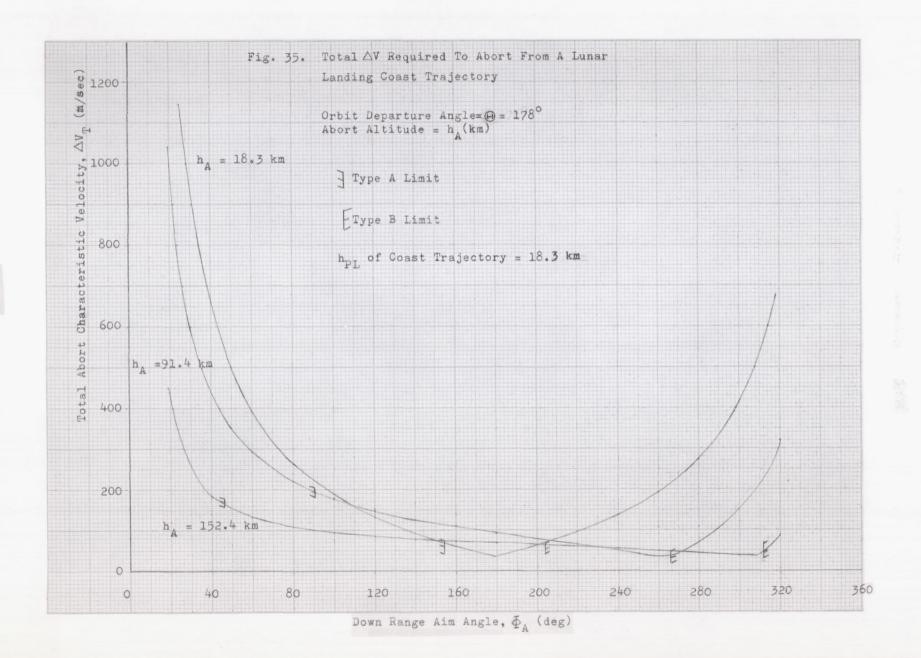


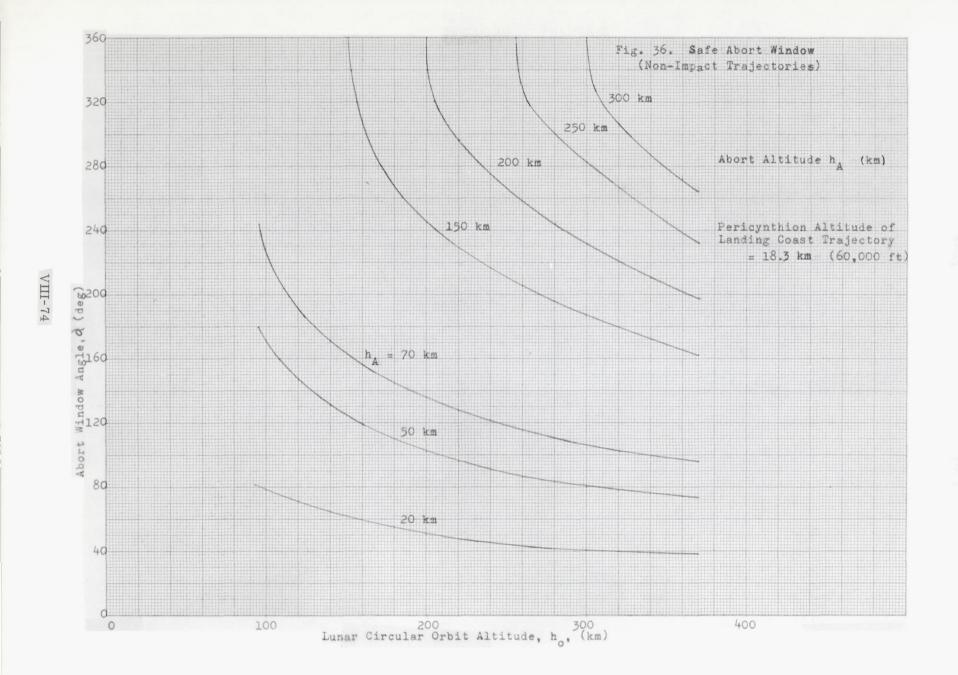
Fig. 32. Typical Lunar Orbit Rendezvous Profile

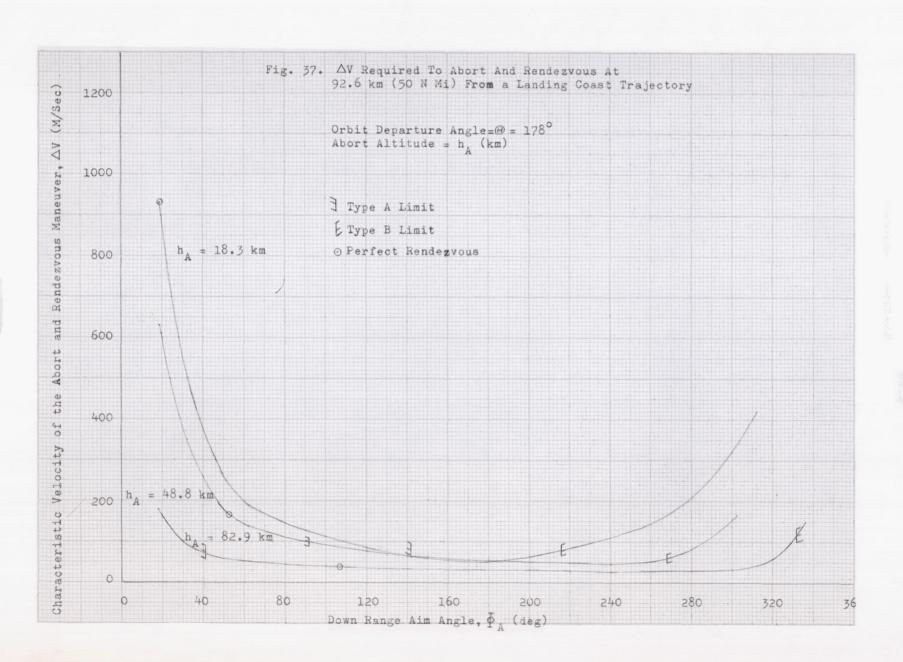


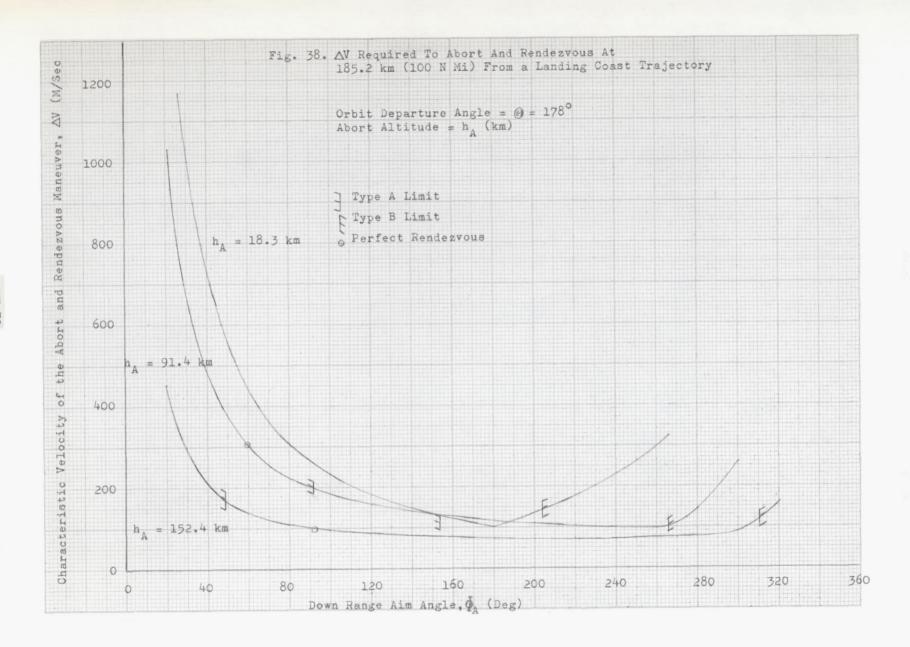


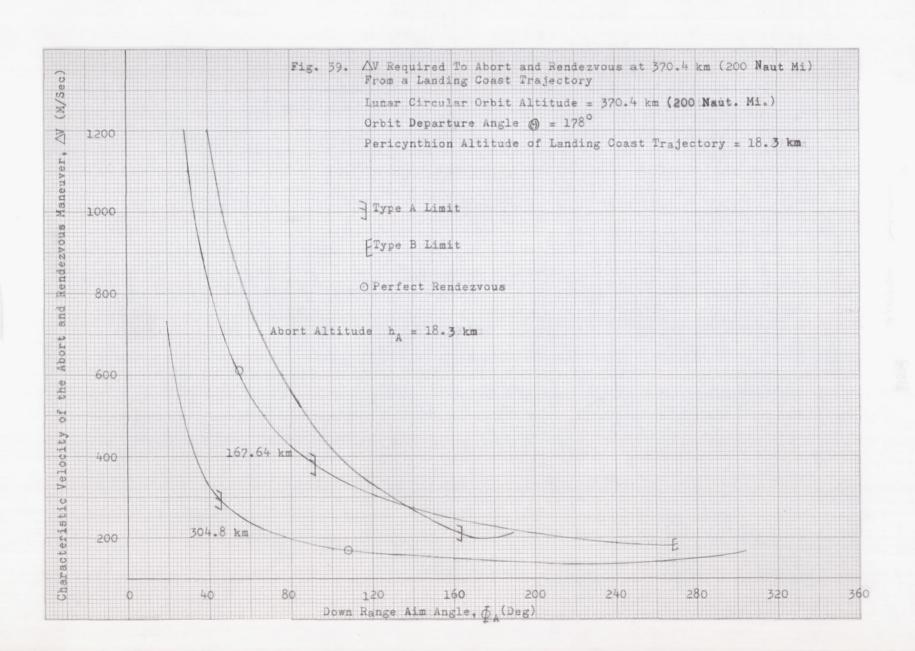


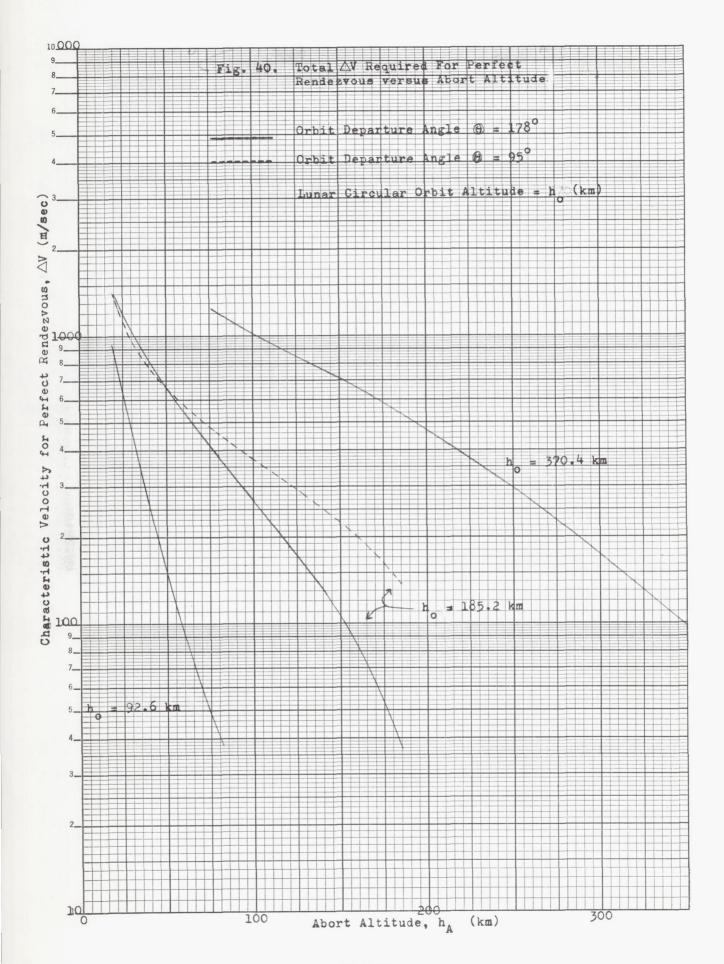


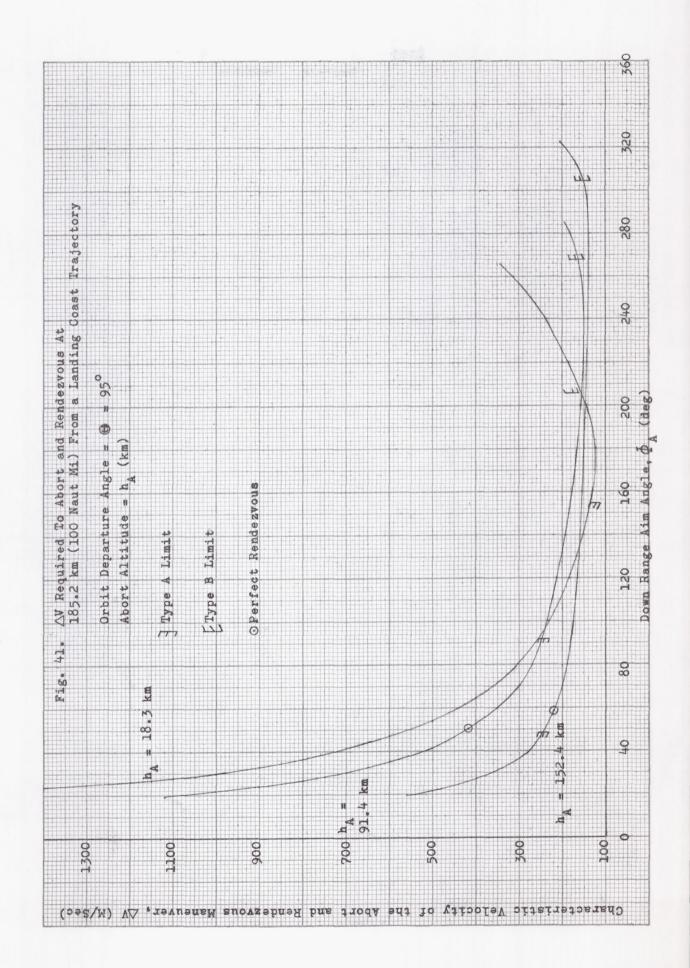


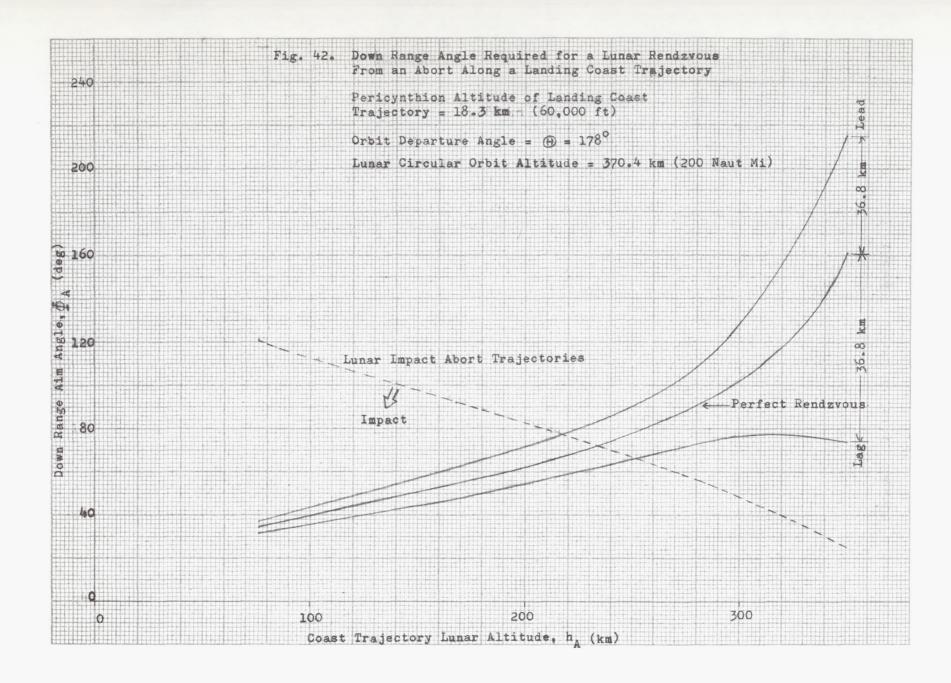


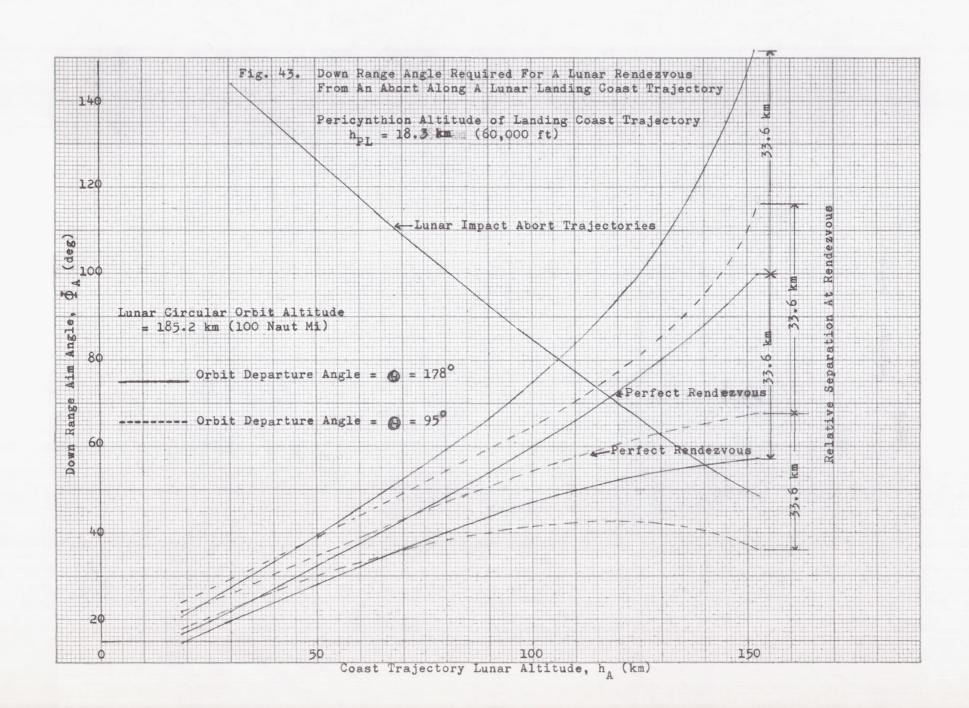


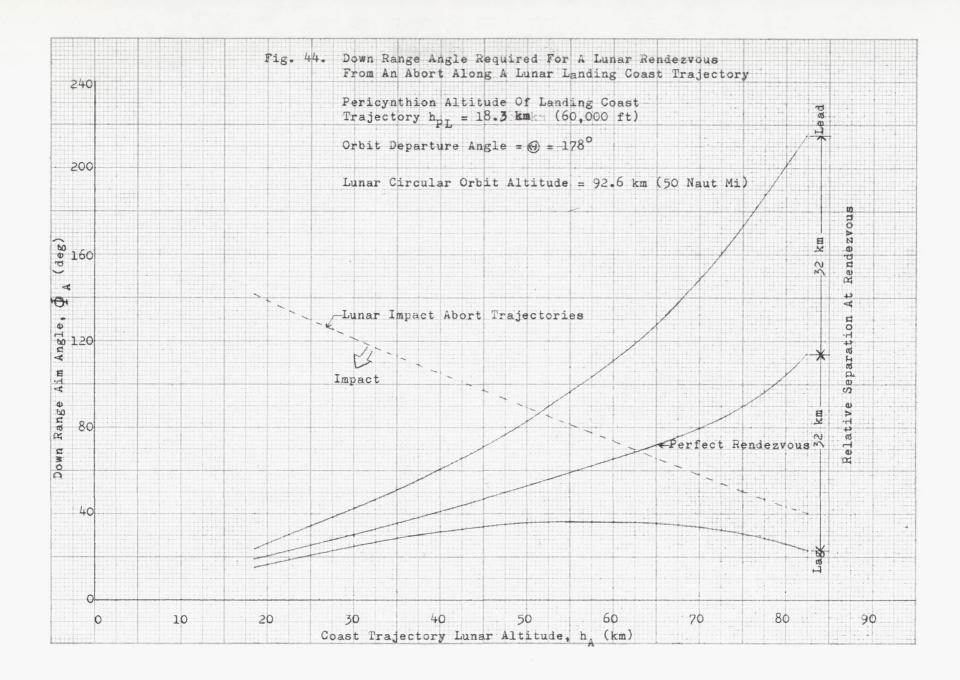


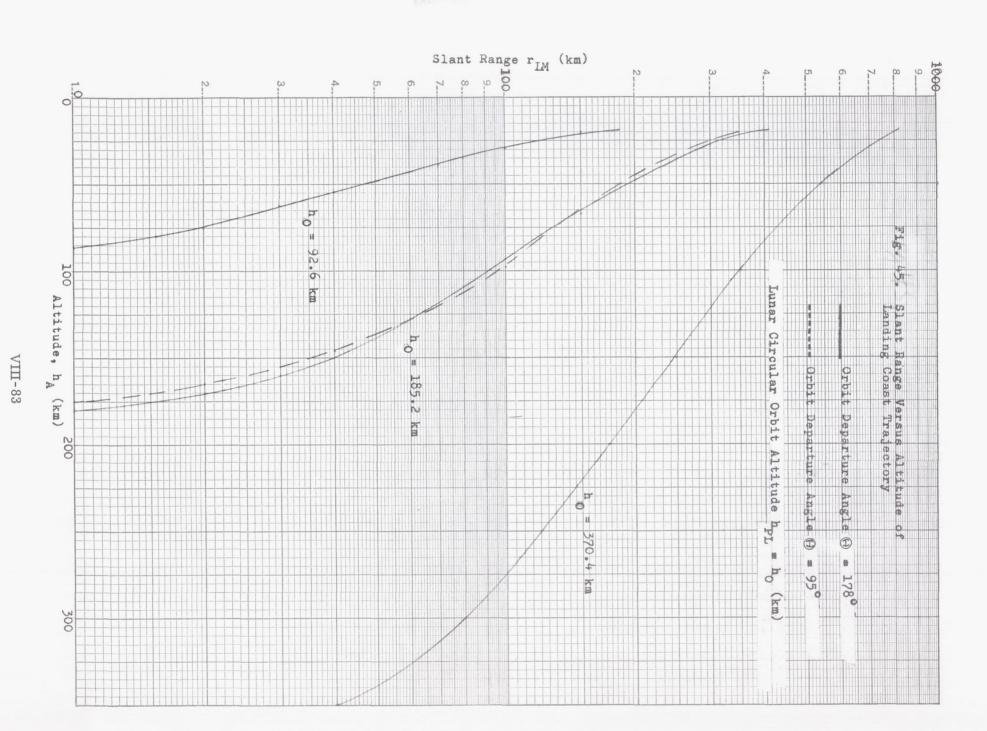


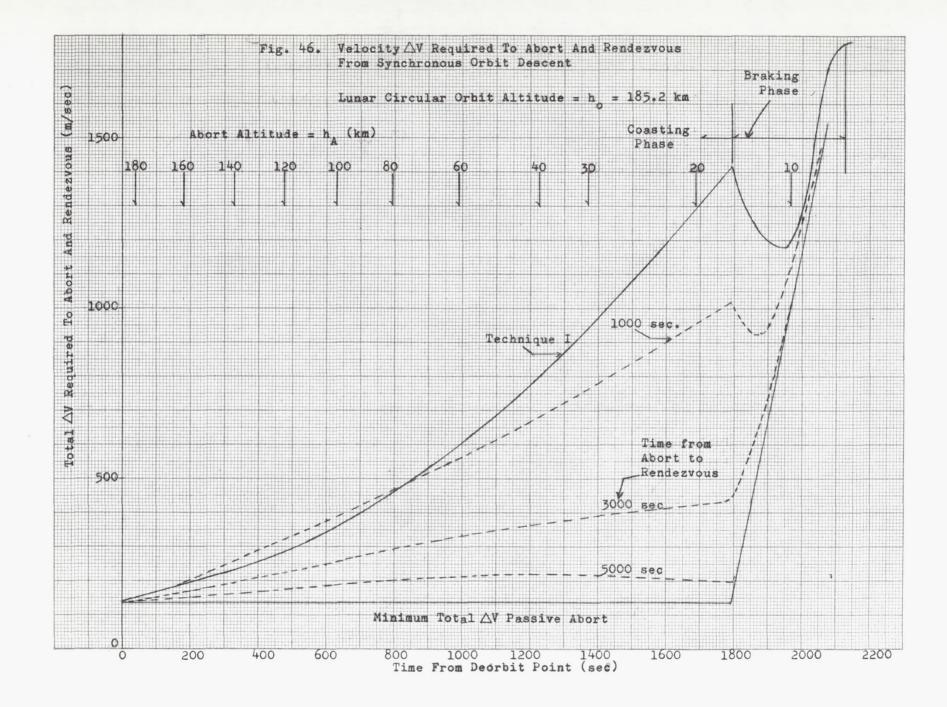


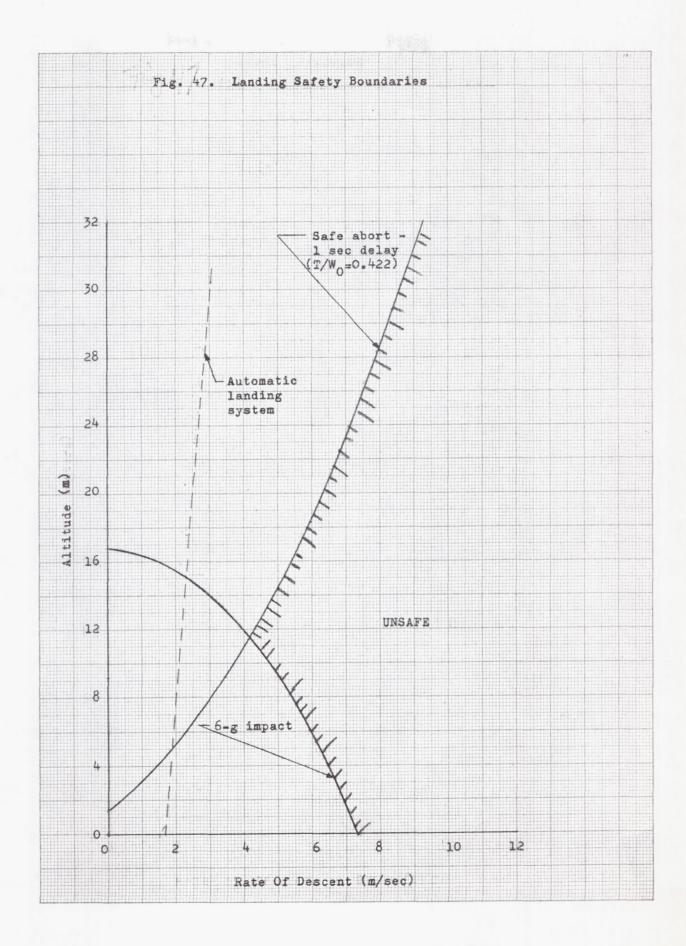


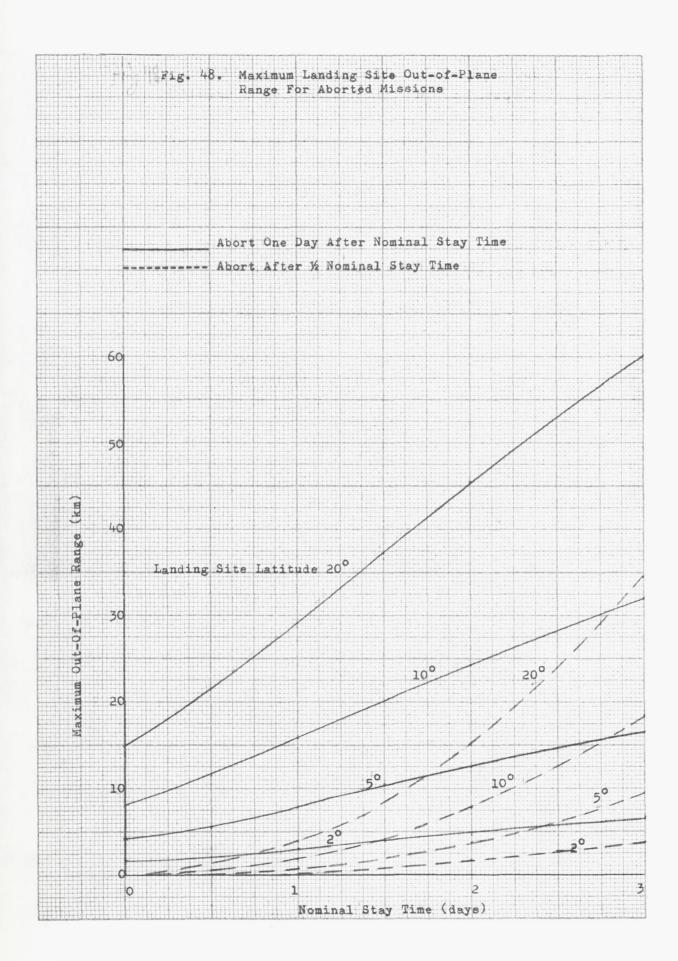


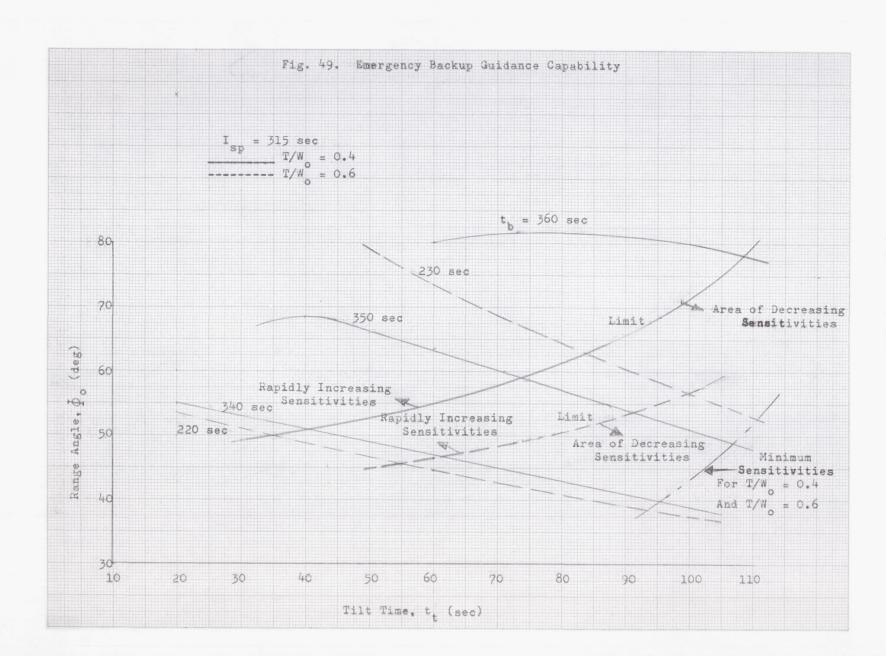


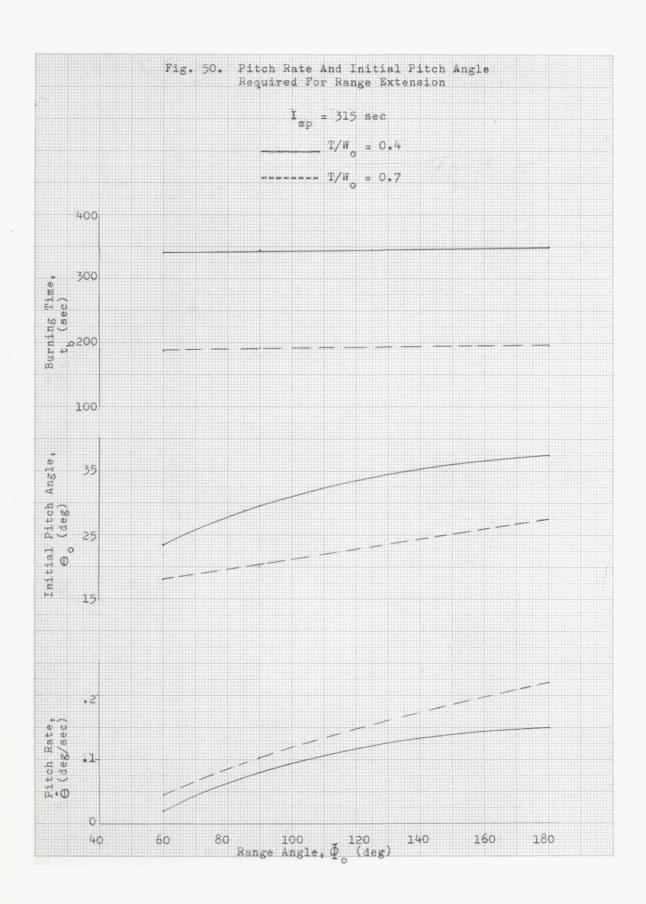












CHAPTER IX

MOON-TO-EARTH TRANSFER

Prepared by:

F. Santora, R. Salinger and D. Kuhn Martin Company (Baltimore) Aerospace Mechanics Department March 1963

		Page
Α.	Injection Requirements for Moon-to-Earth Trajectories	IX-1
В.	Midcourse Guidance and Energy Requirements	IX-7
	Illustrations	IX-9
	List of Illustrations	IX-11

IX. MOON-TO-EARTH TRANSFER

Chapter V focused attention on the techniques for ascending from the earth's surface to the translunar injection point where a ballistic trajectory that satisfies various mission constraints is established. Chapter VI then presented a catalogue of circumlunar trajectory data that specified the injection condition for the ballistic trajectory around the moon with a return to the vicinity of the earth. Another class of translunar trajectories which do not return ballistically to the vicinity of the earth, namely approach trajectories (Chapter IV, Section A), is catalogued in Subsection A-2 of this chapter.

When the objective of the mission is accomplished, whether it be exploration, surveillance, or logistics, etc., it may be desirable to return the vehicle to earth. (This requirement is mandatory if the mission is manned.) Therefore, there are also injection requirements at the moon that must be satisfied if the spacecraft is to return to the vicinity of earth. Two techniques exist whereby these lunar injection conditions can be achieved. The first is a "direct departure technique" in which the spacecraft is boosted directly from the lunar surface to the transearth injection point, inferring lunar landing missions only. In the second technique, the vehicle is in a lunar parking orbit or establishes one prior to injection into a transearth trajectory--hence it is called the "orbital departure technique." Because of the limited data available for the first technique, and since orbital departure is more general, in that the direct departure technique can be regarded as a special case of the orbital departure technique, only the second technique is discussed in this chapter.

Transearth trajectory data is catalogued in Section A in the same manner as was the circumlunar data. It will be seen that the flight times back to earth are for the most part unrestricted, thereby easing the timing problem for returning to specific earth sites. This same transearth catalogue can also be interpreted as a translunar catalogue. The interpreted trajectory data represents the approach class of translunar trajectories. For this class of lunar trajectories, two major improvements over the circumlunar class are realized, namely:

- (1) A wider choice of translunar flight time is now available.
- (2) Any lunar site or feature is accessible for landing, surveillance or rendezvous purposes.

The use of the catalogue material for mission planning is demonstrated for transearth trajectories by the first sample mission in Chapter XI and for the interpreted translunar trajectories by the second sample mission in that chapter.

Transearth trajectory energy requirements for guidance are briefly discussed in Section B and they exhibit essentially the same trends as presented in Chapter VI, Section C. Since navigation, tracking, and guidance techniques for transearth and translunar trajectories are identical, the discussion in Chapter VI applies. However,

abort during the transearth phase is somewhat of a misnomer since the only action that can be taken is to maneuver to "speed up" the return or to change the transearth trajectory inclination to ensure arrival at a given earth landing site. The velocity impulse requirement to accomplish these two maneuvers separately is given in Chapter XI.

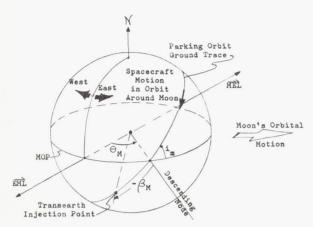
A. INJECTION REQUIREMENTS FOR MOON-TO-EARTH TRAJECTORIES

The data given in this chapter presents the injection requirements for returning from the moon to earth by use of a specific lunar departure technique, namely, the "orbital departure technique." In it, the spacecraft is assumed to be in a circular orbit around the moon. At the proper position in the orbit, the vehicle is accelerated by rocket burning to the desired injection conditions for a transearth trajectory which is ballistic and returns the spacecraft safely to the immediate vicinity of the earth. Again, as in Chapter VI, the data has been generated by the Voice technique except that the translunar portion of the Voice program was eliminated. Thus, the nomenclature and parameters referring to lunar trajectories that have been presented in previous chapters remain unchanged, the moon is assumed spherically symmetric and satellite motion around the moon occurs in a restricted two-body orbit. The effect of perturbations on the orbit, such as lunar triaxiality, and the attractions of the earth and sun have been discussed briefly in Section B of Chapter VII. Departure from elliptic orbits around the moon has not been considered since these orbits seem to offer few advantages over circular lunar orbits. Some disadvantages of elliptic lunar orbits include: (1) the more complicated navigation and guidance that is required for establishing elliptic orbits of arbitrary orientation around the moon, and (2) the possibility of vehicle impact with the moon for elliptic orbits with low pericynthion altitudes if perturbing forces act for a long time. Also, the addition of two new trajectory parameters by elliptic orbits would make the cataloguing of transearth trajectories almost impossible.

1. The Transearth Trajectory Catalogue

As was mentioned above, the spacecraft is assumed to be in circular orbit around the moon. The vehicle may have been placed into this orbit either at the terminal phase of a translunar trajectory, or by ascending from the lunar surface. Since in the general case there are no launch azimuth restrictions on the moon, and since an infinite number of lunar orbit orientations can be established by means of translunar trajectories, the parameters of the initial circular orbit around the moon are completely arbitrary from an operational viewpoint. Only optimization with respect to some aspect of the entire trajectory and mission constraints governs the selection of nominal orbital parameters. Therefore, it is desirable to obtain transearth injection requirements for an arbitrary injection point near the moon.

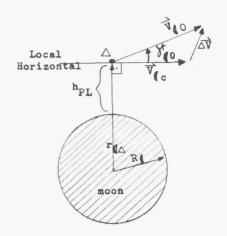
The catalogue again uses the MOP (moon's orbital plane), which is a plane of symmetry, as a reference plane and employs the trajectory parameters defined in Chapters IV and VI. As an aid to understanding the material in this chapter, the following sketch illustrates the geometry of a transearth injection near the moon:



Here is shown the lunar ground trace of the circular lunar orbit which is called the parking orbit as in the case of earth departure. The orbit is inclined to the MOP by the angle i_m , $0 \le i_m \le 90$ °, and the spacecraft's motion in this orbit is as indicated. The lunar satellite, as shown, may be regarded as being in a retrograde orbit relative to the MOP (i.e., its motion is "westward" or against the component of lunar rotation in the MOP). Since i_m varies only between 0° and 90°, the "eastward" or "westward" satellite motion around the moon must be specified together with the value of i_m. "North" is defined as in the direction of the angular momentum vector of the moon's orbital motion around the earth, and the "East" and "West" directions are defined with respect to the MOP by the same convention used for earth departure. These directions are not to be confused with the selenographic cardinal direction given in Chapter III. The intersection of the parking orbit plane with the MOP is designated by the angle $\theta_{\rm M}$ (-180° \leq $\theta_{\rm M}$ \leq 180°) which is measured positively eastward from the earthmoon line (EML) to the descending node of the parking orbit relative to the MOP. The values of i_{m} , θ_{M} specify the orientation of the circular lunar orbit, while its orbital radius r orbital central angle $\beta_{\mbox{\scriptsize M}},$ and "eastward" or "westward" spacecraft motion specify the location of the spacecraft in the orbit at any time.

The injection into the transearth trajectory takes place at a central angle -180° $\leq \beta_{M0} \leq$ 180°, where β_{M0} is measured positively toward north from the descending node. Transearth injection is also assumed to be in the direction of the spacecraft's motion. At the transearth injection point, and after the spacecraft has been accelerated, in addition to i_m , θ_M and β_{M0} , the param-

eters shown in the following sketch are needed for complete specification of the injection.



where

 $V_{\mbox{\scriptsize 1}}0$ is the transearth injection velocity in the selenocentric lunar equatorial coordinate system

 $^{
m h}_{
m PL}$ is the transearth injection altitude $^{
m h}_{
m PL}$ $^{
m r}_{
m M}$ $^{
m r}_{
m M}$

is the transearth injection flight path angle with respect to the lunar local horizontal.

It is also assumed that during transearth injection the spacecraft is accelerated instantaneously, or a velocity impulse ΔV is applied, as shown above.

 $\overrightarrow{\nabla}_{Q0} = \overrightarrow{\nabla}_{Qc} + \triangle \overrightarrow{\nabla}$

where $\overrightarrow{V}_{\boldsymbol{Q}}$ c is the circular orbital velocity corresponding to the radius $r_{\boldsymbol{Q}}$ in the selenocentric coordinate system $\mathbf{x}_{\boldsymbol{Q}}$ y $\mathbf{z}_{\boldsymbol{Q}}$. The effect of finite burning time and finite thrust-to-weight ratio on the fuel requirements of transearth injection is discussed in Chapter VII. The material presented in this catalogue is for $\mathbf{v}_{\boldsymbol{Q}} = \mathbf{0}^{\circ}$, and hence the transearth injection altitude $\mathbf{h}_{\mathbf{PL}}$ is also the pericynthion altitude, $|\Delta \overrightarrow{\mathbf{v}}|$ is colinear with $|\overrightarrow{\mathbf{v}}_{\boldsymbol{Q}}|$ and can be added algebraically to $|\overrightarrow{\mathbf{v}}_{\boldsymbol{Q}}|$ to obtain $|\overrightarrow{\mathbf{v}}_{\boldsymbol{Q}}|$; Δ V is considered an injection condition.

When the space vehicle approaches earth on the transearth trajectory, its inclination to the MOP, i_{VTE}, is defined in the same way as in Section A, Chapter VI. The value of i_{VTE}, $-180^{\circ} \leq i_{VTE} \leq 180^{\circ} \text{ is considered a trajectory parameter.}$

The transearth trajectories have been similar ly catalogued as the circumlunar trajectories in Chapter VI. They have been graphically recorded in Figs. 1 to 90 for specific mission constraints

of i_{m} , lunar parking orbit inclination, $R_{\bigoplus \emptyset}$, earthmoon distance in terms of earth radii, h_{PL} , transearth injection and parking orbit altitude, and hpE, the vacuum perigee altitude of the transearth trajectory. The transearth catalogue includes data for only one value of $h_{\rm PL}$, namely $h_{\rm PL}$ = 185.2 km. The parking orbit inclination, im, is varied from 5° to 90° and the transearth perigee altitude h_{DF} = 183 km. Although this altitude is not in any safe re-entry corridor, it can be considered so since the small change required in \mathbf{h}_{PE} for a safe re-entry corridor will have insignificant effects on the trajectory parameters. Again, as was the case in Chapter VI, R_{eff} is varied from 56 ER (earth radii) to 64 ER, which are the minimum lunar perigee radius and maximum lunar apogee radius, respectively, that can be encountered because of the eccentricity of the moon's orbit around the

In addition to the transearth injection conditions of i_m , θ_M , β_{M0} , ΔV and h_{PL} , the flight time t_p from transearth injection to perigee is recorded. Although the symbol t_p denoted the flight time from the translunar injection to pericynthion in Chapter VI, it will become obvious in the next subsection why the same symbol was chosen here. The data contained in the catalogue is also given as a function of i_{VTE} but for the independent parameter of θ_M .

Table 1 gives the contents of the catalogue apportioned between the three trajectory constraints of i_m , $R_{\bigoplus d}$ and transearth injection direction.

TABLE 1				
Case	R⊕¢ (ER)	i m (deg)	Injection Direction	Figures
1 2 3 4 5 6 7 8 9 10 11 12 13 14	56 56 56 56 56 56 60 60 60 60 64 64 64 64	5 15 30 60 90 5 15 30 60 90 5 15 30 60	Westward	1 to 3 6 to 8 11 to 13 16 to 18 21 to 23 26 to 28 31 to 33 36 to 38 41 to 43 46 to 48 51 to 53 56 to 58 61 to 63 66 to 68
15 16 17 18 19 20	64 60 60 60 60	90 5 15 30 60 90	Westward Eastward Eastward Eastward Eastward Eastward	71 to 73 76 to 78 79 to 81 82 to 84 85 to 87 88 to 90

Trajectory data is given by the following variables as a function of $i_{\mbox{\scriptsize VTE}}$ for each of the above constraints:

- (1) t_p
- (2) △V
- (3) β_{M0}

The angle θ_M is not given as such in the figures, but rather with an additional subscript TE to ease the interpretation of the data when considering translunar trajectories as discussed in the next subsection. Therefore, when considering moonto-earth transfers, the appropriate symbol is θ_{MTE} with the same definition as θ_{M} . The parameter θ_{MTE} is always given in the field of the graph.

The majority of catalogued data is for a westward transearth injection or retrograde relative to the MOP. This selection is based on the assumption that most approaches to the moon from a translunar trajectory will be in a westward direction and,thus, the presented data is more useful for the mission planner. However, some eastward transearth injection data is presented for $R_{\Theta \ell} = 60 \text{ ER}$, mainly for comparison purposes with westward injections $R_{\Theta \ell} = 60 \text{ ER}$ and rough approximations for other values of $R_{\Theta \ell}$.

The trends in each of the three major trajectory variables as shown in the catalogue are discussed below:

(1) $t_{\rm p}$ --Flight time from transearth injection near the moon to vacuum perigee. Flight time is given in Figs. 1, 6, 11, 16, 21, 26, 31, 36, 41, 46, 51, 56, 61, 66, 71, 76, 79, 82, 85 and 88. It is immediately observed that for values of i_m < 30° a discontinuous region exists on the graphs for certain values of $\theta_{\rm MTE}$, and as the region is approached, flight times increase very rapidly. This region has been denoted 'Impractical Region' in the catalogued figures. Actually this "impractical region" also exists for larger im's but is not as pronounced since only a smaller range of $\theta_{\mbox{\scriptsize MTE}}{}^{\mbox{\scriptsize I}}{}^{\mbox{\scriptsize s}}$ are affected. The discontinuity represents the situation where return times to earth become impractical or where the spacecraft escapes from the sphere of influence of the earth and moon into a heliocentric orbit. The sketch below illustrates this latter phenomenon for a trajectory in the MOP ($i_m = 0$ °) and both a westward and eastward transearth injection. When the vehicle exits the lunar volume of influence, its velocity relative to the moon is $\vec{\nabla}_{\mathbf{Q}} \triangle$. However, when its velocity relative to earth $V_{\bigoplus \triangle}$ is found by adding the moon's velocity, $\overrightarrow{V}_{\text{mf}}$, about the

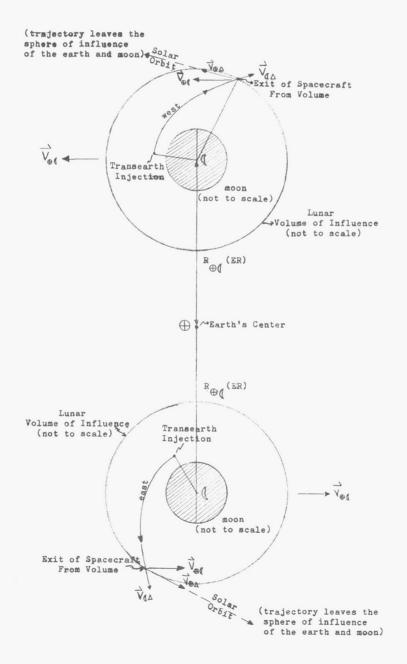
earth, the spacecraft is moving away from

the earth with sufficient energy to leave the sphere of influence of the earth and moon and be captured by the sun.

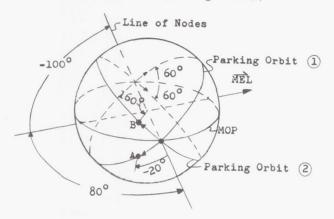
The figures show that the spacecraft can be made to return to earth in 50 hr or, if desired, 150 hr for any value of $i_{\rm m}$ and $R_{\rm eff}$, and for one fixed value of $h_{\rm PL}$, return time is not restricted to the degree as was the case for circumlunar trajectories of Chapter VI.

(2) $\triangle V$ --Velocity impulse required to inject the spacecraft into a transearth trajectory. The value for this variable is found in the figures immediately following the flight time figures. As expected, the higher the $\triangle V$ requirement, the lower the flight time. Another point worth mentioning is the fact that the minimum $\triangle V$ required is approx-

- imately 800 m/sec regardless of the values of $R_{\bigoplus \emptyset}$, i_m , or $\theta_{\rm MTE}$
- (3) $\beta_{\rm M0}$ --Orbital central angle of the transearth injection point, measured postively toward the north from the descending node, -180° $\leq \beta_{\rm M0} \leq$ 180°. Assuming for the moment that a return time to earth has been selected for given values $\theta_{\rm MTE}$ and i along with the return inclination i_{VTE}, the required $\Delta {\rm V}$ can be found. The final variable that completely describes the injection is the injection position $\beta_{\rm M0}$, as defined above. It is determined by entering the catalogue with the additional mission constraints of i_{VTE}, $\theta_{\rm M}$, and i_m.



The material given in the catalogue can be extended significantly by use of symmetry about the MOP, and it is important that an understanding of this extension procedure be achieved. It is illustrated by means of an example. Assume that im = 60°, $\theta_{\rm MTE}$ = 80°, iVTE = 40°, tp = 80 hr, ΔV = 1700 m/sec, $\beta_{\rm M0}$ = -20° and the transearth injection is westward. This situation is shown in the following sketch (parking orbit 1).



Since the MOP is a plane of symmetry, another parking orbit ② can be established that has the same value of i_m, 60°, but having an ascending node that is now coincident with the descending node of parking orbit ①. If the injection point B has the same orbital central angle as A from the line of nodes, the transearth trajectory established from parking orbit ② is a mirror image of the transearth trajectory established from parking orbit ①. Therefore the transearth trajectory data of parking orbit ① can be used for parking orbit ② by means of a few simple rules, for interpreting the catalogued data, namely:

$$\theta_{\mathrm{MTE}}$$
 ② = θ_{MTE} ① ~ 180° = -100° or (1a)

$$\theta_{\mathrm{MTE}}$$
 (1) + 180° = 260°

$$\beta_{\mathrm{M0}}$$
 ② = 180° + β_{M0} ① = 160° (1b)

$$i_{\rm VTE}$$
 ② = $-i_{\rm VTE}$ ① = -40° (1c)

$$\triangle V$$
 ② = $\triangle V$ ① = 1700 m/sec (1d)

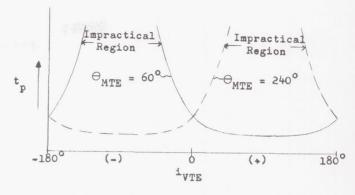
$$i_{m} ② = i_{m} ① = 60^{\circ}$$
 (1e)

$$t_p @ = t_p @ = 80 hr$$
 (1f)

both transearth injections are westward.

The next sketch illustrates the above procedure for a typical t_p versus $i_{\mbox{\scriptsize VTE}}$ curve similar to Fig. 1 in the catalogue.

The "impractical region" has been shifted to the right and the curves are a mirror image about $i_{\rm VTE}$ = 0°.



The extension of the catalogued transearth data by means of conservation of energy to other values of $^{\rm h}_{\rm PE}$ and $^{\rm V}_{\rm (0)}$ can probably be performed for small changes in $^{\rm h}_{\rm PL}$. However, due to the low velocity of the spacecraft relative to the moon, trajectory parameters other than $\rm V_{\rm (0)}$ would be affected, notably the flight time t $_{\rm p}$. Thus the formula given by Eq (2) of Section A, Chapter VI for change in near-earth injection altitude of circumlunar trajectories is applicable for a smaller range of lunar injection altitudes. Before definite recommendations can be made on the useful range of injection altitudes, a comparison of empirically determined parameters with Voice and integrated trajectories is required.

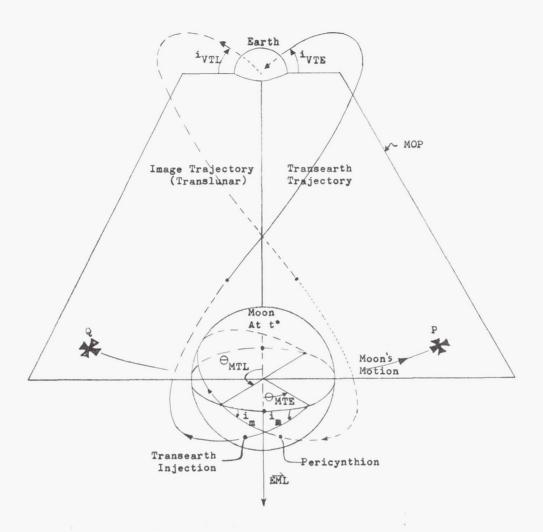
2. Interpretation of Transearth Trajectory Data as Translunar Trajectory Data

The symmetry discussed above can also be employed in interpreting moon-to-earth trajectories as earth-to-moon trajectories, as can be visualized by means of the following sketch which shows the moon at the time of transearth injection t*. At this time, the orientation of the parking orbit about the moon is specified by imand $\theta_{\rm MTE}$. During the moon-to-earth transfer, the moon changes position from t* to the point P; and on arrival at earth the transearth trajectory has an inclination ivTE.

If a mirror were placed along the \overline{EML} perpendicular to the MOP, an image trajectory would be seen. When the moon is at P, its image is at Q and the spacecraft in the image trajectory is also at earth. Now if the motion of the moon were to be reversed, i.e., if it were to move from P to its initial location at t*, the motion of the spacecraft in the transearth trajectory would also be reversed. However, when viewing the image of this lunar reverse motion it is evident that as P moves towards t*, its image Q is also moving toward t*, and the spacecraft moves from the earth toward the moon along the image trajectory.

This image situation is identical to the actual translunar situation since Q moves in the same direction as does the moon in its orbital motion. Thus the transearth trajectory may be interpreted as a translunar trajectory. † The following rules

[†]For instance, if the transearth trajectory is direct north the translunar trajectory is also direct north.



regarding this interpretation can now be made:

for
$$i_{VTE}$$
 use i_{VTL} (2a)

for
$$\theta_{\mathrm{MTE}}$$
 use 180° - θ_{MTL} (2b) where

 $\boldsymbol{\theta}_{\mbox{MTL}}$ locates the descending node of the parking orbit of the translunar trajectory

for
$$\beta_{\mathrm{M0}}$$
 (transearth) use 180° - β_{M0} (2d)

for
$$\triangle V$$
 (transearth injection) use $\triangle V$ (see definition in Chapter VI) (2e)

for
$$t_p$$
 (transearth) use t_p (translunar) (2f)

Furthermore, a fixed value of $i_{\mbox{VTL}}$ may represent either an inject north or inject south case, i.e., the image trajectory can be reflected below

or above the MOP as well. For instance, in the above sketch the translunar injection is direct north. Since the MOP is a plane of symmetry, the image or translunar trajectory can also be reflected below the MOP to obtain a direct inject-south case for which the trajectory parameters at the moon must be interpreted properly. The rules governing the interpretation for the opposite

for
$$i_{\rm VTE}$$
 use $i_{\rm VTL}$ (3a)

for
$$\theta_{\mathrm{MTE}}$$
 use $-\theta_{\mathrm{MTL}}$ (3b)

for
$$\beta_{\mbox{M0}}$$
 (transearth) use - $\beta_{\mbox{M0}}$ (trans-lunar) (3d)

†For instance, if the transearth trajectory is direct north, the translunar trajectory is opposite, i.e., direct south (see example in Fig. 4 of catalogue).

case

for $\triangle V$ (transearth injection) use $\triangle V$ (see definition in Chapter VI) (3e)

for t_{p} (transearth) use t_{p} (translunar) (3f)

for V_0 use V_0 (3g)

If the transearth trajectories in the catalogue are interpreted as translunar data, the injection conditions at earth need further discussion. The transearth data is for an injection altitude h_0 of 183 km, and the injection flight path angle $\boldsymbol{\gamma}_0$ is 0° . The injection velocity V_0 is included in the catalogue along with the injection position $\psi_{\boldsymbol{\theta}}$ (see Chapter VI for definition). The function ψ_0 is discontinuous when i_{VTI} is 0° or 180° due to a singularity in the equations of the Voice program when $i_{\rm VTL}$ = 0° or 180°. However, this feature does not detract from the usefulness of the data for mission planning purposes since the value i_{VTL} = 180° represents unlikely retrograde injections, and the singularity $i_{\ensuremath{\mathrm{VTI}}}$ = 0° invalidates Voice data for mission planning if $i_{\rm VTL} \leq 10$ for the inject-south or the inject-north cases.

The translunar injection conditions of h_0 , V_0 , ψ_0 and γ_0 can be extended to include other injection conditions by the use of the empirical relationships, Eqs (1) and (2), given in Chapter VI, Section A.

As pointed out previously, the translunar trajectories in this Chapter are not of the circumlunar class but of the approach class (Chapter IV). Two major advantages are to be gained by the use of the approach class of translunar trajectories.

- (1) The freedom in selecting landing sites or surveillance areas
- (2) The relative freedom in choosing a flight time to the moon. Although accessibility of lunar areas is vastly improved by the use of these trajectories, the problems associated with mission abort near the moon before entering lunar orbit make this approach more risky.

B. MIDCOURSE GUIDANCE AND ENERGY REQUIREMENTS

The navigation and guidance techniques presented in Chapter VI are also applicable to the transearth phase of a lunar mission and therefore will not be discussed further. However, there are some brief comments to be made regarding the energy requirements of this phase.

For circumlunar trajectories it is very difficult to determine the velocity impulses ΔV TOT for the transearth portion of the trajectory because midcourse corrections are applied during

the translunar phase. These corrections may be designed to return the errant trajectory back to a nominal trajectory or to ensure arrival at a specific aim point near the moon (not necessarily matching a nominal). Therefore the transearth trajectory depends on the accuracy of these translunar midcourse corrections and the off-nominal conditions of $i_{\rm m}$, $\theta_{\rm M}$, $h_{\rm PL}$ and the moon. It was emphasized in Chapter VI that very stringent requirements exist on the trajectory at given instants of time if mission specifications are to be fulfilled.

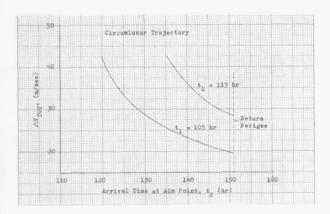
The sensitivity of transearth vacuum perigee to variations in pericynthion altitude, hpl. varies over a wide range, and a factor of 10 is not unreasonable. Not only does the return vacuum perigee altitude vary, but the transearth inclination, i_{VTE} , and the time of re-entry also vary, making the task of returning to a prescribed point on earth even more difficult. Unless midcourse corrections are made to reach the correct pericynthion altitude at the right time and orientation, the distortion in the transearth trajectory may require large transearth midcourse guidance corrections. A circumlunar trajectory will thus require multiple midcourse guidance corrections, one or more during the translunar phase, one at or near pericynthion, and one or more during the transearth phase.

1. Energy Requirements for Transearth Portion of Circumlunar Trajectories

If the first guidance concept given in Chapter VI with the aim point at pericynthion is used, then difficulties arise in simultaneous control of the four prime variables i $_{\rm m}$, $_{\rm M}$, $_{\rm PL}$ and t $_{\rm p}$ at pericynthion which, in turn, control the transearth trajectory. Most likely a statistical approach will be used to determine the transearth guidance requirements for this concept. For the second concept, which is designed to return the spacecraft to the nominal trajectory prior to reaching the moon, the difficulty may arise from the small differences between the required velocity corrections and the accuracy to which the spacecraft's velocity vector is known at the time of correction.

In order to gain at least some insight to the transearth energy requirements, it is assumed that the final translunar midcourse guidance correction (for a typical circumlunar trajectory of Chapter VI) by use of guidance concept 2 is not made. In this case the spacecraft continues its trajectory around the moon with no further corrections until it is on the transearth portion some distance from the moon. The transearth midcourse correction is assumed at t_1 = 105 hr after translunar injection, 106,000 km from the moon. This correction is designed to return the spacecraft to the nominal transearth trajectory at various times t_2 which vary from 120 hr after injection to perigee. The total mission time (from injection to perigee) is approximately 151 hr

and the magnitude of the final translunar correction which is not made is $\Delta V_{_{_{\bf V}}}$ of 0.7 m/sec. The following sketch shows the total corrective velocity requirements for the above conditions.



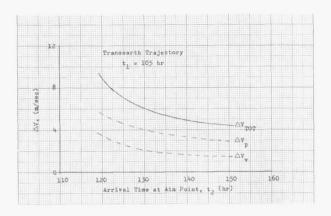
The magnitude of the required corrections, although felt to be quite conservative, indicates the need of controlling the translunar trajectory as closely as possible. The omission of a $\Delta \rm V_{\rm o}$ of 0.7 m/sec correction during the translunar trajectory at t = 50 hr results in a required 20 m/sec correction (at $\rm t_1$ = 105 hr) on the transearth trajectory. Also included in the sketch is data for an initial transearth midcourse correction at $\rm t_1$ = 115 hr. The data shows the expected trends of reduced $\Delta \rm V_{\rm TOT}$ for corrections made as early as possible and reduction of the total $\Delta \rm V_{\rm TOT}$ as the aim point approaches transearth vacuum perigee.

The initial correction times (t_1) assumed ensure that the vehicle position at t_1 is sufficiently beyond the effect of the moon's gravitational field to allow reasonable prediction of position and velocity at perigee. The previous sketch illustrates the necessity of obtaining ample position and velocity data as soon as possible after entering a region where reasonably accurate return midcourse guidance corrections can be computed.

2. Requirements for Transearth Trajectories Originating at the Moon

For transearth trajectories established from a lunar orbit, errors arise mainly from the ability of the guidance system to control the injection velocity vector. Although the correct position at transearth injection is also important, the intrinsic nature of the guidance concept to be used tends to keep position errors small. This is especially

true if the guidance technique uses a phantom satellite as the aim point as discussed in Chapter V. The standard deviation in velocity, i.e., the 1σ error in the velocity, is assumed to be 0.3 m/sec in each coordinate direction, x_v , y_v , z_v ,



where x_{vv} is along the local horizontal in the flight direction, z_{v} is in the direction of the local vertical and y completes the right-handed Cartesian coordinate system by defining a lateral direction normal to the trajectory plane. Injection velocity errors reflect a three-dimensional 99% probability (3.368 σ). The velocity error at transearth injection is propagated to a position corresponding to the point at t_1 = 105 hr used in the circumlunar case above. The previous sketch presents the initial (position) velocity correction ($\triangle V_p$), the final (velocity) correction (ΔV_{V}) and ΔV_{TOT} , the total impulse required. As in the translunar case, the initial correction, made at the 105-hr point, corrects the position of the spacecraft so that it intercepts the nominal transearth trajectory at a predetermined aim position and time. This aim point has been varied from the 120-hr point to perigee on the sketch and the final correction at the aim point reorients the spacecraft's velocity vector along the nominal trajectory with the correct magnitude. The data presented in the sketch represents the highest midcourse energy requirements and as noted, it exhibits the same trends as the circumlunar trajectory of the previous sub-

Guidance accuracy requirements have been discussed qualitatively in Subsection C-2c of Chapter VI with some reference to quantitative data given in that subsection. Again the discussion applies to midcourse guidance and energy requirements of translunar as well as transearth trajectories.

ILLUSTRATIONS

LIST OF ILLUSTRATIONS

Figure	Title	Page
1	Flight Time Versus Return Inclination (Inject West - Retrograde)	IX-17
2	ΔV Required For Transearth Injection Versus Return Inclination	IX-18
3	Transearth Injection Point Versus Return Inclination	IX-19
4	Injection Velocity Versus Translunar Inclination	IX-20
5	Translunar Injection Position Versus Translunar Inclination	IX-21
6	Flight Time Versus Return Inclination (Inject West - Retrograde)	IX-22
7	ΔV Required For Transearth Injection Versus Return Inclination	IX-23
8	Transearth Injection Point Versus Return Inclination	IX-24
9	Injection Velocity Versus Translunar Inclination	IX-25
10	Translunar Injection Position Versus Translunar Inclination	IX-26
11	Flight Time Versus Return Inclination (Inject West - Retrograde)	IX-27
12	ΔV Required For Transearth Injection Versus Return Inclination	IX-28
13	Transearth Injection Point Versus Return Inclination	IX-29
14	Injection Velocity Versus Translunar Inclination	IX-30
15	Translunar Injection Position Versus Translunar Inclination	IX-31
16	Flight Time Versus Return Inclination (Inject West - Retrograde)	IX-32

Figure	Title	Page
17	ΔV Required For Transearth Injection Versus Return Inclination	IX-33
18	Transearth Injection Point Versus Return Inclination	IX-34
19	Injection Velocity Versus Translunar Inclination	IX-35
20	Translunar Injection Position Versus Translunar Inclination	IX-36
21	Flight Time Versus Return Inclination (Inject West - Retrograde)	IX-37
22	ΔV Required For Transearth Injection Versus Return Inclination	IX-38
23	Transearth Injection Point Versus Return Inclination	IX-39
24	Injection Velocity Versus Translunar Inclination	IX-40
25	Translunar Injection Position Versus Translunar Inclination	IX-41
26	Flight Time Versus Return Inclination (Inject West - Retrograde)	IX-42
27	ΔV Required for Transearth Injection Versus Return Inclination	IX-43
28	Transearth Injection Point Versus Return Inclination	IX-44
29	Injection Velocity Versus Translunar Inclination	IX-45
30	Translunar Injection Position Versus Translunar Inclination	IX-46
31	Flight Time Versus Return Inclination (Inject West - Retrograde)	IX-47
32	ΔV Required For Transearth Injection Versus	TX-48

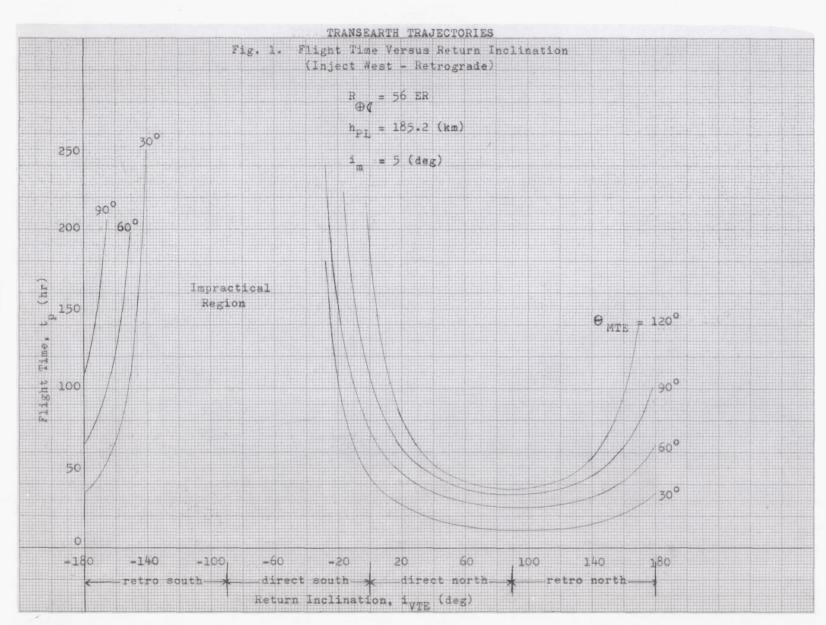
Figure	Title	Page
33	Transearth Injection Point Versus Return Inclination	IX-49
34	Injection Velocity Versus Translunar Inclination	IX-50
35	Translunar Injection Position Versus Translunar Inclination	IX-51
36	Flight Time Versus Return Inclination (Inject West - Retrograde)	IX-52
37	ΔV Required For Transearth Injection Versus Return Inclination	IX-53
38	Transearth Injection Point Versus Return Inclination	IX-54
39	Injection Velocity Versus Translunar Inclination	IX-55
40	Translunar Injection Position Versus Translunar Inclination	IX-56
41	Flight Time Versus Return Inclination (Inject West - Retrograde)	IX-57
42	ΔV Required For Transearth Injection Versus Return Inclination	IX-58
43	Transearth Injection Point Versus Return Inclination	IX-59
44	Injection Velocity Versus Translunar Inclination	IX-60
45	Translunar Injection Position Versus Translunar Inclination	IX-61
46	Flight Time Versus Return Inclination (Inject West - Retrograde)	IX-62
47	ΔV Required For Transearth Injection Versus Return Inclination	IX-63
48	Transearth Injection Point Versus Return Inclination	IX-64

Figure	Title	Page
49	Injection Velocity Versus Translunar Inclination	IX-65
50	Translunar Injection Position Versus Translunar Inclination	IX-66
51	Flight Time Versus Return Inclination (Inject West - Retrograde)	IX-67
52	ΔV Required For Transearth Injection Versus Return Inclination	IX-68
53	Transearth Injection Point Versus Return Inclination	IX-69
54	Injection Velocity Versus Translunar Inclination	IX-70
55	Translunar Injection Position Versus Translunar Inclination	IX-71
56	Flight Time Versus Return Inclination (Inject West - Retrograde)	IX-72
57	ΔV Required For Transearth Injection Versus Return Inclination	IX-73
58	Transearth Injection Point Versus Return Inclination	IX-74
59	Injection Velocity Versus Translunar Inclination	IX-75
60	Translunar Injection Position Versus Translunar Inclination	IX-76
61	Flight Time Versus Return Inclination (Inject West - Retrograde)	IX-77
62	ΔV Required For Transearth Injection Versus Return Inclination	IX-78
63	Transearth Injection Point Versus Return Inclination	IX-79

Figure	Title	Page
64	Injection Velocity Versus Translunar Inclination	IX-80
65	Translunar Injection Position Versus Translunar Inclination	IX-81
66	Flight Time Versus Return Inclination (Inject West - Retrograde)	IX-82
67	ΔV Required For Transearth Injection Versus Return Inclination	IX-83
68	Transearth Injection Point Versus Return Inclination	IX-84
69	Injection Velocity Versus Translunar Inclination	IX-85
70	Translunar Injection Position Versus Translunar Inclination	IX-86
71	Flight Time Versus Return Inclination (Inject West - Retrograde)	IX-87
72	ΔV Required For Transearth Injection Versus Return Inclination	IX-88
73	Transearth Injection Point Versus Return Inclination	IX-89
74	Injection Velocity Versus Translunar Inclination	IX-90
75	Translunar Injection Position Versus Translunar Inclination	IX-91
76	Flight Time Versus Return Inclination (Inject East - Direct)	IX-92
77	Δ V Required For Transearth Injection Versus Return Inclination	IX-93
78	Transearth Injection Point Versus Return Inclination	IX-94
79	Flight Time Versus Return Inclination (Inject East - Direct)	IX-95

ILLUSTRATIONS (continued)

Figure	Title	Page
80	Δ V Required For Transearth Injection Versus Return Inclination	IX-96
81	Transearth Injection Point Versus Return Inclination	IX-97
82	Flight Time Versus Return Inclination (Inject East - Direct)	IX-98
83	ΔV Required For Transearth Injection Versus Return Inclination	IX-99
84	Transearth Injection Point Versus Return Inclination	IX-100
85	Flight Time Versus Return Inclination (Inject East - Direct)	IX-101
86	ΔV Required For Transearth Injection Versus Return Inclination	IX-102
87	Transearth Injection Point Versus Return Inclination	IX-103
88	Flight Time Versus Return Inclination (Inject East - Direct)	IX-104
89	ΔV Required For Transearth Injection Versus Return Inclination	IX-105
90	Transearth Injection Point Versus Return	IV - 106



20

-60

-20

Return Inclination, ivok (deg)

-140

-180

-100

60

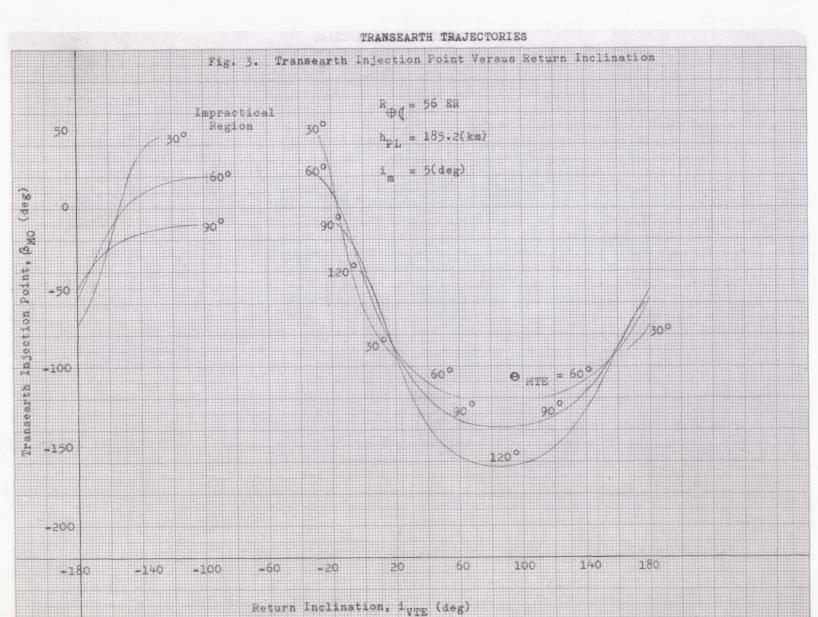
100

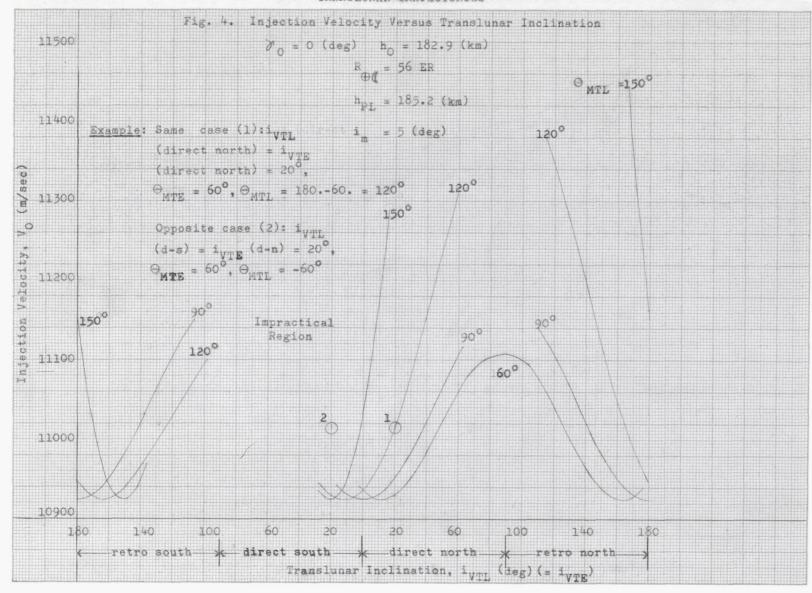
140

180

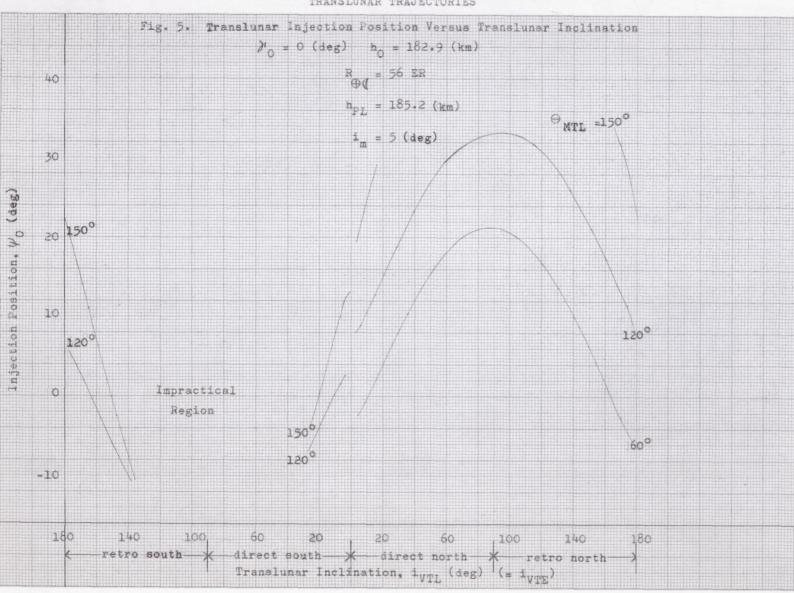
Fig. 2. AV Required For Transearth Injection Versus Return Inclination

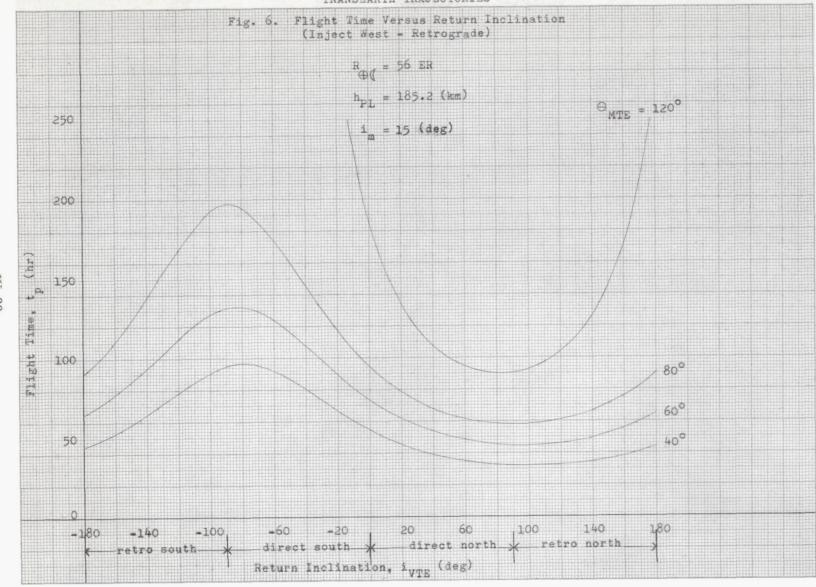


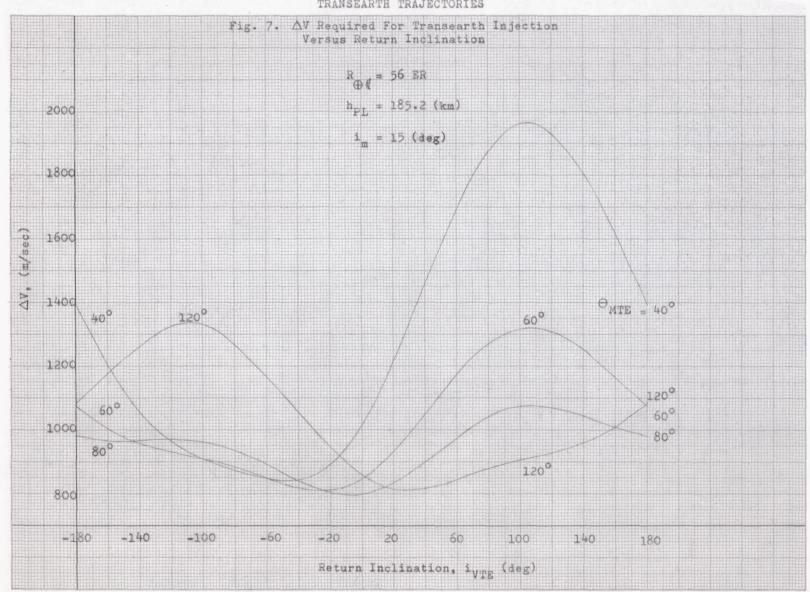




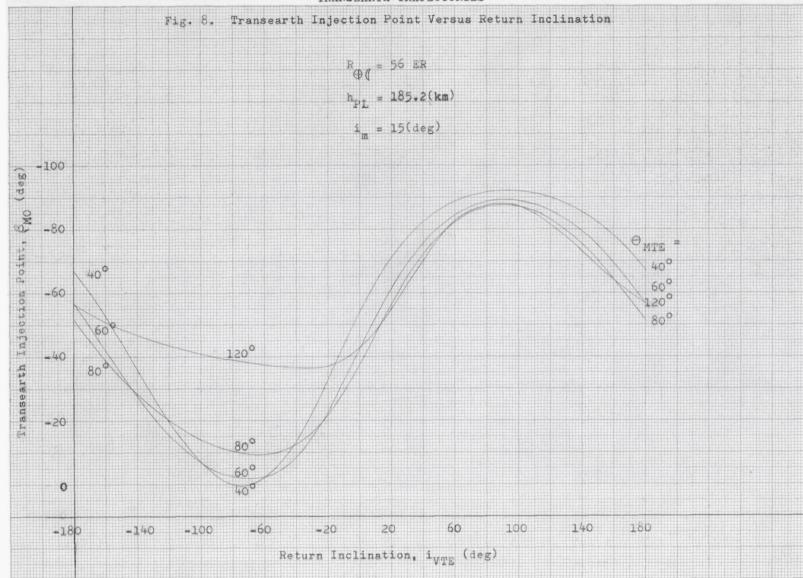
X-20

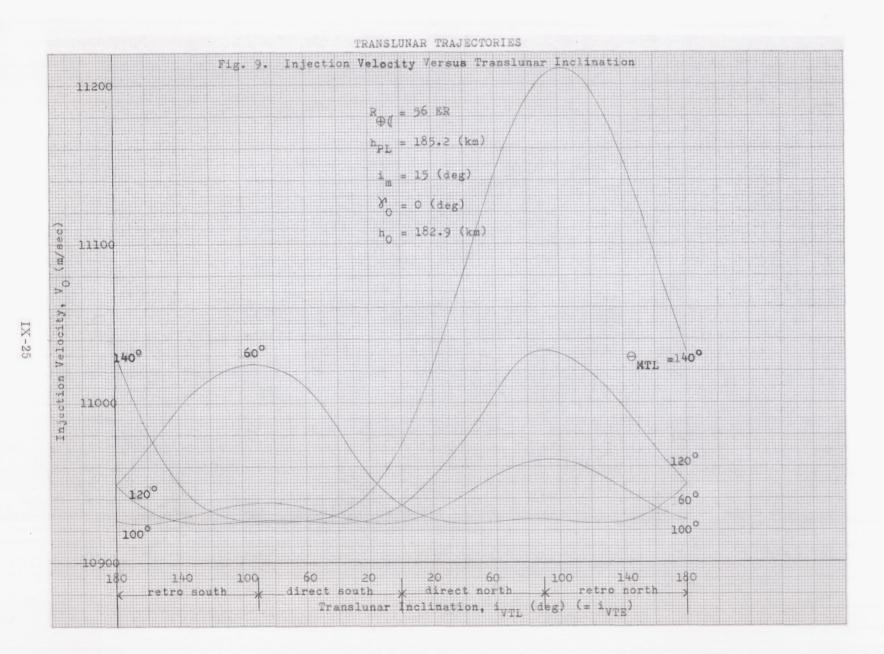


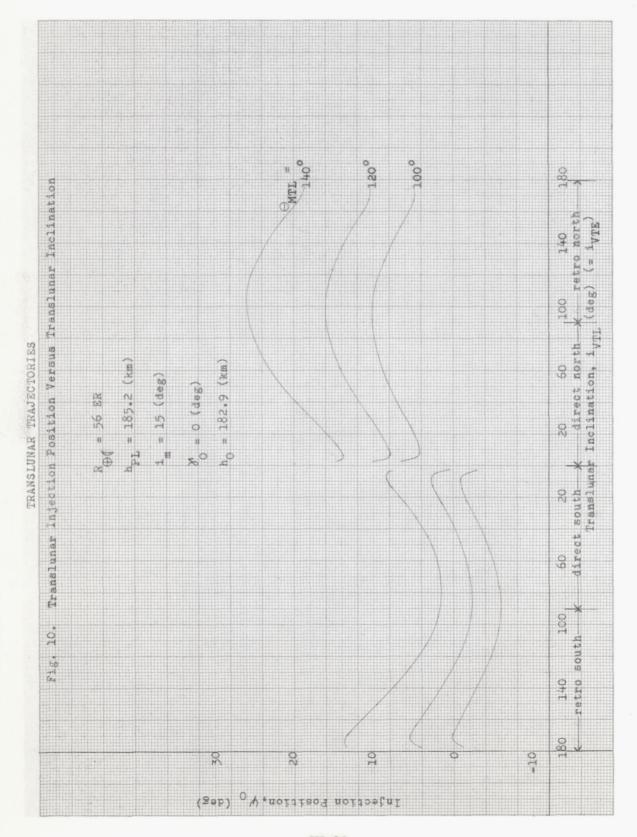


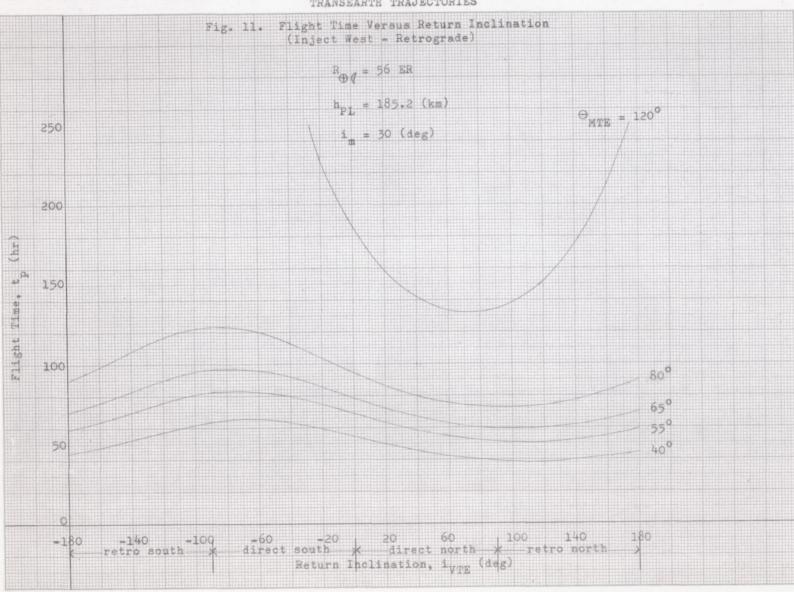


TRANSEARTH TRAJECTORIES

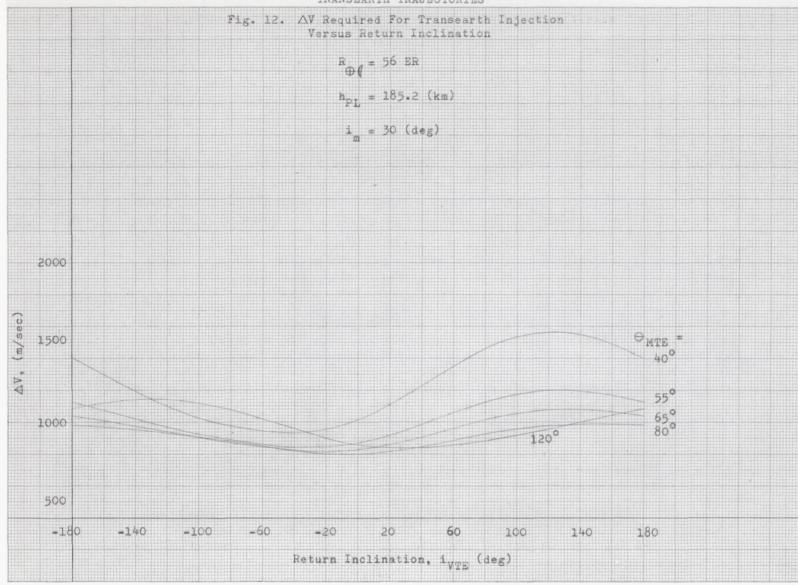


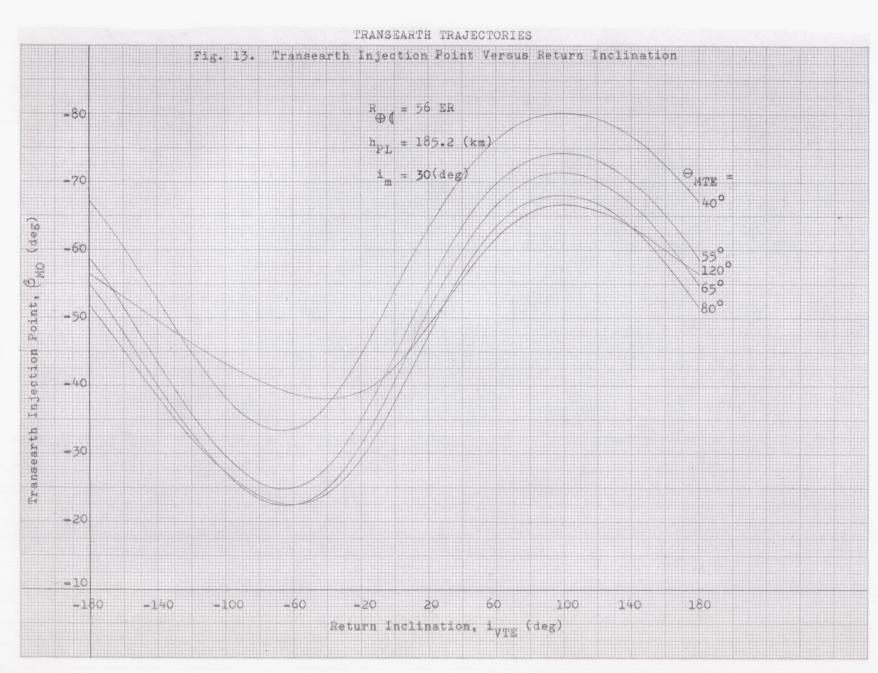




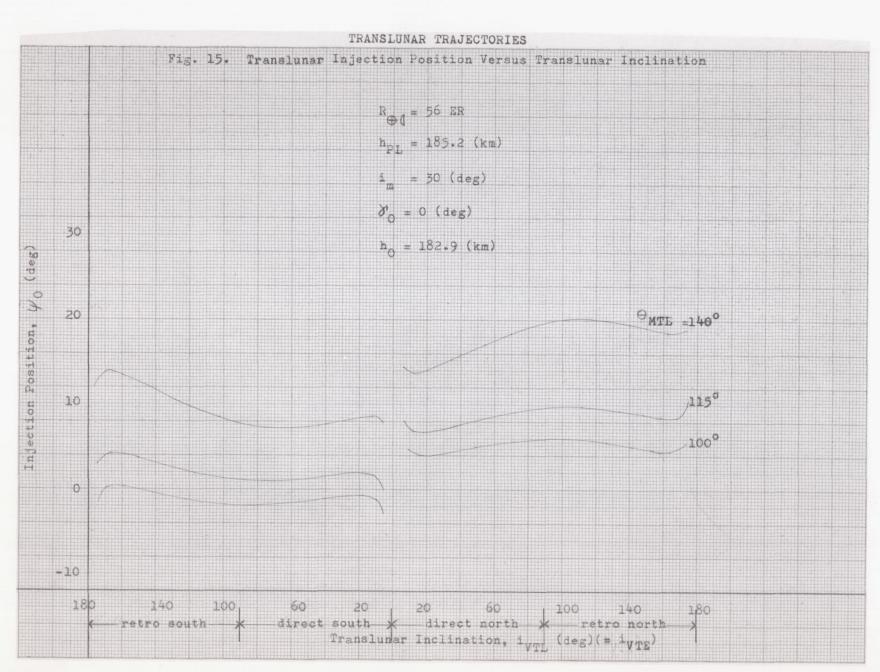


TRANSEARTH TRAJECTORIES

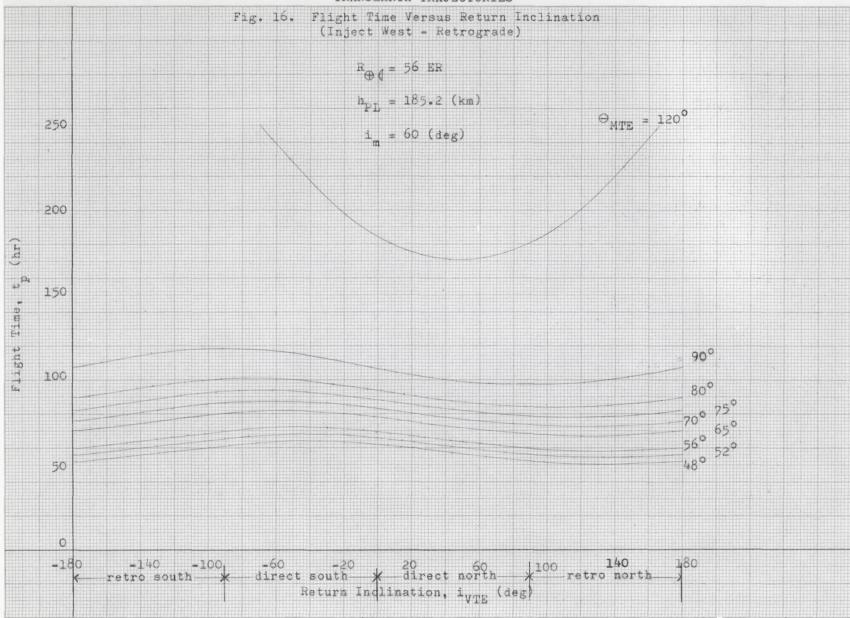


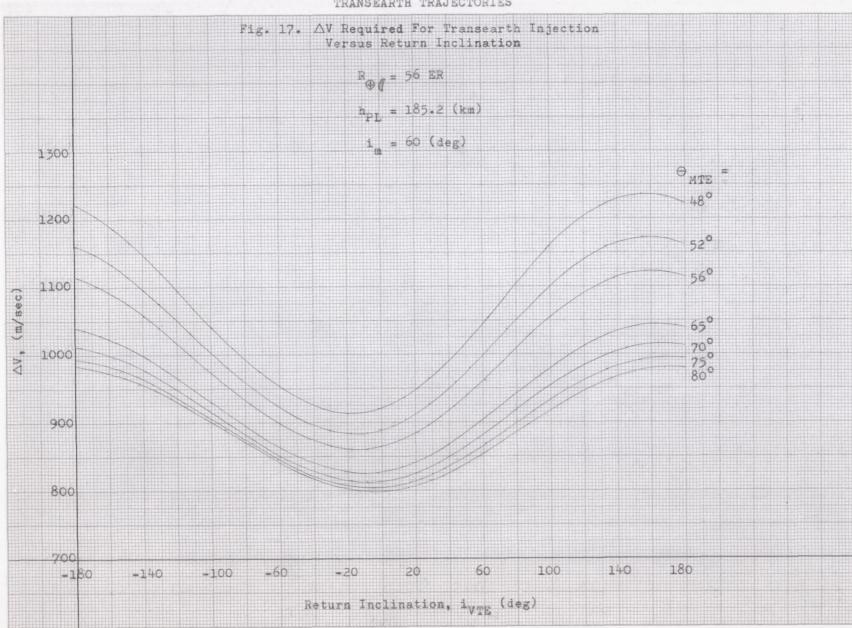


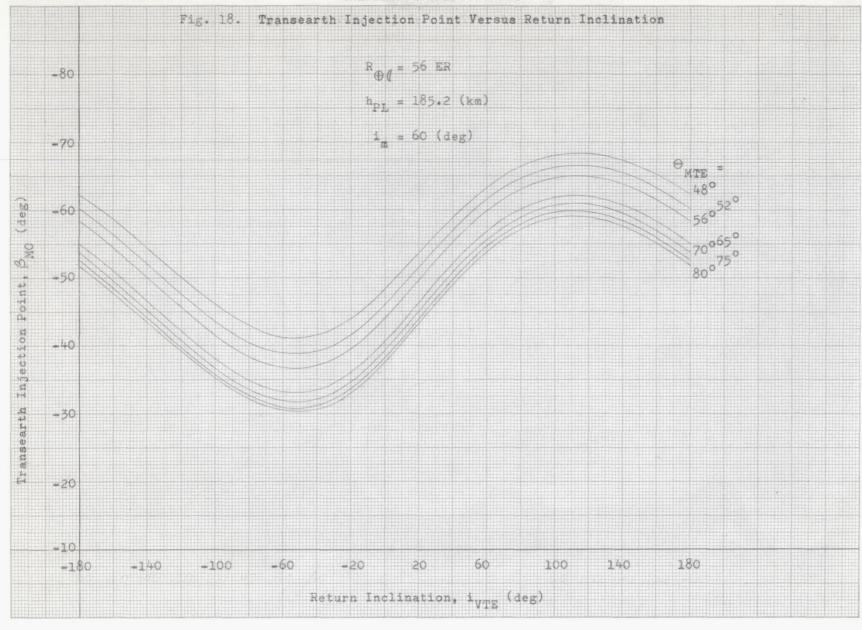
IX-30



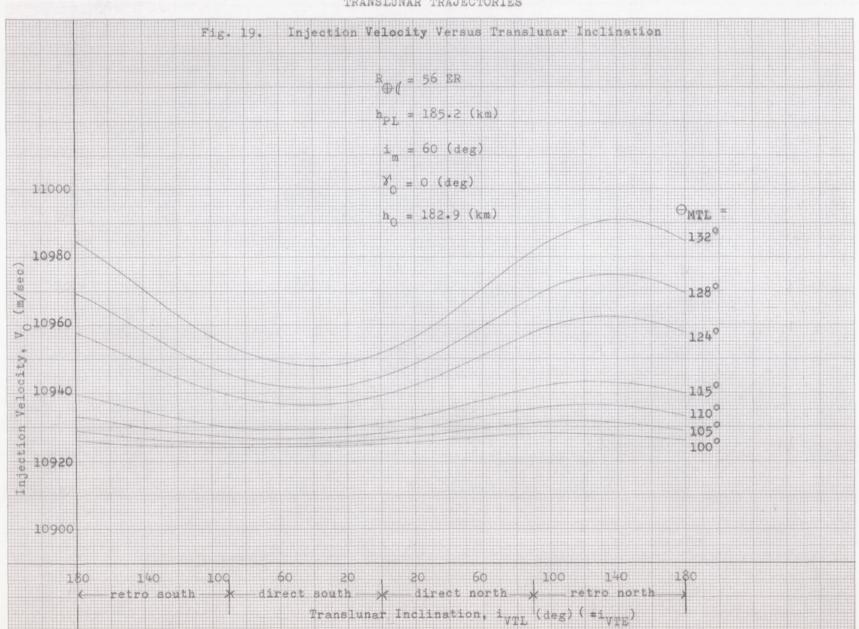
TRANSEARTH TRAJECTORIES

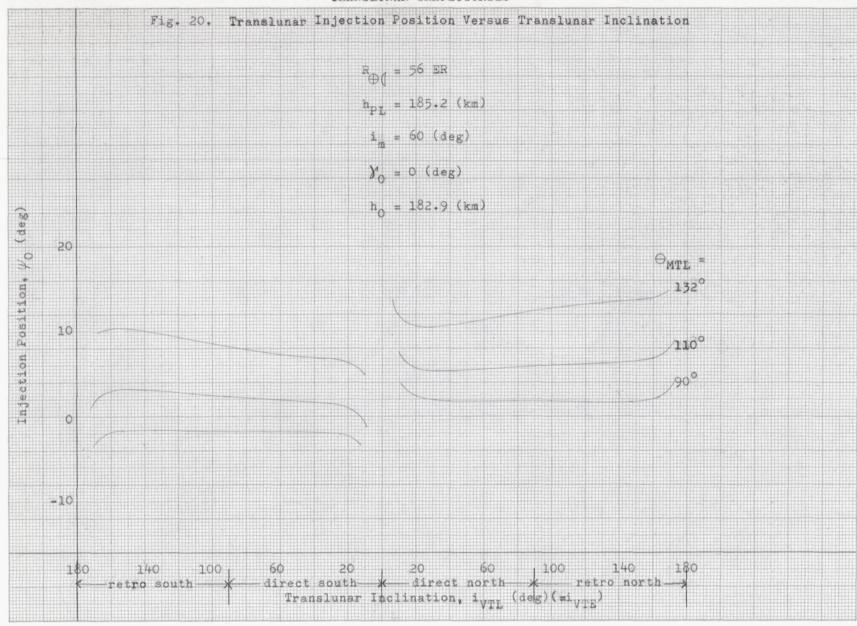


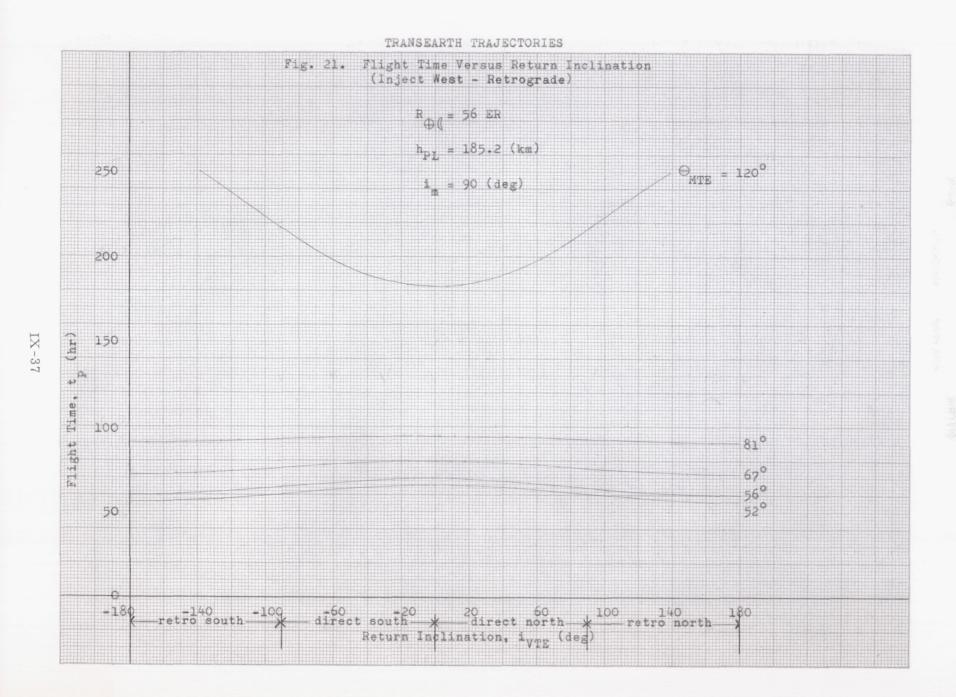


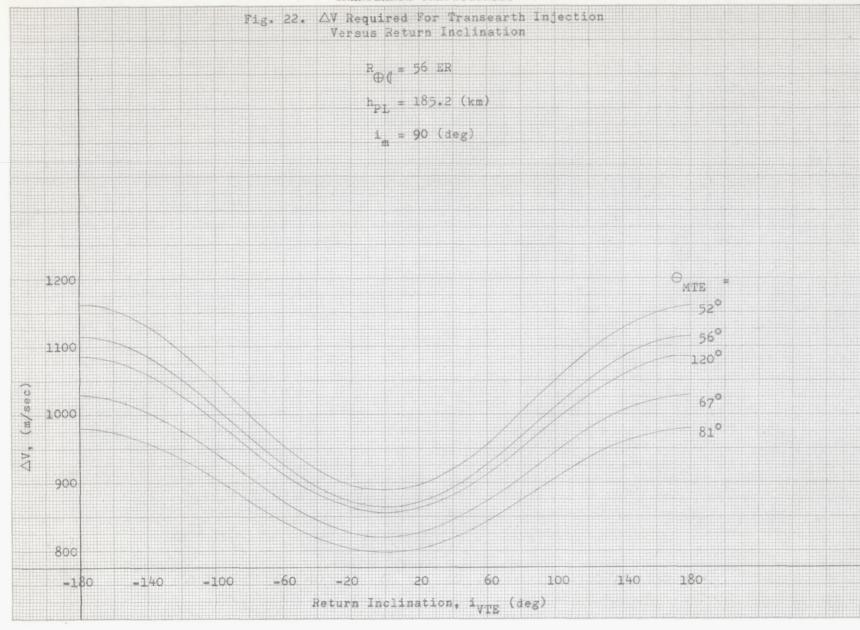


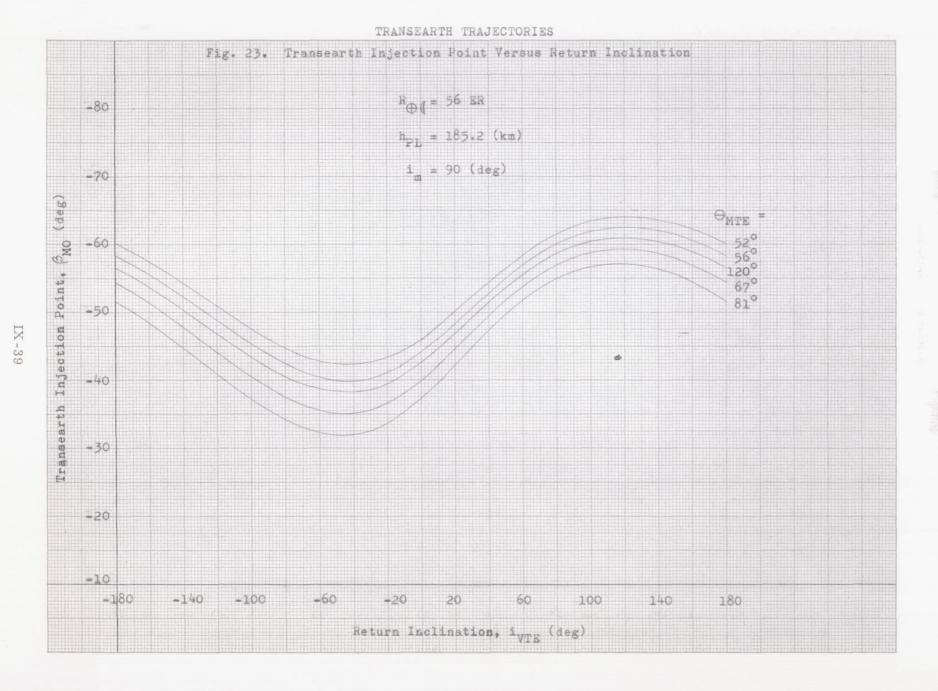
TRANSLUNAR TRAJECTORIES

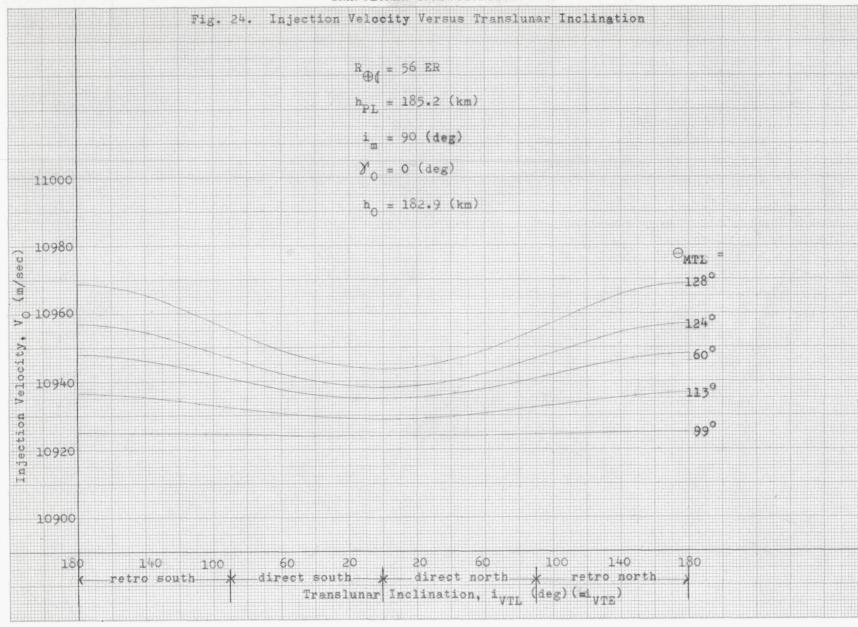


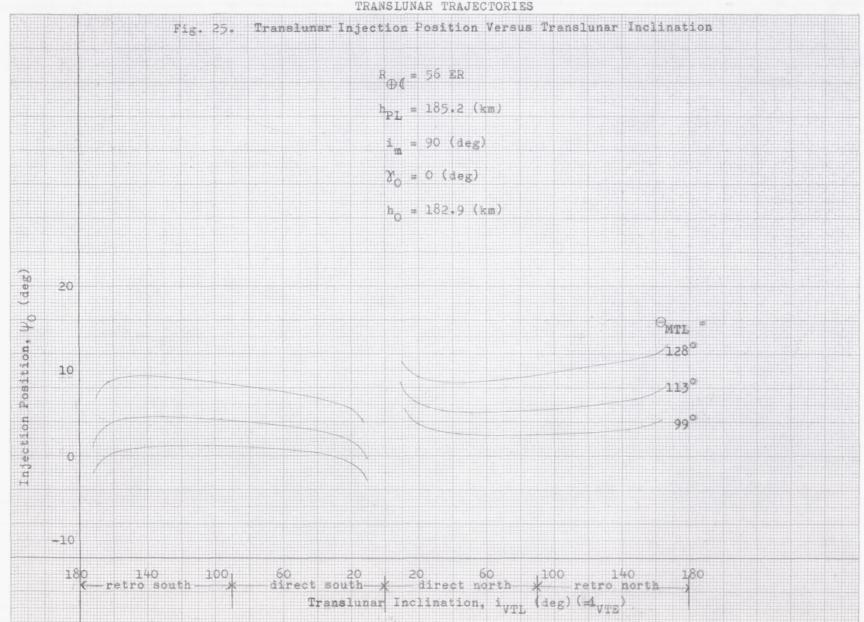


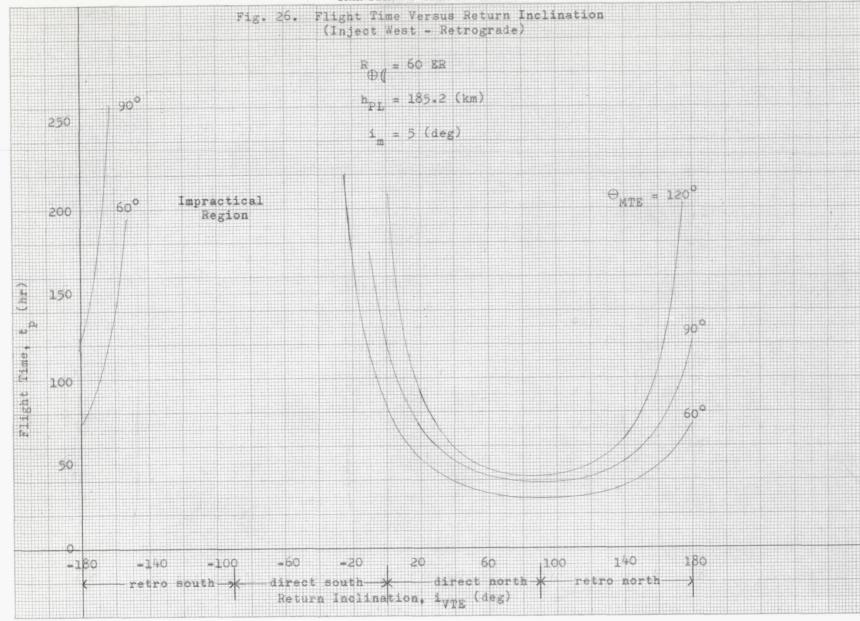


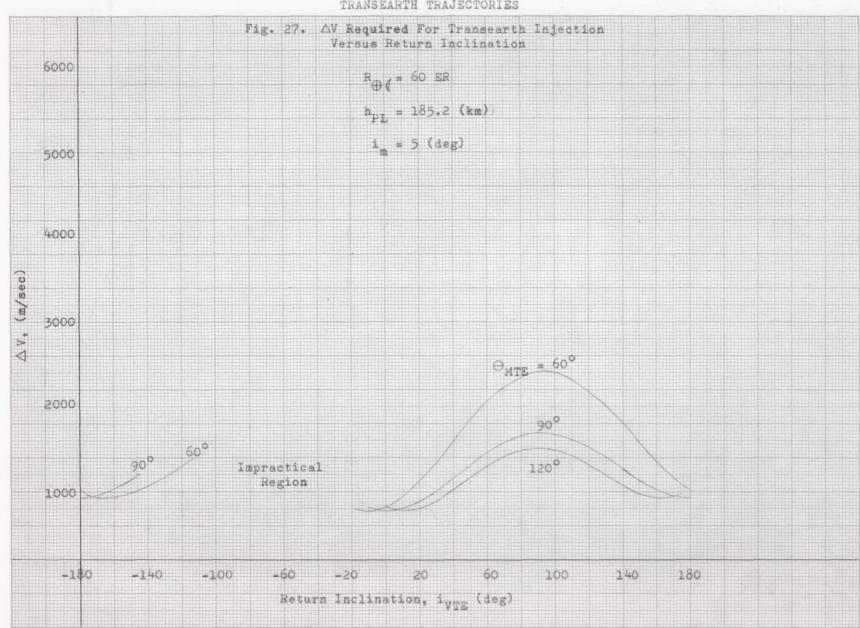


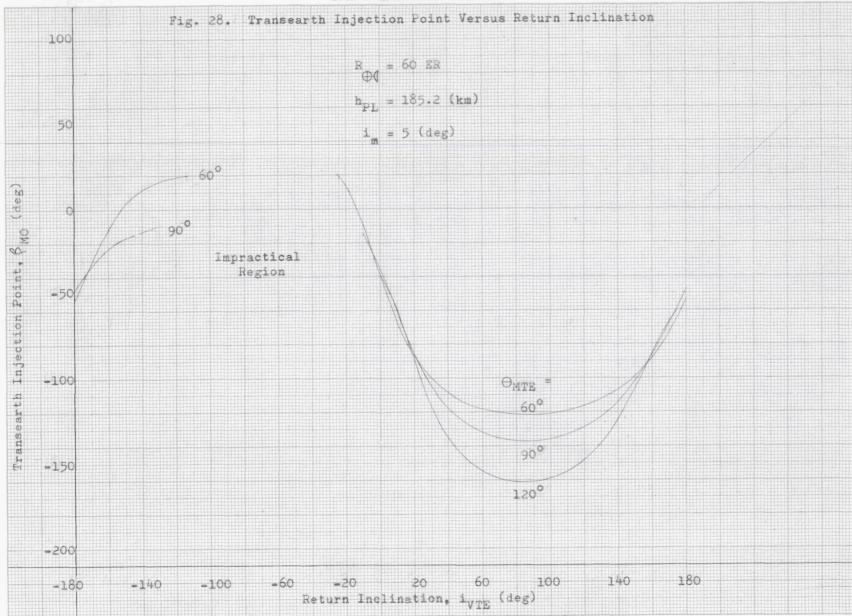


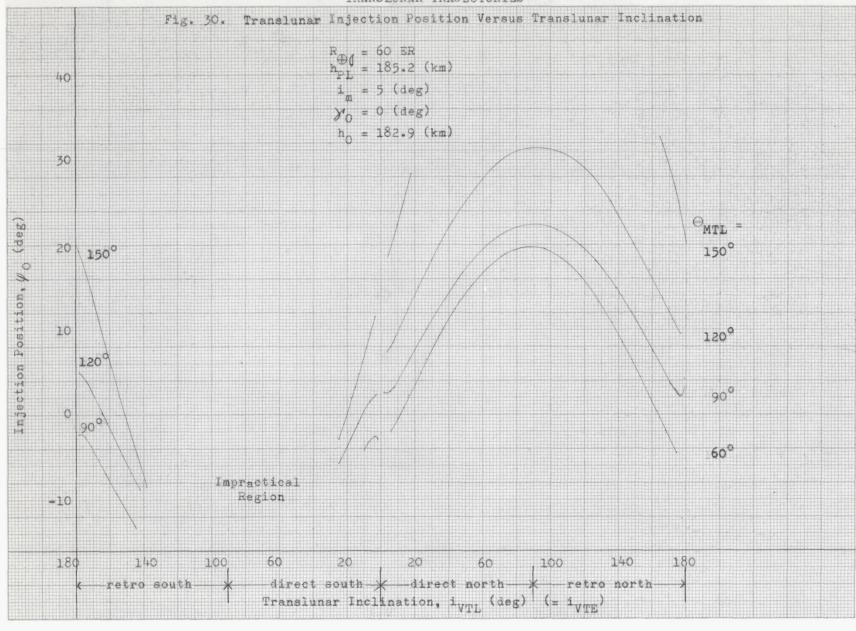


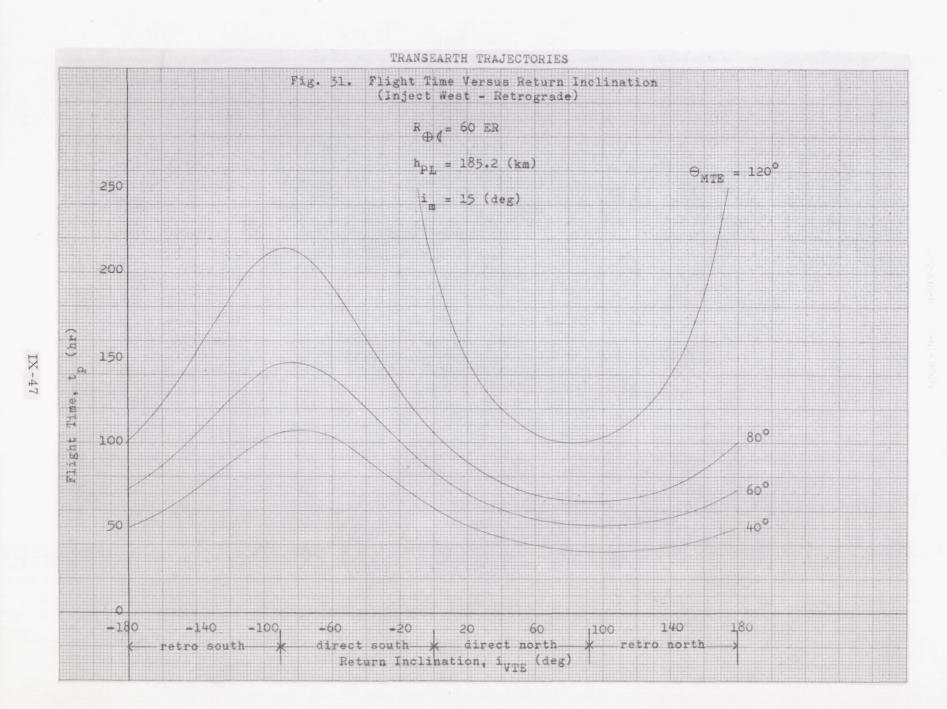


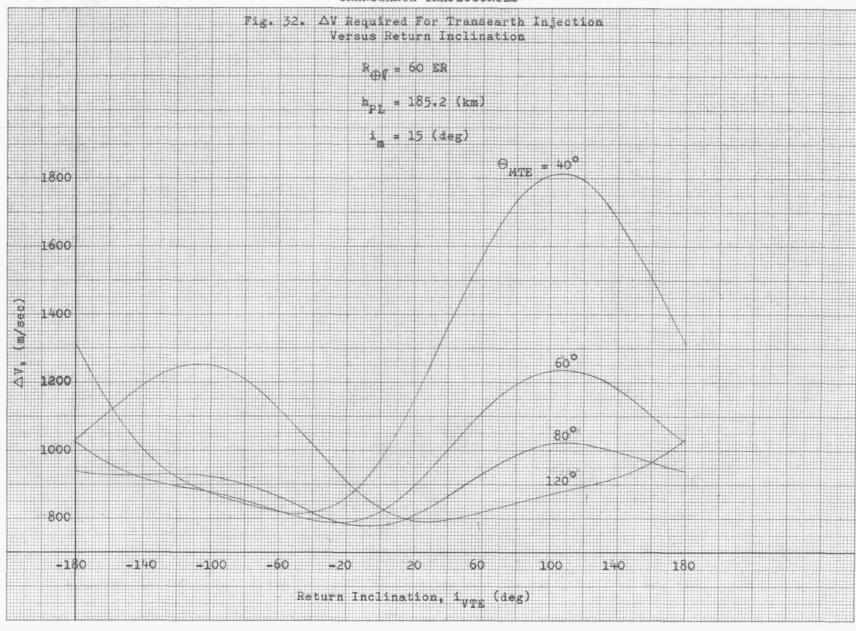




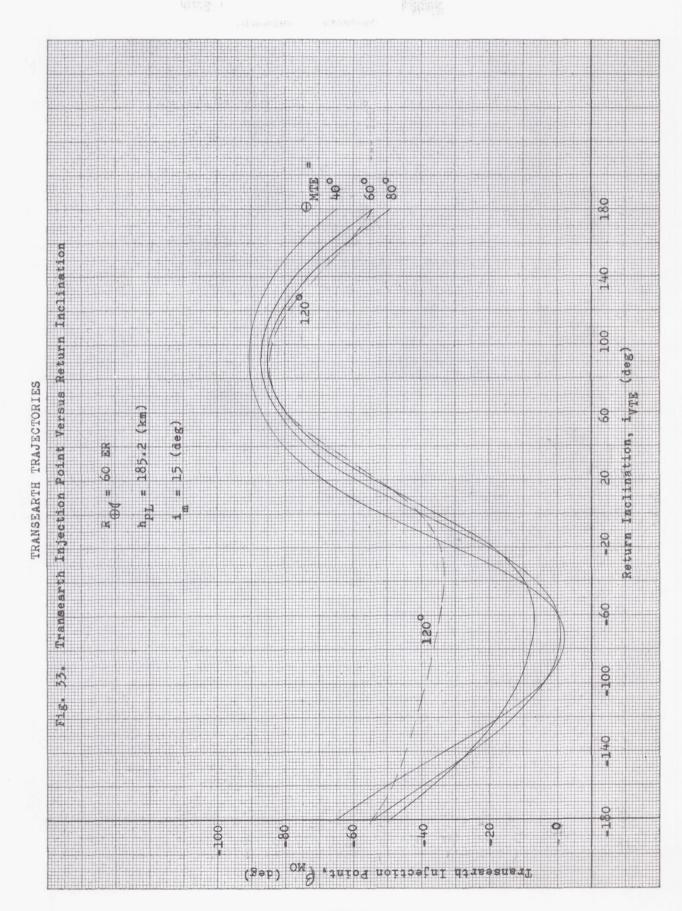


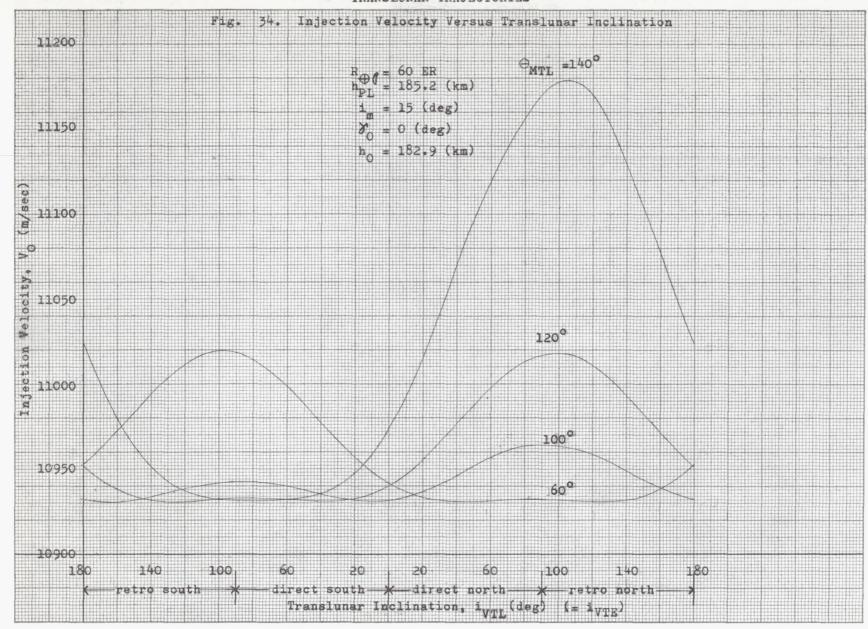


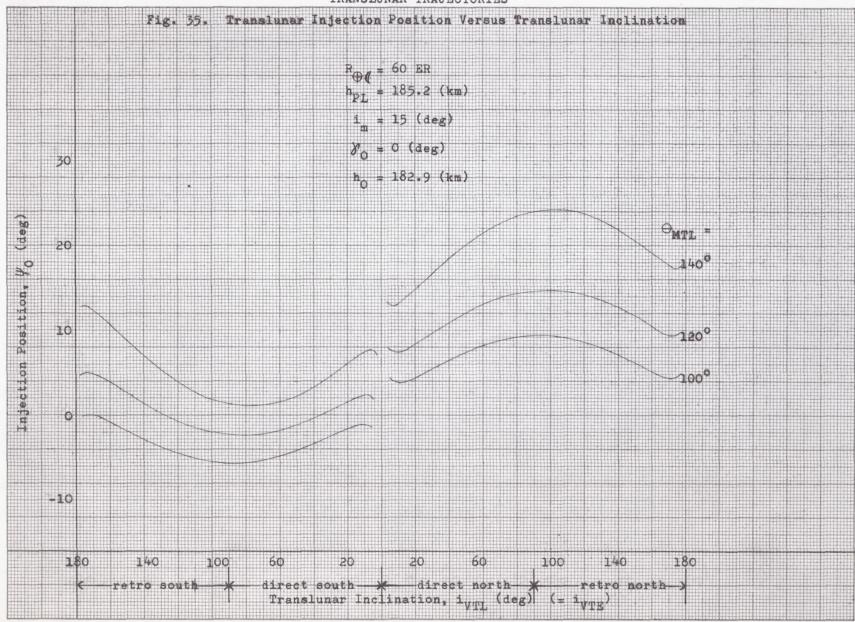




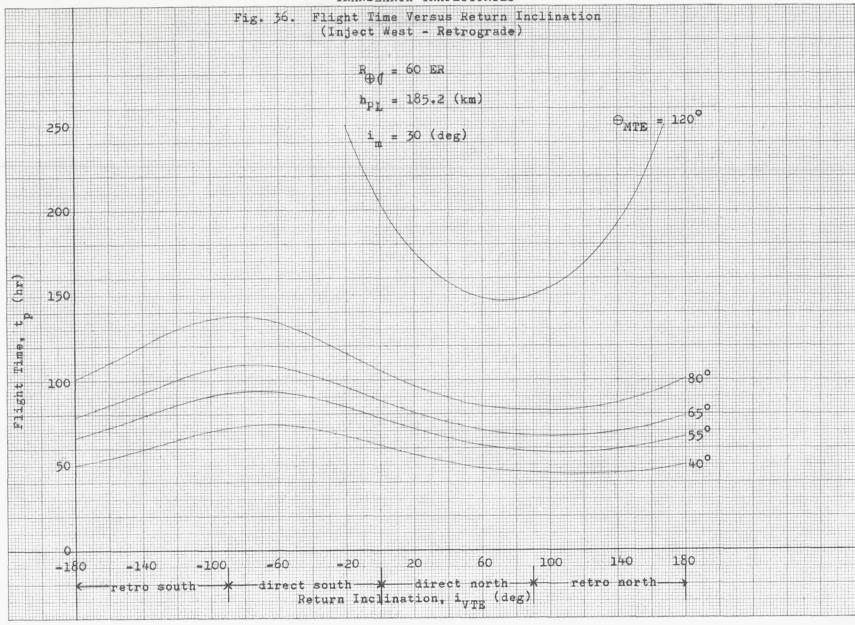
IX-48

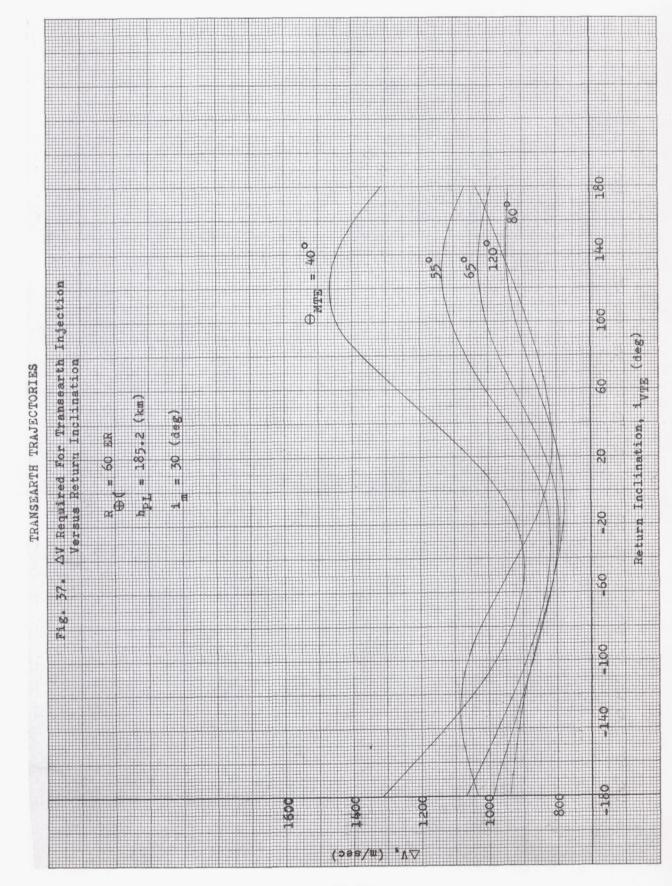


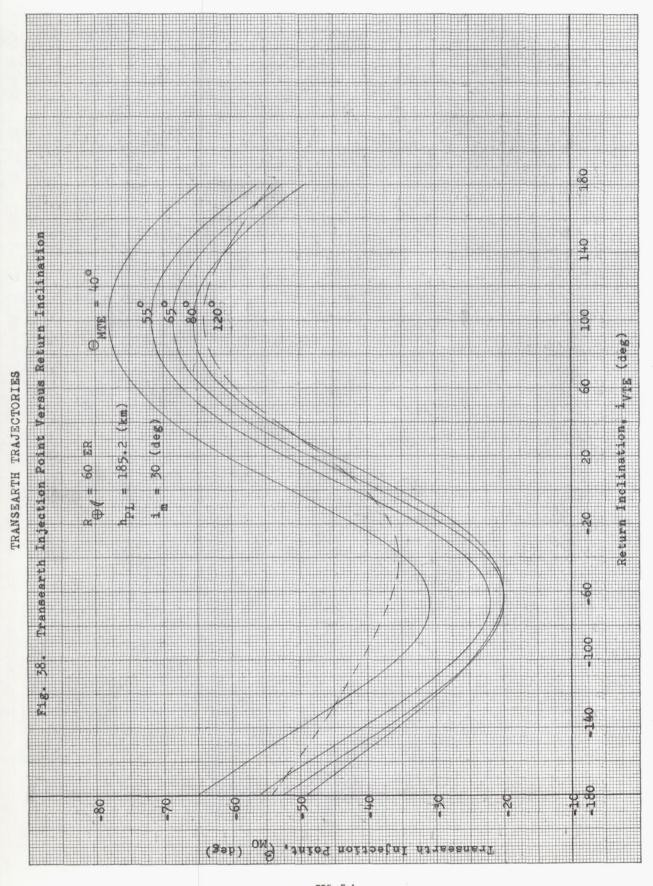


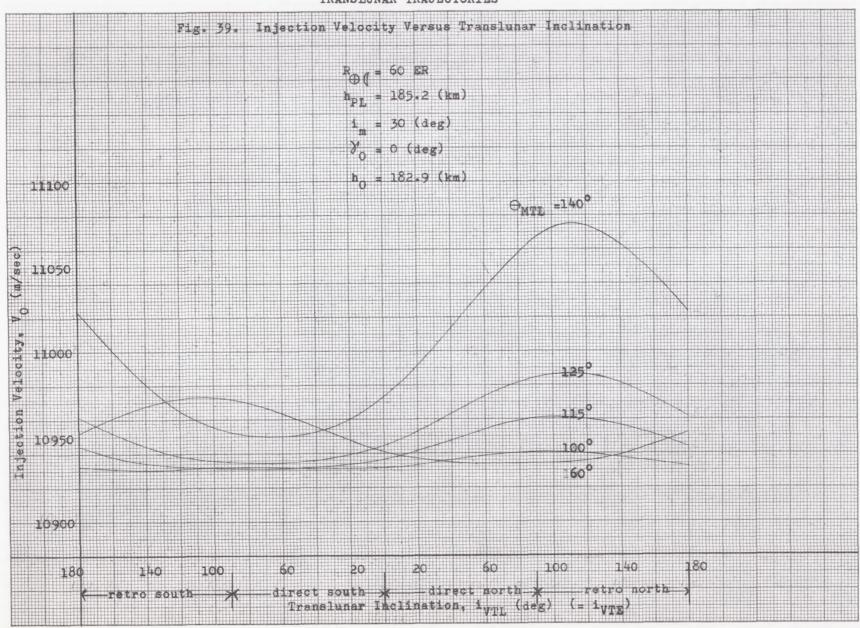


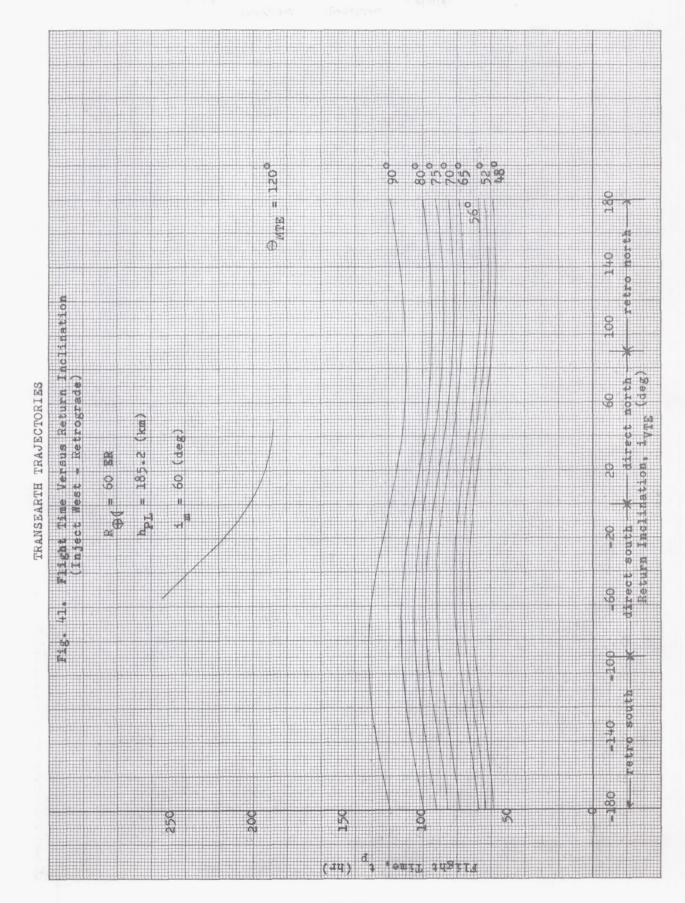
IX-51

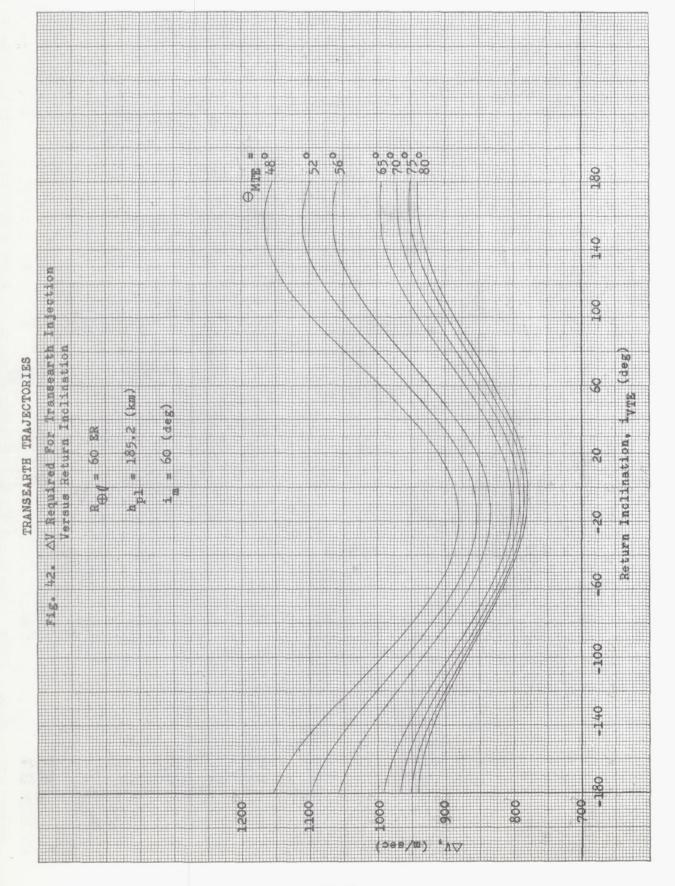


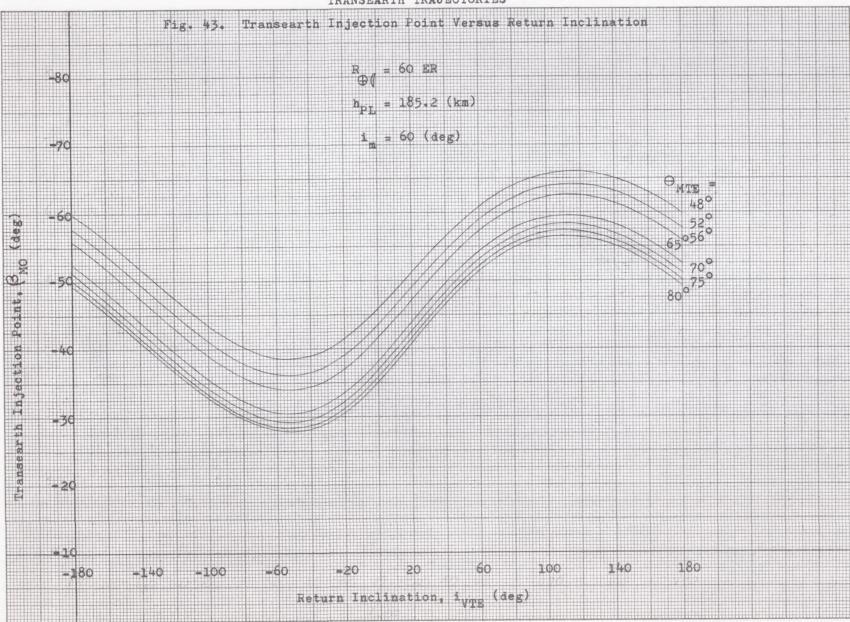


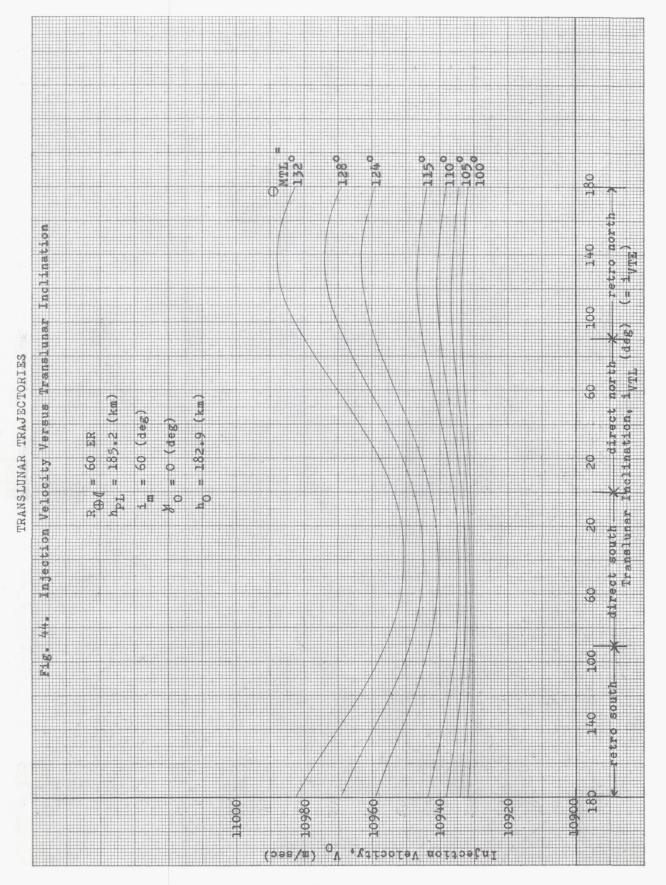


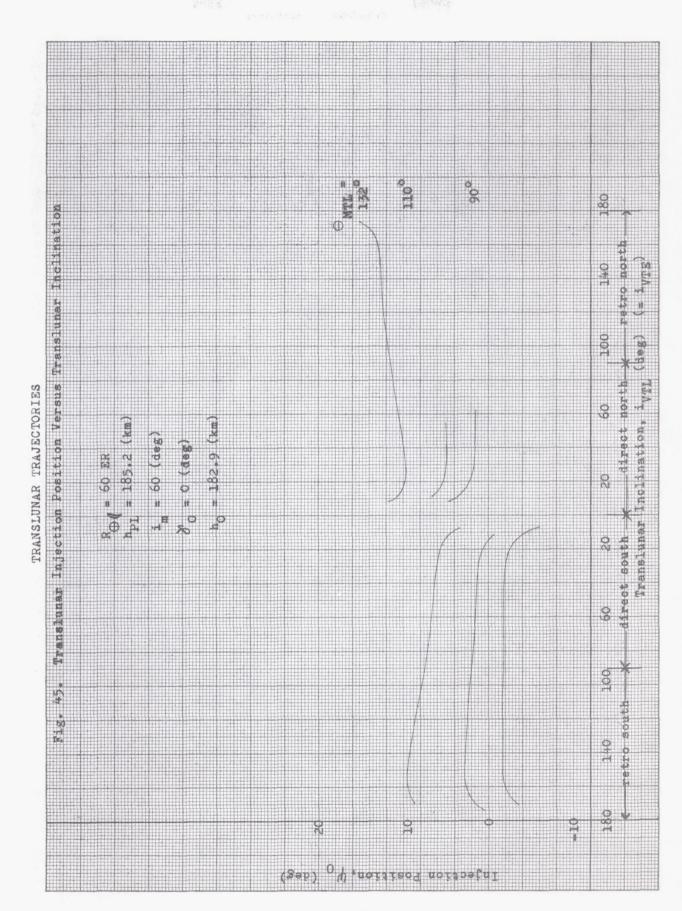










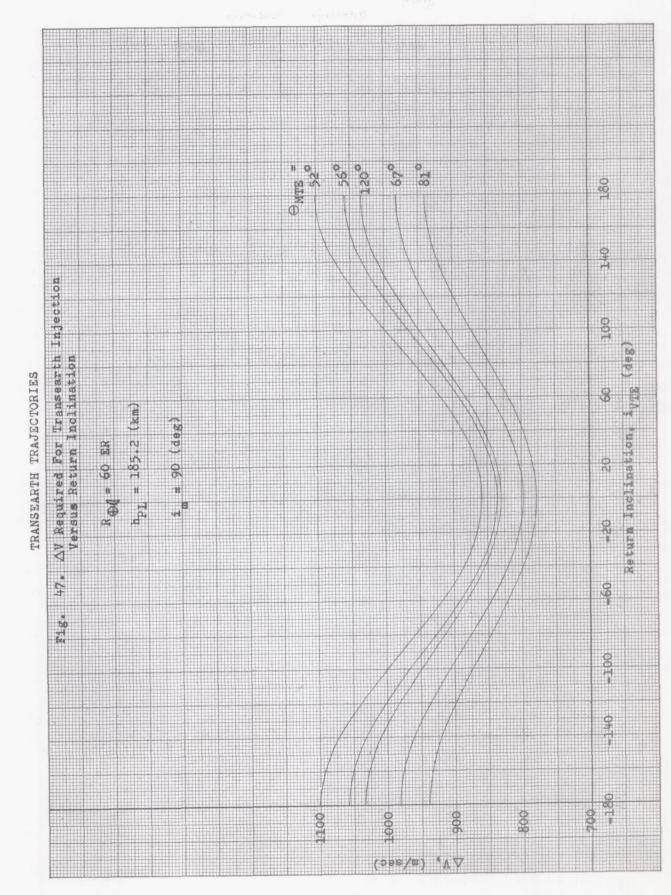


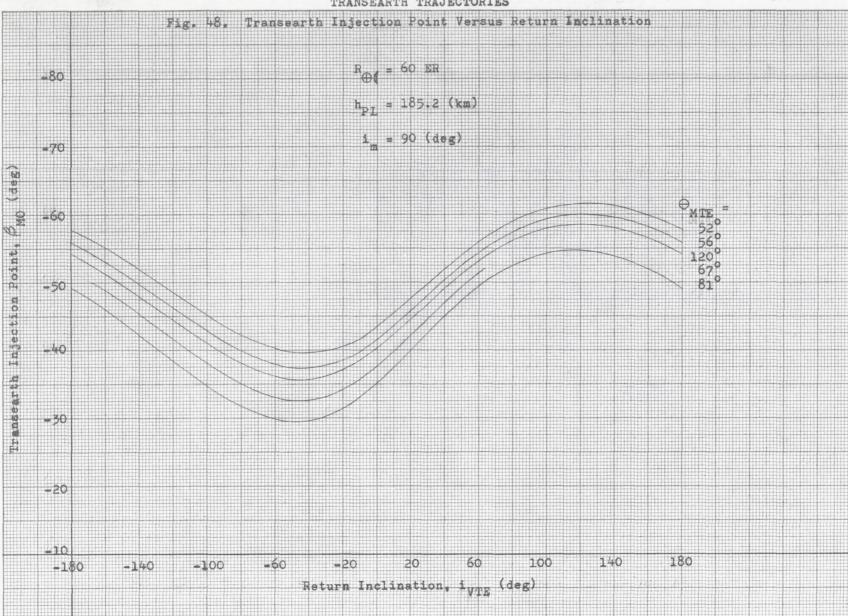
-retro morth

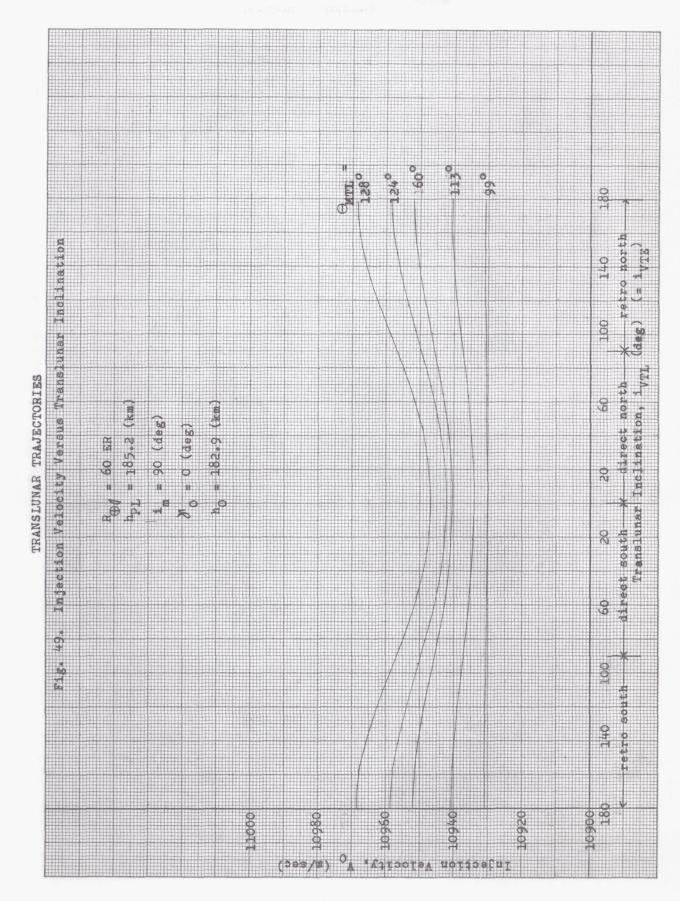
direct mouth X direct north X Return Inclination, 1 vyk (deg)

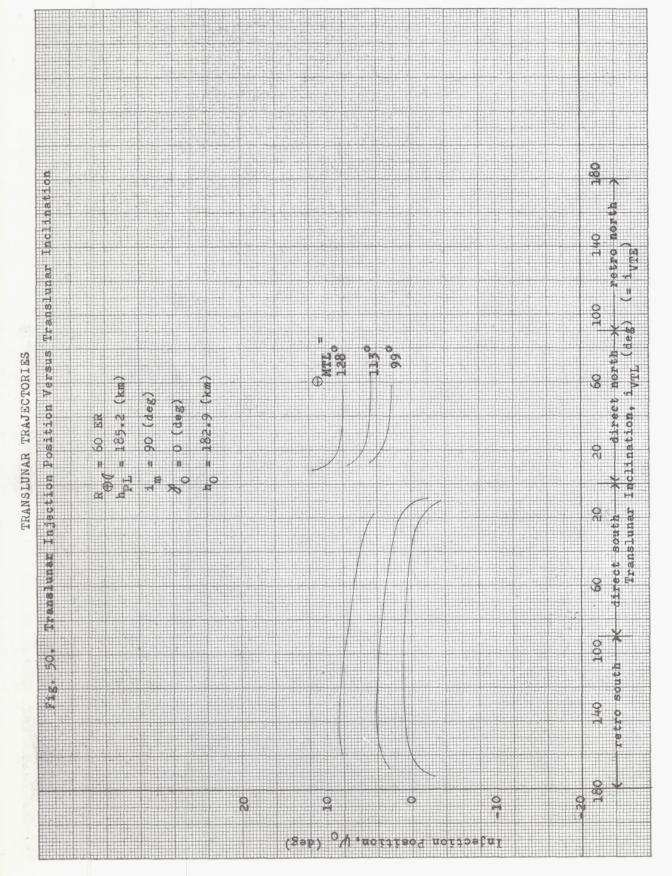
retro south

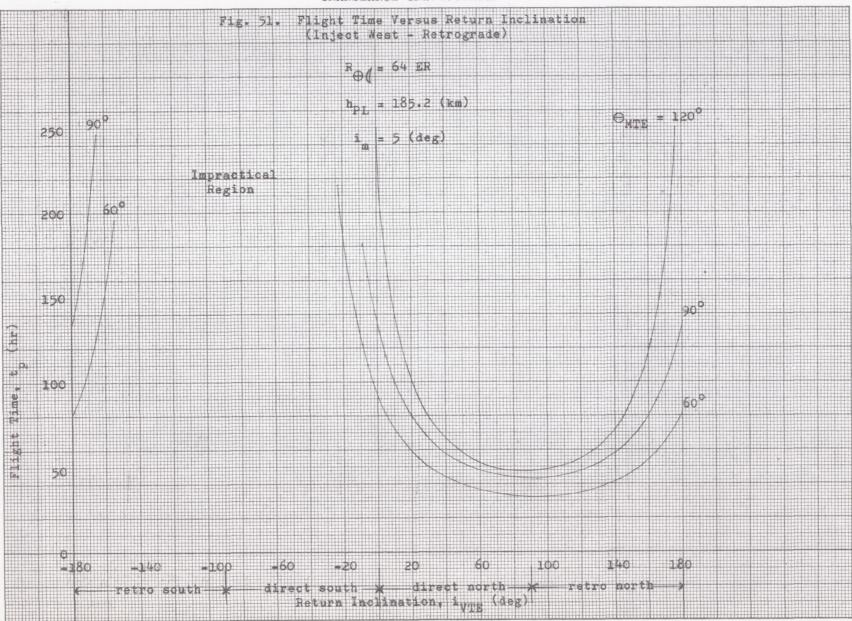
IX-62

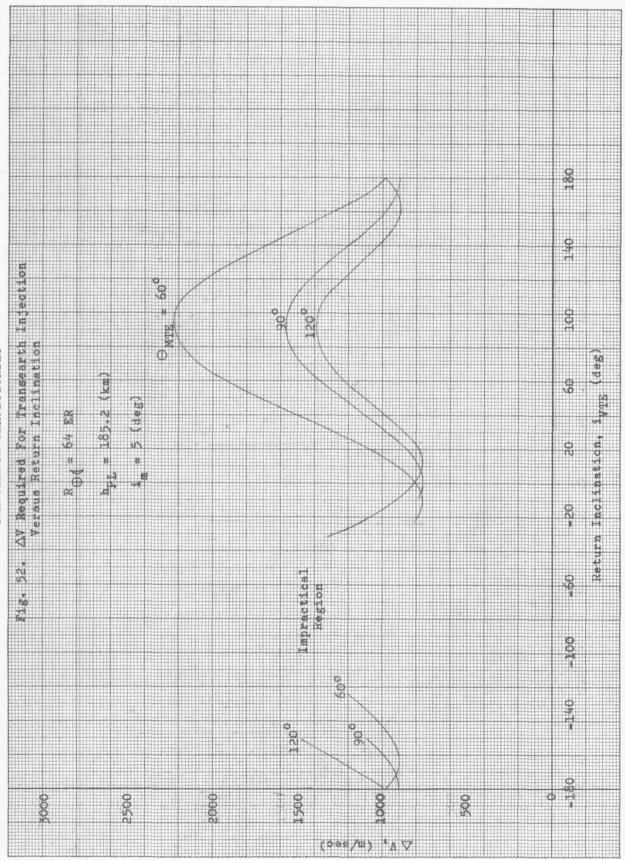


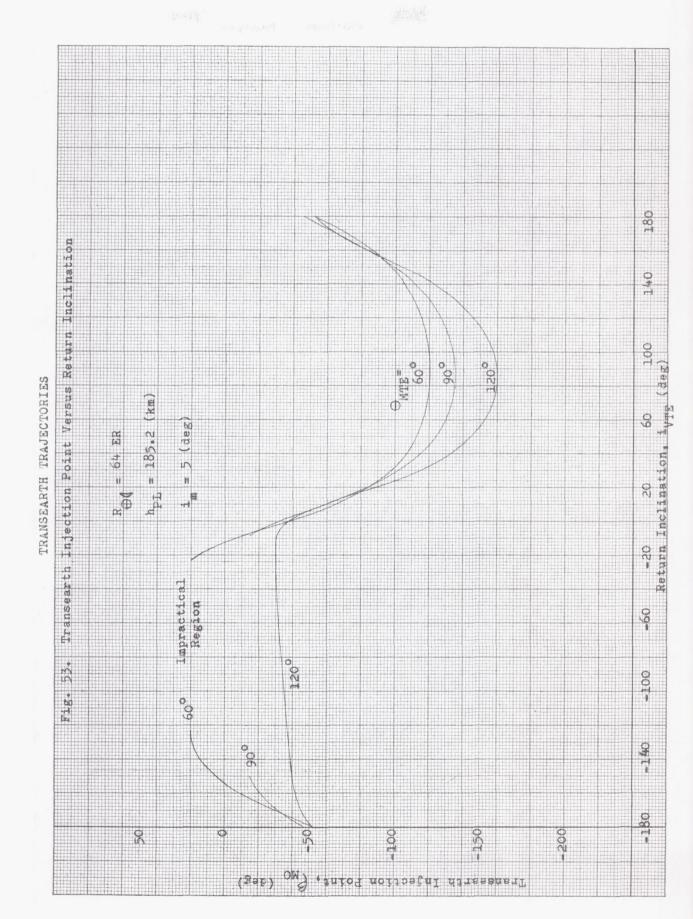


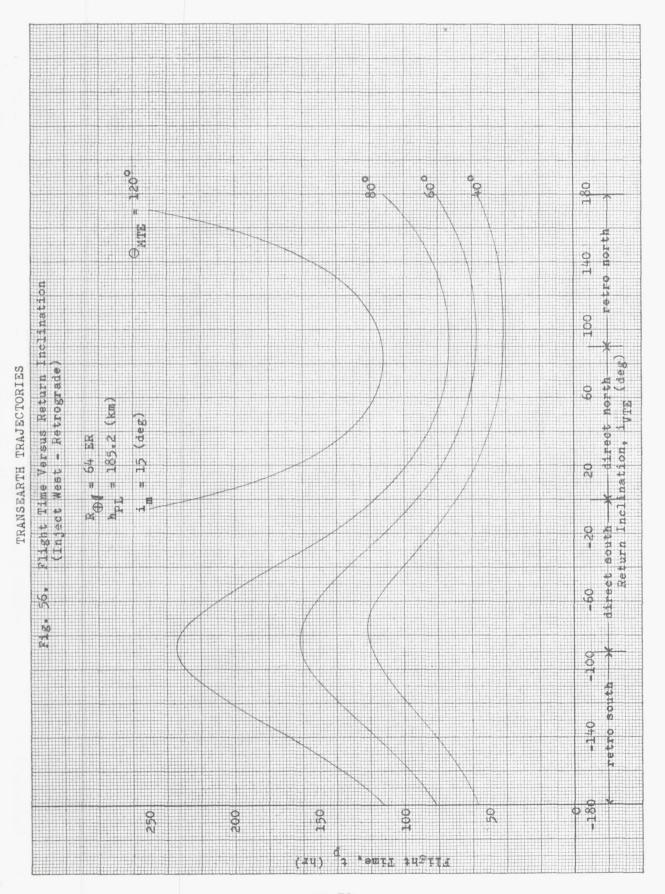


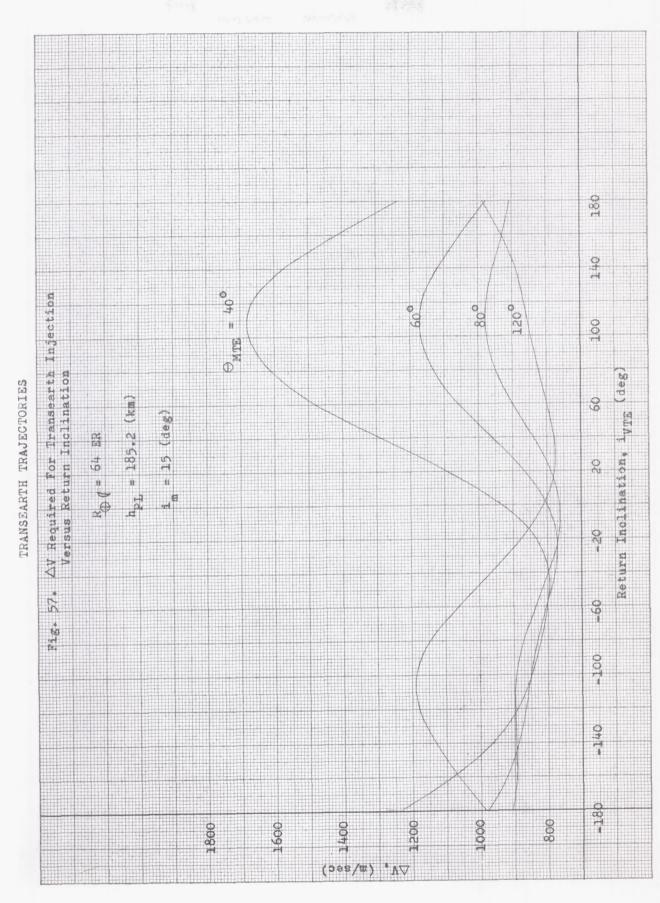




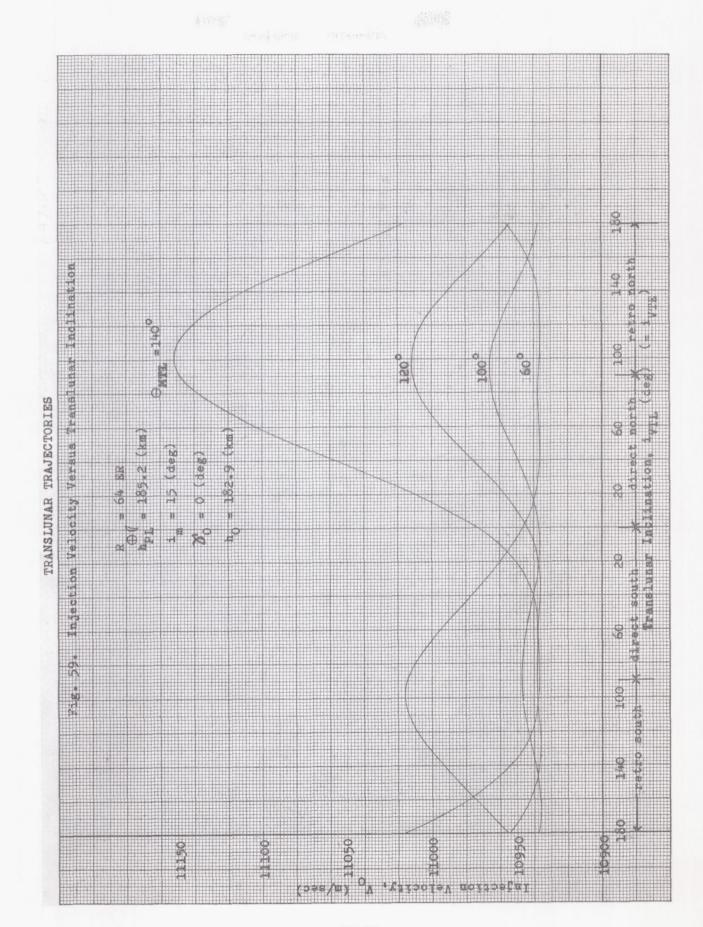


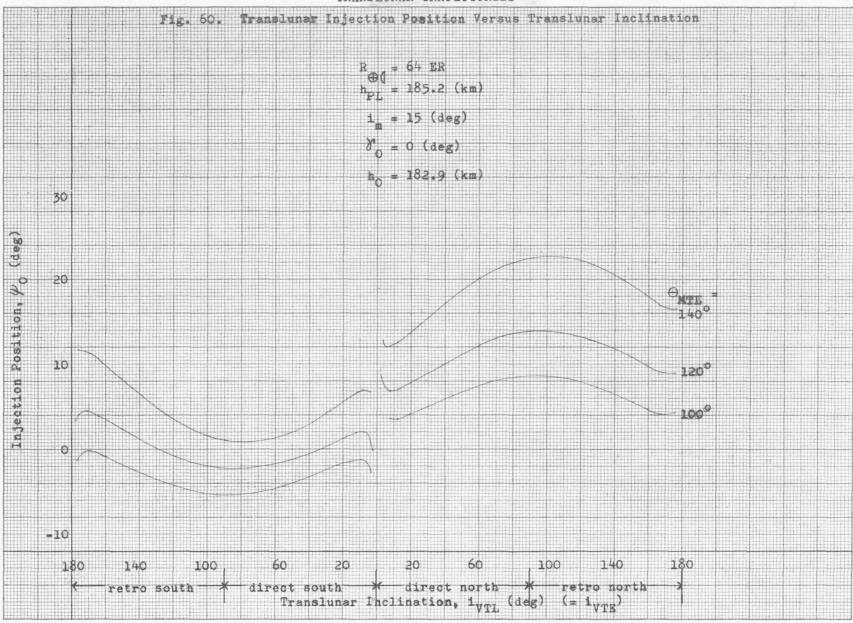


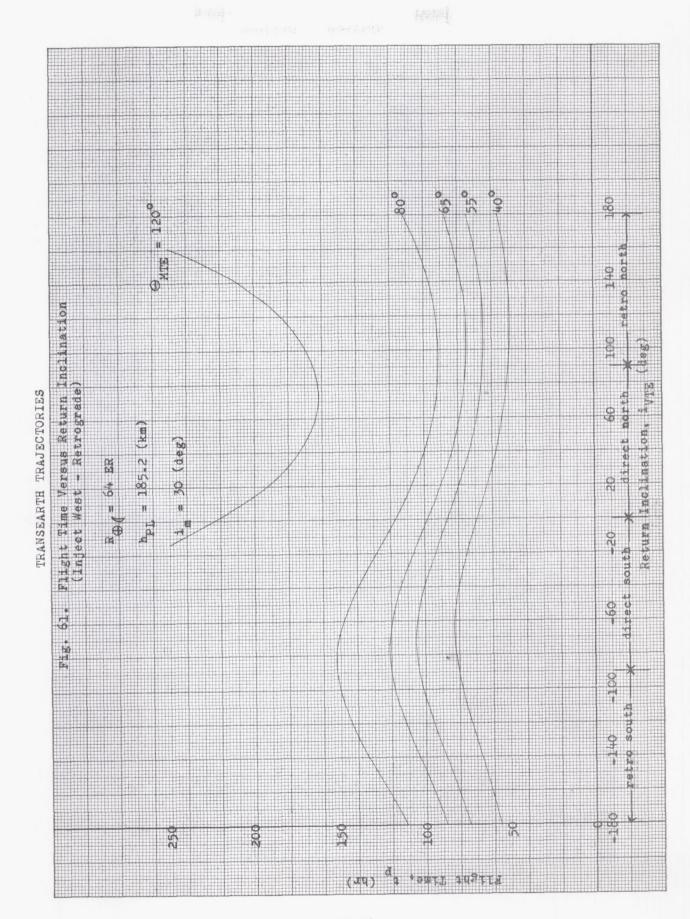


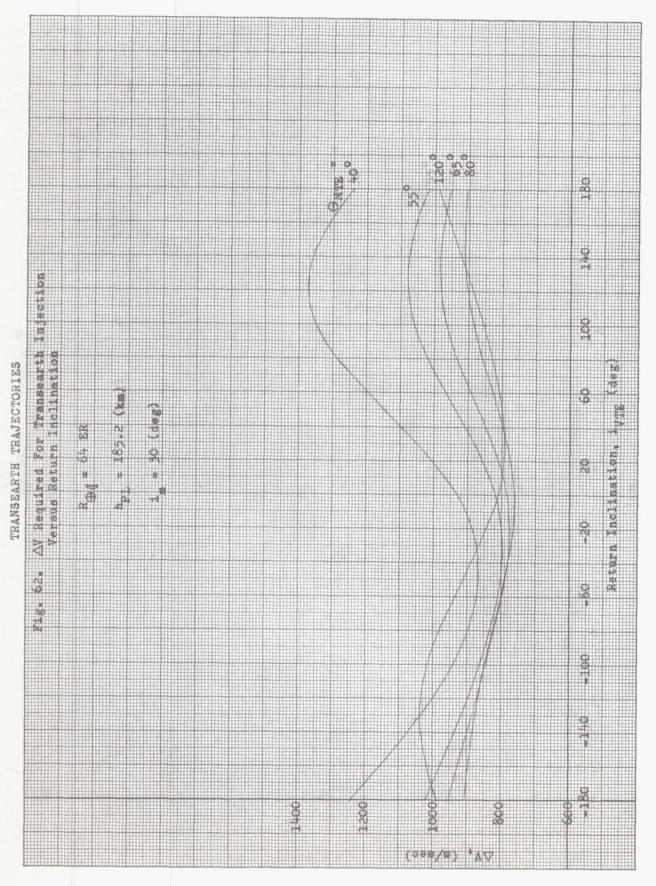


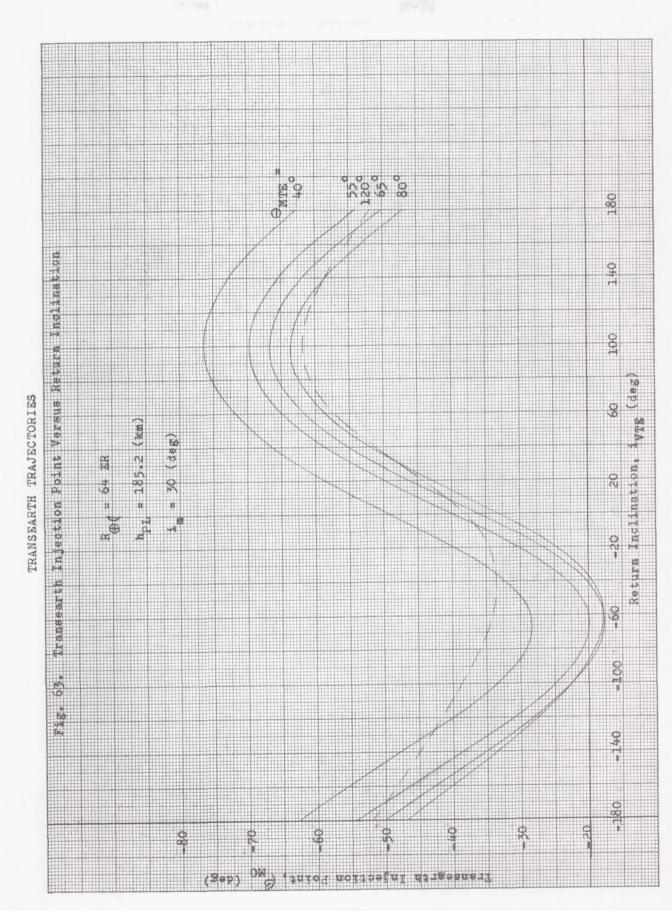
IX-73

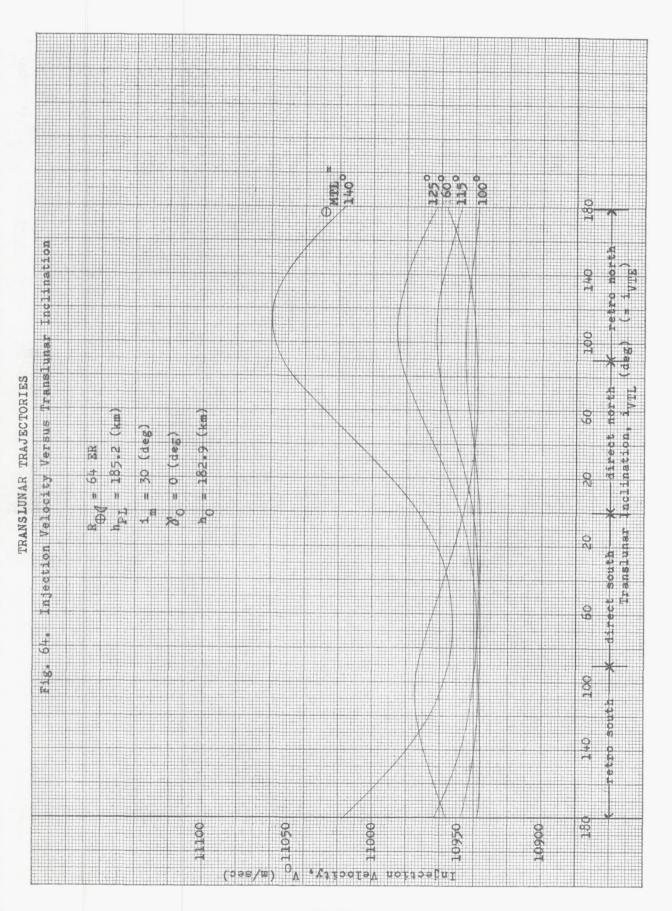


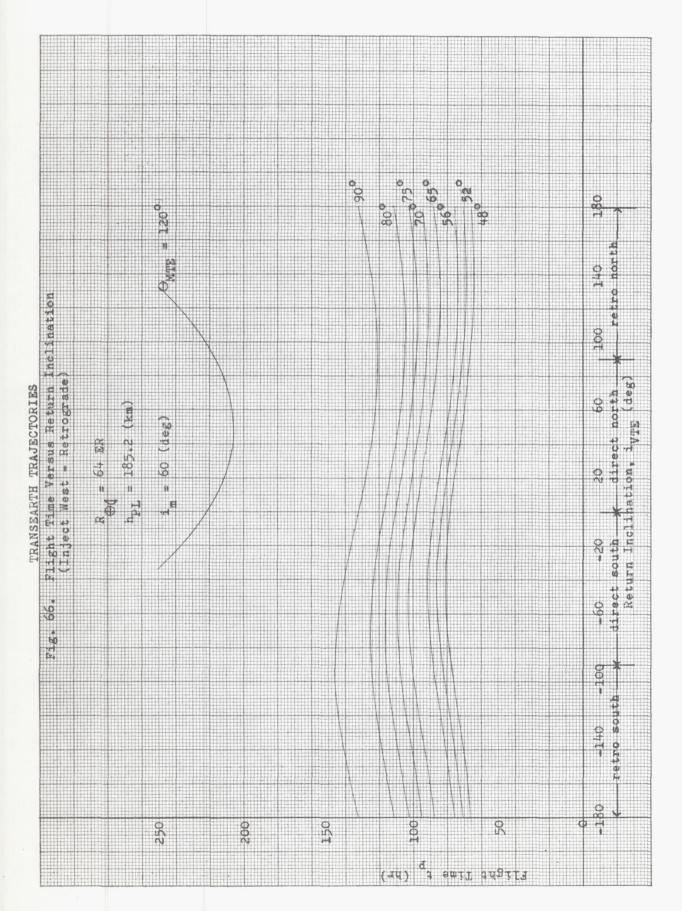


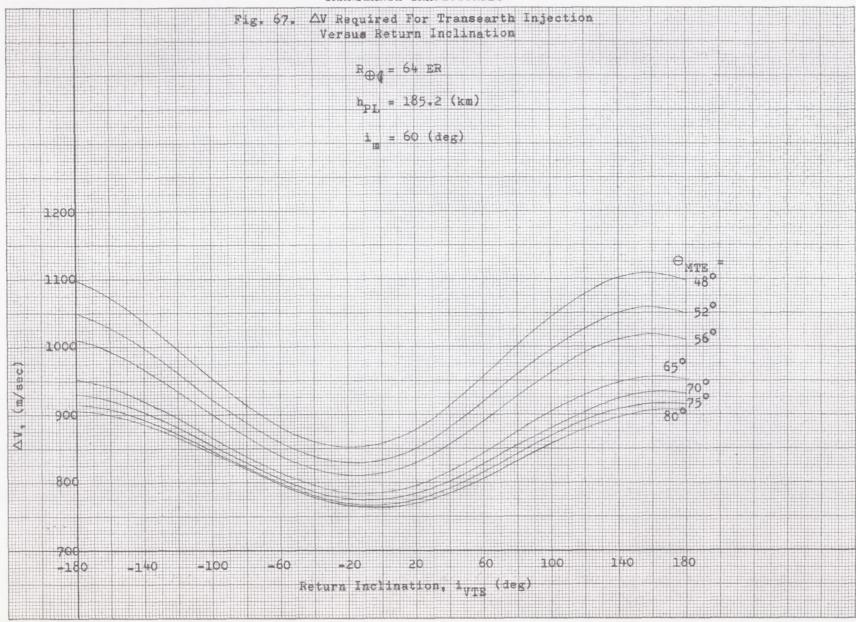


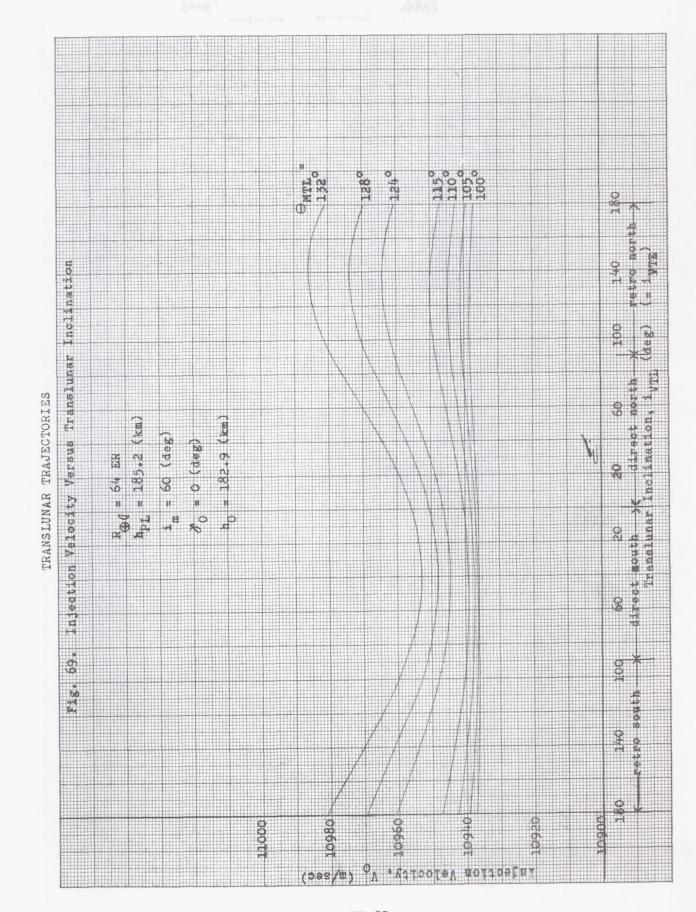


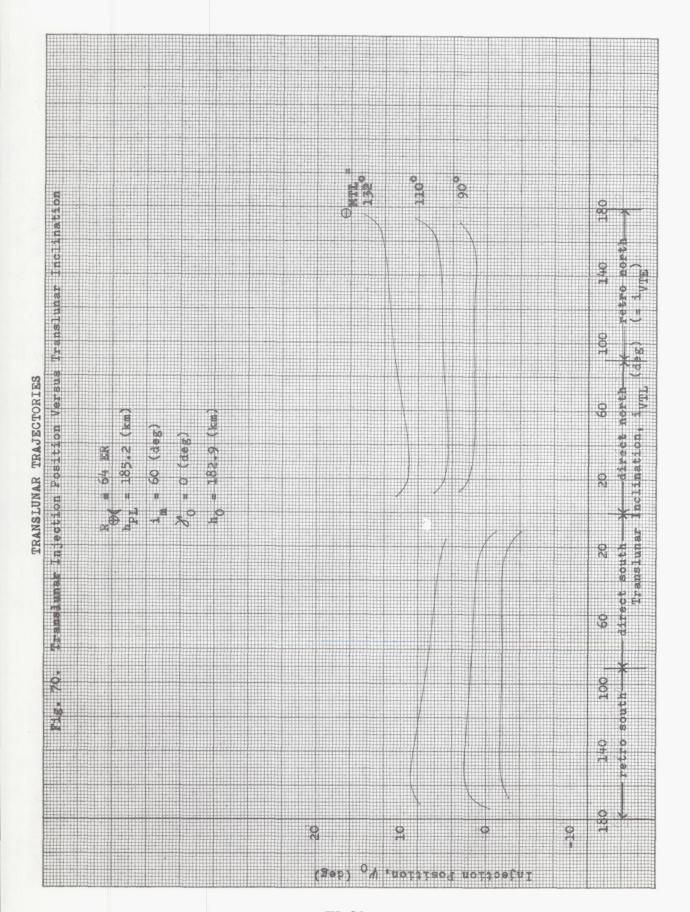


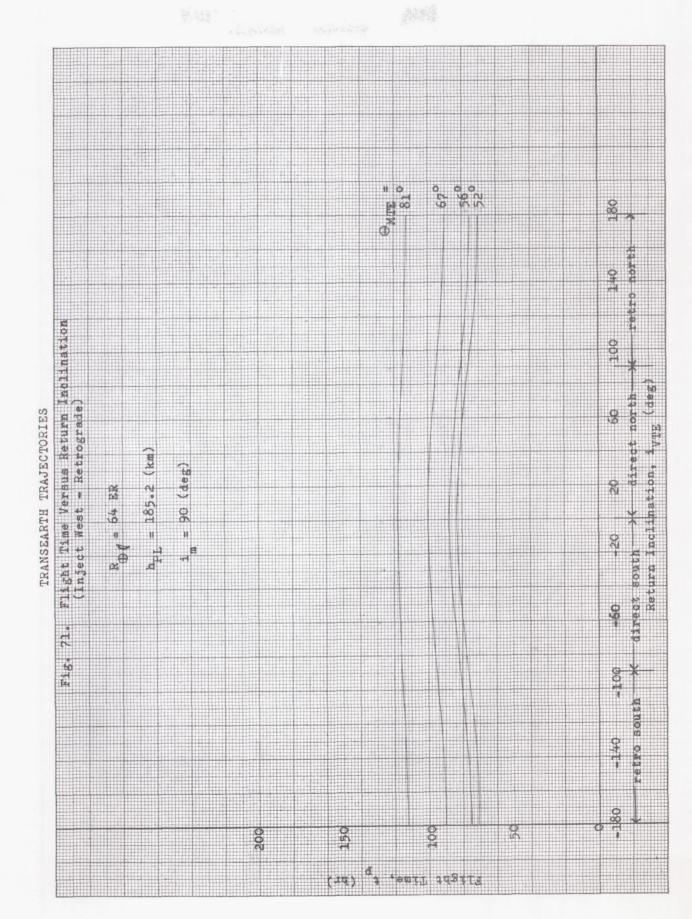


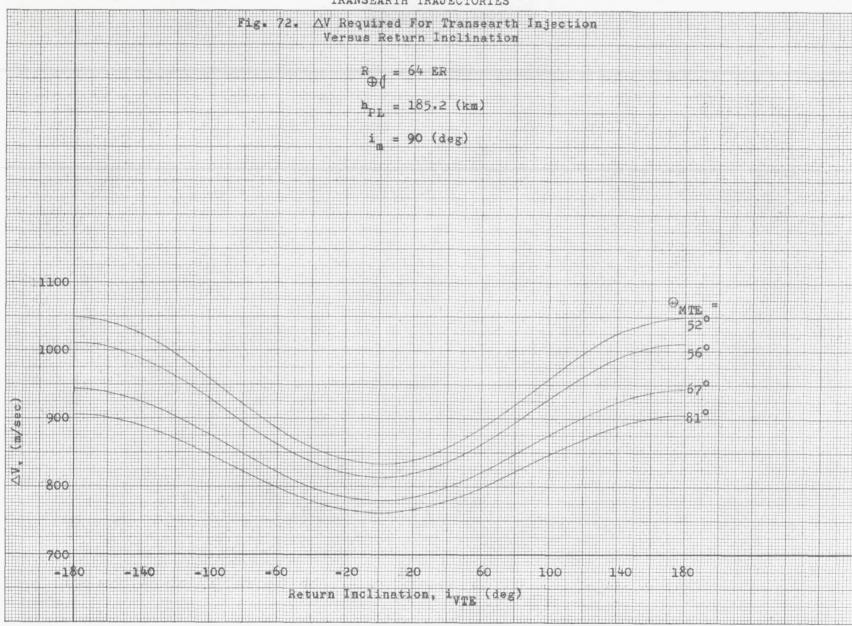


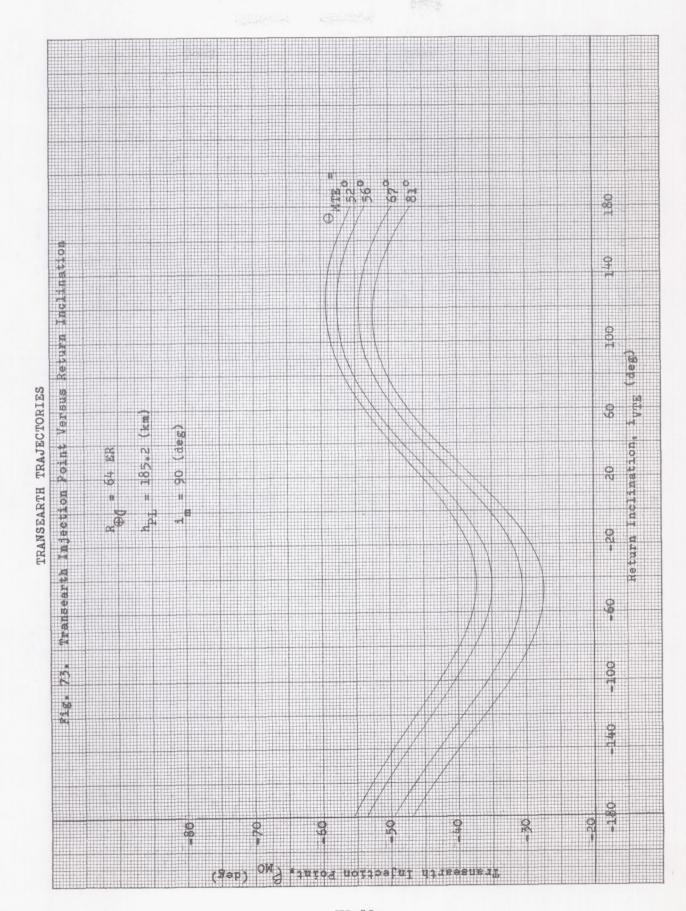


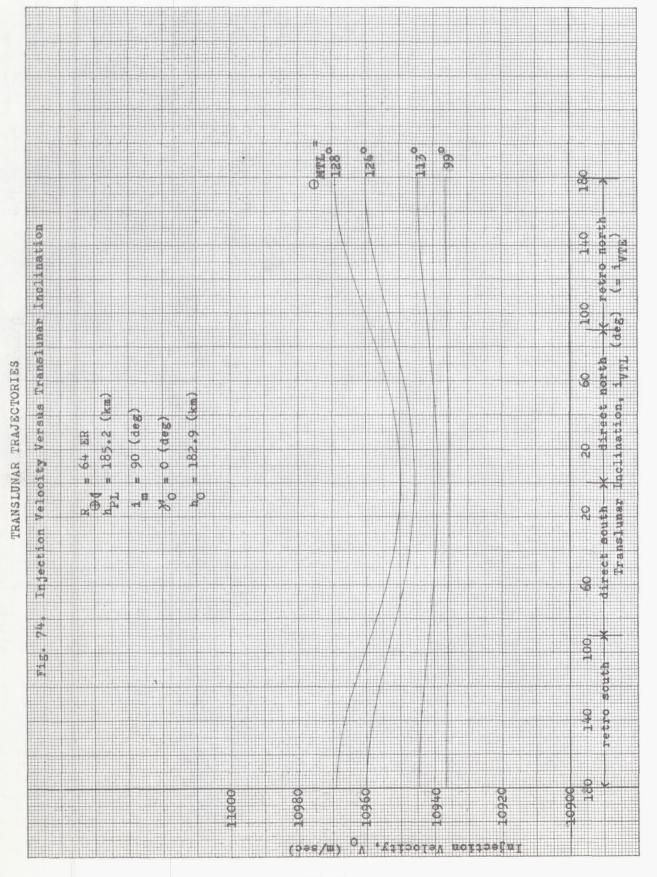


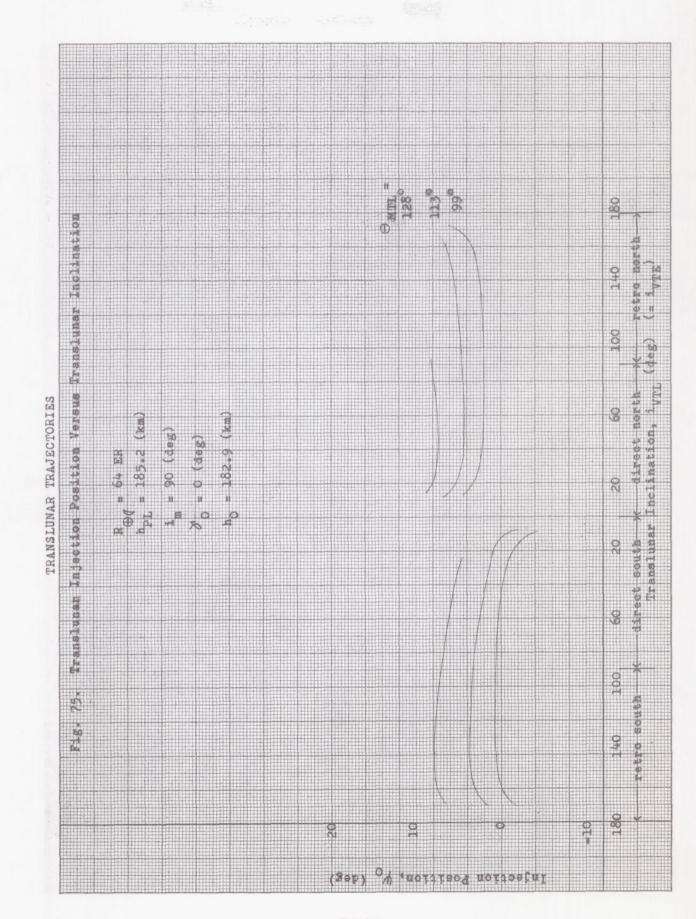


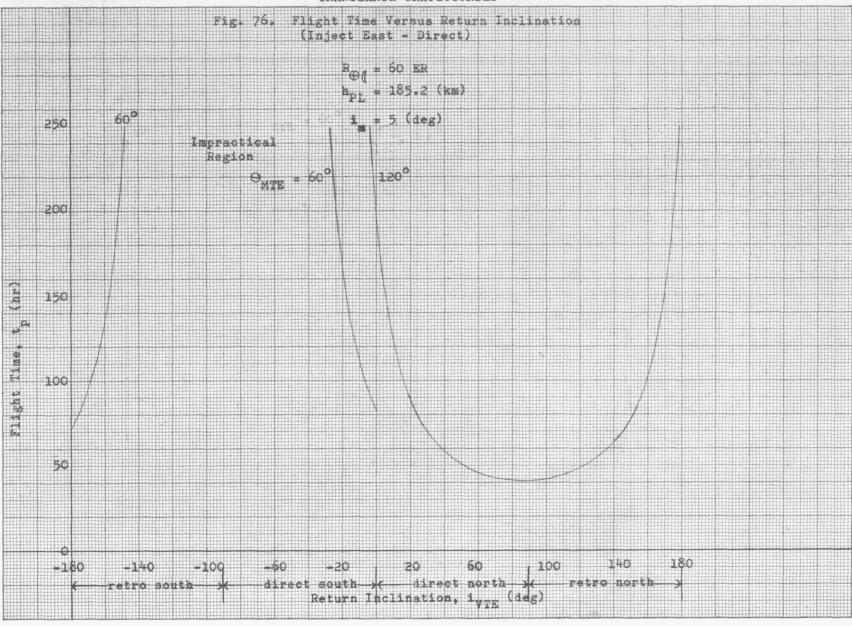




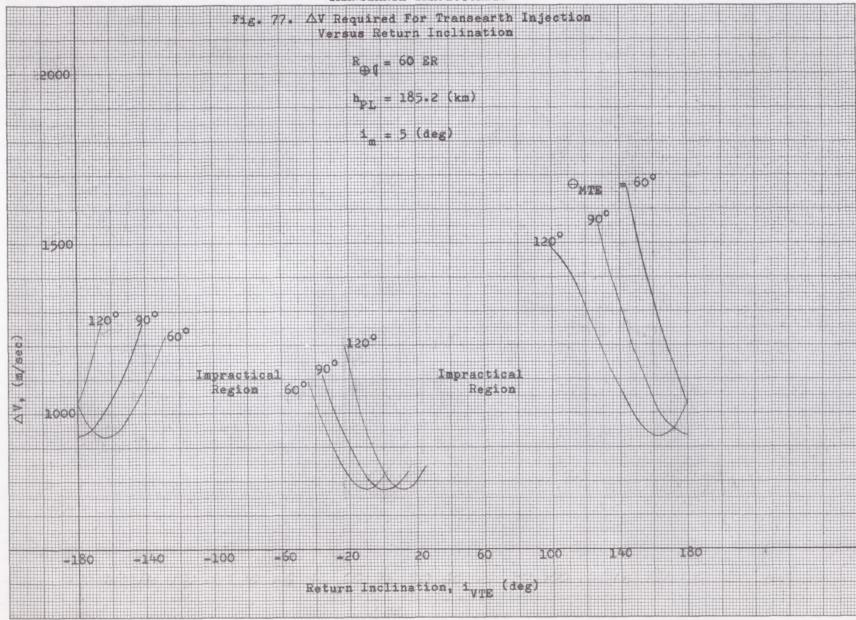




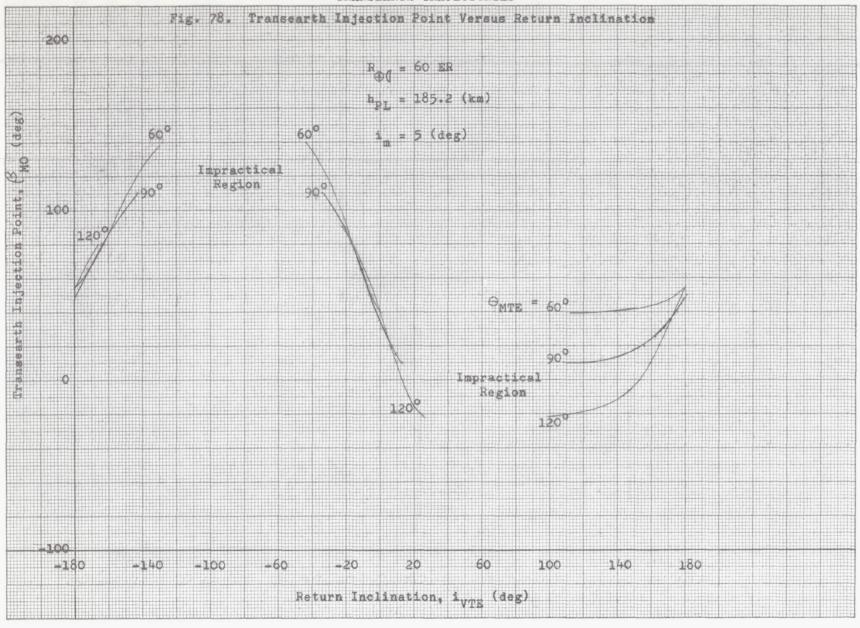




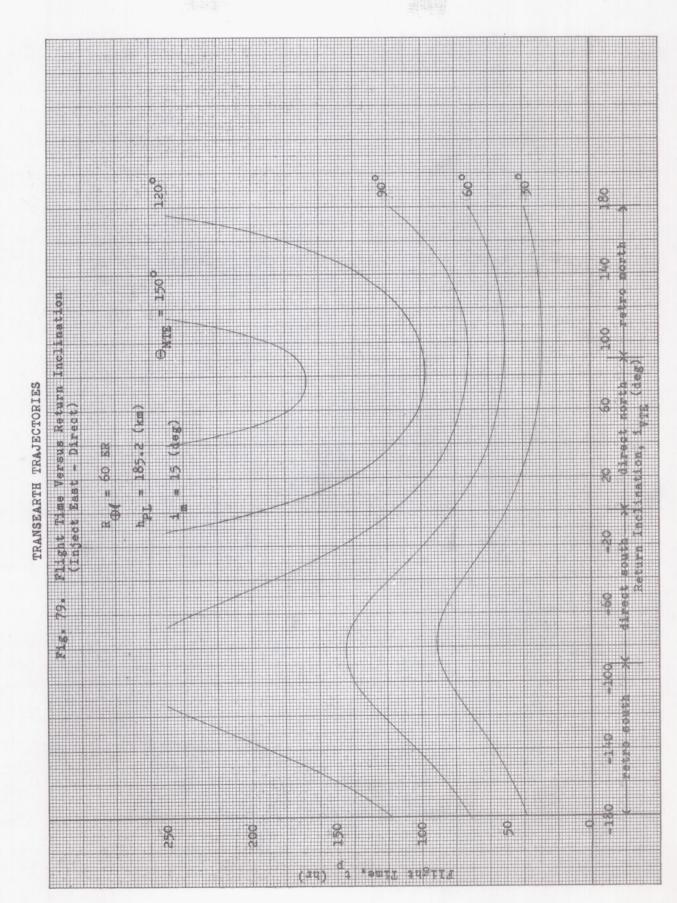
IX-92

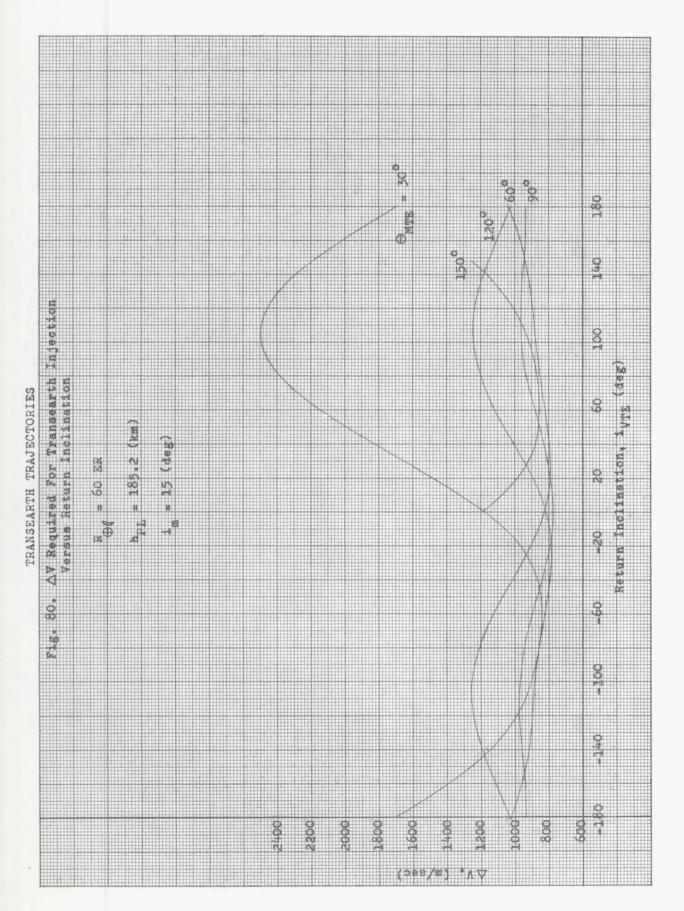


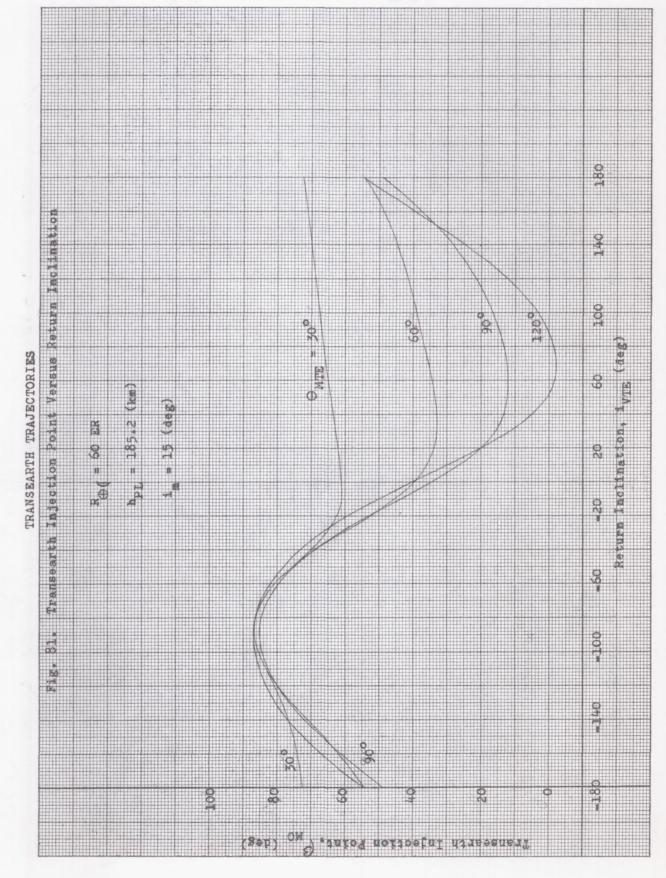
IX-93

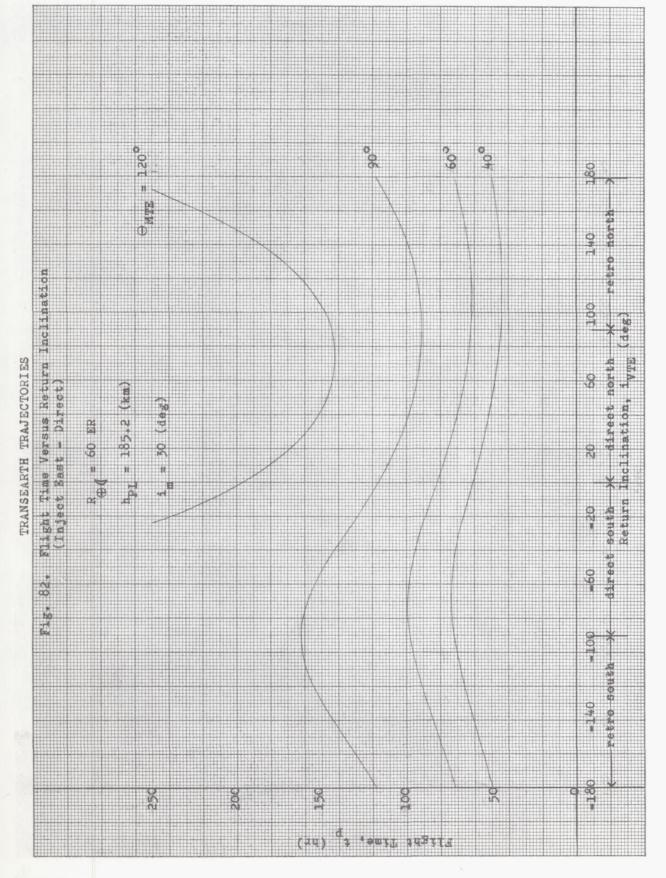


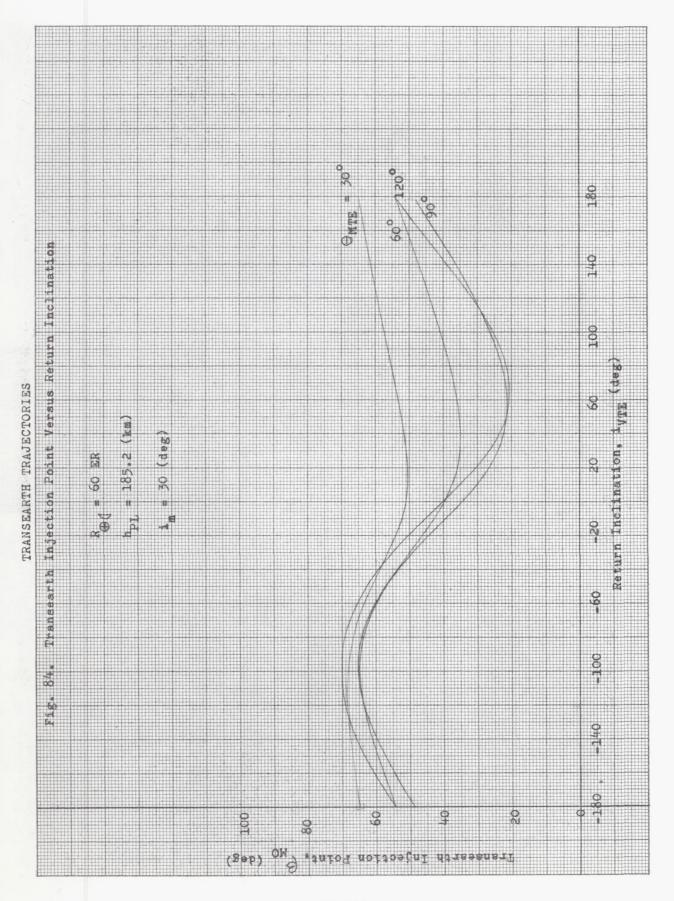
IX-94

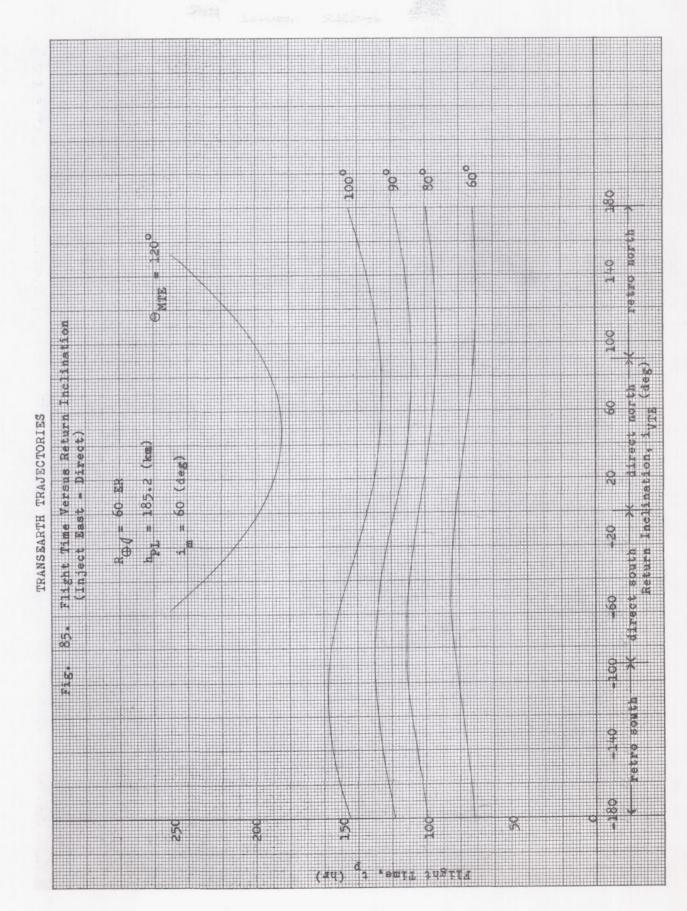


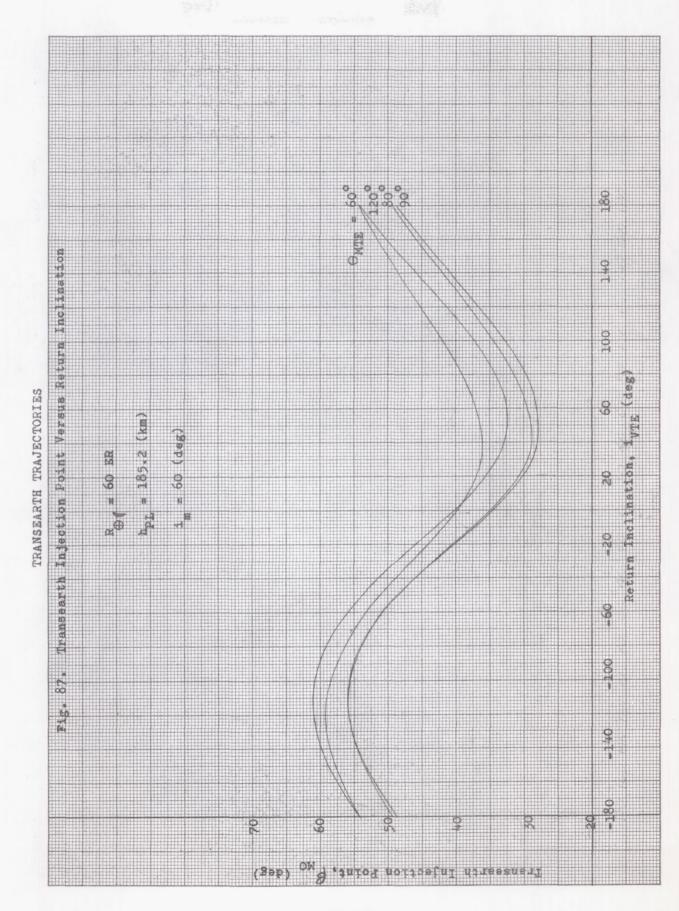


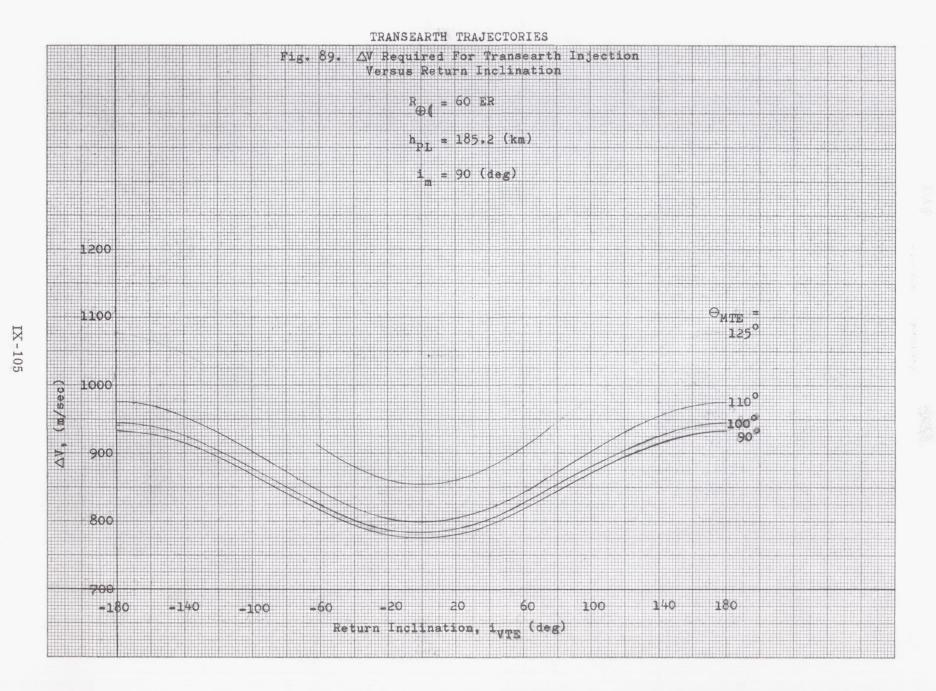


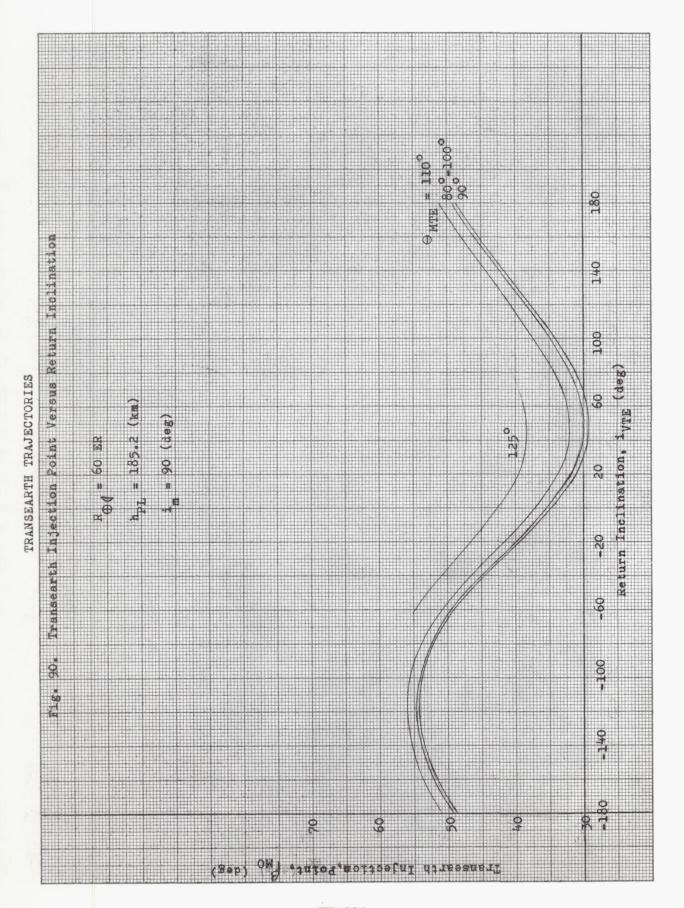












CHAPTER X

EARTH RETURN

Prepared by:

F. Santora and F. Martikan Martin Company (Baltimore) Aerospace Mechanics Department March 1963

		Page
Α.	Landing at a Specific Earth Site	X-1
В.	Re-Entry by Atmospheric Deceleration	X-2
C.	Re-Entry by Rocket Deceleration or a Combination of Atmospheric and Rocket Deceleration	X-18
D.	References	X-24
T1111	strations	X-27



X. EARTH RETURN

This chapter presents the flight mechanics and guidance aspects of earth return. The material is discussed mostly in qualitative form, with the required trajectory equations and methods of solution given. For re-entry into the earth's atmosphere the limiting factors in the selection of the trajectory are not so much the ultimate aerodynamic performance of the re-entry vehicle, which could be augmented by rocket acceleration or deceleration, but the properties of the earth's atmosphere itself, which provide two design limits:

- (1) Upper limit on the steepness of re-entry because of high decelerations.
- (2) Lower limit on the steepness due to high aerodynamic heating or a "skipping" out of the atmosphere if insufficient dissipation of the vehicle's kinetic energy occurs.

A complete description of earth return would thus include a description of the earth's atmosphere, the aerodynamic forces and the resulting decelera-tion and heating of the re-entry vehicle. The properties of the earth's atmosphere have been discussed briefly in Chapter II and in more detail in Chapter II of Ref. 1. The form of the aerodynamic lift and drag terms, which become numerically very large during re-entry, has been given in Section B of Chapter IV. The present chapter discusses the techniques of re-entry, the timing of re-entry for specified lunar mission constraints, and the aerodynamic performance of and trajectory requirements for the re-entry vehicle. The aerodynamic heating aspect of re-entry (with equations for estimating convective, conductive, radiative heating in hypersonic flow and the flow field around the vehicle, thus giving the heat balance and temperature for portions of the re-entry vehicle) has been given in Chapter IX of Ref. 1, and Chapter XII of Ref. 2. Aerodynamic heating is of prime concern during a re-entry; practically all of the vehicle's kinetic energy must be dissipated in the form of heat. Most materials can only absorb a fraction of this heat energy without melting or evaporating; consequently the dissipated kinetic energy must be made to heat the gas around the body rather than the body itself.

Section A of this chapter discusses qualitatively the timing of the return and the transearth and translunar trajectory parameters which are affected by this timing if landing at a specific earth site is desired.

Section B discusses re-entry by atmospheric deceleration. In this technique a large portion of the kinetic energy of the re-entering space vehicle is converted to heat by the action of atmospheric drag until the speed of the vehicle is slow enough to permit a landing without damage to the structure and the occupants, if any. The aerodynamic maneuvering capability of the vehicle is discussed in Subsection B-4 and the techniques for guiding the re-entry vehicle to a landing in Subsection B-5.

Section C discusses earth re-entry by use of rocket and/or atmospheric deceleration to reduce

the space vehicle speed from the supercircular approach speed of $\simeq 11~\rm km/sec$ to a circular orbit velocity of $\simeq 8~\rm km/sec$. The vehicle may then remain in earth satellite orbit until such time that re-entry from orbit to a specific landing site can be accomplished. An important part of this technique, the determination of call-down frequency, has been discussed in some detail and the conditions for a recall to a specific site have been derived.

This chapter completes the discussion of the different phases of a lunar trajectory which was started with earth departure in Chapter V. The material in these chapters consisted of a discussion of techniques and requirements for each trajectory phase, as well as an attempt to catalogue all earth-to-moon trajectories of interest from Cape Canaveral and moon-to-earth trajectories from lunar satellite orbits to an arbitrary earth landing site. The task remains to combine the material on vehicle environment in Chapter II, on the geometry in Chapter III, the dynamics of Chapter IV and the detailed discussion of the trajectory phases in Chapters V to X and then to illustrate the application of this material to the preliminary design of a specific lunar mission. This task will be taken up in Chapter XI.

A. LANDING AT A SPECIFIC EARTH SITE

For manned and many unmanned lunar missions, operational concepts dictate the recovery of the spacecraft after the completion of the mission. Planning for recovery of the spacecraft will be based on landing in one of a few relatively small areas since only small areas on earth can provide adequate tracking facilities during reentry and the recovery forces and facilities can be deployed in only a few restricted areas. In addition, the climate, the terrain and political considerations will also limit the available landing areas. Even abort trajectories can be planned to result in vehicle return to specified landing areas as discussed in Section D of Chapter VI. Only dire emergencies will require indiscriminate earth return and landing, namely when the survival of the space vehicle crew depends on it.

Once one or more landing sites have been selected, the timing of the mission must be designed to result in a landing at that site. For lunar missions the timing is a major problem and it is the first one attacked as illustrated by the two sample missions in Section G of Chapter XI. The timing problem can be solved during earth departure, at injection by choice of a suitable flight time, on the moon, or by use of parking orbits on earth return. In any case, timing depends on the particular trajectory class selected (see Chapter IV for further definition and classification of lunar trajectories).

With a circumlunar trajectory class that is designed to directly re-enter the earth's atmosphere at the end of the transearth portion of the trajectory, a major timing problem arises since

for a direct re-entry the landing will occur soon after re-entry and, therefore, will require that the landing site be close to the re-entry trajectory plane. Therefore the circumlunar mission must be planned at the time of launch (from earth) to possess a total flight time that allows the designated landing site to rotate beneath the transearth trajectory plane at re-entry or at least within the maneuvering capability of the reentry vehicle. For a given lunar arrival date or time of the month, the earth-moon distance R $_{\mbox{\it GM}}$ may be assumed constant for a few hours before and after the arrival date.

The allowable i_{VTL} (Section D, Chapter XI) and the resulting $i_{\mbox{\scriptsize VTE}}$ for a given $h_{\mbox{\scriptsize PL}}$ also remain essentially constant. With these mission constraints, there is a corresponding total flight time, T (from launch to injection -- to pericynthion -to earth re-entry). Now, if the earth landing site is not in the correct position relative to the transearth plane at re-entry (which is the general case) an adjustment in T is necessary. One way of obtaining this adjustment without the expenditure of energy is to alter \mathbf{h}_{PL} since it is the only remaining parameter that affects T for a given arrival date. This is most clearly illustrated in Fig. 1 for two designated landing sites, namely, Australia and Edwards AFB. It is worthwhile to note here that the maximum and minimum hpl. required to acquire these two sites occur either at the maximum southerly or maximum northerly declination. Furthermore, note that the re-entry range required to reach the sites varies considerably.

If the mission specifically states that $\rm h_{PL}$ remains constant, then the adjustment in T must be achieved by means of a transearth adjustment maneuver as explained in Section E, Chapter XI. This midcourse maneuver does not alter the transearth inclination $\rm i_{VTE}$ but only advances or delays the time at which re-entry occurs.

An alternative to the transearth adjustment maneuver is to allow the spacecraft to arrive at earth without consideration to site location. At approximately the time of perigee, an orbital entry maneuver is executed which places the spacecraft in a close earth orbit where the spacecraft stays until the proper position of the landing site relative to the vehicle is achieved, before deorbit, re-entry, and a landing is attempted.

The discussion thus far implicitly assumes that the acquisition of a particular lunar satellite orbit orientation defined by the i_m - θ_M relationship (see Section A of Chapter XI) is not a mission requirement. However, if the spacecraft must have a specific i_m - θ_M combination, then i_{VTE} will depend on and be in error with the desired i_{VTE} . Thus, in addition to making adjustments in total flight time to time a given landing site, it also becomes necessary to make a transearth planar change Δ i_{VTE} for the three cases mentioned above. This maneuver and the

corresponding energy requirements are discussed in detail in Section E of Chapter XI.

For a transearth trajectory that originates at the moon and returns a spacecraft to earth, the problem of returning to a specific earth site is not as formidable as for the circumlunar class since flight time is not constrained (see Chapters IX and XI). There are certain ramifications, however, especially if the lunar departure is conducted from a pre-established orbit resulting from lunar rendezvous or parking orbit requirements. In this case the return time can still be controlled but the return inclination $i_{\mbox{\scriptsize VTE}}$ may have to be adjusted.

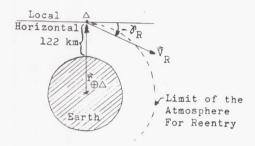
In summary, the timing problem associated with returning a spacecraft to a designated earth landing or recovery area can be solved at different times during the mission. For circumlunar trajectories the problem may be resolved at launch or in parking orbit prior to translunar injection, along the transearth trajectory, or at the completion of a mission (parking orbit at earth return). In the case of transearth trajectories established at the moon, the timing problem is resolved prior to lunar liftoff or lunar orbit departure. It must be remembered that in connection with the timing problem, it can be generally stated that a transearth midcourse correction of $i_{\rm VTE}$ is also required.

B. RE-ENTRY BY ATMOSPHERIC DECELERATION

A very efficient technique for recovery of lunar space vehicles after completion of the mission is to decelerate the re-entry vehicle by dissipating most of its kinetic energy in the earth's atmosphere without application of rocket thrust. For this re-entry technique there is a weight penalty in providing a heat shield, which protects the vehicle by absorbing some of the heat generated, but this weight penalty is far less than that of the fuel required to reduce the vehicle velocity by rocket deceleration. Atmospheric deceleration of a vehicle returning from a lunar mission presents a more severe problem than it does for an earth satellite. This fact is caused by the different speeds of the vehicles--11 km/sec for the lunar vehicle and 8 km/sec for the earth vehicle. However, the use of ablative heat shields in contrast to radiative and heat sink-type heat shields makes it possible to re-enter the earth's atmosphere with supercircular speeds, i.e., speeds in excess of 8 km/sec, at least from the point of view of theoretical thermodynamics. No vehicle has as yet been re-entered and recovered intact at supercircular speeds.

The re-entry portion of a trajectory is characterized by the dominance or large size of the aerodynamic forces as compared to the gravitational force on the vehicle. Since most re-entry trajectories are extremely short as compared to earth satellite orbits, for conventional lunar vehicles the presence of the atmosphere can be neglected until the vehicle altitude first drops below 122 km. Of course, just as in the case of earth satellites, the upper limit of the sensible atmosphere depends on the ballistic coefficient $B = C_{\rm D}A/2{\rm M}$ of the vehicle, the flight path angle γ

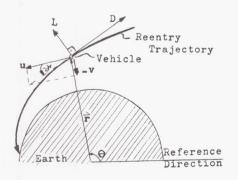
and the velocity V of the vehicle. The approach trajectory above 122 km for conventional lunar vehicles and conventional return may be considered ballistic and the initial conditions of the re-entry trajectory may be characterized by the re-entry velocity $V_{\mbox{\scriptsize R}}$ and the re-entry flight path angle $\gamma_{\mbox{\scriptsize R}}$ occurring at an altitude of 122 km as illustrated in the following sketch:



Nothing prevents the use of the equations of motion as given in Section B of Chapter IV and the initial re-entry conditions to obtain the entire trajectory by numerical integration on a digital computer. However, nonlifting vehicles with fixed aerodynamic coefficients, as well as lifting vehicles with variable aerodynamic coefficients, introduce many trajectory parameters, so that a very large number of numerically calculated trajectories must be obtained before definite trends can be established. In order to obtain an idea of re-entry trajectory characteristics, approximate analytical methods are preferable to numerical solutions just as the Voice technique enabled the determination of ballistic lunar trajectories more quickly and efficiently than numerical integration of the more complicated equations of motion. There exists no analytic solution of the full equations of motion, hence the qualifying statement that the analytic solutions are only approximate.

1. Equations of Motion for a Shallow Re-entry

Consider re-entry into the atmosphere of a spherically symmetric planet and let the atmosphere be spherically symmetric in concentric layers about the planet and be stationary with respect to the planet. Neglect lateral aerodynamic forces as well as thrust forces. The resulting descent is planar and one can introduce plane polar coordinates $r_{\bigoplus \Delta}, \ \theta_{\bigoplus \Delta} \equiv r, \theta.$ The sketch below shows the components of aerodynamic lift, aerodynamic drag and velocity in this coordinate system.



Hence the two component equations of motion in the plane polar coordinate system are as follows:

$$-\frac{dv}{dt} = g - \frac{u^2}{r} - \frac{L}{M} \cos \gamma + \frac{D}{M} \sin \gamma \qquad (1)$$

$$\frac{du}{dt} + \frac{uv}{r} = -\frac{D}{M} \left(\cos \gamma + \frac{L}{D} \sin \gamma\right)$$
 (2)

where

t = time

g = local acceleration due to gravity

M = vehicle mass (constant)

 γ = flight path angle at any time.

In order to obtain an approximate analytical solution, Chapman (Ref. 3) introduces a Z-function.

$$Z = \frac{\rho_{\infty}}{\alpha \left(\frac{2 \,\mathrm{M}}{\mathrm{C}_{\mathrm{D}} \,\mathrm{A}}\right)} \sqrt{\frac{\mathrm{r}}{\beta}} \,\,\overline{\mathrm{u}} \tag{3}$$

where

 ρ_{∞} = free stream atmospheric density, $\frac{\text{kg}}{\text{m}^3}$

$$C_D$$
 = drag coefficient, $C_D = \frac{D}{\frac{1}{2} \rho_m V^2 A}$

$$v^2 = u^2 + v^2 =$$
 vehicle velocity squared

A = vehicle reference area

 β = logarithmic atmospheric density gradient in units of m⁻¹

$$= -\frac{\mathrm{d}}{\mathrm{d}r} \left(\ln \rho_{\infty} \right) = \frac{1}{\rho_{\infty}} \frac{\mathrm{d}\rho_{\infty}}{\mathrm{d}r} = \frac{\overline{\mathrm{M}} g}{B^{*} \Gamma}$$

$$R^*$$
 = 8.31439 x $10^3 \frac{\text{joules}}{\text{°K-kg}}$ = gas constant

T = local temperature of the ambient atmosphere in °K

m = molecular weight of the atmosphere

 $\frac{u}{u} = \frac{u}{\sqrt{gr}}$ is a dimensionless horizontal velocity parameter.

Chapman (Ref. 3) then makes the assumption that the re-entry is shallow (or γ is small during entry), so that $\cos \gamma \cong 1$, $\sin \gamma \cong \gamma$, $V \cong u$, $|(L/D) \tan \gamma|$ << 1.

With the shallow re-entry consumption, the introduction of \overline{u} as the independent and Z as dependent variable, the two equations of motion (1) and (2) reduce to a single ordinary nonlinear second-order differential equation. This transformed equation of motion is given here together with the physical interpretation of the terms:

$$\overline{u} Z'' - (Z' - \frac{Z}{u}) = \frac{1 - \overline{u}^2}{\overline{u} Z} \cos^4 \gamma$$
vertical component of drag force
$$- \sqrt{\beta r} \frac{L}{D} \cos^3 \gamma$$
lift force
$$(4)$$

with the initial conditions

$$Z(\overline{\overline{u}}_i) = Z_i \frac{dZ}{d\overline{u}}(\overline{u}_i) = \left(\frac{dZ}{d\overline{u}}\right)_i$$
 (4a)

The author then examines the structure of Eq (4) with the initial conditions representing re-entry conditions and finds that three dimensionless parameters determine the motion during shallow re-entry: the re-entry velocity parameters $(\overline{V}_R)_i = (V_R/\sqrt{gr})_i$, the lift parameter L/D $\sqrt{\beta r}$ and the perigee parameter

$$F_{PE} = \frac{\rho_{PE}}{2\left(\frac{2 M}{C_D A}\right)} \sqrt{\frac{r_{PE}}{\beta}}, \qquad (4b)$$

where the subscript "PE" refers to vacuum perigee of the earth return trajectory.

These parameters are then utilized to find safe re-entry corridor depths (for a complete definition of re-entry corridor see Subsection B-3) that are extremely useful in comparing various re-entry vehicle configurations and trajectories. Deceleration load factors, guidance requirements, re-entry range, heating rates and L/D effects can also be accurately determined from these parameters.

Luidens (Ref. 4) presents closed form solutions of many engineering parameters of interest for

specific re-entry trajectories such as constant angle of attack, constant altitude, constant net acceleration, modulated roll trajectories, etc.

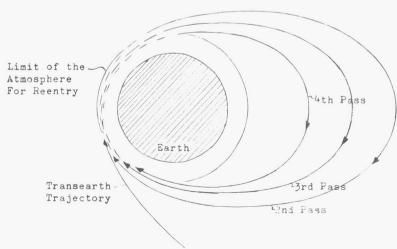
Of course, attention should be given to the assumptions made in the above references to ensure applicability to re-entry trajectories in question. Only the general results obtained in Refs. 3 to 14 are discussed in this chapter and the reader is referred to these references for complete details and mathematical developments.

2. Qualitative Description of Re-entry

The equations governing re-entry as well as the results obtained from these equations by numerical or analytical methods point out the importance of the flight path angle γ_R at re-entry (h $_R$ = 122 km for conventional vehicles). It is always negative since otherwise the vehicle could not lose altitude and re-enter.

If $|\gamma_R|$ is large, the initial approach to the earth's atmosphere is very steep and actual reentry is accomplished in a matter of seconds. This situation is analogous to a bullet being brought to a complete stop in a very short time. The result is a tremendous deceleration that is beyond both human and structural endurance.

If $|\gamma_{\rm R}|$ is very small, the approach to the earth's atmosphere is very shallow, the equation of motion, Eq (4), applies directly and this case may be likened to the ricochet of a bullet; i.e., for highly elliptic, parabolic and hyperbolic approaches the vehicle "skips" out of the atmosphere in a still highly eccentric orbit. The phenomenon of skipping out has been suggested by Chapman (Ref. 5) as a technique to re-enter the earth's atmosphere very slowly, and multiple-pass atmospheric deceleration entries are of interest for several reasons, one of which is that they provide a means of minimizing aerodynamic heating. For example, in an entry which first makes a number of supercircular passes through the outer edge of the atmosphere until the velocity is reduced to circular velocity and then completes the subcircular portion of entry with a sizable positive (see sketch) L/D, the decelerations experienced (and the rates of aerodynamic heating) can be kept relatively small.



It is shown in Ref. 3 that for ballistic entries (L/D = 0) six supercircular passes would be required to keep the maximum heating rates about the same as those experienced during the terminal subcircular portion of entry. Since each pass is followed by a substantial period wherein the structure may cool as the vehicle orbits in preparation for a subsequent atmospheric pass, this method provides an attractive possibility for utilizing the combined heat sink and radiative capability of the structure. If the re-entry body is a lifting vehicle (L/D \neq 0), then it can be rolled during the atmospheric portion of the trajectory to produce a side force which changes the inclination and nodal line of the vehicle orbit in inertial space. This maneuver which does not require rocket fuel may correct any small timing and trajectory errors.

At least two important problems arise for multiple-pass atmospheric re-entries: they could require multiple passes through the Van Allen radiation belt, and they require an especially accurate re-entry guidance system (to produce the desired trajectory). For these two reasons, such a re-entry technique is considered somewhat impractical at this time.

However, there is a region of moderate values of $|\gamma_R|$ which allows the vehicle to re-enter in a single pass, provided that the heating and/or deceleration are not excessive for the returning vehicle.

The preceding qualitative discussion indicates that the direction of the re-entry velocity vector \overrightarrow{V}_R must be controlled so that the penetration is neither too steep nor too shallow to assure the planned re-entry. Thus for a given type of reentry, be it single pass or multiple pass, there exists a small region of $V_R,\ \gamma_R$ which enables this particular type of entry. This region can be described by the concept of re-entry corridor which is defined in detail in the next subsection.

The effect of γ_R on the type of re-entry has been discussed above. As for ${\rm V_R}$, as ${\rm V_R}$ increases the re-entry corridor becomes narrower because with increasing ${\rm V_R}$ more kinetic energy must be dissipated prior to landing; hence the heating and deceleration encountered by the vehicle become more severe. To remain in the reduced re-entry corridor, the supercircular atmospheric entry required for a direct return from the moon necessitates a much more accurate guidance system than that required for the circular entry of close earth satellites.

3. Definition of Corridor Depth

A safe re-entry corridor depth as proposed by Chapman (Ref. 5) depends on the "undershoot" and "overshoot" boundaries peculiar to the configuration of the re-entry vehicle. The undershoot boundary is defined as the steepest approach to the atmosphere that the vehicle can undertake without exceeding structural or human deceleration limits during the re-entry phase. Usually the maximum deceleration, also called the maximum load factor, of 10 $\rm g_0$ is specified.

The overshoot boundary is referred to as the "shallowest" approach that can be taken with a particular vehicle to be captured by the atmosphere within one revolution around the earth, i.e., the single pass re-entry. These boundaries are illustrated in the next sketch by assuming two near-parabolic conic sections (which are representative of transearth trajectory paths prior to the re-entry phase) intersecting the earth's atmosphere. One conic section represents the undershoot boundary trajectory, and the other the overshoot boundary trajectory. If the earth and its atmosphere are ignored for the moment, then the initial conic trajectories continue to their respective vacuum perigees as shown by the dashed lines in the sketch. These conic trajectories are normally referred to as "vacuum trajectories.

Since re-entry is considered to occur at h_R = 122 km with a nearly constant V_R , the difference in γ_R results in vacuum perigee of the overshoot boundary which is usually higher than that of the undershoot boundary. Thus, the safe re-entry corridor can also be defined by a safe corridor depth, namely the difference in vacuum perigee altitudes Δh_{PE} = h_{PE}_1 - h_{PE}_2 the two vacuum trajectories.

The procedure that is used in obtaining the undershoot boundary is to change the configuration or to trim the lifting body re-entry vehicle close to its maximum lift-to-drag ratio $(L/D)_{\rm max}$ at the re-entry point. This trim attitude is maintained until the maximum load factor or heating rate is encountered.

There are several methods that can be used to establish an overshoot boundary. For example, there is the "single pass overshoot," defined as the maximum vacuum perigee altitude at which the vehicle can enter at maximum negative lift coefficient (-C) and land within a range of max

one earth's circumference from the entry point. Another method uses the same technique (- $^{\rm C}{}_{\rm L}$ max

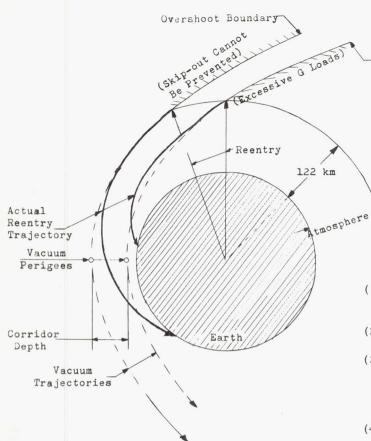
but the overshoot boundary is based on an abrupt shortening in range to impact. The difference in overshoot γ_R between these two methods is approximately 0.05°, which is equivalent to approximately 1 km in corridor depth.

Still another method defines the -C $_{\rm L}$ overshoot boundary as the maximum perigee altitude at which the vehicle can enter at -C $_{\rm L}$ and remain within the atmosphere (h \leq 122 km). This boundary lies somewhere between that of the two former

within the atmosphere (h \leq 122 km). This boundary lies somewhere between that of the two former methods, and the major point to recognize is that the above overshoot methods have negligible effects on the corridor depths.

A final method considers the possibility of an emergency situation in which knowledge of the exact re-entry conditions is not available. Define the aerodynamic lift coefficient $\rm C_L$ by $\rm C_L$ =

 $\frac{L}{\frac{1}{2}\,\rho_{_{\infty}}\,\,\mathrm{V}^2\,\,\mathrm{A}}$ and denote its maximum value by $\mathrm{C}_{L_{\max}}$.



The positive $C_{L_{\max}}$ overshoot boundary is defined

as the maximum perigee altitude for which the vehicle can enter at positive $\mathbf{C}_{\mathrm{L}_{\mathrm{max}}}$ to the point

where $_{\gamma}$ = 0° (arbitrary) at which time -C $_{\rm L_{max}}$ is

applied and the vehicle is able to remain within the atmosphere. The purpose of introducing this definition is to illustrate the reduction in corridor depth that would occur if entry into the atmosphere without precise flight path angle information were necessary. For example, in this emergency, the vehicle would have to enter at positive lift until it is determined (from a load factor time history, e.g.) that an overshoot condition exists. Once this is determined, negative lift would then be applied. This overshoot boundary is approximately 9 to 13 km below the negative C boundary. From

Chapman (Ref. 3), it is possible to determine undershoot and overshoot boundaries as a function of the lifting body re-entry vehicle's L/D, and ballistic parameter, W/C_DA = $\rm g_0/2B$. Figure 2 shows both boundaries with the undershoot boundary limited to 10 $\rm g_0$. It is assumed that C_L and C_D are constant, and that V_R = 10.67 km/sec at h_R = 122 km. The C_L, C_D relationships used are those presented in Ref. 5. It is further assumed that C_L max

applied negatively on the overshoot boundaries and (L/D)_{max} on the undershoot boundaries result in the maximum corridor depths. In Fig. 2 both boundaries are shown, thereby allowing the corridor depth to be determined directly. The associated YR is also included in the figure.

Although the results of such a parametric presentation are limited by the particular selection of ${\bf C_L}$ and ${\bf C_D}$, important trends can nevertheless be established from Fig. 2:

(1) Corridor depth is independent of W/C_DA if W/C_DA is the same for undershoot and overshoot boundaries.

Undershoot Boundary

(2) Overshoot perigee altitude is primarily a function of $W \, / \, C_L \, A$ attainable.

(3) Undershoot perigee altitude for a constant value of W/C_DA is decreased significantly by relatively low values of L/D. As L/D increases beyond 1.0, the benefits become less.

(4) For ballistic re-entry (i.e., L/D = 0), the corridor depth is only 12.8 km for a 10-g₀ maximum undershoot boundary.

The effect of $\rm V_R$ on corridor depth is shown in Fig. 3, which was also obtained from Ref. 5. The corridor depth variation with $\rm V_R$ to a 10-g_0 undershoot boundary is presented for several values of L/D.

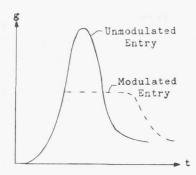
A deceleration-limited undershoot boundary is affected not only by the maximum value of g_0 selected, but also by the particular way in which the L/D is monitored. The material presented thus far has concerned re-entry at constant lift and drag coefficients. Grant (Ref. 6) and Levy (Ref. 7) have indicated that substantial increases in corridor depth can be gained by employing variations of $C_{\rm L}$ during re-entry. Such re-entries are commonly referred to as modulated re-entries.

For a spacecraft entering the atmosphere at a given initial V_R , γ_R , W/C_DA and L/D, the deceleration varies directly as the dynamic pressure $q=\frac{1}{2}\,\rho_\infty\,V^2$ for an unmodulated re-entry. As the vehicle descends into the atmosphere, the dynamic pressure and, hence, the deceleration increase to a maximum value and then decrease. A typical deceleration time-history for an unmodulated entry is shown in the next sketch. To maintain the maximum deceleration at a value lower than the peak value of the unmodulated entry (see dashed curve in following sketch), the coefficient C_R of the resultant aerodynamic force R, C_R =

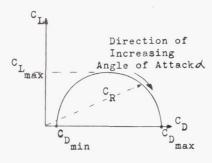
 $\frac{R}{\frac{1}{2}\rho_{\infty}V^{2}A}$, is continuously decreased to compen-

sate for the increase in dynamic pressure.

The term 'modulated re-entry' is somewhat ambiguous since it is necessary to modulate lift during almost all lifting re-entries at some time



prior to landing in order to stay within the design limitations of the vehicle or to avoid atmospheric exit to extreme altitudes. Modulated re-entries, therefore, refer to re-entries in which lift and/or drag are modulated prior to the first maxima of load factor or heating rate. Constant L/D reentries are those in which \mathbf{C}_{L} and \mathbf{C}_{D} are constant only until the initial maxima of load factor or heating rate are reached. Typically, a drag polar or \mathbf{C}_{L} versus \mathbf{C}_{D} curve for a particular vehicle takes the form shown in the sketch below.



It was found by Grant that, for a given vehicle configuration entering at given values of V_R , γ_R , the lowest possible maximum deceleration can be obtained if entry is initiated at the value of CR for and CR is continuously decreased to the value at $\boldsymbol{C}_{\ensuremath{\boldsymbol{D}_{min}}}$. This result suggests the ratio ${\rm C_R}$ at ${\rm C_D_{min}}$ to ${\rm C_R}$ at ${\rm C_L_{max}}$ as a parameter with which to correlate the maximum reduction in peak acceleration. The ratio of minimum load factor $\mathbf{g}_{0~\mathrm{max}}$ for modulated entries to $\mathbf{g}_{0~\mathrm{max}}$ for unmodulated entries is shown in Fig. 4 as a function of the ratio of C_R at C_D to C_R at C_{Lmax} wide range of values of V_R , γ_R , M/C_DA , and L/D_{max} . It is also interesting to show this ratio, $(g_{0 \text{ max}}) \mod/(g_{0 \text{ max}})$ unmod, as a function of $(L/D)_{max}$. This is done in Fig. 5 for a typical family of vehicles that are modulated from ${
m C}_{
m max}$ to C_L = 0 and $C_{L_{\max}}$ to $(L/D)_{\max}$. Observe the appreciable gains up to an $\left(\text{L/D}\right)_{\text{max}}$ value of unity after which it is evident that diminishing returns occur. The data presented in Fig. 5 can then be

factored with Chapman's results for constant C $_{\rm L}$, C $_{\rm D}$ (Fig. 2) to give the 10-g $_{\rm 0}$ modulated reentry corridors. Figure 6 presents such results for the case of modulation from C $_{\rm L}$ to C $_{\rm L}$ = 0.

Comparison of Figs. 2 and 6 indicates the large improvements in corridor depths that are obtained through re-entry modulation. For example, the 10-g_0 single-pass re-entry corridor for a vehicle with L/D = 1.0 and W/CDA = $4790 \, \frac{\text{nt}}{\text{m}^2} \, (100 \, \text{lb/ft}^2)$

is increased from 96 km to 226 km by modulation.

The maximum load factor has been the only determining parameter of the undershoot boundary in the results presented. In some instances, aerodynamic heating may represent more severe limitation than load factor in determining the vehicle's boundary. In such cases, the heating rate-limited $(q_{_{\hbox{\scriptsize H}}})$ or total heat-limited $(Q_{_{\hbox{\scriptsize H}}})$ re-entry corridors would replace the overshoot corridor and possibly the undershoot corridor as well. This is based on the fact that, as the overshoot boundary is approached, the amount of total convective heat absorbed at the stagnation point increases almost exponentially for all longitudinal ranges, since the vehicle is required to spend a greater portion of the flight trajectory in the atmosphere. An increase in the total heat load would eventually result in exceeding the original heat shield material design limit, thereby restricting the allowable range as the boundary is approached. Since the amount of heat absorbed for a given γ_R

varies with longitudinal range, the allowable limit is encountered at different entry angles for various values of re-entry range.

These factors led to the development of an "operational corridor" concept (Ref. 8) wherein the overshoot boundary is defined as the minimum entry angle for which the heat-load limit was not exceeded. This concept is illustrated in Fig. 7. Note that the heat-limited overshoot boundary is a function of the maximum required re-entry range. In other words, if the re-entry range required to fulfill operational considerations is large, the heat limit may define the overshoot boundary. This is altogether possible when reference is again made to Fig. 1 where required range can easily reach 16,000 km for lunar returns.

4. Re-entry Maneuvering Capability

After re-entry within the safe re-entry corridor is assured, the problem of landing at a specific site can be solved. In the case of a lifting re-entry body, the vehicle uses its aerodynamic characteristics as a means for maneuvering both longitudinally and laterally from the re-entry corridor to the site, whereas, in the case of a ballistic (nonlifting body) re-entry, either rocket burning prior to re-entry or a variable configuration can be used to obtain some maneuverability.

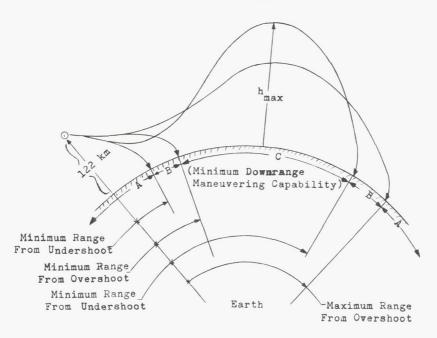
a. Longitudinal maneuverability

The longitudinal maneuvering capability or maneuvering in the re-entry trajectory plane is primarily a function of the vehicle's L/D_{max}

In the following sketch minimum and maximum range trajectories of a vehicle are shown entering along the undershoot and overshoot boundaries of the

re-entry corridor. The range segment marked "A" cannot be reached from any point in the corridor, whereas the segment denoted by "B" can be reached only from restricted portions of the corridor. Segment "C", entitled "Minimum Downrange Maneuvering Capability," gives the range segment that can be reached from any initial conditions within the corridor. The actual values of maximum and minimum

 $h_{\rm max}$ = 122 km and $h_{\rm max}$ = 740 km are shown. It can be seen that the maximum range depends on the allowable $h_{\rm max}$. Also superimposed on Fig. 8 are the 10-g₀ and 6-g₀ load factor limits which verify that the minimum range obtainable is primarily dependent on the allowable load factor.



range from overshoot and minimum range from undershoot depend strongly upon the control techniques used to obtain them. For example, the overshoot re-entries are performed initially at negative $\mathbf{C}_{\mathbf{L}_{\max}}$. This value must be modified

after single-pass entry is assured or the vehicle will experience excessive load factors. The manner in which lift is modified by the control system then determines the maneuverability that is obtained. For ranges greater than 10,000 km, the maximum altitude, $h_{\rm max}$, attained with undershoot maximum range trajectories, is larger than $h_{\rm R}$ = 122 km (which results in skip re-entry trajectories); and for ranges greater than 22,000 km, penetration of the inner Van Allen radiation belt takes place since $h_{\rm max} > 740$ km. Therefore, the particular control technique used to restrict $h_{\rm max}$ becomes the determining factor of maximum undershoot range and therefore "minimum downrange maneuvering capability" as well.

In order to gain an insight to the longitudinal reentry range capability, Fig. 8 is presented. In this figure, longitudinal range as a function of L/D is shown for the parameter γ_R . The assumptions used in this figure are that V_R = 11 km/sec, W/C_DA

= 3350 $\frac{\text{newton}}{\text{m}^2}$ (= 70 lbf/ft²), h_R = 122 km, and L/D

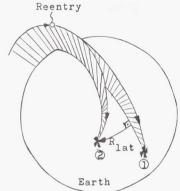
= constant (constant angle of attack trajectory). In addition to the range information, conditions for

b. Lateral maneuverability

The recovery problem implies the ability to return the vehicle to some desired point on the earth's surface. For direct entry from a lunar or deep space mission, considerable variations in re-entry point, re-entry angle, and re-entry plane must be anticipated. The re-entry vehicle must, therefore, not only possess the ability to control its longitudinal range but its lateral or cross range as well. In fact, the lateral range capability of a vehicle during entry may be more important than its longitudinal range capability. Reference 15 shows that under certain conditions a lateral range capability of $\pm 90~{\rm km}$ can possibly allow a variation in time of re-entry of more than three hours and variation in re-entry plane inclination i $_{\rm VE}$ of as much as $\pm 13^{\circ}$.

Lateral range is defined as the perpendicular distance measured along the surface of the earth from the landing point to the vertical plane containing the original re-entry trajectory without lateral maneuvers (see sketch).

References 15, 16, 17 and 18 discuss the lateral maneuvering problem and resulting maneuvering envelopes also referred to as "footprints"; the reader is referred to these reports for details. However, for the purposes of this handbook, the following empirical equation is given which estimates the lateral range $R_{\rm lat}$ for constant L/D re-entries:



- 1 Landing site ~ no lateral maneuvering
- 2 Landing site ~ with lateral maneuvering Rlat ~ Lateral range

$$R_{lat} = (L/D) \ln (\tilde{V}_R) R_{\bigoplus} \sin \xi \sin \Phi_c + 1150 (L/D)^{1.78} \sin 2\xi \text{ (km)}$$
 (5)

where

 $R_{\bigoplus}^{=}$ radius of the equivalent spherical earth in km

 Φ_{C} = central angle to impact in degrees

 ξ = bank angle in degrees

 $V_{\rm p}$ = the re-entry speed in m/sec

Equation (5) is applicable for bank angles $\xi < 80^{\circ}$.

For a first order approximation to the maximum lateral range associated with a specific vehicle, the following assumptions can be made (see Ref. 17) ξ = 45°, $\Phi_{\rm C}$ = 90°, $V_{\rm R}$ = 11 km/sec, R_{\bigoplus} ≈ 6370 km which reduces Eq (5) to the following:

$$(R_{lat})_{max} \approx 1500 (L/D) + 1150 (L/D)^{1.78} (km)$$
 (6)

Equation (6) is shown in Fig. 9 and, as expected, the higher the $\rm L/D$, the greater the range capability.

Equation (5) can also be used to calculate approximate maneuvering envelopes, but first it is necessary to have consistent values of $\Phi_{\rm C}$ and ξ . This may be achieved by making use of Fig. 8 which

may be achieved by making use of Fig. 8 which gives the longitudinal range capability. If the L/D values shown in Fig. 8 are considered to be the vertical component of L/D, then each of these L/D's can be related:

$$\xi = \cos^{-1} \frac{(L/D) \text{ Fig. 8}}{(L/D) \text{ vehicle}}$$

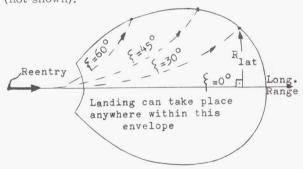
Thus, if a vehicle L/D is selected, Fig. 8 can be interpreted as giving range versus bank angle for various re-entry angles, i.e.,

$$\xi(\deg) = \frac{\text{longitudinal re-entry range in km}}{111 \text{ km/deg}}$$

(7)

Now if Eqs. (5), (6) and (7) are used jointly, then approximate maneuvering envelopes similar to the one shown in the next sketch can be generated. This empirical method implies that ξ is established at the time of re-entry.

Two maneuvering envelopes developed by this method are included in Figs. 10 and 11 for γ_R = -5.5° and γ_R = -7.75° , respectively. It should be kept in mind that these envelopes are for reentries in which bank angles, C_L and C_D , are maintained at constant values throughout the reentry. The envelopes clearly show the effectiveness of L/D in increasing the size of the maneuvering envelope. By comparing Figs. 10 and 11, an indication of the effect of corridor depth on the envelopes can also be obtained. The lower the $(L/D)_{\rm max}$ of a vehicle, the greater is the reduction in maximum lateral range with increasing corridor depth. This reduction in lateral range is less affected for vehicles with $(L/D)_{\rm max} > 0.5$ (not shown).



Of course, the information presented here is somewhat restrictive, but the same procedure can be followed to suit specific needs. However, when investigating vehicle capability beyond preliminary stages, it is obvious that such methods are insufficient.

In summary, the more significant factors that influence the maneuvering capability of a given vehicle of fixed $(L/D)_{max}$ are:

- (1) A reduction in the maximum allowable load factor increases the minimum longitudinal range a vehicle can achieve. Since the load factor increases with bank angle due to the centrifugal force, there is a limiting bank angle for a given load factor tolerance of the vehicle. The corridor depth decreases with increasing values of the limiting bank angle but the minimum longitudinal range is relatively insensitive to it.
- (2) The maximum allowable apogee altitude, h_{max}, limits the maximum range of constant L/D skip trajectories. However, if lift and drag are varied to control atmospheric exit conditions, the restriction on range becomes primarily a function of the (L/D)_{max} of the vehicle. High L/D's allow more modulation or reentry trajectory shaping than low L/D's.

- (3) The minimum allowable dynamic pressure, dictated by a requirement for aerodynamic control, limits the maximum range of some classes of nonexit trajectories.
- (4) The range guidance and control technique has a strong influence on the maximum longitudinal and lateral range capability and also on the minimum longitudinal range.

5. Re-entry Guidance Techniques

A vehicle directly entering the earth's atmosphere upon return from a deep space or lunar mission has an enormous amount of kinetic energy. Subsection B-4 demonstrated that during the dissipation of this energy by aerodynamic drag for lifting re-entry vehicles, a certain degree of maneuverability is available after re-entry. This section is concerned with the control of the vehicle's energy to acquire a specific landing site or recovery area without exceeding deceleration or heating limits.

There are a number of possible techniques that may be employed to guide the vehicle to a preselected landing site; they are commonly classified into (1) guidance using a nominal trajectory, implicit techniques, and (2) guidance using predictive capabilities, explicit techniques. A survey of guidance

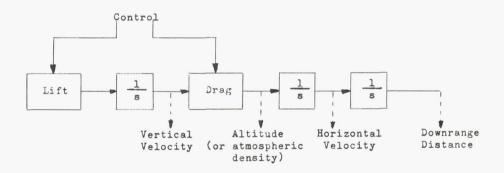
and control methods is given by Wingrove (Ref. 19). The more promising and well-known techniques are listed in the table below, and they are qualitatively discussed in order.

Group I Group II (implicit) (explicit)

- (1) Reference trajectory techniques
- (2) Linear prediction techniques ν
- (3) Re-entry optimum trajectory steering technique
- (4) Repetitive prediction steering techniques
- (5) Equilibrium glide steering techniques

The above classification does not imply that all guidance techniques fall under only one or the other group.

Before discussing these various techniques it is desirable to understand the relationship of control and trajectory dynamics as seen on the following block diagram taken from Ref. 19. This diagram represents the equations of motion in a simplified form, illustrating the relationship of the control forces to the trajectory variables.



The lift force is essentially in the vertical direction, affecting the rate of change of vertical velocity. The integration 1/s of the vertical velocity gives the variation in altitude (or, what is more important, the variation in atmospheric density). This change in density affects the drag force and thus affects the rate of change of horizontal velocity. An integration of horizontal velocity gives variation in the range along the trajectory.

To control longitudinal range, the rate at which horizontal velocity is changing must be controlled; thus the drag must be controlled. Drag can be regulated principally by either changes in the con-

figuration (i.e., by trim changes or by extending a drag brake) or by changes in atmospheric density. For example, if at any time in the trajectory the range must be extended, the lift force is increased in the vertical direction to raise the vehicle into a less dense atmosphere, thus reducing the rate of change of horizontal velocity and extending the longitudinal range.

The applicability and desirability of any guidance system or technique is weighed by the relative advantages or disadvantages with regard to (1) the ability to handle off-design re-entry conditions, (2) the on-board computer requirements, (3) the

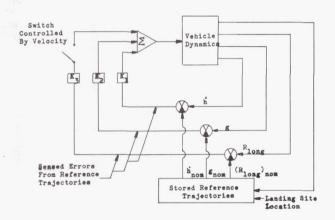
flexibility to maintain trajectories with minimum heating or acceleration, (4) the information the guidance equation gives to the crew if manned.

a. Implicit guidance techniques

In Group I techniques, guidance by use of a nominal trajectory, the trajectory state variables (i.e., V, h, u, R) along the nominal trajectory are precomputed and stored on board. The variations in the measured variables from the stored values are used in guidance either to control the nominal trajectory (path control) or to establish a new trajectory to reach the destination (terminal control).

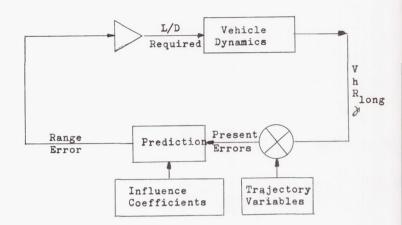
(1) Reference trajectory technique

This type of guidance method controls re-entry by use of stored reference trajectories. Such systems have been studied extensively for circular re-entries (Refs. 18, 20, 21 through 27) and supercircular re-entries (Refs. 28 and 29). The technique is explained with the aid of the next sketch, from Ref. 29.



A nominal trajectory, or one in which the vehicle re-enters with the specified conditions, is selected and stored in the control system. During the actual flight, the observed or measured conditions are compared with those of the reference trajectory and the deviation of the observed from the nominal conditions, or the errors, are obtained. In the guidance system these error signals are amplified by constant-gain elements K_1 , K_2 , K_3 and the sum of the weighted errors is used to specify the L/D to be used to force the actual vehicle conditions to conform to those of the reference trajectory. Typically, feedbacks found to be most effective as an outer loop control were the altitude rate h, deceleration g and range R.

This is essentially a third-order feedback system. Other measurements that may be used for



feedback control are shown in the following chart taken from Wingrove (Ref. 19):

The left column of the chart shows those devices which might be used to sense the various feedback terms.

As is discussed below in Subsection b(2), damping the trajectory is especially important for those velocities greater than circular satellite velocity, where the vehicle can either skip back out of the atmosphere or exceed a given deceleration limit.

This type of guidance technique has the drawback that a large quantity of trajectory data needs to be stored in the airborne computer.

(2) Linear prediction techniques

In addition to the more simplified guidance approach taken above, prediction of critical reentry quantities has been used (Refs. 29 through 34) to improve or augment the control logic of the reference trajectory approach. The block diagram of a typical linear prediction scheme shown below is from Foudriat (Ref. 29).

The similarity between it and the reference trajectory technique is quite evident. The stored trajectory variables are compared with the present flight conditions and the errors are obtained. However, instead of using a constant weighting function, a set of influence coefficients calculated by the adjoint technique (Ref. 31) is used to predict the effect of these present errors on the end conditions. This predicted final value in range is then used to control the L/D of the vehicle.

Thus, whereas the reference trajectory technique forces the vehicle to fly a single trajectory, the prediction technique selects one of many trajectories which terminate at the desired destination.

This guidance law is only good for the linear region near the nominal trajectory. To handle conditions far removed from the nominal, overcontrol is needed to assure that the landing site

Measuring Devices	First-Order Feedback	Second-Order Feedback	Third-Order Feedback	Fourth-Order Feedback
	<u>1</u> s		1 s	1 s
Inertial guid- ance unit or tracking sys- tem	Vertical ve- locity	Altitude	Horizontal velocity	Downrange
Accelerometer	Drag accelera- tion rate	Drag accelera- tion	Integration of drag ac- celeration	Second integration of drag acceleration
Temperature sensor	Atmospheric or skin tempera- ture rate	Atmospheric or. skin tempera- ture		
Pressure Sensor	Atmospheric pressure rate	Atmospheric pressure		

remains within the maneuvering capability of the re-entry vehicle. Also overcontrol is needed because the prediction may be in error because of navigational errors, atmospheric density variations, aerodynamic trim variation of re-entry vehicles, and other uncertainties. The overcontrol can be achieved by multiplying the $\delta(L/D)$ determined by the sensitivity coefficients by a constant gain factor K (K>1). Thus the control equation is:

Control (L/D) = $(L/D)_{nominal} + K \delta(L/D)$ (8)

It should be pointed out that the prediction of supercircular re-entry range suffers from a problem similar to that for the reference trajectory; that is, the control of range in the supercircular portion will cause the vehicle to skip out of the atmosphere. At present, no solution has been obtained which avoids this.

(3) Re-entry optimum trajectory steering technique

Since published work is somewhat limited in this area, only a cursory discussion is given here.

An ideal guidance scheme should determine the trajectory which minimizes the heat input to the body surface, constrain the flight path to one having acceptable acceleration limits and specified landing position and finally, provide signals to the control system to accomplish such a re-entry trajectory. This technique is similar in some respects to the linear prediction scheme given above except that the gains of the control system are optimized.

A promising technique for achieving such an optimum guidance system employs the calculus of variations. In past years, resort to variational techniques for providing guidance equations has been practically impossible due to the complicated nature of the indirect methods and their associated split boundary conditions. Tedious iteration schemes are an unfortunate necessity for obtaining extremal paths by the indirect methods of variational calculus.

Recently, several breakthroughs have occurred which show promise of applying direct methods of variational calculus to future guidance systems. Nearly simultaneously, Kelly (Refs. 35 and 36) and Bryson, et al. (Refs. 35 through 38) published methods incorporating direct variational techniques for obtaining extremal solutions with an associated reduction in computing time. Both methods make use of the system of equations adjoint to the small perturbation equations about a nominal trajectory. This adjoint system yields influence coefficients which, in turn, correct the nominal trajectory in an optimum fashion. Convergence of the method to the true optimum is accomplished by "steepest descent" methods. Other work in this area is found in Refs. 39 and 40.

These direct variational methods are actually linearized solutions to the Mayer problem of the indirect method of the calculus of variations. The approximation involves replacing the nonlinear trajectory equations of motion by a nominal trajectory and a linear, small perturbation system of equations. The adjoint of equations of the direct method

corresponds to the Euler-Lagrange equations of the indirect method and the influence coefficients in the direct method correspond to the Lagrange multipliers in the indirect method. The significant advantage of the direct method is its ability to determine near optimum solutions in relatively few computer cycles.

To apply a direct variational technique to the re-entry vehicle, an on-board computer would be programmed to determine the lift commands which, in turn, would be inputs to the control system. Boundary conditions consisting of position, rate and attitude data would be provided to the computer by either on-board sensing devices or ground control links. To account for errors in the system (primarily input position and rate data), the trajectory could be continually optimized from the vehicle's present position to the desired landing site. The system would become increasingly accurate as the landing site is approached. The significant advantage of this technique lies in its ability to guide the vehicle in a manner which would optimize some pertinent trajectory parameter such as minimizing the heat input to the body, minimizing flight time, etc.

All implicit guidance techniques have the disadvantage of the limited amount of information available for pilot displays. Available pilot information depends on the particular guidance equations used, and implicit guidance techniques give information only with respect to the nominal trajectory at the particular time and not the future trajectory. This problem of pilot display can be eliminated if explicit guidance techniques are used as discussed in the next subsection, B-5b.

b. Explicit guidance techniques

Studies of guidance techniques employing fixed trajectories about which perturbations are made, have indicated that a successful landing from circular velocity can be accomplished if the deviations of the actual initial conditions of entry are close enough to the values stored in a computer memory, and if a sufficient number of perturbation variables are employed in the computation. This approach is inherently limited, however, to the variety of initial conditions and degree of trajectory diversification capable of being stored in the computer memory.

In Group II techniques, or explicit guidance techniques using predictive capabilities, a number of trajectories within the typical maneuver boundary can be chosen. From observed or measured trajectory variables the guidance system predicts continuously the trajectory by which the vehicle will reach the desired landing site without exceeding design limits and without the use of a stored nominal trajectory. An explicit guidance technique is desirable inasmuch as the re-entry guidance system will be required to handle wide variations in abort and earth return conditions and also considerable deviation from established atmospheric standards. In addition to increased flexibility, a continuous prediction system affords an advantage in its direct application to a display of predicted flight conditions and hazardous situations to the pilot in a manner in which maximum control is afforded.

The main problem with any continuous-prediction technique is the complexity of the equations employed to mechanize the prediction. To maintain accuracy and speed in spite of limited input information and restrictive amounts of computing equipment, a satisfactory compromise must be realized.

(1) Repetitive prediction steering technique

Perhaps the most feasible technique thus far proposed is the repetitive prediction steering technique studied by Foudriat (Ref. 29), Wingrove and Coate (Ref. 41), and Bryant and Frank (Ref. 8).

Additional studies of this technique may be found in Refs. 40, 42 and 43.

This technique involves, essentially, a fast solution of the simplified approximate equations of motion of the vehicle during re-entry. By inserting a desired L/D ratio and solving these equations for range, a comparison may be made between the predicted range and the actual range as determined in the guidance computer, and appropriate changes can be made in vehicle angle of attack in order to bring the predicted range in line with that desired. If this operation can be accomplished with sufficient speed, genuine closed-loop range control is possible. Studies conducted thus far indicate that such a system is feasible.

The complete equations of motion for a vehicle entering the earth's atmosphere are by nature complex and difficult to solve even with large high-speed digital computers. The feasibility of inflight solution of these complete equations for the purpose of controlling range, deceleration and heat absorption becomes questionable because of the restrictions placed upon the size and complexity of airborne computers. It is, therefore, both mandatory and desirable to simplify the mathematical and computational requirements of the reentry guidance and control technique.

For example, this simplification can be accomplished by Chapman's method which has reduced the equations of motion to a single, ordinary, nonlinear differential equation of second order by rejecting terms which contribute only negligibly to the solution and by the introduction of a transformation of variables (see Subsection B-1), and the method has been developed further by Bryant and Frank (Ref. 8).

Assumptions. The assumptions made in the development of the Chapman equation restrict its application to a particular range of altitudes and initial conditions which are, however, within the range of extremes predicted for lunar missions. The basic assumptions used in the development of the simplified equation of motion are repeated below:

- Atmosphere and planet are spherically symmetric.
- (2) Variations in atmospheric temperature and molecular weight with altitude are negligible compared to any variation in density.

- (3) Rotational rate of the earth and its atmosphere are negligible compared to the velocity of the vehicle.
- (4) The small change in distance from the center of the earth is negligible compared to the fractional change in velocity in a given increment of time.
- (5) The flight path angle γ is sufficiently small so that the component of drag is large compared to the component of lift in the horizontal direction.

Predictions of longitudinal and lateral range for flight within the atmosphere are obtained by the following equations (Ref. 8), respectively.

$$R_{\text{long}} = \sqrt{\frac{R_{\bigoplus}}{\beta r}} \int_{\overline{u}_{i}}^{\overline{u}_{f}} \frac{\cos y \cos \Delta A}{Z} d\overline{u}$$

$$R_{\text{lat}} = \sqrt{\frac{R_{\bigoplus}}{\beta r}} \int_{\overline{u}_{i}}^{f} \frac{\cos y \sin \Delta A}{Z} d\overline{u}$$
(9)

where the symbols have been defined in Subsection B-1, and where ΔA is the change in azimuth from the initial re-entry trajectory plane

$$\Delta A = \int_{\overline{u}_{i}}^{\overline{u}_{f}} \left[\frac{C_{L} \sin \Phi_{c}}{C_{D} \overline{u}} + \frac{\cos \Delta A \cos \gamma \tan (R_{lat}/R_{\oplus})}{Z \sqrt{\beta r}} \right] d\overline{u}$$
(11)

where $\Phi_{\rm c}$ is the longitudinal re-entry range (from the point of re-entry to the landing site).

Equation (10) was first used in Ref. 17 and its solution determines the range traveled over the earth's surface, measured normal to the initial re-entry trajectory plane. The load factor or deceleration in units of \mathbf{g}_0 along the flight trajectory may be found from:

$$LF = \frac{\sqrt{\beta r} \overline{u}Z}{\cos y} \sqrt{1 + (\frac{L}{D} - \tan y)^2} (g_0) (12)$$

and the total time to re-enter in seconds is given by:

$$t_{\rm R} = 27 \int_{\overline{u}_{\rm i}}^{\overline{u}_{\rm f}} \frac{-\cos \gamma}{uZ} d\overline{u} \text{ (sec)}$$
 (13)

Finally, the total heat absorbed by the re-entry vehicle in kg-cal, measured at the stagnation point on a hemispherical heat shield, is determined by the following equation, as derived by Chapman (Ref. 5):

$$Q_{\text{H (convective)}} = 4000 \, A_{\text{H}} \, \left(\frac{\text{M}}{R_{\text{C}} \, \text{A} \, C_{\text{D}}}\right)^{1/2} \, .$$

$$\sqrt[\overline{u}]{\int_{\overline{L}} \frac{(\overline{u})^{3/2}}{Z^{1/2}} \, d\overline{u} \, (\text{kg-cal})}$$

where

M = mass of the re-entry vehicle.

 ${\rm A}_{\rm H}$ = aerodynamic heating reference area.

 R_C = radius of curvature of the heat shield.

A = reference area for drag and lift.

This completes the list of equations necessary for that portion of the predicted trajectories that remain within the atmosphere. These equations are applicable only to atmospheric flight, because of limitations imposed by the assumption that dr/r | < < | du/u | which can be shown to be equivalent to restricting the minimum value of Z in Eqs (3) and (4). This minimum value of Z is approximately 0.001, which corresponds to an altitude of from 91.44 km to 88.4 for velocities between 11 km/sec and 7.8 km/sec; in combination with a positive flight path angle, it can be used to define (the initial conditions for) a skip. If, at any time during the evaluation of Eq (4), the magnitude of Z decreases below 0.001, that part of the prediction is terminated. The prediction is completed by matching a Keplerian ellipse to the atmospheric exit conditions $(\gamma_e, \overline{u}_e)$ calculated at Z = Z_{\min} , which are simultaneously initial conditions for the skip portion of the trajectory.

The following Keplerian orbit equations are then used to compute the ballistic or skip portion of the trajectory:

Central angle

$$\beta_{e} = \tan^{-1} \left[\tan \gamma_{e} \left(\frac{\overline{u}_{e}^{2}}{\overline{u}_{e}^{2} - 1} \right) \right]$$
 (14)

Longitudinal range during ballistic flight (R_{long})

$$(R_{long})_b = 2 R_{\oplus} \left[\pi - \beta_e \right]$$
 (15)

where $\beta_{\rm e}$ is measured in radians in Eq (15)

Ballistic flight lateral range (R_{lat})

$$(R_{lat})_b = R_{\bigoplus} \left\{ \sin^{-1} \left[\sin i \sin (\Delta + \beta_e) \right] \right\}$$
 (16)

where

$$i = \cos^{-1} \left[\cos \Delta A_b \cos (R_{lat})_b / R_{\oplus} \right]$$
 (17)

and

$$\Delta = \sin^{-1} \left[\cos \left(R_{lat} \right)_b / R_{\bigoplus} \right) / \sin i$$
 (18)

where ΔA_b is the change in azimuth during ballistic flight.

The apogee radius r_{max} is determined for each skip trajectory by the following Keplerian orbit expression:

$$r_{\text{max}} = R_{\oplus} \left(\frac{\overline{u}_{e}^{2}}{1 - \left[1 - \overline{u}_{e}^{2} \left(2 - \frac{\overline{u}_{e}^{2}}{\cos^{2} \gamma_{e}}\right)^{1/2}\right]} \right)$$
(19)

The solution of Eqs (14) through (19), therefore, provides the predicted values of longitudinal and lateral range for the skip or ballistic portion of the trajectory.

These values for ballistic flight are added to the range traveled up to the final conditions for the ballistic portion ($Z = Z_{min}$) to obtain a predicted range from the vehicle's present position to the point of second entry following the skip. Since the second re-entry occurs with a velocity less than circular -- and at flight path angles on the order of -3° to -5°--it is relatively simple to determine the vehicle's maneuvering potential. General statements concerning vehicle performance in this part of the trajectory can be made with some confidence. For this reason, constant values of longitudinal and lateral range are added to the skip range to account for the second reentry. These constant values can be determined so that they are approximately centrally located in the vehicle's maneuver envelope.

The total values of predicted longitudinal and lateral range are obtained by adding ranges for the atmospheric, the ballistic (if any), and the fixed second re-entry portions of the trajectory. The reader is referred to Ref. 8 for details on guidance computer mechanization.

This approach, in addition to providing a maximum allowable margin of error for the skip maneuver, greatly reduces the numerical integration load on the computer, inasmuch as integration need be provided only for a comparatively small portion of the trajectory when the point of atmospheric exit during the first re-entry is being predicted. The saving in time can be well spent in providing either more predictions per second or in decreasing the integration step size thereby increasing prediction accuracy.

The use of Chapman's equation makes the control of skip trajectories feasible, even in light of the extreme sensitivities involved in control of ballistic flight exit (or second re-entry) conditions.

Longitudinal range control can be achieved for all entries in the prescribed lunar-return guidance corridor, except along the absolute overshoot boundary, where longitudinal range is limited to 9300 km or less. In addition, accurate control of lateral range is possible with a fixed-angle-of-attack vehicle by controlling the direction of the roll angle commanded for longitudinal range control.

No knowledge of the vehicle's altitude or of the atmospheric properties is needed for accurate range control. The system has been found to operate successfully, even when comparatively large variations in atmospheric density and vehicle lifting characteristics are imposed.

The operation of such a guidance system starts with a prediction of the longitudinal range and lateral range that would be obtained if the present vehicle L/D and bank angle ξ were held constant. The location of the predicted landing site is compared with that of the desired landing site and a second prediction is made for a larger or smaller value of ξ or L/D. The bank angle and attitude commands are transmitted to the autopilot and maintained until the next prediction is made at which time the entire procedure is repeated.

(2) Equilibrium glide steering technique

When considering explicit guidance techniques for re-entry, one of the more obvious selections is based on the concept of equilibrium glide. This technique has several features which recommend its investigation:

- (1) The relationship between range and velocity is simple.
- (2) It has been studied extensively for subcircular re-entries.
- (3) The range-velocity relationship suggests that it may be applicable to super-circular velocities.

The application of the basic equilibrium glide equation to supercircular speeds has also been studied (Ref. 44). Although it can be shown that the same equation is applicable at this speed, one must use it to steer the vehicle to a target which is associated with a velocity slightly greater than \overline{u} = 1. Unfortunately small perturbations away from the equilibrium glide conditions at supercircular velocity are divergent in nature rather than convergent, as in the subcircular case. This is readily seen from the equation of frequency

for a perturbed trajectory $\omega_n^2 = \beta r \frac{(1 - \overline{u}^2)}{(D/W)^2}$. From the term $(1 - \overline{u}^2)$, the training

From the term $(1-\overline{u}^2)$, the trajectory oscillations possess static stability below circular velocity $(\overline{u}<1)$ and are statically unstable for $\overline{u}>1$. Stability augmentation techniques must be added to prevent this divergence. Some method of transition, such as constant altitude, from supercircular to subcircular equilibrium glide must also be provided.

The use of the equilibrium glide technique for

re-entries appears feasible, but longitudinal range reduction (in comparison with those techniques which provide a skip capability) and increased total convective heat transfer are characteristics of this approach.

If the application of the equilibrium glide principle to the re-entry guidance of a lunar vehicle is considered, then several guidance laws are required, each one being applicable to a segment of the total re-entry trajectory. That portion of the trajectory when the vehicle decelerates from approximately 99.5% of circular orbital velocity to approximately Mach 5 is considered first, then the application of the equilibrium glide principle to the supercircular portion, and finally the control of the skip (if any) is considered.

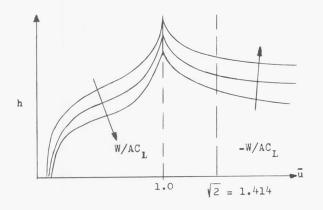
Subcircular equilibrium glide. A quantitative understanding of the equilibrium glide may be gained by considering a dynamic system of the re-entry vehicle alone with the vehicle flying in such a way that the lift and the fictitious centrifugal force just balance the gravitational force. Drag is constantly reducing velocity and since both lift and centrifugal acceleration are proportional to velocity squared, they tend to decrease. Lift is also proportional to density, so that the balance can still be maintained with constant L/D if the vehicle descends into denser air as it slows down. This type of flight will be called an equilibrium glide. An equilibrium glide trajectory has the following general characteristics:

- (1) Altitude is always decreasing.
- (2) Flight path angle is small.
- (3) The rate of descent is always increasing at a rate which is small compared to lift/mass.
- (4) Lift and drag coefficients are constant.
- (5) Velocity is always decreasing.

The equilibrium glide has a number of properties which make it especially attractive as a tool in re-entry guidance, namely

- (1) Altitude is a function only of velocity and lift coefficient.
- (2) Since the heating rate is assumed to depend only upon velocity and atmospheric density, it too is a function only of velocity and lift coefficient.
- (3) The distance traveled between any two velocity states depends only upon the velocities and the lift/drag ratio.
- (4) Explicit and simple expressions for the above relationships can be derived.
- (5) All constant L/D trajectories (subcircular velocity) approach equilibrium glide as time progresses because of natural damping of vertical oscillations. This permits the application of the equilibrium glide expression to the latter portion of any constant L/D trajectory.

If equilibrium glide conditions exist, i.e., the lift plus centrifugal force balances the gravitational force, the atmospheric density will be a function only of velocity for any given lift coefficient. Knowing the relationship between atmospheric density and altitude, we can plot a family of altitude versus normalized velocity (\overline{u}) curves for various lift coefficients. A family of such curves is illustrated in the following sketch.



Suppose that, at a given velocity and lift coefficient, the vehicle is above the altitude shown in the sketch. Then, its lift will be less than if it were on the equilibrium curve because the density will be lower. However, the vehicle cannot remain at this altitude because gravity will reduce the altitude. Moreover, drag will be lower at the higher altitude so that velocity will drop more slowly. Hence, the slope of the altitude versus velocity curve will change in such a way as to bring the vehicle toward the equilibrium curve. This effect may be viewed as a feedback action tending to keep the vehicle on an equilibrium glide. This reasoning leads to the hypothesis that the equilibrium glide is a physically realistic as well as mathematically convenient type of trajectory.

Supercircular equilibrium glide. The equilibrium glide concept has been developed from the study of re-entry vehicle behavior at velocities less than circular orbit velocity. The possibility of extending this concept into the supercircular velocity region now suggests itself. In this region the centrifugal force exceeds the gravitational force and negative lift is needed to balance the vertical forces. Negative lift can be obtained either by flying a lifting body upside down or trimming at negative angles of attack.

As the vehicle decelerates from parabolic velocity to circular orbital velocity on such an equilibrium glide, the centrifugal acceleration drops from 2g to 1g while the lift acceleration changes from -1g to zero. Thus, to maintain the balance of forces, lift will always be numerically less than the centrifugal force. Because of this, and because both lift and centrifugal acceleration are proportional to velocity squared, altitude must increase as the vehicle decelerates. In this respect, the supercircular equilibrium glide differs from the subcircular case. As a consequence of this difference, maximum heating rate occurs at maximum velocity in the supercircular glide.

One of the most desirable properties of the subcircular equilibrium glide (the tendency of any constant L/D trajectory to approach equilibrium conditions) is absent in the supercircular region. In fact the tendency is just the opposite. This behavior is illustrated by supposing that, at a given velocity and lift coefficient, the vehicle is above the altitude shown in sketch. Then its lift will be numerically less than it would be if it were on the equilibrium curve because the density will be lower. The lift, which is negative, is then insufficient to balance the centrifugal acceleration and the vehicle rises even farther from the equilibrium curve. Thus, although the forces are in equilibrium when the vehicle is on the curve, any disturbance in the equilibrium causes the vehicle to rise or fall at an ever-increasing rate. In this sense, flight at constant negative lift coefficient is inherently unstable in altitude. The significance of these rates of divergence is that the control system must be faster than these rates if damping of the divergence is to be obtained. In other words, the guidance system must incorporate stability augmentation at supercircular velocities. In this velocity region the guidance system functions in such a way as to bring the vehicle over a specified point on earth at a specified u (which would be approximately

1.0005). The guidance system calculates the L/D command needed to do this, which together with the actual rate of climb and actual lift and drag accelerations, is incorporated into an error function which changes angle of attack in such a way as to bring the vehicle onto an equilibrium glide at the command L/D.

The equilibrium glide concept is not applicable at circular speed. Between \overline{u} = 1.05 and \overline{u} = 0.995 a different type of trajectory, possibly constant altitude, is desirable.

Skip range control. The range covered after re-entry can be substantially increased by skipping out of the atmosphere and re-entering a second time. The behavior of the vehicle outside the atmosphere can be described by the relatively simple and closed form equations of a Keplerian orbit. Thus, if the desired point of re-entry is specified, the desired path angle at exit can be calculated from the vehicle's velocity and position at exit. The atmosphere does not end abruptly, so the exact instant of exit is undefined. This difficulty is overcome by continuously maintaining the flight path angle at a value such that, if the atmosphere should disappear at that instant, the vehicle would follow the Keplerian orbit to the re-entry point. The required path angle changes with time, and aerodynamic forces are required to bring about the change. As the vehicle gains altitude, the available aerodynamic force diminishes. It should be clear that the accuracy of such a system need only be within the maneuvering capability of the vehicle from the initial conditions of the second re-entry. This is true since it is proposed that equilibrium glide control be used to control range during the second entry.

In the actual use of such a system, the range to the target, based on expected re-entry conditions, would be used to select the skip mode or supercircular equilibrium glide mode of control prior to re-entry. If the skip mode is selected, a subsequent switch to equilibrium glide must be made

prior to the second re-entry.

In addition it appears that this particular technique is easily adapted to a closed form predictive system. Instead of integration of the equations of motion, the closed-form system employs an approximate explicit solution in which all or part of the possible trajectories are considered.

The major drawback of the discussed explicit guidance techniques is the fact that the equations of motion and the equations for controlling the re-entry trajectory must be simplified considerably in order to permit closed-form solutions. Great care must be taken in not simplifying the equations too much for too large a portion of the total re-entry trajectory, so that not enough maneuverability remains to acquire the landing site with the remaining maneuverability of the vehicle during the final portion of the trajectory. The maneuverability envelope or footprint, decreases drastically with altitude and velocity as the re-entry progresses and the kinetic energy of the vehicle has been progressively diminished, and there is a constant danger of missing the desired landing site.

C. RE-ENTRY BY ROCKET DECELERATION OR A COMBINATION OF ATMOSPHERIC AND ROCKET DECELERATION

Atmospheric deceleration requires that a large portion of the kinetic energy of the vehicle be converted to heat. An alternative method that can be used is to reduce the kinetic energy of the space vehicle to that of a circular earth orbit by application of rocket thrust or a combination of atmospheric deceleration and rocket thrust. This latter method has the major disadvantage of requiring additional fuel, tankage or even extra rocket engines for the deceleration. However, its advantages include that actual earth re-entry can be performed from satellite speeds and is consequently simpler, and the lateral and longitudinal maneuverability of the vehicle can be limited if the provisions (attitude control fuel, life support equipment, etc.) allow the space vehicle to remain in earth orbit until the landing site rotates with the earth into a favorable position relative to the vehicle.

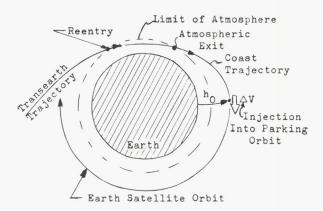
Perhaps the simplest rocket deceleration technique consists of a direct reduction of the speed of approach of the transearth trajectory to circular satellite speed. An estimate of the fuel requirements for this maneuver can be obtained by assuming the approach speed of the vehicle as parabolic and that the required velocity reduction ΔV occurs impulsively. The difference between the parabolic and circular speeds at the radius r then gives the necessary velocity reduction:

is the initial mass of the vehicle, for various orbital altitudes $h_0 = r_0 - R_{\bigoplus}$, where R_{\bigoplus} is the radius of the equivalent spherical earth. The mass ratios ζ were computed from the rocket equation

$$\Delta V = g_0 I_{sp} \ln \left(\frac{\zeta}{1 - \zeta} \right)$$
 (21)

for fuel specific impulses $I_{\rm sp}$ = 300 sec and $I_{\rm sp}$ = 400 sec. The figure shows that the fuel expenditure for a pure rocket deceleration maneuver is very high and not too practical for the early lunar vehicles. Thus, a 22,000-newton re-entry vehicle requires approximately 11,500 newtons fuel for circularizing maneuvers with $I_{\rm sp}$ = 400 sec and about 12,600 newtons fuel with $I_{\rm sp}$ = 300 sec.

More fuel economy can be achieved if a combination of atmospheric and rocket deceleration is used to achieve the parking orbit as suggested by Sommer and Short (Ref. 9). In this combination technique, the atmosphere is re-entered briefly to take advantage of atmospheric deceleration. However, the vehicle is subsequently guided out of the atmosphere. (See sketch below.)



After exit with velocity, $\rm V_e$, the vehicle coasts to the apogee of the Keplerian orbit, which is controlled by the exit velocity, where an accelerating velocity impulse $\Delta\,\rm V$ is applied. This maneuver ensures that re-entry does not take place on the descending arm of the coast trajectory, but that the vehicle continues in the circular parking orbit until the landing site is in a favorable position with respect to the satellite.

To allow a direct comparison of the two rocket deceleration techniques, Fig. 13 gives the mass ratio ζ for circularizing the Keplerian coast trajectory for atmospheric exit velocities ranging from 7300 m/sec to 7900 m/sec for three parking orbit altitudes h_0 = 740, 555, and 370 km and for two values of specific impulse, $I_{\rm sp}$ = 400 sec and 300 sec. The results of the calculations shown in the figure indicate that if the vehicle is guided to exit velocities equal to or a little greater than circular satellite velocities, the fuel weight penalty is kept within practical bounds. For example, for a 22,000-newton re-entry vehicle, approximately 1500 newtons of fuel are required for the circularizing maneuver at h_0 = 740 km.

Both the technique of pure rocket deceleration and that of combined rocket and atmospheric deceleration require an additional impulse to deorbit

from the parking orbit. This impulse varies with the parking orbit altitude and the allowable dispersions from the nominal re-entry trajectory due to dispersions in atmospheric density and the variations in aerodynamic performance of the reentry vehicle. Typically, for deorbit altitudes below 300 km, a high deorbit pulse with $\Delta V_d \simeq$ 500 m/sec will bring the vehicle in steeply and quickly with little dispersions and less maneuvering capability but higher deceleration, while a low deorbit pulse with $\Delta V_{\rm d} \simeq 100$ m/sec results in a long glide with long re-entry times, large dispersions and higher heating. Any reduction in velocity below $\Delta\,V_{\rm d}\simeq 100$ m/sec results in dispersions which may be a very significant portion of the total re-entry vehicle maneuvering capability. For deorbit altitudes above 300 km, the corresponding values of deorbit $\Delta\,V_{\rm d}$ are probably slightly larger and the re-entry range is somewhat longer for the same limiting values of $\gamma_{\rm R}$, the flight path angle at re-entry, which define the re-entry

The re-entry from the parking orbit altitude which occurs from satellite orbital velocities has been discussed fully, both from a theoretical and numerical standpoint, in Chapter IX of Ref. 1.

An important problem in maneuverable reentry vehicle performance is the ability to recall the vehicle to a specified landing site after the vehicle has been decelerated to the circular orbit velocity. Both the orbital phase and the descent phase contribute to the determination of calldown frequency tables which may be regarded as a measure of vehicle performance. Such tables are useful for answering typical parking orbit design questions such as:

- (1) What orbital characteristics are needed to have call-down on a certain revolution for a given landing site and maneuvering capability?
- (2) How long is the waiting time for recall at any time during the parking orbit phase.
- (3) How much do dispersions in initial conditions and orbital dispersions affect the call-down frequency?
- (4) What combinations of orbital, vehicle, and landing site parameters allow vehicle recall once a day, once every three days, or some other time period?

The need to obtain call-down frequencies quickly, preferably by use of a digital computer, is obvious.

Orbital trajectory calculations can be found in Chapters III and IV of Ref. 1, while the re-entry has been discussed to some extent in the present chapter and specifically for re-entry from satellite orbital speeds in Chapter IX of Ref. 1. However, as indicated above, the design of parking orbit parameters for earth return requires the combination of the orbital and descent phases. This can be accomplished in two ways:

- (1) Integrate the equations of motion numerically as was done by Rosamond (Ref. 45) for instance, who considers the touchdown accuracy of retrorocket recovered satellites (no aerodynamic maneuverability during re-entry) by minimizing the effect of rocket burnout errors, which are initial conditions in our case, through proper selection of the deorbit thrust application.
- (2) Use the results of general perturbation theories during the orbit phase (Refs. 46, 47 and Chapters IV and V of Ref. 1 to give but a very few), together with reentry results as given here in Chapter IX of Ref. 1, and by Mandell (Ref. 48)). This approach has been taken by Jensen, Townsend, et al.(Ref. 49), but these authors restrict themselves to polar orbits or arbitrarily inclined orbits with small lateral maneuverability. An improved version of this method suitable for hand calculation has been given in Chapter IX of Ref. 1.

The intent of the present discussion is to give a general method for obtaining call-down frequencies from circular orbits efficiently and quickly by use of a digital computer through introduction of the concept of ground swath to account for lateral maneuverability. The method is thus the most general; it applies for any orbital altitude, inclination, arbitrarily large lateral and longitudinal maneuverability during re-entry, as well as any launch and landing site location. The call-down equations have been programmed on the IBM 7094 at the Martin Company. Basic assumptions, derivations of the equations, as well as some results are presented below.

1. Assumptions for Computing Call-Down.

a. Initial conditions

Initial conditions, which occur at the end of the rocket burning designed to achieve the circular parking orbit, consist of the geodetic latitude, longitude, and direction of motion at the initial point. Small errors in these quantities, however, should not affect the call-down frequency significantly since the effect of these errors on the deorbit position is not cumulative.

b. Orbital conditions

The satellite is represented by a mass point in a circular orbit with a given inclination i_{VE} , $0^{\circ} \leq i_{VE} \leq 180^{\circ}$, and mean radius r_{0} . The altitude h_{0} of the circular orbit is defined as its mean equatorial altitude, i.e.,

$$h_0 = r_0 - R_e,$$
 (22)

where ${\bf r}_0$ is the mean geocentric radius and ${\bf R}_e$ the equatorial radius of the earth. The major forces acting on the satellite are due to earth oblateness and atmospheric drag. Only secular changes in the satellite orbit will be considered important. Short and long periodic changes due to oblateness and drag as well as the effect of

other gravitational bodies, solar radiation pressure, mass irregularities in the earth, and small thrust forces have been neglected since they do not affect the call-down frequency appreciably.

The main effect of atmospheric drag is to decrease the mean orbital radius and to increase the mean motion. The radius on the j-th revolution $\mathbf{r}_{\mathbf{j}}$ is given in terms of quantities in the (j-1)th

$$r_{j} = r_{j-1}^{2} - 4\pi B_{\text{eff}} \rho_{j-1} r_{j-1}^{2},$$
 (23)

where

$$B_{eff} = F_{a0} \frac{\rho \text{ dispersed}}{\rho \text{ standard atmosphere}}, \frac{C_D^A}{2 \text{ M}}$$

is the effective ballistic coefficient, F_{a0} (h, i_{VE}) the atmospheric oblateness correction factor (Ref. 50), C_D the drag coefficient, A the frontal area of the satellite, M its mass, and ρ the neutral atmospheric density computed from the 1961 U.S. Standard Atmosphere (Refs. 51 and 52).

The factor $\frac{\rho}{\rho}$ standard atmosphere was introduced to enable simulation of constant dispersions in atmospheric density from the standard. Drag decay histories for various ballistic coefficients with the option to introduce atmospheric oblateness and dispersions in density can be obtained along with the call-down frequency. The change in period on the j-th revolution corresponding to the decrease in radius is

$$\Delta \tau_{j} = -\frac{12 \pi^{2}}{\sqrt{\mu}} \quad B_{\text{eff}} \rho_{j-1} r_{j-1}^{2.5},$$
 (24)

where μ = GM_{\bigoplus} is the gravitational constant of the earth, G the universal gravitational constant and M_{\bigoplus} the mass of the earth.

The secular effects of earth oblateness are summarized by the regression rate of the node,

$$\frac{d\Omega}{dt} = \dot{\Omega} = -540 \text{ J}_2 \left(\frac{R_e}{r_0}\right)^2 \cos i_{VE}, \quad (25)$$

where J_2 = 1082.28 x 10^{-6} is the constant associated with the second zonal harmonic term in the expansion of the earth's gravitational potential, and a correction to the nodal period of the satellite,

$$\Delta \tau_{\beta} = -\frac{3\pi}{\sqrt{\mu}} r_0^{1.5} J_2 \left(\frac{R_e}{r_0}\right)^2 \frac{7 \cos^2 i_{VE}^{-1}}{4}, (26)$$

which can be derived from Struble (Ref. 47). The secular oblateness corrections are assumed independent of the secular drag effects, i.e., they are constant in a given parking orbit simulation on the computer.

Small dispersions from nominal in-plane orbit injection conditions can be simulated by introducing a further correction to the period, $\Delta\tau_{\rm d}$,

for k revolutions. These injection dispersions may be significant due to their cumulative effect on the satellite deorbit position.

c. Descent conditions

For a landing of the re-entry vehicle to be possible, the orbital plane has to be "near" the intended landing site and the satellite must be in the "correct" orbital position as given by the central angle from the ascending node. The concepts "near" and "correct" will be described quantitatively in Subsection 2.

The actual physical picture during re-entry is the following: We have a point landing site. There is a re-entry region at orbital altitude from which the re-entry vehicle may reach this point, and all possible re-entry trajectories funnel toward it. Since the earth is roughly spherical and the satellite moves in an almost central force field, the shape of this re-entry region changes considerably with orbital position as well as altitude. For call-down studies, it is much more convenient to use a maneuvering envelope which is independent of orbital position and is defined as the locus of points on earth that can be reached by aerodynamic or thrust maneuvering from a fixed deorbit position which coincides with the instantaneous satellite position. This envelope may be reduced in size by constraints of total heat, maximum heating rate, or estimated dispersions during re-entry. Each point inside and on the envelope can be defined on a nonrotating earth by a longitudinal range in the orbit plane from deorbit, and a lateral range Rlat perpendicular to the orbit plane, with lateral ranges in the direction of the satellite angular velocity vector considered positive. The point on the nonrotating earth is related to one on a rotating earth by the descent time $t_{\rm d}$ and the angu-

lar velocity of the earth $\omega_{\mathbf{p}}$.

The assumption that the maneuvering envelope is independent of orbital position corresponds to assuming that the effect of atmospheric rotation during re-entry is negligible. We define calldown as the condition when the landing site, which is on a rotating earth, is within the maneuvering envelope of the re-entry vehicle. The altitude-dependence of the maneuvering envelope can be taken into account by introducing several envelopes for the expected deorbit altitude ranges. We assume further that each irregular maneuvering envelope is approximated by several maneuvering rectangles. Two corners of this rectangle are defined by $(R_{long})_{min}$, the corresponding $(t_{d})_{min}$, and $(R_{lat})_{max}$ as well as $(R_{lat})_{min}$, respectively. Similarly, the other two corners are given by $(R_{long})_{max}$, $(t_{d})_{max}$, $(R_{lat})_{max}$, and $(R_{lat})_{min}$. This definition is possible since t_{d} is only very weakly dependent on R_{lat} .

A measure of landing site "nearness" is $(R_{lat})_{max}$ and $(R_{lat})_{min}$ which form a ground swath around the satellite ground track. One condition for call-down is that the geocentric parallel of latitude of the landing site ϕ_f^t intersect the ground swath (Figs. 14 and 15). The problem of finding this intersection is one of spherical trigonometry: Given the geocentric latitude (or declination) of the landing site ϕ_f^t , the orbit inclination i_{VE}^t , and the

lateral range R_{lat} , find the central angle β and inertial longitude λ of the intersection, as measured relative to the same ascending node. The solution of this problem is (Ref. 53, p 42):

$$\sin \beta = \frac{\sin \phi_{\rm f}^{\rm f} - \cos i_{\rm VE} \sin R}{\sin i_{\rm VE} \cos R}$$

$$\sin \, \lambda = \frac{- \, \sin \, i_{\rm VE} \, \sin \, R + \cos \, i_{\rm VE} \, \cos \, R \, \sin \, \beta}{\cos \, \phi_f^I}$$

$$\cos \lambda = \frac{\cos R \cos \beta}{\cos \phi_f^{\dagger}} \tag{27}$$

where \mathbf{R}_{lat} is positive in the direction of the orbital angular velocity, and

$$R = \frac{360 R_{lat}}{2 \pi R_{e}} \text{ (deg)}$$
 (28)

Three possible cases may arise:

(1) Both $(R_{lat})_{max}$ and $(R_{lat})_{min}$ yield

 $|\sin\beta| > 1$. No intersection occurs and we have either a call-down on each revolution or no call-down at all. These cases can be easily distinguished by the values of ϕ_f^t , i_{VE} and R_{lat} .

(2) Either $(R_{lat})_{max}$ or $(R_{lat})_{min}$ yield $|\sin\beta| > 1$. Two intersections occur near the apex, the northernmost or $|\sin\beta| > 1$. Two intersections occur near the apex, the northernmost or southernmost points of the ground track (see Fig. 15). The quadrants of β can be determined easily by the landing latitude and the relative position of the intersection with respect to the ascending node. Call the smaller value β_1 , the larger value β_2 , and their difference $\Delta\beta=\beta_2-\beta_1$ (29)

The quadrants of the corresponding values of λ , λ_1 and λ_2 , can be determined by use of Eqs (27), and the condition that they differ at most by one from the quadrant of β . Define:

$$\Delta \lambda = \lambda_2 - \lambda_1$$
 with $\Delta \lambda > 0$ for $i_{VE} < 90$ °, $\Delta \lambda < 0$ for $i_{VE} > 90$ °. (30)

(3) If both $(R_{lat})_{max}$ and $(R_{lat})_{min}$ yield $|\sin\beta| \le 1$, then there are four intersections of the landing parallel of latitude with the ground swath. These intersections may be reduced to sets of two intersections by specification of a northerly or southerly approach to the landing site. Each set may now be treated separately with quadrant determination as in Case (2).

If $(R_{lat})_{max} = (R_{lat})_{min} = 0$, then the two ground swath intersections reduce

to one ground track intersection which is given by letting $\sin R = 0$ and $\cos R = 1$ in Eqs (27):

$$\sin \beta = \frac{\sin \phi_{f}^{!}}{\sin i_{VE}},$$

$$\sin \lambda = \frac{\cos i_{VE} \sin \beta}{\cos \phi_{f}^{!}}, \cos \lambda = \frac{\cos \beta}{\cos \phi_{f}^{!}}$$
(31)

The second factor in determining call-down, the "correct" orbital position, is of more importance than the correct time of deorbit, since the longitudinal range in the orbit plane imposes constraints on the location of the deorbit point. The lateral maneuverability of the re-entry vehicle offers some flexibility in the choice of deorbit point as given by $\Delta\beta=\beta_2-\beta_1$ in Figs. 14 and 15, but

in most cases this is not enough to counteract reentry atmospheric dispersions, guidance and control system errors and timing errors in the deorbit point due to density dispersions in orbit. Especially in near-polar orbits, when $\Delta\beta \rightarrow 0$, additional longitudinal range is necessary to overcome these factors and to add somewhat to the call-down frequency by imposing less severe constraints on the deorbit point location. The quantitative evaluation of the correct orbital position will be deferred until the next section.

2. Derivation of the Call-Down Conditions

There are two equations for determining call-down, one giving the position of the orbit plane with respect to the landing site and the other giving the satellite position in orbit. In each case there are conditions that have to be met for call-down to take place. The longitudinal range capability of the re-entry vehicle places constraints on the satellite position, while the lateral range capability places constraints on both orbit plane and satellite position. In the following these equations and constraints will be derived and a method for obtaining call-down frequencies from those two equations and three constraints will be given.

Consider the angular displacement in longitude of the initial point as measured from the vernal equinox, an inertial reference direction (see Fig. 16).

$$\omega_{\{i\}} t_0 = \Omega_0 - \lambda_0 + \lambda_i, \tag{32}$$

where: t_0 is the initial time; λ_0 the longitude; and ϕ_0^1 the geocentric latitude of the initial point; ω_0 the rotational rate of the earth about its axis, ω_0^+ 4.178074 x 10⁻³ deg/sec; Ω_0 the longitude of the ascending node at the initial time; and λ_1 the longitude of the initial site with respect to Ω_0 . At landing on the m-th day, the angular displacement in longitude is given by (see Fig. 17):

$$\omega_{\bigoplus} t_{f} = \Omega_{0} - \lambda_{f} + 360m + \lambda_{1} + \Delta \lambda_{M} + n\Omega,$$
(33)

where the subscript f refers to the landing site,

m is the integral number of sidereal days (1 sidereal day $^{\circ}$ 86164.1 sec), n the number of orbital revolutions from injection to deorbit, and $\Delta\,\lambda_{M}$ the difference in longitude between λ_{1} and the landing site. It can be seen from Eq (30) and Fig. 17 that one condition for call-down is

$$0 \le \Delta \lambda_{M} \le \Delta \lambda. \tag{34}$$

Equations (32) and (33) can be combined to yield $\omega_{\bigoplus} \ (t_f - t_0) = \lambda_0 - \lambda_f - \lambda_1 + 360 \, \text{m} + \text{n} \, \dot{\Omega} + \lambda_1 + \Delta \lambda_M. \tag{35}$

The time from the initial point to landing is:

$$t_f - t_0 = n \tau_0 + \sum_{j=0}^{n} (n - j + 1) \Delta \tau_j + k \Delta \tau_d + t_d,$$
 (36)

where τ_0 is the initial orbital period including oblateness effects and the second term gives the atmospheric drag effects on the period. Now we can solve Eqs (35) and (36) implicitly for n by elimination of (t_f-t₀) between them to obtain:

$$n = \frac{\lambda_0 - \lambda_f - \lambda_i + 360 \text{ m} + \lambda_1 + \Delta \lambda_M}{\omega_{\oplus} (\tau_0 - \frac{\Omega}{\omega_{\oplus}})}$$

$$- \frac{t_d + k \Delta \tau_d}{(\tau_0 - \frac{\Omega}{\omega_{\oplus}})}$$

$$- \frac{\sum_{j=0}^{n} (n - j + 1) \Delta \tau_j}{(\tau_0 - \frac{\Omega}{\omega_{\oplus}})}.$$

$$(37)$$

Another expression can be obtained for n by considering the total central angle from injection to deorbit:

$$n = \frac{\beta_i}{360} + p + \frac{\beta_1}{360} + \frac{\Delta \beta_M}{360} - \frac{R_{long}}{2\pi R_e}, \quad (38)$$

where β_i is the central angle of the initial point, p is the number of revolutions from the ascending node of β_i to the one of β_1 , and $\Delta\beta_M$ is the difference in central angle between β_1 and the landing point. Equation (8) and Fig. 4 suggest the second call-down condition:

$$0 \le \Delta \beta_{\mathbf{M}} \le \Delta \beta$$
, (39)

with a third condition for call-down imposed by the longitudinal maneuverability

$$(R_{long})_{min} \le R_{long} \le (R_{long})_{max}.$$
 (40)

The problem of obtaining call-down frequencies for an orbiting vehicle reduces to solving for the values of n from Eqs (37) and (38) for each value of m, up to the maximum number of days in orbit, q, and subject to the constraints given by Eqs (34), (39) and (40).

However, there are several difficulties. The quantities $\Delta\lambda_M$, $\Delta\beta_M$ and $R_{long.}$ in Eqs (37) and (38) are unknown, as well as the values of n and p for each value of m. In addition, Eq (37) can be solved for n only by an approximation procedure since n occurs in the summation on the right-hand side as well as on the left-hand side.

We propose to determine the lateral maneuvering effectiveness first by considering two cases:

- (1) Entry into the ground swath with $\Delta\lambda_{\rm M}$ = 0, $\Delta\beta_{\rm M}$ = 0 in Eqs (37) and (38).
- (2) Exit from the ground swath with $\Delta \lambda_{M} = \Delta \lambda$, $\Delta \beta_{M} = \Delta \beta$ in the same equations.

The approximation procedure to obtain n consists

of transferring the term
$$-\frac{\mathbf{t_d} + \mathbf{k} \triangle \tau_d}{(\tau_0 - \frac{\dot{\Omega}}{\omega_{\oplus}})}$$
 from

Eq (37) to Eq (38), and computing

$$(n_0)_1 = \frac{\lambda_0 - \lambda_f - \lambda_i + 360 \,\mathrm{m} + \lambda_1}{\omega_{\oplus} (\tau_0 + \frac{\dot{\Omega}}{\omega_{\oplus}})}$$
 (41)

in Case 1 as well as

$$(\mathbf{n}_0)_2 = (\mathbf{n}_0)_1 + \frac{\Delta \lambda}{\omega_{\oplus} (\tau_0 - \frac{\dot{\Omega}}{\omega_{\varpi}})}$$
 (42)

in Case 2 for each value of m. Here $(n_0)_1$ and $(n_0)_2$ are the number of revolutions from the time the initial point passes through the ground track to the entry and exit of the landing point from the ground swath, respectively. The effects of drag have been neglected in Eqs (41) and (42). However, the values of $(n_0)_1$ and $(n_0)_2$ obtained from Eqs (42) and (43) for a given m permit us to calculate drag effects by replacing n by $(n_0)_1$ and $(n_0)_2$ in the drag term of Eq (37),

$$\Delta n_{D} = -\frac{\sum_{j=0}^{n} (n - j + 1) \Delta \tau_{j}}{(\tau_{0} - \frac{\dot{\Omega}}{\omega_{\oplus}})}$$
(43)

Now we can compute for each day in orbit

$$(\mathbf{n}_{0} + \Delta \mathbf{n}_{D})_{1} = \frac{\lambda_{0} - \lambda_{f} - \lambda_{i} + 360 \,\mathrm{m} + \lambda_{1}}{\omega_{\bigoplus} (\tau_{0} + \frac{\dot{\Omega}}{\omega_{\bigoplus}})}$$

$$- \frac{(\mathbf{n}_{0})_{1}}{(\tau_{0} - \frac{\dot{\Omega}}{\omega_{\bigoplus}})}$$

$$(44)$$

and

$$(\mathbf{n}_0 + \Delta \mathbf{n}_D)_2 = \frac{\lambda_0 - \lambda_f - \lambda_i + 360 \,\mathrm{m} + \lambda_i + \Delta \lambda}{\omega_{\bigoplus} (\tau_0 + \frac{\Omega}{\omega_{\bigoplus}})}$$

$$- \frac{(\mathbf{n}_0)_2}{j=0} \left[(\mathbf{n}_0)_2 - j + 1 \right] \Delta \tau_j$$

$$(\tau_0 - \frac{\Omega}{\omega_{\bigoplus}})$$

$$(45)$$

Denote the integral part of $(n_0 + \Delta n_D)_1$ at a given m by I_{m1} and the integral part of $(n_0 + \Delta n_D)_2$ for the same value of m by I_{m2} .

Next we determine the in-plane maneuvering effectiveness by collecting the remaining terms in the other equation. Consider entry of the landing site into the ground swath with minimum longitudinal maneuverability,

$$(n_0 + \Delta n_D)_{1 \text{ min}} = p + \frac{\beta_i + \beta_1}{360} + -\frac{(t_d)_{\min} + k \Delta \tau_d}{(\tau_0 - \frac{\Omega}{\omega_{\bigoplus}})}$$

$$-\frac{(R_{\text{long}})_{\min}}{2 \pi R_e},$$
(46)

and its entry into the ground swath with maximum longitudinal maneuverability,

$$(n_0 + \Delta n_D)_{1 \text{ max}} = p + \frac{\beta_i + \beta_1}{360} + \frac{(t_d)_{\text{max}} + k \Delta \tau_d}{(\tau_0 - \frac{\dot{\Omega}}{\omega_{\oplus}})}$$
$$- \frac{(R_{\text{long}})_{\text{max}}}{2 \pi R_{\Omega}}$$
(47)

Similarly, there are two expressions for the exit of the landing site from the ground swath which can be obtained by adding the term $\frac{\Delta\beta}{360}$ to Eqs (46) and (47), respectively. Take the smallest and largest value of the four values of (n $_0$ + $^\Delta n_D$) just computed and form a range

smallest
$$\left[(n_0 + \triangle n_D) - p \right]$$
,
largest $\left[(n_0 + \triangle n_D) - p \right]$. (48)

The additional assumption has been made here that atmospheric drag acts from the initial point to touchdown, i.e., during n_0 revolutions, rather than from injection to deorbit, or during n revolutions. In most practical cases R_{long} is less than one revolution and this assumption will not affect the call-down frequency appreciably. Furthermore, the drag effects on the dispersed elliptic orbit with period $\tau_j^{} + \Delta \tau_d^{}$ should be essentially the same as those on the nominal circular orbit with period $\tau_i^{}.$

The final step consists of combining lateral and in-plane maneuverability to test for call-down at a given m. Let p in Eq (48) vary between

$$(I_{m1} - 3) \le p \le (I_{m2} + 3)$$
 (49)

and add each of these values of p to Eq (48) to form the seven ranges

smallest
$$(n_0 + \Delta n_D)$$
, (50) largest $(n_0 + \Delta n_D)$

for each p in Eq (49).

Whenever Eq (50) and the range formed by $(n_0 + \Delta n_D)_1$ and $(n_0 + \Delta n_D)_2$ for the same m overlap, there exists a call-down on the day m. Denote each call-down day by m = m_c. For each value of m = m_c obtain

$$n_{\min} = (n_0 + \Delta n_D)_1 \text{ from Eq (44)} - \frac{(t_d)_{\max} + k \Delta \tau_d}{(\tau_0 - \frac{\dot{\Omega}}{\omega_{\bigoplus}})}$$
(51)

$$n_{\text{max}} = (n_0 + \Delta n_D)_2 \text{ from Eq (45)} - \frac{(t_d)_{\text{min}} + k \Delta \tau_d}{(\tau_0 - \frac{\dot{\Omega}}{\omega_{\bigoplus}})}$$
(52)

where n is the number of revolutions from the time the injection point intersects the ground track to the time the deorbit point intersects the ground swath, and accounts essentially for lateral maneuverability. However, the controlling factor of satellite call-down is the in-plane maneuverability from deorbit to landing which places a constraint

$$\frac{\beta_{1}}{360} - \frac{(R_{long})_{max}}{2\pi R_{e}},$$

$$\frac{\beta_{1} + \Delta \beta}{360} - \frac{(R_{long})_{min}}{2\pi R_{e}}$$
(53)

on the satellite position at deorbit during any revolution. The call-down revolutions can be obtained by (1) converting the revolutions from n, which is measured from injection starting at 0, to N, the number of revolutions from the first as-

cending node, where N = 1.0 and (2) by noting for which integral number of revolutions the fractional range (Eq (53)) overlaps the range formed by N $_{\rm min}$ and N $_{\rm max}$ (Eqs (51) and (52) with n converted to N). There may be more than one call-down revolution per day if (N $_{\rm max}$ - N $_{\rm min}$) > 1, which occurs for large lateral maneuverability and for small lateral maneuverability if the landing site is near the northernmost or southernmost points of the ground track. The resulting call-down table for each m = m $_{\rm c}$ consists of N, the altitude, and the time in orbit for both n $_{\rm min}$ and n $_{\rm max}$.

This discussion of call-down frequency ends the qualitative and quantitative description of reentry which uses at least some rocket deceleration during the earth return trajectory phase.

This re-entry technique reduces the demands on the heat shield materials, the guidance accuracy and the aerodynamic performance of the re-entry vehicle itself. On the other hand, a major drawback of this return technique lies in the expenditure of additional fuel and a lesser drawback in the longer time required for completion of the mission.

D. REFERENCES

- Anon., "Orbital Flight Handbook," ER 12684, Martin Company, Space Systems Division (Baltimore) 1963.
- Seifert, Howard S., ed., "Space Technology,"
 John Wiley and Sons, New York, 1959.
 Chapter XII, "Recovery Dynamics--Heat
 Transfer at Hypersonic Speeds in a Planetary
 Atmosphere," L. Lees.
- 3. Chapman, Dean R., "An Approximate Analytical Method for Studying Entry into Planetary Atmospheres," NASA TR R-11, 1959 (supersedes NACA TN 4276).
- Luidens, Roger W., "Flight-Path Characteristics for Decelerating from Supercircular Speed," NASA TN D-1091, 1961.
- Chapman, Dean R., "An Analysis of the Corridor and Guidance Requirements for Supercircular Entry into Planetary Atmospheres," NASA TR R-55, 1959.
- Grant, Frederick C., "Modulated Entry," NASA TN D-452, 1960.
- Levy, Lionel, L., Jr., "Atmosphere Entries with Spacecraft Lift-Drag Ratios Modulated to Limit Decelerations," NASA TN D-1427, 1962.
- 8. Bryant, J. F. and Frank, M. P., "Supercircular Re-entry Guidance for a Fixed L/D Vehicle Employing a Skip for Extreme Ranges," ARS Paper 2489-62, 1962.
- 9. Sommer, Simon C. and Short, Barbara J.,
 "Point Return from a Lunar Mission for a
 Vehicle that Maneuvers Within the Earth's
 Atmosphere," NASA TN D-1142, 1961.

- 10. Grant, Frederick C., "Importance of the Variation of Drag with Lift in Minimization of Satellite Entry Acceleration," NASA TN D-120, 1959.
- Grant, Frederick C., "Analysis of Low-Acceleration Lifting Entry from Escape Speed," NASA TN D-249, 1960.
- 12. Wong, Thomas J. and Slye, Robert E., "The Effect of Lift on Entry Corridor Depth and Guidance Requirements for the Return Lunar Flight," NASA TR R-80, 1960.
- 13. Wang, H. E. and Chu, S. T., "Variable-Lift Re-entry at Superorbital and Orbital Speeds," Aerospace Corp Report TDR -930 (2570-20) TN-2, May 1962 (IAS Paper 62-165, 1962).
- 14. Galman, Barry A., "Direct Re-entry at Escape Velocity," GE-MSVD TIS R60SD357, April 1960 (AAS Preprint 60-86, August 1960).
- 15. Bossevain, Alfred G., "The Effect of Lateral and Longitudinal Range Control on Allowable Entry Conditions for a Point Return from Space," NASA TN D-1067, 1961.
- Baradell, Donald L., "Lateral Range Control by Banking During Initial Phases of Supercircular Re-entries," NASA TN D-1511, 1962.
- 17. Slye, Robert E., "An Analytical Method for Studying the Lateral Motion of Atmosphere Entry Vehicles," NASA TN D-325, 1960.
- Young, John W., "A Method for Longitudinal and Lateral Range Control for High-Drag Low-Lift Vehicle Entering the Atmosphere of a Rotating Earth," NASA TN D-954, 1961.
- Wingrove, Rodney C., "A Survey of Atmosphere Re-entry Guidance and Control Methods," IAS Paper No. 63-86, 1963.
- 20. Reismann, H. and Pistiner, J. S., "Design and Evaluation of a Re-entry Guidance System," Astronautica Acta, Vol. VI, Fasc 2-3, July 1960, pp 79 to 114.
- 21. General Electric Company, "Flight Control Study of a Manned Re-entry Vehicle," WADD Technical Report 60-695, Vols. I and II, July 1960.
- 22. Cheatham, D. C., Young, J. W. and Eggleston, J. M., "The Variation and Control of Range Traveled in the Atmosphere by a High-Drag Variable-Lift Entry Vehicle," NASA TN D-230, 1960.
- 23. Teague, Roger, "Flight Mechanics of Reentry After Flight by Means of Various Lifting Techniques," NASA MNN-M-AERO-4-60, 1960.
- 24. Shahan, R. L., "Re-entry Guidance for Manned Spacecraft," paper presented at

- ARS-IRE, 15th Annual Technical Conference, Cincinnati, Ohio, April 1961.
- 25. Friedenthal, M. J., Love, J. A. and Neustadt, L. W., "Feasibility Study of an Acceleration Monitoring Guidance System for Lifting Re-entry Vehicles," STL Report 9572-0006-MU-000, October 1961.
- Edge, C. F. and Hechtman, E. P., "Control Loop Simulation for Energy Management," Proc Aerospace Forum II Session, IAS Meeting, New York, 22 to 24 January 1962.
- 27. Wingrove, Rodney C. and Coate, Robert E., "Lift-Control During Atmosphere Entry from Supercircular Velocity," Proc IAS National Meeting on Manned Space Flight, St. Louis, Missouri, 30 April to 2 May 1962.
- 28. Wingrove, Rodney C., "A Study of Guidance to Reference Trajectories for Lifting Re-entry at Supercircular Velocity," NASA TR-151, 1963.
- 29. Foudriat, Edwin C., "Guidance and Control During Direct-Descent Parabolic Reentry," NASA TN D-979, 1961.
- 30. Webber, A. L., "Investigation of the Instrumentation of an Atmospheric Re-entry," Report T-218, MIT Instrumentation Laboratory, September 1959.
- 31. Foudriat, Edwin C., "Study of the Use of a Terminal Controller Technique for Reentry Guidance of a Capsule-Type Vehicle," NASA TN D-828, 1961.
- 32. Rosenbaum, Richard, "Longitudinal Range Control for a Lifting Vehicle Entering a Planetary Atmosphere," ARS Preprint 1911-61, August 1961.
- 33. Bryson, Arthur E., and Denham, Walter F., "A Guidance Scheme for Supercircular Reentry of a Lifting Vehicle," ARS Preprint 2299-61 (ARS Journal, Vol. 32, June 1962. pp 894-8).
- 34. North, Raymond, and Speyer, Jason, "Control System for Supercircular Entry Maneuvers," IAS Paper 62-3, January 1962.
- 35. Kelly, H. J., Kapp, R. E., and Moyer, H., "Successive Approximation Techniques for Trajectory Optimization," IAS Symposium on Vehicle System Optimization, November 28 to 29, 1961.
- 36. Kelly, H. J., Gradient Theory of Optimal Flight Paths, ARS Journal Vol. 30, pp 947 to 953, October 1960.
- 37. Bryson, A. E., Denham, W. F., Carroll, F. J., and Mikami, Kinya, "Determination of Lift or Drag Programs to Minimize Reentry Heating," Journal of the Aero/Space Sciences, Vol. 29, No. 4, April 1962.

- 38. Bryson, A. E., and Denham, W. F., "A Steepest Ascent Method of Solving Optimum Programming Problems," Raytheon Co., Missile and Space Division, Report BR-1303, August 1961.
- 39. Speyer, J. L., "Optimization and Control Using Perturbation Theory to Find Neighboring Optimum Paths," presented at the SIAM Symposium on Multivariable Linear Control System Theory, Boston, Mass., November 1 to 2, 1962 (to be published in series on control of the Society for Industrial and Applied Mathematics).
- 40. "A Study of Energy Management Techniques for a High Lift Vehicle," General Electric Company, Air Force Systems Command Technical Documentary Report ASD-TDR-62-77, Vols. 1 and 2, June 1962.
- 41. Wingrove, Rodney C., and Coate, Robert, E., 'Piloted Simulator Tests of a Guidance System Which Can Continuously Predict Landing Point of a Low L/D Vehicle During Atmosphere Re-entry," NASA TN D-787, 1961
- 42. Dow, Paul C., Jr., Fields, Donald P., and Scammell, Frank H., "Automatic Re-entry Guidance at Escape Velocity," ARS Preprint 1946-61, August 1961.
- 43. Lear, Inc., "A Study of Selected Control-Display Problems for Manned Aerospace Vehicles," Lear Engineering Report GR-1405, ASD Technical Report, March 1962.
- 44. Hildebrand, R., "Manned Re-entry at Supersatellite Speeds," IAS Paper No. 60-83, 1960.
- 45. Rosamond, D. L., "Satellite Recovery Techniques for Optimization of Touchdown Accuracy," Journal of the Aero/Space Sciences, Vol. 28, No. 3, March 1961.
- 46. Kozai, Y., "The Motion of a Close Earth Satellite," Astronomical Journal, Vol. 64, No. 9, November 1959.
- 47. Struble, R.A., "The Geometry of the Orbits of Artificial Satellites," Archive for Rational Mechanics and Analysis, Vol. 7, No. 2, 1961.
- 48. Mandell, D. S., "Maneuvering Performance of Lifting Re-Entry Vehicles," ARS Journal, Vol. 32, No. 3, March 1962.
- 49. Jensen, J., Townsend, G. E., Kork, J., Kraft, J. D., "Design Guide for Orbital Flight," McGraw-Hill, New York, 1962.
- Lee, V. A., "Atmosphere-Oblateness Correction Factor for Circular Satellite Orbits," ARS Journal, Vol. 32, No. 1, January 1962.
- 51. Cole, A. E., Court, A., Kantor, A. J.,
 "Standard Atmosphere Revision to 90 km,"
 Geophysics Research Directorate, Air Force

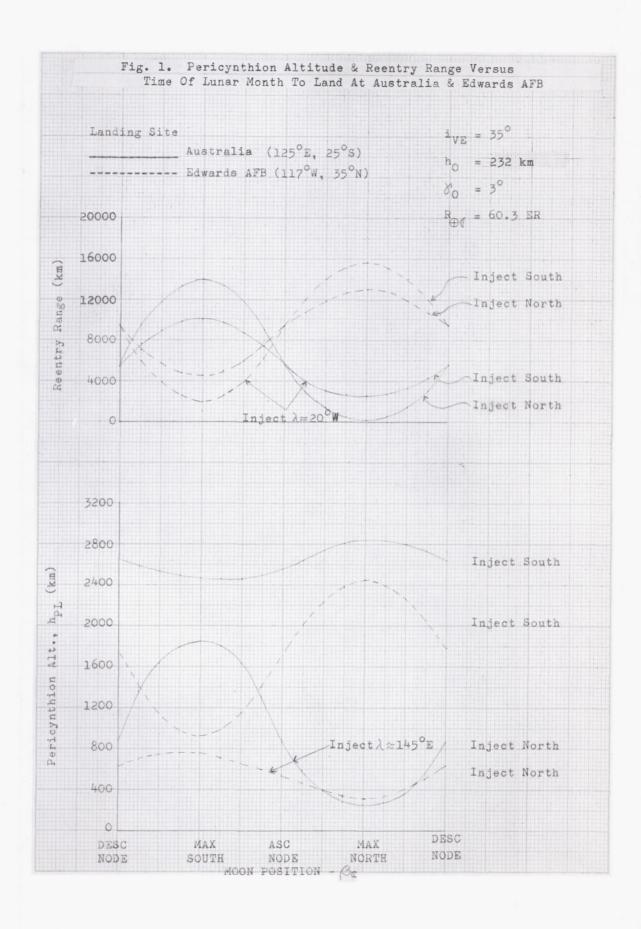
- Research and Development Command, Bedford, Mass., 28 March 1961.
- 52. Champion, K. S. W., and Minzner, R. A.,
 "Proposed Revision of United States Standard
 Atmosphere, 90-700 km," Geophysics Research Directorate, Air Force Research and
- Development Command, Bedford, Mass., 11 December 1961.
- 53. Chauvenet, W., "A Manual of Spherical and Practical Astronomy," Vol. 1, Dover Publications, Inc., New York, 1960.

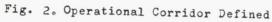
ILLUSTRATIONS

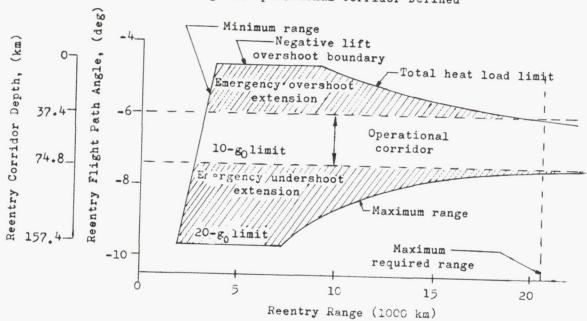
Figure	Title	Page
1	Pericynthion Altitude & Reentry Range Versus Time of Lunar Month to Land at Australia & Edwards AFB.	X-29
2	Operational Corridor Defined	X-30
3	Effect of Entry Velocity on Corridor Depth	X-31
4	Correlation of the Maximum Reduction in Peak Deceleration with the Aerodynamic Resultant-Force Coefficient	X-32
5	Modulation Effectiveness for Lifting Vehicles	X-33
6	10-g $_0$ Undershoot Corridor Boundaries for an Entry Velocity of 10.7 km/sec Lift Modulated from C $_{ m L}$	
	to $C_L = 0$	X-34
7	Single Pass Overshoot and 10-g ₀ Maximum Undershoot Corridor Boundaries for a Reentry Velocity of 10.7 km/sec	X-35
8	Longitudinal Range Capability	X-36
9	Estimated Maximum Lateral Range for Super-Circular Reentry	X-37
10	Maneuvering Envelope	X-38
11	Maneuvering Envelope	X-39
12	Fuel Required for Rocket Deceleration from Parabolic to Circular Velocity	X-40
13	Fuel Required to Obtain a Circular Orbit as a Function of Exit Velocity and Specific Impulse of Fuel for a Combination Rocket and Aerodynamic Deceleration.	X-41
14	Southerly Approach to a Landing (Case 3 of Descent Conditions)	X-42

ILLUSTRATIONS (continued)

Figure	Title	Page
15	Approach to a Landing Near the Northern Most Point of the Satellite Ground Track (Case 2 of Descent Conditions	X-43
16	Displacement in Longitude at the Initial Time	X-44
17	Displacement in Longitude at Landing	X-45







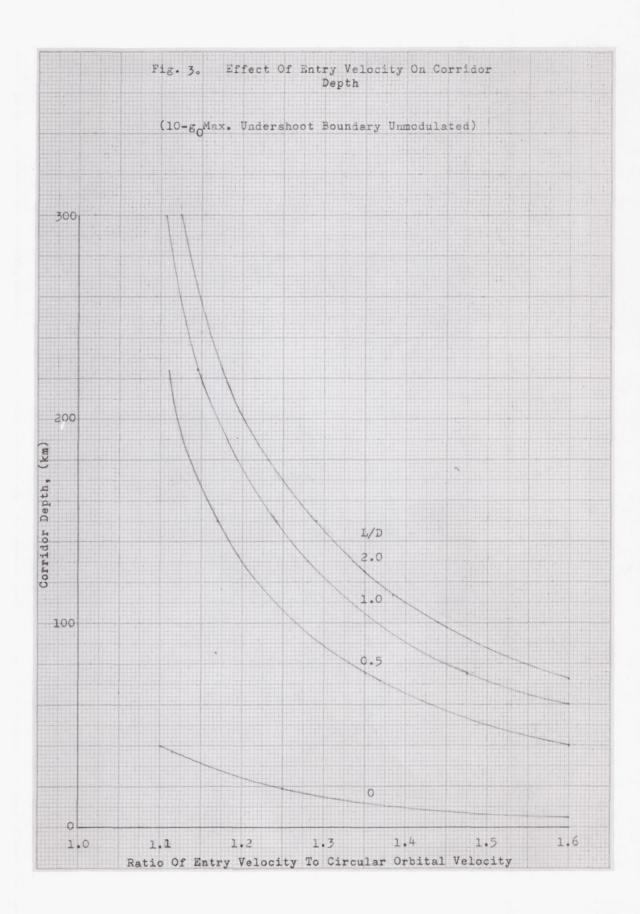
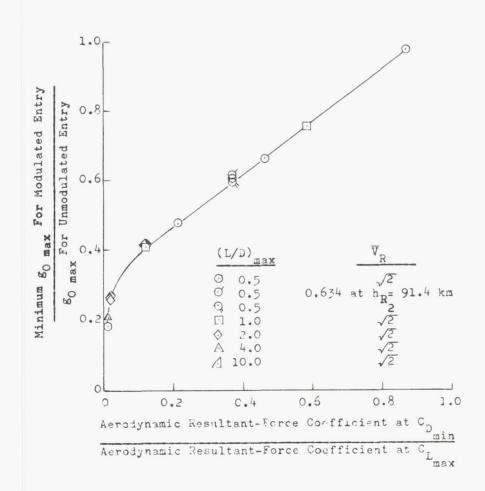


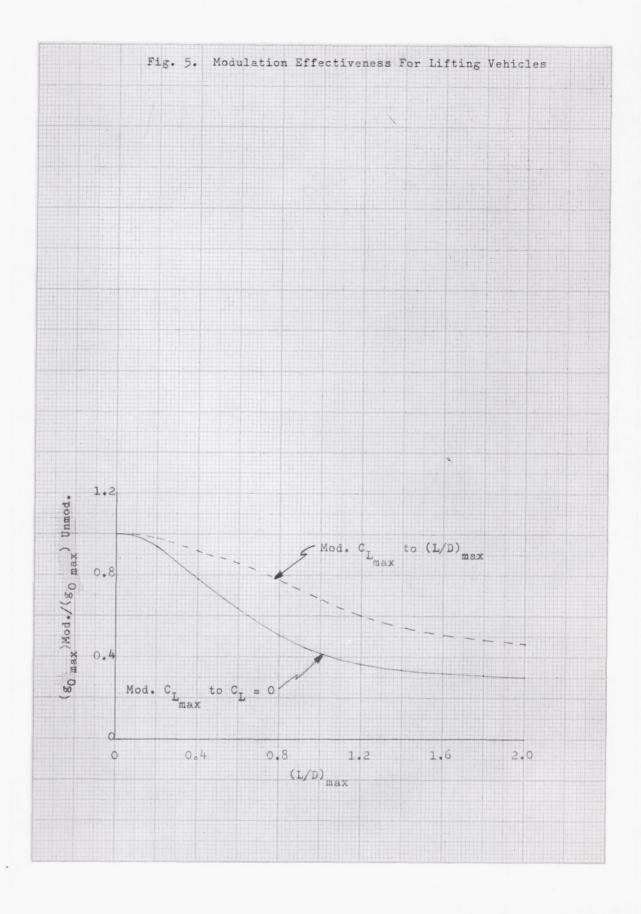
Fig. 4. Correlation Of The Maximum Reduction In Peak Deceleration With The Aerodynamic Resultant-Force Coefficient

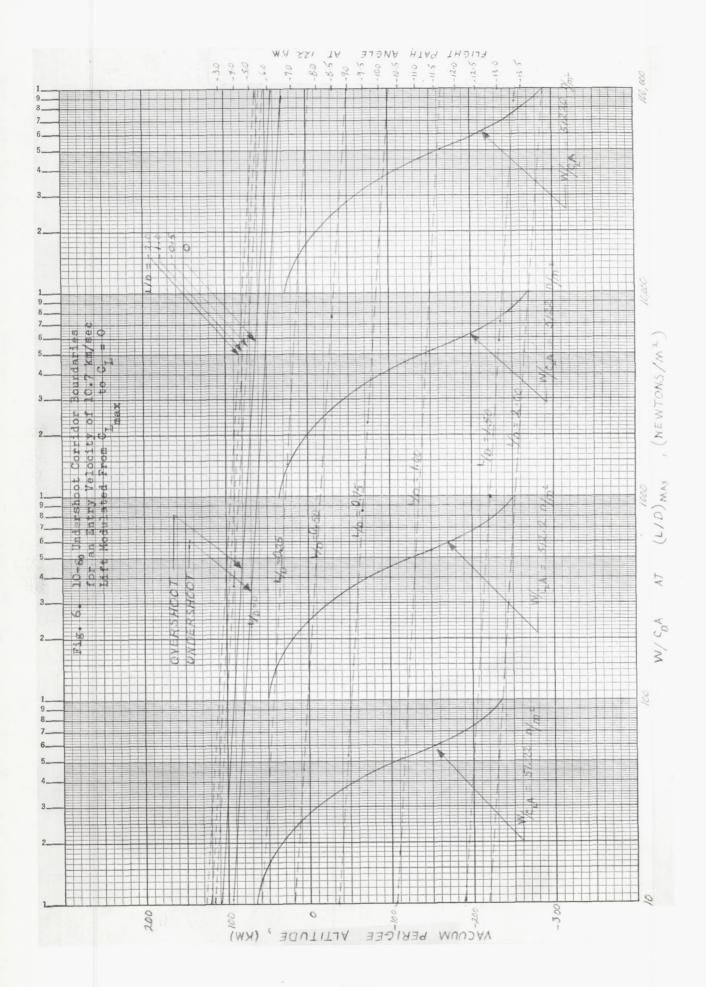
Reentry Conditions:

$$h_R = 122 \text{ km}$$

=5.7° > ∂_R' > -9.2°, $(L/D)_{unmod} = (L/D)_{max}$, $(L/D)_{mod} = L/D \text{ at } C_{L_{max}}$,
315 kg/_m2 < M/C_DA at $(L/D)_{max}$ < 6600 kg/_m2







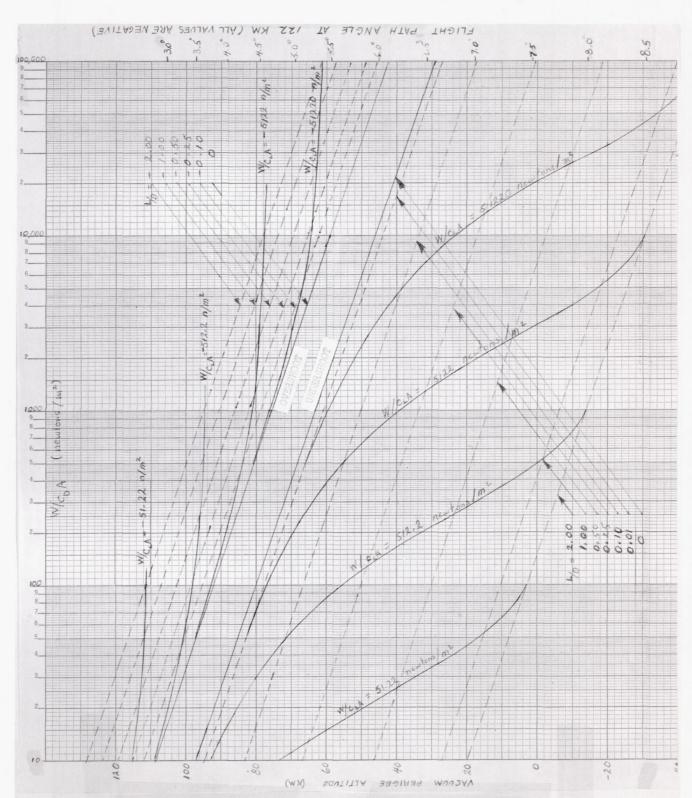
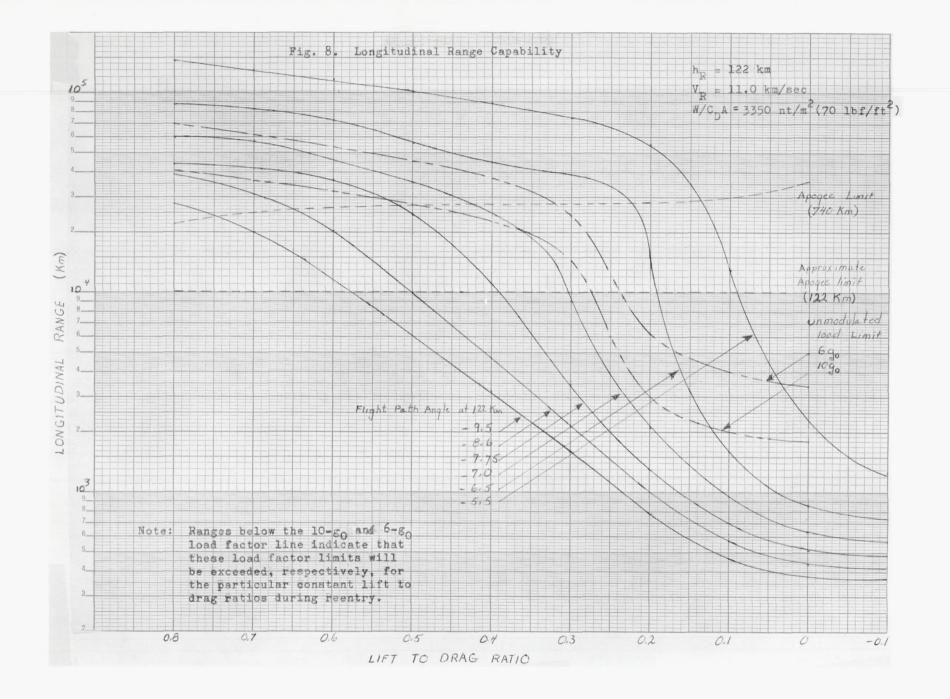
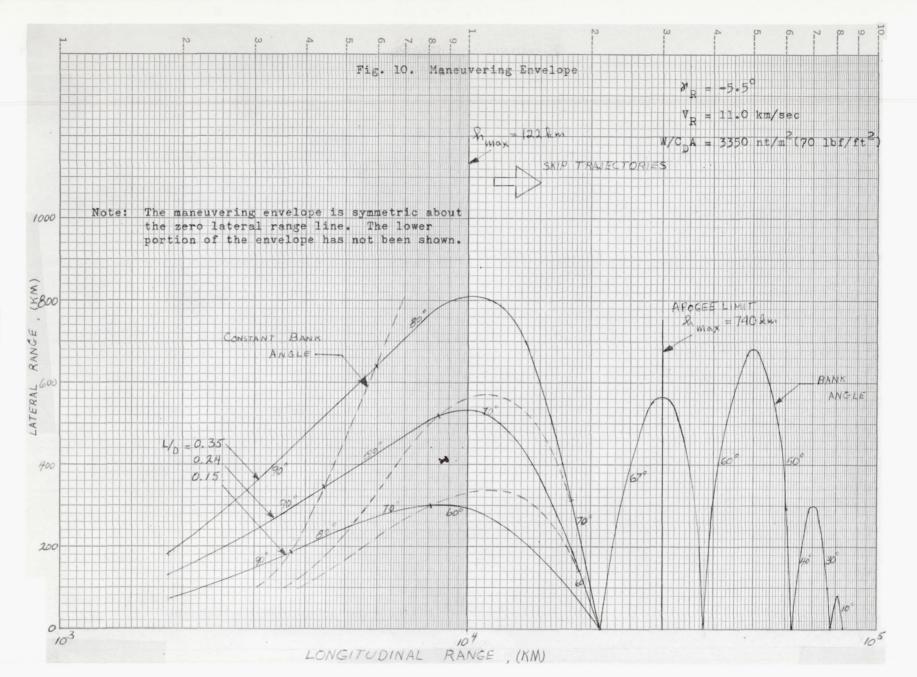
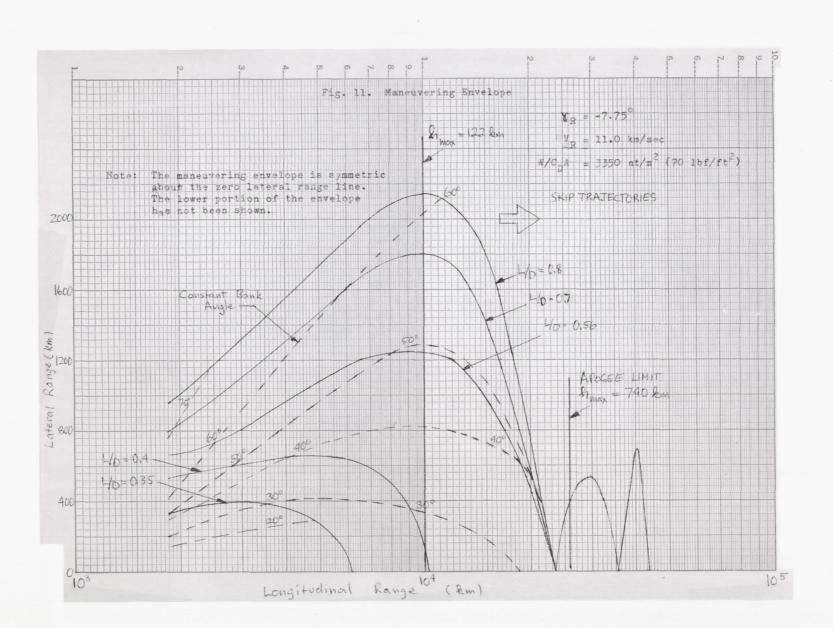


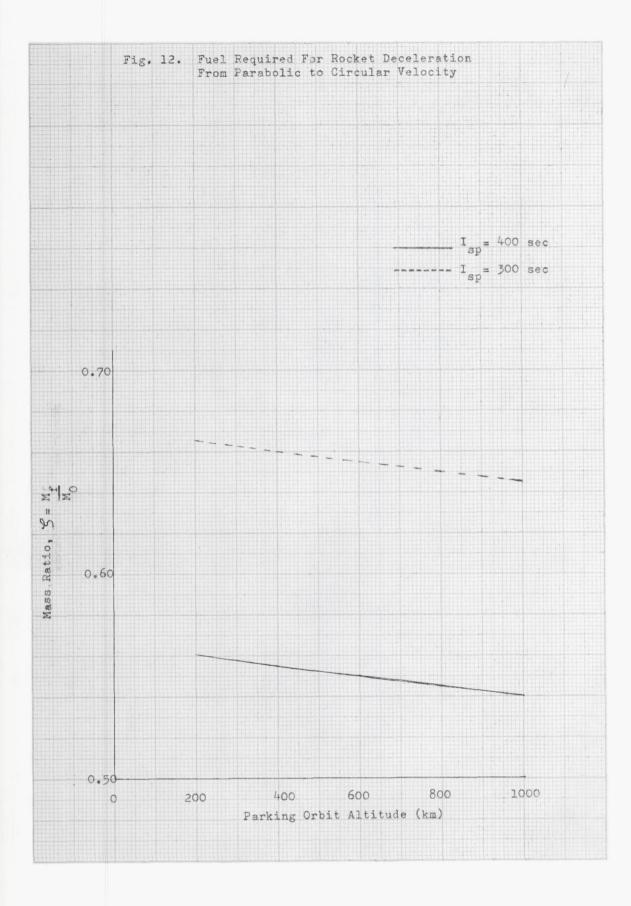
Fig. 7. Single Pass Overshoot and 10-g_O Maximum Undershoot Corridor Boundaries For a Reentry Velocity of 10.7 km/sec











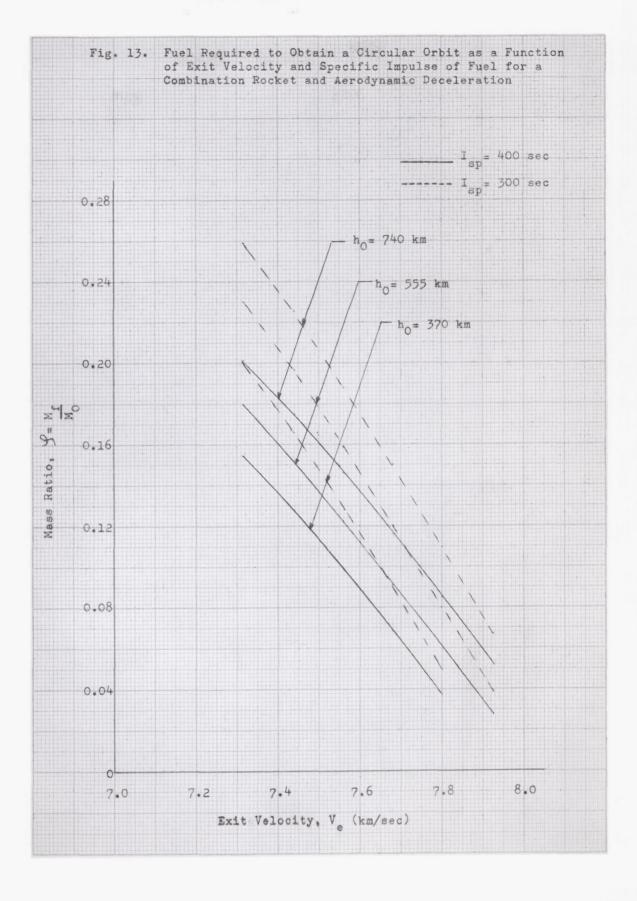


Fig. 14. Southerly Approach to a Landing (Case 3 of Descent Conditions)

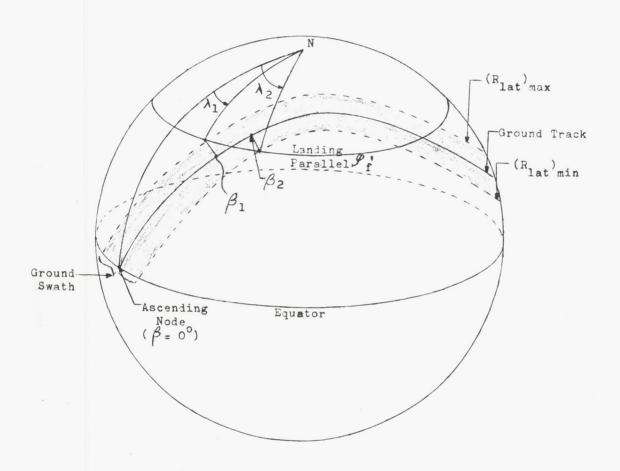


Fig. 15. Approach to a Landing Near the
Northern Most Point of the Satellite
Ground Track (Case 2 of Descent Conditions)

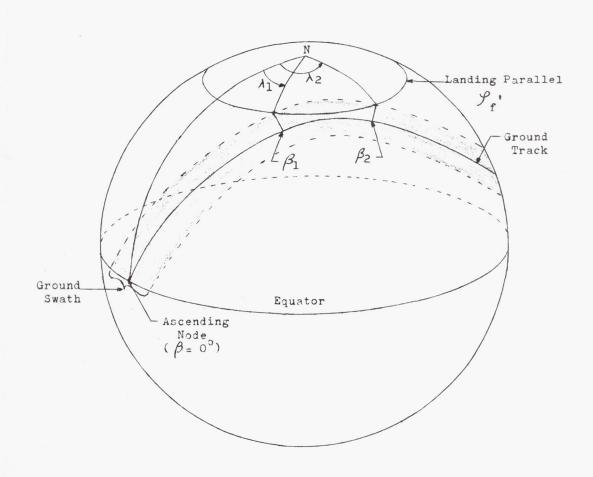


Fig. 16. Displacement in Longitude at the Initial Time

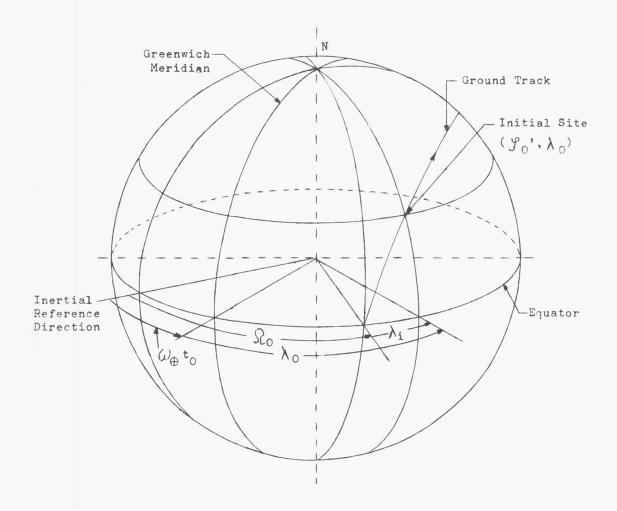


Fig. 17. Displacement in Longitude at Landing

